

**The use of bimolecular fluorescence  
complementation (BiFC) to investigate the functional  
implications of neuropeptide Y receptor dimerisation  
and beta-arrestin recruitment**

**Laura Elise Kilpatrick, MSc., BSc.**

**Thesis submitted to the University of Nottingham for the  
degree of Doctor of Philosophy**

**September 2014**

## **Abstract**

Recent advances in the understanding of the major class of cell surface G protein coupled receptors (GPCRs) have added complexity to their molecular pharmacology. Firstly GPCRs signal not only through G proteins but also other partners such as  $\beta$ -arrestins - adaptors initially characterised for roles in desensitisation and endocytosis. The second is that GPCRs can form homodimers or heterodimers between different subtypes. The functional significance of dimerisation remains debatable, with part of the controversy surrounding an inability to directly assign pharmacological properties to dimers, or receptor-effector complexes, of known molecular composition.

This thesis explores the use of bimolecular fluorescence complementation (BiFC), as a means to address this problem. In BiFC, protein-protein interactions are identified by complementary fluorescent protein fragment tags, which refold and generate a fluorescent signal upon association. As BiFC is irreversible it therefore identifies receptor complexes of known composition. The Y receptor family, which respond to neuropeptide Y (NPY), and related hormones peptide YY and pancreatic polypeptide, were chosen as model GPCRs to explore the use of BiFC in identifying  $\beta$ -arrestin interactions and investigating the behaviour of receptor dimers. The 4 cloned Y receptor subtypes share G protein coupling pathways, but less is known about their relative recruitment of  $\beta$ -arrestins and regulation by endocytosis. Moreover, potential heterodimerisation (e.g. Y1/Y5) has largely unproven physiological roles in central feeding and appetite regulation.

First, BiFC based high content imaging assays were established to quantify the pharmacology of  $\beta$ -arrestin2 recruitment to Y receptor subtypes, and demonstrate the correlation between this process and agonist induced endocytosis (Chapter 3). Targeted mutagenesis, demonstrated the shared involvement of key intracellular receptor domains in arrestin recruitment and internalisation. Fluorescence recovery after photobleaching, and fluorescence

correlation spectroscopy were used to measure the diffusion of fluorescent Y receptor complexes and demonstrated that NPY stimulation slowed receptor motility, reconciling with the propensity of these receptors to undergo endocytosis (Chapter 4). The use of a novel BiFC system allowed, for the first time, this slowed motility to be correlated with the behaviour of defined Y receptor- $\beta$ -arrestin signalling complexes.

To study dimerisation, BiFC was used to constrain Y1 receptor subtypes as homo or heterodimers of precise composition. Quantitative plate reader imaging of recomplemented YFP measured BiFC dimer internalisation as an indirect readout of  $\beta$ -arrestin recruitment and dimer function (Chapters 5 and 6). Constraining Y1 receptor and  $\beta$ 2-adrenoceptor BiFC homodimers had no effect on agonist promoted internalisation. Selective mutagenesis of residues within a single protomer of each dimer illustrated that occupation of a single ligand binding site and the presence of one phosphorylated C terminal domain was sufficient. These results also implied symmetrical binding of  $\beta$ -arrestin to Y1 receptor dimers, an observation supported by the earlier single molecule imaging techniques.

Finally, constrained Y1/Y5 receptor BiFC heterodimers showed modified pharmacology not evident for other heterodimer combinations (Y1/Y4, Y1/ $\beta$ 2AR). The most striking alterations were a switching of the behaviour of Y5 subtype selective antagonists from surmountable (at the Y5 receptor) to insurmountable inhibition of NPY stimulated internalisation of the Y1/Y5 dimer; while in contrast Y1 antagonists became ineffective in inhibiting Y1/Y5 dimer responses. These observations suggest selective allosteric interactions between the respective Y1 and Y5 receptor protomers. Previous attempts to develop anti obesity agents that selectively target either the Y1 or Y5 receptor subtype, have lacked long term clinical efficacy. However identification of novel pharmacology of the Y1/Y5 dimer, and a strategy to screen for selective antagonism of this pairing using the BiFC system, may be a way to identify future therapeutic treatments for obesity.

## Acknowledgements

Firstly I would like to send my sincerest gratitude to my supervisor Dr Nicholas Holliday, not only for everything he has done throughout the course of my PhD but the three years prior to that. I could not have undertaken this PhD without his guidance, enthusiastic encouragement, knowledge and above all patience over the last 7 years. I would also like to thank him for taking an interest in my career development when he really didn't have to, and all the opportunities that have since come my way, such as presenting at international conferences and post doctoral appointments are in no small part due to him.

My thanks also go to the British Pharmacological Society for funding my thesis through their A.J Clark studentship.

I would also like to thank Dr Steve Briddon and Professor Steve Hill for their understanding and patience during my time it has taken me to write this thesis. In addition I would also like to thank Dr Briddon for all his help with FCS and PCH.

ICS has been a fantastic place to work for the last 7 years, and I would like to send a general thank you to all members past and present for all the advice, scientific support, encouragement and cakes! In particular thank you to June McCulloch and Marleen Groenen for keeping the lab and tissue culture running so smoothly and Tim Self for microscopy training.

I would particularly like to thank Dr Leigh Stoddart for so much professional and personal advice that I really should be paying her consultancy rates; Dr Joelle Goulding and Dr Karolina Gherbi for all their advice and support and for helping me conquer Endnote and pagination respectively without destroying my computer; and a special tack så mycket to Dr Sarah-Jane Watson.

I would like to thank my entire family, particularly my Mum and Dad for their endless encouragement and support through all of my many doubts, my brother Neil and sister in law Manda, and my two nieces Isobel and Erica for putting all my stresses into a Peppa Pig shaped perspective. Additionally I'd like to express

my gratitude to all my friends outside of science who have no idea really of what I do but are still incredibly supportive, particularly, Helen Mackness, Anna Barber and Helen Osborne who when asked by Professor Brian Cox what my PhD was about replied ‘Something to do with Science...’

I apologise if these acknowledgements are rather long, but as I was writing them I realised that it is very rare that you get an opportunity to publicly thank people in print. I’m not sure I’ve ever experienced so many highs and lows as during the PhD, but I know it would have been impossible to have done any of this without all the support I have been so fortunate to have had along the way. So to paraphrase the greatest Doctor of them all (The Eleventh):

‘Every life is a pile of good things and bad things. The good things don’t always soften the bad things but vice versa the bad things don’t always spoil the good things and make them unimportant. And you all definitely added to my pile of good things.’

## Abbreviations

**cPP Aib NPY**- pancreatic polypeptide (1-17) (Ala<sup>31</sup>, Aib<sup>32</sup>) neuropeptide Y  
(18-36)

**AC** - adenylyl cyclase

**β2AR** -β2 adrenoceptor

**BiFC**-Bimolecular fluorescence complementation

**BIBO3304 trifluoroacetate**- *N*-[(1*R*)-1-[[[4-[[[(Aminocarbonyl) amino] methyl] phenyl] methyl]amino]carbonyl]-4-[(aminoiminomethyl) amino] butyl]-α-phenyl-benzeneacetamide ditrifluoroacetate

**BRET**- bioluminescence resonance energy transfer

**BSA**- bovine serum albumin

**cAMP**- adenosine-3',5' cyclic monophosphate

**CGP71683 hydrochloride**- *N*-[[*trans*-4-[[[(4-Amino-2-quinazolinyl) amino] methyl]cyclohexyl]methyl]-1-naphthalene sulfonamide hydrochloride

**DMEM**-Dulbecco's modified Eagle's medium

**DMSO**-dimethyl sulphoxide

**DPM**-disintegrations per minute

**EC<sub>50</sub>** - concentration required for 50% maximal responses

**ERK**-extracellular signal related protein kinase

**FBS**- foetal bovine serum

**FCS**-fluorescence correlation spectroscopy

**FRAP**- fluorescence recovery after photobleaching

**FRET**- fluorescence resonance energy transfer

**GDP**- guanosine diphosphate

**GFP**- green fluorescent protein

**GPCR**- G protein coupled receptor

**GRK**- GPCR related kinase

**GTP**- guanosine 5' triphosphate

**HBSS**-HEPES buffered saline solution

**HEK293**- Human embryonic kidney, clone 293

**ICL**- intracellular loop

**IP<sub>3</sub>**- inositol 1,4,5-trisphosphate

**Isoprenaline**- isoprenaline hydrochloride; (4-[1-Hydroxy-2-[(1-methyl ethyl)amino]ethyl]-1,2-benzenediol hydrochloride)

**L182,504**-5,5-Dimethyl-2-(2,3,4,9-tetrahydro-3,3-dimethyl-1oxo-1*H*-xanthen-9-yl)-1,3-cyclohexanedione

**LB**-Luria broth

**MAPK**-mitogen activated protein kinase

**NPY**-neuropeptide Y

**NPY5RA972**-*N*-[4-Methyl-9-(1-methylethyl)-9*H*-carbazol-3-yl]-4-morpholinecarboxamide

**PBS**-phosphate buffered saline

**PCH**-photon counting histogram

**pIC<sub>50</sub>**- concentration required for 50% inhibition of responses (IC<sub>50</sub>) expressed as a negative logarithm

**pK<sub>b</sub>** -equilibrium dissociation constant; the concentration of antagonist required to occupy 50% of receptors expressed as a negative logarithm

**PIP<sub>2</sub>**-phosphatidylinositol 4,5-bisphosphate

**PKA/C**-protein kinase A or C

**PLC**-phospholipase C

**PP**-Pancreatic polypeptide

**Propranolol**-Propranolol hydrochloride; (*RS*)-1-[(1-Methylethyl)amino]-3-(1-naphthalenyloxy) -2-propanol hydrochloride

**PYY**-peptide YY

**ROI**-region of interest

**Salbutamol**-salbutamol hemisulphate;  $\alpha^1$ -[[[(1,1-Dimethylethyl) amino] methyl]-4-hydroxy-1,3-benzenedimethanol hemisulfate

**Salmeterol**-salmeterol xinofoate; 4-Hydroxy- $\alpha^1$ -[[[6-(4-phenylbutoxy)

hexyl]amino]methyl]-1,3-benzenedimethanol 1-  
hydroxy- 2- naphthalene carboxylic acid salt

**TM**-transmembrane

**vYFP**-venus yellow fluorescent protein

**Yc**-carboxyl fragment of venus yellow fluorescent protein (173-238)

**Yn**-amino fragment of venus yellow fluorescent protein (2-172)

**WT**-wildtype

**Y1**- rat Neuropeptide Y Y1 receptor subtype

**Y2**-rat Neuropeptide Y Y2 receptor subtype

**Y4**-human Neuropeptide Y Y4 receptor subtype

**Y5**-human Neuropeptide Y Y5 receptor subtype

## Table of contents

Chapter 1: Introduction .....	1
1.1 The G protein coupled receptor superfamily .....	1
1.2. Structural properties of GPCRs.....	5
1.3 The role of conserved motifs in maintaining the inactive state of Class A GPCRs.....	12
1.4 Structural changes in GPCRs upon ligand induced activation .....	13
1.5 The G protein cycle .....	17
1.6 Termination of GPCR activation – the classical role of arrestins.....	20
1.7 The role of $\beta$ -arrestin in signalling.....	32
1.8 The NPY Y receptor family .....	34
1.9 Aims of this thesis:.....	52
Chapter 2: Materials and methods.....	54
2.1 Materials .....	54
2.2 Methods.....	55
2.2.1 Molecular biology .....	55
2.2.2 Cell culture .....	81
2.2.3 [ <sup>125</sup> I] PYY competition binding studies.....	84
2.2.4 [3H]cAMP accumulation assay .....	86
2.2.5 Automated platereader assays.....	89
2.2.6 Specific platereader assay methods .....	95
2.2.7 Confocal microscopy.....	96
2.2.8 Fluorescence correlation spectroscopy (FCS).....	97
2.2.9 Fluorescence recovery after photobleaching (FRAP) .....	102

2.2.10 Data analysis .....	104
2.2.11 FCS .....	109
2.2.12 Calculating diffusion coefficients from FRAP recovery curves .....	112
2.2.13 Statistical analysis .....	112
Chapter 3: Measurement of $\beta$ -arrestin2 recruitment and endocytosis of fluorescently tagged NPY Y receptors using high content imaging and automated analysis.....	119
3.1 Introduction .....	119
3.2 Aims of this chapter.....	129
3.3 Results.....	130
3.4 Discussion .....	158
Chapter 4 – The use of fluorescence correlation spectroscopy alongside bimolecular fluorescence complementation to investigate the effects of $\beta$ -arrestin recruitment on the membrane mobility of NPY receptors.....	177
4.1 Introduction .....	177
4.2 Aims of this chapter:.....	183
4.3 Results.....	184
4.4 Discussion .....	209
Chapter 5 – The combined use of Snap labelling and BiFC to discretely constrain GPCRs as homodimers of precise composition in order to probe the pharmacological consequences of dimerisation .....	221
5.1 Introduction .....	221
5.2 Chapter aims.....	234
5.3 Results.....	235
5.4 Discussion .....	266

Chapter 6 – The use of BiFC to constrain GPCRs as heterodimers of precise composition in order to investigate potential dimer specific modified pharmacology .....	280
6.1 Introduction .....	280
6.2 Aims of this chapter .....	295
6.3 Results.....	296
6.4 Discussion .....	328
Chapter 7: Final discussion .....	343
References .....	354

## Chapter 1: Introduction

### 1.1 The G protein coupled receptor superfamily

G-protein coupled receptors (GPCRs) represent the largest group of membrane receptors found in the human genome, numbering over 800 unique members (Benovic and von Zastrow, 2014) and are integral to a vast number of physiological processes including vision, cardiac function, neurotransmission, appetite, immune responses and olfaction (Wolfe and Trejo, 2007). GPCR targets comprise 30-50% of drugs currently marketed (Garland, 2013), and their cognate ligands encompass not only classical neurotransmitters such as the monoamines, but also peptides, proteins, lipids, glycoprotein hormones, ions and sensory signals such as photons, odorants and taste ligands (Musnier et al., 2010),(Fung JJ, 2009). Following activation by ligand binding, GPCRs traditionally couple at their cytoplasmic elements to heterotrimeric G proteins ( $G_{\alpha\beta\gamma}$ ). The signalling cascades produced can have rapid short term physiological effects via the production of second messenger molecules as well as long term effects via changes in gene expression.

#### 1.1.1 The pharmacological principles of GPCR signalling

GPCRs can be activated by binding endogenous ligands naturally occurring in the body, such as adrenaline to the  $\beta$ 2-adrenoceptor or neuropeptide Y (NPY) to the NPY Y1 receptor. The site that an endogenous ligand binds to is termed the orthosteric binding site. Exogenous ligands (eg. drugs) are also capable of binding to this site and activating GPCRs, often by mimicking the effect of the endogenous ligand, such as Isoprenaline binding to the  $\beta$ 2-adrenoceptor (Sato et al., 1996). The ability of a ligand to bind to a receptor is termed its *affinity*, while the ability of a ligand to stabilise an active receptor complex once bound is termed (intrinsic) *efficacy*. The *potency* of a ligand is a more empirical term that relates to the concentration of ligand required to produce a functional effect (e.g.

determined by the  $EC_{50}$  value (effective concentration for 50 % response on a concentration response curve). Potency depends on both ligand affinity and efficacy at the target receptor, but also on properties of the system, for example the number of receptors present, or the extent of signal amplification between the receptor and the measured endpoint.

Ligands that activate GPCRs and lead to the induction of biological responses are termed *agonists*. Agonists which show high efficacy are **full** agonists, and can often produce maximal responses whilst occupying only a small proportion of expressed receptors, because of receptor reserve due to signal amplification (Figure 1.1, A). A **partial** agonist shows lower efficacy at inducing responses in relation to a full agonist. This sub maximal response, relative to a full agonist, occurs even when the agonist occupies the entire receptor population. An **inverse** agonist binds to receptors at the orthosteric binding site, but stabilises the inactive conformation of the receptor. Thus, if receptors show constitutive activity (by adopting an active conformation in the absence of agonist) inverse agonists can induce functional responses opposite to that of an agonist.

An *antagonist* is a ligand which inhibits agonist mediated receptor responses without activating the receptor itself. True antagonists therefore have affinity for the receptor but no positive efficacy, though inverse agonists (with “negative” efficacy) also behave as antagonists in inhibiting agonist effects. Competitive antagonists bind to the same receptor orthosteric ligand binding site as the agonist (B). They sterically block agonist binding, meaning that higher concentrations of agonist are required to outcompete the antagonist occupancy (assuming reversible binding in both cases), resulting in reduced potency of this agonist in the presence of antagonist. In functional assays, the effect of competitive antagonists will be seen as rightward parallel shifts of agonist concentration response curves with no effect on maximum responses – known as surmountable antagonism. Antagonism may also be insurmountable, in that no amount of agonist can overcome the inhibition observed to regain the maximal

response (C). This antagonism can occur because of irreversible covalent binding of the antagonist to the receptor orthosteric binding site, or because the antagonist is non-competitive, and binds to a topographically distinct allosteric site.

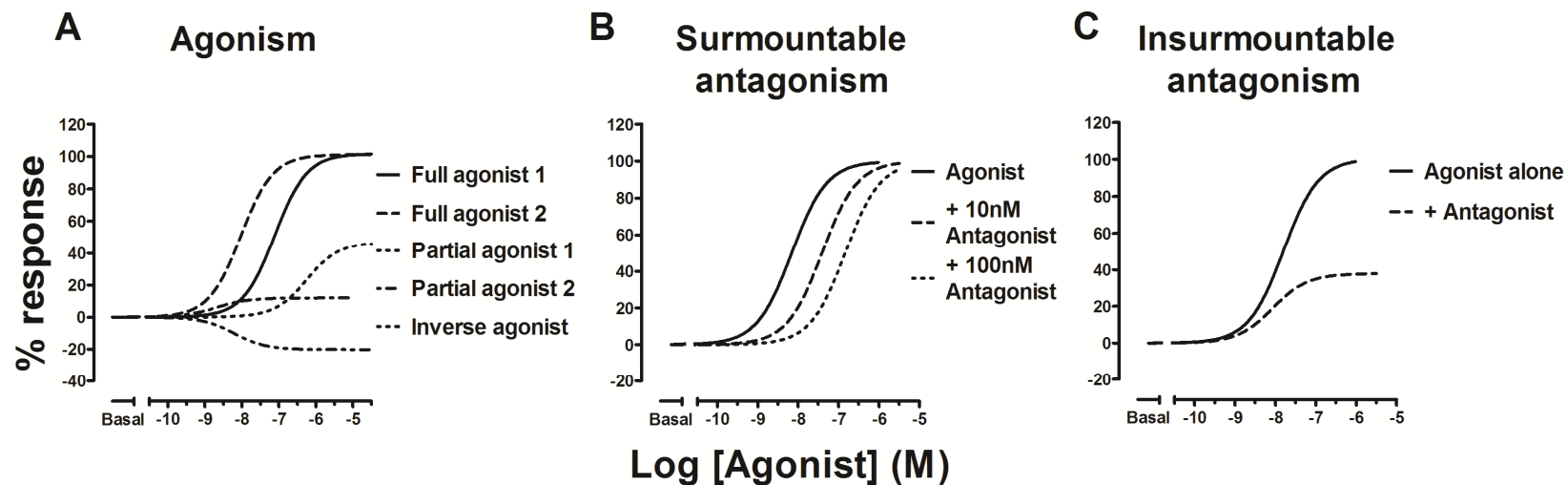


**Figure 1.1: The principles of agonist and antagonist pharmacology at GPCRs**

An agonist is a ligand that stabilises a GPCR conformation which activates the receptor resulting in a biological response (A). Full agonists show high efficacy at inducing maximal responses, whereas partial agonists have lower efficacy and can only induce submaximal responses irrespective of the degree of receptor occupation. An inverse agonist can bind and inhibit constitutively active receptors, inducing a response opposite to that of an agonist at the same receptor. Surmountable competitive antagonists (B) are able to bind to the same orthosteric ligand binding site as the agonist, but do not result in receptor activation, consequently sterically blocking agonist binding. In the presence of increasing concentrations of competitive antagonist, higher concentrations of agonist are required to out compete the antagonist, resulting in a parallel rightward shift in observed agonist concentration response curves. Antagonism may also be insurmountable, in that no amount of agonist can overcome the inhibition (C). This antagonism can be due to an antagonist covalently binding to the receptor orthosteric binding site or binding to a topographically distinct site termed the allosteric site. In functional assays insurmountable antagonism manifests as a drop in the magnitude of the observed maximum response.

## 1.2. Structural properties of GPCRs

### 1.2.1 GPCR Classes

GPCRs are composed of seven helical transmembrane domains (TM I-VII), 3 intracellular (ICL 1-3) and extracellular loops (ECL 1-3), an extracellular amino terminal and an intracellular carboxyl tail (Figure 1.2) (Unal et al., 2012). Electron cryo-microscopy of 2D crystals of bovine rhodopsin, suggested that the 7 transmembrane helices are arranged in a counterclockwise formation with TM3 tilted towards the centre of the helical bundle (Unger and Schertler, 1995). This orientation was confirmed from the first crystal structure of rhodopsin (Palczewski et al., 2000) and later GPCR crystal structures. An additional amphipathic helix (helix 8) is found at the end of TM7 and lies parallel to the cytoplasmic face of the plasma membrane (Kirchberg et al., 2011). In rhodopsin, Helix 8 connects the transmembrane helical bundle to the receptor C terminal tail via two palmitoylated cysteine residues at Cys322 and Cys323.

Both within and between GPCR families, sequence analysis has shown that particularly the N and C terminal domains can vary greatly. GPCRs can be divided into three major structural classes – A, B and C (Pierce et al., 2002). The largest group, Class A, comprises of 19 subgroups that includes rhodopsin, the opioid family ( $\kappa$ ,  $\gamma$ ,  $\mu$ ,  $\delta$ ), the adenosine family (A1, A<sub>2A</sub>, A<sub>2B</sub>, A3), the muscarinic family (M<sub>1</sub>-M<sub>5</sub>) and the two receptor families used in this thesis - neuropeptide Y (Y1, Y2, Y4 and Y5), and adrenoceptors ( $\alpha$ 1A, 1B, 1D;  $\alpha$ 2A, 2B, 2C and  $\beta$ 1-3). Class A GPCRs typically have a short extracellular N terminus, with ligand binding occurring at the extracellular loops (peptide ligands) or within transmembrane helices that form a ligand binding pocket (e.g. adrenaline at the B2AR (Strader et al., 1989, Rasmussen et al., 2007b)).

Class B receptors include those for gastrointestinal peptide hormones, such as glucagon and vasoactive intestinal peptide receptors (Pierce et al., 2002). The N terminal domain is typically the site of ligand binding, and contains six cysteine

residues that form disulphide bridges that facilitate this (Grace et al., 2004). Class C receptors include the metabotropic glutamate receptor and GABA<sub>B</sub> receptors (Pierce et al., 2002). They are particularly characterised by an elaborate N terminal ligand binding region, composed of a Venus flytrap domain which can assume a variety of conformations depending upon the presence or absence of agonists and antagonists (Kniazeff J, 2004). As discussed in more detail later in the thesis (chapters 5 and 6), class C GPCRs have been shown to form obligate dimers in order to function, partly via interactions of these Venus fly trap domains.

The typical structure of a Class A GPCR is shown in Figure 1.2 and has been confirmed from crystal structures (Venkatakrisnan et al., 2013). The first Class A GPCR to be crystallised was rhodopsin, long considered the model GPCR for Class A basal and active conformations. Crystal structures were obtained from primary retinal tissue of the inverse agonist bound (11-*cis*-retinal) form representative of the inactive state (Palczewski et al., 2000) and a constitutively active opsin form, representing the active state (Jager et al., 1996). This structure is not strictly active rhodopsin as the opsin does not have 11-*trans* retinal bound, the active isomer produced by light activation. Although many of the structural motifs involved in receptor activation are highly conserved amongst Class A GPCRs, rhodopsin responses are unique in that they are essentially 'all or nothing'. This is due to the covalently tethered ligand and requirement for photon induced isomerisation of the covalently bound retinal from a inverse agonist conformation (11-*cis*) to an active *trans* conformation, which is sufficient to cause full rhodopsin activation (Jager et al., 1996) (Kobilka and Deupi, 2007).

Crystallisation of inactive rhodopsin provided an early template for modelling other GPCR structures, but has now also been followed by the successful crystallisation of 18 other GPCR conformations. Crystal structures of inactive inverse agonist/ antagonist bound Class A receptors have been obtained for human muscarinic M2 (Haga et al., 2012), rat muscarinic M3 (Kruse et al., 2012),

human histamine H1 (Shimamura et al., 2011), human adenosine A<sub>2A</sub> (Jaakola et al., 2008) and the opioid receptor family (Wu et al., 2012), (Manglik et al., 2012) and (Granier et al., 2012)). in addition to the Class B receptor corticotrophin releasing factor receptor-1 (Hollenstein et al., 2013) and the transmembrane domain of the Class C metabotropic glutamate receptor 5 (Dore et al., 2014).

However the largest range of crystal structures has been obtained for the  $\beta$ 2-adrenoceptor. Unlike rhodopsin,  $\beta$ 2-adrenoceptors readily convert between a range of inactive and active conformations, with multiple ligands with differing efficacies able to stabilise distinct receptor sub states (Bockenbauer et al., 2011), and a level of basal constitutive activity not seen for rhodopsin (Rasmussen et al., 2007b). Crystal structures have been obtained for the inactive receptor form bound to the partial agonist carazolol (Cherezov et al., 2007), (Rasmussen et al., 2007b, Rasmussen et al., 2007a), and for the active agonist bound form stabilised using a nanobody (Rasmussen et al., 2011a) or bound to the G protein heterotrimer (G<sub>s</sub>) (Rasmussen et al., 2011b).

Interestingly crystallisation has implied that some Class A GPCRs form homodimers, such as the ligand free  $\beta$ 1AR (Huang et al., 2013) inactive antagonist bound chemokine CXCR4 receptors (Wu et al., 2010) and  $\mu$  (Manglik et al., 2012),  $\kappa$  (Wu et al., 2012) and  $\delta$  opioid (Granier et al., 2012) receptors. However crystal structures are a 'snapshot' of a particular receptor conformation, normally obtained under artificial conditions (solubilised, purified protein with substantive modification of the receptors by mutagenesis to improve stability) (Warne et al., 2008), therefore the functional relevance of dimerisation remains controversial (see Chapter 5 and Chapter 6).

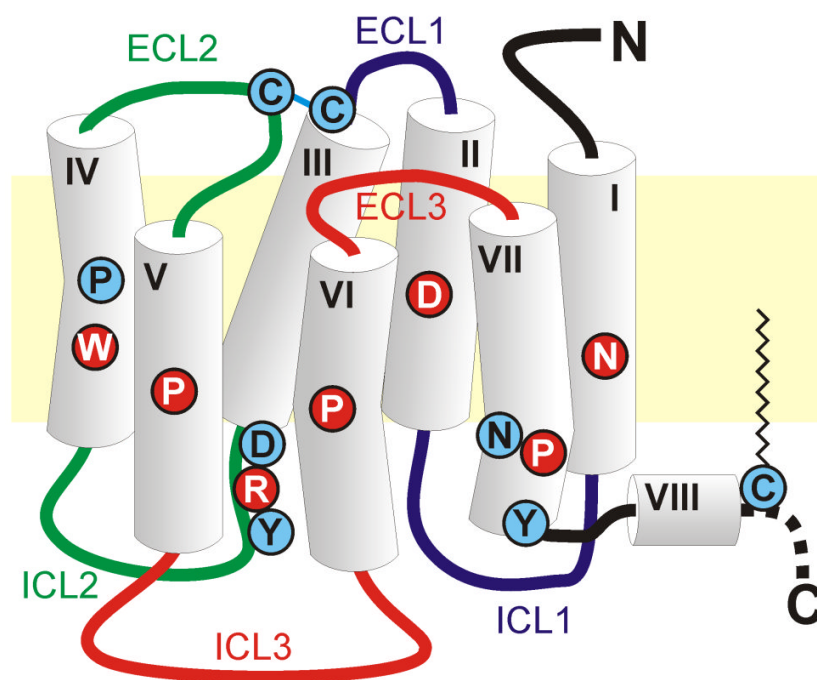


**Figure 1.2: Schematic of GPCR 7 transmembrane helical structure.**

Residues conserved in the primary sequence of all Class A rhodopsin like GPCR's (seen in red). They include the Asn1.50 (TM1) and Asp2.50 (TM2); Arg3.50 (TM3) a key residue of the 'ionic lock' and part of the conserved E (D) RY motif and Pro7.50 (TM7) of the NPxxY motif. Furthermore Trp4.50 on TM4 is conserved in 97% of Class A GPCR's, and forms an interhelical hydrogen bond with Asn2.50. Residues in blue are conserved in the majority of class A GPCR's and include a cysteine (Cys3.25) at the top of TM3 which forms a stabilising disulphide link with ECL2; Asp3.49 and Tyr3.51 of the E (D) RY motif (TM3) and Asn7.49 and Tyr7.53 of the NPxxY motif (TM7).

Residue numbers are as stated for the human  $\beta$ 2-adrenoceptor using the Ballesteros-Weinstein numbering system (Ballesteros and Weinstein, 1995).

## **1.2.2 The structural features of GPCRs**

The traditional view of GPCR activation is the ternary complex model consisting of a GPCR bound to agonist in a high affinity state which is simultaneously stabilised by effector proteins binding to the intracellular face of the receptor (Kenakin and Christopoulos, 2013, Samama et al., 1993). Agonists can activate receptors as their binding results in conformational changes of the receptor transmembrane domains, disrupting the molecular interactions holding the receptor in its low energy inactive state. However the existence of multiple receptor conformations and the phenomena of constitutive activity and biased agonism, means the reality is likely to be far more complex.

### **1.2.2.1 Transmembrane helices and the ligand binding pocket**

The transmembrane domains of Class A GPCRs are typically 25-35 amino acids long, and form stable alpha helices that transverse the plasma membrane. Mutations introduced into the helices can disrupt the formation and alignment of the helical bundle (Unal et al., 2012). The transmembrane helices are broadly responsible for transducing conformation changes brought about by ligand binding, downwards to the intracellular face of the receptor. Across the transmembrane helices of all GPCRs, structural diversity is most concentrated at the extracellular half of the helical bundle. For this half, homology estimates from all GPCR structures suggest only 6% of residues are conserved, compared to 26% for the intracellular half of the helical bundle (Katritch et al., 2012).

Analysis of available crystal structures suggests there is a network of interhelical contacts principally between residues of TM3 (eg. 3.32, 3.36 using Ballesteros Weinstein numbering (Ballesteros and Weinstein, 1995)), TM6 (eg. 6.48, 6.51) and TM7 (eg. 7.39) that position the helices to form a ligand binding cradle (Venkatakrishnan et al., 2013). Additionally, the highly conserved residues Asn1.50 of TM1 and Asp2.50 on TM2 form a hydrogen bond network with residues in TM2 and 7 (Figure 1.2). Furthermore Trp4.50 on TM4 is conserved in

97% of Class A GPCR's, and forms an interhelical hydrogen bond with Asn2.40 of TM2 which 'locks' TM3 within the helix bundle as a 'structural hub'. A hydrogen bond network involving a cluster of water molecules extending from the ligand binding pocket into the cytoplasmic ends of the transmembrane helices is found in both rhodopsin and carazolol bound  $\beta$ 2-adrenoceptor crystal structures (Scheerer et al., 2008), (Rosenbaum et al., 2007).

It is worth noting that although the primary sequence of residues of the binding pocket may vary, all GPCR ligands, be that peptide, lipids or monoamines, occupy a similar 'pocket' within the receptor structure. This indicates that there are conserved structural elements which are crucial to binding and receptor activation. However subtype selective residues of the ligand binding pocket can confer some specificity by contacting elements of the ligand directly. The ligand binding cleft of  $\beta$ 2-adrenoceptors carries a negative charge centred around Asp 3.32 (Cherezov et al., 2007), (Rasmussen et al., 2007a) which reconciles with observations from mutagenesis studies. It has been suggested that this residue contacts the positive amine found on the endogenous  $\beta$ -adrenoceptor catecholamine ligands adrenaline and noradrenaline (Sato et al., 1999) and the synthetic analogue isoprenaline (Savarese and Fraser, 1992). This residue is also responsible for binding positive amine moieties of the ligand for other monoamine receptors such as muscarinic acetylcholine (Page et al., 1995) , histamine (Jongejan et al., 2005) and dopamine D2 (Lan et al., 2006). Additionally Ser5.42 and Ser5.46 residues of TM5 of the  $\beta$ 2-adrenoceptor are responsible for binding the hydroxyl groups found on the catechol ring of catecholamine ligands (Sato et al., 1999). When these residues are mutated, receptor affinity for the full agonist isoprenaline is decreased by 10-25 fold (Strader et al., 1988). Phe6.51 found in TM6 has also been shown to interact with the phenyl ring of adrenaline (Strader et al., 1989).

### **1.2.2.2 The extracellular loop 2 (ECL2)**

The available crystal structures of Class A GPCRs have implied that the access of ligand to the binding pocket may also be regulated, often by the ECL2 domain. The  $\beta$ 2-adrenoceptor has a large, solvent exposed ECL2 that creates a channel to allow small water soluble ligands downwards access to a binding pocket buried within the TM helical bundle (Cherezov et al., 2007) as described above. The importance of the ECL2 in governing the charge distribution and shape of the channel leading to the ligand binding site, may define ligand specificity. For example the crystal structure of the  $\beta$ 1-adrenoceptor has shown that the ECL2 is also heavily involved in defining ligand access. Both  $\beta$ 1 and  $\beta$ 2AR subtypes have relatively high fidelity in the amino acids residues that line each ligand binding pocket, with the only two residues different in  $\beta$ 1AR (Val4.56, Phe7.35) and  $\beta$ 2AR (Thr4.56, Tyr7.35) functionally equivalent. However marked differences have been observed in the sequence of their ECL2 regions, suggesting that it is the access to the ligand binding pocket that differs (Rosenbaum et al., 2007). Regulated ligand access by ECL domains is supported by evidence from the crystal structures obtained from receptors with diffusable ligands, such as the spingosine 1 phosphate receptor (S1P) (Hanson et al., 2012) or GPR40 (Srivastava et al., 2014). For these receptors the ECLs, in conjunction with the amino terminus, block the extracellular face of the receptor to ligands. In order to access the binding pocket, ligands must traverse the lipid bilayer in order to enter laterally. However the degree of influence the ECLs exert over ligand binding itself can differ with GPCR or ligand. When binding large peptide ligands, such as NPY, the ECLs can directly participate in this process. For example Asp6.59 is highly conserved across the NPY Y receptor family. Mutation of this residue resulted in a drastic loss of agonist binding affinity (Walker et al., 1994, Merten et al., 2007). However functional activation of Y receptors by agonist still requires engagement with the helical core. Even for some receptors with small molecule ligands, direct participation of the ECLs has been observed. For the adenosine A<sub>2A</sub> receptor for

example, interaction of adenosine with Phe5.29 located in ECL2 is necessary for high affinity binding (Katritch et al., 2012).

Additionally disulphide bridges formed between the ECLs and transmembrane domains have been suggested to contribute to stabilising the highly ordered secondary structure of the receptor (Peeters et al., 2011, Katritch et al., 2012). Several are subtype specific, but one that appears to be highly conserved across all known GPCR Class A structures is between cysteine residues of ECL2 and TM3 (Cys3.25; (Venkatakrisnan et al., 2013)) which has been suggested to anchor the extracellular side of TM3 close to the proposed ligand binding site to minimise the movement of its extracellular end during receptor activation.

### **1.3 The role of conserved motifs in maintaining the inactive state of Class A GPCRs**

A range of non covalent interactions, predominantly found in the central transmembrane helical core, are believed to play a role in stabilising the inactive state of Class A GPCRs. Of these, two motifs have been found to be highly conserved across rhodopsin-like receptors.

#### **1.3.1 The DRY motif of TM3**

The Glu/Asp-Arg-Tyr (E/DRY) motif is centred around Arg3.50 of the  $\beta$ 2-adrenoceptor at the bottom of TM3 (Figure 1.2) and is found in 75% of all Class A GPCRs (Rasmussen et al., 2007a). Insights from the crystal structure of inactive rhodopsin have shown that ionic salt bridges form both within this motif (Glu/Asp with Arg) and between Arg3.50 and residues of TM6 (Glu6.30 and Thr6.36; (Scheerer et al., 2008)). This 'ionic lock' has been proposed to constrain rhodopsin in an inactive conformation and has also been observed in crystal structures of ligand free  $\beta$ 1AR (Huang et al., 2013), inactive dopamine D3 (Chien et al., 2010) and inactive adenosine A2A bound to certain antagonists (Dore et al., 2011). However the significance of the ionic lock for other Class A GPCRs remains debatable. Mutagenesis of DRY motif residues resulted in constitutive activity of

in  $\beta$ 2AR and  $\beta$ 1AR receptors in the absence of agonist (Scheer et al., 2000), (Ballesteros et al., 2001). Molecular dynamic modelling has also suggested a highly stable ionic lock in  $\beta$ 1AR (Greasley et al., 2002) and  $\mu$  opioid receptors (Kolinski and Filipek, 2010). However an intact ionic lock has not been observed in crystal structures of inactive  $\beta$ 2AR (Cherezov et al., 2007). This may however be a consequence of the crystallisation process and the addition of large protein modification (such as nanobodies (Rasmussen et al., 2011a)) to stabilise the structure. For receptors such as  $\beta$ 2AR that have been shown by NMR spectroscopy to adopt a variety of intermediate conformations (Nygaard et al., 2013), crystallisation can only provide a 'snapshot' of the particular conformation stabilised during crystallisation. Interestingly data from molecular dynamic modelling has suggested that for dynamic receptors, such as  $\beta$ 2AR, the fidelity of the ionic lock may also be dynamic (Romo et al., 2010) or ligand dependent (Bhattacharya et al., 2008).

### **1.3.2 The NPxxY motif**

The NPxxY motif (Asn-Pro-X-X-Tyr) is found at the junction between TM7 and helix 8 (Asn7.49 to Tyr7.53) and is highly conserved in Class A GPCRs. The Tyr residue within this motif interacts with a conserved Phe residue (Phe6.52) in TM6 via its aromatic side chains (Park et al., 2008). Additionally residues in the NPxxY motif mediate a hydrogen bond network with residues in TM1 and TM2 (Balaraman et al., 2010) and Trp 6.48 in the CWxP motif in TM 6 (see Figure 1.2) (Bhattacharya et al., 2008). Mutations of the extended NPxxY(x)<sub>5,6</sub>F motif have also been shown to effect receptor behaviour beyond activation, such as receptor expression, sequestration and ligand affinity (Fritze et al., 2003).

### **1.4 Structural changes in GPCRs upon ligand induced activation**

Conformational changes in multiple domains, involving many of the residues holding the inactive state, are required to disrupt the molecular interactions typically holding the receptor in its low energy inactive state.

#### 1.4.1 Movement of transmembrane helices

Observations from the crystal structures of inactive and active  $\beta$ 2AR have shown that the largest change in the TM domains upon activation is a 14Å outward movement of the intracellular ends of TM6 (Rasmussen et al., 2011a). Additionally there is a smaller movement and helical extension of the cytoplasmic end of TM5. These movements are driven by ligand binding to the extracellular regions of these helices pulling them inwards in a rocking motion which subsequently displaces the intracellular ends. This suggests that local changes surrounding the ligand binding site translate to far greater movement of the intracellular domains of the helices (Venkatakrisnan et al., 2013).

Breakage of the DRY motif also facilitates the rotation of TM6 around a conserved proline (Pro 6.50) that moves it away from TM3 towards TM5 (Dunham and Farrens, 1999). This rotation of TM6 is also observed for  $\beta$ 2AR (Ghanouni et al., 2001) leading TM5 and 6 to rearrange their side chains by aromatic stacking so that TM5 interacts with the Trp residue in the CWxP motif of TM6 (Holst et al., 2010). This rotation of TM6 is also confirmed by solid state NMR, whereby an inward rotation of the extracellular side of TM6 close to the ligand binding site occurs, but a substantial outward rotation of the intracellular domain is observed (Ding et al., 2013). An additional rotation of TM7 around another conserved proline (Pro 7.50), caused an inward movement of this helix towards TM3 closing the entrance to the ligand binding site of both  $A_{2A}$  and  $\beta$ 2 structures (Jaakola et al., 2008), (Cherezov et al., 2007). In rhodopsin, the network of water molecules forming hydrogen bond interactions in TM2, 3, 6 and 7 are disrupted to allow rapid toggling to the active state and to reinforce the helical deformation of TM7 (Palczewski, 2006). Although this network is not seen in the  $\beta$ 2-adrenoceptor crystal structures, this may be due to inadequate resolution (Rasmussen et al., 2011a).

Importantly for downstream signalling, movement of helices 3, 5 and 6 sterically facilitates the binding of effector proteins such as G proteins, by creating a crevice in the intracellular face of the receptor (Nygaard et al., 2013).

#### **1.4.2 The CWxP transmission switch**

The transmission switch, also called the rotamer toggle switch, works in conjunction with the movements of TM3 and TM6 and breakage of the ionic lock. The Pro6.50 residue of the CWxP motif in TM6 causes a kink of the intracellular end of this helix so that it moves outward from TM3 (Bhattacharya et al., 2008) and towards TM5. This tilted TM6 helix is now stabilised via an interaction with the Tyr residue of the NPxxY motif in TM7 (Scheerer et al., 2008). The CWxP motif therefore effectively links conformational changes at the ligand binding site with movements of TM5 and 6 via the rearrangement of the interface that exists between TM3, 5 and 6 (Deupi and Standfuss, 2011).

#### **1.4.3 The DRY motif 'ionic lock'**

The largest change upon receptor activation, suggested by crystallisation of rhodopsin, is a 11.4 Angstrom movement outward of the intracellular ends of TM6 away from TM3, resulting in the breakage of the 'ionic lock' between the conserved Arg3.50 of TM3 and Glu6.30 of TM6. The 'ionic lock' residues in rhodopsin compensate for this energy expenditure by forming new stabilising hydrogen bonds with residues in TM5 (Arg3.50 to Tyr 5.64) and TM6 (Glu6.30 to Lys5.66). However the importance of the ionic lock in the activation of other GPCRs remains debatable as crystal structures of active (Rasmussen et al., 2011a) and G protein bound (Rasmussen et al., 2011b)  $\beta$ 2AR all contained intact ionic locks. However the Arg3.50 residue of this motif is highly conserved across Class A GPCR sequences, suggesting it may fulfil an additional role. The position of this residue at the cytoplasmic end of TM3, in conjunction with the movement of TM5 and 6 means this residue is able to directly interact with the carbonyl backbone

of the C terminus of the G protein  $\alpha$  subunit seen in crystal structures (Scheerer et al., 2008) and solid state NMR (Ding et al., 2013).

#### **1.4.4 NPxxY motif**

In the inactive receptor, a hydrophobic barrier of TM2,3 and 6 separates a water mediated hydrogen bond network within the receptor TM domains from the DRY motif. The movement of TM6 brought about by receptor activation, breaks the interaction of the NPxxY motif with helix 8, connecting the hydrogen bond network with the DRY motif at the cytoplasmic end of TM3 (Fritze et al., 2003), (Park et al., 2008).

#### **1.4.5 Intracellular loops**

The agonist induced movement of TM5 and 6, creates a space on the intracellular face of the receptor to allow ICL2 and 3 residues to interact with G proteins. Evidence from the crystal structure of  $\beta$ 2AR- $G_s$  complex has suggested that receptor activation causes a 6Å displacement of the  $G_\alpha$  subunit towards the  $\beta$ 2AR C terminal and transmembrane core (Rasmussen et al., 2011b). No changes were observed for the  $G_{\beta\gamma}$  subunits. Interaction of receptor ICL2 with the N terminus of the  $G_\alpha$  subunit led to substantial changes in the highly conserved G protein P loop that surrounded the  $\beta$  phosphate of GDP, suggesting the key step promoting GDP release (Figure 1.3; see description of the G protein cycle in section 1.5). These results were also confirmed by peptide amine hydrogen deuterium exchange mass spectroscopy (Chung et al., 2011) suggesting that these changes in G protein interaction are not a consequence of the protein modifications required for crystallisation. Interestingly this study also found evidence for pre coupling of inactive GDP bound G proteins and the  $\beta$ 2AR intracellular domain, which may reconcile with the constitutive activity of a fraction of receptors in the absence of agonist. ICL2 has also been proposed to be important for determining the selectivity of GPCR-G protein interactions. For the thyrotropin receptor (TSHR) for example, residues 525-527 of ICL2 drive agonist induced coupling to  $G_{\alpha_s}$ , but

residues 528-532 direct  $G_{\alpha q}$  coupling (Kosugi et al., 1994). Additionally the protease activated receptor 1 (PAR1) has been shown to couple to multiple G protein subtypes  $G_{q/11}$ ,  $G_{i/o}$  or  $G_{12/13}$  (see section 1.5.1) However mutagenesis studies have shown that five key residues within ICL2 direct coupling to the  $G_{(q/11)}$  subtype exclusively (McCoy et al., 2012).

Multiple studies have also implied the importance of ICL3 for G protein coupling. In rhodopsin, mutation of several hydrophobic residues in this region reduced the activation rate of the cognate G protein transducin, by 90% (Acharya et al., 1997). For TSHR, ICL3 in conjunction with the intracellular domain of TM6, has been shown to directly interact with multiple residues within the G protein structure (Huang et al., 2005). However to date no clearly defined G protein consensus motif within ICL3 has been identified. Moreira (2014) has suggested that this may be a consequence of ICL3 being one of the least conserved regions of Class A GPCRs meaning that coupling selectivity would be impossible to detect from the primary structure alone. In addition even closely related GPCR subtypes show notable discrepancies in the secondary structure adopted by ICL3 (reviewed in (Moreira, 2014)).

### **1.5 The G protein cycle**

There are two principle classes of G proteins – the small monomeric class which are comprised of 3 main branches Ras, Raf and Rap which act as GTPases (Cherfils and Zeghouf, 2013) and the larger heterotrimeric G proteins.

Heterotrimeric G proteins are historically the principle mechanism by which GPCR activation, through binding of extracellular stimuli, results in the initiation of intracellular signalling cascades (Oldham and Hamm, 2008). These G proteins are comprised of three subunits termed  $\alpha$ ,  $\beta$  and  $\gamma$  (Figure 1.3). In the inactive G protein these subunits are complexed together as a heterotrimer with  $G_{\alpha}$  bound to guanosine diphosphate (GDP). Following ligand binding, the now activated GPCR can in turn activate its cognate G protein via the exchange of GDP for guanosine triphosphate (GTP) at  $G_{\alpha}$ . The G protein heterotrimer then dissociates

into  $G_{\alpha}$ -GTP and  $G_{\beta\gamma}$  subunits, which are able to positively and negatively regulate downstream effectors, leading to the regulation of second messenger molecules such as cyclic AMP, cyclic GMP, inositol trisphosphate, diacylglycerol and intracellular calcium. Cessation of G protein activation comes via the hydrolysis of GTP for GDP at the  $G_{\alpha}$  subunit, facilitated by the intrinsic GTPase activity of  $G_{\alpha}$ , meaning that G protein dependent signalling is self limiting. Amplification is inbuilt as a single agonist molecule binding to a single receptor is capable of activating a large pool of G proteins and inducing the production of a cascade of second messenger molecules, which can lead to pharmacological properties such as receptor reserve (Chabre and le Maire, 2005).

### **1.5.1 G protein dependent signalling**

There are at least 20 subtypes of  $G_{\alpha}$  subunit, which group G proteins into four main classes –  $G_s$ ,  $G_{i/o}$ ,  $G_q$  and  $G_{12}$  (Premont and Gainetdinov, 2007). These classes are, to a greater or lesser extent, activated selectively by different GPCRs. Receptors that preferentially couple to the  $G_{\alpha_s}$  subtype include activated  $\beta$ 2AR (Gilman, 1984), which has been implicated in the control of vascular and airway smooth muscle relaxation, blood vessel dilation and bronchodilation (Johnson, 2006).  $G_{\alpha_s}$  activation stimulates adenylyl cyclase leading to the production of the second messenger molecule cyclic AMP (cAMP). cAMP itself activates cAMP dependent protein kinase (PKA) which phosphorylates cytosolic targets such as ion channels (Gray et al., 1998), nuclear targets such as the transcription factor cAMP response element binding protein (CREB), leading to changes in gene transcription, and in the case of the  $\beta$ 2AR, proteins that regulate smooth muscle tone. cAMP can also inhibit the release of  $Ca^{2+}$  ions from intracellular stores and in the case of  $\beta$ 2AR activation this also leads to the relaxation of airway smooth muscle (Johnson et al., 2005). The novel cAMP mediators, termed Epac1 and Epac2 can act alone or in concert with PKA. They are guanine nucleotide exchange factors for Ras-like small GTPases, which catalyse the exchange of GDP for GTP and can regulate multiple processes including ion transport, neuronal

responses and vesicle trafficking ((Grandoch et al., 2010)). Finally, the coupling of Gs with adenylyl cyclase and the production of cAMP has typically been observed at the plasma membrane.

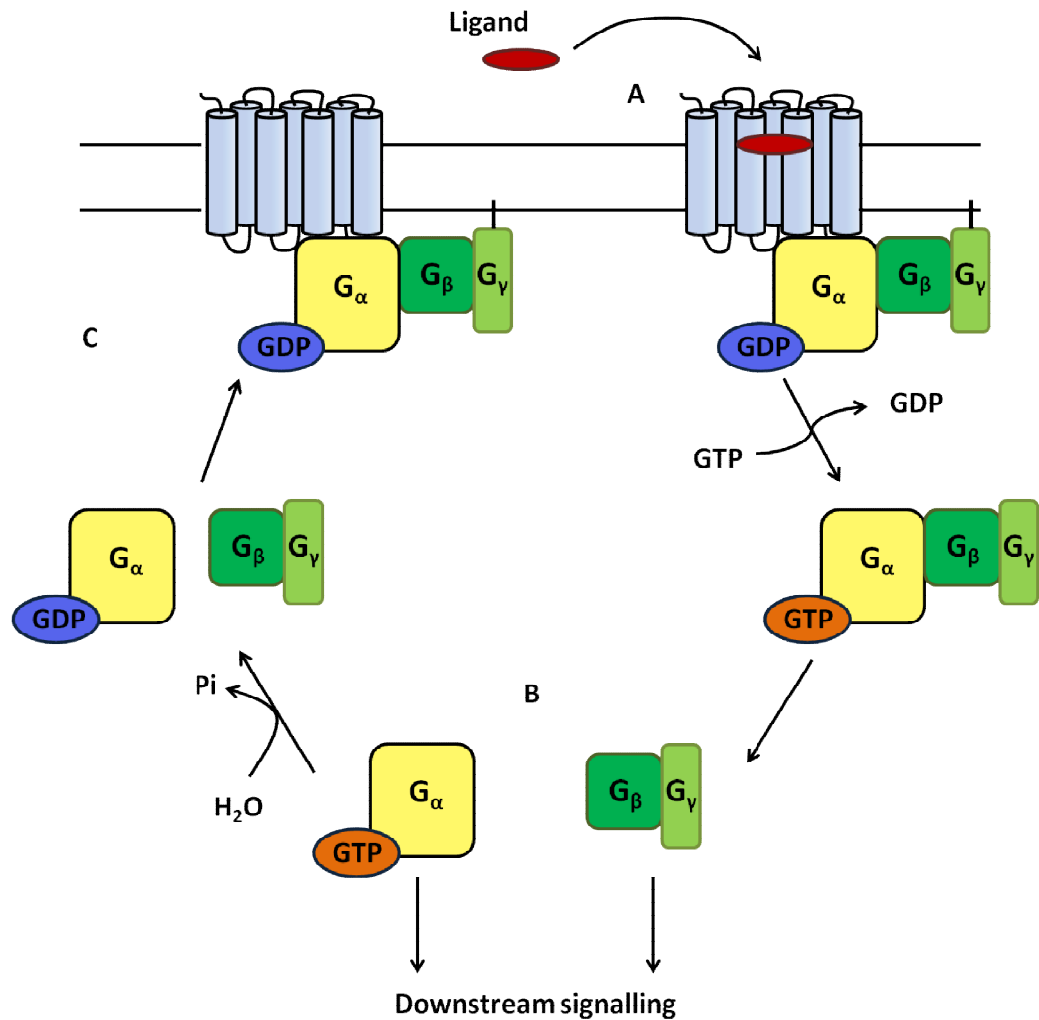


**Figure 1.3: The heterotrimeric G protein cycle**

Upon binding ligand (red), GPCRs undergo a series of conformational changes that promotes the binding of heterotrimeric G proteins to the intracellular face of the receptor and the exchange of GDP for GTP at the G $\alpha$  subunit (A). GTP binding causes dissociation of the G $\alpha$  and G $\beta\gamma$  subunits, whereby both can then interact with downstream signalling partners (B). Signalling is terminated upon hydrolysis of GTP to GDP, facilitated by the intrinsic GTPase activity of G $\alpha$  subunit. The G $\alpha$  and G $\beta\gamma$  subunits then reform the trimer structure.

However evidence is now emerging that internalised  $\beta$ 2-adrenoceptors (see section 1.6.2) can continue to signal within endosomes with a more sustained profile of cAMP production observed (Vilardaga et al., 2014).

Conversely receptors signalling through the  $G_i$  subunit, such as the NPY receptor family, adenosine  $A_1$  and  $A_3$  receptors and the opioid receptors  $\mu, \delta$  and  $\kappa$ , induce inhibition of adenylyl cyclase and subsequent cAMP production, ultimately inhibiting protein kinase A activation (Michel et al., 1998). Additionally receptors of the Neuropeptide Y family have been shown to signal via  $G_i$  to activate inwardly rectifying potassium GIRK ion channels in rat thalamic neurons (Sun et al., 2001).

The  $G_q$  subunits are modulated by receptors including the muscarinic  $M_1, M_3$  and  $M_5$  leading to activation of phospholipase  $C_\beta$  and subsequent production of the second messengers diacylglycerol (DAG) and inositol trisphosphate ( $IP_3$ ).  $IP_3$  released into the cytosol can act on  $IP_3$  ligand gated calcium channels located on the membrane of the endoplasmic reticulum, leading to release of calcium from intracellular stores (Ferris and Snyder, 1992). DAG chiefly activates protein kinase C, which can regulate receptor desensitisation. Physiological effects include vasoconstriction in the circulatory system and contraction of smooth muscle cells in the digestive and urinary systems via various effectors (Rang, 2003).

The  $G_{12/13}$  subunits regulate actin cytoskeletal rearrangement via Rho guanine exchange factors (GEFs) activating the small G protein Rho (Wang et al., 2006). An example of this is the activation of  $G_{12/13}$  via stimulation of the thrombin receptor results in platelet shape changes (Offermanns et al., 1994).

### **1.6 Termination of GPCR activation – the classical role of arrestins**

The regulation of processes involved in GPCR activation right through to receptor recycling or degradation allows spatial and temporal control of GPCR signalling. Regulation can occur at several points in the pathway but here I will focus on those mechanisms that directly affect GPCRs.

Cessation of signalling induced by the activation of GPCRs occurs by a process called desensitisation. Heterologous desensitisation occurs independently of ligand binding, with phosphorylation of receptor intracellular loop and C terminal residues by protein kinases A and C (Luttrell and Gesty-Palmer, 2010). Homologous desensitisation is targeted to ligand activated receptors and is the classical function of the accessory protein  $\beta$ -arrestin. Key serine and threonine residues in the receptor C terminus and the third intracellular loop are phosphorylated by G protein-coupled receptor kinases (GRKs) (Luttrell and Lefkowitz, 2002), with GRKs showing greater affinity for activated GPCRs (Premont and Gainetdinov, 2007). GRK phosphorylation alone is not enough to drive receptor desensitisation; it instead chiefly increases the affinity of  $\beta$ -arrestins for receptors (Luttrell and Lefkowitz, 2002). These rapidly translocate from the cytosol to dock at the receptor phosphorylated residues, sterically blocking receptor coupling to additional G proteins even in the continued presence of agonist (Premont and Gainetdinov, 2007), leading to receptor desensitisation and endocytosis into intracellular vesicles. The interaction of  $\beta$ -arrestins with GPCRs was first visualised using GFP tagged  $\beta$ -arrestin2 recruitment to the  $\beta$ 2AR (Barak et al., 1997b). Real time measures of this interaction (further discussed in Chapter 3) have been made using resonance energy transfer methods, for thyrotropin releasing hormone receptors or vasopressin V2 receptors (Kocan et al., 2008), dopamine D2 (Masri et al., 2008), orexin (OXR2) (Hasbi et al., 2004) and angiotensin AT<sub>1</sub> receptors (Hansen et al., 2004). Additionally BRET was used to investigate the kinetics of this interaction following agonist stimulation for the NPY receptor subtypes Y1, Y2, Y4 and Y5 (Berglund et al., 2003b).

There are 4 subtypes of arrestin - arrestin 1 (visual) and 4 (cone) are predominantly expressed in visual tissue (Luttrell and Gesty-Palmer, 2010). The function of arrestins was first identified in rhodopsin, whereby visual arrestin, alongside rhodopsin targeted GRK1, was shown to be crucial to desensitisation of

photon activated rhodopsin (Wilden et al., 1986) and steric inhibition of the specialised G protein transducin (Krupnick et al., 1997b). Lohse et al identified a molecule analogous to visual arrestin ( $\beta$ -arrestin) that was also involved in the desensitisation of other activated GPCR's following their phosphorylation by GRK's, using  $\beta$ 2-adrenoceptor as a model system (Lohse et al., 1990). COS-7 cells transfected with this protein inhibited function of GRK phosphorylated  $\beta$ 2-adrenoceptor compared to control cells. This inhibition was 20-40 times more effective at GRK phosphorylated  $\beta$ 2-adrenoceptors than nonphosphorylated receptors (Lohse et al., 1990). Subsequently  $\beta$ -arrestin1 (arrestin2) and  $\beta$ -arrestin2 (arrestin3) isoforms have been identified which are ubiquitously expressed (Luttrell and Gesty-Palmer, 2010) and share 78% sequence homology with one another (DeWire et al., 2007) as well as sequence and structural homology with the two visual arrestins (Kendall and Luttrell, 2009). Observations have suggested that GPCRs may show a bias for  $\beta$ -arrestin subtype; for example the activated  $\beta$ 2-adrenoceptor preferentially binds  $\beta$ -arrestin 2 over 1 (Moore et al., 2007). Both subtypes have been implicated in regulating GPCR endocytosis, for example through overexpression of  $\beta$ -arrestin2 leading to increased agonist induced sequestration of  $\beta$ 2-adrenoceptor and conversely expression of a dominant negative form of  $\beta$ -arrestin2 inhibiting this process (Ferguson et al., 1996).

### **1.6.1 The molecular interactions facilitating $\beta$ -arrestin binding to GPCRs**

Crystal structures have revealed that  $\beta$ -arrestins show structural similarities with one another. This common domain structure is also shared to an extent by the  $\alpha$ -arrestin proteins, which are an ancestral relative of  $\beta$ -arrestins.  $\alpha$ -arrestins are involved in intracellular trafficking processes, but their ability to regulate GPCRs remains largely unclear (Puca and Brou, 2014). This suggests that the shared motifs are likely to reflect the similar roles of these proteins in intracellular trafficking (Gurevich and Gurevich, 2013).

Arrestins are comprised of two concave domains; the N domain (8-180 residues) comprised of a single  $\alpha$  helix and the C domain (188-362 residues) made up of 2 short helices and an extended C tail connected by a flexible linker (Gurevich and Gurevich, 2006). Visual and  $\beta$ -arrestins are constrained in the basal state by a series of intramolecular interactions. The polar core primarily stabilises the inactive conformation via electrostatic attractions between a series of highly conserved charged residues Asp27, Arg170, Lys171, Asp292, Asp299 and Arg394 (rat  $\beta$ -arrestin 2) that make up the polar core (Xiao et al., 2004). Alanine substitution of any of these residues resulted in an arrestin mutant that is able to bind to unphosphorylated receptor (Vishnivetskiy et al., 2000). Additionally charge reversal of the Arg170 residue disrupted the delicate balance of the polar core leading to an arrestin form that is able to bind unphosphorylated active receptor. These observations suggested that the polar core of arrestin is responsible for recognising the phosphorylation status of the receptor, and drives conformational change when it is disrupted on binding negatively charged phosphorylated receptor residues. This has recently been demonstrated in the crystal structure of  $\beta$ -arrestin1 in complex with a V2 receptor C tail phosphopeptide (Shukla et al., 2013). An additional feature of inactive arrestin structure is hydrophobic interactions that occur between the N terminal  $\beta$  strand 1 (residues 103-111),  $\alpha$  helix 1 (9-14) and the last  $\beta$  strand of the C terminus (373-380) (Xiao et al., 2007), (Gurevich and Gurevich, 2004) termed the 3 element interaction.

The agonist induced activation of GPCRs and the subsequent phosphorylation of their C terminal domain by GRKs, facilitates arrestin recruitment and engagement with the intracellular face of the receptor. Arrestin has been shown to exhibit highest affinity binding for active phosphorylated receptors (Bayburt et al., 2011),(Vishnivetskiy et al., 2011). For example studies on visual arrestin *in vitro* have shown low affinity binding to unphosphorylated active receptors or inactive phosphorylated receptors, with 20 fold increased binding observed for active

phosphorylated receptors (Gurevich and Gurevich, 2004). Initial studies involving C terminal truncations of  $\beta$ 2-adrenoceptors (Bouvier et al., 1988), resulted in receptors with delayed agonist induced desensitisation. The authors postulated that this was due to the receptor being sensitive to phosphorylation of residues within this receptor domain by GRK's. Further C terminal truncation studies in other GPCRs such as complement 5A (Braun et al., 2003), rhodopsin (Kisselev et al., 2004), prostaglandin EP4 (Neuschafer-Rube et al., 2004) have supported this assertion. Removal of the Y1 receptor C terminal, alongside mutation studies identified a region within the rat Y1 (Ser352 to Lys360; (Holliday et al., 2005)) and human Y1 sequences (Met355 to Thr362; (Ouedraogo et al., 2008)) that contains a putative 'phosphorylation motif' that facilitates desensitisation,  $\beta$ -arrestin2 binding and ultimately Y1 receptor internalisation. Additionally studies of  $\beta$ -arrestin recruitment to the NPY Y1 receptor have implied that mutation of these sites led to severely impaired  $\beta$ -arrestin2 recruitment (Kilpatrick et al., 2010). Interestingly for both the Y1 receptor and rhodopsin, there does not seem to be a single 'magic bullet' residue that when phosphorylated drives internalisation, rather a minimum number of residues must be phosphorylated (Kilpatrick et al., 2010) (Doan et al., 2006) (Shukla et al., 2013).

Observations from the  $\beta$ 2-adrenoceptor have also suggested that different GRK subtypes can phosphorylate distinct receptor sites (Nobles et al., 2011). These 'phosphorylation barcodes' might lead to distinct signalling outcomes, by stabilising different  $\beta$ -arrestin conformations. Similar observations from  $G_{q/11}$  coupled  $M_3$ -muscarinic receptors have suggested that phosphorylation profiles may be tissue/cell specific and might contribute to the differential effects of the same receptor observed in different tissues (Butcher et al., 2011).

NMR spectroscopy studies have indicated that visual arrestin binding to inactive phosphorylated rhodopsin results in small movements of the polar core and the 3 element interaction described above (Zhuang et al., 2013). However the arrestin C tail remains constrained. Binding of visual arrestin to active unphosphorylated

rhodopsin, resulted in conformational changes of the 3 element interaction alone resulting in increased local mobility of this region. No changes in the conformation of the C terminal tail were observed. However in this context, arrestin is not fully activated, suggesting further global conformational changes are required. All these observations indicated that arrestin has two independent 'sensors' recognising the phosphorylation and activation states of the receptor (Gurevich and Gurevich, 2004), (Nobles et al., 2007) (Zhuang et al., 2013) with both elements needed for transition of arrestin to the fully active state (discussed further in Chapter 5).

Binding to active phosphorylated receptors, results in major global conformational changes in both the N and C domain of arrestin (Zhuang et al., 2013), (Hanson et al., 2006), (Vishnivetskiy et al., 2011). The elucidation of the crystal structure of  $\beta$ -arrestin1 bound to a GPCR C terminal phosphopeptide (consisting of a B2AR chimera containing the vasopressin V2 receptor C terminus which stably interacts with  $\beta$ -arrestin due to a cluster of phosphorylation sites) has supported many of the previous indications of structural changes inherent to activation (Shukla et al., 2013). The burying of charged residues in the arrestin polar core is energetically unfavourable. Phosphate residues attached to the activated GPCR C terminal tail by GRK's, are 'guided' by lysine residues 10 and 11 to the 'phosphate sensor' of the polar core (Gurevich and Gurevich, 2004) where upon engagement disrupts the delicate balance of the core. These lysine residues face opposing directions on the  $\beta$ -strand I, so that when they migrate they disrupt the hydrophobic 3 element interactions. This leads to a pronounced movement of the arrestin C tail (Palczewski et al., 1991), (Hanson et al., 2006), (Vishnivetskiy et al., 2010), (Zhuang et al., 2013), (Kim et al., 2012) that has also been observed in crystal structures of receptor bound visual arrestin (Kim et al., 2012) and GPCR phosphopeptide bound  $\beta$ -arrestin1 (Shukla et al., 2013). The arrestin C tail is then available to interact with accessory partners such as clathrin and adaptin. In addition an extensive 20° rotation of the N and C terminal domains relative to

one another was seen in the active  $\beta$ -arrestin1 structure and driven by the hinge domain between the N domain and  $\alpha$  helix I. Shukla et al. (2013) have suggested that this rearrangement may expose large interaction interfaces in the arrestin structure for binding signalling partners ((Shukla et al., 2013)).

Additional interactions also occur between arrestin residues and regions of the receptor also implicated in G protein binding. Hydrogen-deuterium exchange mass spectroscopy (HDX-MS) has suggested that the finger loop domain of  $\beta$ -arrestin1 can directly engage with a  $\beta$ 2AR chimera containing the vasopressin V2 receptor C terminus (Shukla et al., 2013). The finger loop is inserted into the space between TM3, 5 and 6 created by  $\beta$ 2AR activation and the residue Lys 77 crosslinks with a fellow lysine residue in ICL3 of the receptor.

Arrestin residues in the N terminal domain  $\beta$  strands V and VI (49-90) and C terminal  $\beta$  strands XV and XVI (237-268) have been implicated in determining the difference in specificity of visual arrestin or  $\beta$ -arrestin1 binding to GPCRs (Vishnivetskiy et al., 2011). Of these only 35 residues differ between the two subtypes, but visual arrestin shows almost exclusive preference for binding rhodopsin, whereas  $\beta$ -arrestin1 shows more promiscuity for GPCRs. Simultaneous swapping of these regions switched the receptor binding preference of  $\beta$ -arrestin1 to that of visual arrestin (Vishnivetskiy et al., 2004). Selective mutation studies implicated 5 specific N terminal and 9 specific C terminal residues as being largely responsible for this arrestin-GPCR specificity by directly contacting the receptor (Vishnivetskiy et al., 2011). BRET measurements showed that alanine substitution of these residues abolished binding of  $\beta$ -arrestin1 to dopamine D2 or muscarinic M2 receptors, but only decreased binding to  $\beta$ 2AR. This discrepancy suggested that interface between arrestin and GPCR cytoplasmic domains may vary with GPCR.

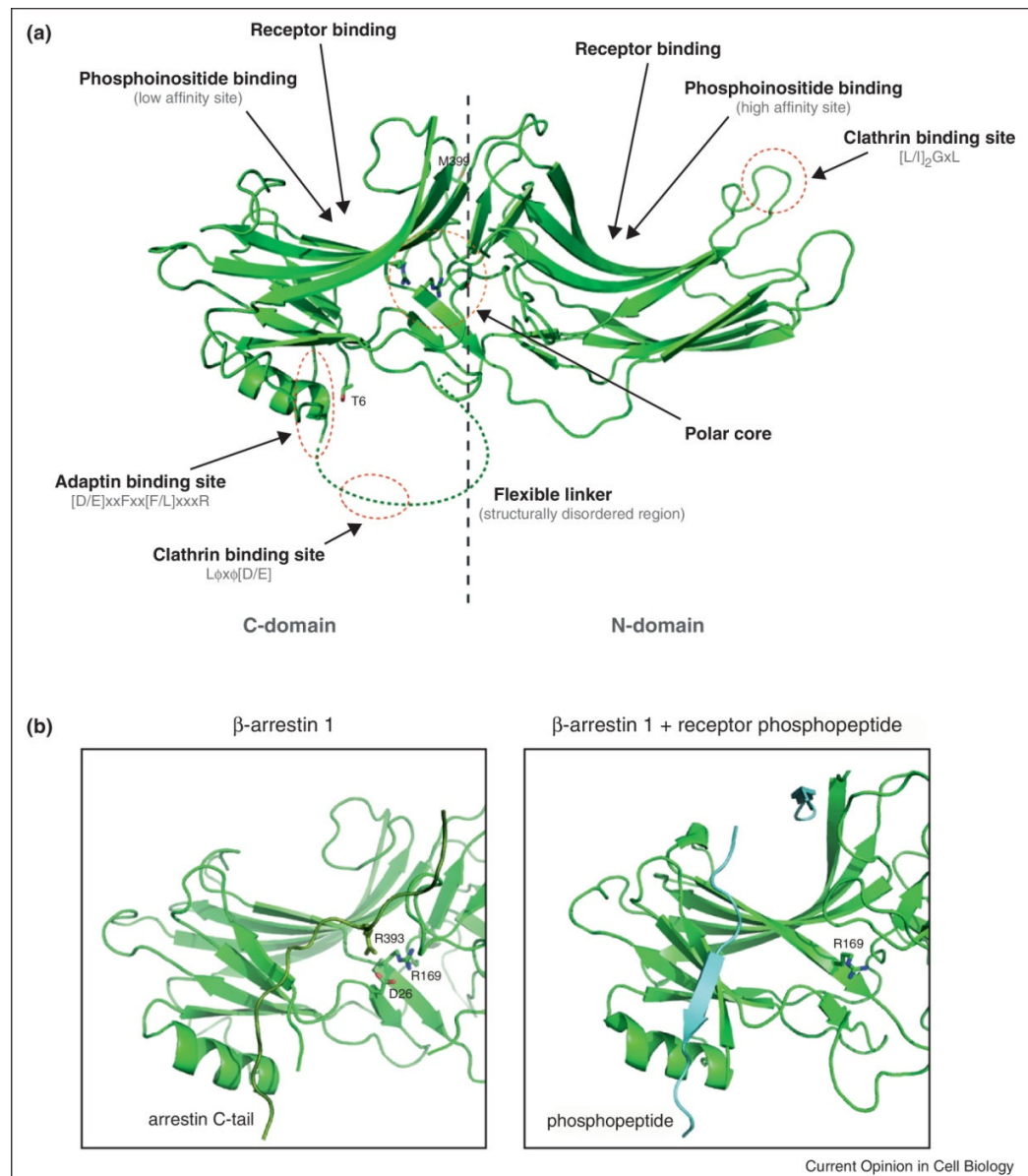


**Figure 1.4: The key structural elements of  $\beta$ -arrestin showing residues which mediate GPCR trafficking**

A ribbon diagram is shown of the structure of  $\beta$ -arrestin1, with N and C domains identified alongside the polar core. Motifs implicated in the binding of G protein, phosphoinositides, clathrin, and  $\beta$ -adaptin are also shown (A). Panels B and C show the 'inactive' (apo- $\beta$ -arrestin1) and 'active' ( $\beta$ 2AR/V2R phosphopeptide bound)  $\beta$ -arrestin1 structures. Engagement of the phosphopeptide (shown in blue), disrupts the charge balance of the polar core centred around Arg169, causing displacement of the  $\beta$ -arrestin C tail and global rearrangement of both N and C terminal domains. The C tail is then free to bind members of the endocytic machinery.

Figure taken from (Kang et al., 2014).

### **1.6.2 The role of arrestins in receptor trafficking**

Intracellular trafficking is a homeostatic mechanism by which cells regulate signalling and functional responses to stimuli through the transit of receptor proteins between the cell surface and various intracellular vesicular compartments.. This process is particularly significant for GPCRs due to the wide range of structurally diverse ligands to which they bind and the diverse physiological functions they regulate (Hanyaloglu and von Zastrow, 2008). Typically in response to agonist, receptors are rapidly removed from the cell surface and internalised into intracellular compartments. This process is termed endocytosis, and can take distinct forms. For the majority of GPCRs including,  $\beta$ 2-adrenoceptors and the NPY Y receptor family, this process is dependent on the protein clathrin and  $\beta$ -arrestins (see below 1.6.2.1).

However it should also be noted that clathrin independent endocytosis has been observed for a range of membrane proteins including but not limited to transforming growth factor  $\beta$  receptors, autocrine motility factor receptors and interleukin-2 receptors (reviewed in (Le Roy and Wrana, 2005)). One mechanism of this is the formation of membrane buds termed caveolae (60-80nm in diameter) that consist of the cholesterol binding protein caveolin 1 and glycolipids (Doherty and McMahon, 2009). The GTPase dynamin mediates the fission of these caveolar vaginations from the plasma membrane into the cell where they can fuse with endosomes.

The importance of  $\beta$ -arrestin recruitment in receptor endocytosis can also differ with subtype. For example  $\beta$ -arrestin2 is crucial to the internalisation of  $\beta$ 2-adrenoceptors (Tsao and von Zastrow, 2001). However for PAR1 receptors, although they are dependent on  $\beta$ -arrestin for desensitisation, both constitutive and agonist induced internalisation is independent of  $\beta$ -arrestin (Paing et al., 2002).

Following endocytosis, receptors are sorted and either recycled back to the cell surface or degraded in lysosomes. Here I will focus on the mechanism of endocytosis that requires  $\beta$ -arrestin recruitment and is clathrin mediated.

#### **1.6.2.1 Clathrin mediated endocytosis and receptor sorting**

Upon activation, the C tail of arrestin is released allowing arrestin to act as a molecular scaffold for adaptor proteins involved in the internalisation of receptors.  $\beta$ -arrestin2 can interact directly with clathrin and direct receptors to clathrin coated pits (approximately 100nm in diameter) for their subsequent endocytosis (Goodman et al., 1996) via the engagement of a clathrin binding motif (LIEFD) found in the  $\beta$ -arrestin2 C tail (Kang et al., 2009). The endocytic adapter AP-2 also interacts with the  $\beta$ -arrestin2-GPCR complex (Laporte et al., 1999) via a C tail motif ([D/E]xxFxx) in  $\beta$ -arrestin2 that interacts with the  $\beta$ 2 subunit of AP-2. AP-2 promotes the recruitment of clathrin and the targeting of receptors to pits composed of a polyhedral lattice of clathrin heavy and light chains (Figure 1.5). The recruitment of AP-2 is aided by interaction of  $\beta$ -arrestin2 with phosphoinositides (IP<sub>6</sub>) with both high and low affinity binding sites found in the N and C terminal arrestin domains respectively (Kang et al., 2014) (Figure 1.4).

These accessory proteins bound to  $\beta$ -arrestin2 drive the sequestration of receptors inside the cell via clathrin coated pits (Figure 1.5). These pits enable receptors to be sequestered into the cell by the small G protein dynamin, whereupon they enter the endosomal trafficking network (Kendall and Luttrell, 2009). The longevity of the GPCR-arrestin interaction can determine the fate of the sequestered receptor (Kendall and Luttrell, 2009). Receptors with greater affinity for  $\beta$ -arrestin2 (such as the  $\beta$ 2-adrenoceptor) rapidly dissociate from each other following internalisation, due to arrestin de-ubiquitination (see 1.6.2.2 below) (Wolfe and Trejo, 2007), (Kendall and Luttrell, 2009). They then re-sensitise and recycle back to the plasma membrane (Kendall and Luttrell, 2009). Those receptors with equal affinity for  $\beta$ -arrestin 1 and 2 (such as the V2

Vasopressin receptor) remain in complex due to the continued presence of stabilising ubiquitin (Luttrell and Lefkowitz, 2002), (Kendall and Luttrell, 2009), (Shenoy and Lefkowitz, 2003). Following early endosomal sorting (Moore et al., 2007), receptors are then slowly recycled or sorted and degraded in lysosomes (Kendall and Luttrell, 2009). This downregulation decreases the proportion of receptors at the plasma membrane and is a process allowing longer term modulation of receptor signal duration and magnitude (Kendall and Luttrell, 2009) (Moore et al., 2007).

#### **1.6.2.2 The role of post translational modifications in trafficking**

GPCR trafficking is also regulated by post translational modifications and binding to other trafficking proteins. For example both  $\beta$ -arrestin2 and  $\beta$ 2AR are ubiquitinated by the E3 ubiquitin ligase Mdm2 which increases GPCR internalisation (Shenoy and Lefkowitz, 2003), (Kommaddi and Shenoy, 2013). Mdm2 binding is also facilitated by the binding of the small protein parken to  $\beta$ -arrestin2 (Ahmed et al., 2011). The covalent attachment of a Small Ubiquitin-like Modifier protein (SUMO) to Lys 400 in the  $\beta$ -arrestin2 C tail has also been shown to increase  $\beta$ 2AR endocytosis (Wyatt et al., 2011). Additionally nitrosylation at Cys410, has been shown to enhance the association of  $\beta$ -arrestin2 with clathrin heavy chains leading to accelerating the rate of sequestration (Ozawa et al., 2008). Some GPCRs such as human  $\beta$ 2AR, bovine rhodopsin and the M2 muscarinic receptors are also subject to palmitoylation (Escriba et al., 2007) whereby one or more palmitate molecule is covalently attached to C terminal receptor cysteine residues. Palmitoylation has been suggested to aid the delivery of some GPCRs to the plasma membrane. For example mutation of palmitoylation sites in the follicle stimulating hormone receptor have been shown to decrease receptor surface expression by 10-30% (Uribe et al., 2008).

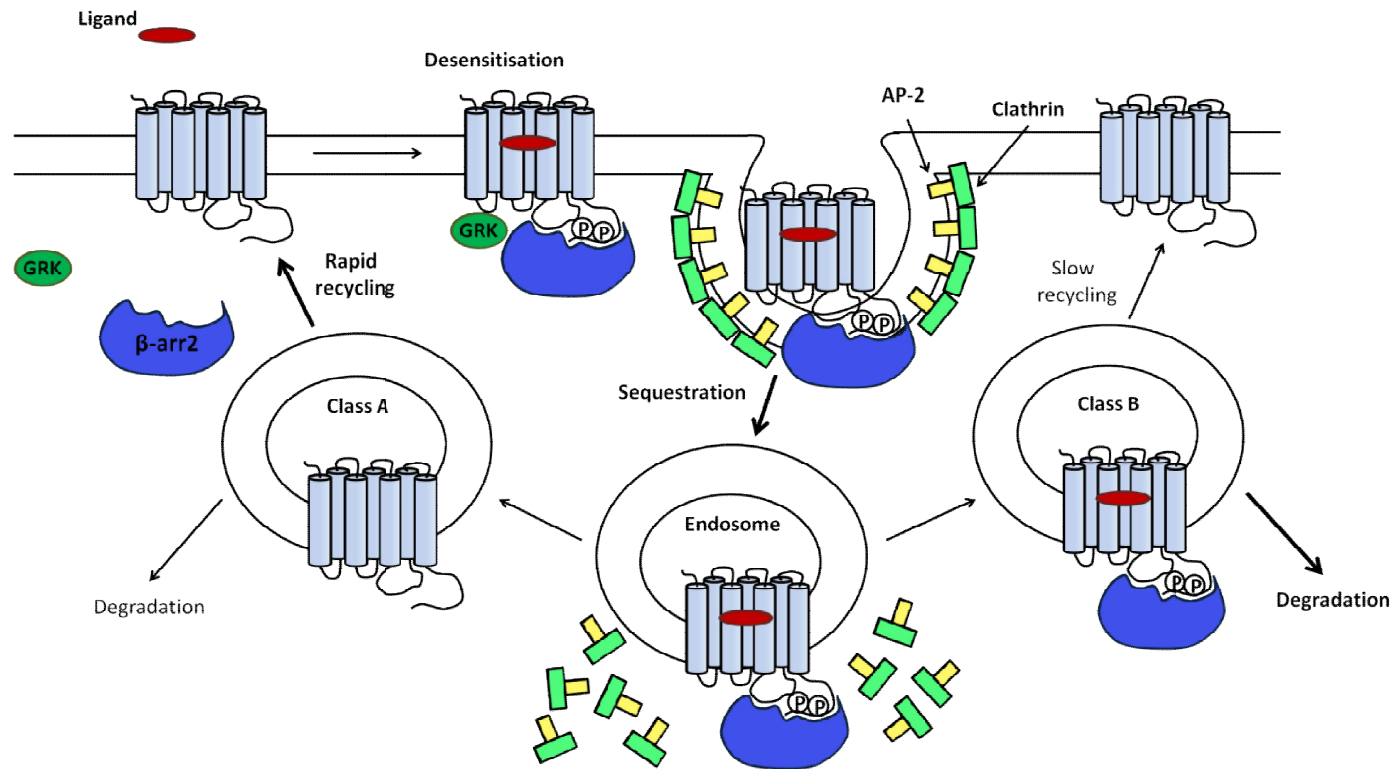


**Figure 1.5: The molecular machinery involved in GPCR desensitisation and internalisation**

Agonist binding to its cognate GPCR leads to conformational changes within the GPCR helical domains that facilitate receptor activation. G protein coupled receptor kinases (GRK's) are recruited to the activated receptor and phosphorylate the receptor at key serine or threonine residues in its C terminal domain. These phosphates can act as docking sites to facilitate the recruitment of  $\beta$ -arrestin to the receptor.  $\beta$ -arrestin desensitises the receptor by sterically hindering further G protein coupling to the GPCR.  $\beta$ -arrestin can then act as a molecular scaffold for a variety of molecules essential to GPCR internalisation such as clathrin and AP-2. Following sequestration into the cell the internalised receptor has one of two fates, partly influenced by the strength of its association with arrestin. Class A receptors, such as  $\beta$ 2-adrenoceptors, readily dissociate from  $\beta$ -arrestin and rapidly recycle to the plasma membrane. Class B receptors, such as the V2 vasopressin receptor, form stable complexes with  $\beta$ -arrestin which are then slowly recycle or are degraded. Preferential pathways are shown in bold.

Figure adapted from (Kendall and Luttrell, 2009)

### 1.7 The role of $\beta$ -arrestin in signalling

The role of  $\beta$ -arrestin in GPCR desensitisation and internalisation is now well established. However evidence now suggests that  $\beta$ -arrestins themselves can also act as signalling components in their own right (Rajagopal et al., 2010) and can interact with a wide range of signalling partners including but not limited to protein kinases such as c-Src, p38 and ERK1/2 (Xiao et al., 2007), (Shukla et al., 2008), (Song et al., 2009), phosphodiesterase (PDE) 4 to accelerate cAMP degradation (Baillie et al., 2003) and diacylglycerol kinases to assist the quenching of diacylglycerol dependent signalling (such as PKC) (Nelson et al., 2007).

$\beta$ -arrestin activated ERK has been suggested to impact translational regulation as it is sequestered in the cytoplasm unlike G protein dependently activated ERK which translocates to the nucleus and activates transcription factors (Gesty-Palmer et al., 2006), reviewed in (Musnier et al., 2010). This suggests that G protein dependent and G protein independent activation of ERK can result in distinct functional outcomes via the stabilisation of different receptor 'active' conformations or 'ligand selective states' (Shukla et al., 2008). The concept of biased agonism offers the potential to be able to pharmacologically separate and direct signalling pathways depending on the ligand used and could represent a novel therapeutic agent (Shukla et al., 2008). The role of  $\beta$ -arrestin in signalling has driven the interest in the identification of ligands that selectively bias signalling towards these G protein independent pathways. For example ligands that have inverse agonist activity at the  $\beta_2$ -adrenoceptor for adenylyl cyclase activation (ie. inhibit  $G_s$  coupling) are capable of activating MAPK (Azzi et al., 2003) with increased ERK phosphorylation following propranolol stimulation and ICI118551. Using a dominant negative mutant of  $\beta$ -arrestin and mouse embryonic fibroblast  $\beta$ -arrestin knockouts, this partial activation of ERK was shown to be  $G_\alpha$  independent but  $\beta$ -arrestin dependent. The authors propose that the phenomena of G protein independent activation of MAPK occurs when GPCR-G protein coupling is ablated or inhibited by particular ligands, suggesting that different

ligands can stabilise different active states of the receptor and 'bias' signalling towards a G protein dependent or independent pathway. The  $\beta$ 2-adrenoceptor ligand carvedilol has been shown to bias signalling to G protein independent pathways (Wisler et al., 2007). For example, stimulation of the  $\beta$ 2-adrenoceptor with carvedilol led to a distinct receptor phosphorylation profile to that seen for the unbiased agonist isoprenaline indicative of a differential recruitment of GRK subtypes (Nobles et al., 2011). The phosphorylation 'barcode' resulting from carvedilol binding promotes a conformation of receptor- $\beta$ -arrestin2 that favours G protein independent signalling pathways.

Parathyroid hormone receptor (PTH1R) ligands can activate  $G_s$  and also  $G_{q/11}$ , and internalise in a  $\beta$ -arrestin dependent manner. Parathyroid hormone stimulation induces MAPK activation with a rapid G protein dependent phase followed by a prolonged G protein independent phase (Gesty-Palmer et al., 2006). RNA silencing and the use of G protein inhibitors showed that this prolonged MAPK activation was  $\beta$ -arrestin dependent and wholly distinct from G protein involvement. Biased agonism was also observed at the PTH1R, as the inverse agonist for  $G_s$  and  $G_q$ , PTH-1A, can still stimulate prolonged MAPK activity in HEK293 cells again confirmed by RNA silencing to be  $\beta$ -arrestin dependent.

The impact of biased agonism, therefore requires greater elucidation to tease out potential effects of signalling crosstalk, however it does provide the potential to improve therapeutic selectivity. For example the angiotensin II receptor ligand TRV027 has been shown *in vitro* to selectively bias signalling towards  $\beta$ -arrestin dependent pathways (Violin et al., 2010). This bias was translated to early clinical studies in humans where TRV027 treatment was shown to have cardioprotective effects in both healthy volunteers and those suffering from systolic heart failure which was selective for the renin-angiotensin system (Violin et al., 2014). TRV027 is currently in phase IIb clinical trials in acute heart failure.

## 1.8 The NPY Y receptor family

### 1.8.1 Peptide ligands

The endogenous ligands of the NPY receptors are neuropeptide Y (NPY), peptide YY (PYY) and pancreatic polypeptide (PP). They are all 36 amino acid peptides with an amidated C terminal tyrosine (Figure 1.6A; (Babilon et al., 2013). Although PYY and PP only share 70% and 50% sequence homology with NPY (Cerdeira-Reverte and Larhammar, 2000) they have been proposed to share a common defined U shaped tertiary structure comprising of an extended N terminal polyproline helix followed by an amphipathic  $\alpha$  helix, connected by a  $\beta$  turn (Michel et al., 1998). This structure has been derived from the crystal structure of avian PP resolved in 1981 (Blundell et al., 1981). An alternative structure has also been proposed based on the nuclear magnetic resonance (NMR) structure of human NPY in the presence of membrane mimicking micelles (composed of dodecylphosphocholine) (Bader et al., 2001). This structure also contains the alpha helical regions as before, but the N terminus shows greater flexibility and lacks the U shaped fold. The authors propose that this model may more likely reflect the physiological status of NPY and other related peptides.

NPY is the most abundant neuropeptide in the brain, with greatest expression found in the hypothalamus (Bai et al., 1985) where it is primarily produced in the arcuate nucleus (Morris, 1989) (Fetisov et al., 2004). NPY is also expressed in the periphery as a co-transmitter in postganglionic sympathetic neurones and the adrenal medulla, with circulating human plasma levels estimated to be 5-19pmol/L (Onuoha et al., 2000). Additionally NPY and noradrenaline are co-released from central catecholamine neurons during nerve stimulation (Illes and Regenold, 1990).

In contrast to NPY, peptide YY (PYY) and pancreatic polypeptide (PP) are both hormones, with PYY released from endocrine L cells most widespread in the distal ileum and colon, but present throughout the gastrointestinal tract (Ekblad and

Sundler, 2002). PP is exclusively expressed by pancreatic F type cells (Adrian et al., 1978). Both NPY and PYY can be cleaved by endogenous dipeptidyl peptidase IV in the periphery to generate the truncated forms NPY<sub>3-36</sub> and PYY<sub>3-36</sub> (Borowsky et al., 1998).

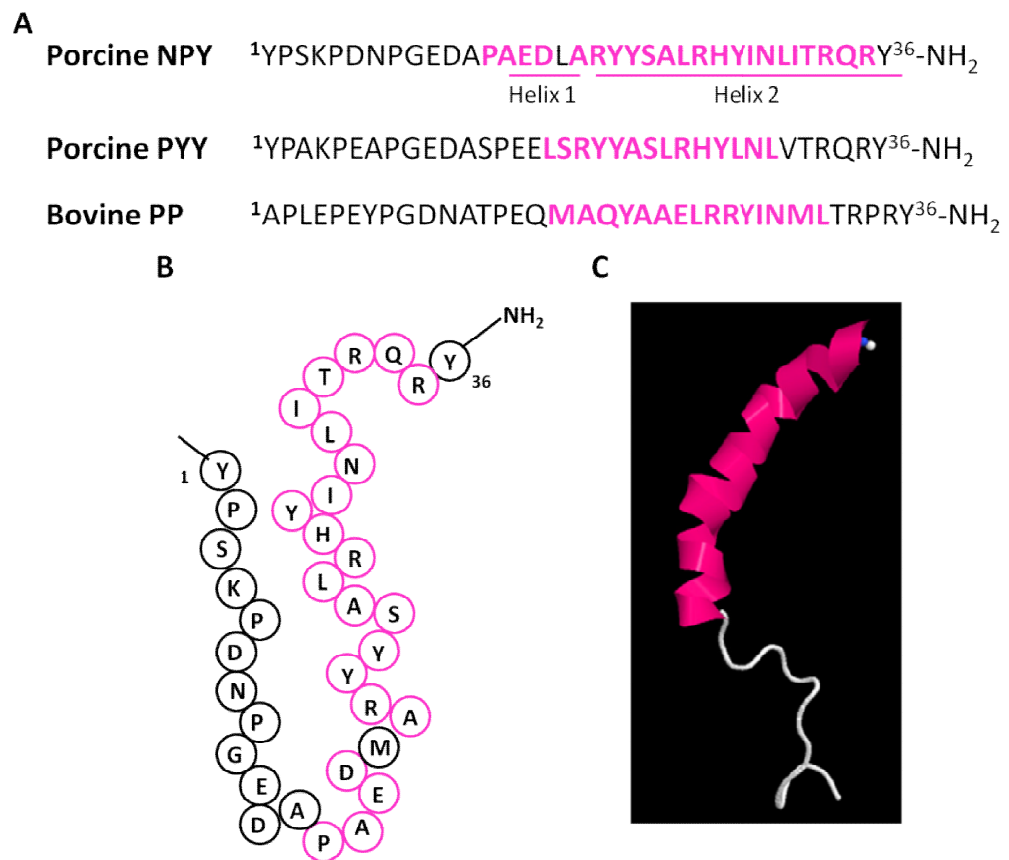


**Figure 1.6: The sequence and structural models proposed for NPY**

Panel **A** shows the 36 amino acid length sequence of porcine NPY and PYY and bovine PP. Residues highlighted in pink show the location of alpha helical regions within the sequence (panel **B**). A topographical interpretation of NPY showing the defined U shaped structure predicted from the crystal structure of avian pancreatic polypeptide. The alpha helical regions are again indicated in pink. Panel **C** shows the structure as predicted from nuclear magnetic resonance imaging of human NPY in the presence of membrane mimicking micelles, whereby the N terminal domain is shown to be relatively flexible and is more likely to reflect the peptide's physiological form.

Figure adapted from (Babilon et al., 2013) with panel **C** taken from the Protein Data Bank<sup>1</sup>with the structure derived from (Monks et al., 1996).

<sup>1</sup> <http://www.rcsb.org/pdb/explore/jmol.do?structureid=1RON>, last updated 13-07-2011; page accessed 12-12-2014.

### **1.8.2 NPY Y receptor family**

The NPY Y receptor subtypes are Class A GPCRs, with four functional subtypes in man termed the Y1, Y2, Y4 and Y5 (Michel et al., 1998). A further subtype, the y6, has been identified but is a truncated form that is not expressed in primates (Rose et al., 1997). Structural domains are relatively consistent between subtypes, with the exception of the Y5 subtype which has a short C terminal domain and a larger ICL3. All 5 receptor subtypes couple to G<sub>i/o</sub> proteins, and are capable of binding to a similar array of ligands. However subtypes differ in their endogenous and synthetic ligand selectivity, which is likely a reflection of the relatively low sequence homology of 27-32% (Michel et al., 1998, Sjodin et al., 2006).

#### **1.8.2.1 Y1 receptor**

The Y1 receptor is expressed in a wide range of species, with more than 92% sequence homology observed for human, rat, pig, guinea pig, mouse and cattle (Michel et al., 1998) (see Figure 1.7). The Y1 subtype shows a wide distribution throughout the body, but the greatest concentrations are found within regions of the hypothalamus, namely the arcuate nucleus, paraventricular and dorsomedial nuclei (Fetissov et al., 2004). Y1 receptors are also expressed in vascular smooth muscle cells, adipose tissue, kidney and the gastrointestinal tract (Michel et al., 1998). Y1 receptors are able to bind both NPY and PYY with high affinity (Cabrele and Beck-Sickinger, 2000), but show reduced affinity for PP (Gehlert and Gackenhaimer, 1997). This subtype is also able to bind the NPY analogue Leu<sup>31</sup>, Pro<sup>34</sup> NPY (Fuhlendorff et al., 1990) with high affinity

BIBO3304 is a highly selective Y1 antagonist exhibiting 2600 fold selectivity over Y2, Y4 and Y5 receptors (Wieland et al., 1998). The closely related non peptide antagonist BIBP3326 also shows high selectivity for the Y1 subtype over other Y receptors but also shows relatively high affinity binding (K<sub>i</sub> 79nM) for neuropeptide FF receptors (Mollereau et al., 2001). The dimeric C terminal NPY

analogue GR231118 has also been suggested to be a highly potent antagonist at the Y1 receptor (Ishihara et al., 1998), however it is worth noting that this was when compared to selectivity at the Y2 subtype. Additionally GR231118 has been shown to be a potent agonist at human Y4 (Parker et al., 1998) and to a lesser extent rat Y5 and Y2 receptors as well showing affinity for neuropeptide FF receptors (Mollereau et al., 2001). Caution should therefore be taken when assuming the selectivity of these antagonists in assays where multiple subtypes may be present.

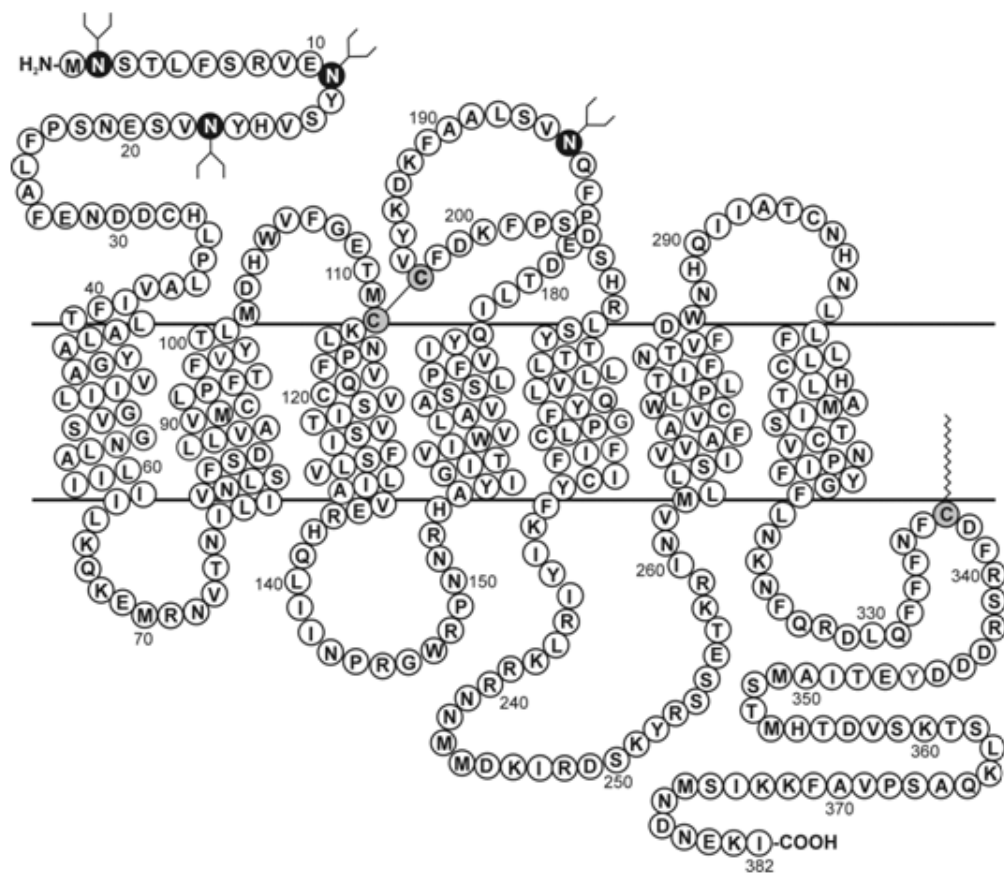


**Figure 1.7: The rat Y1 receptor sequence**

A snake plot showing the structure of the rat Y1 receptor. Amino acids are numbered according to cDNA sequence. The presence of a disulphide bridge between TM3 and ECL2 is predicted (residues Cys112 to Cys197) in addition to receptor palmitoylation at Cys337.

Figure courtesy of Dr Nick Holliday.

### **1.8.2.2 Y2 receptor**

The Y2 receptor subtype is predominantly expressed in the central nervous system, particularly within the arcuate nucleus of the hypothalamus (Dumont et al., 1998), whereby their activation at presynaptic junctions can inhibit the release of the neurotransmitters NPY and glutamate (Klapstein and Colmers, 1993). The Y2 receptor is also expressed in spleen, liver, blood vessels, white and brown adipose tissue and the gastrointestinal tract (Michel et al., 1998).

The Y2 receptor shows similar affinities for NPY and PYY and lower affinity for PP (Michel et al., 1998). However unlike the Y1 receptor, the Y2 receptor is also capable of binding the truncated forms NPY<sub>3-36</sub> and PYY<sub>3-36</sub> with high affinity (Keire et al., 2000) and has low affinity for Leu<sup>31</sup>, Pro<sup>34</sup> NPY (Gerald et al., 1995).

### **1.8.2.3 NPY Y4**

Expression of the Y4 receptor subtype is largely localised to the gastrointestinal tract, but has also been documented in the hippocampus and hypothalamus (Dumont et al., 1998), (Lindner et al., 2008). Like the Y2 receptor, the Y4 subtype has been suggested to mediate the satiety effects of PP and perhaps also PYY (Sainsbury et al., 2003). The Y4 receptor is a “PP-selective” receptor, binding PP with high affinity (Gehlert et al., 1997) (Tough et al., 2006) and showed reduced affinity for NPY and PYY and Leu<sup>31</sup>, Pro<sup>34</sup> NPY (Gehlert et al., 1996b). The NPY C terminal analogue GR231118 has also been shown to be a potent agonist at human Y4 receptors (Parker et al., 1998).

### **1.8.2.4 NPY Y5**

The highest expression for the Y5 subtype is seen in the brain, specifically the hippocampus and hypothalamus (Parker and Herzog, 1999). Both the mRNA and protein expression of the Y5 receptor overlaps with that of the Y1 receptor in these regions of rat brains (Parker and Herzog, 1999) with immunohistochemistry further confirming distinct receptor co-expression within the same cells and nerve fibres of this brain region (Wolak et al., 2003). Additionally both receptors

are located on chromosome 4q31-q32, and share an overlapping gene structure (Nguyen et al., 2012).

The rank order of potency of Y5 receptors for endogenous ligands is  $NPY \geq PYY \geq PP$  (Michel et al., 1998). However this subtype is relatively non-selective, and is capable of responding to both  $NPY_{3-36}$  and  $PYY_{3-36}$  (Gerald et al., 1996) and also  $[Leu^{31}, Pro^{34}]$  NPY (Balasubramaniam, 1997), analogues traditionally used to define Y1 versus Y2 receptor pharmacology. However synthetic ligands have also been created that selectively target the Y5 subtype with high affinity, in comparison to other Y receptors such as the agonists  $cPP(1-17)(Ala^{31}, Aib^{32})$  (17-36) NPY (Dumont et al., 2003) and  $dTrp^{32}NPY$  (Balasubramaniam et al., 1994) and antagonists such as CGP71683 (Criscione et al., 1998), NPY5RA972 (Block et al., 2002) and L152,804 (Kanatani et al., 2000) (see chapter 6).

### **1.8.3 Peptide binding to NPY receptor subtypes**

The Y1, Y2 and Y5 subtypes differ the most in sequence homology, but yet share high affinity binding to the same ligand NPY, suggesting that the small proportion of conserved residues are important to ligand binding (Sjodin et al., 2006). All 3 subtypes have been shown to interact with the amidated C terminal domain of NPY and PYY, but differ in their interaction with the N terminus. The Y1 subtype requires a complete N terminal domain of NPY (Larhammar et al., 1992) reflected in its lack of affinity for the N terminal truncated forms  $NPY_{3-36}$  and  $PYY_{3-36}$ . However the Y2 and Y5 receptor subtypes have equal affinity for NPY, PYY and  $NPY_{3-36}$  and  $PYY_{3-36}$ , suggesting the N terminal portion of the peptide is not as crucial.

Ligand binding to NPY receptor subtypes has been suggested to occur within the transmembrane helical bundle and also involve extracellular loop residues. Extensive mutagenesis of the human Y1 receptor was used to characterise residues important to binding both peptide agonists and non peptide antagonists (Kannoa et al., 2001, Sjodin et al., 2006). Mutation of the highly conserved Tyr100 to alanine led to a complete loss of NPY binding (Kannoa et al., 2001, Sautel et al.,

1995). This residue is a tyrosine or serine in the Y2 and Y5 receptors respectively, and the hydroxyl group both these amino acids contain has been proposed to interact with the amidated C terminus of the peptide ligand directly (Sjodin et al., 2006). The TM6 residues F286 and His298 have also been implicated in ligand binding (Kannoa et al., 2001). Mutation of the Y1 receptor specific residue Asn116 (TM3) has also been shown to produce a 35 fold decrease in binding of the Y1 selective antagonist SR120819A (Sjodin et al., 2006). Asp286 at the interface of TM6 and ECL3 of Y1 and Y4 receptors has also been shown to form a salt bridge with Arg35 of NPY and PP (Merten et al., 2007). This residue in Y2 and Y5 receptors is also conserved but instead interacts with Arg33 of the peptide, and requires an additional interaction of Asp199 in ECL2 to Arg25 of the peptide for high affinity binding (Lindner et al., 2008). This suggests that some residues have a shared importance for ligand binding across the subtypes, but subtype specific residues are also involved. Babilon et al. (2013) have suggested that the Y1 and Y4 subtypes may have distinct ligand binding modes to that seen for the Y2 and Y5 subtypes based on these mutation studies and may reflect the closer sequence homology of this receptor pairing (Babilon et al., 2013).

#### **1.8.4 Physiological implication of NPYergic peptide signalling**

The NPY receptor subtypes have been implicated in a range of physiological processes such as feeding responses, energy expenditure, anxiolysis, nociception, circadian rhythms, bone metabolism, inflammation, and cognitive impairment (reviewed in (Holzer et al., 2012)). NPY can also act in conjunction with noradrenaline in perivascular sympathetic neurons to promote vasoconstriction (Wahlestedt et al., 1990b). In addition, aberrations in receptor expression have also been seen in cancer. Overexpression of NPY receptor subtypes have been implicated in ERK signalling driven proliferation and migration of a variety of tumours, with overexpression of Y1 and Y2 receptors seen in human breast carcinomas, and glioblastomas respectively and Y5 receptors in a range of cancer cell lines (Sheriff et al., 2010). Both Y1 and Y5 subtypes have also been shown to

mediate NPY effects on stimulating vascular endothelial growth factor secretion from endothelial cells and subsequent angiogenesis in breast cancer cell lines (Medeiros and Jackson, 2013).

However the physiological role of the NPY receptor subtypes that has historically attracted the most pharmacological interest is their control of appetite, (Zhang et al., 2011) - specifically the regulation of centrally mediated food intake and satiety, and processes such as lipid metabolism, and insulin secretion.

The arcuate nucleus, a major hypothalamic centre for appetite regulation, is responsible for innervating the majority of the hypothalamus, with chemical and neuronal signals generated in the periphery also integrated here. As well as expressing all 4 of the functional NPY receptor subtypes, (Dumont et al., 1998), the arcuate nucleus also expresses receptors for the orexigenic hormone ghrelin (Willesen et al., 1999), the satiety adipose hormone leptin (Elmquist et al., 1998) and insulin (Marks et al., 1990). NPY release from arcuate neurons can be temporally controlled by these receptors depending on the energy expenditure balance, with insulin and leptin able to inhibit NPY secretion and ghrelin stimulate it (Zhang et al., 2011). NPY is a potent stimulator of hyperphagia, with its release correlated with food intake in rodents (Clark et al., 1984), (Kalra et al., 1991) in a circadian fashion (Akabayashi et al., 1994). Direct injection of NPY into hypothalamic regions of rats results in a dose dependent increase in food intake (Stanley and Leibowitz, 1985), (Stanley et al., 1986), (Leibowitz et al., 1988), (Zarjevski et al., 1993). Through both its central actions and peripheral sympathetic nerve release, increased NPY signalling is also implicated in other processes of energy homeostasis which result in weight gain and increased fat storage, such as hyperinsulinemia, insulin hyper responsiveness, insulin resistance in skeletal muscle, increased de novo lipogenesis in white adipose tissue and suppressed thermogenesis in brown adipose tissue (reviewed in (Zhang et al., 2011)). Therefore increased NPYergic tone has been implicated as one of the signalling pathways in the development and persistence of obesity.

Elevation in circulating NPY levels have been observed in obese women (Baranowska et al., 2005) when compared to healthy women. Obese rats fed a high fat diet for 22 weeks have increased mRNA expression of NPY in the hypothalamus (Huang et al., 2003). Similar increases have also been seen for obese rats with defective leptin signalling (Stephens and Caro, 1998) in keeping with the inhibitory role of leptin on NPY secretion previously documented.

Both PYY and PP have been shown to be secreted following food ingestion and act in the periphery as satiety factors. Once secreted, PYY is cleaved to its predominant form PYY<sub>3-36</sub>, allowing selective binding to Y2 receptors and to a lesser extent Y5 (Holzer et al., 2012). PYY and PYY<sub>3-36</sub> binding to Y2 receptors in the enteric nervous system have been shown to inhibit colonic transit in mice (Wang et al., 2010). PYY and PYY<sub>3-36</sub>, together with co-released peptides from ileal and colonic cells, such as GLP-1, inhibit gastric acid secretion and mediate the 'ileal brake' that slows gastric emptying in response to food entering the small intestine (Field et al., 2010). PP can also inhibit gastric emptying via the vagus nerve (Field et al., 2010) , peristalsis (Fujimiya and Inui, 2000) and intestinal electrolyte and water secretion via binding to Y4 receptors expressed on the intestinal epithelium (Tough et al., 2006).

Therefore the control of central feeding responses is a delicate balance between the brain-gut axis involving multiple signalling inputs that can have both synergistic and opposing physiological effects. which are partly mediated by the Y family of receptors.

#### **1.8.4.1 Y1 and Y5 receptor roles in stimulating food intake**

Interestingly Y receptor subtypes can be grouped based on their roles in feeding responses. The Y1 and Y5 subtypes mediate NPY induced orexigenic responses, with both originally identified as 'feeding receptors' (Haynes et al., 1998). Significantly reduced mRNA expression levels of Y1 and Y5 receptors in the hypothalamus have been observed for rodents that are resistant to diet induced obesity (compared to control obese animals)(Huang et al., 2003) suggesting the

role of both receptors in obesity development. Direct administration of NPY into the hypothalamus of Y1 receptor knock out mice led to decreases in feeding responses. However germline knock out models of the Y1 receptor in mice surprisingly do not show substantial changes in spontaneous feeding (Kushi et al., 1998), (Howell et al., 2003) but more subtle reductions in hyperphagia compared to wildtype controls (Pedrazzini et al., 1998).

However paradoxically, Y1 receptor germline knock outs developed late onset obesity suggested to be due to decreased metabolic rate. This was also associated with hyperinsulinemia with increased circulating insulin suggested to increase adipose tissue glucose storage (Kushi et al., 1998). Similar development of late onset obesity have also been seen Y5 receptor knock out mice (Marsh et al., 1998), (Higuchi et al., 2008), suggesting they may be a degree of compensation between the Y1 and Y5 subtypes in respect to feeding responses (Nguyen et al., 2012). However significant reductions in feeding were seen in Y1 receptor deficient ob/ob mice (Pralong et al., 2002) in addition to a significant decrease in body weight, suggesting that deficiency in Y1 receptor mediated effects is more pronounced in physiological conditions of high NPY concentrations.

The intravenous administration of a range of Y1 receptor agonists in rats, such as [DArg<sup>25</sup>]NPY, stimulates increased food intake (Mullins et al., 2001). Prolonged stimulation led to significant increases in body weight and fat gain (Mullins et al., 2001), increased lipogenesis (Henry et al., 2005), and circulating insulin levels (Gao et al., 2004). Similar effects have also been observed when using Y5 receptor selective agonists such as [Ala<sup>31</sup>, Aib<sup>34</sup>] NPY which were able to significantly increase feeding behaviour in rats (Cabrele et al., 2000). The Y5 receptor chimeric agonist 2-36 [K4,RYYSA19-23]PP (McCrea et al., 2000) also was able to dramatically increase food intake in a rat model.

Therefore activation of both Y1 and Y5 receptor subtypes has both been implicated in the stimulation of food intake *in vivo*. Potential compensatory

effects between these two subtypes have been proposed instead to be due to coregulation of feeding responses. In support of this concurrent germline and hypothalamic knock out of both Y1 and Y5 receptors in mice, resulted in decreased spontaneous and fast induced food intake when fed a high fat diet suggesting a coordination between these subtypes (Nguyen et al., 2012). This coordination has also been suggested to be via the Y1 and Y5 receptors forming heterodimers that are able to modulate one another (Gehlert et al., 2007) and result in altered pharmacology compared to either receptor acting alone (see Chapter 6).

#### **1.8.4.2 Y2 and Y4 receptor roles in satiety**

Conversely the activation of Y2 and Y4 receptor subtypes has been implicated in the induction of satiety. Gut derived peptides such as PYY and PP, are satiety signals that can trigger the termination of feeding via binding to both receptor subtype (Batterham et al., 2003b, Batterham et al., 2002). Therefore agonist therapies that target either subtype were attractive targets for anti obesity treatments (see section 1.8.6.2).

Mice models with germline knock out of Y2 receptors show increased food intake (Naveilhan et al., 1999), (Sainsbury et al., 2002). Knock out studies have shown discrepancies in respect to effects on body weight, with both increases (Naveilhan et al., 1999) and no changes observed (Sainsbury et al., 2002) but is likely due to either differences in the mice model used, experimental stress affecting typical mice feeding behaviour or differential effects seen in the central or periphery (Zhang et al., 2011). For example, hypothalamic deletion in adult mice has resulted in significant increases in food intake, weight gain and fat deposition (Shi et al., 2010). This group also showed by deleting Y2 receptors only expressed on NPYergic neurons, that the Y2 receptors can regulate NPY expression in an autocrine manner in the arcuate nucleus (Shi et al., 2010).

Knock out studies of the ligand PYY, resulted in mice developing an obese phenotype with (Batterham et al., 2006) or without any significant change in

feeding (Wortley et al., 2007). Another study suggested that PYY knock out may result in hyperinsulinemia (Boey et al., 2006) similar to effects after Y1 receptor deletion. Conversely, overexpression of PYY in mice models leads to marked inhibition of diet induced obesity (Boey et al., 2006). Crossing this line with an ob/ob line can rescue the obese phenotype with significant reductions on weight gain, adiposity and improved glucose tolerance observed. These *in vivo* models therefore suggest that PYY and PYY derivatives play a substantial role in the control of feeding responses via activation of the Y2 receptor.

Although Y4 receptors are expressed in the brain regions implicated in appetite regulation, its primary endogenous agonist, PP is exclusively expressed in the pancreas and is released prior to PYY via vagal cholinergic mechanisms (Schwartz et al., 1978). The extent of PP release is in proportion to the calorific load, leading to inhibition of exocrine function, stimulation of gastric motility and gastric secretion (Zhang et al., 2011). However Zhang et al., 2011, have suggested that many of the anorexigenic effects in the CNS attributed to PP are actually due to binding of NPY to the Y4 subtype (Zhang et al., 2011) , although this seems unlikely based on the reduced affinity of the Y4 receptor for NPY (Chapter 3, Figure 3.9) (Gehlert et al., 1997).

Germline deletion of Y4 receptors in mice resulted in a lean phenotype with reduction in body weight and adiposity but no change in food intake (Sainsbury et al., 2003). The authors suggest reduction in body weight is driven by changes in energy expenditure and metabolic rate. A synergistic effect on reduced adiposity and increased energy expenditure was observed when both the Y4 and Y2 receptors were ablated (Zhang et al., 2010). Therefore as for the Y1-Y5 receptors in respect to orexigenic effects, coregulation between Y2 and Y4 receptors may be involved in anorexigenic effects.

### **1.8.5 Obesity –the health and socioeconomic implications**

As of 2013, it was estimated that 61.9% of adults and 28% of children aged 2-15 in the UK are overweight or obese <sup>2</sup>. Obesity rates have also vastly increased globally over the past three decades (Finucane et al., 2011) with suggestions that prevalence is correlated to socioeconomic state. Obesity is typically defined by an individual having a body mass index (BMI) in excess of 30 kg/m<sup>2</sup>, compared to 18.5-25 kg/m<sup>2</sup> for a healthy individual (Mitchell et al., 2011). Measurements of waist circumference are also used to evaluate individual health risks. Medical complications associated with obesity cost the NHS more than £5 billion pounds each year and include higher incidences and morbidity rates of coronary heart disease, hypertension, type 2 diabetes, cognitive dysfunction, sleep apnea, non alcoholic liver disease and many forms of cancer including thyroid, colorectal, renal, pancreatic, oesophageal, ovarian and breast (reviewed in (Mitchell et al., 2011)).

A gap exists in the market for pharmacotherapies targeting obesity, as social drives by governments and health officials in promoting healthier lifestyles and exercise have been largely unsuccessful. Diet and exercise programmes are also often ineffective for maintaining long term weight loss. Surgical intervention in the form of bariatric surgery is not only costly (private health care estimates range from £5000-£15,000) but carries a high risk of internal bleeding, thrombosis and pulmonary embolism <sup>3</sup> with mortality rates in the USA estimated at 1:1000 patients. Additionally the NHS will only consider patients with a BMI in excess of 35 as eligible.

In order to obtain food and drug administration (FDA) approval in the USA, drug treatments in phase trials must show a sustained weight loss of approximately 5% of total body weight, which could significantly improve the quality of life for

---

<sup>2</sup> <https://www.gov.uk/government/policies/reducing-obesity-and-improving-diet> authored by the Department of Health and Jane Ellison MP, March 25<sup>th</sup> 2013. Accessed 01-09-2014.

<sup>3</sup> <http://www.nhs.uk/conditions/weight-loss-surgery/Pages/Introduction.aspx>; page last reviewed 05-11-2013. Accessed 01-09-2014.

obese individuals. However as obese individuals are likely to require these therapies chronically, their safety profiles must be beyond dispute. Currently the majority of anti obesity agents have been withdrawn from market due to a lack of efficacy or concerns over safety. Only orlistat, a pancreatic lipase inhibitor, is currently approved for long term use, however many patients cannot tolerate its gastrointestinal side effects. The noradrenaline and dopamine stimulators diethylpropion and benzphetamine have been approved for short term use (12 weeks) in the USA, but there are concerns over potential drug abuse in longer term use (Cheung et al., 2013). Sibutramine, a noradrenaline/5-HT reuptake blocker was withdrawn from the market in 2010 due to major cardiovascular effects (Cheung et al., 2013). Rimonabant, a cannabinoid 1 receptor antagonist was also withdrawn worldwide due to significant psychiatric side effects such as suicide. As of June 2014, the FDA had postponed the approval of the combined therapy Contrave following phase III trials, due to worries over long term cardiovascular risks. Therefore there is a large currently unmet demand for anti obesity therapies that are effective and safe.

### **1.8.6 Targeting the NPY receptor subtypes in anti obesity therapies**

#### **1.8.6.1 The Y1 and Y5 subtypes**

The primary aim of many pharmacotherapies to treat obesity was in inducing reductions in food intake. Historically, the first focus on anti-obesity agents targeted at Y receptors was on inhibiting NPY orexigenic effects modulated through the Y1 and Y5 receptors, by the use of highly subtype selective antagonists. A number of Y1 receptor selective antagonists have been developed, which bind with high affinity. Direct injection of BIBO3304 or 1229U91 into the paraventricular nucleus of lean or obese rats inhibited NPY induced hyperphagia (Kanatani et al., 1996). However the therapeutic use of these Y1 receptor antagonists in the clinic was limited due to their poor bioavailability in both oral and peripheral administration (Kanatani et al., 2001) restricting their use to

pharmacological research. An orally active compound J-104870 when administered via the intracerebroventricular and intraperitoneal route was able to inhibit hypothalamic NPY induced food intake in Zucker fatty rats (Kanatani et al., 1999) leading to significant reduction in weight gain and lipid accumulation in the liver (Ishihara et al., 2002). A similar antagonist, J-115814 also showed similar effects on NPY induced feeding (Kanatani et al., 2001), however its therapeutic use has been limited due to cardiovascular toxicity (Fermini and Fossa, 2003).

A range of Y5 selective antagonists have also been developed that have shown high selectivity and the ability to inhibit NPY and/or Y5 agonist induced hyperphagia in rats. Of these CGP71683A showed high efficacy in both acute and chronic administration, however it also showed cross reactivity with muscarinic and serotonin 5-HT receptors raising the potential for physiological side effects (Criscione et al., 1998). Additionally GW438014A showed high efficacy, but poor oral bioavailability (Daniels et al., 2002). MK-0557 showed promise in mice studies with chronic administration suppressing high fat diet and  $dTrp^{32}NPY$  induced obesity in mice (Erondu et al., 2006). However this efficacy did not translate to human clinical trials, where a 1 year trial with MK-0557 treatment induced no meaningful clinical weight loss. Clinical trials with Velneperit (S-2367) in 656 patients also showed limited human efficacy with no clinically significant weight loss observed compared to placebo (George et al., 2014). Therefore both Y1 and Y5 selective antagonists showed promise as inhibitors of agonist induced hyperphagia in rodent studies, but translating this to human trials has so far been unsuccessful. The potential coregulation of Y1 and Y5 receptors in the control of central feeding responses in rats (Nguyen et al., 2012) suggests pharmacological targeting of both subtypes simultaneously, may provide a therapeutic alternative (discussed further in chapter 6).

#### **1.8.6.2 The Y2 and Y4 subtypes**

The roles of Y2 and Y4 receptors in satiety, also suggest that agonists targeting either subtype may have therapeutic potential in treating obesity. Administration

of PYY<sub>3-36</sub> in rats, mice and humans (Batterham et al., 2002), (Batterham et al., 2003a) reduced food intake and/or body weight. These effects were abolished in Y2 deficient mice (Batterham et al., 2002) or in the presence of the Y2 selective antagonist BIIIE0246 (Abbott et al., 2005), suggesting the anorexic effects of PYY<sub>3-36</sub> are driven by activation of Y2 receptors. Long term 7-56 day administration of PYY<sub>3-36</sub> or another Y2 peptide agonist produced sustained reductions in body weight and adiposity but transient changes in feeding in obese rodents whether given daily (Ortiz et al., 2007) or continuously (Pittner et al., 2004). This suggested that long term changes in weight are driven by alterations in energy expenditure as opposed to long term decreases in feeding (Zhang et al., 2011). Unlike leptin administration, where obese patients tended to develop resistance to treatment over time, PYY<sub>3-36</sub> appeared to remain effective in clinical trials (Batterham et al., 2003a). However the therapeutic use of PYY<sub>3-36</sub> in humans is currently limited as i.v. administration of high doses has been documented to cause nausea and vomiting (Sloth et al., 2007), but well tolerated doses appear to have decreased efficacy in decreasing food intake. Additionally Allison et al., 2006, have also suggested that PYY<sub>3-36</sub> treatment may have long term effects on bone mass (Allison and Herzog, 2006).

Peripheral administration of physiological doses of PP also produces rapid satiety in fasted normal weight mice (Asakawa et al., 1999). Administration in Y4 knock out mice abolishes the anorexic effects of PP confirming the specific role of Y4 receptors in these responses (Balasubramaniam et al., 2006). Peripheral administration of physiological doses of PP in healthy men decreased rapid and transient food intake (Batterham et al., 2003b). Repeated treatment in ob/ob mice leads to decreased body weight and food intake (Asakawa et al., 1999). Circulating PP levels in humans have been correlated with some disease states. Patients with Prader Willi syndrome who are morbidly obese, with hyperphagia have very low concentrations of PP (Zipf et al., 1981), but peripheral administration of PP can result in decreased food intake (Berntson et al., 1993)

for these patients, suggesting a potential therapeutic option if issues of bioavailability and peptide life span can be improved.

Whilst combination treatments of PYY<sub>3-36</sub> and PP have shown no additive effects on reducing food intake in mice or humans, the shared roles of Y2 and Y4 receptors in satiety mechanisms suggests that other methods of co-targeting this pairing may be effective (McGavigan and Murphy, 2012). One such compound was obinipitide, a synthetic dual analogue of PYY<sub>3-36</sub> and PP. The poor bioavailability of obinipitide, whereby daily or twice daily subcutaneous injections were required, made it unsuited to long term use (McGavigan and Murphy, 2012), however improved anorectic effects were observed suggesting that 'Y2/Y4 complexes' (potentially in the form of heterodimers) might still be a valid target for anti obesity therapies.

Y receptor family targeted therapies in anti obesity treatment, have therefore shown potential but there is a need to increase efficacy *in vivo* whilst retaining bioavailability. Suggested coregulation, potentially reflecting receptor dimerisation, between subtypes also increases the complexity of developing selective therapies due to the potential impact of compensatory mechanisms or novel signalling. Therefore investigating the pharmacological consequences of dimerisation would be of benefit to potentially improve therapeutic targeting.

### 1.9 Aims of this thesis:

Whilst the preferential coupling of all Y receptor subtypes to the  $G_i$  class of G proteins is well established, less is known of their relative abilities to interact with  $\beta$ -arrestins and the role this interaction plays in regulating receptor intracellular trafficking, which may underlie substantive functional differences between the subtypes. To this end, **Chapter 3** makes a systematic comparison of Y receptor  $\beta$ -arrestin association and intracellular trafficking, developing high content imaging assays to quantify agonist and antagonist pharmacology. In particular it will characterise the association of Y receptor subtypes with  $\beta$ -arrestins using a technique known as bimolecular fluorescence complementation (BiFC), which is capable of identifying receptor signalling complexes of precise composition.

**Chapter 4** develops these methods further in conjunction with single molecule imaging techniques, such as fluorescence correlation spectroscopy (FCS), to characterise the mobilities and stoichiometry of Y receptor complexes, and the influence of ligand occupancy. For the first time, the combination of FCS and BiFC approaches is used to describe the behaviour of molecular Y receptor-arrestin complexes at the plasma membrane.

The potential of GPCRs to form dimers is now widely accepted, but the functional importance in respect to signalling protein interaction, modified receptor trafficking and signalling is still in debate. This evidence is discussed in detail in **Chapters 5 and 6**, in which a novel BiFC based imaging system is described which constrains GPCRs as dimers of precise composition, allowing pharmacological responses to be directly attributable to defined GPCR dimer populations. **Chapter 5** will explore the influence of Y receptor and  $\beta$ 2AR homodimerisation on one functional readout – receptor endocytosis. Selective protomer mutagenesis will be used to investigate the functional requirements for ligand binding site occupancy, receptor activation and phosphorylation within the dimer – allowing conclusions to be drawn about the stoichiometry of  $\beta$ -arrestin2 recruitment to the dimer interface. **Chapter 6** extends this technique to investigations of Y1

receptor heterodimer pharmacology, demonstrating that heterodimerisation between Y1 and Y5 receptors, the key co-expressed “feeding” receptors, selectively influences both agonist and antagonist pharmacology.

## Chapter 2: Materials and methods

### 2.1 Materials

pcDNA3.1zeo(+) and pcDNA4/TO(+) DNA vectors, HEK293T/TR cells, OptiMEM, lipofectamine and the selection antibiotics zeocin and blasticidin were from Invitrogen (Paisley, UK). pCMV FLAG vector was from Agilent (Santa Clara, CA, USA). All oligonucleotide primers were synthesised by Eurogentec (Seraing, Belgium). The GenElute™ gel extraction, PCR purification, miniprep and maxiprep kits were purchased from Sigma Aldrich (Gillingham, UK). Restriction enzymes, fast shrimp alkaline phosphatase, T4 DNA ligase and pJET cloning kit were obtained from Fermentas (St Leon-Rot, Germany). 1kb DNA ladder was purchased from Promega (Madison, WI). Additional molecular biology reagents were also purchased from Sigma Aldrich (Gillingham, UK). DNA sequencing was carried out by the DNA sequencing laboratory, School of Life Sciences, University of Nottingham.

All cell culture plasticware was purchased from Fisher Scientific (Loughborough, UK) with all medium reagents from Sigma (Gillingham, UK). The SNAPSurface™ Alexa Fluor 647 was obtained from New England Biolabs (Hitchin, UK). The compounds Neuropeptide Y (NPY), peptide YY (PYY), pancreatic polypeptide (PP), Pro NPY ((Leu<sup>31</sup>, Pro<sup>34</sup>) NPY), NPY<sub>3-36</sub> and cPP (1-17)(Ala<sup>31</sup>, Aib<sup>32</sup>) NPY (18-36) were purchased from Bachem (Bubendorf, Switzerland). The compounds dTrp<sup>32</sup> NPY, BIBO3304 trifluoroacetate, CGP71683 hydrochloride, NPY5RA972, L182,504, isoproterenol hydrochloride (isoprenaline), salmeterol, salbutamol hemisulphate, propranolol hydrochloride, ICI 118,551 and forskolin were all obtained from Tocris Cookson (Avonmouth, Bristol, UK). Both [<sup>3</sup>H] Adenine and [<sup>14</sup>C] cAMP were purchased from Amersham Biosciences UK (Buckinghamshire, UK), the poly prep columns and Dowex AC '50' 50W-4X resin from Bio-Rad (Hercules, CA), and imidazole was from Applichem (Darmstadt, Germany), [<sup>125</sup>I] PYY and scintillation fluid from Perkin Elmer (Groningen, Netherlands) and scintillation vials from

Sarstedt (Nümbrecht, Germany). Whatman GF/B filters (Size 2<sup>1/4</sup> x 12<sup>1/4</sup> inches) were purchased from Brandel Inc (Maryland, USA).

All compounds were stored as single use aliquots at -20°C diluted in aqueous stock with the exception of the Y receptor antagonists BIBO3304, CGP71683, NPY5RA972, L182,504 and the β2-adrenoceptor agonists formoterol and salmeterol which were diluted in DMSO. Non-dissolved stock compounds were stored as instructed either at room temperature (β2-adrenoceptor ligands eg. isoprenaline), 4°C (non peptide Y receptor ligands eg. L182,504) or -20°C (peptide ligands eg. NPY, PP).

All other chemicals if not directly stated were obtained from Sigma Aldrich (Gillingham, UK).

## **2.2 Methods**

### **2.2.1 Molecular biology**

A summary of all constructs used is provided in Table 2.3. Rat Y1 receptor and β2-adrenoceptor cDNAs were provided by Professor T Schwartz of the University of Copenhagen, Denmark. Human Y2, Y4 and Y5 receptor, D2L dopamine and human arrestin cDNAs were obtained from the Missouri S&T cDNA resource centre ([www.cDNA.org](http://www.cDNA.org))

#### **.2.2.1.1 Amplification of DNA**

##### **2.2.1.1.1 Using sited directed mutagenesis to generate a C terminal phospho-site negative mutant of the NPY Y1 receptor**

PCR-based site directed mutagenesis (Quikchange) was used to selectively mutate specific serine and threonine residues in the C terminal domain of the rat NPY Y1 receptor cDNA sequence (Genbank reference number: Z11504). This phospho-site deficient mutant was termed Y15A after the number of alanine mutations that were introduced. Mutagenesis reactions were performed using Accuzyme, a 5'-3' DNA polymerase (Biolone, London, UK). This enzyme also has 3'-

5' exonuclease proofreading activity whereby nucleotide mismatches identified in the newly synthesised DNA are excised and the correct base pair inserted. Accuzyme can amplify large regions of DNA (up to 5kbp) with high fidelity producing blunt ended products.

#### **2.2.1.1.1.2 Mutagenesis primer design**

Two sets of complementary primers were designed to introduce 5 amino acid changes into the template cDNA strand in succession. The specific amino acid codons were identified and mutated to a codon used frequently in human cells to account for species specific codon usage bias. Primer sequences contained 12-15 conserved bases either side of the mutated codons and both forward and reverse primers recognised the same sequence on opposite template DNA strands. The forward primer sequence was identical to the coding strand of the template DNA (except for the introduced mutations), with the reverse primer the reversed and complemented sequence of this (see Table 1). A further consideration in primer design was GC base content, with a figure of 40-60% desirable for stable binding of primer sequences to template DNA. Where possible, primer sequences ended with a GC clamp to promote specific primer binding (due to the stronger triple hydrogen bonding of G and C bases). The melting point of primers was also considered (dependent on the degree of GC content and primer length) with temperatures of 58-62°C preferred in order to minimise the chance of secondary annealing. When generating the Y15A mutant, sequential rounds of mutagenesis were required. 3 mutations were introduced in the first round. This mutant (when confirmed as correct with sequencing) was used as the template for the second round of mutagenesis to introduce the 2 additional mutations. The same protocol was followed for both rounds. All primers were purchased from Eurogentec and are detailed in Table 2.1.

### **2.2.1.1.1.3 PCR-based site directed mutagenesis protocol**

Reactions were prepared in 200µl PCR tubes consisting of 25ng template DNA (pCMV FLAG Y1-Yc first round), 125ng of forward and reverse primers (1µl each), 200µM dNTP's (2µl), AccuBuffer buffer (5µl; supplied with enzyme; 60mM Tris-HCl, 6mM (NH<sub>4</sub>)<sub>2</sub>SO<sub>4</sub>, 10mM KCl, 2mM MgSO<sub>4</sub>; pH 8.3) and 2.5 units of Accuzyme (not added to the starting mix) in double distilled water (ddH<sub>2</sub>O) to give a total volume of 50µl. A negative control reaction was also set up containing all components except Accuzyme. Reactions were carried out using a thermocycler block (Mastercycler gradient, Eppendorf, UK). The initial step, whereby double stranded template DNA was denatured to single stranded DNA, was performed at 95°C for 30 s (see Figure 2.1). The temperature was then decreased (typically to 58-60°C for mutagenesis reactions; for 1min), and Accuzyme added at this point. This "HotStart" procedure, following the first round of denaturation and primer annealing to the template, minimised non specific DNA amplification by Accuzyme. The annealing temperature was varied depending on the primer used but was typically 5°C less than the melting temperature of the primer to allow specific primer hybridisation. Finally the extension step was performed (68°C for 10min; equating to approximately 1.5min per kbp) whereby the DNA polymerase synthesised a new complementary DNA strand from the primer sequence in a 5' to 3' direction. This sequence of cycles (denaturation, annealing and elongation) was repeated 18 times, with the newly synthesised fragment DNA (containing the region to be amplified) now also acting as the template DNA. Following completion of all cycles, tubes were cooled and held at 4°C.

Samples were then treated with the restriction enzyme Dpn I for 2hr at 37°C, 20 min at 60°C. Dpn I can only cleave methylated DNA (ie the original template DNA), therefore digestion with this enzyme will leave the unmethylated mutated DNA intact as a circular plasmid for efficient transformation. 2µl of each Dpn I digested sample was then transformed into XL-1 competent cells (see section 2.2.1.7.1), grown on a small scale and purified (miniprep; section 2.2.1.8) before

being screened using restriction enzyme digestion (section 2.2.1.3). If the isolated DNA was of an expected size, the sample was then sequenced to confirm the presence or absence of the desired mutations. (Figure 2.2; section 2.2.1.2).

If correct, the DNA was ligated into fresh plasmid vector. This was to prevent unwanted mutations that may have been introduced elsewhere during the mutagenesis process being carried over into the DNA. DNA in fresh vector was then transformed into XL-1 cells and then grown up on a larger scale (maxiprep; section 2.2.1.9).

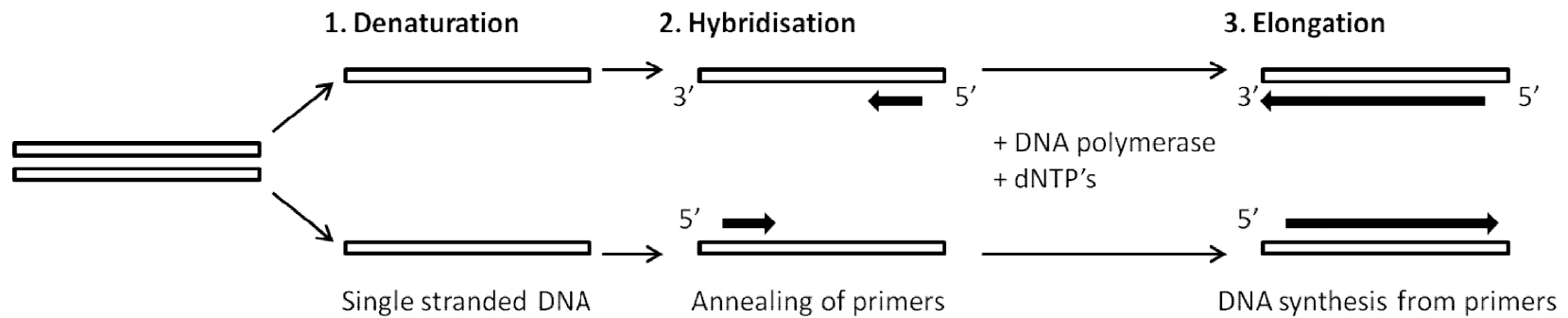
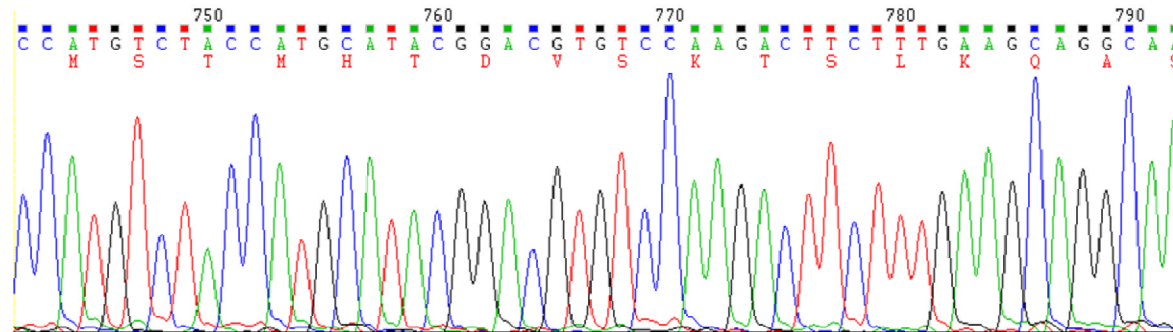


**Figure 2.1: The principles of using polymerase chain reaction (PCR) to amplify specific regions of DNA**

PCR begins with an initial high temperature step, whereby double stranded template DNA is denatured to become single stranded (**denaturation**). The reaction is then cooled to facilitate annealing of short oligonucleotide forward and reverse primers to complementary sequences in the two DNA strands (**hybridisation**). DNA synthesis using the thermostable polymerase begins from these primers in a 5' to 3' direction (**elongation**). This entire cycle is repeated with the newly synthesised double stranded DNA fragment (containing the desired region to be amplified) now acting as the template. Every cycle doubles the amount of DNA synthesised in the previous cycle.

Wildtype NPY Y1 receptor sequence:



Mutated NPY Y1 Phosneg receptor sequence (Y15A):

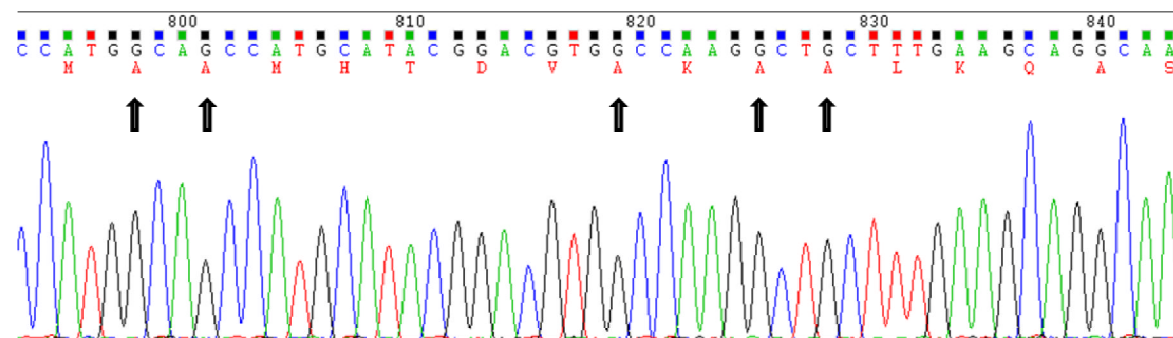


**Figure 2.2: A sequence chromatogram showing the positions of selective mutations introduced into the rat NPY Y1 receptor sequence**

The top sequence shows the wildtype rat NPY Y1 receptor sequence (amino acid residues 350-367). The lower sequence shows the position of alanine mutations of selective serine and threonine residues within the NPY Y1 receptor (mutations indicated by arrows). This phospho-site deficient mutant receptor was termed Y15A after the number of mutations introduced. This chromatogram was created using Chrom as 2.

#### 2.2.1.1.1.4 Amplification of the Human NPY Y5 receptor using polymerase chain reaction (PCR)

In this case, the polymerase chain reaction (PCR) was used to amplify the entire human NPY Y5 receptor cDNA (residues 2-444). The PCR protocol was similar to that used for site directed mutagenesis with some modifications. Here a different high fidelity DNA polymerase, PWO (Roche, Burgess Hill, UK) was used. PWO is also a 5'-3' DNA polymerase with 3'-5' exonuclease proofreading activity.

#### 2.2.1.1.1.5 Primer design

Two complementary primers (34-40 bases) were designed to anneal to the start and end of the human NPY Y5 receptor sequence (Genbank Reference number: NM\_006174.2). They were also designed to introduce a Bam HI (GGATCC) and a Not I (GCGGCCGC) restriction enzyme site prior to the start and after the end of the Y5 sequence respectively (Figure 2.3). The initiation methionine codon was removed from the start of the Y5 sequence so that the receptor could ultimately be inserted continuously into the pCMV vector downstream of a FLAG tag (Figure 2.5; see section 2.2.1.3.2.1). The stop codon was also removed to allow C terminal fluorescent protein fragment tags to be added, and the position of the NotI site was designed so that it located the Y5 sequence in frame with the fluorescent protein tag in the vector on cloning

Forward: 5' G AGT GGA TCC GAT TTA GAG CTC GAC GAG TAT TAT AAC 3'

Receptor codons: *Bam HI* D L E L D E Y Y N

Reverse: 5' ATT AGC GGC CGC CAT ATG AAG ACA GTG TAT AAG G

Receptor codons: *Not I* M H L C H I L

#### Figure 2.3: PCR primer design for amplifying the human NPY Y5 receptor

The forward primer sequence is detailed in the top section, alongside the corresponding Y5 receptor codon sequence. The initiation methionine codon has been omitted. The second section shows the reverse primer reversed and complemented to the final part of the Y5 sequence, excluding the STOP codon. Restriction enzyme consensus sites are underlined.

#### **2.2.1.1.1.6 PCR protocol**

Reactions were prepared in 200µl PCR tubes, comprised of 25ng template cDNA (p3.1neo human Y5 receptor), 600nM each of forward and reverse primers, 200µM dNTP's (final concentration), PWO buffer (5µl; supplied with enzyme; 10mM Tris-HCl, 25mM KCl, 5mM (NH<sub>4</sub>)SO<sub>4</sub>, 2mM MgSO<sub>4</sub>; pH 8.9) and 0.5µl PWO enzyme (added at a later point) in ddH<sub>2</sub>O to make a total volume of 50µl. Using the thermocycler block, a similar protocol was followed as for site directed mutagenesis, with PWO polymerase following an initial HotStart primer annealing step. 25 cycles of PCR were performed, with an annealing temperature of 58°C and an extension step at 72°C for 90sec. (for the last 15 cycles, 5 sec was added to the extension time each cycle). Following the completion of all cycles, tubes were cooled and held at 4°C.

Following the completion of the PCR cycles, the DNA was visualised using gel electrophoresis, and the size of the fragment accessed (section 2.2.1.4). If correct, the fragment band was excised and purified (section 2.2.1.5.1).

#### **2.2.1.1.1.7 Ligation of PCR generated human NPY Y5 receptor cDNA into pJET vector**

The PCR Y5 receptor cDNA fragment was first subcloned into the vector pJET1.2 (CloneJET PCR cloning kit, Fermentas). Ligation of the PCR cDNA blunt-ended product into the pJET vector disrupts the expression of a gene encoding the restriction endonuclease enzyme *eco46/R*. This enzyme is typically lethal to host *E coli* cells therefore only bacterial clones with insert containing plasmids are capable of growth.

pJET ligation reactions were performed in 0.5ml Eppendorf tubes consisting of 10µl 2x pJET ligation buffer containing polyethylene glycol to improve the efficiency of blunt end ligations (supplied with enzyme), 1µl pJET vector (50ng), 1µl purified PCR product and 1µl T4 DNA Ligase in nuclease free water to give a total volume of 20µl. Reactions were incubated for 30min at 22°C, before being transformed into XL-1 cells (section 2.2.1.7.1). DNA was then grown up on a small

scale and purified (miniprep; section 2.2.1.8), before being screened using restriction enzymes (section 2.2.1.3) and gel electrophoresis (section 2.2.1.4). PCR derived DNA was then sequenced and if correct, ligated into fresh vector (firstly pcDNA3.1 zeo or pcDNA4 TO containing (between KpnI and BamHI) a Kozak sequence prior to the initiation methionine residue and FLAG tag) using a restriction digest (Bam HI/Not I; sections 2.2.1.3 and 2.2.1.6) before fluorescent protein tags could be inserted downstream (using a Not I / Xba I restriction digest; section 2.2.1.3). Complete constructs were then cultured on a larger scale (maxiprep; section 2.2.1.9) to be used in mammalian cell transfections (section 2.2.2.1).

#### **2.2.1.2 DNA sequencing**

The sequences of all engineered DNA were checked for any alterations that may have been erroneously introduced, and that mutations purposely introduced were present (Figure 2.2). The appropriate forward and reverse primers for that particular construct (dependent on the vector cDNA used; see Table 1) were used. All sequencing was undertaken by the DNA sequencing laboratory at the University of Nottingham.

#### **2.2.1.3 Restriction digestion**

Restriction enzymes recognise and bind to a specific small sequence of nucleotides (termed restriction sites) and subsequently cleave DNA into fragments. Typically constructs were digested with two different restriction enzymes (a 'double digest') at either end of the 'insert' DNA (eg. receptor, fluorescent protein tag). The same enzyme pair was used to digest the 'vector' DNA ultimately receiving the insert (eg. pCMV FLAG, pcDNA3.1 zeo Snap). The enzymes chosen also produced complementary 'sticky ends', whereby an overhang stretch of unpaired nucleotides was left following digestion. The different 'sticky ends' left by double enzyme digestion of both insert and vector

DNA are complementary and can subsequently be joined together in only one orientation using T4 DNA ligase (see section 2.2.1.6).

When performing a restriction digest, 2µg of DNA (in a total volume of 20µl) was added to a sterile 0.5ml Eppendorf tube along with 2µl of 10x fast digest buffer (supplied with enzyme) and digested with 1µl of each restriction enzyme (Fast Digest; Fermentas). This reaction was incubated for 1hr at 37°C, followed by 20min at 65°C and 5min at 80°C to heat inactivate the restriction enzymes.

Digested DNA was then identified and isolated using gel electrophoresis (Figure 2.8; see section 2.2.1.4).

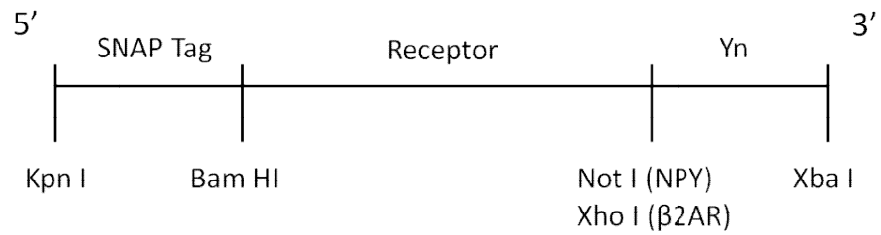
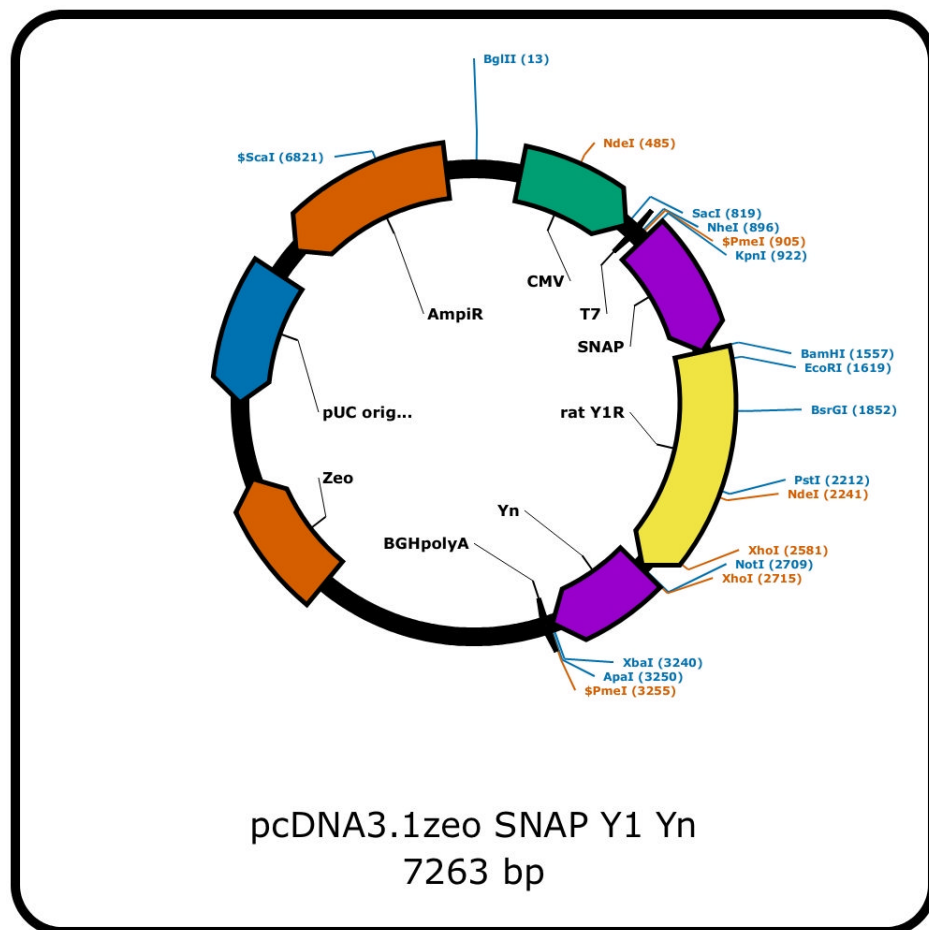
#### **2.2.1.3.1 Generation of a Snap tagged receptor construct**

Receptor cDNA was inserted into a pcDNA 3.1zeo plasmid already containing the Snap tag sequence (181 amino acids; see Table 2.3). This vector was previously made by Dr Holliday. A short sequence derived from 5HT<sub>3</sub> receptor derived signal sequence (amino acids MRLCIPQVLLALFLSMLTGPGEGRK) was added upstream of the Snap tag sequence to facilitate insertion of the receptor protein into the membrane during translation. This construct was also tagged at the C terminus with an N terminal fragment of Venus YFP (Yn; residues 2-173).

This p3.1zeo Snap vector (see Figure 2.4) contained a human cytomegalovirus (CMV) promoter, which is a strong promoter that expresses well in a variety of mammalian cell lines and allowed for a high level of receptor expression. This vector also contained a polyadenylation signal (bovine growth hormone derived; bGH poly A) which is a transcription termination sequence that aids expression in eukaryotic cells as well as sites for sequencing primers (T7 promoter and bGHrev; see section 2.2.1.2). Sites of antibiotic resistance for the selection of both transformed bacterial cells (ampicillin) and transfected mammalian cell lines (zeocin; see Table 2.2 for details) were also included.

All cDNAs of interest were inserted into the vector in frame downstream of the Snap tag, via the multiple cloning site (MCS) which contained several restriction enzyme sites (Figure 2.4). Receptor cDNAs were placed between BamHI and XhoI

( $\beta$ 2AR), or BamHI and Not I (Y1) restriction sites, due to the presence of an internal Xho I site in the Y1 sequence. Inserted receptor cDNA sequences lacked the initiation methionine codon and the 3' STOP codon to allow the addition of a Venus Yellow Fluorescent Protein (vYFP) fragment (N terminal 2-173 termed Yn; these numbers equated to the native Green Fluorescent Protein (GFP) sequence (Kilpatrick and Holliday, 2012) ). This fragment was placed between Not I / Xho I and Xba I restriction sites yielding LRPLE (Y1) or LE ( $\beta$ 2AR) amino acid linkers.

**A****B**

**Figure 2.4 pcDNA3.1 zeo Snap Y1-Yn construct**

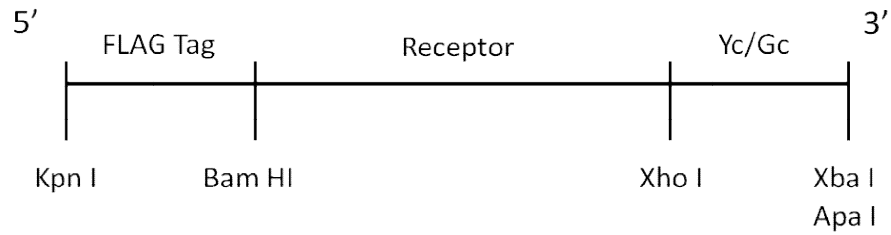
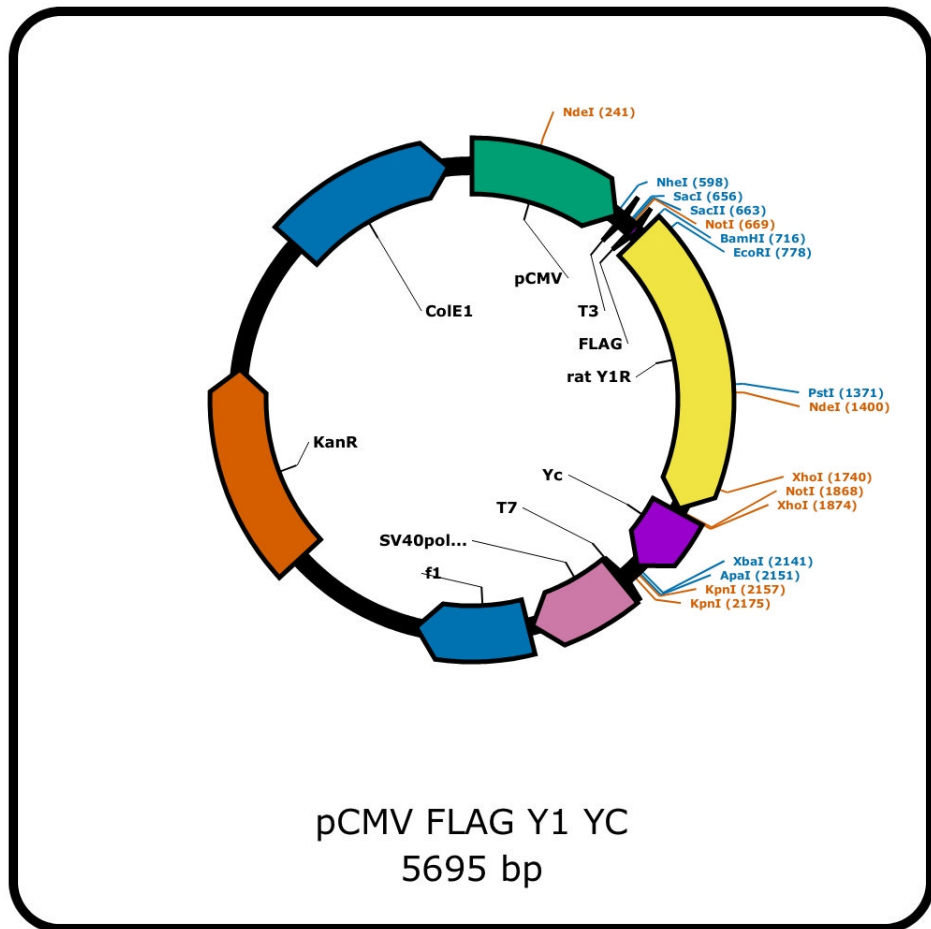
Panel A shows a schematic of the multiple cloning site restriction enzyme sites used to generate receptor-Yn constructs in pcDNA3.1 zeo Snap vector. Panel B shows a vector map of the pcDNA3.1 zeo Snap Y1-Yn. NPY Y1 receptor cDNA (shown in yellow) was inserted into the pcDNA 3.1 zeo vector downstream of a Snap sequence (purple). A BiFC fragment tag (Yn; purple) was inserted downstream of the receptor cDNA, giving the Snap-receptor-Yn in frame cDNA. Additional features contained in the vector are also included and key single and remaining double cut restriction enzyme sites indicated.

### **2.2.1.3.1.2 Exchanging C terminal fluorescent protein fragment tags on FLAG tagged receptor constructs**

#### **2.2.1.3.1.2.1 pCMV FLAG Receptor-Yc / Gc**

Enzymatic digestion was used to ultimately insert receptor cDNAs into a pCMV FLAG vector also containing a C terminal fragment of Venus YFP (termed Yc throughout). This vector contained a FLAG tag epitope (MDYKDDDDK), which gave the option to identify this receptor construct by techniques such as antibody live labelling (Figure 2.5). This vector also contained a pCMV promoter to allow for high receptor expression, and polyadenylation signals (Simian1 virus 40 (SV40) derived) to aid eukaryotic protein expression.

The NotI enzyme could not be used when cloning receptor cDNA in the correct orientation into the pCMV FLAG vector, because of an additional NotI site upstream of the FLAG tag. To account for this receptor cDNA was first inserted into a p3.1zeo vector between Bam HI and Not I (NPY Y1) or Xho I ( $\beta$ 2AR) restriction sites (see figure 2.5). Receptor cDNA sequences lacked the initiation methionine codon and the 3' STOP codon to allow the addition of a C terminal vYFP fragment (173-238; termed Yc) or a C terminal superfolder GFP fragment (173-238; Gc) between Not I / Xho I and Xba I restriction sites using a LRPLE linker. The GFP sequence used had previously been engineered to contain superfolder mutations S30R, F99S, N105T, M153T and V163A (Pedelacq et al., 2006). The entire receptor-Yc construct was then inserted into the pCMV FLAG vector, downstream of the vector FLAG tag via a Bam HI and Apa I digest.

**A****B**

**Figure 2.5 pCMV FLAG Receptor-Yc/Gc construct**

Panel A shows a schematic of the multiple cloning site restriction enzyme sites used to generate receptor-Yc constructs in pCMV FLAG vector. Panel B shows an example vector map of the pCMV FLAG Y1-Yc. NPY Y1 receptor cDNA (shown in yellow) was inserted into the pCMV vector downstream of a FLAG tag. A BiFC fragment tag (Yc; purple) was inserted in frame downstream of the receptor cDNA. Additional features contained in the vector are also included and key single and remaining double cut restriction enzyme sites indicated.

#### **2.2.1.3.1.2.1.2 pcDNA4 TO FLAG Receptor-GFP**

Receptor cDNA tagged with a full length superfolder GFP tag (GFP) was inserted into the pcDNA4 TO vector downstream of a FLAG tag epitope (MDYKDDDDK). The pcDNA4 TO vector contains a pCMV promoter in conjunction with two tetracycline operator sequences (see figure 2.6) inserted between the TATA box and the transcription initiation start site. This sequence was identical to that of pcDNA 3.1zeo with the exception of the tetracycline operon sequence. As for pcDNA3.1zeo, the vector used for cloning contained a Kozak sequence, start methionine and FLAG tag placed between KpnI and BamHI of the multiple cloning sequence.

Receptor cDNA sequences lacked the initiation methionine codon and the 3' STOP codon to allow the C terminal addition of full length superfolder GFP placed between Not I and Xba I restriction sites after an LRPLE linker (see Figure 2.6).

#### **2.2.1.3.3 Adding C terminal fragment tags to $\beta$ -arrestin2 constructs**

Human  $\beta$ -arrestin1 or 2 cDNA (Genbank reference NM\_004041 or NM\_004313), containing a Kozak sequence (GCCACC) prior to the initiation methionine residue and no STOP codon (as described in Kilpatrick et al 2010), was inserted into the pcDNA3.1zeo vector using enzymatic digestion with EcoRI and Not I (Figures 2.7). The pcDNA3.1zeo vector was previously described in section 2.2.1.3.1. A N terminal vYFP fragment (residues 2-173; Yn) or an N terminal GFP fragment (2-173; Gn) was added in frame downstream of the  $\beta$ -arrestin2 cDNA [creating a QRPLE linker] and placed between Not I and Xba I restriction sites.

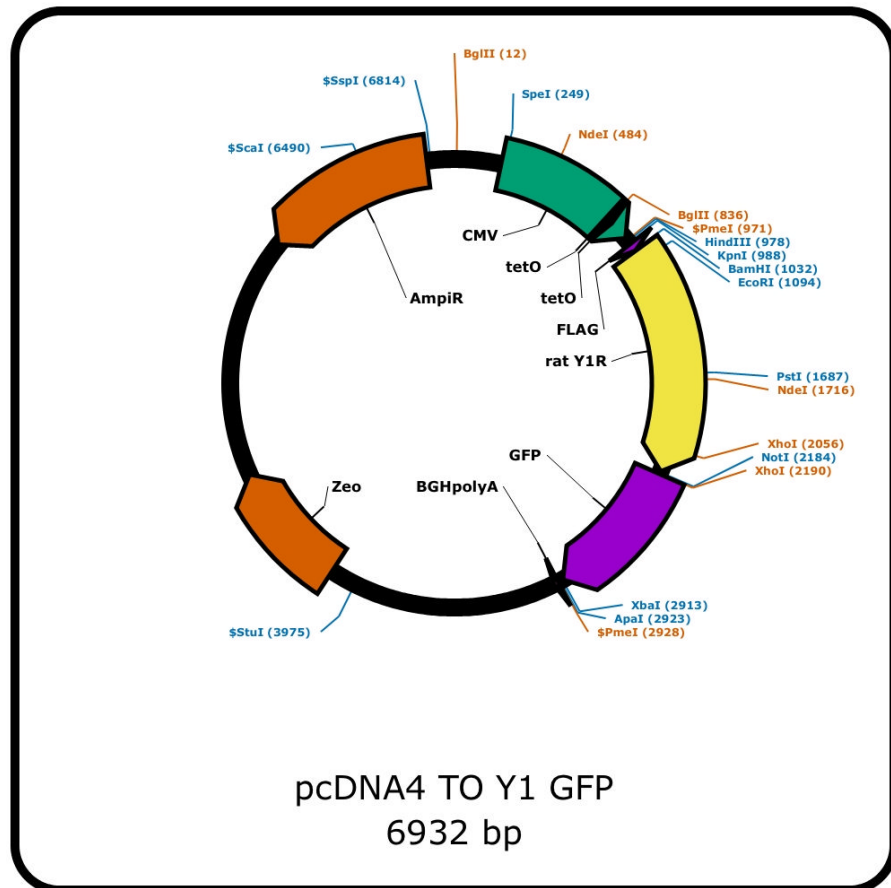
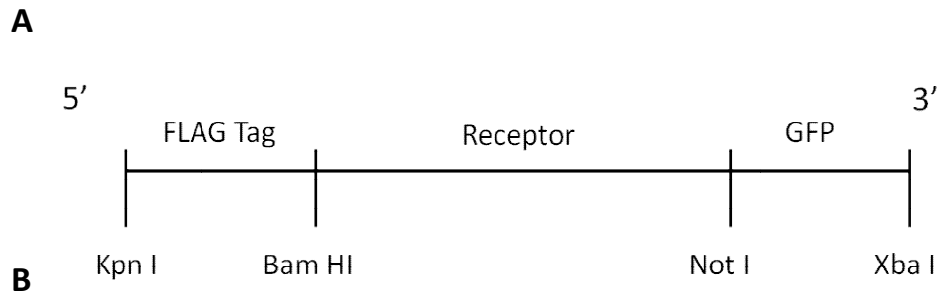


**Figure 2.6 pcDNA4 TO FLAG Receptor-GFP construct**

Panel A shows a schematic of the multiple cloning site restriction enzyme sites used to generate receptor-GFP constructs in p4 TO FLAG vector. Panel B shows an example vector map of the pcDNA4 TO FLAG Y1-GFP. NPY Y1 receptor cDNA (shown in yellow) was inserted into the pCMV vector downstream of a FLAG tag. A full length superfolder GFP tag (purple) was inserted in frame downstream of the receptor cDNA. Additional features contained in the vector are also included and key single and remaining double cut restriction enzyme sites indicated.

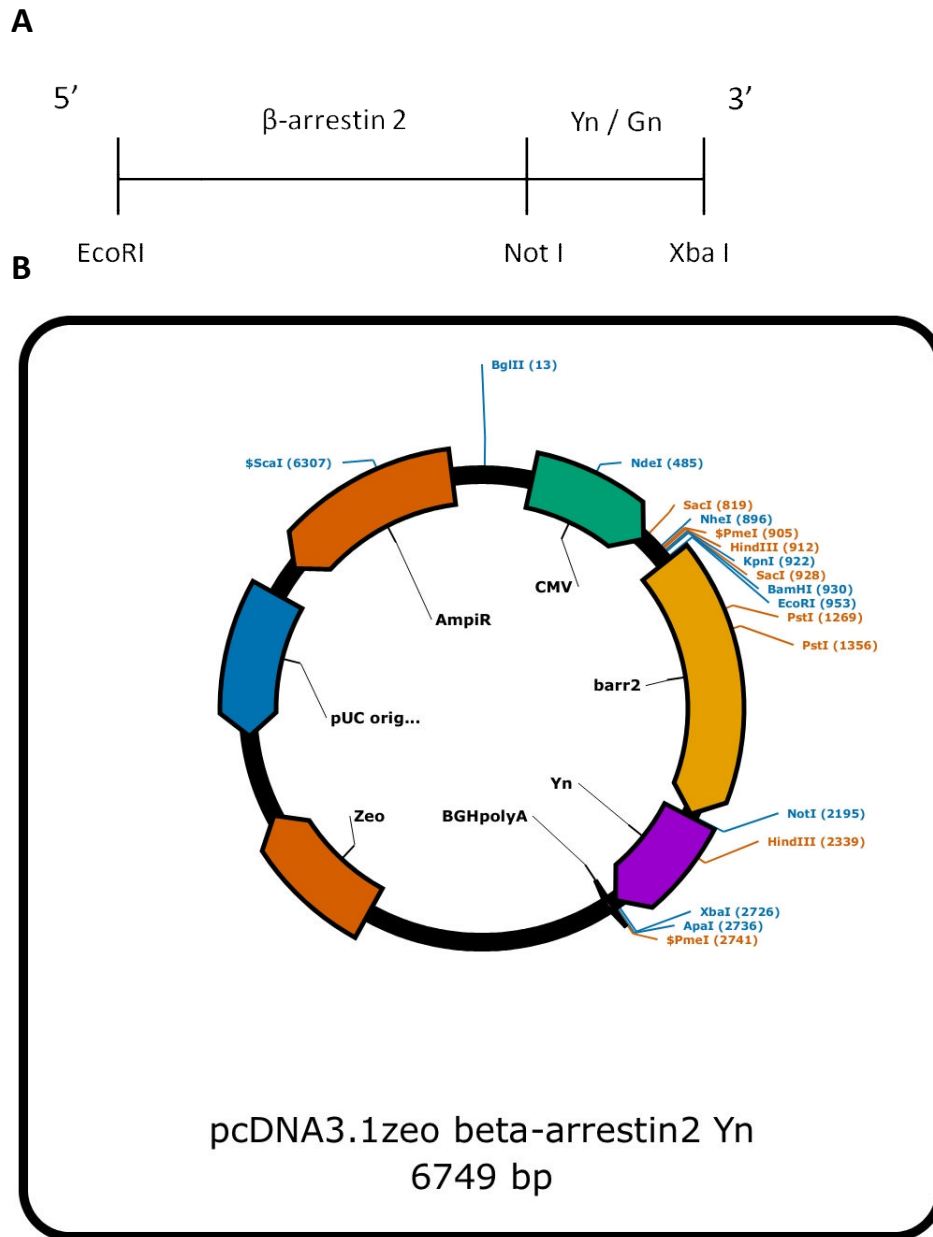


**Figure 2.7 pcDNA3.1 zeo  $\beta$ arrestin2-Yn/Gn construct**

Panel A shows a schematic of the multiple cloning site restriction enzyme sites used to generate  $\beta$ -arrestin-Yn constructs in pcDNA3.1zeo vector. Panel B shows an example vector map of the pcDNA3.1zeo  $\beta$ -arrestin2-Yn.  $\beta$ -arrestin2 cDNA (shown in orange) was inserted into the pcDNA3.1zeo vector downstream. A BiFC fragment tag (Yn; purple) was inserted in frame downstream of the  $\beta$ -arrestin cDNA. Additional features contained in the vector are also included and key single and remaining double cut restriction enzyme sites indicated.

#### **2.2.1.4 Visualisation and isolation of DNA using agarose gel electrophoresis**

Gel electrophoresis allows the separation of DNA molecules based upon their size by applying an electric field through an agarose gel matrix. Smaller negatively charged DNA molecules move faster through the pores of the gel, towards the positive electrode of the electric field, than larger DNA molecules.

A gel was prepared consisting of 1% agarose (Sigma Aldrich) dissolved in TBE buffer (89mM Tris HCl, 89mM Boric acid, 2mM EDTA (ethylenediaminetetraacetic acid); pH 7.6). The mixture was allowed to cool to touch whereupon ethidium bromide ( $0.1\mu\text{g ml}^{-1}$ ) was added. Ethidium bromide is a chemical agent which intercalates into DNA. Upon exposure to ultraviolet light, ethidium bromide bound to DNA is intensely fluorescent, allowing DNA to be visualised as discrete bands on the gel. The gel was then left to set, prior to being placed into an electrophoresis tank and covered entirely with TBE buffer. DNA samples were mixed with blue loading buffer (0.25% w/v bromophenol blue, 50% v/v glycerol in TBE) and loaded. 5 $\mu\text{l}$  of 1kb DNA ladder (Promega) was also added as a molecular weight marker. The gel was run at 80V for 30-45 minutes until sufficient migration of the DNA was achieved to separate the bands of interest..

DNA was visualised using an UV light box (Syngene GVS-30 transilluminator) and if required the DNA band of the correct size excised. A representative gel showing a variety of constructs used throughout this thesis and the DNA bands obtained following their restriction digestion can be seen in figure 2.8.

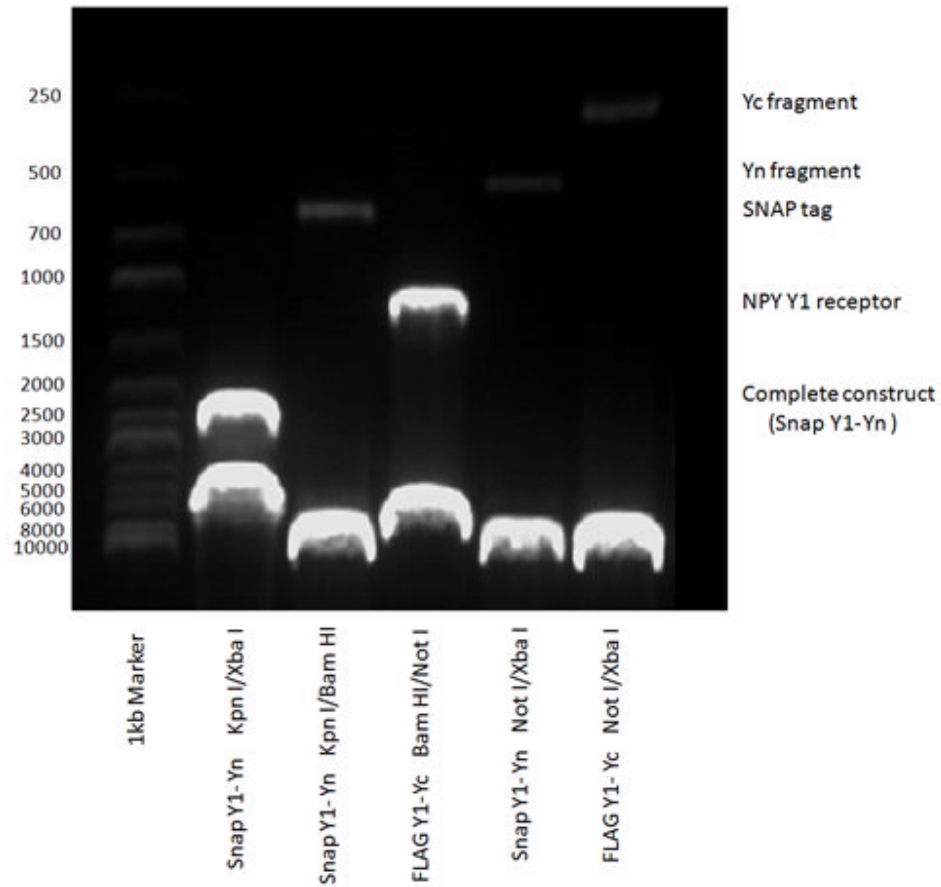


**Figure 2.8: A representative agarose gel showing various restriction digests of p3.1zeo Snap-Y1-Yn or pCMV FLAG Y1-Yc constructs.**

A 1kb marker was included to allow molecular weights (in base pairs) to be estimated (lane 1). In lanes 2 and 3, the pcDNA3.1zeo Snap Y1-Yn construct (2  $\mu$ g throughout) was digested with 2 different restriction enzyme pairs. Digestion with KpnI and XbaI yielded the complete construct (ie. Snap, Y1 receptor plus Yn tag; approximately 2300bp) and its corresponding vector band (pcDNA3.1zeo, 5000 bp). Alternatively digestion with KpnI and BamHI, liberated the Snap tag (at approximately 600bp) and the vector band (pcDNA3.1zeo, Y1 receptor and Yn tag). Other examples show the isolation of the Y1 receptor (lane 4; approximately 1200bp), the Yn fragment (lane 5; approximately 500bp) and the Yc fragment (lane 6; approximately 250bp) alongside their corresponding vector bands.

### **2.2.1.5 Preparation of insert and vector cDNA for ligation**

#### **2.2.1.5.1 Gel extraction of insert DNA**

Restriction digested DNA fragments for ligation were separated by agarose gel electrophoresis and isolated using a gel extraction kit (Sigma Aldrich). This method of DNA purification is a silica gel-based which uses column chromatography. The gel slice containing the desired DNA fragment was weighed in a sterile Eppendorf and 3 gel volumes of gel solubilisation solution added and the tube incubated for 10 min at 60°C. The chaotropic salts in the solubilisation solution disrupt the ordered structure of water molecules surrounding the DNA. This creates a hydrophobic environment that promotes the binding of the DNA phosphate backbone to the silica of the spin column whilst proteins and other contaminants do not bind and are washed away. One gel volume of isopropanol was then added to the solubilised gel solution to increase specific binding of the DNA to the column. Column preparation solution was added to the binding column and the column centrifuged for 1min at 12,000rpm. The solubilised gel solution was then added and centrifuged for 1 min at 12,000rpm facilitating the binding of the DNA to the silica filter of the column. A solvent based wash solution, containing 70% ethanol was added to remove any contaminants without affecting DNA binding (DNA does not dissolve in ethanol solution). A further 2min centrifuge at 12,000rpm removed any excess ethanol. The DNA was then unbound from the silica of the column upon addition of 40µl ddH<sub>2</sub>O and a 1min centrifugation at 12,000rpm. The DNA was now in solution and ready to use in ligation reactions.

#### **2.2.1.5.2 Preparation of vector DNA**

Following double digest with restriction enzymes, 2 µg vector DNA was treated with shrimp alkaline phosphatase (SAP; 2µl SAP buffer (supplied with enzyme ; 100mM Tris-HCl, 50mM MgCl<sub>2</sub>, 1M KCl, 0.2% Triton-X-100, 1mg ml<sup>-1</sup>; pH 8.0) and 2µl SAP) for 2hr at 37°C. The purpose of SAP treatment is to remove phosphates

from exposed nucleotides at the ends of the linearised plasmid DNA in order to prevent self-ligation. In order to be used in ligation reactions, the vector DNA was purified using a PCR clean up kit (Sigma Aldrich) following the manufacturer's instructions. Like the gel extraction kit (as described in section 2.2.1.5.1) it uses silica spin columns to remove contaminants such as excess salts and protein. Vector DNA was eluted in 40µl ddH<sub>2</sub>O.

### **2.2.1.6 Ligations**

The insert and vector preparations (as described in sections 2.2.1.5.1 and 2.2.1.5.2.1) were ligated together in a 3:1 insert:vector molar ratio. DNA concentrations in both preparations were calculated assuming an 80% yield from the gel purification (insert; I) and PCR clean up (vector; V) protocol, and starting from 2µg of DNA:

$$2\mu\text{g DNA} \times (\text{size of isolated I or V} / \text{size of original plasmid in its entirety}) \times 0.8 \\ = \text{concentration of I or V DNA isolated in the } 40\mu\text{l elution.}$$

50ng of vector DNA was deemed optimal for use in ligations to produce single circular plasmids. A 1:3 ratio of vector to insert was used, therefore assuming 50ng of vector contains x moles, the following equation was used to calculate the correct amount of insert DNA required:

$$\text{ng of insert needed} = 3 \times 50\text{ng} \times (\text{size of I} / \text{size of V})$$

The actual volume in µl of vector and insert to be added was then calculated (based on the number of moles required and the actual concentration present in the eluate). Positive and negative ligations were set up in 0.5ml Eppendorf tubes, with ddH<sub>2</sub>O added in place of insert to the negative control (but all other components present). 1µl of 10x T4 Ligase buffer (supplied with the enzyme) and 1µl T4 DNA ligase were added to give a total volume in ddH<sub>2</sub>O of 10µl per ligation reaction. Reactions were performed at 16°C for 16 hours.

5µl of both positive and negative ligations were transformed in XL-1 competent cells as described in section 2.2.1.7.1.

### 2.2.1.7 Preparation of competent cells

The XL-1 strain of *E.coli* is suitable for making chemically competent cells as mutations have been introduced that make it more amenable for DNA uptake. Mutations in *recA* recombinase minimises recombination of the introduced plasmid DNA with host DNA and increases the stability of inserts. The lack of *endA* nuclease improves the quality of purified plasmid DNA isolates. A *hsdR17* mutation knocks out EcoK 1 methylase, which prevents cleavage of transformed plasmid DNA by endogenous endonucleases. The gene encoding tetracycline resistance (on the F' episome) has also been introduced.

Agar plates were produced using 35 grams of Luria Bertani (LB) agar powder (Sigma Aldrich) dissolved in 1L of ddH<sub>2</sub>O which was sterilised by autoclaving. The mixture was allowed to cool to hand hot and tetracycline was added at a concentration of 10 µg ml<sup>-1</sup> before being poured into Petri dishes and allowed to set. The XL-1 strain *E.coli* cells were streaked out onto these LB agar plates using sterile apparatus with the aim of obtaining single colonies. Plates were incubated overnight at 37°C. The next day a single colony was inoculated into 5ml of sterile LB broth containing 10µg/ml<sup>-1</sup> tetracycline and grown overnight at 37°C with shaking at 225rpm. On the third day this 5ml preparation was added to 20ml of 2YT medium and incubated at 225rpm until cell growth had reached a density of OD<sub>600</sub> = 0.2-0.8. The entire 20ml preparation was then poured into a 1L flask containing 80ml 2YT medium plus 10µg ml<sup>-1</sup> tetracycline. This solution was further agitated until OD<sub>600</sub> = 0.5-0.9 before being diluted to 250ml using 2YT medium. Cells were grown until a precise density of OD<sub>600</sub> = 0.6 was obtained and the solution rapidly cooled in ice water to arrest further growth. The solution was centrifuged for 15 min at 4,000rpm at 4°C and the subsequent pellet was resuspended in 50ml Tfb I solution (30mM potassium acetate, 50mM MnCl<sub>2</sub>, 64mM KCl, 10mM CaCl<sub>2</sub> and 15% glycerol; pH 5.8) on ice with gentle shaking. The solution was further centrifuged for 8min at 4,000 rpm at 4°C, the supernatant poured off and the pellet resuspended in 10ml cold Tfb II buffer (10mM 3-(N-

morpholino) propanesulphonic acid (MOPS), 1mM KCl, 75mM CaCl<sub>2</sub> and 15% glycerol; pH 7.4) on ice with gentle shaking. 400µl resuspension was aliquoted into pre chilled microcentrifuge tubes, snap frozen in liquid nitrogen and stored at -80°C until required.

#### **2.2.1.7.1 Transformation of DNA into competent *E.coli* cells**

Transformation is the process of introducing plasmid DNA into *E coli* cells. By treating cells using a heat shock process and with chemicals, they become competent to take up DNA.

Aliquots of competent cells (described in section 2.2.1.7) were gently thawed on ice and 100µl of cell suspension per transformation was added to pre-chilled Eppendorf tubes. 1.5µl of β-mercaptoethanol (1.4M in H<sub>2</sub>O) was then added to each tube. β-mercaptoethanol is a reducing agent which increases the efficiency of transformations by inactivating surface nucleases and making the cell wall permeable to nucleic acids (Brzobohaty and Kovac, 1986). Cells were incubated on ice for 10min before 5µl of a ligation reaction or 10ng circular plasmid DNA was added to the tube and mixed by swirling. The reaction mix was then incubated on ice for 30min, to allow the DNA to associate with the competent cells. Following this, cells were heat shocked for 45 s at precisely 42°C to facilitate uptake of DNA by the competent cells. The length of time and the temperature used are critical to the efficiency of the transformation. Reaction tubes were then returned to ice for 2min before 400µl LB broth was added to each tube. Tubes were then incubated for 1hr at 37°C with gentle shaking at 225rpm. Following this 100µl transformation mix was plated onto LB agar plates containing the correct selection antibiotic for the specific plasmid being transformed (eg. 75µg ml<sup>-1</sup> ampicillin or 30µg ml<sup>-1</sup> kanamycin). Plates were then grown overnight at 37°C and the next day colony growth assessed. Only those cells that have taken up the introduced plasmid DNA express the appropriate antibiotic resistance protein required to grow. 2 single colonies were then picked and each inoculated into 5ml of LB broth containing the appropriate selection antibiotic (75µg ml<sup>-1</sup>

ampicillin or  $30\mu\text{g ml}^{-1}$  kanamycin). These miniprep cultures were then grown overnight at  $37^{\circ}\text{C}$  with gentle shaking at 225rpm.

#### **2.2.1.8 Small scale (miniprep) isolation and purification of cDNA**

The purpose of performing a miniprep is to further amplify and then isolate the plasmid vector from the transformed bacteria. Purification of the DNA was performed using a silica binding spin column protocol using alkaline-SDS lysis according to the manufacturer's instructions (Sigma Aldrich). A 3ml sample of the overnight preparation was pelleted by centrifugation for 5 min at 5,000rpm. The resulting pellet was resuspended in hyperosmotic sucrose resuspension buffer containing RNase that degrades RNA in the preparation.

The cells were then lysed using an alkaline solution containing sodium dodecyl sulphate (SDS), a very strong detergent, which solubilises the lipid bilayer of the cells and denatures any proteins that may be bound to the desired plasmid DNA. This lysis solution contains NaOH, a strong base that disrupts the hydrogen bond network intrinsic to DNA base pairing of chromosomal DNA essentially denaturing it into single stranded DNA. However the supercoiled nature of the plasmid DNA means it is not irreversibly affected. The solution was then neutralised using a buffer containing potassium acetate (KOAc). The larger chromosomal DNA, proteins and cell debris do not renature correctly and instead aggregate into an insoluble precipitate, whereas the plasmid DNA remains soluble. This neutralisation step also added chaotropic binding salts that facilitated plasmid DNA binding to the silica of the spin column. The solution was then centrifuged for 10min at 12,000rpm to form a pellet to remove any contaminants.

The binding column was prepared by being placed into a centrifuge tube and 500 $\mu\text{l}$  column preparation solution added before centrifugation at 12,000rpm for 1min. The neutralised lysate was then added to the column and centrifuged again at 12,000rpm to promote binding of the plasmid DNA to the silica filter of the column. The filter was then washed using a solution containing solvent (80% ethanol) which dissolves residual salts and other contaminants from the

preparation (then eluted in the supernatant). The plasmid DNA is unaffected and remains bound to the column. The column was re-spun again for 2min at 12,000rpm to remove any residual ethanol. The plasmid DNA was then eluted from the column using 100 $\mu$ l ddH<sub>2</sub>O or Tris-EDTA (TE; 10mM Tris HCl, 0.1mM EDTA; pH 8.0). The resulting miniprep (approximate concentration of 50ng/ $\mu$ l) was then digested using restriction enzymes in order to screen whether they contained the correct plasmid DNA, or stored at -20°C for later use.

#### **2.2.1.9 Large scale (maxiprep) isolation and purification of DNA**

If screening of a miniprep produces a correct result, a larger yield of cDNA may be required for use in cellular transfections. This was achieved using a maxiprep kit (Sigma Aldrich) according to the manufacturer's instructions. Many of the buffer solutions are of a similar composition to those used in the miniprep kit.

A 'starter' culture consisting of 20 $\mu$ l of the correct miniprep clone (not purified) was placed in a 20ml tube containing 5ml LB broth plus the required antibiotic (75 $\mu$ g ml<sup>-1</sup> ampicillin or 30 $\mu$ g ml<sup>-1</sup> kanamycin) and grown for eight hours during the course of the day at 37°C with gentle shaking (225rpm). This starter culture was then added to a 500ml conical flask containing 120ml sterile LB broth containing the appropriate antibiotic (75 $\mu$ g ml<sup>-1</sup> ampicillin or 30 $\mu$ g ml<sup>-1</sup> kanamycin) and grown overnight at 37°C with gentle shaking (225rpm).

The following day, the overnight culture was centrifuged for 15 min at 4,000rpm at 4°C. The pellet was then resuspended in a resuspension buffer, a hyperosmotic sucrose solution containing RNase to degrade any RNA that may be present in the preparation. An alkaline detergent solution composed of NaOH and SDS, was added and centrifuge tubes inverted 6 times to mix the contents. The lysis solution was left on for 3min, until the solution was clear and viscous.

The solution was then neutralised using a chilled solution containing potassium acetate. The larger chromosomal DNA, proteins and cell debris precipitate into an insoluble cluster, whereas the plasmid DNA remains soluble in the supernatant. A binding solution was then added and centrifuge tubes inverted once before the

contents were immediately poured into the barrel of a prepared filter syringe and left to sit for 5min, whilst binding columns were prepared. Half of the lysate was expelled into the tube, before centrifugation at 4,000rpm and the eluate discarded. The second half of the lysate was then added to the binding column and the process repeated. This resulted in the plasmid DNA becoming bound to the filter of the column. The filter was washed with two wash solutions, the first for 2 min at 4,000rpm and the second with a solution containing solvent (80% ethanol) for 5min at 4,000rpm. This second solution removes residual salts and other contaminants from the purified DNA which remains in the filter.

The binding column was then removed and placed in a clean 50ml collection tube. 3ml of elution solution was then added and the tube centrifuged for 5min at 4,000rpm. Ethanol precipitation was then performed to further concentrate and purify the eluted DNA. 3M sodium acetate (pH 5.0) was added in a 1:10 ratio (300 $\mu$ l, giving a final concentration of 0.3M) to the 3ml DNA elute. The Na<sup>+</sup> ions neutralise the negative charges on the DNA sugar phosphate backbone and subsequent addition of chilled 100% ethanol as a 2.2 x volume (7.2ml) displaces the less polar water molecules surrounding the DNA phosphates. The plasmid DNA precipitates out of this solution, and can be collected following centrifugation for 20min at 4,000rpm. This was followed by adding 1ml of chilled 70% ethanol and the solution centrifuged for 10min at 4,000rpm, to remove any residual salt from the precipitated DNA. The resulting supernatant was removed and the pellet re-centrifuged to remove residual ethanol. The pellet was then left to air dry for approximately 20min. The pellet was then resuspended in TE buffer (10mM Tris-HCl, 1mM EDTA; pH 7.4) and concentration and purity determined using a spectrophotometer (BioPhotometer, Eppendorf) with absorbance read at 260nm (the wavelength at which double stranded DNA absorbs light). This absorbance was converted to a DNA concentration using the calibration for double stranded DNA (1 AU = 50 ng / ml). Protein peak absorption was also measured at 280nm, and the ratio between these two values (260/280nm)

indicated the purity of the sample DNA. A ratio of 1.7-1.9 was desired, as it was indicative of relatively pure double stranded DNA. The volume of the preparation was then adjusted to a stock DNA concentration of 1 $\mu$ g/ $\mu$ l in TE buffer.

## **2.2.2 Cell culture**

### **2.2.2.1 Cell lines and passaging**

The base cell line typically used for bimolecular fluorescence complementation (BiFC) studies of constrained GPCR dimers, were HEK293T cells stably expressing clonal Snap modified receptor fused to a N terminal fragment of Venus YFP (2-172; Yn) (see Figure 2.4). Additionally cell lines were also generated using this Snap receptor-Yn cell line, co-transfected with a mixed population of FLAG tagged receptor cDNA (lacking the STOP codon) within the pCMV FLAG vector (see Figure 2.5). The complete dual transfect cell line is therefore referred to as Snap receptor-Yn / FLAG receptor-Yc.

The cell lines used for BiFC studies of receptor:  $\beta$ -arrestin association were also dual transfects stably expressed in HEK293T cells, as described previously ((Kilpatrick et al., 2010)). These consisted of a clonal population of  $\beta$ -arrestin2-Yn  $\beta$ -arrestin1-Gn or  $\beta$ -arrestin2-Gn (Figure 2.7), co-expressed with a mixed population of FLAG receptor -Yc or -Gc(Figure 2.5).

Additionally HEK293TR tetracycline inducible cell lines were also used in some experiments. Here receptor-GFP cDNA sequences were placed in the pcDNA4/TO vector downstream of the FLAG epitope (Figure 2.6). Receptor expression was induced following treatment with tetracycline (see section 2.2.2.4).

All cell lines were grown in Dulbecco's modified Eagle's medium (DMEM) supplemented with 10% foetal bovine serum (FBS) in 75 cm<sup>2</sup> tissue culture flasks (T75s) at 37°C and 95% O<sub>2</sub>/5% CO<sub>2</sub>. Medium was supplemented with maintenance concentrations of the appropriate antibiotic required for the transfected constructs in that cell line (see Table 2.2). Cells were only grown up to 80% confluency prior to passaging to prevent cell detachment. When

passaging cells the presence of residual FBS can deactivate trypsin, therefore cells were first washed with PBS followed by treatment with 1ml trypsin (0.25% w/v in Versene; Lonza Wokingham Ltd (Wokingham, UK)). Trypsin is a serine protease that facilitates cell detachment by hydrolysing proteins that enable cells to adhere to the culture flask. Washing the flask surface with 10ml DMEM prevented trypsin from further proteolysis and allowed detached cells to be collected. Cells were then centrifuged then resuspended in 5ml DMEM. For cell passaging, and an appropriate volume of cell suspension added to a T75 flask to give a required dilution ratio typically of 1:5-1:20. Maintenance concentrations of appropriate antibiotic were also included (see Table 2.2).

For experiments, 100µl cell suspension was loaded onto a haemocytometer and the number of cells within a 1mm<sup>2</sup> area counted (25x0.04mm<sup>2</sup> squares totalling 0.1µl volume). The average number of cells per ml was calculated by multiplying the number of cells by 10,000. This cell suspension was then resuspended in an appropriate volume of DMEM to give the required cell density. Prior to seeding, the wells of an appropriate plate were coated with poly-D-lysine (10 µg ml<sup>-1</sup> in double distilled H<sub>2</sub>O; filter sterilised using a 0.2µm filter) for 30min at room temperature before being aspirated and washed with DMEM.

Typically cells were seeded the day before experimentation with the exception of cells under the tetracycline repressor system (eg. HEK293TR Y1-GFP) or cells used for cAMP accumulation experiments (see Table 4 for details).

#### **2.2.2.2 Transfection**

Transfection is the process of introducing DNA into a recipient eukaryotic cell and, for stable transfection, the integration of this DNA into the host cell's genome. Stable transfections were undertaken using lipofectamine (Invitrogen) and the appropriate cell line (HEK293T or HEK293TR cells) to generate mixed populations. Cells were grown to 70% confluence in T25 flasks and the media replaced with 1.2 ml OptiMEM (Invitrogen). Mixtures of 2 µg DNA in 200µl OptiMEM and 18 µl lipofectamine also in 200µl OptiMEM, were prepared

separately and then combined to allow lipofectamine:DNA complexes to form over 1hr at room temperature. At the end of the incubation, a further 800 $\mu$ l OptiMEM was added to the DNA-lipofectamine reaction, which was then mixed by vortexing. The entire 1.2 ml DNA-lipofectamine mixture was then carefully added to the T25 flask of cells and left for 24 h at 37°C and 95% O<sub>2</sub>/5% CO<sub>2</sub>. The next day, cells were passaged using the standard protocol described (in section 2.2.2.3) and seeded at a 1:5 ratio. The appropriate antibiotic was also added at concentration required for selection (Table 2.2).

### **2.2.2.3 Dilution cloning**

Dilution cloning was used to generate HEK293T clonal cell lines expressing Snap modified receptor constructs, namely Snap Y1-Yn, Snap Y1Y99A-Yn and Snap  $\beta$ 2ARYn, and the  $\beta$ -arrestin1-Gn or  $\beta$ -arrestin2-Gn base lines. These clonal cell lines were then either expressed alone or used to create a dual stably transfected cell line for use in BiFC dimer experiments. Mixed populations of cell lines generated by stable transfection (2.2.2.1) were passaged (2.2.2.3) and counted (2.2.2.1). Serial dilutions were created whereby an appropriate aliquot of cell suspension was added to a universal containing 20ml DMEM and the appropriate antibiotic required to give dilutions of ~200 cells per 20ml and ~20 cells per 20ml. Of each dilution, 200 $\mu$ l per well was seeded onto a clear flat bottomed 96 well plate with the aim to place 1 cell per well. Cells were left to grow until they had reached approximately 50% confluency, with growth medium (containing the required antibiotic for selection) replaced regularly. Only wells containing colonies grown from a single foci were selected, with growth medium removed and cells washed with 100 $\mu$ l PBS followed by treatment with 50 $\mu$ l trypsin. Gentle pipetting was used to detach and collect cells, which were added to an individual well of a 24 well plate containing 1.5ml DMEM. Cells were then grown to approximately 70% confluency with cell morphology assessed, before being moved to 6 well plates. Additionally 100 $\mu$ l cell suspension of each clone was seeded onto 2 wells of a poly-D-lysine coated 96 well plate to allow clones to be

screened for receptor expression. Screening was achieved using Snap tag labelling (see section 2.2.5.4) and imaging using an IX Ultra confocal plate reader. The growth of positive clones was expanded in T75 flasks before being frozen. The clone showing appropriate levels of receptor expression was either used alone in experiments, or co-transfected with FLAG and Yc tagged receptor constructs to generate mixed population BiFC dimer cell lines (eg. Snap Y1-Yn (clone) / FLAG Y1-Yc (mixed)).

#### **2.2.2.4 Induction of receptor expression using tetracycline**

For receptor constructs expressed in HEK293TR cells (e.g. Y1-GFP), receptor expression was induced following treatment with tetracycline ( $1\mu\text{g ml}^{-1}$ ) 24 h prior to experimentation. The promoter of pcDNA4/TO contained two operon sites (see figure 2.6) that are typically bound by the repressor protein co-expressed in HEK293TR cells. This repressor control mechanism subsequently prevents receptor transcription initiation. Treatment with tetracycline led to a de-repression process, whereby the repressor protein is now bound by tetracycline. This leads to the dissociation of the repressor protein from the tetracycline operon sites, allowing receptor transcription to commence from the pCMV promoter (Yao et al., 1998).

### **2.2.3 [ $^{125}\text{I}$ ] PYY competition binding studies**

#### **2.2.3.1 Membrane preparation**

Crude membranes were freshly prepared from HEK293T or 293TR (following tetracycline induction) cell lines, grown to 70% confluent in T75 flasks. All equipment and buffers were kept on ice whilst membranes were prepared. Medium was aspirated from flasks, and cells washed using PBS. 15ml of membrane preparation buffer (25mM HEPES, 10mM  $\text{Na}_2\text{EDTA}$  and 0.1mM AEBSF; pH 7.4) was fired at the cells to detach them from the flask. The cell suspension was added to a Dounce homogeniser. A further 5ml of membrane preparation buffer was used to wash the surface of the T75 flask to collect any remaining

cells. This 5ml of suspension was also added to the homogeniser. The entire suspension was then homogenised 15 times using a pestle to break down cell architecture. The suspension was then centrifuged for 20min at 40,000x g and the resulting pellet resuspended in 15ml of membrane resuspension buffer (25mM HEPES, 1mM Na<sub>2</sub>EDTA and 0.1mM AEBSF; pH 7.4) and added to the homogeniser. A further 5ml was used to wash the centrifuge tube and collect any remaining cells. The homogenisation process was repeated and the resulting suspension centrifuged again for 20min at 40,000x g. The resulting pellet was resuspended in 4ml of membrane resuspension buffer and placed in a homogeniser. The suspension was homogenised 50 times, before being placed on ice until needed.

### 2.2.3.2 Assay protocol

Experimental incubation buffer consisted of 25mM HEPES, 2.5mM CaCl<sub>2</sub> and 1.0mM MgCl<sub>2</sub>, 0.1% BSA and 0.01% bacitracin (pH7.4). Bacitracin was included in the assay buffer as a metalloproteinase inhibitor.

For GTPγS displacements, saponin was also included in the assay buffer at a final concentration of 30μg/ml<sup>-1</sup>, in order to permeabilise cell membranes and allow access of the GTPγS to micelles (Cohen et al., 1996).

400μl of assay incubation buffer was added first to each experimental tube. Serial dilutions of competing non radioactive ligands (at 10x final concentration) were made up in assay incubation buffer and then added as a 50μl aliquot in duplicate to the appropriate tube and tubes vortexed. GTPγS dilutions were not made up until needed due to its instability. A stock volume of [<sup>125</sup>I] PYY was diluted in incubation buffer to give a final experimental concentration per tube of 15pM. The volume for dilution was determined for each experiment, to account for the decreasing activity of the radioligand as it decays. Firstly the activity of stock (in Bq) was calculated using the equation:

$$1. \left( \frac{\text{stock used } (\mu\text{l})}{\text{total volume stock } (\mu\text{l})} \right) \cdot \text{stock size (in Bq)} \cdot e^{-D \cdot \frac{\ln 2}{t_{1/2}}}$$

where D is the difference in days between the assay date and the reference date, and  $t_{1/2}$  is the half life of Iodine-125

Radioactive activity required per tube (500  $\mu$ l) was then calculated using the equation:

2. Assay concentration (15pM)/2\*specific activity of radioligand (81.4 Bq/fmol).

The dilution volume was finally calculated using the equation:

3. (Equation 1/ Equation 2)\*volume of radioligand per tube (25 $\mu$ l)

This 25 $\mu$ l aliquot of diluted [ $^{125}$ I] PYY was added to the side of each assay tube (ie. not directly to the assay buffer to avoid cross contamination with the competing ligands) and tubes vortexed. 10 $\mu$ l aliquots of [ $^{125}$ I] PYY were saved for later calibration of the gamma counter counting efficiency. A 25 $\mu$ l aliquot of diluted cell membranes was then added to all assay tubes (except the designated blanks), and tubes vortexed. The stock volume of diluted membranes was vortexed every 6 tubes to prevent settling. Therefore each assay tube contained a total volume of 500 $\mu$ l consisting of:

400 $\mu$ l assay incubation buffer

50 $\mu$ l cold ligand

25 $\mu$ l diluted [ $^{125}$ I] PYY

25 $\mu$ l diluted membranes

Competition binding assays were carried out for 90 minutes at 21°C with gentle shaking. Membrane bound ligand was then separated by filtration through Whatman GF/B filters pre-soaked in 0.3% polyethyleneimine solution using a Brandel cell harvester. Retained radioactivity was quantified using a gamma counter (Packard Cobra II, Perkin Elmer, Waltham, MA, USA).

#### **2.2.4 [ $^3$ H]cAMP accumulation assay**

Typically in response to receptor activation, the enzyme adenylyl cyclase converts ATP to cAMP and pyrophosphate. Therefore the production of cAMP can be used as a readout of the activity of adenylyl cyclase. To facilitate this [ $^3$ H] adenine can

be used to label pools of intracellular adenine nucleotides, such as ATP ( $[^3\text{H}]\text{ATP}$ ) which is then converted to  $[^3\text{H}]\text{cAMP}$ . In response to the activation of receptors coupled to the  $G_i$  class of G proteins, such as  $\gamma$  receptors, the  $G_\alpha$  subunit inhibits adenylyl cyclase and subsequent  $[^3\text{H}]\text{cAMP}$  production. Measuring  $[^3\text{H}]\text{cAMP}$  production in response to agonist stimulation gives an indication of the degree of receptor induced inhibition with sequential column chromatography used to recover  $[^3\text{H}]\text{cAMP}$  from  $[^3\text{H}]\text{ATP}$  (Donaldson et al., 1989).

#### **2.2.4.1.1 Dowex columns**

A slurry of Dowex AC '50' 50W-4X resin mesh 200-400 (1:1 (v/v)) with distilled water was mixed under constant stirring and 2.4ml of this suspension was added to each Bio-Rad 'Poly-prep' column. Columns were regenerated prior to each experiment using 10ml 1M HCL, followed by 2 washes of 10ml distilled water. Columns were cleaned after each experiment using 10ml 1M NaOH followed by 2 washes of 10ml distilled water.

#### **2.2.4.1.2 Alumina columns**

Columns were prepared when 0.6g of Neutral alumina WN-3 was added to each Bio-Rad 'Poly-prep' column. Both prior to and after each experiment, columns were washed twice with 10ml 0.1M imidazole.

#### **2.2.4.2 Assay protocol**

The assay protocol was adapted from (Donaldson et al., 1989). Due to the large number of cells required for each assay, HEK293T cells were cultured in 175cm<sup>2</sup> flasks (T175). Cells were seeded onto poly-D-lysine coated 24 well plates two days prior to experimentation at a density of 100,000 cells per well in a total volume of 500 $\mu\text{l}$  (see section 2.2.2.3). On the day of the experiment, cells were loaded with 100 $\mu\text{l}$  of serum free DMEM containing 1 $\mu\text{l}$   $[^3\text{H}]\text{adenine}$  per well (2  $\mu\text{Ci/ml}$ ; ie. 25 $\mu\text{l}$   $[^3\text{H}]\text{adenine}$  in 2.5ml DMEM per plate) added using a 10ml Eppendorf combitip. Plates were incubated for 2hr at 37°C/5% CO<sub>2</sub> to allow incorporation of  $[^3\text{H}]\text{adenine}$  into intracellular pools of adenine nucleotides. Following this,

extracellular [<sup>3</sup>H]adenine was removed by washing once with 400µl of serum free DMEM and replaced with 400µl DMEM/0.1% BSA containing 1mM rolipram (a phosphodiesterase IV inhibitor). Antagonists, where used, were added at this stage at an appropriate concentration, and plates incubated for 30 min at 37°C/5% CO<sub>2</sub>. Serial dilutions of desired agonist were made up in a vehicle buffer of DMEM/0.1% BSA. A 50µl aliquot of agonist was added to designated wells, along with a negative control of vehicle alone. Cells were preincubated with agonist for 10min at 37°C/5% CO<sub>2</sub>, before the addition of 50µl per well of forskolin (final concentration 30 µM) in serum free DMEM. Plates were then incubated for a further 1hr at 37°C/5% CO<sub>2</sub>. Reactions were terminated using 50µl concentrated HCL added to all wells, followed by the addition of 100µl of [<sup>14</sup>C] cAMP solution per well (0.25µl [<sup>14</sup>C] cAMP in 2.5ml ddH<sub>2</sub>O per plate). The addition of [<sup>14</sup>C] cAMP, allowed the percentage recovery sample cAMP during column chromatography to be estimated and corrected for. Therefore 3 vials containing 100µl of [<sup>14</sup>C] cAMP alone from the day of the assay, representing 100% recovery controls, were saved to be read at a later date alongside the corresponding plate. Assay plates were frozen and stored at -20°C in a radioactivity designated freezer prior to recovery of [<sup>3</sup>H]cAMP and [<sup>14</sup>C]cAMP using sequential column chromatography.

#### **2.2.4.3 [<sup>3</sup>H] cAMP and [<sup>14</sup>C] cAMP recovery**

Sequential chromatography using prepared Dowex and Alumina Biorad columns, was used to isolate [<sup>3</sup>H] cAMP from [<sup>3</sup>H] ATP. This method was based on that described by (Salomon et al., 1974). Columns were prepared as described above (2.2.7.1), during which time assay plates were thawed at room temperature. The whole well contents, totalling 650µl, was transferred to Dowex columns and left to drip through. The resin of the Dowex columns, though negatively charged themselves absorb the negatively charged nucleotides, cAMP, AMP, ADP and ATP delaying their passage through the column. Upon washing the columns with 3ml distilled water, the more negatively charged molecules, ATP and ADP are repelled

by the negatively charged Dowex and forced through the column. The less negatively charged AMP and cyclic AMP are retained in the Dowex column. The Dowex columns were then placed over the alumina columns. The addition of 6ml distilled water per Dowex column facilitated the elution of cAMP ( $[^3\text{H}]$  cAMP,  $[^{14}\text{C}]$  cAMP and unlabelled cAMP) into the alumina column. Alumina columns were then placed directly over scintillation vials, with 5ml 0.1M imidazole added to each column to allow the elution of cAMP from the column into the vial (due to the induced rise in pH). 8ml of scintillation fluid was added to each vial, in addition to the 3 100% recovery vials saved from the day of the experiment. All vials were then counted using a  $\beta$  scintillation counter capable of simultaneous dual counting of  $[^3\text{H}]$  and  $[^{14}\text{C}]$ .

The scintillation fluid added to each vial contains phosphors which have luminescence properties. Upon decay  $[^3\text{H}]$  and  $[^{14}\text{C}]$  radioisotopes emit  $\beta$ -particles, which transfer energy absorbed by the phosphor. They then re-emit this as photons, which are counted to give counts per minute (cpm). The use of a control radioactive sample alongside each vial, allowed the efficiency of the mix of scintillation fluid/elution to be determined. From this cpm values were corrected to give estimated disintegrations per minute (dpm) values. The use of dual counting of samples relies on the two radioisotopes decaying with different energies from each other. The  $\beta$ -particles emitted by  $[^{14}\text{C}]$  have more energy than those produced by  $[^3\text{H}]$ , and are therefore recognised as distinct species by the scintillation counter producing a separate value for each isotope's disintegration.

## **2.2.5 Automated platereader assays**

### **2.2.5.1 Agonist induced internalisation of HEK293TR GFP tagged receptors**

HEK293TR cells stably expressing FLAG-tagged receptor-GFP constructs were seeded onto poly-D-lysine coated 96 well clear flat bottomed black sided plates (Greiner 655090, Greiner Bio-One, Stonehouse, UK) two days prior to assay at a density of 20,000 cell per well. The next day cells were treated with 1  $\mu\text{g}/\text{ml}$

tetracycline to induce receptor expression (see section 2.2.2.4). On the day of experiment, cells were washed once with medium consisting of HEPES buffered saline solution (HBSS; 147mM NaCl, 5 mM KCl, 1.3mM CaCl<sub>2</sub>, 1mM MgSO<sub>4</sub>, 10mM HEPES, 2mM NaCH<sub>3</sub>COCO<sub>2</sub>; pH 7.45) supplemented with 0.1% bovine serum albumin (BSA). This was then replaced with 100µl per well of HBSS. BSA was included in the assay vehicle to prevent the peptide ligands from sticking to the plasticware. Vehicle (HBSS) or agonist additions were made to triplicate wells and incubated at 37°C for times as indicated. Following this, cells were washed with phosphate buffered saline (PBS) and fixed in 3% paraformaldehyde (PFA)/PBS for 10min at room temperature. Cells were then washed with PBS for 5min followed by nuclei staining using H33342 (bisbenzimidazole H 33342 trihydrochloride; Sigma Aldrich; 2µg ml<sup>-1</sup> in PBS) for 15min at room temperature. Wells were then washed twice with PBS before being imaged using an IX Ultra confocal plate reader (Molecular Devices). A Plan Fluor 40x NA0.6 extra long working distance air objective with a pinhole set to 4 was used to image four central sites per well. 405nm (DAPI; cell nuclei) and 488nm (GFP) laser excitation were used. Laser powers and gains were kept constant for all experiments (see Table 2.6).

#### **2.2.5.2 Bimolecular fluorescence complementation (BiFC)**

Bimolecular fluorescence complementation (BiFC) is a fluorescence based technique which can be used to investigate defined protein-protein interactions. A fluorescent protein is split into 2 non fluorescent halves N and C terminal fragments. These fragments can be covalently fused to proteins of interest eg. receptor-Yc and β-arrestin2-Yn (Kilpatrick et al., 2010). Upon interaction of the tagged proteins, the two fragment tags are brought into close proximity facilitating their association and refolding into the full length vYFP. The chromophore matures, which then produces a fluorescent signal that acts as a readout of the interaction of the two tagged proteins (Kerppola, 2009).

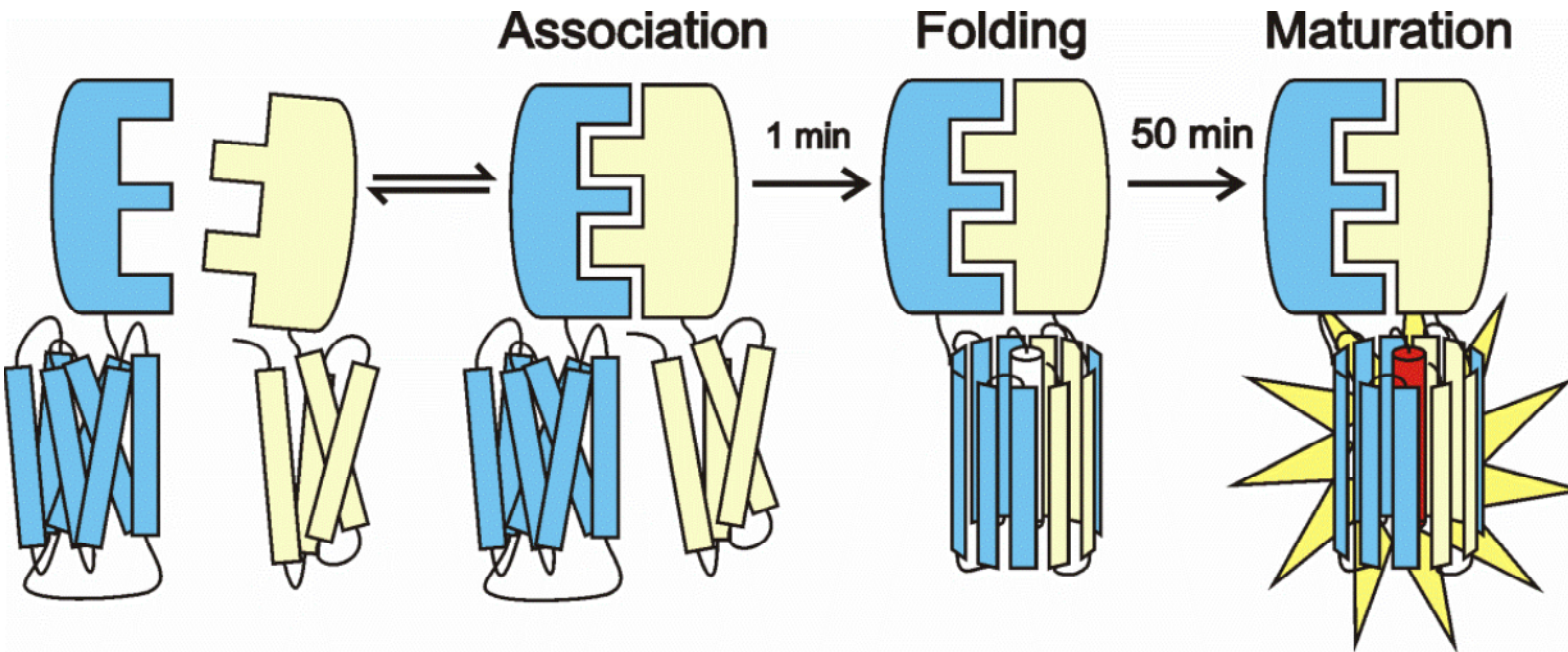


**Figure 2.9: The principle of bimolecular fluorescence complementation (BiFC)**

Two proteins of interest can be covalently tagged with complementary fragments of vYFP. Following interaction of the tagged proteins, these fragments re-associate and re-fold to form full length vYFP. Following chromophore maturation, observed fluorescence acts as a readout of protein-protein interaction.

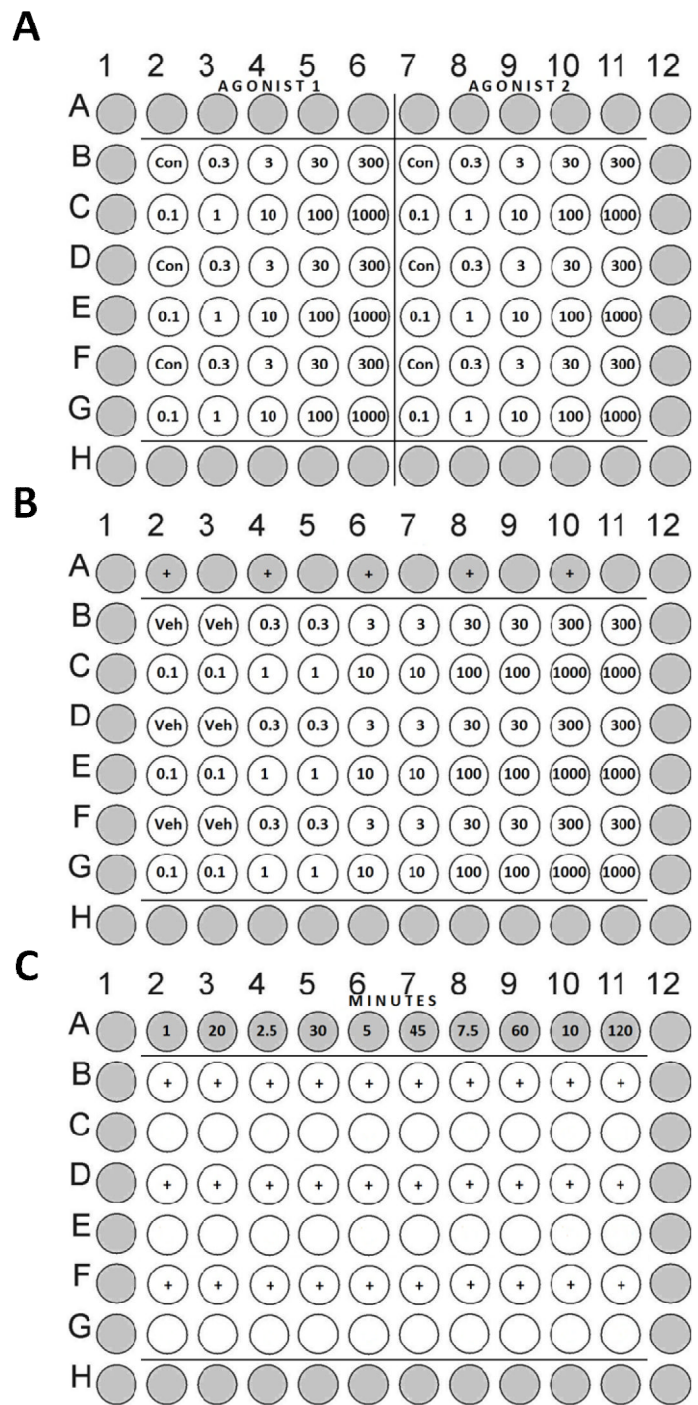


**Figure 2.10: Example plate layouts used in automated plater reader assays**

Representative plate layouts used for agonist concentration response courses (A) and antagonist pretreatment followed by agonist stimulation (B; + representing antagonist treated columns). All values are stated as nanomolar concentrations. An example layout of a timecourse experiment is also shown (C) with agonist treated wells indicated (+).

### **2.2.5.3 Measuring the interaction of $\beta$ -arrestin2 with NPY Y receptors using BiFC**

HEK293T cells stably co-expressing a mixed population of FLAG-NPY Y receptor-Yc and clonal  $\beta$ -arrestin2-Yn (Y1/A2) or  $\beta$ -arrestin-Gn (Y1/A1G, Y1/A2G) were seeded the day prior at a density of 40,000 cells per well onto poly-D-lysine coated 96 well clear bottomed black sided plates (Greiner 655090). Cells were washed with serum free DMEM/0.1% BSA (vehicle) and replaced with 100 $\mu$ l per well. Plates were incubated for 20min at 37°C/5% CO<sub>2</sub>. Agonists or vehicle control were added to the appropriate-triplicate wells to give a final concentration range of 10<sup>-10</sup> to 10<sup>-6</sup>M and incubated for 60min at 37°C/5% CO<sub>2</sub>. Cells were then washed, fixed and nuclei stained as described in section 2.2.3.1. Plates were also imaged using an IX Ultra confocal platereader, fitted with a Plan Fluor 40x NA0.6 extra long working distance air objective, with 405nm (DAPI; cell nuclei) and 488nm (YFP; BiFC signal) laser lines used for excitation. A larger pinhole diameter of 7 was used for imaging recomplemented YFP to improve the signal to noise ratio.

### **2.2.5.4 Receptor visualisation of Snap tagged receptors**

The Snap tag is a 20 kDa mutated version of the human DNA repair protein O<sup>6</sup>-alkylguanine transferase (hAGT). Physiologically this enzyme removes alkyl groups on the O<sup>6</sup> position of guanine bases of DNA and covalently transfers them to an internal cysteine residue (Pegg, 2011). This property has been exploited for use in tagging recombinant proteins by engineering hAGT to react with exogenous benzylguanine substrates covalently bound to a fluorophore (BG-AF647 throughout). This leads to irreversible labelling of the Snap tag with the fluorescent probe allowing direct visualisation of N terminally Snap modified receptors. Snap surface labels are membrane impermeant, therefore only receptors that have been successfully trafficked from the endoplasmic reticulum or Golgi apparatus and are subsequently expressed at the cell surface (with extracellular Snap tag) are labelled.

## Red Channel

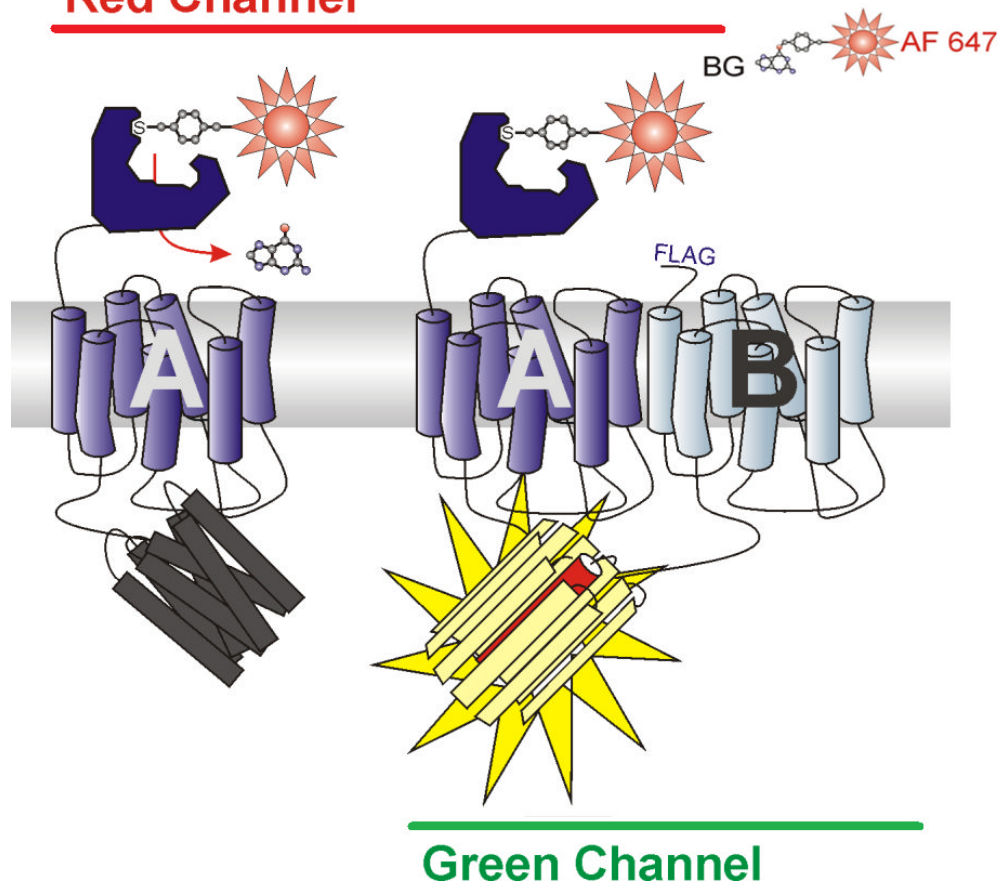


**Figure 2.11: The principle of combining Snap labelling and BiFC to study the interaction of two receptor protomers.**

The schematic illustrates how HEK293T cells were stably transfected with a clonal GPCR protomer (A) expressing an N terminal Snap tag. The Snap tag is a small polypeptide based on a mammalian DNA repair protein, which irreversibly transfers the alkyl group of a membrane impermeant fluorophore conjugated substrate (AF-647) to a cysteine residue of the tag sequence allowing the surface expression of Snap labelled receptor to be imaging using the Cy5 filter settings of a confocal plareader (B). To investigate the internalisation of receptor dimers, Snap-protomer A can be co-expressed with an additional FLAG labelled protomer B. Both protomers (A and B) are tagged at their C terminus with a fragment of YFP. Receptor dimerisation brings the two fragments into close proximity whereupon they can refold into recomplemented YFP. This produces a fluorescent signal that identifies a discrete interaction between receptors of known composition ('BiFC dimer').

### **2.2.5.5 Agonist induced internalisation of BiFC constrained GPCR dimers**

For BiFC dimer experiments, Snap 647 labelling of Snap-Receptor-Yn (termed protomer A; Figure 2.11) allowed the simultaneous imaging of this population with the BiFC dimer population (complementation between Snap Receptor-Yn / FLAG Receptor-Yc protomers A+B; recomplemented YFP) in the same cell. This allowed the responses of the BiFC dimer population to be compared with the protomer A population (be that monomers, dimers or oligomers).

HEK293T cells stably co-expressing Snap-receptor protomer A-Yn alongside a mixed population of FLAG-tagged receptor protomer B-Yc were seeded onto poly-D-lysine coated 96 well clear flat bottomed black sided plates (Greiner 655090) on the day before experiment at a density of 40,000 cells per well. On the day of experiment, cells were treated with serum supplemented DMEM containing 0.2 $\mu$ M Snap AF647 for 30min at 37°C/5% CO<sub>2</sub>. Wells were then washed with HBSS/0.1% BSA before being replaced with 100 $\mu$ l per well of HBSS / 0.1% BSA. Vehicle or agonist were added as a 20 $\mu$ l aliquot typically at a final concentration range of 10<sup>-10</sup> to 10<sup>-6</sup>M to triplicate wells and incubated at 37°C for times as indicated. Cells were then fixed and nuclei stained as described previously (2.2.3.1). Plates were imaged using an IX Ultra confocal platereader, fitted with a Plan Fluor 40x NA0.6 extra long working distance air objective, with a pinhole set to 7 using 405nm (DAPI; H33342 cell nuclei) and 488nm (FITC; YFP BiFC signal) and 647nm (Cy5; Snap AF647 label) laser excitation.

### **2.2.6 Specific platereader assay methods**

#### **2.2.6.1 Assays requiring pretreatment with antagonist**

Where antagonist pre-treatment was required after the initial wash, the contents of wells of even numbered columns was replaced with 100 $\mu$ l of HBSS/0.1% BSA containing the appropriate concentration of antagonist (see Figure 2.10, plate layout B). To the wells of odd numbered columns, 100 $\mu$ l of medium alone was

added. Plates were incubated for 30min at 37°C/5% CO<sub>2</sub>, prior to agonist addition. From this point on the assay protocol followed that of section 2.2.3.1.

#### **2.2.6.2 Timecourse assays**

To assess the timecourse of agonist induced internalisation of receptor constructs, the same protocol as for section 2.2.5.3 or 2.2.5.5 was followed until the replacement of well volumes with 100µl per well of HBSS/0.1% BSA. 100nM NPY was then added as a 20µl aliquot to the centre of wells in rows B D and F at an appropriate time point, such that incubations finished concurrently. The time intervals chosen were 30, 20, 15, 12, 10, 8, 6, 4, 2, and 1min (see plate layout). Assay medium was quickly removed, by flicking the well contents into a sink. Cells were immediately fixed as described in 2.2.3.1.

#### **2.2.7 Confocal microscopy**

HEK293T Snap-receptor cell lines were seeded onto poly-D-lysine coated 8 well clear plates (Nunc Lab-Tek, Thermo-Fisher Scientific, UK) at a density of 50,000 cells per well. The next day, live cells were labelled with 0.2µM Snap AF647 as previously described (see section 2.2.3.4), washed twice with HBSS/0.1% BSA (vehicle) and treated with either 300µl vehicle or 100nM NPY in HBSS/0.1% BSA for 30 min at 37°C. Images were taken using a Zeiss LSM 510 (Carl Zeiss Ltd., Welwyn, UK) fitted with a 63x Plan Aplanachromat NA 1.4 oil objective using Argon 488nm (Recomplemented vYFP) and HeNe 633nm (SNAP-surface AF647) laser lines for excitation.

Multitrack settings were utilised, so that the sample was illuminated sequentially with the distinct laser excitations to prevent bleed-through from one to the other. Long pass and band pass emission spectra are detailed in Table 2.5.

A pinhole diameter of 1.5 Airy units was set for the longest wavelength acquired (633 nm / long pass 650nm) and the optical slice subsequently matched for the shorter wavelength (488nm / BP 505 – 550 nm). This pinhole size was larger than the optimal pinhole size of 1 Airy unit in order to improve the signal to noise ratio

when imaging BiFC fluorescence. Microscope detector gains and amplifier offsets were consistently adjusted within data groups to enable comparison between control and treated samples and prevent oversaturation. All images were taken at 1024x1024 pixels per frames with 8 averages limiting total laser exposure per acquisition to approximately one minute.

When using HEK293TR receptor-GFP cell lines, cells were seeded two days prior to assay at a density of 20,000 cells per well. The next day receptor expression was induced following the addition of  $1\mu\text{g ml}^{-1}$  tetracycline (see section 2.2.2.4). Cells were also imaged using a Zeiss LSM 510 fitted with a 63x Plan Apochromat NA 1.4 oil objective using an Argon 488nm laser line for excitation and emitted light collected via a 505-550nm bandpass filter, using a pinhole diameter of 1 Airy unit. Gains and offsets were consistently adjusted within data groups to prevent oversaturation. All images were taken at 1024x1024 pixels per frame with 8 averages.

### **2.2.8 Fluorescence correlation spectroscopy (FCS)**

Fluorescence correlation spectroscopy (FCS) is a technique which measures the diffusion of fluorescently tagged moieties through a fixed confocal volume of approximately  $0.25\mu\text{m}^3$ . As fluorescent particles pass through this volume, they produced time dependent fluctuations in intensity which were analysed to generate information concerning the mobility, concentration and molecular brightness of these particles (Figure 2.12; see Chapter 4).

#### **2.2.8.1 Calibration**

FCS measurements were performed using a Zeiss Confocor 2 fluorescence microscope fitted with a c-Apochromat 40x NA 1.2 water immersion objective lens. Calibration was required to ensure the optimal position of the beam path and to confirm a detection volume of Gaussian shape. Calibration was first performed using rhodamine 6G (Invitrogen,  $D_{\text{R6G}}$ ; known diffusion coefficient,  $D = 3 \times 10^{-6} \text{ cm}^2 \text{ s}^{-1}$ ).  $10^{-2}\text{M}$  stock solutions of Rhodamine 6G was diluted to  $10^{-6}\text{M}$  and

$10^{-8}$ M aliquots in ultrapure fluorescence free water. 300 $\mu$ l of each dilution was placed into separate wells of an 8 well plate and left for 5min before calibration. The plate was placed over the objective, and firstly centred on the well containing the  $10^{-6}$ M solution. Both the lower then upper surface of the 8 well plate were determined using the reflection beampath and the focal position set 200 $\mu$ m above the upper surface as the defined well bottom.

A beampath was then selected which gave the correct laser excitation, dichroic mirror and emission filter for detecting GFP tagged receptors. An Argon laser set to 25% output, with a pinhole diameter of 1 Airy unit was used. When calibrating using  $10^{-6}$ M rhodamine, a laser power of 0.3% was used and the collar correction adjusted to give a count rate of 200-250 kHz. The position of the pinhole was then scanned and automatically optimised by the machine in both the x and y axis alongside adjustment of the collimator position (z axis). The x,y and z values were recorded for each experiment, with the x and y values not expected to widely vary. The objective was then centred over the well containing the  $10^{-8}$ M rhodamine solution and the laser power increased to give a count rate of approximately 50-70 counts per molecule. Rhodamine calibration measures of 3 x 15 seconds reads were then carried out using a range of laser powers (5-1%). The first read was used to bleach immobile species within the sample in order to obtain a more stable trace in the absence of systematic decreases in mean intensity over the recording time. However in reality, bleaching for rhodamine is minimal (due to its fast diffusion), and was therefore included as a control for measurements of fluorescent protein tagged cells where bleaching is much more prevalent. The calibration autocorrelation curves were then fitted using the inbuilt analysis software (Zeiss AIM, Jena, Germany) to a one component 3D diffusion model with the structural parameter set to free (see section 2.2.11.1 for further details of equations used). All counts per molecule and structural parameters for each laser power used were recorded in order to confirm that the system was calibrated correctly and to calculate the parameters required for

analysis post experiment. The structural parameter is a value that is extremely sensitive to correct calibration as it is the ratio of the height to waist radius of the confocal volume. For correct rhodamine calibration this value should be approximately 5 for a Gaussian detection volume (independent of the laser power used).

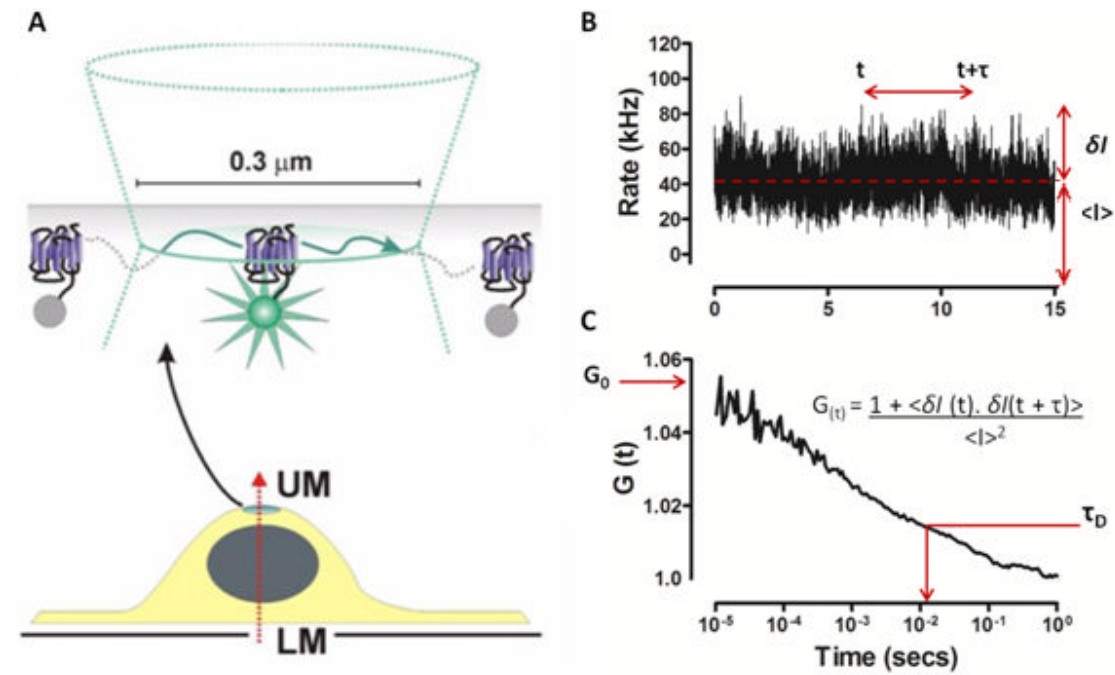


**Figure 2.12: The principles of fluorescence correlation spectroscopy (FCS)**

The confocal volume was positioned on the upper membrane of the cell (A) and the diffusion of fluorescently tagged molecules through the confocal volume was detected. These time dependent fluctuations in fluorescent intensity were measured (B) and analysed to give quantitative data concerning the mobility and concentration of these fluorescent particles (C).

### **2.2.8.2 Measuring the diffusion of superfolder GFP tagged receptors using FCS**

HEK293TR cells expressing FLAG receptor-GFP were seeded on poly-D-lysine coated 8 well plates (Nunc Lab-Tek, Thermo Fisher Scientific, UK) at a density of 20,000 cells per well. The next day receptor expression was induced upon tetracycline addition ( $1\mu\text{g ml}^{-1}$  see section 2.2.2.4). FCS experiments were performed two days post seeding. On the day of the assay, cells were washed with HBSS/0.1% BSA. Well contents were then replaced with 400 $\mu\text{l}$  per well vehicle and cells pretreated with either vehicle or 100nM NPY for 15min at 37°C/5% CO<sub>2</sub>. Following this plates were placed over the objective (previously calibrated as detailed in section 2.2.5.1) and fluorescent cells (of approximately equivalent brightness) were selected from live imaging using a Zeiss Axiocam HR camera with GFP exposure set to 700ms. To prevent bleaching, a low laser power (0.1%) was used to place the xy position of the focal volume over the centre of a nucleus. The z position of the confocal volume was determined by performing a z scan which, for plasma membrane limited tagged receptors, produced 2 peaks defining the upper and lower membranes of the cell. The focal volume was then placed at the z position on the upper membrane. When recording autocorrelation fluctuations, the laser power was increased to 0.3% (0.61 kW/cm<sup>2</sup>) and a 15sec prebleach was performed followed by 2 x 15sec reads.

### **2.2.8.3 Measuring the diffusion of FLAG receptor-Gc and $\beta$ -arrestin2-Gn complexes using FCS**

HEK293T cells co-expressing a mixed population of FLAG receptor-Gc and clonal  $\beta$ -arrestin2-Gn were seeded on poly-D-lysine coated 8 well plates at a density of 50,000 cells per well the day before experimentation.

On the day of the assay, cells were washed with HBSS/0.1% BSA (vehicle). Well contents were then replaced with 400 $\mu\text{l}$  per well of vehicle and cells pretreated with 100nM NPY for 1 h at 37°C/5% CO<sub>2</sub>.

Fluorescent cells were again selected from live imaging using a Zeiss Axiocam HR camera. However GFP exposure during selection was increased to 1000 ms, to account for the reduced signal to noise ratio of recomplemented GFP. A defined plasma membrane was difficult to identify for GFP BiFC cells, therefore the xy position of the confocal volume was placed over an area of high intensity fluorescence corresponding to internalised receptor within perinuclear recycling compartments. Following cell selection, a z scan was performed as before but the confocal volume was now placed slightly offset of the fluorescence intensity peak representing the upper membrane. From this point, the same assay protocol was followed as for full length GFP tagged receptors (section 2.2.8.2).

### **2.2.9 Fluorescence recovery after photobleaching (FRAP)**

Fluorescence recovery after photobleaching (FRAP) is a technique that can be used to quantify the 2D diffusion of fluorescently tagged molecules. Additionally FRAP can also provide estimates on the respective proportions of mobile and immobile fluorescent molecules present. In FRAP the fluorescent molecules present on a small region of interest (ROI) on a cell, are irreversibly photobleached using a high intensity laser power. Subsequent recovery of fluorescence due to the lateral diffusion of non bleached fluorescent molecules into the bleached area are recorded and estimates of diffusion coefficients calculated (Ishikawa-Ankerhold et al., 2012).

#### **2.2.9.1 Using FRAP to measure the diffusion of GFP tagged receptors**

HEK293TR cells expressing native or mutant Y1 receptor-GFP were seeded on poly-D-lysine coated 8 well plates (Nunc Lab-Tek) at a density of 20,000 cells per well. The next day receptor expression was induced using tetracycline addition ( $1\mu\text{g ml}^{-1}$  see section 2.2.2.4). FRAP experiments were performed two days post seeding.

### **2.2.9.2 Using FRAP to measure the diffusion of Y1 receptor/ $\beta$ -arrestin2 BiFC complexes**

For FRAP investigations using HEK293T cells coexpressing Y1 receptor and  $\beta$ -arrestin constructs tagged with superfolder GFP complementary fragments (e.g. Y1/A2G) cells were seeded on poly-D-lysine coated 8 well plates (Nunc Lab-Tek) at a density of 40,000 cells per well. FRAP experiments were performed the following day.

### **2.2.9.3 FRAP experimental protocol**

FRAP experiments were performed using a Zeiss LSM710 laser scanning microscope using a 63x Plan-Apochromat NA 1.4 oil objective. Argon 488nm (full length or recomplemented GFP) laser excitation was used with emitted light collected between 493 -558nm. On the day of the assay, cells were washed with HBSS/0.1% BSA. Well contents were then replaced with 400 $\mu$ l per well of vehicle and cells pretreated with either vehicle or 100nM NPY for 15min (GFP tagged constructs) or 60min (GFP fragment tagged constructs) at 37°C/5% CO<sub>2</sub>. Slides were then transferred to a heated stage and left to equilibrate at 37°C. A 1.4 $\mu$ m<sup>2</sup> ROI (radius 0.66 $\mu$ m; red circle in Figure 2.13) was placed on the lower plasma membrane adjacent to the coverglass. 10 images were then acquired at 0.5sec intervals (512x512 pixels) to provide a baseline value of fluorescence intensity for the ROI. The region of interest was then bleached using 50 iterations of 100% laser power. Fluorescence recovery was then measured for 90 (full length GFP) to 120 sec (recomplemented GFP). Following this ROIs were also placed on an area of the coverslip containing no cells (background ROI; blue circle) and an adjacent cell of comparable fluorescence intensity to the cell investigated (representative cell; green circle). These representative ROI's allowed background fluorescence and the amount of non bleached fluorescent signal lost during imaging (background bleaching) to be corrected for in recovery curves. A one phase exponential model was used to fit FRAP recovery curves (see section 2.12).

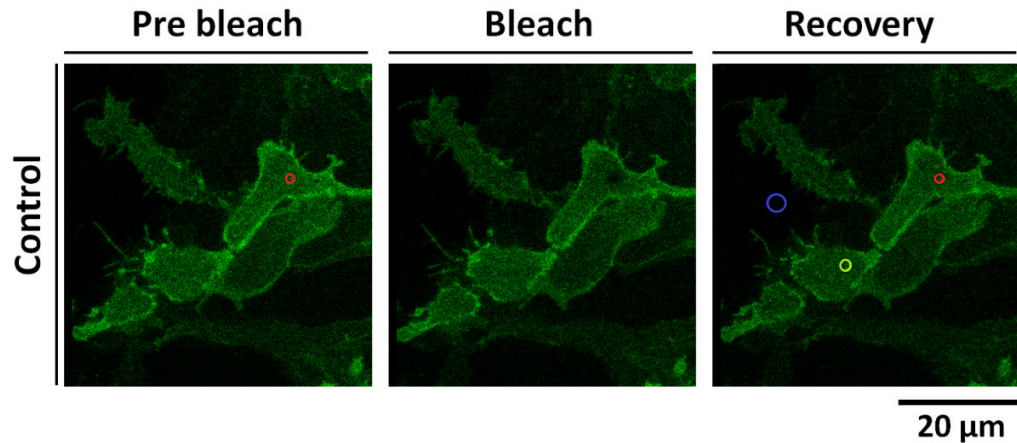


**Figure 2.13: Representative images showing the placement of ROI used in FRAP**

Representative images show a FRAP experiment being performed on Y1-GFP cells. The circular area on the lower plasma membrane approximately  $1.3\mu\text{m}$  to be photobleached is shown in red (Prebleach panel). Following bleaching, this area is now seen as a black spot (bleach panel). Following the recording of fluorescence recovery, representative (green) and background (blue) reference ROIs are drawn (recovery panel).

## 2.2.10 Data analysis

### 2.2.10.1 [ $^{125}\text{I}$ ] PYY competition binding

As each ligand concentration was performed in duplicate, the average gamma count was used. Non specific binding, comprising less than 5% of total specific binding was subtracted from the data. Specific disintegrations per minute molecule (dpm) were converted to fmol/mg using the formula:

$$\text{Specific cpm} * (1/60) * (100 / \text{CE}) * 1000 / \text{protein} * (1 / \text{SA})$$

Where 60 is the factor to convert counts per minute to counts per second.

Where CE = counting efficiency (%), based on the day's reference [ $^{125}\text{I}$ ] PYY aliquot, protein = amount of protein ( $\mu\text{g}$ ) in membrane aliquot, and SA = specific activity (81.4 Bq / fmol).

$\text{IC}_{50}$  values were calculated from displacement curves fitted using non linear least squares regression in GraphPad Prism 5.02. The Cheng Prusoff equation was used to convert  $\text{IC}_{50}$  measurements to  $\text{pK}_i$  values where appropriate:

- $K_i = IC_{50} / (1 + [L]/K_d)$

where [L] is the concentration of free radioligand and  $K_d$  the dissociation constant of the radioligand derived from homologous displacements of PYY for the receptor.

Homologous PYY displacements were used to derive approximate estimates of Bmax values (in pmol mg<sup>-1</sup> membrane protein) using the equation:

- $B_{max} = TSB \times IC_{50} / [L]$

where TSB is the total specific binding in the absence of agonist and [L] the radioligand concentration used.

To convert disintegration counts to fmol/mg the counting efficiency of the gamma counter was firstly determined using the equation:

$$1. = \frac{\text{Observed counts from reference volume (Bq)}}{\text{activity of radioligand on count day}} \times 100$$

The concentration of radioligand per assay in fmol/mg was then calculated using the equation:

$$2. = \left(\frac{1}{A}\right) \cdot \text{Equation 1.} \cdot \left(\frac{1000}{B}\right) \cdot \left(\frac{1}{C}\right)$$

where A = the half life of the radioligand

B = protein amount within the assay volume used (µg/tube).

C = the known specific activity of the radiolabel (81.4 Bq/fmol).

All values are quoted as means ± s.e.m throughout.

### 2.2.10.2 Inhibition of cAMP accumulation

To determine the efficiency of the column chromatography, the average of the 3x 100% recovery vials per experiment was used to give the expected [<sup>14</sup>C]-cAMP dpm values assuming 100% column efficiency (the '100% recovery dpm'). To correct for column efficiency, the [<sup>14</sup>C] dpm value from each individual column was divided by this 100% 'recovery dpm' to give the fraction recovered from that column (the recovery fraction). The corrected [<sup>3</sup>H] dpm value for each column was then determined by dividing the [<sup>3</sup>H] dpm obtained from the counter by this

recovery fraction. All cAMP data presented in this thesis are expressed as corrected [<sup>3</sup>H] dpm values obtained from raw data which has been normalised using negative (unstimulated cells representing 0% basal values) and positive controls (wells stimulated with 30µM forskolin only representing 100% values) to allow different assay plates to be compared. Normalised dpm values from multiple experiments were pooled and then plotted against agonist concentration with bottom values constrained to 100% and Hill slopes set equal to 1. Antagonist K<sub>b</sub> values were calculated as for section 2.2.9.1.2.

### **2.2.10.3 Automated image analysis of plate reader images**

The images acquired using the IX Ultra confocal plater reader (see section 2.2.3; Figure 2.14) can be analysed using various algorithms (MetaXpress 2.0, Molecular Devices) to provide quantitative data of receptor internalisation. All images acquired were 16 bit greyscale, meaning each pixel is represented as a number from 0 (black) to 65535 (white). Images of receptor internalisation (Example images from Y1-GFP receptor internalisation are shown in Figure 2.14; panel A and B) or BiFC images of NPY Y receptors interacting with β-arrestin were analysed using a granularity algorithm which identified regions of internalised fluorescence as 'granules' of 3-15 µm in diameter (Figure 2.14 panel C; white spots). Additionally fluorescence intensity thresholds were set to negative (vehicle) and positive plate controls (top concentration of full agonist used). The addition of a nuclear stain H33342 identified nuclei, allowing all data to be expressed on a per cell basis (Figure 2.14 panel C; green masks). Internalised vesicles were assigned to an identified nucleus based on proximity.

All values were averaged from triplicate wells (4 sites imaged per well; ie. 12 sites of data obtained per point). Granularity analysis gives several parameters such as granule count, intensity and area which all produced similar results. All data presented derived from measurements of granule count per cell. BiFC receptor dimer images were also analysed using the granularity algorithm.

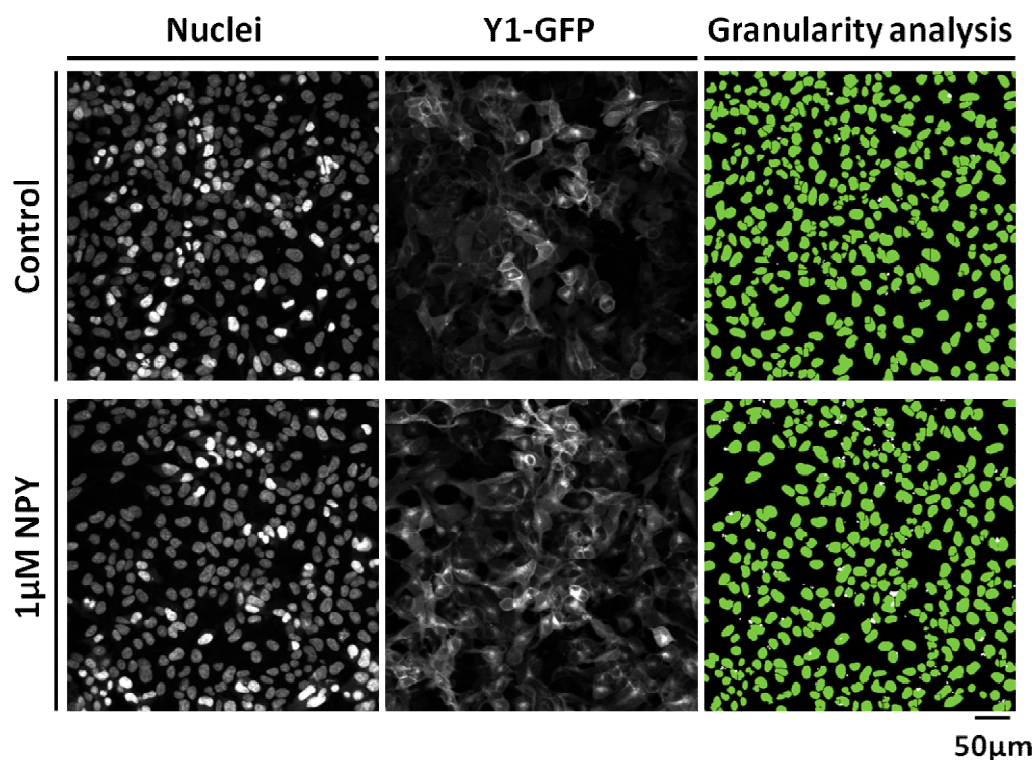


**Figure 2.14: Representative images of automated confocal imaging and quantitative analysis of Y1-GFP receptor internalisation in response to NPY stimulation**  
 Representative images show Y1-GFP receptors stably expressed in HEK293TR cells following control (HBSS/0.1% BSA) or 1μM NPY stimulation (30min at 37°C/5%CO<sub>2</sub>). The inclusion of a nuclear stain (H333442) identified nuclei (granularity analysis panel; green spots). Concurrent use of a granularity algorithm on sets of paired images allowed the quantification of internalised fluorescence on a per cell basis. This fluorescence was identified as granules of 3-15μm in diameter (Granularity analysis panel; white spots). Stimulation with 1μM NPY resulted in marked internalisation of Y1-GFP receptors. This was reflected in an increase in the number of intracellular granules quantified when compared to control images.

For both Snap 647 images (Snap labelled receptor population; Snap Receptor-Yn) and BiFC dimer images (Snap Receptor-Yn / Receptor-Yc population) granule size was kept consistent; for investigations using Y receptors granule size was set to 3-15μm in diameter, with granule size set to 2-15μm in diameter for β2AR receptors. Fluorescence intensity thresholds differed for the two wavelengths used, but were again set based comparison between negative (vehicle) and

positive (1 $\mu$ M NPY for NPY Y receptors and 10 $\mu$ M Isoprenaline for  $\beta$ 2AR receptors) plate controls.

All automated image analysis data was exported as an Excel spreadsheet and analysed using GraphPad Prism 5 (Prism 5.02; GraphPad Software Inc, San Diego, CA).

#### **2.2.10.3.1 Concentration response curves measured using plate reader assays**

Data was normalised to the top concentration of the specific full agonist used (eg. 1 $\mu$ M NPY for NPY Y1 receptors or 10 $\mu$ M Isoprenaline for  $\beta$ 2AR). Concentration response curves were fitted to pooled data from at least 3 individual experiments using non linear least squares regression (Prism 5.02; GraphPad). Additionally some data sets were expressed where appropriate as percentage fold increase over basal with all data constrained at basal values to 100%. Hill slopes were fitted freely but constrained to a maximum of 2. If a maximum response could be defined agonist pEC<sub>50</sub> values were stated (expressed as  $-\log EC_{50}$ ; pEC<sub>50</sub>) as mean  $\pm$  standard error of the mean and responses fitted as defined by the equation:

$$\text{Response} = \frac{R_{\text{max}} \cdot [\text{Agonist}]^n}{[\text{Agonist}]^n + EC_{50}^n}$$

Where R<sub>max</sub> is the maximum response and n is the Hill Slope.

#### **2.2.10.3.2 Antagonist pretreatment**

Responses following antagonist pretreatment were analysed using the Gaddum equation to determine the affinity of the competitive antagonist used. Firstly the concentration ratio (CR) was determined as the ratio of the agonist EC<sub>50</sub> value in the absence and presence of a particular concentration of antagonist ([B]). The antagonist equilibrium dissociation constant (K<sub>b</sub>) was then calculated using the equation:  $K_b = [B] / (CR - 1)$

The K<sub>b</sub>, equilibrium dissociation constant represents the concentration of antagonist required at equilibrium to occupy 50% of receptors. Each individual K<sub>b</sub> value from independent experiments was pooled and expressed as mean  $\pm$  standard error of the mean.

#### 2.2.10.3.4 Timecourse of stimulation

Timecourse experimental data were analysed using single phase association kinetics using Prism 5. A latency period (typically of 2 minutes) was included where appropriate to account for the delay between agonist addition and initial response, as indicated in the relevant Figure legends.

#### 2.2.11 FCS

##### 2.2.11.1 Autocorrelation analysis

In FCS the pinhole of the microscope objective can be positioned to create a Gaussian shaped confocal detection volume ( $\sim 0.25\text{fl}$ ) on a region of interest, such as the plasma membrane of a cell. As fluorescently tagged moieties diffuse through this volume they produce time dependent fluctuations in detected fluorescent intensities. Autocorrelation analysis compares the size of a fluctuation ( $\delta I$ ) with the mean fluorescent intensity ( $\langle I \rangle$ ) at time  $T$  with that of a subsequent fluctuation at time  $T+\tau$ . Using the whole range of  $\tau$  values, the autocorrelation function ( $G(\tau)$ ) can be derived, which is then normalised to the square of the mean intensity measured ( $\langle I \rangle$ ). The autocorrelation function is thus:  $G(\tau) = 1 + \langle \delta I(T) \cdot \delta I(T+\tau) \rangle / \langle I \rangle^2$  (Figure 2.12C).

Non linear curve fitting of data derived from the autocorrelation function using a biophysical model, was used to produce an autocorrelation decay curve (see Figure 2.12, panel C). From this curve, specific parameters of the fluorescent particles within the confocal detection volume can be defined, namely the average dwell time ( $\tau_D$ ) representing the halfway point of the  $G(\tau)$  decay (Bridson and Hill, 2007) and the average particle number  $N$ , from its inverse relationship to the autocorrelation function at time zero ( $G_0$ ).

Experimental calibration using a fluorophore with a known diffusion coefficient, in this case rhodamine 6G ( $D = 3 \times 10^{-6} \text{ cm}^2 \text{ s}^{-1}$ ), alongside the structural parameter obtained in calibration, allowed the volume and waist radius of the confocal volume to be determined per experiment ( $\omega_0 = (4D \cdot \tau_D)^{1/2}$ ). This volume, in

conjunction with individual  $\tau D$  values allowed the diffusion coefficients ( $D$ ) of the fluorescently tagged receptor or complex to be calculated using the equation  $D = \omega^2_0 / 4\tau D$ . The concentration of 2D limited fluorescent particles (ie. receptors expressed in plasma membranes) within the confocal detection volume, was derived using the equation  $N / (\pi\omega^2_0)$ .

The model chosen for curve fitting of calibration reads was 1x3D free, as it incorporates movement in x,y and z dimensions. Very rapid fluctuations ( $< 10 \mu s$ ) were also recorded of excited fluorophore electrons exhibiting delayed decay and emission. This property, termed the triplet factor, was accounted for by a pre-exponential term (not shown) in the 1x3D model chosen (1x3D + Triplet):

$$G(\tau) = 1 + \frac{1}{N} \cdot \sum_{i=1}^m \cdot f_i \cdot \left(1 + \frac{\tau}{\tau_{Di}}\right)^{-1} \cdot \left(1 + \frac{\tau}{S^2 \cdot \tau_{Di}}\right)^{-\frac{1}{2}}$$

In addition to components already described,  $m$  is the total number of components (in this case  $m=1$ ),  $f_i$  is the fractional contribution that component  $i$  attributes to the curve (in this case 1), and  $S$  is the structural parameter related to the shape of the confocal volume.

A 2D model, was used to fit traces of GFP tagged receptors and BiFC complexes as this model only incorporates diffusion in x and y within the plasma membrane.

This model also incorporates a fast pre-exponential component ( $< 10 \mu s$ ) that accounts for on-off transitions in fluorescence, termed 'blinking', that is a consequence of the photophysics of GFP. In this fit, the number of components ( $m$ ) was 2. The following equation was used for fitting traces to a 2D model:

$$G(\tau) = 1 + \frac{1}{N} \cdot \sum_{i=1}^m \cdot f_i \cdot \left(1 + \frac{\tau}{\tau_{Di}}\right)^{-1}$$

This model typically gave two dwell times,  $\tau D_1$  and  $\tau D_2$ , as well as  $f_i$  in terms of the percentage each component contributes to the overall amplitude of the autocorrelation curve at  $G_{(0)}$  ( $\tau D_1$  % and  $\tau D_2$  %).

### **2.2.11.2. Photon counting histogram (PCH)**

In a subset of FCS experiments, the raw fluctuation measurements were also exported and analysed using photon counting histogram (PCH) analysis (Chen et al., 1999). Unlike autocorrelation analysis which describes the temporal behaviour of fluorescence fluctuations, PCH analysis is concerned with the variations that occur in the amplitude of excitation intensity in different parts of the confocal volume. PCH analysis can provide information on molecular brightness ( $\epsilon$ ) and an alternative calculation of particle concentration. When performing PCH analysis, the fluorescence trace is divided into bins of a specific time. For diffusion of receptor GFP (dwell time  $\sim 40$  ms) for example, a bin time of 1 ms was chosen throughout to be less than the dwell time of the fluorescent species but to exclude more rapid time dependent fluctuations attributed to the photophysics of the fluorophore.

The photon counts in each bin were counted, with a frequency histogram generated with the x axis representing the number of photon counts  $k$  and the y axis the number of bins containing those counts  $k$ . This histogram deviates from an expected Poisson distribution due to the uneven illumination of the confocal volume, whereby the greatest excitation is found in the centre of the volume. This deviation from the ideal Poisson distribution can be measured in PCH analysis, and a fit modelled on the number ( $N$ ) and the molecular brightness ( $\epsilon$ ) of fluorescent species.

PCR calibration reads (rhodamine) were fitted to a 1 component model. The purpose of this calibration was to provide a first order correction value ( $F$ ), which accounts for deviation from a Gaussian observation volume when using single photon rather than 2 photon excitation (Huang et al., 2004). This value was then used in the analysis of experimental data, using 1 or 2 component PCH models with a bin time set to 1msec.

### 2.2.12 Calculating diffusion coefficients from FRAP recovery curves

A one phase exponential model was used to fit FRAP recovery curves using data previously corrected for background fluorescence and global bleaching of the image (Zen 2010 software, Zeiss, Jena, Germany). The following equation was used:

- $I(t) = I_0 - I_1 \cdot e^{-t/T_1}$

$I_0$  is the final intensity value of recovered fluorescence,  $I_1$  is the amplitude of the recovered fraction,  $T_1$  is an exponential decay time and  $t$  equals time.

$t_{1/2}$  times of recovery were calculated using the equation:

- $t_{1/2} = T_1 \ln 0.5$

Percentage of mobile fractions (F1) were calculated using:

- $F1 = 100 \cdot I_1 / (I_B - I_A)$

where  $I_B$  is the initial fluorescence intensity pre bleaching and  $I_A$  is the fluorescence intensity recorded post bleaching.

Diffusion coefficients of fluorescence recovery were calculated using the equation:

- $D = \text{radius of bleached area}^2 / 4 \cdot t_{1/2}$

### 2.2.13 Statistical analysis

Multiple comparisons between data sets were compared using GraphPad Prism one way analysis of variance (ANOVA) and Dunnett's post tests to determine statistical significance (Chapters 3, 5 and 6). For FCS, PCH and FRAP measurements (Chapter 4), a normal distribution of diffusion co-efficient data was not assumed, and the non parametric Kruskal-Wallis test followed by Dunn's post test was used to determine statistical significance between groups.

Student's unpaired t tests were used to test significance in all other experiments.

All data throughout is expressed as mean  $\pm$  standard error of the mean (s.e.m).

**Table 2.1: Oligonucleotide primers used for polymerase chain reactions and mutagenesis reactions**

Receptor	Primer sequence	T <sub>m</sub> (°C)	% GC	Length
<b>PCR</b>				
Human Y5 - Forward	GAGT <b>GGATCC</b> GATTTAGAGCTCGACGAGTATTATAAC	70	43	37
Human Y5 - Reverse	ATTAG <b>CGGCCG</b> CATATGAAGACAGTGTATAAGG	73	47	34
<b>Mutagenesis rat Y1 Phosneg (Y15A)</b>				
First round forward (3 mutations)	GCATACGGACGTGGCCAAGGCTGCTTTGAAGC	79	59	32
First round reverse	GCTTCAAAGCAGCCTTGCCACGTCCGTATGC			
Second round forward (2 mutations)	CTATAGCCATGGCAGCCATGCATAC	68	52	25
Second round reverse	GTATGCATGGCTGCCATGGCTATAG			

Bolded regions show restriction enzyme sites.

**Table 2.2: The use of antibiotics in maintaining cells in culture**

		Antibiotic resistance			
Parent cell line	Cell line	cDNA Construct	Receptor plasmid	Concentration	Experimental use
HEK293T	Zeocin	Snap Y1-Yn; $\beta$ arrestin2-Yn	pcDNA 3.1 zeocin	200 $\mu$ g ml <sup>-1</sup>	BiFC constrained dimers, $\beta$ -arrestin2 association
HEK293T	Neomycin (G418)	Y1-Yc; $\beta$ 2AR-Yc	pCMV FLAG	0.8mg ml <sup>-1</sup>	BiFC constrained dimer, BiFC $\beta$ -arrestin2 association
HEK293TR	Blasticidin	For tetracycline operon	pcDNA4/TR	5 $\mu$ g ml <sup>-1</sup>	Internalisation, FCS

A table summarising the antibiotics used in routine cell culture, the parent cell line plasmid they select for and the selection concentration used.

**Table 2.3: Table of tagged constructs used throughout this thesis.**

Host vector	N terminal tag	cDNA insert	C terminal tag	Bacterial resistance	Mammalian resistance	Tetracycline inducible	Plasmid map
<b>pcDNA3.1 zeocin</b>	Snap	Y1 (rat)	Yn	Ampicillin	Zeocin	No	Figure 2.4
	Snap	Y15A (rat)	Yn	Ampicillin	Zeocin	No	
	Snap	$\beta$ 2AR (human)	Yn	Ampicillin	Zeocin	No	
		$\beta$ -arrestin2	Yn	Ampicillin	Zeocin	No	Figure 2.7
		$\beta$ -arrestin2	Gn (sf)*	Ampicillin	Zeocin	No	
		$\beta$ -arrestin2LIEFD	Gn (sf)	Ampicillin	Zeocin	No	
		$\beta$ -arrestin1	Gn (sf)	Ampicillin	Zeocin	No	
<b>pCMV</b>	FLAG	Y1 (rat)	Yc	Kanamycin	Neomycin	No	Figure 2.5
	FLAG	Y1	Gc (sf)	Kanamycin	Neomycin	No	
	FLAG	Y16A	Yc	Kanamycin	Neomycin	No	
	FLAG	Y16A	Gc (sf)	Kanamycin	Neomycin	No	

	FLAG	Y15A (rat)	Yc	Kanamycin	Neomycin	No	
	FLAG	Y1Y199A(rat)	Yc	Kanamycin	Neomycin	No	
	FLAG	Y4 (human)	Yc	Kanamycin	Neomycin	No	
	FLAG	Y5 (human)	Yc	Kanamycin	Neomycin	No	
	FLAG	$\beta$ 2AR (human)	Yc	Kanamycin	Neomycin	No	
	FLAG	$\beta$ 2ARN322A (human)	Yc	Kanamycin	Neomycin	No	
	FLAG	$\beta$ 2ARY326A (human)	Yc	Kanamycin	Neomycin	No	
<b>pcDNA4/TO</b>	FLAG	Y1 (rat)	GFP (sf)	Ampicillin	Zeocin	Yes	Figure 2.6
	FLAG	Y4 (human)	GFP (sf)	Ampicillin	Zeocin	Yes	
	FLAG	Y5 (human)	GFP (sf)	Ampicillin	Zeocin	Yes	
	FLAG	Y2 (rat)	GFP (sf)	Ampicillin	Zeocin	Yes	
	FLAG	Y2H155P (rat)	GFP (sf)	Ampicillin	Zeocin	Yes	Figure 2.6

\*sf abbreviation refers to superfolder GFP

**Table 2.4: Table detailing the parameters required for seeding of cells depending on the experimental use.**

Cell seeding				
Plate layout	Cell density/cell	Volume/well	Day plated	Experimental use
<b>96 well</b>				
HEK293T	40, 000	100 µl	Day prior	Platereader experiments
HEK293TR	20, 000	100 µl	2 days prior	Platereader experiments
<b>24 well</b>				
HEK293T	100, 000	500 µl	2 days prior	Inhibition of cAMP accumulation
<b>8 well</b>				
HEK293T	50, 000	300 µl	Day prior	Confocal microscopy, FCS, FRAP
HEK293TR	25, 000	300 µl	2 days prior	Confocal microscopy, FCS, FRAP

**Table 2.5: Laser excitation and emission spectra for use with the IX Ultra confocal plate reader**

	Laser excitation	Fluorophore emission	Laser power	Laser gain
<b>H33342 (cell nuclei)</b>	405nm	447/60nm	40%	500
<b>BiFC (recomplemented YFP or GFP)</b>	488nm	525/50nm	50%	550
<b>Receptor-GFP (superfolder)</b>	488nm	525/50nm	30%	500
<b>Snap receptor</b>	647nm	685/40nm	35%	500

**Table 2.6: Laser excitation and emission spectra for use with a confocal Zeiss LSM 510**

	Laser excitation	Laser type	Emission filter	Laser power	Gain
<b>BiFC (recomplemented YFP or GFP)</b>	488nm	Argon	BP 505-530nm	3%	850-1000
<b>Receptor-GFP (superfolder)</b>	488nm	Argon	BP 505-530nm	3%	800-900
<b>Snap receptor</b>	633nm	Helium-Neon	LP650nm	15%	800-900

BP = band pass filter; LP = long pass filter

## **Chapter 3: Measurement of $\beta$ -arrestin2 recruitment and endocytosis of fluorescently tagged NPY Y receptors using high content imaging and automated analysis**

### **3.1 Introduction**

#### **3.1.1 The importance of fluorescence based imaging techniques**

Fluorescence based imaging techniques provide the opportunity to visualise cellular proteins, such as GPCRs, in their native environment at a single cell level. Recent advances in both the fluorescence proteins themselves and imaging techniques have allowed the spatial and temporal resolution of protein-protein interactions in living and fixed cells. This is particularly important as many of these interactions are involved in the regulation of a wide range of physiological processes. For example the recruitment of  $\beta$ -arrestins has been implicated in regulating GPCR desensitisation, endocytosis, and subsequent trafficking (see Chapter 1; section 1.6) as well as directing signalling in their own right to produce therapeutically relevant outcomes (Chapter 1, section 1.7).

A variety of techniques have been used to selectively visualise receptors and other proteins in cells. Some of these are theoretically applicable to receptors in their native environment. For example antibodies conjugated to fluorophores offer potentially high labelling as they selectively recognise a small receptor peptide epitope expressed on the target protein. However this epitope must be of high enough selectivity to minimise non specific binding and antibodies (particularly those that are monoclonal) are expensive. In respect to GPCRs, fluorescent ligands are an alternative label as they both identify receptor expression and act as a pharmacological probe (Kuder and Kiec-Kononowicz, 2008). However a caveat of this technique is that the addition of a fluorescent label can adversely affect the affinity of a ligand for its target receptor, and the localisation of ligands and their receptors may

differ during intracellular trafficking. However fluorescent imaging of proteins within a cell, more often requires genetic modifications to target proteins. Snap tagging can be used to attach a fluorophore to the protein itself. This is a modified form of a DNA repair enzyme, which covalently binds a synthetic probe (most often a fluorophore) transferred from a benzyl guanine substrate, and can be inserted as genetically engineered tag attached to the target protein (see Chapter 5 for further details on Snap tag labelling). This technique minimises non specific labelling as the probe is chemically inert in respect to other proteins. Genetically encoded full length fluorescent protein tags also offer an alternative method of labelling, and do not require the addition of exogenous substrates. Both fluorescent protein (typically 27 kD) and the Snap tag enzyme (20 kD) represent substantive modifications to the labelled receptor, which may potentially affect function. As the fluorescent protein is encoded alongside that of the target protein, labelling is theoretically of a 1:1 stoichiometry. However to improve their effectiveness as biological labels, naturally occurring fluorescent proteins have required engineering.

### **3.1.2 The engineering of fluorescent proteins for use in biological assays**

The isolation and subsequent cloning of green fluorescent protein (GFP) from the jellyfish species *Aequorea Victoria* (Prasher et al., 1992) combined with advances in microscopy, has revolutionised the imaging of biological processes in single cells. Fluorescent proteins have also been isolated from other species, such as DsRed from the sea anemone *Discosoma* (Patterson, 2007). The elucidation of the crystal structure of GFP revealed a 11 stranded beta barrel wrapped around a central alpha helix (Figure 3.1, A; Ormo et al., 1996)). Each strand consists of 9-13 residues linked by inter-strand loops. During maturation the chromophore is buried inside the beta barrel, ultimately resulting in the production of fluorescence. A photon hitting the chromophore excites an electron from its ground state to an excited energy state. When the electron falls back to its lower state, it loses energy either by emitting a photon or from heat or vibration (Figure 3.1B). This emitted

photon is of lower energy and therefore a longer wavelength than the excited photon. This is manifested as a difference (in terms of the frequency or wavelength) in the maximum peaks observed for the fluorescence absorption and emission spectra. This difference is termed the Stokes shift (Figure 3.1C).

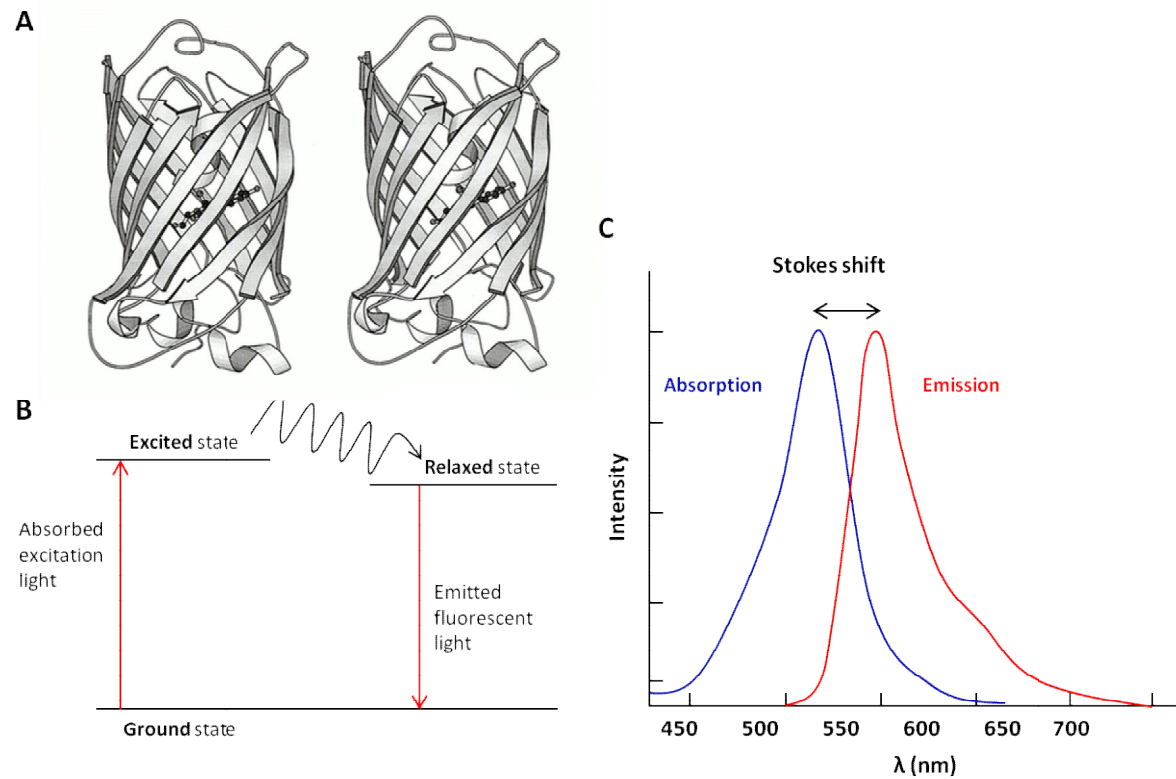


**Figure 3.1: The tertiary structure of GFP**

The tertiary structure of GFP is shown in A, with the central residues that form the chromophore shown as a ball and stick representation (A). The 11  $\beta$  strands surrounding the chromophore are also shown. Panel B shows the principle of electron excitation and emission. Absorption of light by the chromophore excites an electron from a ground state of energy to a higher energy state. The energy lost upon returning to a relaxed state is emitted as photons of a longer wavelength than that originally absorbed. This shift in frequency or wavelength of light is illustrated in C and is termed the Stoke's shift.

Figure A was taken from (Tsien, 1998).

Maturation of the chromophore in GFP and GFP derived polypeptides is a multistep process consisting of a folding step, followed by the formation of the native conformation of the protein and finally oxidation of an internal tripeptide which becomes the core of the chromophore (Ser65-Tyr66-Gly67; (Heim et al., 1995)). However wildtype GFP has some properties that make its use as a biological label in mammalian cells unsuitable, such as a relatively low quantum yield and poor folding and maturation at 37°C (Patterson, 2007). To address some of these limitations, selective mutations were introduced into the wildtype GFP sequence. An initial mutation at serine residue 65 to threonine resulted in GFP with increased quantum yield and crucially a single excitation peak which lessens potential ultraviolet excitation, avoiding damage to living cells (Heim et al., 1995). An additional mutation was then introduced at F64L which resulted in accelerated chromophore maturation at 37°C and was termed eGFP (Cormack et al., 1996). The rate of folding, chromophore maturation, fluorescence intensity and thermostability of the protein at 37°C was further improved by additional mutation of the eGFP sequence. These included the 'cycle 3' mutations (F99S, M153T and V164A) which increased fluorescence intensity compared to wildtype GFP due to improved folding efficiency (Cramer et al., 1996) as well as substitutions at residues S30R, Y39N, N105T, Y145F, I171V and A206V. All wildtype GFP derived fluorescent proteins have a tendency to form dimers, albeit at high ( $\mu\text{M}$ ) concentrations. This property is undesirable in biological assays, as it can lead to the atypical localisation and disrupted function of any labelled proteins. Therefore a lysine substitution was also introduced at alanine residue 206 (A206K) which inhibited the formation of GFP dimers (Zacharias et al., 2002). These 11 mutations resulted in a GFP variant, that was more suitable for use in fluorescence based biological assays and was termed superfolder GFP (Pedelacq et al., 2006). As for A206K, the A206V substitution was introduced, based upon theoretical modelling of dimeric GFP, to hinder the probability of superfolder GFP forming dimers (Pedelacq et al., 2006). The S30R substitution is the greatest contributor to increasing folding rate and

efficiency at 37°C by mediating the formation of an electrostatic network of residues in  $\beta$  strands 1, 2, 5 and 6. This increased the inherent stability of the structure even when fused to a poorly folding protein partner. These mutations ultimately resulted in the fluorescence intensity of GFP being 60% greater than that of eGFP with no changes to either excitation or emission spectra.

Both the eGFP and GFP forms can be used as biological tags to label proteins of interest, such as GPCRs, in order to investigate the pharmacological properties of these receptors.

### **3.1.3 GFP variants – Yellow Fluorescent Protein**

The eGFP sequence has been further engineered to produce coloured variants with different excitation and emission spectra (from blue to orange). This is typically done by substituting residues in the immediate environment surrounding the chromophore with residues that are spatially similar. Of these the yellow variant (eYFP) was produced by a substitution of a threonine residue that lies close to the chromophore at position 203 with tyrosine (T203Y). However eYFP has a relatively slow folding and maturation rate at 37°C, as well as being sensitive to pH and halides. Therefore additional mutations were introduced to address these limitations resulting in the variant form Venus YFP (vYFP) (Nagai et al., 2002). The principle mutation, F46L is responsible for increasing the rate of folding and chromophore maturation at 37°C by accelerating the oxidation of Tyr66 residue within the internal tripeptide at the core of the chromophore. This F46L mutation is specific to YFP, as the same mutation introduced into eGFP and other GFP variants had no effect upon maturation. 4 additional ‘folding mutations’ were also introduced; F64L, M153T, V163A, S175G which are also shared with other GFP variants. All enhanced folding and maturation at 37°C by introducing highly flexible smaller side chains outside the  $\beta$  barrel structure within the connecting loop regions. These 4 mutations were also effective at decreasing pH and halide sensitivity of vYFP. However they did not have any significant effect upon fluorescent intensities, when compared to eGFP (100%), with

relative brightness values being 151% for eYFP and 156% for vYFP respectively.

### **3.1.4 The use of fluorescent proteins**

Full length fluorescent proteins have been expressed in a wide range of species including mammalian, nematode, plant, insect, fungi and yeast cells (reviewed in (Tsien, 1998) ). Theoretically GFP derived proteins can be expressed in any cell amenable to genetic modification (Hu et al., 2002). The intrinsic fluorescence of these proteins means there is no requirement for external substrates. Additionally unlike immunolabelling techniques (such as antibody conjugates) no cell permeabilisation or fixation is required. Fluorescent protein expression appears to be well tolerated by live cells, and is easily detected using standard FITC excitation and emission filters (for GFP) on a fluorescence microscope.

Arguably the most successful use of fluorescent proteins has been in directly labelling proteins of interest in order to visualise their subcellular location. The gene encoding the fluorescent protein is fused in frame with that of the gene encoding the target protein, (Kallal and Benovic, 2000). The resulting chimera is then expressed in the cell, effectively in a 1:1 stoichiometry. Protein-GFP fusions have been successfully identified in a range of organelles including secretory vesicles, the endoplasmic reticulum, Golgi apparatus, mitochondria, peroxisomes and nucleus (reviewed in (Tsien, 1998)). They have also been used to label plasma membrane spanning proteins, including GPCRs. The  $\beta$ 2-adrenoceptor was the first GPCR to be successfully labelled with eGFP (Barak et al., 1997a) and was then followed by labelling of GPCRs spanning all classes of the superfamily (reviewed in (Kallal and Benovic, 2000)). For example, both N terminal eGFP (Gicquiaux et al., 2002) and C terminal vYFP (Kilpatrick et al., 2010) tags have been used to investigate the agonist induced internalisation of NPY Y1 receptors.

Fluorescent proteins tags have also been used to study the real time dynamics of protein-protein interactions, such as the recruitment of proteins from the cytosol to the plasma membrane. For example the desensitisation and

endocytosis of many activated GPCRs, has been shown to be dependent upon interaction with  $\beta$ -arrestin (Chapter 1; section 1.6). This association has been visualised at a distinct range of GPCRs such as the  $\beta$ 2-adrenoceptor, dopamine D<sub>1</sub> and angiotensin II type 1A receptors by imaging the fluorescence redistribution of GFP tagged  $\beta$ -arrestin2 from the cytosol to the plasma membrane following receptor activation (Barak et al., 1997b, Zhang et al., 1996). This technique was also sensitive enough to show trafficking of  $\beta$ -arrestin2-GFP to distinct subcellular locations depending on the stability of its interaction with specific GPCRs (Zhang et al., 1996).

### **3.1.5 Protein Complementation Assays**

The use of fluorescent tags to label proteins can provide useful information on their cellular distribution and co-localisation with other structures (for example  $\beta$ -arrestin-GFP with GPCRs). However colocalisation can only imply but not resolve protein-protein interactions. Standard light microscopy is limited in spatial resolution by Abbe's limit which states that a point source of light must form a diffraction limited spot 150 - 250 nm in diameter, depending on wavelength and the numerical aperture of the lens .

However there are a range of fluorescence based techniques that can be used to investigate protein-protein interactions indirectly including fluorescence resonance energy transfer (FRET), fluorescence lifetime imaging microscopy (FLIM), bioluminescence resonance energy transfer (BRET) which can be used singularly or in conjunction with each other (Ciruela et al., 2014). Protein complementation assays (PCA) offer a further option for discretely identifying the molecular composition of protein complexes (Diekmann and Hoischen, 2014). A 'reporter' protein is split into its complementary N and C terminal fragments, which are both fused to proteins of interest. Upon close association of the two proteins, the fragment tags are able to re-fold and produce a readout indicative of specific protein-protein interactions (Kerppola, 2008b, Hu and Kerppola, 2003). Initial assays produced an enzymatic readout, with fragments of  $\beta$ -galactosidase or dihydrofolate reductase used (reviewed in (Kerppola, 2008a, Michnick et al., 2011)).

However in order to visualise many of these interactions an exogenous chromogenic or fluorogenic substrate is required, which can risk disrupting the environment surrounding the PCA complex, for example through cell lysis. Therefore PCA's utilising fluorescent protein fragments were developed which exploit the intrinsic fluorescence produced when fluorescently tagged proteins interact within living cells (Kerppola, 2013, Ghosh et al., 2000). This modification was termed bimolecular fluorescence complementation (BiFC).

### **3.1.6 Bimolecular Fluorescence Complementation (BiFC)**

In bimolecular fluorescence complementation (BiFC), fluorescent proteins (for example vYFP) are split into their complementary N and C terminal fragments. Proteins of interest (such as receptor and  $\beta$ -arrestin2) are covalently tagged with these fragments (see Figure 2.2) which themselves are not fluorescent (Hu et al., 2002). However upon protein association, the fragments are brought into close proximity and refold to reform the full length fluorescent protein (Rose RH, 2010). The resulting fluorescent signal acts as a readout of tagged protein-protein interaction. Fluorescence complementation was initially demonstrated using split eGFP fused to leucine zippers of transcription regulatory proteins both *in vitro* and in *E coli* (Ghosh et al., 2000). This assay was then modified using eYFP fragments to successfully visualise the interaction of Fos and Jun transcription factors *in vitro* and in living transfected mammalian COS cells (Hu et al., 2002). BiFC has now been successfully used in a wide range of cell systems such as bacteria, yeast, insect, plant and mammalian (Kerppola, 2009, Vidi and Watts, 2009) using a wide variety of fluorescent protein fragments (Kodama and Hu, 2012).

As the beta barrel of the fluorescent protein must be present in order to maintain the complex network of polar residues surrounding the chromophore (Ormo et al., 1996), the location of the split point, typically within the loops connecting individual  $\beta$ -strands of the barrel, is crucial to successful complementation. In this work, the fluorescent protein tags generated from vYFP or superfolder GFP (see Chapter 4), contained an overlapping region of residues meaning that  $\beta$  strand 8 was repeated at this

break point in both the N (residues 2-172 termed Yn or Gn) and C terminal (residues 155-238 termed Yc or Gc) fragments. For both vYFP and GFP this break point was between  $\beta$  strands 7-8 (amino acids 154/155) or  $\beta$  strands 8-9 (amino acids 172/173). The use of BiFC fragments with an overlapping region has been shown to aid the refolding process (Hu and Kerppola, 2003) and increase the kinetics of BiFC development when compared to using fragments that lack this overlap (Kilpatrick et al., 2010).

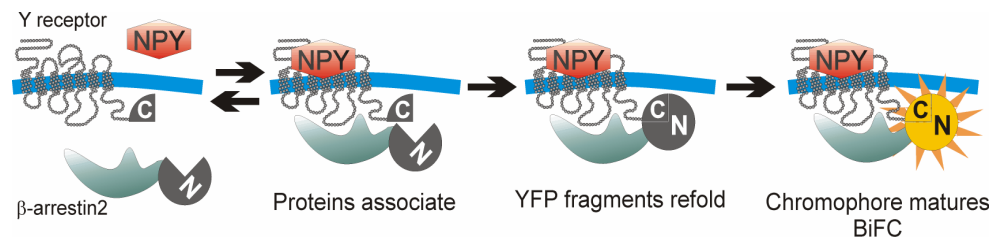


**Figure 3.2: The principle of using BiFC to investigate the interaction of Y receptor subtypes with  $\beta$ -arrestin2.**

Y receptor subtypes were tagged at the C terminal domain with a fragment of Venus YFP (Yc). The complimentary vYFP fragment (Yn) was covalently attached to the C terminus of  $\beta$ -arrestin2. Following addition of the agonist NPY, the receptor then associates with  $\beta$ -arrestin2, bringing the two fluorescent fragments into close proximity allowing them to refold to form the full length YFP. Following a period of maturation, the chromophore then matures to produce a fluorescent signal which can act as a readout of receptor-  $\beta$ -arrestin2 association (Kilpatrick et al., 2010) (see Chapter 2, 2.2.5.3).

One of the reasons for using BiFC in this thesis, as opposed to other PCA's or FRET is that the subcellular localisation of receptor- $\beta$ -arrestin2 complexes could be visualised directly using single wavelength measurements on a standard confocal plater reader. Quantification of this fluorescent 'BiFC signal' using automated analysis provided an indirect measure of the recruitment of  $\beta$ -arrestin2 to activated receptors (Kilpatrick et al., 2010).

### **3.2 Aims of this chapter**

The main aims of this chapter are to undertake a quantitative comparison of the relative abilities of different Y receptor subtypes to recruit  $\beta$ -arrestin2 and undergo regulatory endocytosis. This will be achieved by using GFP tagging of Y receptor subtypes, or YFP BiFC fragment tagging of Y receptor (receptor-Yc) and  $\beta$ -arrestin2 (Yn). The extent to which these two processes (Y receptor internalisation and  $\beta$ -arrestin2 binding) are correlated will be investigated by quantifying agonist and antagonist pharmacology using high content imaging techniques and automated analysis.

Targeted amino acid substitutions in both the Y1 and Y2 receptor sequences of potential  $\beta$ -arrestin interaction motifs, will be performed to investigate whether the molecular mechanisms involved in  $\beta$ -arrestin2 binding and receptor endocytosis are comparable.

### 3.3 Results

#### 3.3.1 The use of full length fluorescent protein tags to investigate the agonist induced internalisation of Y1 and Y2 receptors.

Y1 or Y2 receptor-GFP cDNA was expressed in HEK293TR cells with receptor expression induced using tetracycline 18hr prior to experimentation (see Chapter 2, section 2.2.2.4). To verify expression of Y1-GFP and Y2-GFP constructs, competition [<sup>125</sup>I] PYY binding was initially performed. Displacements of specific binding for Y1-GFP membranes are shown in Figure 3.3. Both agonist (PYY; A) or a non peptide Y1 antagonist (BIBO3304; B) were able to displace specific [<sup>125</sup>I] PYY binding. Compared to the Y1 subtype, Y2-GFP exhibited increased PYY binding affinities, consistent with its documented higher affinity (Gehlert et al., 1996a, Krause et al., 1992). For both Y1 and Y2-GFP, GTPγS was able to inhibit [<sup>125</sup>I] PYY binding by disrupting the formation of the high affinity Y receptor-G protein complex (Figure 3.3, C) (Kilpatrick et al., 2012). Additionally Bmax estimates indicated that expression levels were comparable between both cell lines. This validation of receptor function (in respect to ligand binding and G protein coupling) was important as the addition of the relatively large GFP tag may adversely affect receptor function. The expression of receptor-GFP constructs was also confirmed using confocal fluorescent imaging. In the absence of tetracycline treatment, no GFP fluorescence was observed for any cell line (Figure 3.4). Following treatment with vehicle (HBSS/0.1% BSA; 30min at 37°C) predominantly plasma membrane localised GFP fluorescence was observed for both native and mutant Y1 (A) and Y2-GFP tagged receptors (B). Cells were then stimulated with the endogenous agonist NPY (1μM; 30min at 37°C) and the same region of cells imaged. Marked receptor internalisation was observed for the Y1 receptor-GFP, represented as highly intense punctuate regions of internalised GFP fluorescence (granules). Internalisation was also observed for Y2-GFP receptors following this high concentration of NPY. However detecting more subtle differences in agonist potency between these subtypes required more quantitative automated imaging of receptor internalisation.

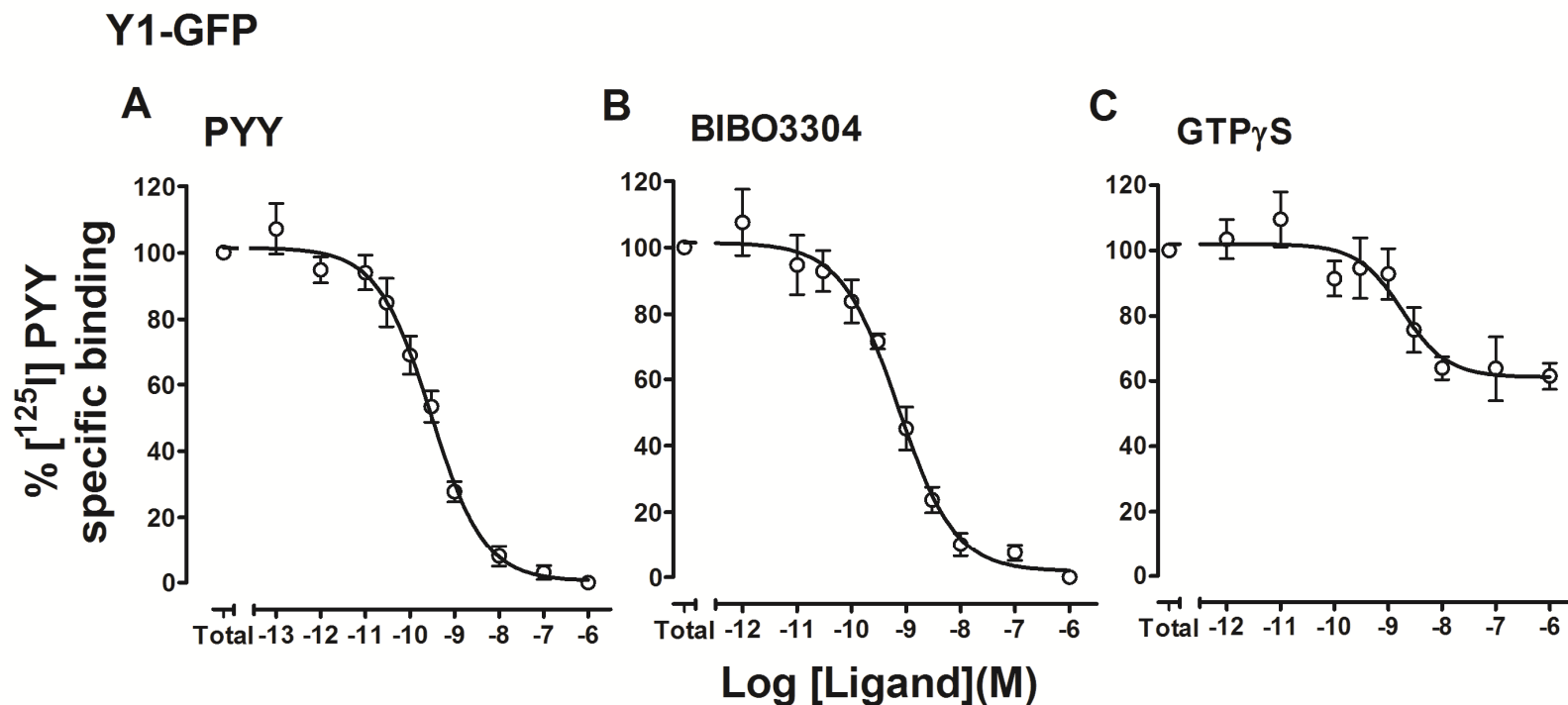


**Figure 3.3: [<sup>125</sup>I] PYY competition binding experiments in HEK293TR cell membranes stably expressing Y1-GFP receptors**

Membranes freshly prepared from HEK293TR cell lines stably expressing Y1-GFP were incubated with [<sup>125</sup>I] PYY (15pM) and increasing concentrations of unlabelled PYY (A), BIBO3304 (B) or GTP<sub>γ</sub>S (C) for 90min at 22°C. Membrane bound radioligand was separated using filtration and quantified using a gamma counter. Competition displacement curves were generated using GraphPad Prism, with pooled data representing 4 independent experiments. Data was expressed as mean ± s.e.m (Hill slope range 0.72-1.0).

**Table 3.1: [<sup>125</sup>I] PYY membrane competition binding parameters derived from Y receptor-GFP and BiFC HEK293T cell lines**

Cell line	PYY	BIBO3304	GTPγS		Bmax
	pIC <sub>50</sub>	pIC <sub>50</sub>	pIC <sub>50</sub>	% inhibition	fmol/mg <sup>-1</sup>
<b>Y1</b>	9.5 ± 0.2		9.0 ± 0.2	68.6 ± 6.7	1500 ± 700
<b>Y16A</b>	9.2 ± 0.1		8.8 ± 0.2	72.9 ± 7.0	2300 ± 100
<b>Y2</b>	10.8 ± 0.1		8.8 ± 0.1	69.2 ± 5.4	2200 ± 300
<b>Y2H155P</b>	10.6 ± 0.1		8.7 ± 0.2	46.9 ± 10.2	2100 ± 200
<b>Y1/A2</b>	9.8 ± 0.1	9.0 ± 0.1	9.1 ± 0.2	58.6 ± 4.1	350 ± 60
<b>Y16A/A2</b>	9.6 ± 0.1	9.1 ± 0.2	9.0 ± 0.1	63.2 ± 1.2	340 ± 30
<b>Y2/A2</b>	11.1 ± 0.1		9.2 ± 0.1	73.8 ± 3.5	1190 ± 120

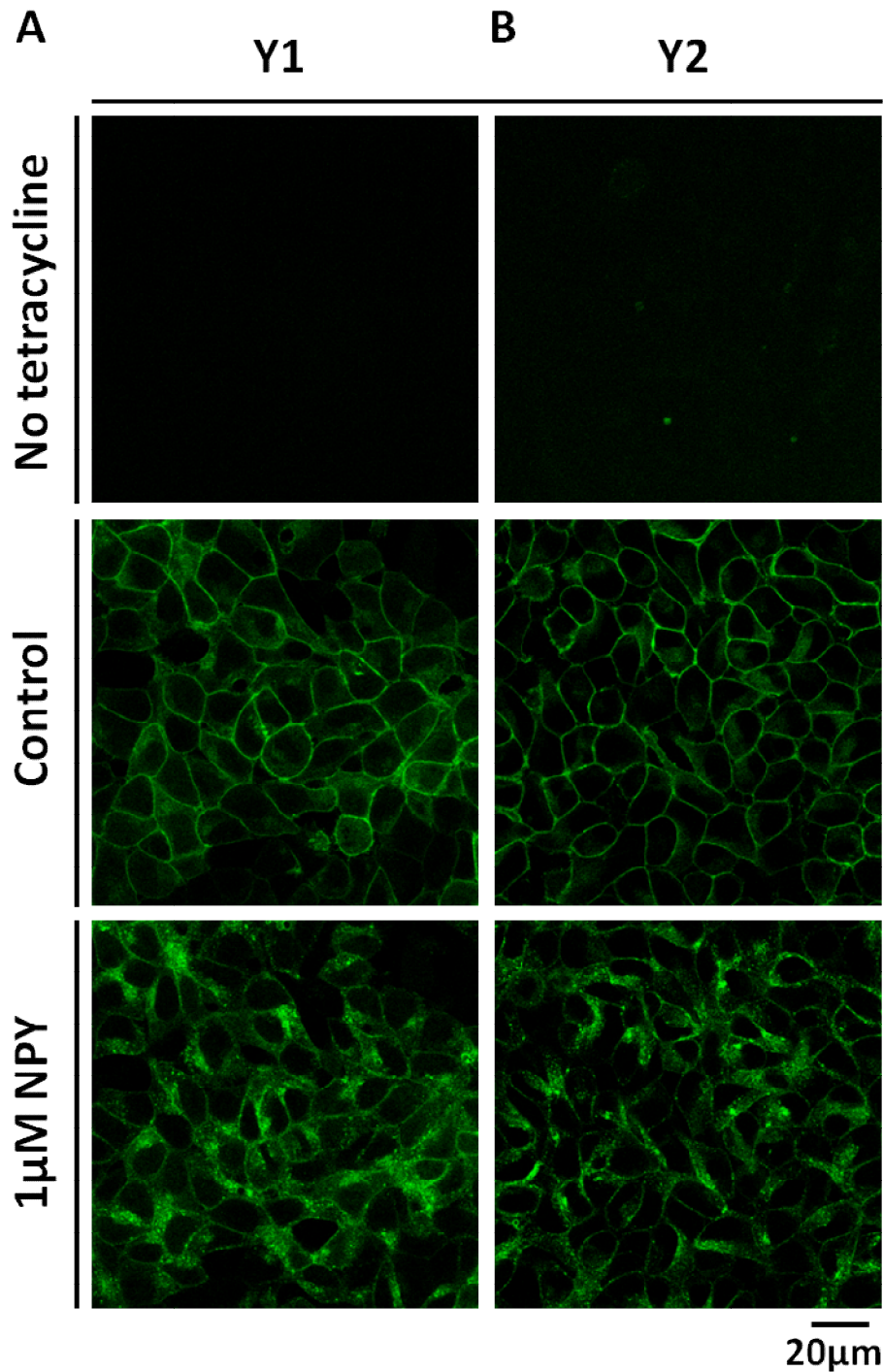
All parameters were obtained from [<sup>125</sup>I] PYY competition membrane binding experiments as described in Chapter 2, section 2.2.3.

Details of receptor mutations are given in the text.

% inhibition of TSB refers to the displacement by 1μM competing ligand, as a % of the total specific binding (TSB) defined in the absence / presence of 1 μM PYY.

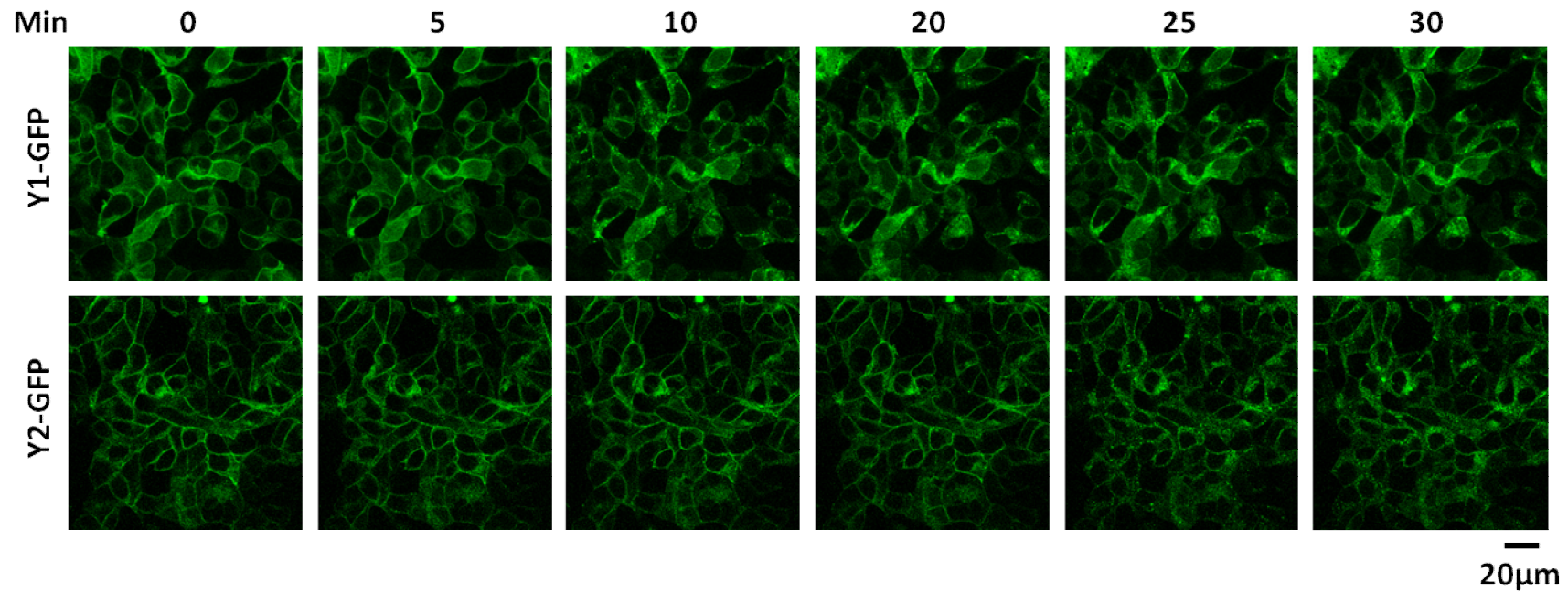
n =3-4 independent experiments

Table was reproduced from (Kilpatrick et al., 2010, Kilpatrick et al., 2012).



**Figure 3.4: The addition of full length superfolder GFP to the respective C termini of both wildtype and mutated Y1 (A) and Y2 (B) receptors, can be used to visualise agonist induced receptor internalisation.**

HEK293TR cells were stably transfected with Y1 (A) or Y2 (B) receptors fused to full length superfolder variant of GFP. No receptor expression was observed in the absence of tetracycline treatment 18hr prior to imaging ( $1 \mu\text{g ml}^{-1}$ ). Cells were treated with vehicle or  $1\mu\text{M}$  NPY (30min at  $37^\circ\text{C}$ ) and imaged live using a Zeiss LSM 510 confocal microscope with laser excitation at 488nm. Images are from the same field of view before ("control") and after NPY treatment - representative of those acquired from 4 independent experiments.



**Figure 3.5: 30min timecourse stimulation of Y1-GFP and Y2-GFP cells with 100nM NPY**

HEK293TR cells stably expressing Y1-GFP or Y2-GFP were stimulated with 100nM NPY over a 30min timecourse. Representative images of the same region of cells were imaged at 5min intervals using a LSM510 confocal platereader.

Firstly a timecourse of NPY stimulation was used to determine an appropriate assay timepoint (Figure 3.5). Both Y1-GFP (A) and Y2-GFP (B) were stimulated over a 30min timecourse with 100nM NPY (37°C) with the same region of cells imaged at 5min intervals. By 10min noticeable internalisation was observed for Y1-GFP that was maintained until 30min. Y2-GFP internalised at a slower rate with noticeable internalisation only seen from 20min stimulation. Additionally timecourse experiments using YFP tagged Y1 receptor, have illustrated rapid NPY induced internalisation ( $t_{1/2}$  2.4min  $\pm$  0.3; n=3) that reaches saturation at 20min (timecourse length 1-120min) (Kilpatrick et al., 2010). A 30min time period was therefore chosen for all future investigations of agonist induced internalisation of both subtypes. Y2-GFP receptor internalisation responses in particular, were noticeably less with 100nM NPY compared to 1 $\mu$ M NPY (Figure 3.4, B) suggesting that quantification of responses could reveal subtle differences in subtype specific ligand potencies.

### **3.3.1.2 The use of automated high content imaging to quantify Y receptor subtype specific ligand pharmacology**

Manual imaging of HEK293T cells expressing Y1 or Y2-GFP constructs using a confocal microscope (Figure 3.4) provided visual validation of receptor expression and internalisation. However this is of relatively low throughput and qualitative images cannot quantify the degree of receptor internalisation without further manual image analysis. In order to address this, fluorescently tagged constructs were imaged in a 96 well plate format using an automated confocal platereader (IX Ultra, MDC). Like a standard confocal microscope, this provided qualitative images that revealed the subcellular location of receptor GFP tagged constructs following vehicle and agonist treatment (Figure 3.6, 3.7A). After stimulation with vehicle (HBSS/0.1% BSA; 37°C), all receptor constructs were localised predominantly to the plasma membrane with a small degree of constitutive internalisation observed for both receptors. Following treatment with NPY, pronounced intracellular regions of highly intense internalised GFP fluorescence were observed for both receptors.

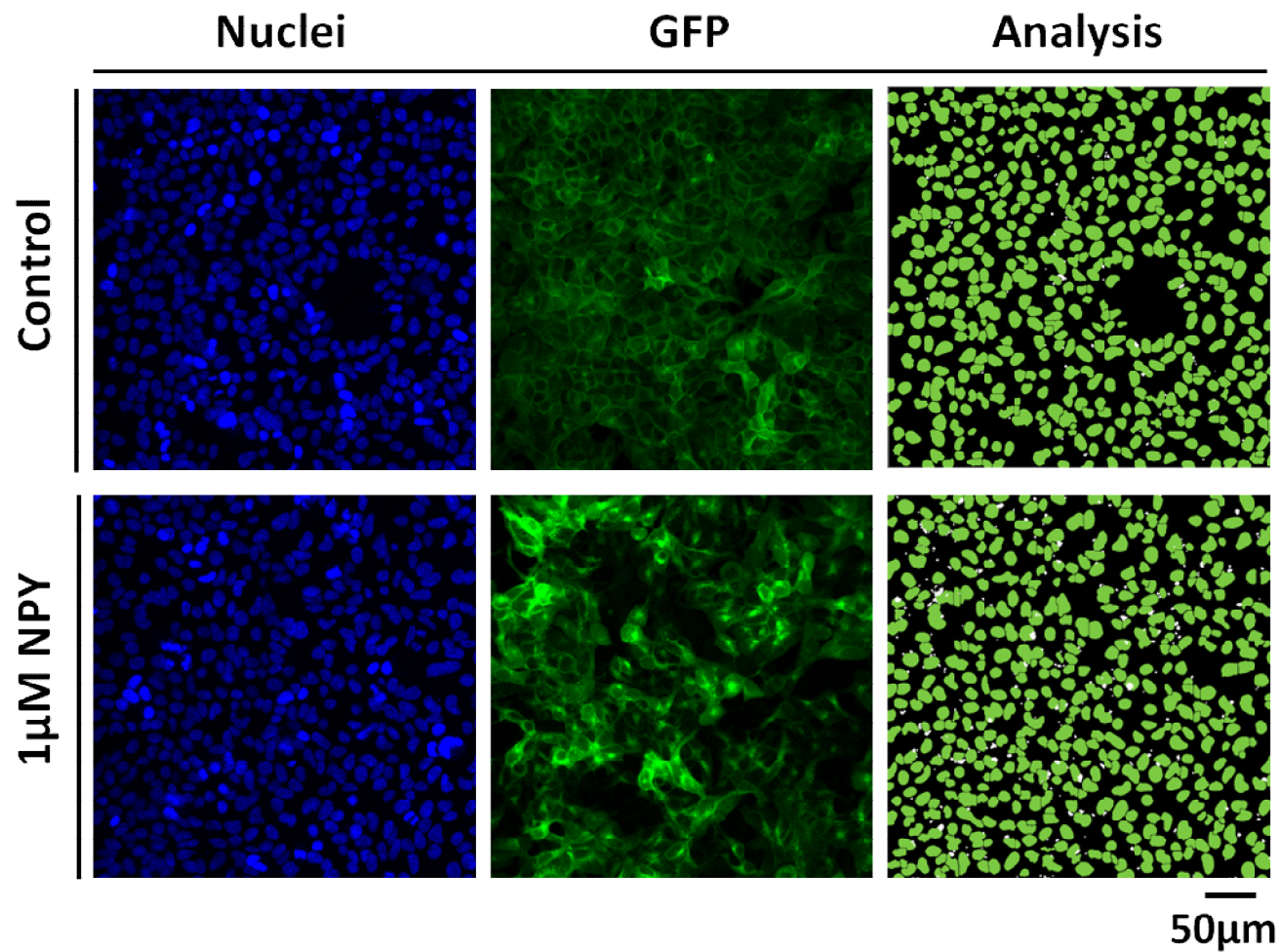


**Figure 3.6: The principle of applying a granularity algorithm to images of Y1-GFP receptor internalisation acquired using a confocal plate reader**

Representative images show Y1-GFP receptors treated with vehicle or 1μM NPY (30 min at 37°C). Cells were fixed, and nuclei stained using H33342. Cells were then imaged using an IX Ultra confocal plate reader, with appropriate laser excitation used for imaging cell nuclei (**Nuclei**) and receptor-GFP (**GFP**). A granularity algorithm was applied (**Analysis**) which identified cells (shown in green) from the parallel image of stained nuclei, in addition to 3-15μm punctuate regions of internalised receptor termed 'granules' (white spots).

A granularity algorithm was then applied to paired nuclei and GFP images. Internalised GFP fluorescent compartments were defined on the basis of diameter (3-15 $\mu$ m) and threshold intensity (see Chapter 2, section 2.2.10.3 for more detail). These punctuate regions termed 'granules' were identified as white spots (Figure 3.6; Analysis). Cell nuclei were identified according to a set diameter range (shown as green spots). This analysis was then used to derive full NPY concentration response courses for Y1 and Y2 receptors (Figure 3.7, B and C). Data was expressed as fold over basal to allow responses of cell lines to be compared. The endogenous agonist NPY was a full agonist stimulating the internalisation of Y1-GFP receptors with a pEC<sub>50</sub> value of  $8.4 \pm 0.2$  (30min at 37°C; n=4; Figure 3.7, B). However NPY was 63 fold less potent in inducing the internalisation of Y2-GFP receptors (n=4) with appreciable internalisation only seen at concentrations in excess of 100nM NPY (Figure 3.7, C). This was in keeping with the noticeable difference in the extent of Y2-GFP internalisation observed in confocal imaging performed using 100nM (Figure 3.5) or 1 $\mu$ M NPY (Figure 3.4).

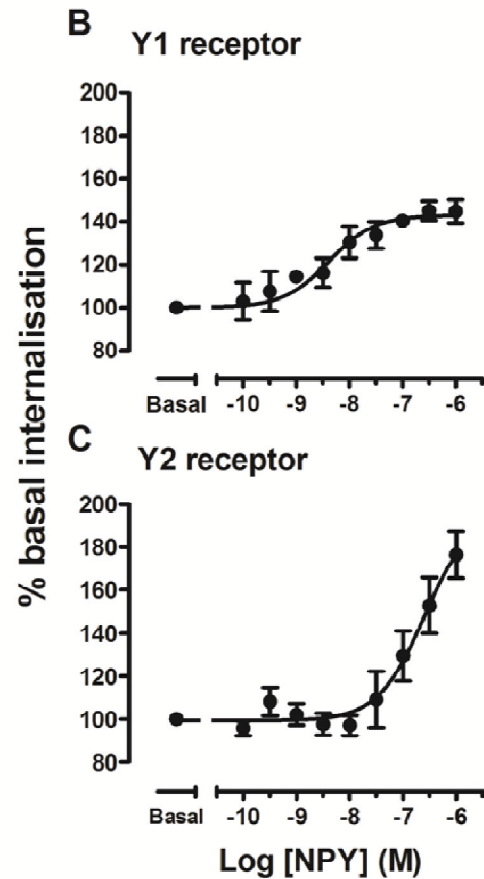
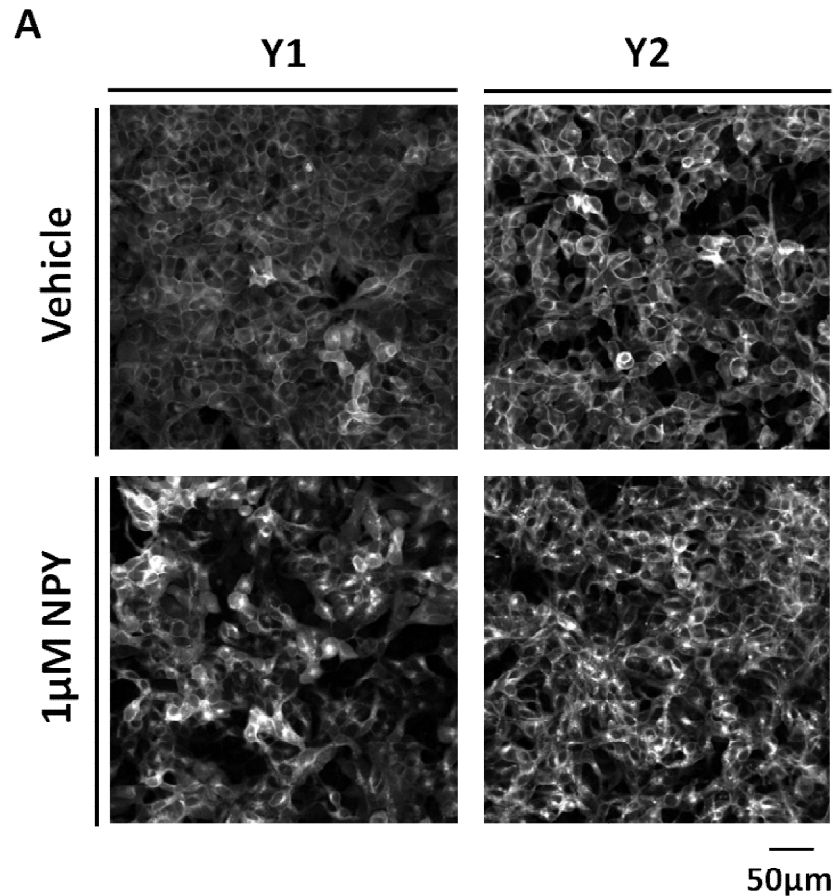


**Figure 3.7: Quantitative analysis of agonist induced internalisation of native and mutant Y receptors**

HEK293TR cells were stably transfected with Y1-GFP or Y2-GFP. Receptor expression was induced following pretreatment with tetracycline ( $1\mu\text{g ml}^{-1}$ ) for 18hr. Y1-GFP or Y2-GFP (A) receptors were treated with either vehicle or  $1\mu\text{M}$  NPY (30min at  $37^\circ\text{C}$ ) and then imaged using an IX Ultra confocal plater reader (only GFP images are shown here). A granularity algorithm was applied to acquired images (as detailed in Figure 3.4). Quantification of receptor internalisation was expressed as the average vesicle count per cell, and was normalised as a percentage above basal responses. Data from at least 3 independent experiments were pooled and NPY concentration response curves derived for Y1-GFP (B) and Y2-GFP (C) receptors.  $\text{pEC}_{50}$  values are stated in the text.

### 3.3.1.3 Subtype selective pharmacology of agonist stimulated Y receptor internalisation

High content imaging was then used to investigate the potency of a panel of ligands at inducing the internalisation of the four cloned Y receptor subtypes (Figures 3.7 and 3.8). Subtype specific ligands were also used to ensure that selectivity was maintained in respect to potency and efficacy following GFP tag addition. The Y4 and Y5 subtypes were also tagged with full length GFP and stably expressed in HEK293TR cells. Receptor expression for all cell lines was induced using tetracycline (1µg/ml) 18hr prior to the assay. All responses were normalised to the reference 1µM NPY for Y1-GFP, Y2-GFP and Y5-GFP and 100nM PP for Y4-GFP respectively. Figure 3.9 shows the initial comparisons for key agonists using these cell lines (with Figure 3.7 NPY data for Y1-GFP (A) and Y2-GFP (B) also included for comparison, normalised this time to the reference concentration). An overall summary of potency data for each receptor-GFP is found in Table 3.2.

Compared to the reference NPY (Figure 3.9, A), pancreatic polypeptide (PP) showed reduced efficacy at inducing Y1 receptor internalisation with a maximal response of  $18.3 \pm 3.3$  % (n=4) when normalised to 1µM NPY responses. A Y1 peptide antagonist GR231118, reported previously to increase Y1 receptor internalisation (Pheng et al., 2003) showed no activity at inducing Y1-GFP internalisation (n=3). In contrast PP was the most potent agonist at promoting Y4 receptor internalisation, with NPY showing comparatively lower potency and efficacy (Figure 3.9, C). The Y4 selective agonist GR231118 showed partial agonism in respect to PP, with a maximal responses of  $28.4 \pm 7.4$  % (pEC<sub>50</sub> of  $7.1 \pm 0.3$ ; n=5).

Y5-GFP internalisation proceeded at a somewhat slower rate compared to other Y receptor subtypes. Therefore a 60min incubation time, rather than 30min, was used when measuring Y5-GFP agonist concentration response curves in order to increase response windows. NPY stimulated internalisation of Y5-GFP receptors with a pEC<sub>50</sub>  $8.0 \pm 0.1$  (D; n=6). PP also showed maximal responses similar to NPY. The Y5 selective agonist cPP (1-17)(Ala,Aib) 18-36

NPY (referred to as cPP-Aib NPY (Cabrele et al., 2000)), was a potent stimulator of Y5-GFP internalisation, maximum responses  $94.6 \pm 1.1$  % (n = 4) relative to that of the positive reference ligand (1 $\mu$ M NPY).

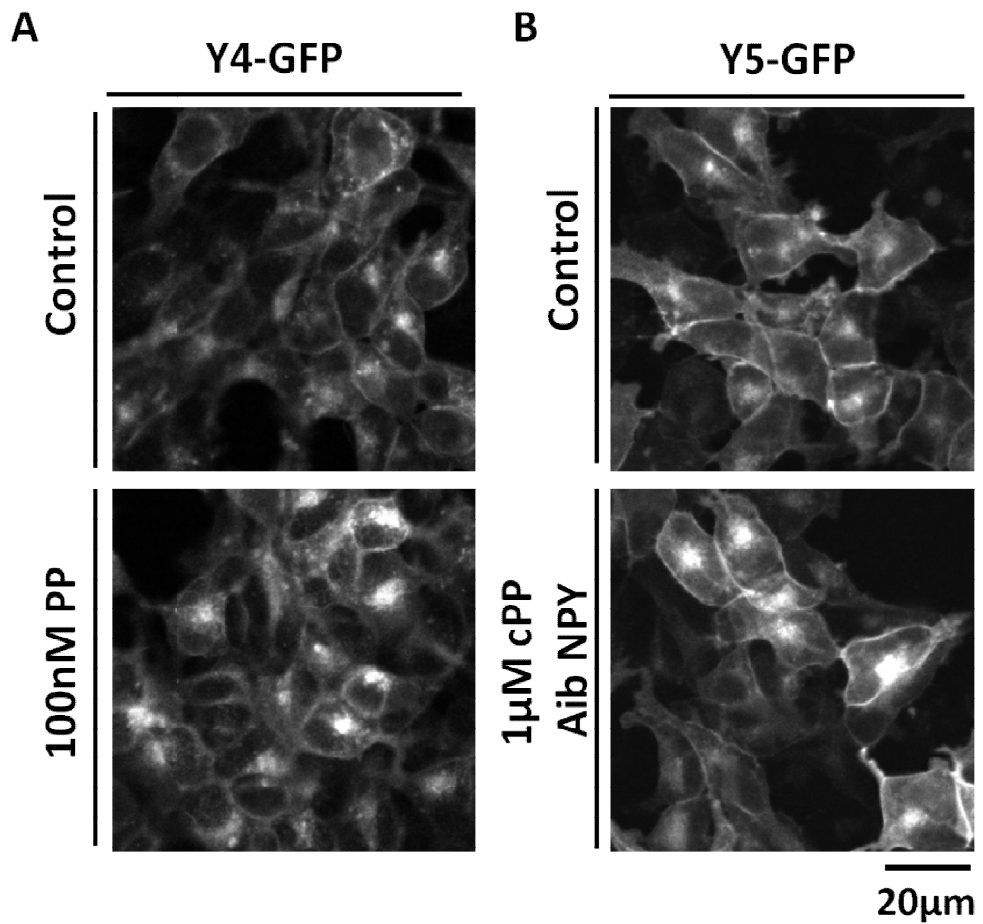


**Figure 3.8: Representative confocal images of Y4-GFP and Y5-GFP receptors stimulated with subtype selective agonists**

Representative images show Y4-GFP or Y5-GFP receptors treated with vehicle or 100nM PP (30min at 37°C) or 100nM cPP-Aib-NPY (60min at 37°C) respectively. Cells were fixed, and nuclei stained using H333342. Cells were then imaged using an IX Ultra confocal platerreader. These images represent a 300x300 pixel cropped region.

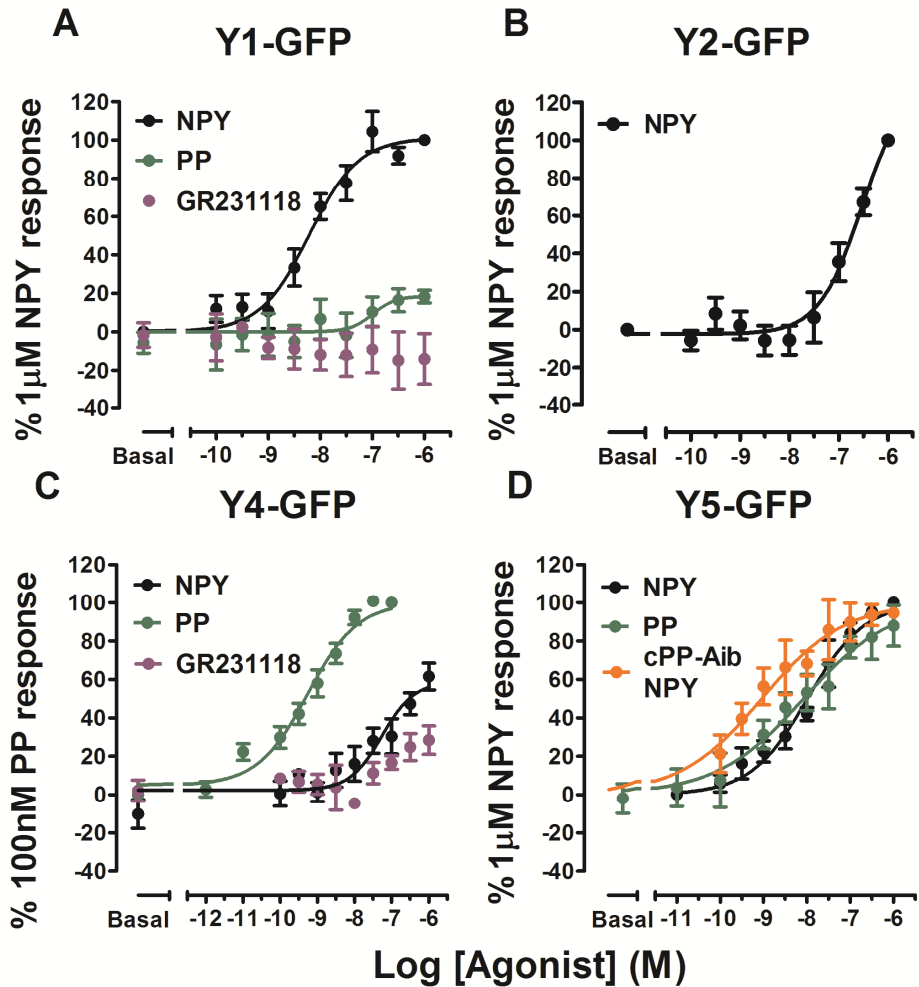


**Figure 3.9: Quantification of the agonist induced internalisation of GFP tagged NPY receptors in response to a panel of ligands.**

Y1, Y2, Y4 and Y5 GFP tagged receptors were stably transfected into HEK293TR cells, with expression induced following pretreatment with tetracycline ( $1\mu\text{g ml}^{-1}$ ) for 18 hr prior to assay. Cells were treated with a panel of subtype selective ligands for 30min for Y1, Y2 and Y4 receptors and 60min for the Y5 subtype. All assays were performed at  $37^\circ\text{C}$ , prior to fixation, nuclei staining and imaging using an IX Ultra confocal platerreader. Granularity analysis of these images allowed for quantification of agonist induced internalisation. All data were normalised to vehicle (basal) and maximal  $1\mu\text{M}$  NPY responses for Y1 (A), Y2 (B) and Y5 receptors (D) and  $100\text{nM}$  PP for Y4 receptor responses (C). Data were pooled from 3-9 individual experiments.

**Table 3.2: Summary of potencies and efficacies of a panel of ligands for stimulating internalisation of GFP tagged NPY receptor subtypes**

Ligand	Y1-GFP		Y2-GFP		Y4-GFP		Y5-GFP	
	pEC <sub>50</sub>	E <sub>max</sub> (%)						
<b>NPY</b>	8.2 ± 0.1	100	N.D	/	N.D	61.4 ± 6	8.0 ± 0.1	100
<b>PP</b>	7.0 ± 0.1	18.3 ± 3.3			9.0 ± 0.2	100	8.1 ± 0.1	94.6 ± 1.1
<b>GR231118</b>	N.D	N.D			7.1 ± 0.3	28.4 ± 7.4		
<b>cPP (Aib ) NPY</b>	N.D	N.D					9.0 ± 0.1	87.8 ± 10.7

All data were expressed as ± standard error of the mean. pEC<sub>50</sub> values were obtained from pooled concentration response curves presented in Figure 3.6. E<sub>max</sub> responses to each ligand were calculated as a percentage of 1µM NPY responses for Y1 and Y5-GFP, and as a percentage of 100nM PP responses for Y4-GFP.

N values for all data 3-4.

N.D = not determined

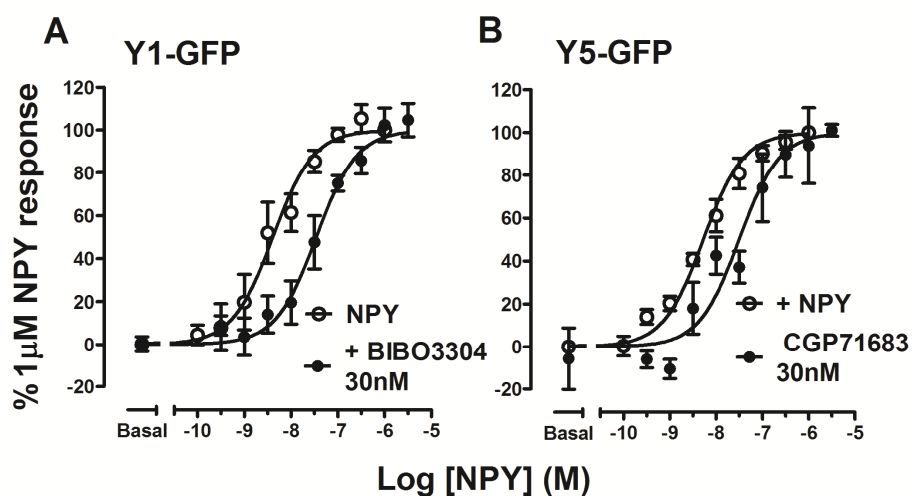


**Figure 3.10: The effect of antagonist treatment on Y1-GFP and Y5-GFP receptors**

HEK293TR cells stably expressing Y1-GFP (A) or Y5-GFP (B) were pretreated for 30min (37°C) with subtype selective antagonists BIBO3304 or CGP71683 (both 30nM) respectively. Both cell lines were then stimulated with a concentration response course of NPY (30min for Y1-GFP and 60min for Y5-GFP; 37°C/5% CO<sub>2</sub>). Cells were then washed, fixed, nuclei stained with H33342 prior to being imaged using a IX Ultra confocal platereader. Granularity analysis allowed the quantification of agonist induced internalisation. All data were normalised to vehicle (basal) and maximal 1µM NPY responses from a minimum of 4 experiments.

Antagonist pharmacology was then investigated for Y1-GFP and Y5-GFP receptors using subtype selective non-peptide antagonists. Cells were pretreated for 30min at 37°C with BIBO3304 (Y1) or CGP71683 (Y5) (Dumont et al., 2000), prior to stimulation with a concentration response course of NPY (30min for Y1-GFP; 60min for Y5-GFP). Both BIBO3304 and CGP71683 exhibited expected rightward parallel shifts of NPY induced receptor internalisation indicative of surmountable antagonism (Figure 3.10; A and B). pK<sub>b</sub> values were estimated at 8.8 ± 0.2 (n=4) and 8.2 ± 0.1 (n=3) for BIBO3304 and CGP71683 respectively.

### 3.3.2.1 Measuring the agonist induced association of $\beta$ -arrestin2 with Y1 receptors using automated imaging of BiFC responses

Quantification of the internalisation of GFP tagged NPY receptors is only an indirect indication of the effects of  $\beta$ -arrestin2 recruitment predicted to underlie their endocytosis (Ouedraogo et al., 2008, Holliday et al., 2005, Berglund et al., 2003b, Kilpatrick et al., 2010). Therefore, BiFC was used to directly measure the association between  $\beta$ -arrestin2 and Y receptors, initially focussing on the Y1 subtype. YFP C (Yc) and N terminal (Yn) fragments were fused to the C terminus of Y1 receptors and  $\beta$ -arrestin2 respectively (Figure 3.2). Stable HEK293T cells were generated that coexpressed clonal  $\beta$ arrestin2-Yn with mixed population Y1-Yc (cell line termed Y1/A2). [<sup>125</sup>I] competition PYY binding in Y1/A2 membranes (Kilpatrick et al., 2010) verified that PYY, BIBO3304 and GTP $\gamma$ S affinities were comparable to those observed for Y1-GFP. The generation of completed YFP fluorescence, indicative of an agonist stimulated association between Y1 receptors and  $\beta$ -arrestin2, was then imaged using an automated confocal platereader (Figure 3.11, A).

120 min timecourse stimulations using 100nM NPY indicated a  $t_{1/2}$  value of 10.4min  $\pm$  1.0 (n=3) in respect to Y1/A2 BiFC development, with responses reaching a sustained plateau at 60min (Kilpatrick et al., 2010). A 60min assay length was therefore chosen to assess the responses to a panel of agonists using the BiFC cell lines. Stimulation with the endogenous agonist NPY lead to a substantial increase in the accumulation of Y1/A2 BiFC complexes localised to intracellular compartments (Figure 3.11; A). Responses to PYY and the selective analogue [Leu<sup>31</sup>, Pro<sup>34</sup>] NPY were equipotent with NPY (Figure 3.11, B; Table 2.3). PP and the metabolite NPY<sub>3-36</sub> showed reduced potency and efficacy in respect to NPY. GR231118, reported previously to increase Y1 receptor internalisation (Pheng et al., 2003) showed no activity in Y1/A2 cells.

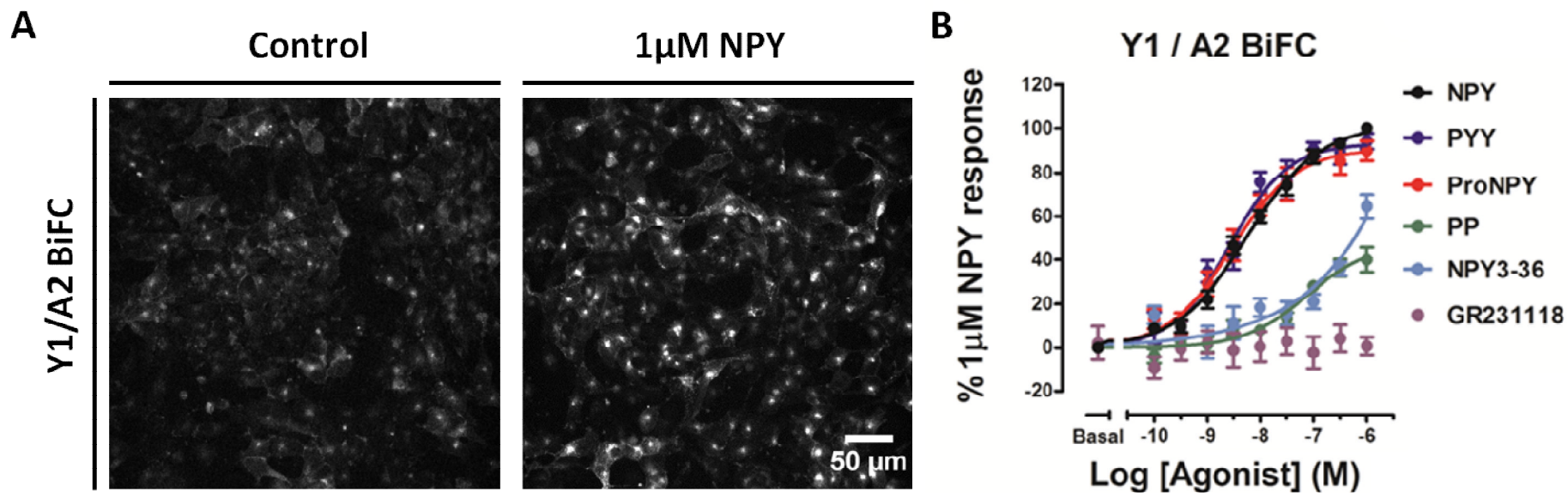


**Figure 3.11: Quantitative analysis of Y1/A2 BiFC agonist pharmacology**

HEK293T cells stably expressing Y1/A2 BiFC constructs were stimulated with a panel of ligands for 60min at 37°C/5% CO<sub>2</sub>, before imaging using a IX Ultra confocal plate reader. Representative images following vehicle and 1 $\mu$ M NPY stimulation are shown in panel A. Quantification of BiFC responses was assessed by applying a granularity algorithm to acquired images. All data were pooled and normalised to plate controls (vehicle and 1 $\mu$ M NPY) and expressed as mean  $\pm$  s.e.m (B). Data were pooled from at least 3 independent experiments.

Pro NPY refers to [Leu<sup>31</sup>, Pro<sup>34</sup>] NPY.

### 3.3.2.2 The use of BiFC to compare Y receptor subtype specific recruitment of $\beta$ -arrestin2

Following the validation of the BiFC assay at the Y1/A2 cell line, it was then used to investigate the agonist selectivity of other NPY receptor subtypes in respect to potency and relative maximal responses. HEK293T cells were stably co-transfected with mixed populations of Y2-Yc or Y4-Yc on top of a clonal population of  $\beta$ -arrestin2-Yn. The Y5/A2 cell line required double dilution cloning as expressing the Y5-Yc receptor as a mixed population resulted in low numbers of cells expressing both BiFC components.

Cell lines were treated with a panel of ligands (60min at 37°C/5%CO<sub>2</sub>) and concentration response curves derived following the quantification of internalised BiFC fluorescence (Figure 3.12). All responses were normalised to a reference compound 1 $\mu$ M NPY for Y1/A2 (A) Y2/A2 (B) and Y5/A2 (D) BiFC and 100nM PP for Y4/A2 (C) BiFC respectively. An overall summary of potencies for each Y receptor subtype is found in Table 2.3.

For the Y1/A2 cell line a rank order of potency of PYY>Leu<sup>31</sup>, Pro<sup>34</sup> NPY>NPY> was observed (Figure 3.11, 3.12A). NPY was also a full agonist at Y2/A2 BiFC but with a reduced potency when compared to Y1/A2 (26 fold less). The rank order of potency observed for Y2/A2 BiFC was PYY>PYY<sub>3-36</sub>>NPY>> Leu<sup>31</sup>, Pro<sup>34</sup> NPY (Figure 3.12, B).

PP was a full agonist at Y4/A2 as expected based on its documented potency (Lundell et al., 1995, Tough et al., 2006) with a 1000 fold increased potency and an increased efficacy compared to PP activity at Y1/A2. Y4/A2 showed a rank order of potency of PP>GR231118> PYY>NPY. Subtype selective activity was observed, in respect to the Y4 selective ligand GR231118 which was able to induce partial BiFC responses at Y4/A2 BiFC cells.

The Y5 subtype selective ligand cPP-Aib-NPY was equipotent to NPY at Y5/A2 cells as expected from its selectivity for this receptor subtype (Dumont et al., 2003). Furthermore PP and NPY<sub>3-36</sub> were also potent agonist.

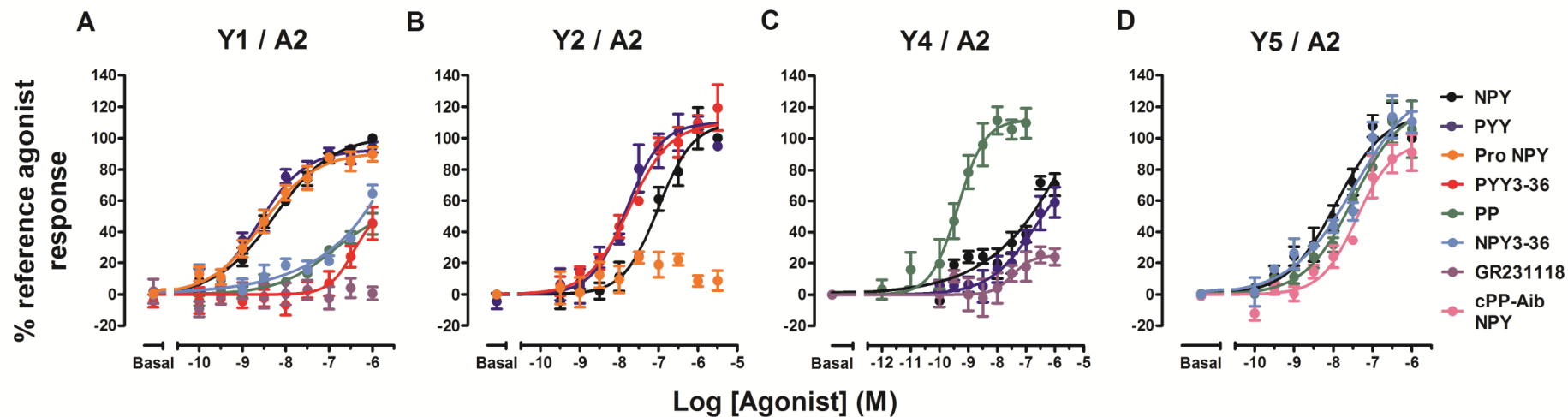


**Figure 3.12: Agonist induced NPY receptor /  $\beta$ -arrestin2 BiFC in response to a panel of ligands.**

HEK293T cells stably co-expressing Y receptor-Yc and  $\beta$ -arrestin2-Yn were stimulated with ligand for 60min at 37°C/5% CO<sub>2</sub>. Ligand responses were measured by performing granularity analysis of images acquired using an automated confocal plater reader. All data were normalised to plate controls of vehicle (basal responses) and maximal reference agonist concentration (1 $\mu$ M NPY for receptor subtypes Y1 (panel A), Y2 (panel B) and Y5 (D) and 100nM PP for the Y4 subtype (C)). All data were pooled from a minimum of 3 independent experiments, and expressed as mean  $\pm$  s.e.m.

**Table 3.3: Summary of potencies and efficacies of a panel of ligands for stimulating the internalisation of NPY receptor/A2 BiFC complexes**

Ligand	Y1/A2		Y2/A2		Y4/A2		Y5/A2	
	pEC <sub>50</sub>	E <sub>max</sub> (%)						
<b>NPY</b>	8.3 ± 0.1	100	7.1 ± 0.1	100	<6.5	70.6 ± 7.2	7.9 ± 0.1	100
<b>PYY</b>	8.5 ± 0.1	95.4 ± 3.4	7.8 ± 0.1	94.8 ± 1.5	6.8 ± 0.1	59.1 ± 9.8		
<b>[Leu<sup>31</sup>,Pro<sup>34</sup>] NPY</b>	8.5 ± 0.1	89.9 ± 4.5	N.D	8.6 ± 6.3				
<b>PYY<sub>3-36</sub></b>	6.4 ± 0.4	45.5 ± 10.4	7.7 ± 0.1	119.3 ± 14.7				
<b>PP</b>	6.3 ± 0.1	40.1 ± 5.8	/	/	9.5 ± 0.3	100	7.5 ± 0.2	105.7 ± 18.0
<b>NPY<sub>3-36</sub></b>	<6.5	64.5 ± 5.5	/	/			7.5 ± 0.2	110.3 ± 6.9
<b>GR231118</b>	/	/	/	/	7.5 ± 0.4	23.9 ± 5.3		
<b>cPP (Aib ) NPY</b>	/	/	/	/	/	/	7.4 ± 0.1	90.5 ± 11.5

All data were expressed as ± standard error of the mean. pEC<sub>50</sub> values were obtained from pooled concentration response curves presented in Figure 3.9. E<sub>max</sub> responses to each ligand were calculated as a percentage of 1µM NPY responses, with the exception of responses at Y4/A2 where they were expressed as a percentage of 100nM PP responses.

N values for all data 3-11.

N.D = not determined

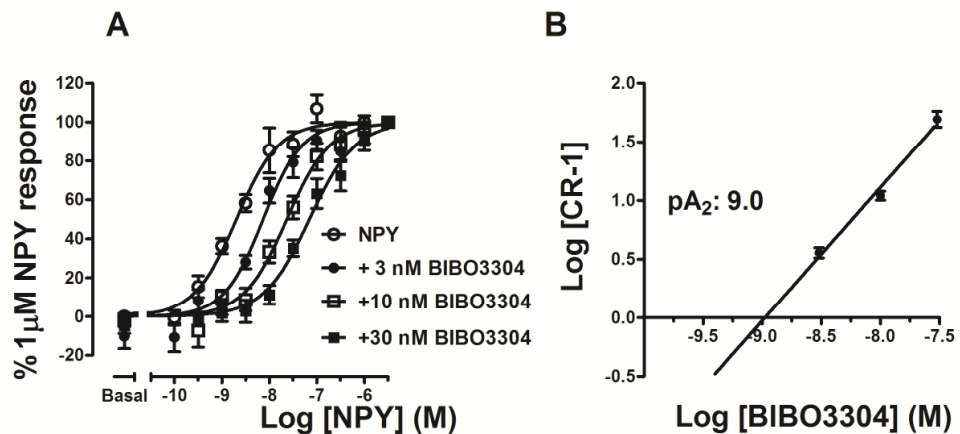


**Figure 3.13: The effect of pretreatment with antagonist on NPY stimulated Y1 / A2 BiFC**

Y1/A2 cells were pretreated with the antagonist BIBO3304 at the concentrations indicated for 30min at  $37^\circ\text{C}/5\% \text{CO}_2$ . Cells were then stimulated with NPY for 60min at  $37^\circ\text{C}/5\% \text{CO}_2$ . Granularity analysis was performed on images obtained using an automated confocal plater reader. Concentration response curves in the presence and absence of BIBO3304 were fitted (A), with a shared minimum, maximum and Hill slope constraints. Concentration ratios in respect to derived  $\text{EC}_{50}$  values were used to construct a Schild plot (B) to determine the  $\text{pA}_2$  value.

Y1/A2 BiFC responses in respect to antagonist pharmacology were also investigated. The Y1 selective antagonist BIBO3304, was able to inhibit the NPY induced Y1/A2 BiFC responses, showing rightward parallel shifts in the NPY concentration response curve indicative of surmountable antagonism (Figure 3.13, A). Schild analysis was used to calculate a  $\text{pA}_2$  value of  $9.0 \pm 0.1$  ( $n=5$ ; B).

### 3.3.3.1 Y1 and Y2 receptor mutants that alter agonist induced internalisation also affect $\beta$ -arrestin2 association to these subtypes

Point mutations were selectively introduced into the Y1 and Y2 receptor sequences (as described in section 2.2.1.1.1.2-3). For the Y1 receptor, an alanine substitution was introduced at Tyr 99 (Y99; see Figure 3.14, A; residue highlighted in blue) located at the top of TM2. This mutation has previously been shown to inhibit NPY binding (Sautel et al., 1995, Sautel et al., 1996). This receptor construct was termed Y1Y99A. Another set of mutations were

also separately introduced into the C terminal domain of the Y1 receptor. Alanine substitutions were made of 6 serine and threonine residues (S352A, T353A, T356A, S359A, T361A, S362A) previously implicated as sites phosphorylated by GRK's in receptor desensitisation (see Figure 3.14, A; residues highlighted in red). Mutation of these residues resulted in a 'phosphorylation negative' receptor that is incapable of  $\beta$ -arrestin2 dependent agonist induced internalisation (Holliday et al., 2005, Ouedraogo et al., 2008, Kilpatrick et al., 2010). This receptor was termed the Y16A receptor. A point mutation was also introduced into the Y2 receptor sequence with histidine residue 155 in the second intracellular loop being substituted with proline (see Figure 3.14, B; residue shown in red). The H155P mutation has been previously shown to enhance recruitment of  $\beta$ -arrestin2 to Y2 receptors (Marion et al., 2006, Ouedraogo et al., 2008) by reconstructing a necessary recognition motif implicated in regulating  $\beta$ -arrestin2 binding and  $\beta$ -arrestin2 mediated receptor internalisation for a variety of Class A GPCRs. This receptor construct was termed Y2H155P.

Competition binding experiments using [ $^{125}$ I] PYY were performed in membranes derived from HEK293TR cells stably expressing either Y16A-GFP or Y2H155P-GFP. Receptor expression was induced using tetracycline treatment 18hr prior to assay. At both receptor constructs, PYY and BIBO3304 were able to displace specific [ $^{125}$ I] PYY binding with comparable affinities to that seen for native Y1-GFP and Y2-GFP respectively (Kilpatrick et al., 2012). Both receptors were also sensitive to GTP $\gamma$ S treatment, and Bmax estimates of receptor expression were comparable to Y1-GFP and Y2-GFP preparations.

Confocal imaging was then performed to investigate the agonist induced internalisation of Y16A-GFP and Y2H155P-GFP receptors. For the phosphorylation negative Y16A mutant, no internalisation was observed in response to 1 $\mu$ M NPY following 30min stimulation (Figure 3.14, C). Internalisation in response to high NPY concentrations (1 $\mu$ M) was observed for mutant Y2H155P-GFP tagged receptors after 30min incubation at 37°C (Figure 3.14, C; Figure 3.15).

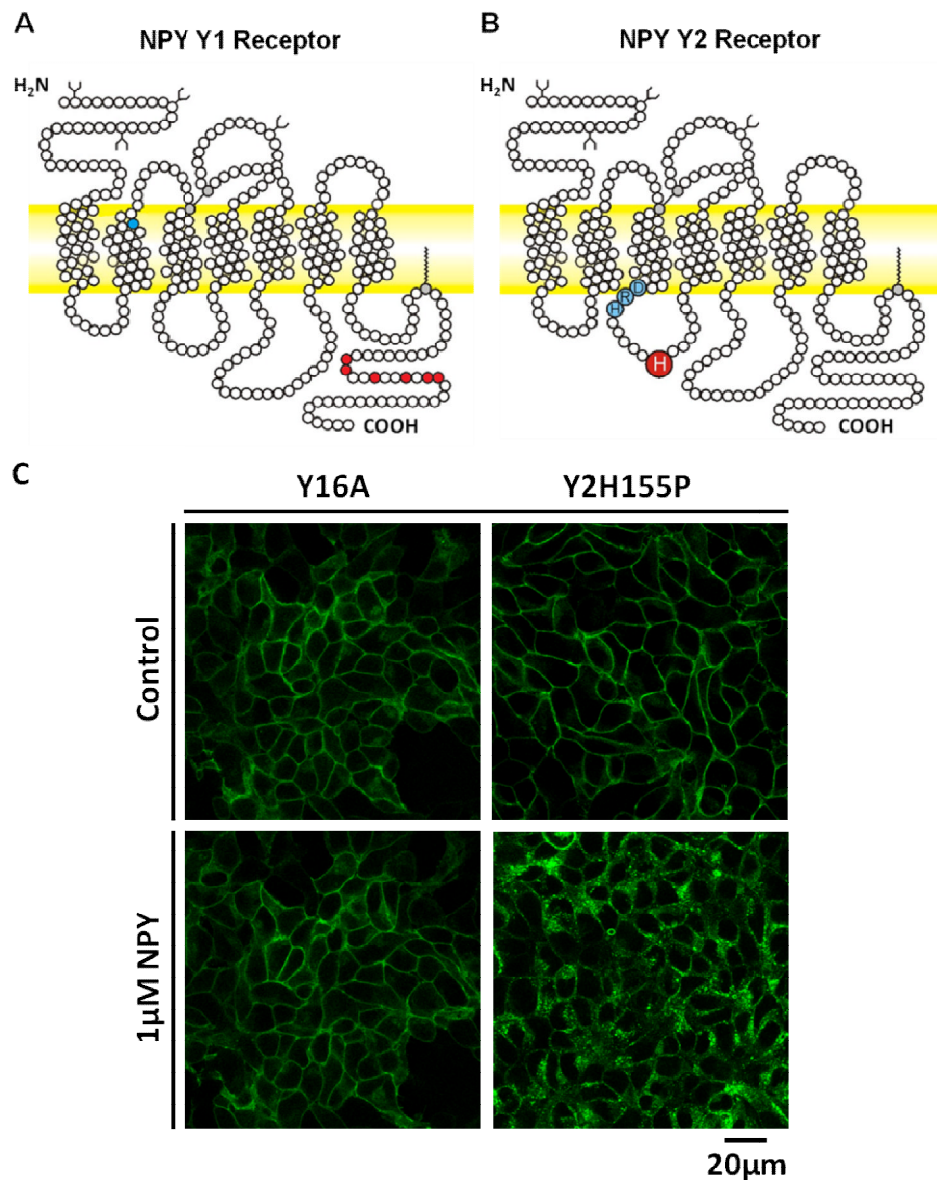


**Figure 3.14: Mutations selectively introduced into the NPY Y1 and Y2 receptor subtypes.**

The Y99A mutation introduced into the NPY Y1 receptor (A) is shown in blue, with the location of six mutations of C terminal phosphorylation residues shown in red. The H155P mutation selectively introduced into the Y2 receptor (B) is shown in red. For reference, the DRH ionic lock motif of the NPY Y2 receptor subtype is shown in light blue. HEK293TR cells were stably transfected with Y16A (A) or Y2H155P (B) receptors fused to full length superfolder variant of GFP. Receptor expression was induced by 18hr pretreatment with tetracycline (1  $\mu\text{g ml}^{-1}$ ). Cells were imaged live in the absence or presence of 1  $\mu\text{M}$  NPY (30min at 37°C) using a Zeiss LSM 510 confocal microscope with laser excitation at 488nm. Images are representative of those acquired from 4 independent experiments. For reference compare with Figure 3.4 for non-mutated Y1-GFP and Y2-GFP images.

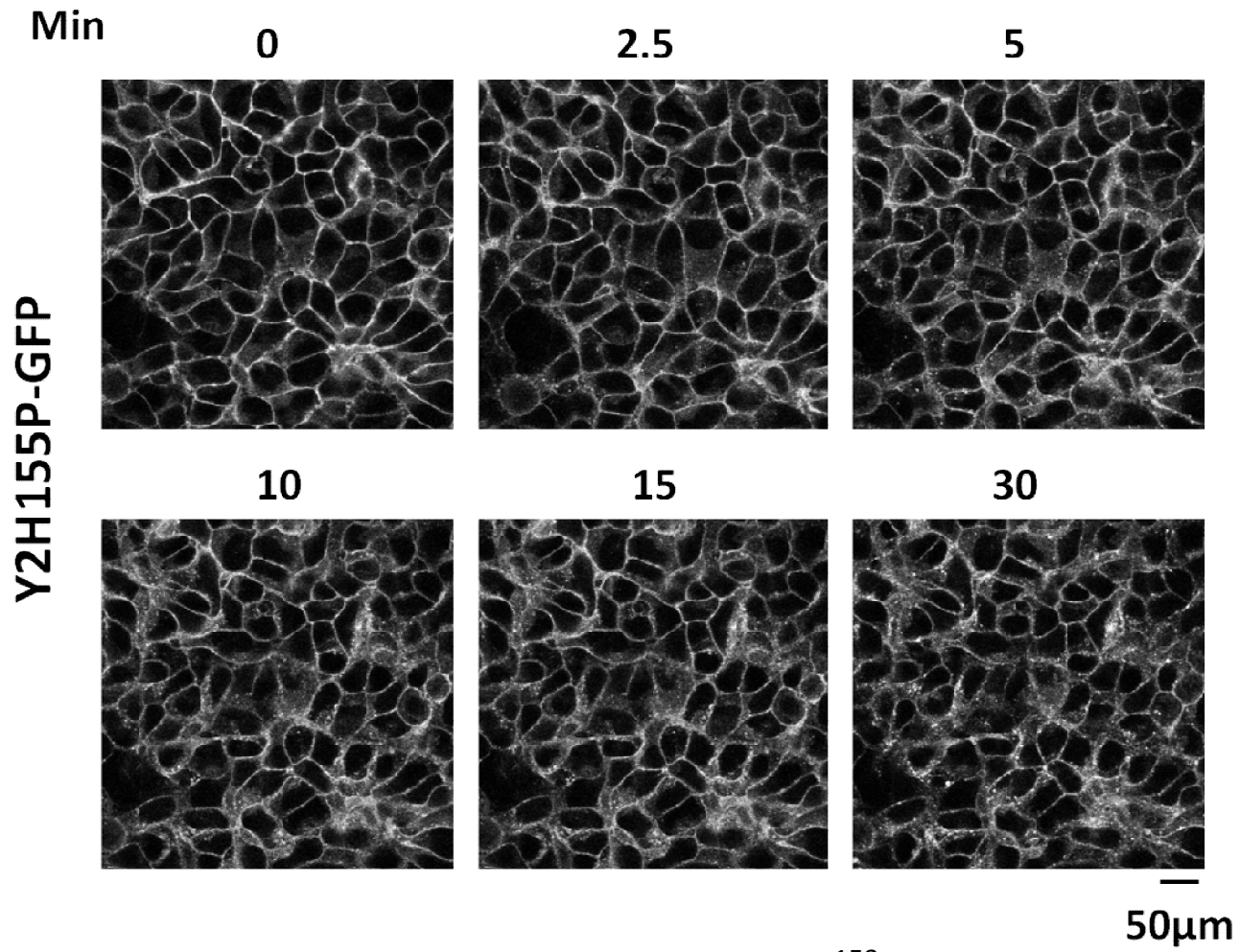


**Figure 3.15: 15min timecourse stimulation of Y2H155P -GFP cells with 100nM NPY**

HEK293TR cells stably expressing Y2H155P-GFP, were stimulated with 100nM NPY over a 15min timecourse.

Representative images are shown of the same region of cells imaged at temporal intervals using a LSM510 confocal microscope.

In order to determine if a 30min agonist incubation (as previously used for Y1-GFP and Y2-GFP) was sufficient, cells were stimulated with 100nM NPY at 37°C with the same region of cells imaged at 2.5min intervals. No internalisation was seen for Y16A-GFP at any timepoint imaged. Noticeable internalisation was observed for Y2H155P-GFP cells from 2.5min incubation times onwards (Figure 3.15 compared to Figure 3.5). Automated imaging using a confocal platereader, in conjunction with a granularity algorithm, allowed NPY induced internalisation to be quantified and compared with those obtained for native Y1 and Y2-GFP. No NPY induced internalisation (30min at 37°C) was observed for Y16A-GFP even at higher concentrations (Figure 3.16, A and B). Conversely the H155P mutation introduced into the Y2 sequence enhanced agonist-stimulated endocytosis of Y2H155P-GFP receptors (A and C), with NPY potencies 18 fold greater when compared to responses at the wildtype Y2 receptor ( $pEC_{50} 7.8 \pm 0.1$ ,  $n=4$ ;  $p < 0.01$ ).

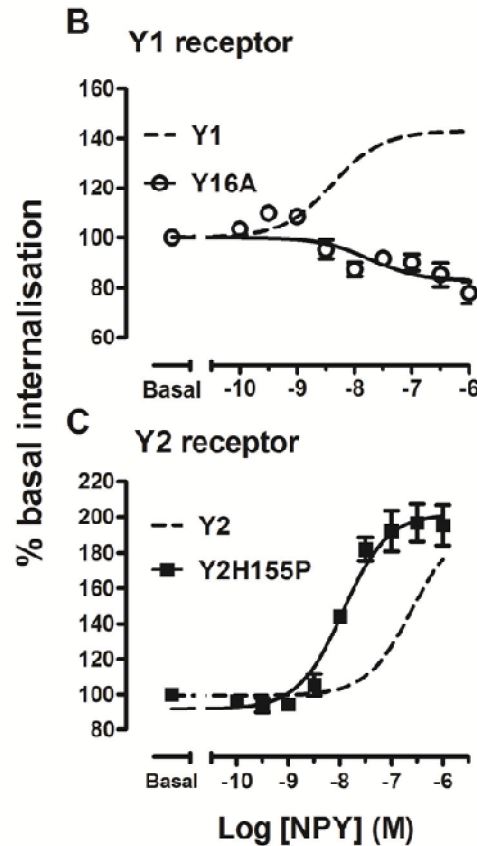
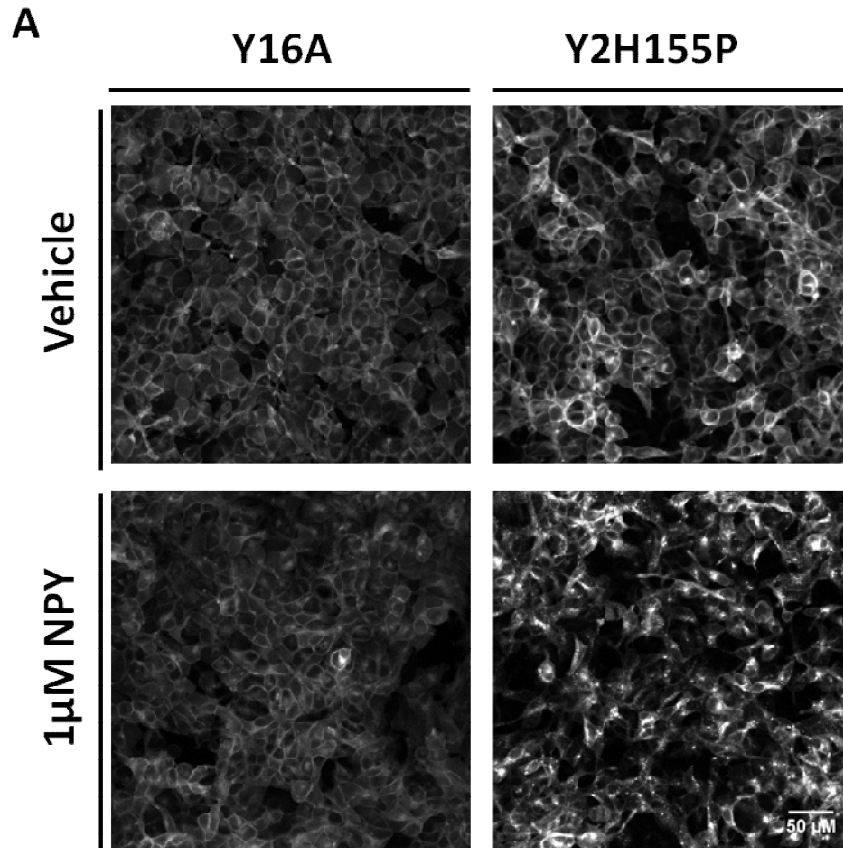


**Figure 3.16: Quantitative analysis of agonist induced internalisation of native and mutant Y1 and Y2 receptors**

HEK293TR cells were stably transfected with Y16A-GFP or Y2H155P-GFP. Receptor expression was induced with tetracycline ( $1\mu\text{g ml}^{-1}$ ) for 18hr. Y16A-GFP or Y2H155P-GFP (A) receptors were treated with either vehicle or  $1\mu\text{M}$  NPY (30min at  $37^\circ\text{C}$ ) and then imaged using an IX Ultra confocal plater reader (only GFP images are shown here). Quantification of receptor internalisation was normalised as a percentage above basal responses. Data from at least 3 independent experiments were pooled and NPY concentration response curves derived for Y16A-GFP (B) and Y2H155P-GFP (C) receptors.  $\text{pEC}_{50}$  values are stated in the text. Responses from native Y1-GFP and Y2-GFP receptors (Figure 3.7B and C) are shown as a dotted line.

### **3.3.3.2 Using automated imaging of BiFC responses to investigate the effect of selective mutations on the association of Y1 receptors with $\beta$ -arrestin2**

Studies using GFP tagged mutant Y16A and Y2H15PP-GFP suggested that these mutations could confer changes in the nature of Y receptor internalisation. The BiFC assay was then used to quantify whether selective introductions of these mutations could also alter  $\beta$ -arrestin2 recruitment.

Firstly, the effect of substituting a tyrosine at residue 99 for alanine (Y99A) in the Y1 receptor sequence was investigated (Y1Y99A/A2; Figure 3.14, A; residue highlighted in blue). This residue has been shown to inhibit agonist binding at the Y1 receptor preventing the use of radioligand binding measurements to estimate ligand affinity and receptor expression (Sautel et al., 1995). The Y16A mutation (previously described in section 3.4.3.1) was also investigated to assess the relative importance of these phosphorylated residues in  $\beta$ -arrestin2 recruitment (Y16A/A2). Displacement of specific [<sup>125</sup>I] PYY binding by PYY and BIBO3304, and sensitivity of this binding to GTP $\gamma$ S suggested that Y16A/A2 constructs were functional in respect to ligand binding with Bmax values comparable to native Y1/A2 (Kilpatrick et al., 2010). HEK293T cell lines stably co-expressing Y1/ $\beta$ -arrestin2 mutant BiFC constructs were stimulated with NPY for 60min at 37°C/5% CO<sub>2</sub> (Figure 3.17). NPY induced BiFC responses were abolished for both Y1Y99A/A2 and Y1Y6A/A2 mutant cell lines.

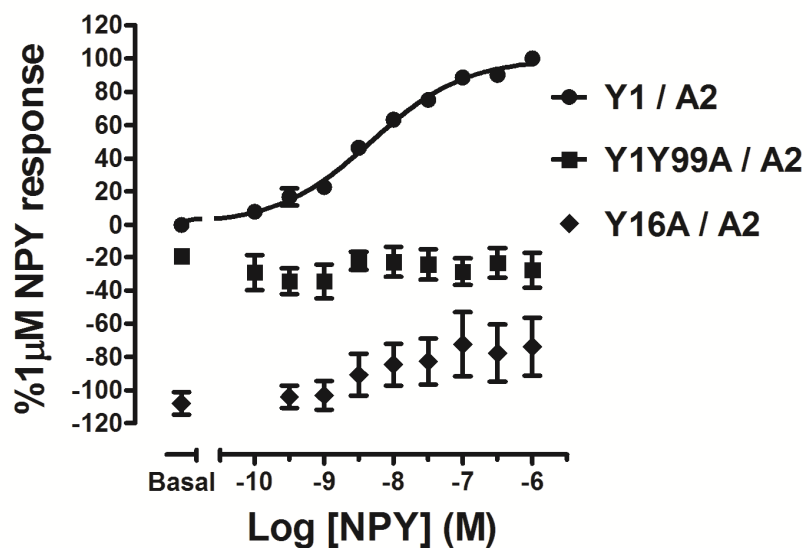


**Figure 3.17: Investigating the effect of selectively introduced mutations on Y1 receptor/  $\beta$ -arrestin2 BiFC**

HEK293T cells stably co-expressing native or mutant Y1/A2 were stimulated with a concentration range of NPY (60min at 37°C/5% CO<sub>2</sub>). Granularity analysis of images acquired using an automated confocal plate reader, allowed the effects on receptor internalisation of mutations affecting ligand binding (Y1Y99A) and receptor phosphorylation (Y16A) to be determined. All data was normalised to wildtype Y1 receptor responses to plate controls (vehicle and 1µM NPY) and expressed as means  $\pm$  s.e.m. Data were pooled from at least 4 independent experiments.

## **3.4 Discussion**

### **3.4.1 Summary of main findings**

High content imaging of fluorescently tagged Y receptor subtypes or Y receptor/ $\beta$ -arrestin2 BiFC complexes in conjunction with automated analysis allowed quantitative pharmacology to be derived from qualitative images. The use of BiFC defined the association of Y receptor/ $\beta$ -arrestin2 as discrete complexes, whose pharmacological responses could be compared to those obtained in respect to Y receptor internalisation. Consistent agonist and antagonist pharmacology was observed for these distinct signalling endpoints, across all 4 Y receptor subtypes investigated, with affinity estimates also comparable with those previously documented for each subtype using alternative assay methodologies.

Quantification of BiFC fluorescence was here able to distinguish between receptor mutations that alter the engagement of  $\beta$ -arrestin activation (Y1H155P) or phosphorylation sensors (Y16A) with the receptor. The use of these selective mutations further supported a shared molecular mechanism underlying both receptor internalisation and  $\beta$ -arrestin recruitment to Y receptors. As supported by previous studies, Y receptor internalisation is therefore likely to reflect an agonist induced recruitment of  $\beta$ -arrestin that subsequently facilitates receptor endocytosis.

#### **3.4.2.1 Y receptor-GFP fusion proteins are functional in respect to ligand binding and cell surface expression**

The addition of C terminal fluorescent protein tags to receptor constructs required validation to ensure receptor expression and function was conserved. The large size of GFP (27kDa) has the potential to alter the expression and function of tagged proteins.. However the addition of superfolder GFP tags to the C terminus of Y1-GFP did not adversely affect ligand binding or receptor expression. [<sup>125</sup>I] PYY competition binding assays (Figure 3.3) confirmed that ligand affinities were comparable to that previously documented for cloned rat Y1 receptors in respect to PYY (Gehlert

et al., 1997) and BIBO3304 (Dumont and Quirion, 2000) binding. The activity of GTP $\gamma$ S in respect to its potency and degree of inhibition was also comparable to previous measures of N terminally HA-tagged Y1 receptors (Holliday and Cox, 2003). Additionally confocal imaging confirmed that Y1-GFP receptors were expressed at the plasma membrane of HEK293T cells (Figure 3.4, A). A small degree of constitutive Y1 receptor internalisation was observed, which was consistent with untagged Y1 receptors using antibody live labelling techniques (Holliday et al., 2005, Lundell et al., 2011). Observations from the Y receptor subtypes Y1, Y2, Y4 and Y5 with full length eGFP or eYFP, showed that receptor expression and ligand binding was unchanged (Bohme et al., 2008). GFP tagging of other Class A GPCRs such as  $\beta$ 2-adrenoceptors,  $\alpha_{1A}$  and  $\alpha_{1B}$ , vasopressin V2 and thyrotropin releasing hormone receptors also resulted in receptors with unaltered ligand binding and second messenger generation (reviewed in (Kallal and Benovic, 2000)). Rapid agonist induced internalisation of Y1-GFP in response to agonist was comparable to that previously observed for Y1 receptors containing no fluorescent tag and measured using alternative methods. Labelling cloned guinea pig Y1 receptors expressed in CHO cells using [ $^{125}$ I] peptide ligands revealed a marked decrease in the proportion of cell surface receptors in response to agonist challenge (Parker et al., 2001, Parker et al., 2002). This was also consistent with observations for endogenously expressed human Y1 receptor internalisation following labelling with a fluorescent NPY derivative and observed using confocal microscopy in SK-N-MC cells (Fabry et al., 2000), C terminal FLAG epitope labelling of human Y1 receptors in HEK derived EBNA-293 cells (Lundell et al., 2011) and HA tagged rat Y1 receptors in HEK293T cells (Holliday et al., 2005, Pheng et al., 2003). Y1-GFP receptor agonist induced internalisation was also comparable to that previously observed for this receptor when containing alternative C terminal (Bohme et al., 2008, Lindner et al., 2009, Kilpatrick et al., 2010) or N terminal (Gicquiaux et al., 2002, Ouedraogo et al., 2008, Lecat et al., 2011) fluorescent protein tags. These comparisons are important, because for example, tagging of the

$\beta$ 2-adrenoceptor with eGFP has previously been shown to decrease the rate of Isoprenaline induced internalisation compared to untagged receptor (McLean and Milligan, 2000). Therefore the addition of a C terminal GFP tag to the Y1 receptor did not appear to adversely affect Y1 receptor expression, ligand binding potency or agonist induced internalisation suggesting this technique was suitable for use in further investigations of Y receptor pharmacology aligned to the internalisation response.

#### **3.4.2.2 Agonist and antagonist pharmacology of Y1-GFP internalisation responses revealed by quantitative imaging and analysis**

Here for the first time, the use of automated confocal imaging and analysis allowed quantitative data of agonist ( $pEC_{50}$ ) and antagonist ( $pK_b$ ) potencies to be extracted from confocal imaging of Y1-GFP internalisation (Figure 3.6). Previous observations of Y1 receptor agonist induced internalisation have derived ligand potencies from alternative measures of Y1 internalisation, for example the use of radiolabelled peptides (Parker et al., 2001, Parker et al., 2002) and anti GFP antibodies (Ouedraogo et al., 2008, Lecat et al., 2011, Gicquiaux et al., 2002) to measure the decrease in surface receptor expression. Using this technique agonist pharmacology for Y1-GFP internalisation could then be compared with previous estimates of Y1 pharmacology, which were broadly similar (Table 3.1) (Krause et al., 1992, Gehlert et al., 1997, Lindner et al., 2009, Kilpatrick et al., 2010). For example, the decreased potency of PP, compared to NPY, at inducing Y1-GFP internalisation was similar to previous observations of the inability of PP to decrease cell surface expression of GFP-Y1 receptors (Gicquiaux et al., 2002) and was expected based on its decreased affinity for the Y1 receptor (Gehlert et al., 1997). Functional antagonism was also observed for Y1-GFP receptor endocytosis. The Y1 selective antagonist BIBO3304 was able to competitively inhibit NPY induced Y1-GFP internalisation with affinity estimates consistent with those from other studies (Michel et al., 1998, Wieland et al., 1998) and reconcilable with the affinity of BIBO3304 at Y1-GFP receptors measured using [ $^{125}$ I] PYY radioligand binding (Table 3.1).

Therefore automated confocal microscopy and analysis of Y1-GFP internalisation allowed agonist and antagonist pharmacology to be investigated and compared to previous measurements. This same technique was therefore validated for use in quantifying ligand pharmacology using both Y receptor internalisation and Y1/ $\beta$ -arrestin2 BiFC responses as functional readouts.

### **3.4.2.3 Advantages and limitations of the platereader approach to measuring Y1 receptor internalisation**

The use of standard confocal microscopy allowed the sub-cellular localisation of GFP tagged Y1 receptors to be visualised at high magnification and resolution (Figure 3.4, A). The internalisation of these labelled receptors could be observed in response to receptor activation with agonist. However quantification of internalisation from these images requires manual analysis which can be time consuming and risks unintended experimenter bias. The use of automated confocal image acquisition and analysis addressed both of these caveats, in addition to also providing high resolution qualitative data of the sub-cellular localisation of GFP tagged receptors (Figure 3.6) and measuring the accumulation of receptor- $\beta$ -arrestin2 BiFC complexes (Figure 3.11, A). For example when using the granularity algorithm, although the fluorescent intensity threshold to detect internalised granules is subjectively defined by the experimenter, these were consistently applied to all images acquired across the entire plate. This allowed quantification of pharmacological responses to both full and partial agonists. The addition of a nuclei stain also allowed results to be expressed on a per cell basis. Additionally automated imaging allowed a greater number of cells to be imaged per field assays can be performed in 96-1536 plate well formats (Auld et al., 2006). However it is worth noting that the granularity algorithm method is to some extent an indirect measure of endocytosis, as although it measures an increase in intracellular receptor-GFP fluorescence as endocytosis proceeds, it does not specifically measure decreases in the cell surface receptor expression. However, automated detection and monitoring

of receptors at the cell surface, using images of confluent cell lines such as HEK293, is very difficult without a separate specific fluorescent marker to define the plasma membrane. Thus granularity represents the most convenient and rapid option to measure receptor endocytosis from automated platereader images.

Additionally in common with manual microscopy there are spatiotemporal limits to the confocal resolution possible. For example both are unable to resolve structures such as clathrin coated pits and can only infer that internalised receptors accumulate in perinuclear recycling compartments. There are also differences between the spatial resolutions possible between the confocal and plate reader formats due to the differences in numerical aperture of the objectives used. The numerical aperture of the 40x objective used in the plate reader format is lower (NA 0.6) than that of the 63x time objective (NA 1.4) used in manual confocal imaging, meaning that some finer details are less likely to be resolved using platereader imaging. Additionally the choice of medium used between the objective and cover glass/plate can account for these differences in resolution, as the immersion oil used at the 63x objective in confocal imaging creates an interface with a greater refractive index which increases the possible resolution of cellular structures.

However despite these factors, automated image acquisition and analysis, was able to generate both qualitative and quantitative data on the internalisation of fluorescently tagged Y receptors and the interaction of Y receptor with  $\beta$ -arrestin2 using BiFC and could indicate the cellular localisation of these fluorescent species.

### **3.4.3 Correspondence between Y receptor internalisation pharmacology and BiFC measurements of $\beta$ -arrestin2 association**

The successful use of automated analysis to quantify agonist induced Y1-GFP receptor internalisation, suggested that this technique could be applied to quantify the upstream signalling process such as the agonist induced recruitment of  $\beta$ -arrestin2 to Y1 receptors measured by BiFC.

### **3.4.3.1 Characteristics of Y1 receptor- $\beta$ -arrestin2 recruitment measured using BiFC**

The same imaging system and analysis algorithm used to quantify Y receptor-GFP internalisation was used in conjunction with BiFC to quantify ligand pharmacology of Y receptor/ $\beta$ -arrestin2 associations. The Y1/A2 BiFC cell line was functional in respect to [<sup>125</sup>I] PYY ligand binding and GTP $\gamma$ S sensitivity, with PYY and BIBO3304 binding affinities similar to those of Y1-GFP (Table 1) and to previous observations (Kilpatrick et al., 2010, Gehlert et al., 1997, Dumont and Quirion, 2000, Holliday and Cox, 2003). Translocation of cytosolic GFP tagged  $\beta$ -arrestin2 to activated Y1 receptors has been shown in HEK293T cells (Holliday et al., 2005, Ouedraogo et al., 2008). BRET assays have also shown that NPY receptor subtypes associate with  $\beta$ -arrestin2 in a concentration dependent manner (Berglund et al., 2003b). However whilst BRET, and other techniques such as FRET, have the advantage of providing a real time readout of  $\beta$ -arrestin recruitment, they are relatively complex requiring exogenous substrates (BRET) or dual wavelength measurements (FRET). The irreversibility of BiFC and the time required for chromophore maturation prevents real time measurements of responses using this technique (Kerppola, 2009, Kerppola, 2013). However the irreversibility of BiFC can be advantageous as it constrains associated proteins (in this case Y receptor and  $\beta$ -arrestin2) as stable molecular complexes of precise composition, generating long lived recomplemented YFP fluorescence indicative of an interaction. This is reflected in the stimulation time used here, as although the initial Y1- $\beta$ -arrestin2 interaction is rapid, the 60 minute incubation time allowed the fluorophore to fully mature resulting in a more stable and intense fluorescent readout. Previous observation using these BiFC fragments suggested that incubation time had no effect on derived agonist potencies, and that longer stimulations only increased the proportion of fluorescent recomplemented YFP observed (Kilpatrick et al., 2010). Analysis of this fluorescence using the granularity algorithm allowed quantification of agonist and antagonist pharmacological responses of Y receptor/ $\beta$ -arrestin2

complexes (Figure 3.11). The derivation of  $pEC_{50}$  potencies also allowed comparisons to be made between BiFC and receptor-GFP internalisation readouts using the same assay format. The use of this same granularity algorithm in conjunction with the same set of BiFC fragments has previously illustrated the agonist induced association of GPR120S and 120L splice variants with  $\beta$ -arrestin2 (Watson et al., 2012). Alternative analysis techniques have also quantified the interaction of  $\beta$ -arrestin2 with  $\beta$ -adrenoceptors (Auld et al., 2006) (also using a larger scale 1536 well plate format) and angiotensin 1 receptors (Porrello et al., 2011). Quantitative analysis of BiFC fluorescence was therefore a valid approach to investigate the pharmacology of  $\beta$ -arrestin2 recruitment to Y receptor subtypes.

Much of the success of BiFC assays is linked to the appropriate choice of BiFC fragment used (Kilpatrick and Holliday, 2012). This factor was previously optimised for vYFP fragments (Kilpatrick et al., 2010), which suggested that C terminal tagging of the Y1 receptor with the 155-238 Yc fragment was most appropriate for sufficient receptor expression. The use of a complementary N terminal fragment tag of  $\beta$ -arrestin2 (1-173) was found to maximise refolding rates at 37°C (Kilpatrick et al., 2010, Nagai et al., 2002, Hu and Kerppola, 2003). This is likely due to the overlapping region repeating a  $\beta$  strand (155-172) within both fragments that facilitates refolding of the complete  $\beta$  barrel structure. Timecourse experiments using both these overlapping and non-overlapping YFP fragments, revealed differences in the rates of complementation (Kilpatrick et al., 2010), with the overlapping pairs showing significantly faster  $t_{1/2}$  values for BiFC development compared to other fragment pairs (10 min  $\pm$  1.0 versus 17.5-20.9min). However it is worth noting that the choice of fragment pair had no effect on observed agonist potencies (Kilpatrick et al., 2010), indicating that the different affinities of these fragments for each other did not alter the agonist driven receptor-arrestin association. Additionally the kinetics of Y1/A2 with overlapping BiFC fragments was slower than that observed for Y1-vYFP internalisation (2.4min  $\pm$  0.3) (Kilpatrick et al., 2010), confirming that NPY stimulation results in the de

novo formation of new BiFC complexes rather than altering trafficking of existing complexes. The use of a series of wash steps supported this assertion in addition to illustrating the irreversible nature of BiFC complementation (comparable results are observed for GFP complementation, see Chapter 4, Figure 4.8) (Kilpatrick et al., 2010). An inevitable consequence of using overlapping BiFC fragments with more efficient folding is the increased propensity for 'bystander' collisions that can lead to higher background levels of fluorescence (Kerppola, 2008b, Kodama and Hu, 2010). There is also a risk in using BiFC assays that the strength of the affinity of the two tags is driving the association of the tagged proteins as opposed to representing a genuine interaction (Kerppola, 2013) – but as indicated above, changing the affinity of the fragments for each other had no effect on the observed agonist pharmacology (15). Under control conditions, some constitutive Y1/A2 fluorescence was observed (Figure 3.11, A), however this reconciled with the constitutive activity previously observed for Y1-YFP receptors, suggesting it is not as a consequence of intrinsic fragment affinity. The lack of basal fluorescence observed for Y16A/A2 BiFC using the same overlapping BiFC fragments (see below) (Kilpatrick et al., 2012), also suggested that constitutive BiFC fluorescence may be receptor, not BiFC, dependent.

#### **3.4.3.2 Agonist and antagonist pharmacology of Y1 receptor-arrestin association closely resembles the profile seen for Y1-GFP receptor internalisation**

NPY was able to induce the association of Y1 receptor/ $\beta$ -arrestin2 BiFC complexes with a potency comparable to that observed for Y1-GFP receptor internalisation (Table 3.2 and 3.3). Confocal images obtained (Figure 3.11, A) were of high enough resolution to suggest that following internalisation, Y1/ $\beta$ -arrestin2 complexes were present in perinuclear compartments within the cytosol. This is reconciled with previous observations for Y1 receptor associations with  $\beta$ -arrestin2 in HEK293T cells (Gicquiaux et al., 2002, Pheng et al., 2003). However no real conclusions can be made on the endocytic trafficking of receptor- $\beta$ -arrestin2 BiFC complexes beyond this point due to

the risk that the irreversibility of complementation is adversely affecting receptor trafficking.

Y1/A2 BiFC responses showed agonist potencies and maximal responses consistent with that observed for NPY at inducing fluorescently tagged Y1 receptor internalisation (Tables 3.2 and 3.3) (Gicquiaux et al., 2002, Lecat et al., 2011, Ouedraogo et al., 2008). Similar to the Y1-GFP receptor, the typically Y4 selective ligand GR231118 did not induce the association of  $\beta$ -arrestin2 and Y1 receptors (Pheng et al., 2003). Responses to PP were also comparable in measures of both Y1 receptor internalisation and  $\beta$ -arrestin2 recruitment. The low potency and efficacy of the N terminal truncated ligands NPY<sub>3-36</sub> and PYY<sub>3-36</sub> reflected the importance of N terminal peptide residues in Y1 receptor binding and activation (reviewed in (Pedragosa-Badia et al., 2013)). BIBO3304 exhibited the expected surmountable antagonism of Y1 / A2 BiFC responses, with affinity estimates consistent with those determined for Y1-GFP and previous affinity measurements for BIBO3304 (Michel et al., 1998, Wieland et al., 1998).

Therefore the BiFC assay gives expected pharmacology for agonist induced recruitment of  $\beta$ -arrestin2 to Y1 receptors that was also comparable to Y1-GFP responses and suggested that the presence of the BiFC tags did not have an adverse effect on measuring the pharmacology of Y1 receptor – arrestin recruitment. The quantification of two assay endpoint measurements (internalisation and  $\beta$ -arrestin2 recruitment) generated comparable ligand pharmacology, suggesting that similar molecular mechanisms underlie  $\beta$ -arrestin recruitment and Y1 receptor internalisation.

### **3.4.4 Similarities between $\beta$ -arrestin recruitment and internalisation pharmacology are preserved for other Y receptor subtypes**

#### **3.4.4.1 The Y2 receptor**

As previously described the Y1 receptor rapidly internalised in response to stimulation with the agonists NPY, PYY and [Leu<sup>31</sup>, Pro<sup>34</sup>] NPY (Y1-GFP, Figure 3.12A). However observations of human (Gicquiaux et al., 2002) and guinea

pig Y2 receptors (Parker et al., 2001) expressed in heterologous cell lines, showed comparatively decreased internalisation in response to agonist. Here NPY induced internalisation of GFP tagged Y2 receptors, and stimulated the formation of Y2/ $\beta$ -arrestin2 BiFC complexes, with comparable potencies obtained for both assay formats (Figure 3.12, B; Table 3.3). However both of these processes only occurred with NPY concentrations in excess of 50nM. This is in accordance with previous observations of Y2 receptor internalisation using N terminal GFP tagged (Ouedraogo et al., 2008), C terminal tagged eYFP (Bohme et al., 2008, Walther et al., 2010) and FLAG tag immunolabelling (Lundell et al., 2011). These groups observed Y2 receptor internalisation only with NPY concentrations of 50-100nM, suggesting that internalisation required a high degree of receptor occupancy (Kilpatrick et al., 2010). However Lundell et al (2011) (Lundell et al., 2011) have suggested that the Y2 receptor internalisation observed in response to high concentrations of NPY is less relevant at the physiological levels of NPY observed *in vivo*. Interestingly the Y2 receptor showed comparable affinity to that of the Y1 receptor for NPY and radiolabelled NPY (Lundell et al., 2011) even though both receptor subtypes share only 30% sequence homology (Akerberg et al., 2010) and substantial different residues implicated in ligand binding (Lindner et al., 2008, Xu et al., 2013). NPY was substantially less potent in stimulating  $\beta$ -arrestin2 recruitment to Y2 receptors when using the BiFC assay (Y2/A2) with responses 26 fold less than observed at Y1/A2. This phenomena was also mirrored when quantifying Y2 receptor internalisation, with NPY responses 63 fold lower than that seen for Y1-GFP (Table 3.2 and 3.3).

The reduction in potency of NPY at inducing the formation of Y2/A2 BiFC complexes or Y2-GFP internalisation does not appear to be due to a complete lack of interaction with  $\beta$ -arrestin2. Colocalisation of Y2 receptors and  $\beta$ -arrestin2 has been observed using BRET (Berglund et al., 2003b, Walther et al., 2010). Monitoring reductions in Y2 receptor plasma membrane expression measured by ELISA showed that overexpression of mCherry- $\beta$ -arrestin2 further enhanced Y2 receptor internalisation. Therefore the decreased

potency for Y2/A2 and Y2-GFP is likely to be a consequence of Y2 receptors having a decreased affinity for  $\beta$ -arrestin2 compared to that observed for the Y1 receptor. This has been implied from BRET studies whereby recruitment of  $\beta$ -arrestin2 to Y2 receptors was both decreased in terms of extent and kinetics when compared to the Y1 subtype ( $t_{1/2}$  23min for Y2 and 3.4min for Y1 respectively) (Berglund et al., 2003b). The reason for this reduced arrestin affinity may lie in the sequence differences between the Y1 and Y2 receptors. Surprisingly interaction does not appear dependent on the Y1 and Y2 receptor C terminal tails, the traditional site for phosphorylation by G protein receptor and other kinases. For example the Y2 receptor contains a region analogous to the Y1 receptor 'phosphorylation motif' (Ouedraogo et al., 2008, Walther et al., 2010) thought to play a key role in the recruitment of  $\beta$ -arrestin2. NPY receptor chimeras consisting of the Y1 receptor substituted with the Y2 receptor C terminal domain, showed significantly increased NPY induced internalisation when compared to wildtype Y1 receptors (Lundell et al., 2011). This indicated that the Y2 receptor C terminus is capable of supporting  $\beta$ -arrestin2 recruitment, so that other Y2 receptor intracellular domains may be affecting the strength of this interaction.

Both PYY and the amino truncated form of PYY3-36 induced the formation of Y2/A2 BiFC with higher potencies than that observed for NPY. This is in line with previous observations of the rank order of potency at the Y2 receptor (Gerald et al., 1995, Matthews et al., 1997, Akerberg et al., 2010). The differences in potency of PYY<sub>3-36</sub> at Y1 versus Y2 receptors likely reflects the differing requirements of each receptor subtype for the N terminal domain of the peptide (Michel et al., 1998). Ligand binding affinity observations suggested that unlike the Y1 receptor, the C terminal peptide portion from residue 13 onwards is sufficient for binding to the Y2 subtype (Lindner et al., 2008). As expected the Y1 selective peptide [Leu<sup>31</sup>, Pro<sup>34</sup>] NPY (Fuhlendorff et al., 1990) showed very low potency at the Y2 receptor, reconcilable with previous measurements of its low binding affinity at this subtype (Matthews et al., 1997, Lindner et al., 2008, Akerberg et al., 2010).

#### 3.4.4.2 Y4 receptor

Stimulation with agonist resulted in internalisation of Y4-GFP receptors and the formation of Y4 receptor/ $\beta$ -arrestin2 BiFC complexes (Figures 3.9, C and 3.12, C). Conflicting reports exist on the ability and kinetics of Y4 receptor internalisation. Initial observations in CHO cells showed no desensitisation or internalisation for C terminal FLAG tag labelled Y4 receptors (Voisin et al., 2000). However observations from several other groups have shown rapid internalisation of Y4 receptors in response to agonist (Tough et al., 2006, Bohme et al., 2008), which were largely comparable to Y1 responses (Parker et al., 2001, Parker et al., 2005). The greatest degree of responses for both endpoint measurements were observed following stimulation with PP. This was expected based on the known high selectivity of Y4 receptors for PP (Bard et al., 1995, Berglund et al., 2001) in contrast to responses observed for the Y1 receptor (Tables 3.2 and 3.3). Observations of HA tagged Y4 receptor internalisation in HEK293 cells in response to PP was also less than observed for Y1 receptors in response to NPY (Tough et al., 2006). BRET observations have also shown that PP can induce concentration dependent recruitment of  $\beta$ -arrestin2 to Y4 receptors (Berglund et al., 2003b) however with a significantly reduced potency compared to that observed using BiFC ( $pEC_{50}$   $7.4 \pm 0.1$  for BRET2 versus  $9.5 \pm 0.3$  for Y4/A2 BiFC). It is worth noting however in the aforementioned BRET study, agonist potencies were consistently lower for all subtypes than their respective binding estimates (Berglund et al., 2003b). The authors postulate that this may be due to an overexpression of GFP-arrestin2 in these studies changing the stoichiometry of receptor-arrestin interactions. However  $\beta$ -arrestin2 was also overexpressed in this BiFC system (as the  $\beta$ -arrestin2-Yn is a stably expressed clonal line) and agonist potencies for all Y subtypes were relatively consistent with those seen for the internalisation of GFP tagged receptors expressed in HEK293T (expressing endogeneous levels of  $\beta$ -arrestin2) and previous estimates of ligand potencies. However observations from BRET are useful as an indicator of the real time rank order of association of  $\beta$ -arrestin2 with Y receptor subtypes (in

terms of  $t_{1/2}$  values), which can only be inferred by BiFC studies from changes in agonist potency.

NPY and PYY showed reduced maximal responses, compared to PP, at inducing Y4/A2 BiFC responses and Y4-GFP receptor internalisation. This is consistent with the reported decreased affinity of these ligands at the Y4 receptor when [ $^{125}$ I] PP is used as the radioligand (Lundell et al., 1995, Lundell et al., 1996, Parker et al., 1998), in comparison to relative affinities at the Y1 and Y5 receptor subtypes (Lindner et al., 2008), and their reduced ability to stimulate Y4 receptor G protein coupling and inhibition of cAMP formation (Tough et al., 2006). GR231118 was a low efficacy agonist at both Y4-GFP and Y4/A2 cell lines. Partial agonism of GR231118 at Y4 receptors has also been documented in functional assays such as stimulation of GTP $\gamma$ [ $^{35}$ S] binding (Tough et al., 2006) and is consistent with previous observations implying it is high affinity Y4 receptor agonist (Parker et al., 1998). Interestingly although GR231118 has similar binding affinities for both Y4 and Y1 receptor subtypes (Matthews et al., 1997, Parker et al., 1998), GR231118 showed no activity at Y1-GFP or Y1/A2 BiFC (Figures 3.9, A and 3.12, A) consistent with its previously documented activity as a Y1 receptor antagonist (Daniels et al., 1995). GR231118 is a dimeric analogue of the C terminal domain of NPY (Tough et al., 2006). The contrasting effects of GR231118 at Y4 and Y1 receptors, suggests that the C terminal portion of NPY is capable of activating the Y4 receptor. However the Y1 receptor requires further engagement with the NPY N terminus, which reconciles with the previous partial efficacy observed at Y1/A2 for NPY $_{3-36}$  and PYY $_{3-36}$  (Table 3.3) and the Y1 selective antagonism observed for the NPY C terminal dipeptide mimic BIBO3304 for Y1-GFP internalisation and Y1/A2 BiFC formation (Lindner et al., 2008).

Both Y4-GFP and Y4/A2 BiFC cell lines therefore showed expected ligand selectivity based on previous observations. The presence of either tag did not adversely affect potency values in respect to receptor internalisation or  $\beta$ -arrestin recruitment.

### 3.4.4.3 Y5 receptor

Both NPY and PP were able to induce the formation of Y5/A2 BiFC complexes and the internalisation of Y5-GFP receptors within a 60 minute time period (Figure 3.6, C) with comparable potencies observed between the different endpoint measurements (Tables 3.2 and 3.3). These NPY potencies were also comparable to those previously observed for this receptor for inositol phosphate accumulation assay in COS-7 cells (Lindner et al., 2008). NPY<sub>3-36</sub> also exhibited high potency in stimulating Y5/A2 BiFC complexes, consistent with the previously documented affinity of N terminal truncated peptides for this receptor subtype (Gerald et al., 1996). The Y5 selective ligand cPP(1-17)(Ala<sup>31</sup>,Aib<sup>32</sup>) (17-36) NPY showed subtype selectivity for Y5 receptors, whereby it was able to induce Y5/A2 BiFC with high potency and efficacy, but showed no activity at inducing Y1/A2 BiFC complex formation. This was expected based on previous observations of the subnanomolar affinity of Ala<sup>31</sup>, Aib<sup>32</sup> containing PP/NPY hybrid peptides at Y5 receptors when compared to other NPY receptor subtypes (Cabrele and Beck-Sickinger, 2000), with this motif crucial for promoting selectivity. The Y5 selective antagonist CGP71683 also showed expected surmountable antagonism at Y5-GFP receptors, suggesting that the presence of the fluorescent protein tag was well tolerated. The only discrepancy in ligand responses observed between measures of  $\beta$ -arrestin2 recruitment and Y5 receptor internalisation was the 43 fold increase in potency seen for cPP(1-17)(Ala<sup>31</sup>,Aib<sup>32</sup>) (17-36) NPY at Y5-GFP.

All stimulations of the Y5 receptor required a 60min assay stimulation in order for sufficient responses to be determined. Similar to the Y4 receptor, the extent and rate of Y5 receptor internalisation has been disputed. Y5-GFP receptors have previously been shown to translocate in a time dependent manner to intracellular compartments following stimulation with PYY (Gehlert et al., 2007) and with internalisation assays using radiolabelled ligand suggested this receptor does undergo internalisation but at a slower rate when compared to Y1 receptors (Parker et al., 2003, Bohme et al., 2008).

BRET studies have shown that the Y5 receptor rapidly associates with  $\beta$ -arrestin2 in response to stimulation with NPY with kinetics comparable to that observed for the Y1 receptor ( $t_{1/2}$  values 4.6min and 3.4min respectively). However BRET maximum responses were decreased for Y5 receptors compared to that of the Y1, suggesting that the Y5 receptor is capable of rapidly recruiting  $\beta$ -arrestin2, but to a lower extent – and that does not translate to rapid receptor internalisation as seen for the Y1 receptor.

One explanation for this discrepancy is the structure of the Y5 receptor, in that it is relatively distinct from other NPY receptor subtypes, with a short C terminus consisting of only 17 amino acids (versus 64 amino acids for the Y1 receptor) and a long intracellular loop 3 over 100 residues longer than the Y1 receptor (Gerald et al., 1996). The ability of the Y5 receptor to internalise, suggests that for this subtype, the third intracellular loop may fulfil the typical role of the C terminus for the other NPY receptor subtypes, particularly as it contains a stretch of serine residues that are potential kinase phosphorylation sites (Berglund et al., 2003b). As a change in potency was only observed for the Y5 selective ligand cPP(1-17)(Ala<sup>31</sup>,Aib<sup>32</sup>) (17-36) NPY, this ligand may stabilise a particular conformation of Y5-GFP that is capable of rapidly recruiting  $\beta$ -arrestin2 (Berglund et al., 2003b), might also recruit other mechanisms to drive internalisation.

This phenomenon has been suggested to account for the constitutive internalisation of C terminal truncated Y1 receptors (Holliday et al., 2005) and muscarinic M2 receptors (Pals-Rylaarsdam et al., 1997). Although further work is required to confirm this, it is possible that the selective change in cPP-Aib-NPY potency reflects that all forms of Y5-GFP receptor internalisation are measured, be that  $\beta$ -arrestin2 dependent or independent, whereas the BiFC assay is directly measuring the association of Y5 receptors with  $\beta$ -arrestin2 only.

#### **3.4.4.4 Summary of responses at Y receptor subtypes**

Measurements of ligand pharmacology derived from the quantification of two distinct functional outputs (receptor internalisation and  $\beta$ -arrestin

recruitment) were relatively consistent across all 4 Y receptor subtypes suggesting that the agonist induced recruitment of  $\beta$ -arrestin2 to Y receptors facilitates receptor endocytosis.

### **3.4.5 The relationship between Y receptor internalisation and arrestin association is supported by the effects of Y1 and Y2 receptor mutations**

Mutations were selectively introduced into the Y1 and Y2 receptor sequences in order to investigate the role of residues implicated in ligand binding (Y1Y99A) or in the molecular mechanisms that facilitate  $\beta$ -arrestin2 recruitment (Y16A, Y2H155P).

#### **3.4.5.1 The effect of mutating a residue implicated in ligand binding (Y1Y99A)**

Mutation studies have implicated 3 hydrophobic residues in transmembrane domains 2 (Y99), 6 (F286) and 7 (H298) that facilitate ligand binding at the Y1 receptor (Walker et al., 1994, Sautel et al., 1995, Sautel et al., 1996, Sjodin et al., 2006, Akerberg et al., 2010). Substitution of these residues with alanine has been shown to abolish binding of peptide ligands. These residues have been proposed to form a 'hydrophobic binding pocket' essential for peptide binding (Sjodin et al., 2006). In this study, mutant Y1Y99A/A2 BiFC complexes did not show agonist induced endocytosis in response to stimulation with NPY (Figure 3.17). This was in marked contrast to responses of wildtype Y1/A2, supporting the importance of this residue in peptide binding at the Y1 receptor. Interestingly this Tyr99 residue is highly conserved across all NPY receptor subtypes, with the exception of the Y5 receptor (Akerberg et al., 2010). Mutation of this residue to alanine in both the Y2 (Akerberg et al., 2010) and the Y4 receptor (Pedragosa-Badia et al., 2013) sequences led to marked alterations in the affinity of the receptor for binding peptide agonists. This suggests Tyr99 may be a crucial contributor to ligand binding for the majority of the NPY receptor family, with a potential hydrogen bond being formed between the hydroxyl group of this tyrosine to the carboxyl terminal amide of peptide ligands such as NPY, PYY and their metabolites (Sautel et al.,

1995, Akerberg et al., 2010, Pedragosa-Badia et al., 2013). The Phe286 and His298 residues are much less conserved across receptor subtypes and the extent of their importance in ligand binding is disputed, with other subtype specific residues thought to be required. The agonist selectivity of Y receptor subtypes may partly be a reflection of this, with specific residues interacting with different residues of each peptide ligand.

#### **3.4.5.2 Mutation of Y1 receptor carboxyl terminal residues implicated in the recruitment of $\beta$ -arrestin2 (Y16A)**

A lack of agonist induced responses were observed for both Y16A-GFP internalisation and Y16A/A2 BiFC responses (Figures 3.16 and 3.17). Radioligand competition binding experiments showed that Y16A constructs were expressed at the cell surface and bound agonist and antagonist peptides normally. The C terminal domain of many GPCR's has been implicated in regulating receptor desensitisation and as a major site of  $\beta$ -arrestin recruitment. The six alanine substitutions sequentially introduced into the C terminal domain of the Y16A (Figure 3.14, A) were located within the Y1 receptor 'phosphorylation motif' that has been proposed to aid high affinity binding of  $\beta$ -arrestin2 (Holliday et al., 2005, Ouedraogo et al., 2008, Kilpatrick et al., 2010). As  $\beta$ -arrestin2 has previously been shown using BRET to readily interact with agonist activated Y receptors (Berglund et al., 2003b), the abolition of NPY responses for Y16A-GFP and Y16A/A2 indirectly suggested that  $\beta$ -arrestin2 recruitment is responsible for Y1 receptor endocytosis. This also reconciles with the shared agonist and antagonist profiles seen for Y receptor internalisation and Y receptor/A2 BiFC responses.

Mass spectrometry experiments have been used to directly identify C terminal residues phosphorylated upon agonist stimulation in vasopressin (Wu et al., 2008), CXCR4 (Busillo et al., 2010) and  $\beta$ 2-adrenoceptors (Nobles et al., 2011). Interestingly for the Y1 receptor, it seems to be the number of residues phosphorylated is more important than the location of these residues. When sequential alanine mutations were introduced into the Y1 receptor C terminal, dramatic reductions in  $\beta$ -arrestin2 recruitment were only seen when a

combination of 4/6 residues were mutated (Ouedraogo et al., 2008, Kilpatrick et al., 2010). Two separate mutant Y1 receptor cell lines containing a different combination of 4 mutated residues, showed similar reductions (approximately a 70% decrease) in  $\beta$ -arrestin2 recruitment (Kilpatrick et al., 2010). Only marginal reductions (approximately 20%) were observed with single substitutions, suggesting there are no 'magic bullet' residues that knockout Y1- $\beta$ -arrestin2 interaction and that different clusters of phosphorylated residues can support this association. This redundancy within the 'phosphorylation motif' was also observed for rhodopsin receptors (Doan et al., 2006) where activity was correlated to the number of C terminal phosphorylation sites as opposed to the identity of the specific residue, and chemokine receptor 5 (Huttenrauch et al., 2005). Interestingly the importance of C terminal phosphorylation in driving recruitment of  $\beta$ -arrestin2 seems to differ within the GPCR superfamily with muscarinic M2 (Gimenez et al., 2012) and neurokinin receptors (Richardson et al., 2003) both capable of desensitising and internalising in a phosphorylation independent manner. The conservation of this 'phosphorylation barcode' may also change with cell type, receptor subtype and the ligand used to activate the receptor (possibly providing a mechanism for signalling pathway bias; (Nobles et al., 2011, Chen et al., 2013). Additional sites distinct from the receptor carboxyl terminal have also been implicated in high affinity binding of  $\beta$ -arrestin2, such as sites in the second (Marion et al., 2006) and third intracellular loop (for example the muscarinic M2 and M3 receptors; (Gimenez et al., 2012, Poulin et al., 2010, Butcher et al., 2011).

#### **3.4.5.3 Mutation of an intracellular loop 2 mutation implicated in the recruitment of $\beta$ -arrestin2 (Y2H155P)**

The H155P mutation selectively introduced into the Y2 receptor sequence enhanced both  $\beta$ -arrestin2 recruitment (Kilpatrick et al., 2010) and Y2 receptor internalisation in response to NPY (Figure 3.16) with potency values substantially greater than those observed for the wildtype Y2 receptor (Table 3.2). In the Y1 receptor sequence this residue is a proline that is conserved in

64% of class A GPCRs (Marion et al., 2006, Shan et al., 2010) and has been implicated as one of the elements within the receptor recognised by  $\beta$ -arrestin2 to determine the receptor activation state (Marion et al., 2006, Shan et al., 2010). Therefore the H155P mutation appears to confer a 'Y1 like' phenotype on the Y2 receptor in respect to agonist induced internalisation, most likely by enhancing  $\beta$ -arrestin2 recruitment. The increased potency of NPY at the Y2H155P vs Y2 receptor is a consequence of this. Additionally this conclusion is supported by previous substitutions of the equivalent proline residue in rhodopsin (Raman et al., 1999), serotonin 2C and  $\beta$ 2-adrenoceptors (Marion et al., 2006) which led to a marked decrease in  $\beta$ -arrestin2 binding and subsequent  $\beta$ -arrestin2 mediated internalisation.

### **3.4.6 Final conclusions**

Here automated imaging was used to successfully quantify the agonist and antagonist pharmacology of internalisation responses across Y receptor subtypes for the first time. These responses largely corresponded with those observed for upstream  $\beta$ -arrestin2 recruitment to the same Y receptor subtypes. Quantification of BiFC fluorescence was here able to distinguish between receptor mutations that alter the engagement of the  $\beta$ -arrestin activation (Y1H155P) or phosphorylation sensors (Y16A) with the receptor, with complementary effects in respect to receptor-GFP internalisation observed. This suggested shared molecular machinery was involved in both these processes, in that internalisation of Y receptor subtypes is likely to be largely driven by the recruitment of  $\beta$ -arrestin2.

The irreversibility of BiFC effectively constrains protein-protein interactions as complexes of precise composition. Subsequent chapters exploit this to allow the investigation of responses that can be directly attributable to this defined complex, such as interactions of GPCRs with  $\beta$ -arrestin2 (Chapter 4) or receptor-receptor homo (Chapter 5) or heterodimerisation (Chapter 6).

## **Chapter 4 – The use of fluorescence correlation spectroscopy alongside bimolecular fluorescence complementation to investigate the effects of $\beta$ -arrestin recruitment on the membrane mobility of NPY receptors**

### **4.1 Introduction**

The Y receptor family has previously been shown in Chapter 3 to be able to internalise in response to agonist, which correlated with  $\beta$ -arrestin2 association (Figures 3.9, 3.12). The role of  $\beta$ -arrestins in facilitating the endocytosis of many GPCRs (Chapter 1, section 1.6) by interacting with components of the endocytic machinery such as clathrin and AP-2 is well established. However  $\beta$ -arrestins have also been shown to act as signalling adaptors in their own right, with ligands able to selectively bias signalling towards  $\beta$ -arrestin dependent pathways (Kenakin and Christopoulos, 2013, Wisler et al., 2007), though the intracellular or plasma membrane location of such signalling complexes is currently unclear. At the plasma membrane for example, the spatial organisation of GPCRs into discrete membrane microdomains, through interactions with the cytoskeleton or the lipid environment (Cordeaux et al., 2008, Padgett and Slesinger, 2010, Insel et al., 2005), may organise intracellular signalling components in close proximity (Corriden et al., 2014). However due to the heterogeneity of these microdomains, and their small size, it is often difficult to study specific complexes, for example receptor/ $\beta$ -arrestin, in microdomains within single cells. One way in which this might be overcome is through the use of single cell imaging techniques such as fluorescence correlation spectroscopy (FCS), photon counting histogram analysis (PCH) and fluorescence recovery after photobleaching (FRAP). Potentially these techniques have great enough spatial resolution to investigate microdomain organisation of GPCR signalling domains, but the drawback has often been to define what is present in the

complex. Application of BiFC in combination with such methods provides one approach, which is explored in this Chapter.

#### **4.1.2 Fluorescence correlation spectroscopy (FCS)**

FCS is a live cell imaging technique used to measure the diffusion of fluorescent species through a defined confocal volume (Schwille, 2001, Diekmann and Hoischen, 2014, Briddon and Hill, 2007) (Figure 4.1, A). As fluorescent species traverse the detection volume they generate time dependent fluctuations in fluorescence intensity that can be analysed to give quantitative data on the nature of fluorescent particles present, including the average particle number and the average dwell time within the volume ( $\tau_D$ ) (Chapter 2, section 2.2.8).  $\tau_D$  in conjunction with the calibrated dimensions of the confocal volume can be used to determine diffusion coefficients ( $D$ ) for the fluorescent species (For equations see Chapter 2, section 2.2.11). Furthermore multiple  $\tau_D$  components isolated in autocorrelation analysis can provide quantitative information about different complexes involving the fluorescent species, where they are distinguished by sufficiently different diffusion rates (for example, free and receptor bound fluorescent ligands (Corriden et al., 2014). This information is extracted from within the detection volume used in FCS ( $\sim 0.25$ fl), comprising cellular regions containing only  $\sim 0.1 \mu\text{m}^2$  of plasma membrane consisting of typically 1-100 fluorescent particles. The diffusional behaviour of fluorescent ligands or GPCRs can then provide insights into the signalling events within these microdomains. For example FCS has been used to study the diffusion of adenosine receptors (Briddon et al., 2004a, Cordeaux et al., 2008),  $\beta_2$ -adrenoceptors (Hegener et al., 2004) somatostatin receptors (Patel et al., 2002) and GABA<sub>A</sub> receptors (Meissner and Haberlein, 2003).

There are limitations that need to be considered when using FCS to measure the diffusion of membrane bound receptors and signalling complexes. Firstly the 2D model used to fit the recorded fluctuations assumes a 2D plasma membrane when in reality it contains topographical 3D features such as clathrin coated pits. Additionally the use of changes in  $D$  to identify alterations

in molecular mass, indicative of events such as receptor dimerisation or clustering of signalling complexes, can often be problematic due to the cube root relationship that exists between changes in mass causing a change in  $D$  (Briddon and Hill, 2007). For example whilst the formation of a GPCR dimer from a monomer is a 2 fold change in mass, this only equates to a 1.25 fold change in  $D$ .

However FCS is sensitive enough to be used where receptor expression is low (such as in native tissues), as the amplitude of the autocorrelation curve is inversely proportional to the concentration of fluorescent particles present within the confocal volume (Diekmann and Hoischen, 2014). The largest limitation to using FCS is that only mobile fluorescent species will produce fluctuations that can be recorded. Therefore immobilised species will not be detected (Diekmann and Hoischen, 2014), for example receptors bound to the cytoskeleton (Lenne et al., 2006) or limited by other membrane components such as caveolae (Insel et al., 2005) and lipid rafts (Padgett and Slesinger, 2010).

#### **4.1.3 Photon counting histogram analysis (PCH)**

The same fluorescent fluctuations recorded in FCS readings can be alternatively analysed in respect to variation in amplitude rather than time. PCH analysis generates an alternative estimate of particle concentration than that determined by autocorrelation analysis, in addition to estimates of molecular brightness ( $\epsilon$ ) of fluorescent species (Chen et al., 1999, Kask et al., 1999). PCH is therefore a more sensitive indicator of changes in the stoichiometry of fluorescent complexes as molecular brightness is proportional to the number of fluorescent molecules within a complex as for example, the transition of a fully labelled GPCR from a monomer to dimer should theoretically result in a doubling of  $\epsilon$  (assuming a 1:1 stoichiometry of protein to fluorescent label).

Therefore FCS and PCH can provide complementary information on the diffusion characteristics and molecular composition of fluorescently tagged complexes such as adenosine A3 receptors (Cordeaux et al., 2008), serotonin

5-HT<sub>2c</sub> receptors (Herrick-Davis et al., 2012) and the biogenic amine  $\alpha_{1b}$ -adrenoceptors,  $\beta_2$ -adrenoceptors, muscarinic M<sub>1</sub> and M<sub>3</sub> and dopamine D1 receptors (Herrick-Davis et al., 2013).

#### **4.1.4 Fluorescence recovery after photobleaching (FRAP)**

FRAP is a technique that can also measure the mobility and molecular dynamics of fluorescently tagged molecules within the membranes of living cells (Bancaud et al., 2009, Axelrod et al., 1976, Dorsch et al., 2009). Since its development in the 1970s, FRAP has now become commonplace to study the dynamics of a wide range of cellular processes such as protein recycling, cytoskeletal dynamics, vesicle transport, cell adhesion and signal transduction (reviewed in (Diekmann and Hoischen, 2014)). Typically in a FRAP assay, fluorescent molecules within a small region of the cell are photobleached using a high power focused laser beam. Photobleaching causes irreversible damage to the chromophore by interrupting the cycle of repetitive excitation and emission so that these molecules can no longer fluoresce. The recovery of fluorescence within the bleached region is attributable to an inward diffusion of unbleached 'bright' fluorescent molecules which are exchanged for their bleached counterparts. This process is recorded over time at a low intensity laser power (Lippincott-Schwartz et al., 2003, McNally, 2008).

FRAP analysis can also provide additional information on the underlying molecular dynamics of the cellular environment, by giving estimates of the proportion of fluorescently tagged receptors that are mobile. This fraction can be significantly affected by the interaction of fluorescently tagged receptors of interest with other intracellular components and microdomains leading to restrictions on free diffusion (Diekmann and Hoischen, 2014). Both the mobile and immobile fractions can be calculated directly from the ratios of fluorescence intensities recorded pre and post bleaching (see Chapter 2, 2.12). The use of representative and background ROI's in addition to the experimental ROI monitors background bleaching over time, and facilitates the calculation of accurate diffusion coefficients ( $D$ ) (Figure 4.4, A; see Chapter 2, 2.12 for further details).

In contrast to FCS, FRAP measurements are made over a larger membrane area (Briddon and Hill, 2007) and are more likely to be influenced by the heterogeneity of the membrane surface. However unlike FCS, FRAP can estimate the proportion of fluorescent molecules which are mobile compared to immobile, providing information on the influence of stable cellular barriers to free diffusion within membrane regions. Therefore both techniques can complement one another to provide information on the micro (FCS) and macro (FRAP) diffusion of cellular complexes.

#### **4.1.5 The development of a novel BiFC pairing using superfolder GFP fragments**

BiFC using YFP fragments has been used previously in FCS studies to investigate the diffusion of adenosine receptor dimers (Briddon et al., 2008), serotonin 5-HT<sub>2C</sub> homodimers (Herrick-Davis et al., 2012) and histamine H<sub>1</sub> receptors (Rose et al., 2010). The irreversible nature of BiFC is potentially advantageous when investigating such interactions as it defines the precise composition of molecular complexes (Kerppola, 2008a, Kilpatrick et al., 2010). However, although YFP BiFC fragments were previously used successfully in Chapter 3 to investigate the  $\beta$ -arrestin2 association with Y receptors, these same constructs are less suited to single molecule imaging techniques. This is due to the high propensity of YFP molecules to spot bleach as they diffuse through the confocal volume (Schwille, 2001). YFP tagged molecules effectively 'disappear' from the confocal volume during the recording leading to artificially reduced dwell times and consequently faster observed diffusion coefficients (Rose et al., 2010, Briddon et al., 2004b, Schwille et al., 2000). This property has been illustrated in assessments of myc tagged H1-YFP receptors, using YFP fluorescence directly, where a steep linear relationship was observed between laser power and  $D$  (Rose et al., 2012).

GFP variants do not show as great an inclination to bleach at low laser powers and would therefore be better suited to FCS assays (Diekmann and Hoischen, 2014), as well as showing other improved photophysical characteristics for measurements (such as a reduced contribution to the autocorrelation trace

from fluorescent protein “blinking” at high frequencies). However the use of split eGFP fragments in complementation assays is problematic, as they show relatively poor complementation efficiencies in living cells under physiological conditions (Hu and Kerppola, 2003). The superfolder variant of GFP has also been developed for BiFC, but the fragments previously chosen (split point between  $\beta$  strands 10 and 11) were designed for spontaneous self assembly (Cabantous and Waldo, 2006). Therefore we proposed that the split point used previously in this (Chapter 3) and other YFP BiFC studies (Kilpatrick et al., 2010, Hu and Kerppola, 2003, Kerppola, 2008a, Rose RH, 2010) could be replicated to generate overlapping superfolder GFP N ( $\beta$  strands 8-9) and C ( $\beta$  strands 7-8) terminal fragments with BiFC properties suitable for monitoring agonist induced Y receptor-arrestin complexes using FCS, FRAP or PCH analysis.

## **4.2 Aims of this chapter:**

The overarching aim of this chapter was to use single molecule imaging techniques to probe the diffusion characteristics of Y1 and Y2 receptor complexes and investigate how these were affected by agonist stimulation, and the differing propensities of these subtypes to undergo agonist induced internalisation. We then aimed to characterise and use the novel superfolder GFP BiFC system to relate these data to defined Y receptor- $\beta$ -arrestin signalling complexes, using  $\beta$ -arrestin mutants to manipulate their interaction with clathrin coated pits.

Finally, in addition to FCS autocorrelation analysis and FRAP, we used PCH to obtain estimates of molecular brightness, in order to provide information on the molecular stoichiometry of Y1 receptors and  $\beta$ -arrestin complexes.

## 4.3 Results

### 4.3.1 The use of FCS and FRAP to investigate the plasma membrane diffusion of agonist stimulated NPY receptors

Initial FCS recordings were performed on unstimulated Y1-GFP receptors expressed in 293TR cells (GFP cell lines as previously described in Chapter 3) (Figure 4.1, B), with the confocal volume placed on the upper plasma membrane. All FCS recordings were performed at 22°C, rather than the 37°C incubation used for internalisation assays, as this decreased temperature is necessary to minimise cell membrane movements and consequent fluctuation artefacts. Fluctuations were fitted to a 2 dimensional model with two components of similar proportions ( $\tau_{D1}$ ,  $\tau_{D2}$  see Table 4.1), which also contains a pre-exponential term (not shown) to correct for rapid ( $< 5 \mu\text{s}$ ) fluctuations arising from photophysics of the fluorophore. The first component yielded a short dwell time ( $\tau_{D1}$ ) of 150-250 $\mu\text{s}$ , which was also interpreted as a consequence of the photophysics of the GFP protein as highlighted in previous studies (Schwille, 2001, Briddon et al., 2004b, Briddon et al., 2008, Licht et al., 2003). The second longer dwell time ( $\tau_{D2}$ ) was therefore interpreted as representing the dwell time and mobility of unstimulated Y1-GFP receptor proteins. Diffusion coefficients were derived from these dwell times normalised to the dimensions of the confocal volume calibrated with Rhodamine 6G on each experimental day.

Y1-GFP expressing cells were then pretreated with vehicle or 100nM NPY for 15min at 37°C, prior to FCS measurements being made at 22°C (Figure 4.1, C). During the initial 37°C period agonist-stimulated internalisation was observed, comparable to that seen previously for the Y1-GFP receptor in manual or automated confocal imaging (Chapter 3, Figures 3.4, 3.7A). Room temperature FCS recordings were made for up to 60min after control or agonist treatments, and no time dependent changes in either particle concentration or  $D$  were observed for Y1-GFP receptors, under control or NPY stimulated conditions, in traces obtained at different points over this period (Figure 4.2, A and B). The data presented henceforth were therefore pooled

over this recording time. FCS reads from the plasma membrane revealed no change in the concentration of Y1-GFP particles after NPY stimulation compared to controls (Figure 4.2, C), despite evident receptor internalisation. However a significant slowing of Y1-GFP lateral mobility was detected with NPY occupancy (Figure 4.2, D, see Table 4.1).

FCS measurements performed here utilised the superfolder variant of GFP previously used to measure the agonist induced internalisation of NPY receptor subtypes in plate reader assays (Chapter 3, Figure 3.9). This engineered variant contained mutations that increased the efficiency and rate of chromophore maturation resulting in a 60% increase in fluorescence intensity when compared to standard enhanced (e)GFP (Pedelacq et al., 2006). As this is the first documented set of FCS experiments using the superfolder GFP variant, its properties were verified by comparing the diffusion of HEK293TR Y1-eGFP receptors to that previously observed for Y1-GFP (superfolder). Using identical acquisition settings, comparable measurements of  $\tau_{D1}$ ,  $\tau_{D2}$ ,  $D$  (Table 4.1) and particle concentrations ( $63.7 \pm 4.2 \mu\text{m}^{-2}$  and  $62.3 \pm 5.0 \mu\text{m}^{-2}$ ;  $n=46-53$ ) were observed for Y1-eGFP in control and NPY stimulated conditions (Figure 4.2, C and D). This was expected given that the addition of superfolder mutations, whilst enhancing GFP folding efficiency, do not alter chromophore photophysics (Pedelacq et al., 2006).

The Y1 antagonist BIBO3304 (Wieland et al., 1998) was previously demonstrated to competitively inhibit NPY induced internalisation of Y1-GFP receptors (Chapter 3, Figure 3.10, A). Pretreatment with BIBO3304 ( $1\mu\text{M}$ ; 15min at  $37^\circ\text{C}$ ) did not significantly change the membrane mobility of Y1-GFP under control conditions (Figure 4.3, B;  $D = 2.32 \pm 0.22 \times 10^{-9} \text{ cm}^2 \text{ s}^{-1}$ ;  $n=28$ ). However BIBO3304 pretreatment was able to inhibit the effect of 100nM NPY treatment on the slowing of Y1-GFP diffusion. BIBO3304 treatment did not significantly affect the particle concentrations of Y1-GFP receptors under control or NPY stimulated conditions (A).

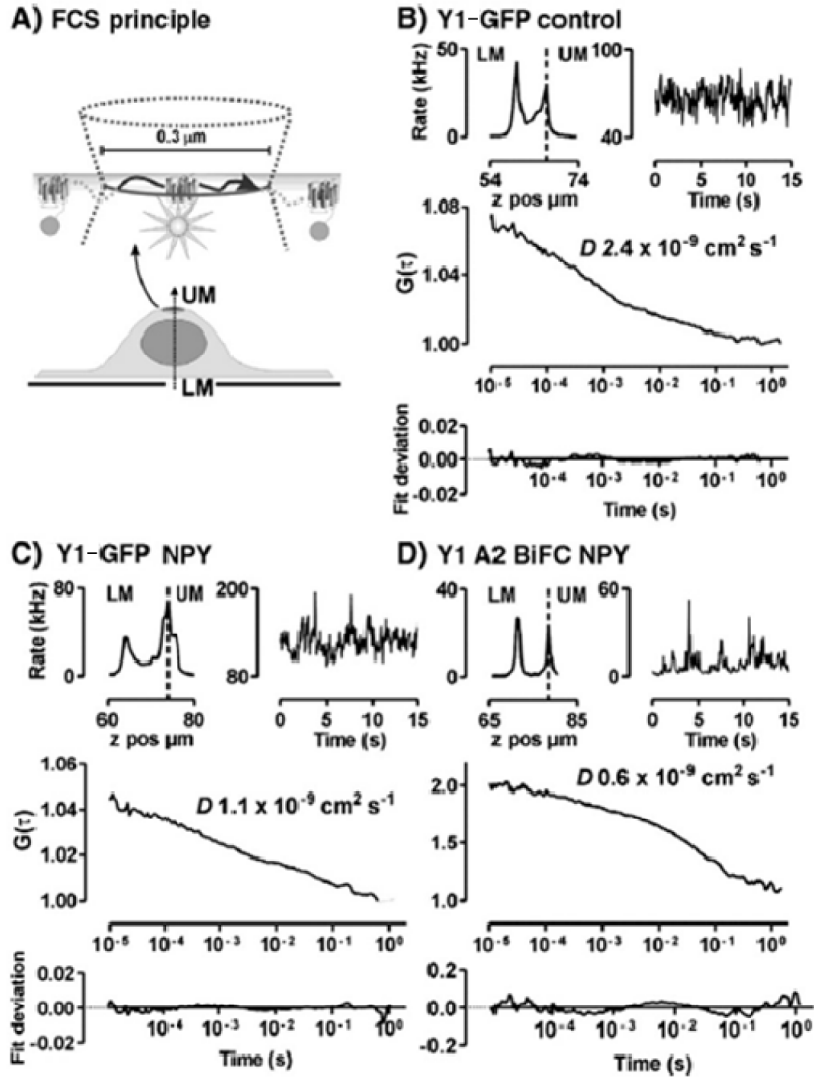


**Figure 4.1: Using FCS to measure the lateral mobility of GFP tagged Y receptors and Y receptor/ $\beta$ -arrestin2 GFP BiFC complexes**

The principle of FCS is shown in the schematic (A), whereby the diffusion of fluorescently tagged moieties through a stationary confocal volume can be measured. Example FCS recordings and autocorrelation analysis are shown for HEK293TR Y1-GFP cells under control (B), or pretreated 100nM NPY (15min at 37°C; C) or for HEK293T Y1/A2G cells pretreated with 100nM NPY (60min at 37°C; D). A confocal z-scan at the x-y location of the cell nucleus gives the upper and lower plasma membranes (UM and LM), shown by the peaks in the top left insets for B-D. The confocal volume was positioned on the upper membrane, and following a 15sec prebleach, fluorescence intensity fluctuations were recorded at 22°C (one 15sec read is shown in top right graphs for B-D). The larger graphs show the resultant autocorrelation curves that can be derived from these fluorescence fluctuations and the fit deviation from a 2 dimensional 2 component diffusional model (Chapter 2, section 2.2.11). Using this model, dwell times of receptor species within the confocal volume could be estimated, and the diffusion coefficient (D) derived from this using the dimensions of the calibrated confocal volume. Pooled data derived from this analysis are shown for Y1 in Figures 4.2 and 4.9 and Tables 1 and 3.

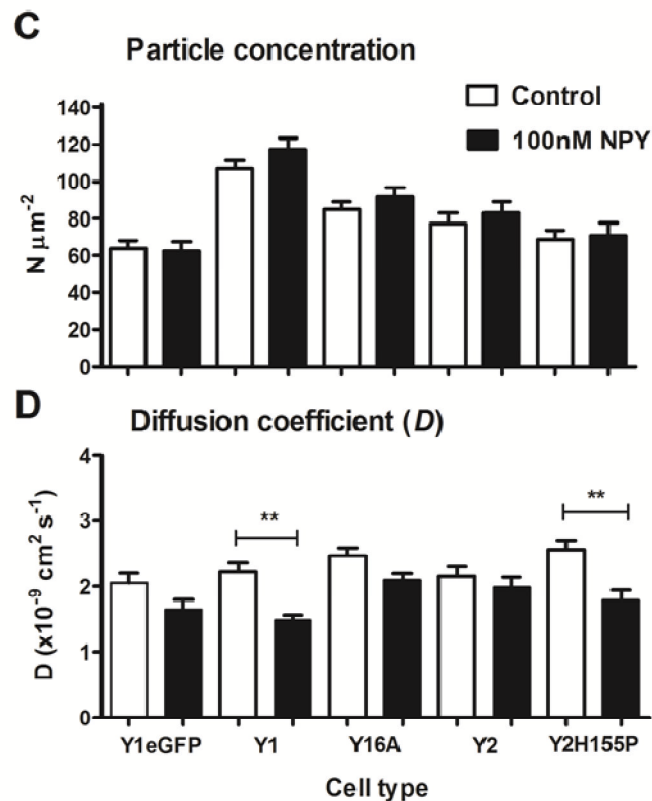
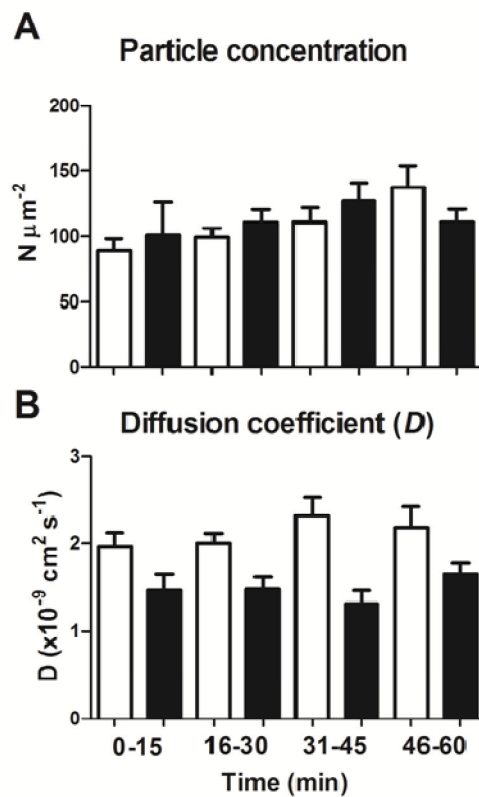


**Figure 4.2: Treatment with agonist results in a slowing of the lateral plasma membrane diffusion of Y receptors that internalise.**

Histograms show pooled data for particle concentrations (A) and diffusion coefficients (B) from FCS measurements (at 22°C) performed on HEK293TR cells expressing Y1-GFP under control or 100nM NPY stimulation (15min pretreatment at 37°C), pooled based on the time of recording. No significant differences were observed in responses over time providing justification for pooling responses across all time points. FCS derived particle concentrations (C) and diffusion co-efficients (D) were then obtained from HEK293TR cells expressing Y1-eGFP (n=53-46 cells), Y1-GFP (n=117-148), Y16A-GFP (n=87-95), Y2-GFP (n=47-50) or Y2H155P-GFP (n=35-51) receptors. Measurements of vehicle treated cells are shown in the open bars with solid bars representing observations from 100 nM NPY stimulated cells (15min pretreatment at 37°C). Significant differences between control or stimulated groups were determined using Kruskal-Wallis tests followed by Dunn's post tests and are indicated by \*\*p<0.01.

**Table 4.1: Summary of FCS parameters for GFP tagged NPY receptor subtypes**

Receptor	Condition	$\tau$ D1	$\tau$ D2		Concentration ( $\tau$ D2)	$D$	n cells
		$\mu$ s	%	ms			
<b>Y1-eGFP (5)</b>	Control	144 $\pm$ 5	46.3 $\pm$ 1.6	40.4 $\pm$ 2.2	63.7 $\pm$ 4.2	2.05 $\pm$ 0.2	53
	100nM NPY	190 $\pm$ 10	49.5 $\pm$ 2.1	59.3 $\pm$ 5.1	62.3 $\pm$ 5.0	1.64 $\pm$ 0.2	46
<b>Y1-GFP (16)</b>	Control	250 $\pm$ 9	41.6 $\pm$ 1.1	40.0 $\pm$ 1.6	102.5 $\pm$ 5.2	2.22 $\pm$ 0.2	148
	100nM NPY	258 $\pm$ 9	39.6 $\pm$ 1.2	60.4 $\pm$ 3.4	117 $\pm$ 6.5	1.48 $\pm$ 0.1	117
<b>Y16A-GFP (7)</b>	Control	230 $\pm$ 8	41.6 $\pm$ 1.4	33.9 $\pm$ 1.8	90.7 $\pm$ 5.4	2.45 $\pm$ 0.1	87
	100nM NPY	244 $\pm$ 8	42.6 $\pm$ 1.2	40.0 $\pm$ 2.0	89.3 $\pm$ 5.1	2.09 $\pm$ 0.1	95
<b>Y2-GFP (4)</b>	Control	223 $\pm$ 11	52.2 $\pm$ 0.6	37.5 $\pm$ 2.2	77.3 $\pm$ 5.7	2.15 $\pm$ 0.2	50
	100nM NPY	265 $\pm$ 12	51.6 $\pm$ 0.6	46.4 $\pm$ 4.8	83.0 $\pm$ 6.0	1.99 $\pm$ 0.2	47
<b>Y2H155P-GFP (4)</b>	Control	213 $\pm$ 11	53.4 $\pm$ 0.6	31.6 $\pm$ 2.1	68.4 $\pm$ 4.8	2.55 $\pm$ 0.1	51
	100nM NPY	260 $\pm$ 16	53.1 $\pm$ 1.3	53.0 $\pm$ 6.2	70.5 $\pm$ 7.3	1.78 $\pm$ 0.2	35

D values were calculated from measurements of dwell time ( $\tau$ D2) using a 2D diffusion model with 2x dwell components. The %  $\tau$ D2 refers to the percentage contribution of the  $\tau$ D2 dwell time component to the autocorrelation curve.

n numbers in parenthesis refers to the number of independent experiments performed, whilst n values in the table refer to the total number of cell recordings. Pooled data are expressed as mean  $\pm$  s.e.m..

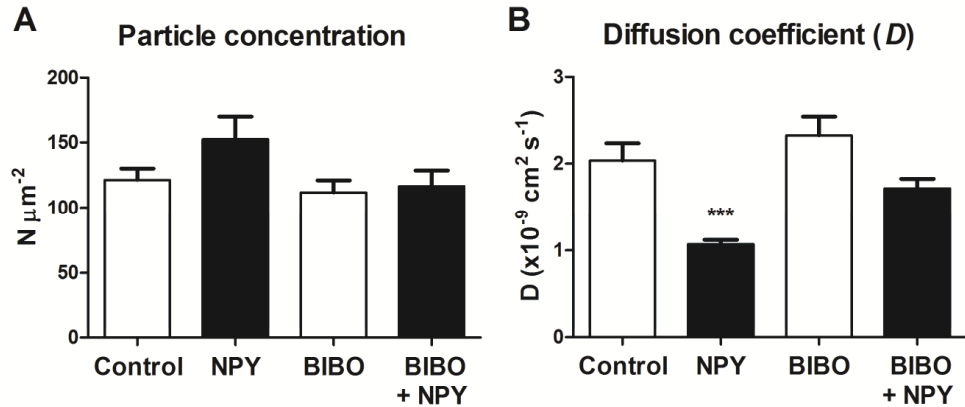


**Figure 4.3: Changes in agonist stimulated membrane Y1-GFP receptor mobility are inhibited by the Y1 selective antagonist BIBO3304**

Histograms showing pooled data for FCS measurements of particle concentrations (A) and diffusion coefficients (B) observed in HEK293TR Y1-GFP cells. Cells were pretreated with BIBO3304 (1 $\mu\text{M}$ ; 15min at 37 $^{\circ}\text{C}$ ) followed by incubation with vehicle (control; open bars) or NPY (100nM; solid bars) for 15min at 37 $^{\circ}\text{C}$ . FCS measurements were then obtained at 22 $^{\circ}\text{C}$  (n=20-29 cells). Significant differences between control and NPY stimulated data groups are indicated by \*\*\* p<0.001 (Kruskal-Wallis, followed by Dunn's post hoc test). Data was pooled from 4 independent experiments.

Previous investigation of HEK293TR cells stably expressing native (Y1 or Y2) or mutant (Y16A, Y2H155P) GFP tagged Y receptor subtypes revealed differences in the extent of their agonist induced endocytosis. Y1 receptors showed rapid internalisation in response to agonist, which was abolished by the selective introduction of 6 alanine mutations (6A) into the Y1 C terminus (Chapter 3, Figure 3.7, B; Figure 3.16). Y2-GFP receptors showed reduced NPY induced internalisation when compared to Y1-GFP (Figure 3.7, A), however the Y2H155P mutation was able to enhance the potency of NPY at inducing Y2 receptor internalisation (Y2H155P; Figure 3.7,C and Figure 3.16). We therefore used these mutants to test whether the observed changes in Y receptor diffusion following agonist exposure could be accounted for by predicted interaction with the endocytosis machinery. In order to maximise the difference in the extent of agonist-stimulated endocytosis by the different receptors, pretreatment with 100nM NPY was used throughout (Chapter3, Figure 3.9). In FCS measurements of Y16A-GFP, NPY pretreatment had no effect on membrane motility, unlike the significant reduction in D observed

for the wildtype Y1 receptor (Figure 4.2, D). Additionally NPY pretreatment did not alter the lateral diffusion of wildtype Y2-GFP, however a significant decrease in the rate of diffusion was introduced by the Y2H155P mutation. However NPY pretreatment had no effect on cell surface particle concentrations of native or mutant Y1 or Y2-GFP receptors (Figure 4.2, C). This was surprising for native Y1-GFP or Y2H155P-GFP receptors given the receptor internalisation previously seen (Chapter 3, Figures 3.7,B, 3.16,C). This observation might be explained by NPY increasing the proportion of the mobile fraction of receptor complexes present at the plasma membrane, particularly as immobile fractions are undetectable by FCS (Briddon and Hill, 2007). This might compensate for the overall loss of Y receptor-GFP from the cell surface as endocytosis proceeds.

In order to investigate the role of the mobile receptor fraction, FRAP experiments were performed on HEK293TR Y1-GFP or Y16A-GFP cells at 37°C (Figure 4.4). A high fraction (approximately 80%) of mobile receptors was observed for unstimulated Y1-GFP, which did not change with NPY stimulation or following the introduction of the 6A mutations (Figure 4.5, B). Similar to observations using FCS, FRAP studies revealed a significant slowing in the rate of Y1-GFP diffusion following NPY stimulation (C;  $D = 0.68 \pm 0.04 \times 10^{-10} \text{ cm}^2 \text{ s}^{-1}$ ; \*\* $p < 0.01$ ;  $n = 23$ ) when compared to vehicle (control;  $D = 0.99 \pm 0.06 \times 10^{-10} \text{ cm}^2 \text{ s}^{-1}$ ;  $n = 19$ ). These  $D$  values were considerably lower (approximately 10 fold) than those obtained using FCS. No effect of agonist on the diffusion of Y16A-GFP receptors was observed using FRAP.

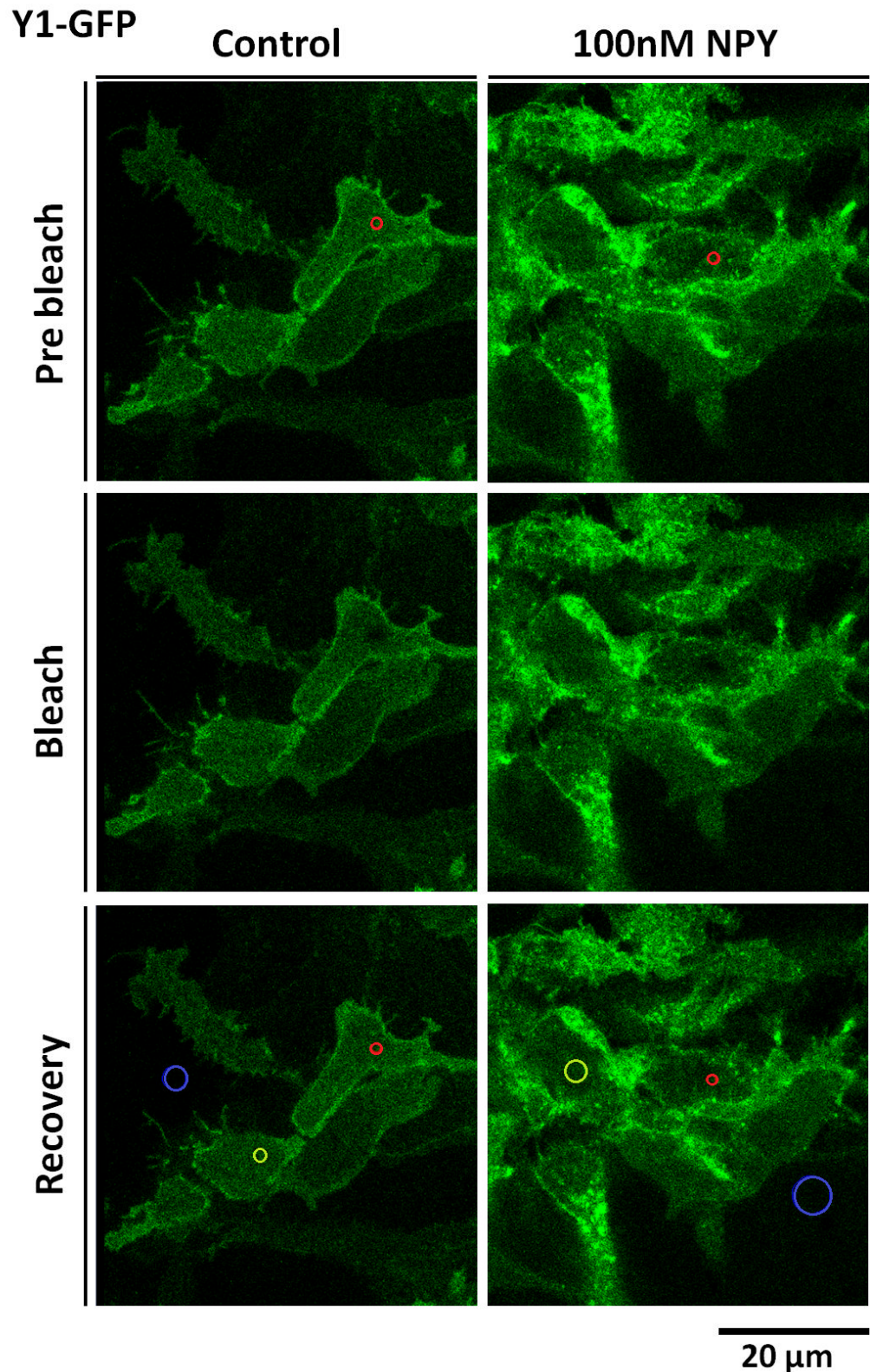


**Figure 4.4: Representative images of a FRAP experiment**

Representative images of FRAP experiments performed on the lower plasma membrane of HEK293TR expressing Y1-GFP receptors under control or agonist stimulated conditions (100nM NPY; 15min). Example images were taken prebleach, immediately post bleach and following a 90sec recovery period.

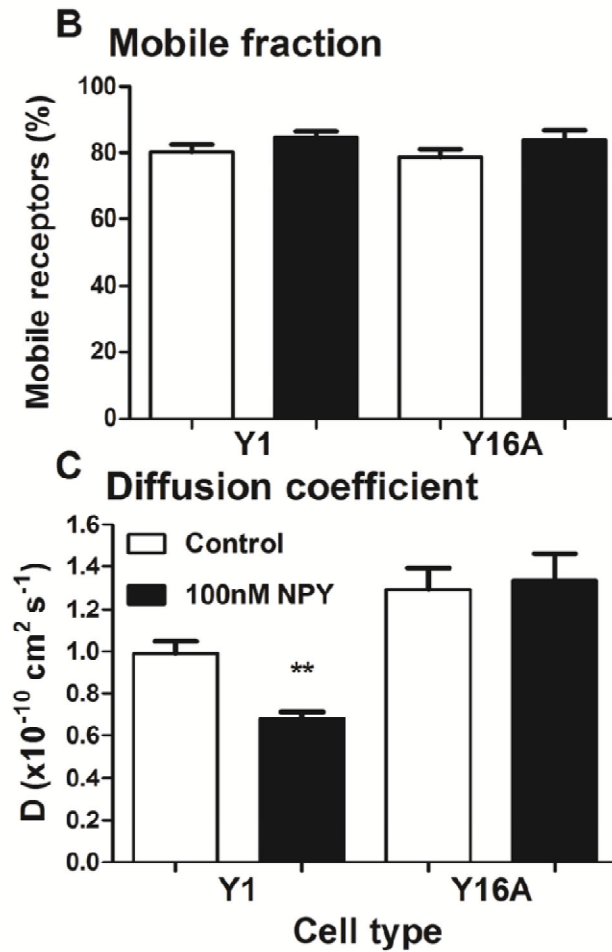
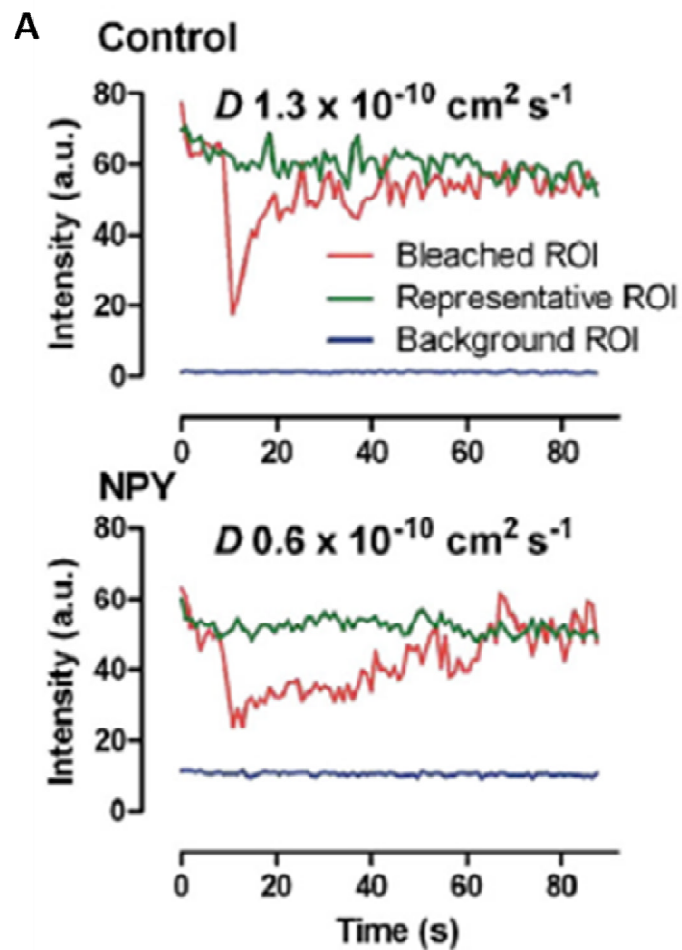


**Figure 4.5: Pooled data derived from FRAP experiments showing the fraction of mobile receptors and estimated diffusion coefficients**

Fluorescence intensity traces are shown over time taken from the bleached (red), representative (green) or background ROIs (blue) indicated in the recovery image from Figure 4.4. Data were fitted to a single phase exponential of recovery (Zeiss Zen 2010 software; see section 2.2.12) and gave estimates of mobile receptor fractions and diffusion coefficients (D) with pooled data (n=19-24 cells; 3 experiments) shown in panels B and C respectively. Significant differences between control or agonist stimulated groups were determined using the Kruskal-Wallis test followed by Dunn's post tests and are indicated by \*\*p<0.01.

#### **4.3.2 The use of superfolder GFP BiFC to detect Y receptor-arrestin complexes using FCS**

A clear correlation was revealed from FCS and FRAP investigations between the agonist induced changes in Y1 or Y2 receptor mobility and the ability of these receptors to undergo agonist induced endocytosis. However the molecular composition of species diffusing through the confocal volume, for example the receptor- $\beta$ -arrestin complexes that might be involved in this pathway, are difficult to define using standard FCS measurements using GFP-tagged receptors.

Therefore methods that identify the actual molecular complexes present within the confocal volume will potentially improve the interpretation of *D* measurements and their changes. To this end, a novel version of BiFC utilising superfolder GFP fragments was created to define Y1 receptor/ $\beta$ -arrestin complexes of defined composition in FCS studies. The use of a mutant form of  $\beta$ -arrestin2 lacking a proposed clathrin binding site (LIEFD; residues 373-377 deleted; termed A2LIEFD throughout (ter Haar et al., 2000, Krupnick et al., 1997a)) was also used to investigate the potential influence of clathrin interaction of diffusion rates of Y1/ $\beta$ -arrestin2. As described in Chapter 3, dual stably transfected HEK293T cells lines were established that coexpressed Y1 receptor-Gc and clonal  $\beta$ -arrestin1 (A1),  $\beta$ -arrestin2 (A2) or  $\beta$ -arrestin2 $\Delta$ LIEFD (A2LIEFD) tagged with the complementary Gn fragment. These cell lines were termed Y1/A1G, Y1/A2G or Y1/A2LIEFDG respectively, with the G representing the superfolder GFP BiFC variant.

[<sup>125</sup>I] PYY binding confirmed that all Y1/ $\beta$ -arrestin GFP BiFC cell lines were able to specifically bind PYY and BIBO3304 with high affinity and were sensitive to GTP $\gamma$ S (Kilpatrick et al., 2012). Bmax values derived from [<sup>125</sup>I] PYY displacements confirmed similar expression levels for Y1/A2G, Y1/ A2G and Y1/A2LIEFD G BiFC cell lines (Table 4.2). Confocal and platereader imaging experiments were then performed using these lines, as described for the YFP BiFC system to detect receptor-arrestin association (Chapter 3, Figure 3.4.2.1). NPY stimulated complementation of the superfolder GFP fragments was

indicated by fluorescence in live transfected HEK293T cells (Figure 4.6), following association of the Y1 receptor with  $\beta$ -arrestin. For the Y1/A2G cell line, minimal intracellular fluorescence was observed under control conditions, however stimulation with 100nM NPY (60min, 37°C/5%CO<sub>2</sub>) generated novel Y1 receptor/ $\beta$ -arrestin2 BiFC complexes that were predominantly localised to intracellular perinuclear compartments and to a lesser extent the plasma membrane (A; Y1/A2G). However under basal conditions some pre existing Y1/A1G BiFC complexes were observed at the plasma membrane (B). After NPY stimulation of Y1/A1G lines, brighter intracellular fluorescent compartments were observed, suggesting both redistribution of pre-existing complexes and *de novo* complementation.

The specificity of the GFP BiFC signal for both arrestin isoforms was verified using control Y16A receptors, which do not recruit arrestin (Chapter 3; Figure 3.17). No BiFC was detected under basal or agonist stimulated conditions for Y16A/A2G or Y16A/A1G (C or D). In these confocal experiments, incorporation of the clathrin binding deletion  $\Delta$ LIEFD into  $\beta$ -arrestin2 also resulted in more cell surface BiFC in the Y1/A2LIEFDG cell line, when compared to Y1/A2G cells, under basal or agonist stimulated conditions (E). However substantial localisation of Y1/A2 $\Delta$ LIEFDG BiFC complexes after NPY stimulation in intracellular compartments was still observed.

**Table 4.2: [<sup>125</sup>I] PYY membrane competition binding parameters derived from Y1-Gc/ $\beta$ -arrestin-Gn constructs**

Cell line	PYY	BIBO3304	GTP $\gamma$ S		Bmax
	pIC <sub>50</sub>	pIC <sub>50</sub>	pIC <sub>50</sub>	% inhibition	pmol/mg <sup>-1</sup>
<b>Y1/A1G</b>	9.5 ± 0.2	9.6 ± 0.1	8.6 ± 0.3	68.5 ± 13.9	0.7 ± 0.2
<b>Y1/A2G</b>	9.2 ± 0.1	9.7 ± 0.1	8.5 ± 0.2	66.7 ± 7.0	0.9 ± 0.4
<b>Y1/A2LIEFDG</b>	9.4 ± 0.1	9.8 ± 0.2	8.5 ± 0.1	54.9 ± 7.0	1.1 ± 0.3

Table taken from (Kilpatrick et al., 2012).

All parameters were obtained from [<sup>125</sup>I] PYY competition membrane binding experiments (using 16pM [<sup>125</sup>I] PYY) as described in Chapter 2, section 2.2.3.

% inhibition of TSB refers to the displacement by 1 $\mu$ M competing ligand, as a % of the total specific binding (TSB) defined in the absence / presence of 1  $\mu$ M PYY.

Details of the  $\beta$ -arrestin2LIEFD deletion are given in the text.

n =3+ independent experiments

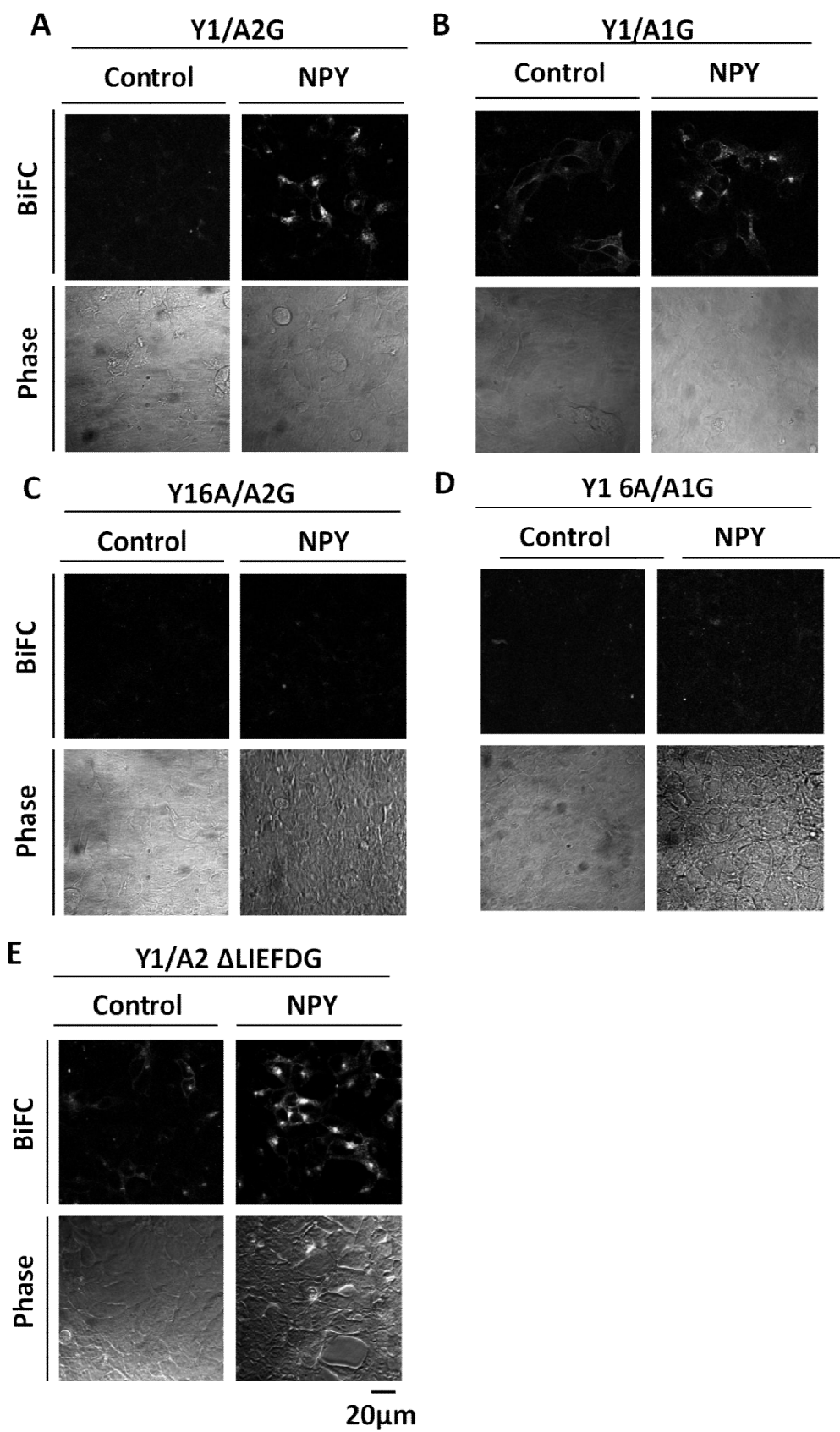


**Figure 4.6: Confocal microscopy images identifying the association of Y1 receptors with  $\beta$ -arrestin2 using split sfGFP BiFC**

Live HEK293T cells stably coexpressing Y1 receptor-Gc and either  $\beta$ -arrestin2-Gn (termed Y1/A2G),  $\beta$ -arrestin1-Gc (Y1/A1G) or  $\beta$ -arrestin2 $\Delta$ LIEFD-Gn (Y1/A2LIEFDG) were imaged using confocal microscopy. Equivalent images were also obtained for phosphorylation deficient mutant Y16A receptor-Gc coexpressed with  $\beta$ -arrestin-Gn (Y16A/A2G or Y16A/A1G). BiFC fluorescence was investigated under both control or agonist simulated conditions (100nM NPY, 60min at 37°C). Acquisition settings were kept consistent across all cell lines from all experiments (from n=3-5).

The kinetics of the agonist stimulated development of Y1/A1G and Y1/A2G BiFC, were quantified using automated confocal plate reader images and granularity analysis (Figure 4.7, A and B). Cells expressing Y1/A1G or Y1/A2G constructs were stimulated with 100nM NPY (60min at 37°C) with  $t_{1/2}$  values for BiFC responses of  $3.0 \pm 0.8$  min (n=4) and  $5.2 \pm 1.4$  min (n=5) respectively (Figure 4.8 A and B). The reversibility of superfolder BiFC responses was also investigated, by washing plates twice after the initial 100nM NPY timecourse stimulation and then leaving cells in media minus agonist for 60min at 37°C prior to fixation. This protocol has previously been shown to be sufficient to enable Y1 receptor-YFP recycling to the plasma membrane after internalisation (Kilpatrick et al., 2010). For both Y1/A1G (A) and Y1/A2G cells (B), the formation of endosomal BiFC complexes was largely irreversible. NPY was equipotent (60min at 37°C) in recruiting  $\beta$ -arrestin1 or 2 to the Y1 receptor (Figure 4.7 C), with  $pEC_{50}$  values of  $8.3 \pm 0.1$  (n=4) and  $8.6 \pm 0.1$  (n=4). Overall these values were also similar to previous potency estimates of agonist induced Y1 receptor / $\beta$ -arrestin association measured using split YFP complementation (Chapter 3, Figure 3.11, B) or internalisation of Y1 receptors tagged with full length YFP (Kilpatrick et al., 2010).

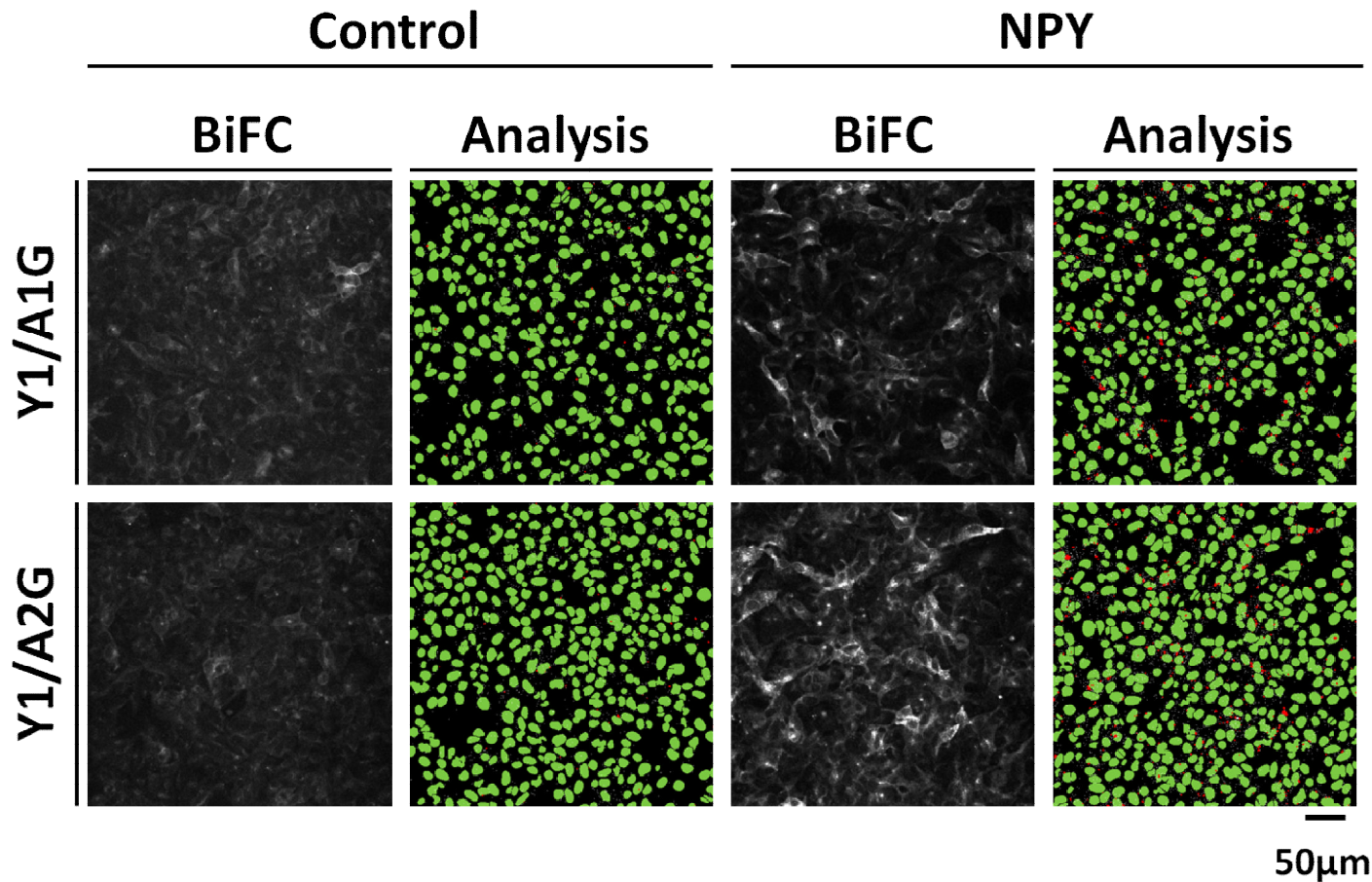


**Figure 4.7:** Representative images of Y1/A1G and Y1/A2G cell lines taken using an IX Ultra confocal plater reader

HEK293T cells stably coexpressing Y1/A1G or Y1/A2G were treated with either vehicle or 100nM NPY (60min at 37°C) prior to fixation, nuclear staining and imaging using a IX Ultra confocal plater reader. The analysis panel shows the use of a granularity algorithm which identified nuclei (green spots; original H33342 images not shown) and BiFC fluorescent compartments (red spots; >3μm diameter). This algorithm allowed the measurement of the average granule intensity on a per cell basis for each image. The quantified pooled data of this data is shown in Figure 4.8 .

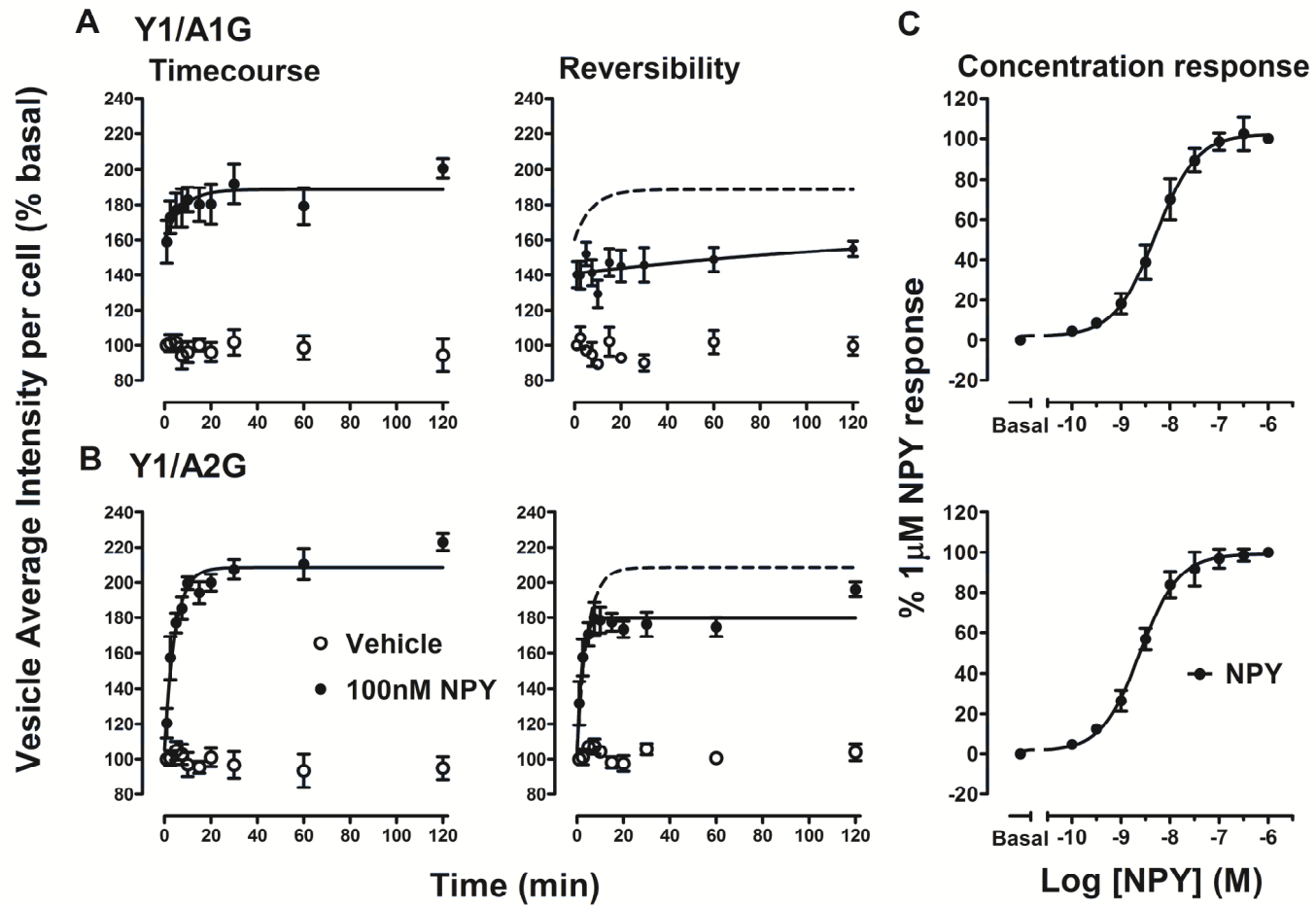


**Figure 4.8: Timecourse, reversibility and concentration response relationships for the association of Y1 receptor and  $\beta$ -arrestin measured using GFP BiFC**

BiFC responses resulting from interactions of Y1 receptors with  $\beta$ -arrestin1 (Y1/A1G; A) or-2 (Y1/A2G; B) were determined from quantitative analysis of automated platereader images. Timecourses of stimulation (n=4-5) were performed over 120min at 37°C with either 100nM NPY (closed circles) or vehicle controls (open circles). Estimated half times were determined from curve fitting to a one phase association and are stated in the text. In reversibility experiments 100nM NPY timecourses were performed as before, but then agonist was removed by washing (2x rinse, 1x60min at 37°C). Cells were then fixed, nuclei stained and imaged using a IX Ultra confocal platereader. BiFC responses from pooled data of washed cells were compared with the original curve fits without agonist removal (dotted line; taken from A or B). Additionally, NPY concentration response curves (C; 60min at 37°C; n=4) were performed for both Y1/A1G and Y1/A2G complexes with pEC<sub>50</sub> values quoted in the text.

**4.3.3 Molecularly defined Y1 receptor-arrestin BiFC complexes show slow lateral mobility**

Y1/A1G and Y1/A2G BiFC cells lines were then used to relate whether the NPY induced changes observed in the diffusion of Y1-GFP receptors could be correlated with the properties of molecular Y receptor-arrestin complexes. FCS measurements were recorded from Y1/A1G and Y1/A2G cell lines following a 60min NPY prestimulation to generate BiFC (100nM; 37°C). Although NPY induced BiFC complexes were predominantly localised to intracellular compartments, the plasma membrane localisation was sufficient to allow FCS recordings to be made. Similar to FCS measurements of GFP tagged Y receptors, a 2 dimensional 2 component model was sufficient to fit recorded fluorescence fluctuations. Comparable  $\tau$ D1 values (representing fluorophore photophysics) were observed for recomplemented superfolder GFP when compared to full length superfolder GFP (Tables 4.1 and 4.3). Particle concentrations observed for GFP Y1 receptor– arrestin BiFC complexes (Y1/A1G, Y1/A2G and Y1/A2LIEFDG) were substantially decreased compared to the higher expressing Y1-GFP receptors (Figure 4.9, A). Similar rates of mobility were observed for NPY stimulated Y1 receptors complexed with either  $\beta$ arrestin1 or  $\beta$ -arrestin2 (see Figure 4.9, B; Table 2). These diffusion coefficients were also comparable to those observed for Y1-GFP

receptors stimulated by NPY and were significantly slower than those observed for Y1-GFP under basal conditions ( $p < 0.01$  \*\* or  $p < 0.001$  \*\*\*).

However deletion of the LIEFD motif within  $\beta$ -arrestin2 had no effect on the diffusion rates of Y1 receptor/ $\beta$ -arrestin2 GFP BiFC complexes. For Y1/A1G and Y1/A2LIEFDG BiFC complexes, preformed BiFC fluorescence was also observed at the plasma membrane under basal conditions (Figure 4.6), allowing FCS measurements under unstimulated conditions to be recorded. There was evidence for a reduction in diffusion compared to unstimulated Y1-GFP receptors, however this change was not significant (Figure 4.9, B).

Likewise, FRAP analysis revealed that the fraction of mobile Y1/A2G and Y1/A2LIEFDG particles formed following 60min 100nM NPY stimulation (37°C) were consistent with that observed for Y1-GFP ( $80.0\% \pm 2.6$  and  $79.6\% \pm 2.6$  respectively;  $n=26-31$ , Figure 4.5, B). Diffusion rates of Y1/A2G and Y1/A2LIEFDG, derived from FRAP analysis, were also comparable to NPY stimulated Y1-GFP expressing cells ( $D=0.63 \pm 0.03 \times 10^{-10} \text{ cm}^2 \text{ s}^{-1}$  and  $0.67 \pm 0.08 \times 10^{-10} \text{ cm}^2 \text{ s}^{-1}$  respectively;  $n=26-31$ ).

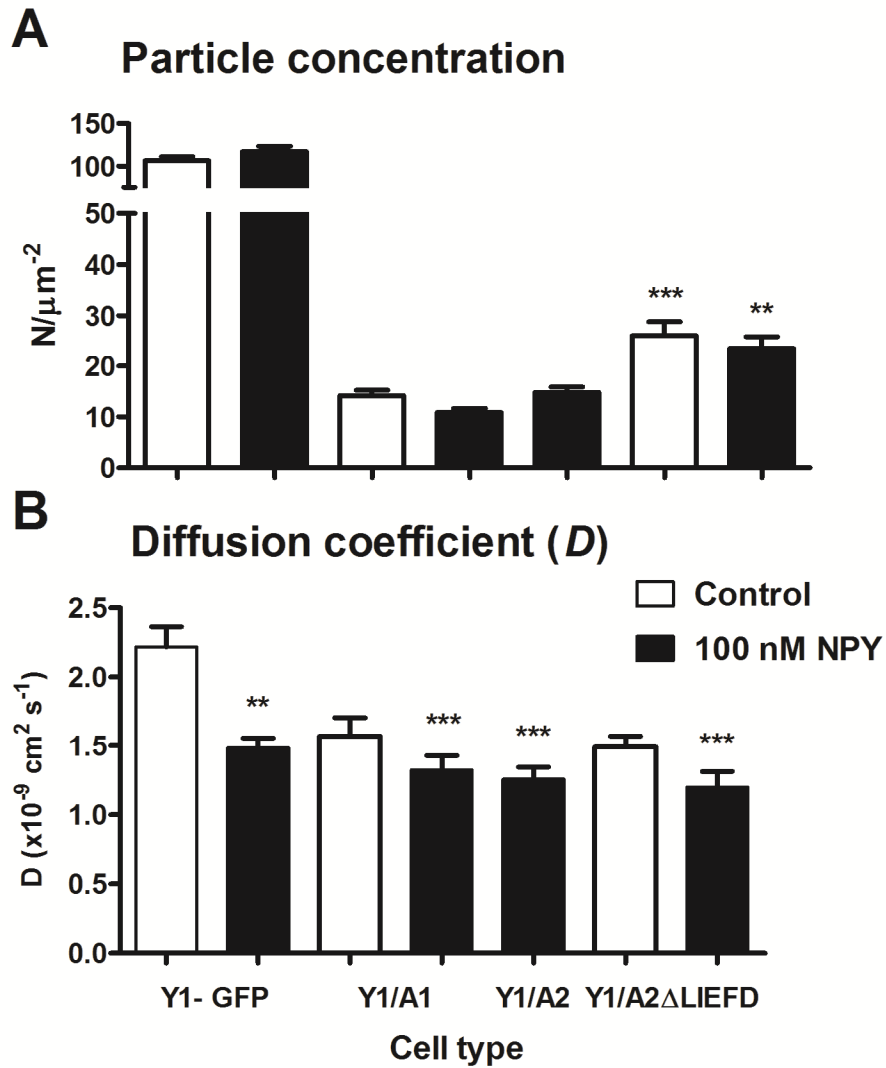


**Figure 4.9: The use of FCS to determine the diffusion of Y1 receptor/ $\beta$ -arrestin2 GFP BiFC complexes**

FCS measurements were taken from the upper membrane of Y1/A1G (control n=21; NPY n=49 cells), Y1/A2G (NPY n=64) or Y1/A2LIEFDG cells (control n=35; NPY n=22). Cells were pretreated with control (open bars) or 100nM NPY (closed bars) for 60min at 37°C prior to FCS measurements at 22°C. Data was pooled for both particle concentrations (A; specific to  $\tau$ D2 component) and diffusion coefficients (B; derived from  $\tau$ D2). Responses were compared with measurements of Y1-GFP receptors acquired under identical conditions. Plasma membrane fluorescence in Y1/A2G cells under control conditions was negligible with no fluctuations able to be recorded. Significant differences in responses refer to comparison with Y1/A2G NPY data (for A) or Y1-GFP control data (for B) using the Kruskal-Wallis test with Dunn's post test ( $p < 0.01$  \*\* or  $p < 0.001$  \*\*\*).

**Table 4.3: Summary of FCS parameters for Y1 receptor /  $\beta$ -arrestin GFP BiFC complexes**

Receptor	Condition	$\tau$ D1	$\tau$ D2		Concentration ( $\tau$ D2)	$D$	n cells
		$\mu$ s	%	ms	$N \mu\text{m}^{-2}$	( $\times 10^{-9} \text{cm}^2 \text{s}^{-1}$ )	
<b>Y1/A1G (4)</b>	Control	246 $\pm$ 20	52.1 $\pm$ 0.8	48.4 $\pm$ 3.7	14.2 $\pm$ 1.1	1.57 $\pm$ 0.1	21
	100nM NPY	279 $\pm$ 29	60.3 $\pm$ 1.4	72.3 $\pm$ 5.6	10.9 $\pm$ 0.8	1.33 $\pm$ 0.1	49
<b>Y1/A2G (9)</b>	100nM NPY	278 $\pm$ 17	63.3 $\pm$ 1.4	72.6 $\pm$ 6.2	9.5 $\pm$ 0.8	1.26 $\pm$ 0.1	64
<b>Y1/A2LIEFDG (4)</b>	Control	259 $\pm$ 17	60.0 $\pm$ 1.6	48.8 $\pm$ 2.3	30.6 $\pm$ 4.8	1.51 $\pm$ 0.1	35
	100nM NPY	254 $\pm$ 11	57.8 $\pm$ 3.4	77.1 $\pm$ 7.0	28.1 $\pm$ 6.1	1.20 $\pm$ 0.1	22

D values were calculated from measurements of dwell time ( $\tau$ D2) using a 2D diffusion model with 2x dwell components.

Pooled data are expressed as mean  $\pm$  s.e.m.

The %  $\tau$ D2 refers to the percentage contribution of the  $\tau$ D2 dwell time component to the autocorrelation curve amplitude.

n numbers in parenthesis refers to the number of independent experiments performed, whilst n values in the table refer to the total number of cell recordings.

#### 4.3.4 The use of PCH analysis to investigate the stoichiometry of Y1-GFP and Y1/ $\beta$ -Arrestin BiFC complexes

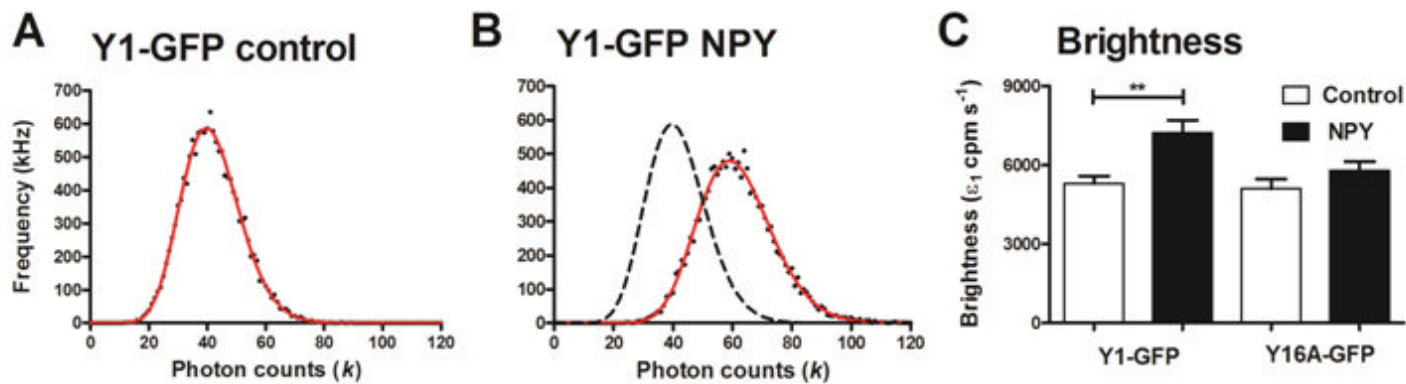
The formation of GPCR dimers, higher order oligomers or signalling clusters microdomains, has the potential to significantly impact GPCR signalling events (addressed in greater detail in chapters 5 and 6). However standard FCS measurements of mobility are relatively insensitive to detecting small changes in molecular mass. (Schwille, 2001). In practice changes in  $D$  need to be more pronounced to reliably reflect changes in molecular mass. However the same fluorescence fluctuations can be analysed using PCH, to generate information on the molecular brightness ( $\epsilon$ ) of each species, in addition to an alternative measure of particle concentration to that derived from autocorrelation (FCS) analysis.

Fluorescence fluctuations recorded from HEK293TR Y1-GFP and HEK293T Y1/A2G BiFC were analysed using PCH (Figure 4.10). Frequency histograms were generated from Y1-GFP data, using a 1ms bin time chosen to be below the dwell time ( $\tau_{D2}$ ) of the diffusing receptors. This distribution was fitted sufficiently with a 1 component model, under basal (A) and 100nM NPY stimulated conditions (B). Stimulation of Y1-GFP with NPY resulted in an increase (albeit not significant) of particle concentrations when compared to basal conditions ( $350 \pm 19 \mu\text{m}^{-2}$  ( $n=57$ ) and  $441 \pm 37 \mu\text{m}^{-2}$  ( $n=47$ ) for vehicle or 100nM NPY stimulations respectively). A significant 1.5 fold increase in particle brightness was observed for Y1-GFP following NPY stimulation (C;  $P < 0.01$  \*\*; Table 4.4). This was consistent with NPY inducing the formation of particles containing more fluorescent receptors. Pretreatment with the Y1 selective antagonist BIBO3304 ( $1\mu\text{M}$ ; 15min at  $37^\circ\text{C}$ ) abolished the NPY induced increase in molecular brightness previously observed (brightness  $\epsilon$  of  $5412 \pm 502$  counts per molecule (cpm)  $\text{s}^{-1}$  in cells treated with BIBO3304 alone versus  $5740 \pm 388$  cpm  $\text{s}^{-1}$  for BIBO3304 followed by 100 nM NPY,  $n=24-28$ ). Under basal conditions, PCH analysis revealed that Y16A-GFP showed similar particle concentrations and molecular brightness to that seen for unstimulated Y1-GFP (Table 4.4). However following NPY treatment, Y16A-

GFP cells did not show a similar increase in molecular brightness or particle number to that observed for native Y1-GFP.

PCH analysis performed on fluctuations obtained from Y1 receptor/ $\beta$ -arrestin BiFC complexes (using Y1/A2G or Y1/A2LIEFDG cell lines) required a model with 2 components for effective fitting (Figure 4.10, D). The predominant species observed for both NPY stimulated Y1/A2G and Y1/A2LIEFDG had particle concentrations of  $97.2 \pm 20.3 \mu\text{m}^{-2}$  (n=18) and  $97.6 \pm 27.5 \mu\text{m}^{-2}$  (n=14) respectively. The molecular brightness of this component for both Y1/A2G and Y1/A2LIEFDG was similar to that observed for unstimulated Y1-GFP (Figure 4.10, E; Table 4.4). PCH analysis also revealed a second component for Y1/A2G and Y1/A2LIEFDG. This component had a 5-8 fold increased  $\epsilon$  compared to the first component, and likely represented aggregated BiFC complexes. However component 2 only constituted  $12.7 \pm 2.4 \%$  (Y1/A2G) or  $8.6 \pm 1.2 \%$  (Y1/A2LIEFDG) of the total particle population (F).

## Y1 receptor GFP



## Y1 / $\beta$ -arrestin2 GFP BiFC

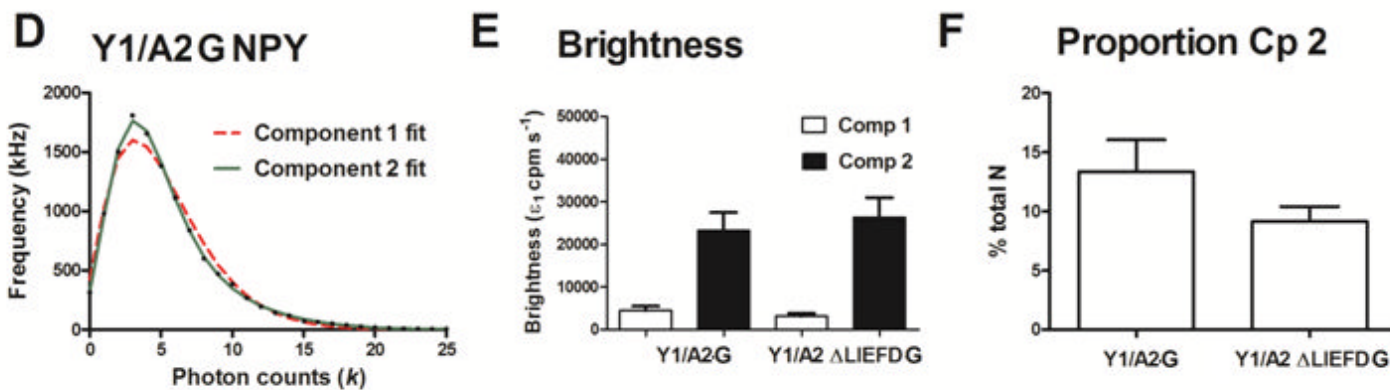


**Figure 4.10: The use of PCH analysis to determine the molecular brightness of Y1-GFP or Y1/ $\beta$ -arrestin2 GFP BiFC complexes**

Panels A and B show representative traces of 1 component PCH fits (red line) of single recordings of Y1-GFP cells following control or 100nM NPY stimulation (from at least 3 individual experiments). Photon counting frequency histograms were created using a bin time of 1ms, from a 15sec read. Pooled data for Y1-GFP (n=47-57) or Y16A-GFP (n=30-43) receptors (C) showed the effect of NPY treatment on particle brightness ( $\epsilon$ ).  $p < 0.01$  \*\* control vs NPY. A 1 component fit was not adequately able to model PCH data from Y1/A2G NPY treated cells (D; red line). Fitting was improved by using a 2 component model (green line) with the proportion of each component determined in the analysis. Both component 1 and 2 (Cp 1, Cp2) showed substantially different molecular brightness values (pooled data shown in E) for NPY stimulated Y1/A2G or Y1/A2 $\Delta$ LIEFDG cells (n=14-19 from 3 individual experiments). No significant difference was found in the proportion of component 2, representing very bright aggregated particles, between Y1/A2G or Y1/A2LIEFDG cells ( $p=0.051$ ).

**Table 4.4: Summary of PCH parameters for Y1-GFP and Y1/ $\beta$ -arrestin2 GFP BiFC complexes**

Receptor	Condition	Concentration ( $N \mu m^{-2}$ )		Brightness ( $\epsilon$ )		n cells
		Component 1	Component 2	Component 1	Component 2	
<b>Y1-GFP (7)</b>	Control	349.9 $\pm$ 18.8	/	5299 $\pm$ 291.4	/	57
	100nM NPY	450.1 $\pm$ 36.9	/	7238 $\pm$ 476.5	/	44
<b>Y16A-GFP (3)</b>	Control	351.2 $\pm$ 29.0	/	5110 $\pm$ 359.1	/	30
	100nM NPY	382.6 $\pm$ 30.3	/	5799 $\pm$ 340.6	/	43
<b>Y1/A2G (3)</b>	100nM NPY	97.2 $\pm$ 20.3	7.6 $\pm$ 1.2	4477 $\pm$ 103.7	23217 $\pm$ 4291	18
<b>Y1/A2LIEFDG (3)</b>	Control	98.0 $\pm$ 19.9	9.8 $\pm$ 1.6	3051 $\pm$ 462.9	12503 $\pm$ 2338	23
	100nM NPY	72.0 $\pm$ 6.9	7.5 $\pm$ 1.7	3190 $\pm$ 690	23349 $\pm$ 4649	14

n numbers in parenthesis refers to the number of independent experiments performed, whilst n values in the table refer to the total number of cell recordings.

/ indicates that traces were fit to a 1 component fit PCH model, therefore a 2 component was not resolved

## 4.4 Discussion

### 4.4.1 Summary of main findings

Here we used FCS and FRAP analysis to investigate the motility of Y receptor complexes at the single cell level. The use of native and mutant Y1 or Y2 receptors revealed that reduced receptor motility at the plasma membrane in response to agonist occupancy was correlated with the relative abilities of these receptors to undergo agonist induced internalisation (see Chapter 3).

A novel superfolder GFP complementation system was then developed to define the specific properties of the signalling complex most likely to be responsible for Y receptor endocytosis– namely Y receptor-arrestin complexes – using FCS and FRAP techniques. The improved photophysical properties of superfolder GFP BiFC allowed its effective use in FCS measurements, and demonstrated that the observed lateral mobilities of Y1-  $\beta$ -arrestin complexes were correlated, as expected with NPY-stimulated Y1-GFP mobility. Although the most likely explanation for the reduced complex mobility is an association with clathrin coated pits, this was not confirmed by the use of the LIEFD mutation to disrupt clathrin binding by  $\beta$ -arrestin2.

PCH analysis allowed the investigation of the molecular brightness of Y1 receptor complexes, suggesting a clustering of receptors occurs following agonist stimulation and prior to endocytosis. The lack of change in molecular brightness seen for Y16A-GFP suggested that this process was driven by association of  $\beta$ -arrestin2. This was also confirmed from the resolution of a clustered second component in PCH analysis of Y1/A2G BiFC, potentially reflecting recruitment of several Y1/ $\beta$ -arrestin2 complexes in clathrin coated pits. Comparable molecular brightness values obtained for Y1-GFP and the first component of Y1/A2G provides some evidence that the mode of binding of  $\beta$ -arrestin2 to the Y1 receptor is symmetrical.

#### **4.4.2 Superfolder GFP showed improved photophysics when compared to YFP, validating its suitability for use in single cell imaging techniques**

The overall aim of this work was for the first time to use a novel version of BiFC utilising split superfolder GFP fragments in combination with FCS. The split YFP BiFC previously used to characterise the association of Y receptors with  $\beta$ -arrestin2 (Chapter 3, Figure 3.12) is less suitable for use in FCS due to the increased propensity of YFP to spot bleach. This has been shown to yield artificially short dwell times ( $\tau_{D2}$ ) generating inaccurate increases in diffusion coefficients, which are less evident for GFP (Herrick-Davis et al., 2013). For example FCS measurements of the diffusion of adenosine A3 receptors tagged with GFP yielded a slower  $D$  of  $1.3 \times 10^{-9} \text{cm}^2 \text{s}^{-1}$  (Corriden et al., 2014) when compared to the corresponding YFP tagged A3 receptor ( $D$  of  $2.1 \times 10^{-9} \text{cm}^2 \text{s}^{-1}$ , unpublished observations by Kilpatrick, LE., 2014). The use of split GFP complementation would therefore be more advantageous in single imaging studies. However previous use of eGFP (split points  $\beta$  strands 7-8) or superfolder GFP fragments (split point  $\beta$  strands 10 - 11) in complementation assays have shown relatively poor complementation in physiological conditions (eGFP) or were designed for spontaneous self assembly respectively (Hu and Kerppola, 2003, Cabantous and Waldo, 2006). Therefore here BiFC fragments were generated from superfolder GFP using the same split point as previously used successfully for YFP complementation (Chapter 3). As this was the first documented use of superfolder GFP in FCS recordings, its use was initially validated in pilot studies by comparison to eGFP widely used in FCS studies, (Corriden et al., 2014, Skakun et al., 2012, Haupts et al., 1998). No significant changes were observed between Y1-GFP (superfolder) or Y1-eGFP in respect to key parameters such as the  $\tau_{D1}$  photophysical component,  $\tau_{D2}$ , the proportion of the  $\tau_{D2}$  component making up the autocorrelation curve or diffusion coefficients (Table 1) - for control or NPY stimulated cells recorded under identical acquisition settings. This indicated that superfolder GFP was a valid alternative to eGFP in FCS recordings. Additionally recomplemented GFP showed comparable  $\tau_{D1}$  values to that of

full length GFP ( $\tau_{D1}$  values; Tables 4.1 and 4.3) indicating similar photophysical characteristics of the native and complemented fluorescent proteins. This has also been observed for full length YFP versus recomplemented YFP in FCS (Herrick-Davis et al., 2012).

#### **4.4.3 FCS and FRAP revealed selective agonist induced slowing in the lateral diffusion of Y receptors which efficiently recruit $\beta$ -arrestins**

Diffusion coefficients measured by FCS for unstimulated Y1 -GFP or Y2 -GFP were broadly comparable to previous estimates of GPCR diffusion measured using FCS and/or FRAP for adenosine A<sub>1</sub> (Bridson et al., 2004b, Bridson et al., 2008), A<sub>2A</sub> (Bridson et al., 2008), A<sub>3</sub> (Cordeaux et al., 2008) receptors,  $\beta$ 2-adrenoceptor (Hegener et al., 2004, Barak et al., 1997b), histamine H<sub>1</sub> (Rose RH, 2010), type 2 bradykinin (Philip et al., 2007), complement C5a (Licht et al., 2003), neurokinin 2 (Cezanne et al., 2004) and  $\mu$  opioid receptors (Golebiewska et al., 2011, Sauliere et al., 2006). Both FCS and FRAP observations showed NPY was able to slow the lateral mobility of Y1-GFP receptors similar to FCS observations of YFP tagged complement C5a receptors (Licht et al., 2003), and the identification of 2 populations of fluorescent agonist species with differing diffusion characteristics when bound to adenosine A<sub>3</sub> receptors (Cordeaux et al., 2008) or  $\beta$ 2-adrenoceptors (Hegener et al., 2004). However this agonist effect does not seem to be universal for all GPCRs as agonist occupancy has been shown to have no effect on the membrane motility of adenosine A1 receptors (Bridson et al., 2008). Additionally observations of the  $\mu$  opioid receptor have suggested that the impact of agonist occupancy on diffusion rates may differ with experimental setup with unchanged effects seen with FCS (Golebiewska et al., 2011) and increases seen with FRAP (Sauliere et al., 2006) (see FCS and FRAP comparison below).

The degree to which native and mutant Y1 or Y2 GFP tagged receptors undergo endocytosis correlated with the extent to which NPY could induce changes in their lateral diffusion characteristics. Both Y1-GFP and Y2H155P-

GFP receptors have been previously shown to readily undergo endocytosis in response to NPY (Chapter 3, Figure 3.7, A and Figure 3.16, C). This is here mirrored in a slowing of their rates of diffusion measured using FCS (Figure 4.2, D) or FRAP (Figure 4.5, C) following agonist stimulation, which was in the case of the Y1 receptor able to be inhibited by antagonist pretreatment. No change was observed for receptors that are less capable (Y2) or unable (Y16A) to undergo agonist mediated internalisation suggesting agonist induced slowing of diffusion is selective to receptors which readily internalise.

However the lack of concomitant changes in the surface particle concentrations of Y1 or Y2H155P-GFP measured by FCS, despite observed NPY induced endocytosis, was surprising. We hypothesised that a simultaneous change in mobile receptor fraction following agonist stimulation might be responsible for preserving FCS particle concentration, but FRAP measurements of Y1 or Y16A-GFP receptors showed no such changes. In fact the high proportion of mobile Y1 or Y16A-GFP receptors was similar to observations using FRAP for  $\beta$ 2-adrenoceptors expressed in HEK293T cells (Barak et al., 1997b, Kaya et al., 2011) and both lipid raft and non raft associated membrane proteins (such as H-Ras and K-Ras) (Kenworthy et al., 2004). One issue that complicates comparison between such measurements is the different spatial scales over which FCS and FRAP investigate fluorescent protein mobility. The circular bleaching area used in FRAP in these experiments ( $1.4\mu\text{m}^2$ ) was approximately 14 times larger than the confocal volume used in FCS. Similarly the estimates of Y receptor diffusion coefficients made by FRAP supported the key finding that NPY stimulation selectively slowed diffusion of Y1-GFP but not Y16A-GFP phosphorylation deficient receptors. However FRAP derived measurements of  $D$  for Y1 receptors (based on fluorescence recovery half times) were an order of magnitude lower than those recorded using FCS.

A larger experimental volume will increase the potential impact of limitors of diffusion, particularly cytoskeletal networks (Kenworthy et al., 2004, Fujiwara

et al., 2002). They can form 'corrals' which effectively divide the plasma membrane into 0.5-1 $\mu$ m regions that can limit the mobility of a diffusing species at the scale of FRAP (and result in the lower measure of  $D$  from FRAP), but will show little effect at the shorter diffusion scale used in FCS. This phenomena has been observed using single particle tracking of gold tagged  $\mu$  opioid receptors (Suzuki et al., 2005). These experiments showed the receptors undergo diffusion largely confined into membrane domains by cytoskeleton fences, but are occasionally able to 'hop' over these compartments (covering distances of 210-730nm). These distinct states of diffusion would thus influence FRAP measurements that cover an area of several corrals, but FCS recordings might simply sample the diffusion within a corral (due to the smaller size of the confocal volume used), and the limiting "fence" and 'hop' diffusion is therefore missed.

Equally using the smaller area sampled by FCS we observed a wide range of individual  $D$  estimates for Y1-GFP controls ranging from 0.60 to 15.36  $\times 10^{-9}$   $\text{cm}^2 \text{s}^{-1}$ , although 90% of values were within 1.02-3.58  $\times 10^{-9}$   $\text{cm}^2 \text{s}^{-1}$ . With the small confocal volume, a high degree of heterogeneity of the membrane regions sampled is expected, in respect to other components present (Kenworthy et al., 2004, Philip et al., 2007, Briddon and Hill, 2007, Licht et al., 2003, Corriden et al., 2014, Lenne et al., 2006).

#### **4.4.4 The use of superfolder GFP BiFC to pharmacologically characterise the interaction of Y1 receptors with $\beta$ -arrestin**

Agonist stimulated reductions in Y receptor mobility correlated with the relative abilities of such receptors to undergo endocytosis, indicating that the interactions of receptors with slow moving clathrin coated pits (CCP) might be responsible. Though these stably associated complexes might be invisible to FCS due to their lack of mobility, it is more likely these interactions occur transiently, relative to the dwell time used in FCS measurements. Thus, CCP trapping might immobilise tagged receptors for part of the dwell time within the volume, resulting in a reduction of the diffusion coefficient  $D$ , rather than

disappearance of the immobile component (Bridson and Hill, 2007, Schwille, 2001, Licht et al., 2003). As Chapter 3 illustrated, it is predicted that Y receptor- $\beta$ -arrestin signalling complexes would be the species associated with CCPs. However the identification of this complex as the responsible component is almost impossible using standard single channel FCS using Y receptor GFP measurements.

For example, changes in molecular mass, such as GPCR-arrestin association, have a limited impact on FCS derived measurements of diffusion alone, as a 2 fold change in  $D$  requires a 8 fold change in molecular mass (Bridson and Hill, 2007). Thus we used the novel superfolder GFP BiFC system to identify Y1 receptors complexed with either  $\beta$ -arrestin1 or 2. In high content and confocal imaging assays, NPY stimulated receptor-arrestin association with similar kinetics, irreversibility (demonstrating de novo complementation; (Kilpatrick et al., 2010)) and potency expected based on the YFP BiFC system characterised in Chapter 3. The equivalency in  $\beta$ -arrestin1 or 2 recruitment was similar to previous indirect measures of the formation of  $\beta$ -arrestin1 or 2 complexes with AP-2 following Y1 receptor agonist induced activation (Ouedraogo et al., 2008).

Some differences between  $\beta$ -arrestin1 or 2 BiFC were observed. In particular, some preformed cell surface and intracellular fluorescence was more evident under basal conditions for Y1 receptor/ $\beta$ -arrestin1 BiFC (but less so  $\beta$ -arrestin2). While this may represent non specific 'bystander' fluorescence driven by the affinity of the two GFP tags for one another (Kerppola, 2008a), this is unlikely as the background fluorescence was significantly inhibited was observed under basal conditions for the GFP BiFC Y16A/ $\beta$ -arrestin1 or 2 cell lines, using the phosphorylation deficient receptor mutant that does not recruit arrestins. Basal levels of BiFC fluorescence are therefore likely to be due to a degree of agonist independent recruitment of  $\beta$ -arrestins to the Y1 receptor in keeping with observations suggesting that for some GPCRs this interaction can occur in the absence of ligand (Kocan et al., 2009, Halls and Cooper, 2010). In addition forced recruitment of  $\beta$ -arrestin2 to V1a or V2

vasopressin receptors in the absence of agonist, resulted in endocytosis of these complexes, suggesting that agonist occupancy of receptors is not essential for inducing the formation of Y1 / $\beta$ -arrestin complexes (Terrillon and Bouvier, 2004).

The ability of Y1/ $\beta$ -arrestin2LIEFDG complexes to undergo NPY induced endocytosis was consistent with additional compensatory clathrin binding sites within  $\beta$ -arrestin2 (Kang et al., 2009, Kern et al., 2009, Kang et al., 2014) (Chapter 1, Figure 1.4 ) and the contribution of adaptor proteins such as AP-2 binding scaffolding with arrestins during endocytosis (Chapter 1, section 1.6.2.1) (Kim and Benovic, 2002, Kang et al., 2014). However in confocal microscopy experiments, there was some evidence of an inhibitory effect of the LIEFD mutation, because increased plasma membrane localisation of the Y1/A2LIEFDG complexes was observed compared to Y1/A2G cells.

Comparable FCS and FRAP derived diffusion rates and proportions of mobile particles were obtained for all agonist stimulated BiFC cell lines investigated, and these were matched with NPY stimulated Y1-GFP measurements. Thus the use of GFP BiFC can define the diffusion of the known molecular receptor-arrestin complex and so support the hypothesis that similar complexes are associated with Y1-GFP receptors following NPY stimulation. *D* estimates of unstimulated Y1/A1G and Y1/A2LIEFDG complexes on the plasma membrane were also obtained, with similarly slow *D* measurements compared to unstimulated Y1-GFP receptors. Therefore, agonist occupancy is potentially not required for these complexes to engage the structures (presumably CCPs) limiting their diffusion.

#### **4.4.5 PCH analysis can provide clues in respect to the molecular composition of NPY stimulated Y1-GFP receptors**

PCH measurements of molecular brightness were also obtained to provide information on the stoichiometry of Y1-GFP receptors under different conditions. Such measurements might reveal the oligomerisation state of these receptors under unstimulated conditions. However this relies on an accurate reference for the brightness of monomeric membrane associated

GFP, which is technically challenging (Kilpatrick et al. 2012). In addition the incomplete maturation of GFP in practice limits the expectation that a 2 fold change in brightness would accompany receptor dimerization. For example, estimates for eGFP or sfGFP constructs expressed in HEK293T cells range from 53-68% maturation (Hallworth and Nichols, 2012, McGuire et al., 2012). Therefore the transition from monomeric to constitutive dimeric Y1-GFP might result only in a 1.3 – 1.5 fold increase in molecular brightness as not all receptor protomers would be tagged with a fully mature GFP molecule that produces fluorescence. However a previous study on a number of other GPCRs has indicated constitutive dimerisation for a range of GPCRs based on a doubling of molecular brightness values when compared to monomeric control in PCH analysis (Herrick-Davis et al., 2013). Given the incomplete maturation of GFP, it is surprising that Herrick-Davis et al (2013) saw such clear cut doubling of  $\epsilon$  when identifying oligomerisation of a range of fluorescently labelled GPCRs (Herrick-Davis et al., 2013). It is also worth pointing out that the bin time used by Herrick-Davis is smaller than that used here (10 $\mu$ s versus 1ms here) therefore it is likely a second contribution to the overall  $\epsilon$  data may be being detected from the faster  $\tau$ D1 component within the fluctuation trace. This is an important consideration, particularly as Herrick-Davis et al used both YFP and GFP tagging when investigating oligomerisation of GPCRs and as described previously, YFP shows an increased propensity to bleach which is often reflected in a fast  $\tau$ D1 component ( $\sim$ 100 $\mu$ s detected by (Briddon et al., 2004a) at the A1 receptors tagged with Topaz (a yellow shifted variant of GFP) and in the data from this group  $\tau$ D1 for YFP ranges from 70-100 $\mu$ s. It would therefore be interesting to see if increasing the bin time would result in such clear changes in  $\epsilon$  and subsequent changes in assumed oligomeric states in their data.

Nevertheless, even with the caveat of GFP maturation being incomplete, there was a clear 1.5 fold increase in Y1-GFP brightness seen in PCH analysis following NPY stimulation, and this is consistent with receptor clustering. Agonist induced changes in brightness were sensitive to antagonist treatment,

thus demonstrating the requirement for Y1 receptor activation. This effect may be due to agonist driving oligomerisation of Y1 receptors, a phenomena observed for other Class A GPCRs (see Chapter 4) and reconcilable with a decreased maturation of GFP resulting in not all Y1-GFP dimers representing two molecules of GFP (ie not a clear cut doubling of  $\epsilon$ ). However FRET observations on Y1 receptor dimerisation suggest that oligomerisation is not ligand dependent (Dinger et al., 2003). Additionally under basal conditions Y16A-GFP and Y1-GFP receptors had similar particle concentrations and brightness values, but only the Y1-GFP showed significant changes following NPY stimulation. The location of the 6 alanine mutations, introduced into the Y1 receptor C terminus, are unlikely to affect potential Y1 receptor oligomerisation per se, particularly when the sites of GPCR dimer interfaces have been largely been predicted to be within the transmembrane helical bundle (Johnston et al., 2012) (see Chapter 4). As the 6A mutation has also been shown to substantially inhibit  $\beta$ -arrestin2 recruitment, these data suggest that the increased molecular brightness of NPY stimulated Y1-GFP particles, in common with their slower diffusion, is an indirect consequence of  $\beta$ -arrestin dependent clustering of receptors prior to entering the endocytosis pathway.

This conclusion was supported by the 5-8 fold brighter second component that was resolved in PCH analysis of BiFC complexes that was not observed for Y1-GFP. This likely represents Y1/ $\beta$ -arrestin GFP BiFC complexes forming clusters that interact with components of the endocytic machinery such as clathrin coated pits (Krupnick et al., 1997a, Goodman et al., 1996, Kim and Benovic, 2002, Holliday et al., 2005, Gicquiaux et al., 2002, Ouedraogo et al., 2008) (Chapter 1, section 1.6.2.1). The approximate waist diameter of the confocal volume used (300nm) suggests that measurements are detecting single clathrin coated pits (approximate 100nm diameter), and that such pits may therefore contain multiple Y receptor/ $\beta$ -arrestin complexes.

#### **4.4.6 Reconciling discrepancies in diffusion characteristics seen in FCS and PCH measurements**

Whilst data obtained using FCS and PCH analysis can often complement each other, there are limitations inherent to each technique. For example the very bright second component resolved using PCH for Y1/A2G and Y1/A2LIEFDG BiFC aggregates, whilst only representing a small proportion of the total particles, may have the greatest influence on overall dwell times seen in FCS. This is partly due to each particle within component 2 (~10 % of the particle number) containing approximately 10 times the unit  $\epsilon$  of component 1, meaning ~50% of the “unit” Y receptor-arrestin BiFC fluorescent complexes at the membrane are actually represented by component 2. In addition the relative contribution of these individual particles to time dependent fluctuations in FCS (is weighted by  $\epsilon^2$  (Schwille, 2001), and so brighter particles have a disproportionately greater influence on measurements of  $\tau_D$

A caveat to PCH analysis that may account for discrepancies with FCS measurements is the use of a 3D model of diffusion when fitting in comparison to the 2D model used in FCS autocorrelation analysis. The complex membrane environment of living cells complicates the use of either model. For example a 2D lipid bilayer will inevitably contain 3D features such as clathrin coated pits, which can differentially affect the absolute measurements. The size of bin time used may also explain some of the PCH discrepancies in particle number, due to potential contributions of the  $\tau_{D1}$  photophysical component to overall data. However this is unlikely to be exerting a significant influence here, as repeating the analysis on the same data set but using a longer bin time (50ms, data not shown) did not change overall estimates of N or  $\epsilon$  obtained for Y1-GFP or Y1/A2G BiFC. Finally despite the requirement of both FCS and PCH techniques for particles to be mobile in order to produce fluorescent fluctuations, the sensitivity threshold of this mobility is lower for PCH analysis. It is therefore likely that some slowly

moving particles that are detected by PCH are not observed in FCS autocorrelation measurements.

#### **4.4.7 PCH analysis revealed a symmetrical mode of recruitment of $\beta$ -arrestin to Y1 receptors**

The precise stoichiometry of GPCR interactions with G proteins is still in debate and is further complicated by the increasingly accepted concept of GPCR oligomerisation (see Chapters 5 and 6 for more detailed discussion). Compelling evidence has suggested that G protein binding can be either symmetric (ie 1:1) (Whorton et al., 2007, Chabre and le Maire, 2005) or asymmetric (2 receptors :1 G protein) (Jastrzebska et al., 2013, Damian et al., 2008, Baneres and Parello, 2003) in nature. However the mode of  $\beta$ -arrestin binding is even more uncertain (Hanson et al., 2007a, Tsukamoto et al., 2010, Sommer et al., 2011, Sommer et al., 2012) and may even change with the proportion of activated receptors that are present (Sommer et al., 2011).

The bilobed structure of  $\beta$ -arrestin (Chapter 1, Figure 1.4; section 1.6.1) suggests an asymmetric 2:1 recruitment to GPCR dimers, with both the phosphorylation and activation 'sensors' of  $\beta$ -arrestin engaging with a different receptor protomer within the dimer (Fotiadis et al., 2006, Sommer et al., 2011). However a symmetric 1:1 (or 2:2) stoichiometry has also been suggested based on experimental studies of rhodopsin (Hanson et al., 2007a, Bayburt et al., 2011). PCH comparisons between Y1-GFP and Y1/ $\beta$ -arrestin BiFC complexes may provide a clue to the mode of  $\beta$ -arrestin binding. This is because equivalent molecular brightness  $\epsilon$  was observed for Y1-GFP and the non clustered component (component 1) of Y1/ $\beta$ -arrestin complexes, suggesting that each fluorescent complex contained similar numbers of GFP particles. Of the available stoichiometries, this is less supported by a model with exclusive asymmetric  $\beta$ -arrestin binding to a receptor dimer. In this model, a single recomplemented GFP molecule per two receptors (ie a dimer) would be predicted in Y receptor-arrestin BiFC particles, and theoretically this would generate a halved brightness compared to two Y1-GFP protomers participating in the same complex. Instead the equivalent brightness is more

easily reconciled with a symmetrical mode of  $\beta$ -arrestin recruitment. However there are several limitations placed on this conclusion, including the confounding effects on incomplete maturation for GFP (described in 4.5.5). It also makes the assumption that with the exception of receptor clustering prior to endocytosis, Y1-GFP oligomerisation is not affected by agonist stimulation, which is in keeping with previous FRET based observations for Y1 dimers (Dinger et al., 2003).

Although the PCH data in this chapter provides some indications of the mode of recruitment of  $\beta$ -arrestin to GPCRs, other approaches are required to probe the stoichiometry of this interaction, particularly when considering dimeric receptors. With this goal in mind, Chapter 5 describes the development of ways to measure the function and pharmacology of BiFC constrained GPCR homodimers, with the roles of individual protomers within the dimer investigated using selective mutagenesis.

## **Chapter 5 – The combined use of Snap labelling and BiFC to discretely constrain GPCRs as homodimers of precise composition in order to probe the pharmacological consequences of dimerisation**

### **5.1 Introduction**

The introduction to this chapter explores the evidence that GPCRs form dimers, or higher order oligomers, and considers their functional relevance - which is still much in debate. Dimerisation can take the form of homodimers, whereby protomers of the same receptor subtype associate, or heterodimers which represent the association of closely or distantly related GPCR family members. Dimerisation may offer new pharmacological targets, with novel pharmacology potentially arising from interaction between the promoter binding sites or modified coupling to downstream effector proteins such as G proteins and  $\beta$ -arrestin (Smith and Milligan, 2010). Precedence for receptor dimerisation exists for some non GPCR mammalian receptor systems such as receptor tyrosine kinases (RTK's) and transcription factors (Helsen and Claessens, 2014, Reich, 2007). Robust agonist induced dimerisation of RTK's leads to their activation by bringing the receptor cytoplasmic tyrosine kinase domains into close proximity to facilitate trans autophosphorylation (Hubbard and Miller, 2007). Both ligand induced homodimerisation, and to a lesser extent heterodimerisation, has also been observed for the non-catalytic Toll like receptor superfamily involved in the innate immune response (Reuven et al., 2014).

#### **5.1.1 The evidence for the existence of GPCR dimerisation**

Evidence for the existence and function of GPCR dimerisation has largely been derived from a number of biochemical, functional and fluorescence approaches.

#### **5.1.1.1 Biochemical and ligand binding evidence**

Biochemical evidence for GPCR dimerisation is abundant in the Class C subclass of GPCRs such as metabotropic glutamate receptor (mGlu5) and GABA<sub>B</sub> receptors (Pierce et al., 2002). For example, mGlu5 receptors have been shown under non reducing conditions to migrate through SDS-PAGE gels with a higher molecular mass than predicted from the monomer, suggesting the formation of larger receptor complexes (Romano et al., 1996). In accordance with this a disulphide bridge has been shown to crosslink two class C receptor subunits at the N terminal extracellular Venus fly trap dimer interface for ligand binding. The monomeric form of Class C receptors is only seen following reduction of this bond (Romano et al., 1996),(Pin et al., 2007). Co-immunoprecipitation experiments confirmed that mGlu5 receptors selectively form homodimers, as no association was observed with the mGluR1a subtype even though they share 60% sequence homology (Romano et al., 1996). A yeast two hybrid screen of another class C receptor, the receptor for GABA ( $\gamma$ -aminobutyric acid), suggested a specific interaction between the GABA<sub>B</sub>R1 and R2 subtypes via an interaction between coiled coil domains in their C terminus (White et al., 1998). Co-immunoprecipitation experiments (Kaupmann et al., 1998, White et al., 1998) confirmed specific heterodimers of co-expressed tagged GABA<sub>B</sub>R1 with GABA<sub>B</sub>R2 detected together.

However biochemical evidence for functional dimerisation of Class A GPCR's remains much more inconclusive. Early evidence came from photoaffinity labelling of muscarinic receptors (Avisar et al., 1983), whereby a potent muscarinic reagent specifically labelled muscarinic binding sites in the brain and heart. Gel electrophoresis suggested these native muscarinic receptors were found to exist as dimers or even higher order oligomers. Co-immunoprecipitation experiments in baculovirus Sf9 cells demonstrated the existence of specific  $\beta$ 2-adrenoceptor monomers and homodimers (Hebert et al., 1996). Hebert et al (Hebert et al., 1998) used [<sup>3</sup>H] palmitate labelling to prove a physical interaction between  $\beta$ 2-adrenoceptors and a mutant form,

C341G that cannot be palmitoylated at the conserved cysteine. This mutant was still immunoprecipitated with the [<sup>3</sup>H] palmitoylated wildtype receptor. However, as acknowledged by the authors, and in common with most co-immunoprecipitation approaches in recombinant cells, this does not imply that the dimer is the predominant functional form of  $\beta$ 2-adrenoceptors. The first evidence of GPCR Class A homodimerisation between two fully functional receptor subtypes came from crosslinking and immunoprecipitation experiments of  $\delta$  opioid receptors tagged with either FLAG or c-myc epitopes (Cvejic and Devi, 1997). The proportion of  $\delta$  opioid receptors existing as dimers was seen to be modulated by ligand, with agonist inducing conversion to monomers. Conversely homodimers of  $\kappa$  opioid receptors, whose existence was confirmed by Jordan and Devi in 1999 (Jordan and Devi, 1999), do not monomerise following agonist stimulation, suggesting dimerisation can have different modes of regulation even within closely related receptor subtypes. A limitation of coimmunoprecipitation approaches that must be considered is the solubilisation of receptors required for protein gel loading may inadvertently promote oligomerisation.

For homodimers, binding of an orthosteric ligand to protomer A or B has been suggested to induce a conformational change within the dimer that can positively or negatively affect the affinity of the same ligand binding to the second orthosteric binding site. This phenomenon has been termed cooperativity (Smith and Milligan, 2010, Casado et al., 2009b). This is allosteric in nature as the second protomer binding site, although identical, is topographically distinct from the first. Modulation of ligand binding affinities or responses of the dimer are therefore driven by interactions occurring across the dimer interface (Kenakin and Miller, 2010). Cooperativity at dimers suggests they may be behaving as a single entity whereby the two binding sites are allosterically linked, seen for thyrotropin (TSH) and lutropin (LH) receptor heterodimers (Urizar et al., 2005). A chimeric receptor unable to bind TSH but capable of binding LH was created and coexpressed with the TSH receptor (unable to bind LH) Under these conditions, LH was able to displace

radiolabelled thyrotropin ligand, suggestive of strong negative cooperativity between the two ligand binding sites of the co-expressed receptors (Urizar et al., 2005).

Chabre has argued that negative cooperativity in binding assays is not necessarily indicative of dimer formation, but could be an artefact of assays performed from membrane preparations in the absence of GTP and G proteins (Chabre et al., 2009). However negative cooperativity has still been observed in the excess of both (Smith and Milligan, 2010). Additionally evidence for negative cooperativity has also been observed in living cells by measuring dissociation kinetics with fluorescent ligands at native adenosine A3 receptors in CHO K1 cells (May et al., 2011) or in native tissues measured using TR-FRET with fluorescent agonists at oxytocin receptors (Albizu et al., 2010).

#### **5.1.1.2 Altered initial expression**

The formation of constitutive dimers has been suggested to occur soon after receptor biosynthesis in order to facilitate correct receptor endoplasmic reticulum export and transport to the plasma membrane by acting as a molecular chaperone (Angers et al., 2002). This is supported by evidence from Class C GPCR's. For example, the GABA<sub>B</sub> receptor splice variants (GABA<sub>B</sub>R1a and GABA<sub>B</sub>R1b) are retained intracellularly as immature glycoproteins due to a C terminal intracellular retention signal preventing them being trafficked to the cell surface (Margeta-Mitrovic et al., 2000). Three separate research groups (Jones KA, 1998), (White et al., 1998), (Kaupmann et al., 1998) each used expressed sequence tags from the GABA<sub>B</sub>R1 sequence to identify another subtype termed GABA<sub>B</sub>R2 with 35% identity. Flow cytometry confirmed that the addition of GABA<sub>B</sub>R2 facilitates surface expression of mature glycosylated GABA<sub>B</sub>R1 (White et al., 1998) with in situ hybridisation showing co-localisation of GABA<sub>B</sub>R1 and R2 in the rat cerebellar cortex (Jones KA, 1998). The GABA<sub>B</sub>R2 subunit masks the intracellular retention signal on the GABA<sub>B</sub>R1 subunit (summarised in (Kniazeff et al., 2002)) so that only via dimerisation is the GABA<sub>B</sub> receptor able to be expressed.

For the Class A group, the requirement for dimerisation for correct receptor expression is less clear. Some evidence of dimers forming during biosynthesis has been obtained, for example for the  $\beta$ 2-adrenoceptor (Hebert et al., 1998), but more research is needed before firm conclusions can be drawn.

### **5.1.1.3 Evidence from effector protein coupling stoichiometries**

The stoichiometry of effector protein binding to GPCR can provide insight into the minimal functional receptor unit that is required to support signalling. The mode of binding of G proteins is beginning to be elucidated, however the recruitment of  $\beta$ -arrestin is still unclear. Binding can take the form of a range of modes including one effector molecule binding to a single GPCR monomer within a dimer (1:2), two molecules bound to each monomer (2:2), both monomers bind to a single effector protein (2:1) or active receptor is only found in its monomeric form bound to one effector (1:1) (Gurevich and Gurevich, 2008). Gurevich and Gurevich suggest that a single model may not be appropriate for all GPCR's and that dimer coupling may differ even over the course of the same receptor's life cycle (Gurevich and Gurevich, 2008).

Using Class C GPCR dimerisation as a model it is worth noting that in GABA<sub>B</sub> receptor dimers only one subunit couples to the G protein alpha subunit, (however these studies did not exclude that binding to the second protomer could occur) (Kniazeff J, 2004, Kniazeff et al., 2002). The model class A GPCR, rhodopsin has been consistently shown by many groups to be monomeric in its dark, unactivated state when detergent solubilised (summarised in (Chabre and le Maire, 2005)). However atomic force microscopy has indicated that rhodopsin is found as highly organised rows of dimers or higher order oligomers in retinal rod outer membrane segments (Fotiadis et al., 2003).

Isolation of rhodopsin monomers in nanodiscs, a synthetic model membrane bilayer, or reconstituted high density lipid (HDL) vesicles illustrated that the monomeric form was capable of functionally coupling to its cognate G protein transducin (Bayburt et al., 2007, Whorton et al., 2008). Similar results have been seen for monomeric  $\beta$ 2AR (Whorton et al., 2007) or  $\delta$  opioid receptors (Kuszak et al., 2009) reconstituted in HDL vesicles alongside the G<sub>s</sub> subunit of

their cognate G protein. These results indicate that, like rhodopsin the monomeric form is the minimal functional unit required for G protein dependent signalling and high affinity agonist binding (Whorton et al., 2007). Similar results were observed for mGluR, whereby isolated monomers in HDL vesicles could functionally couple to G protein when activated by a synthetic allosteric ligand (that binds to the TM bundle) (El Moustaine et al., 2012). However the reconstituted dimeric form was required for glutamate activation, via (the class C specific) venus fly trap ligand binding domains. Therefore even for well documented constitutive dimers, such as mGluRs, monomeric receptor is sufficient to support functional G protein coupling. However these results do not disprove the presence of dimer formation in intact membranes of living cells as for example only one protomer may be fully activated within the dimer (Pellissier et al., 2011). The second protomer also may not directly couple to G protein (as in the GABA<sub>B</sub>R1 subunit) but exert some degree of cooperativity when also ligand bound. A further scenario is that binding of ligand A to a dimer might be different than if it were binding to a monomeric receptor (Birdsall, 2010). The stoichiometry of one G protein binding to a GPCR dimer could arise from altered pharmacology due to allosterism, or competition between the two ligand occupied monomers in the dimer for a shared pool of G protein molecules (Birdsall, 2010).

#### **5.1.1.4 Evidence from GPCR crystal structures**

The recently solved high resolution crystal structures of a range of Class A GPCRs have provided some insight into the potential structural basis of oligomerisation. A range of conformational states have been crystallised for the  $\beta$ 2AR (Rosenbaum et al., 2007, Rasmussen et al., 2007a, Rasmussen et al., 2011a) indicating the receptor binds to G $\alpha$  in a monomeric state (Rasmussen et al., 2011b). However this does not necessarily imply a 1:1 receptor: G protein stoichiometry *in vivo*, as asymmetric binding could still occur whereby one protomer of the dimer engages with the G $\alpha$  subunit, whilst the other protomer binds to G $\beta\gamma$ . Additionally the Class A GPCRs such as the  $\mu$  and  $\kappa$

opioid (Wu et al., 2012, Manglik et al., 2012), the chemokine CXCR4 (Wu et al., 2010),  $\beta$ 1-adrenoceptor (Huang et al., 2013) and the smoothed receptor (Wang et al., 2013) have all crystallised as parallel dimers and/ or tetramers. These structures have indicated the existence of relatively conserved dimer interfaces between protomers. For example the inactive  $\beta$ 1AR dimeric structure suggests that it has two main interfaces, the first involving TM1, TM2, helix 8 and ECL1 and the second TM4, TM5, ICL2 and ECL2 (Huang et al., 2013). TM5 and 6, and to a lesser extent TM1, TM2 and helix 8 have been suggested to be the interfaces of the symmetrical dimers observed for  $\mu$  opioid receptors (Manglik et al., 2012). These multiple interfaces may also facilitate the higher order oligomerisation observed for some GPCRs such as the  $\beta$ 2AR which spontaneously forms tetramers when reconstituted in membranes (Fung JJ, 2009). Care needs to be taken when interpreting the physiological implications of structures seen from crystallisation as they may reflect artefacts of crystal packing (particularly as it is the lowest energy state that is typically most amenable to successful crystallisation), reflect only the conformational state captured during crystallisation, or may be a consequence of the modifications/additions required to stabilise the receptor for crystallisation away from its natural lipid environment (such as the use of nanobodies (Rasmussen et al., 2011a). Nevertheless many of the sites identified in crystal structures have also been previously implicated from biochemical studies (see 5.1.1.5. below) suggesting they may be physiologically relevant.

#### **5.1.1.5 Mutagenesis and functional complementation assays**

Much of the early evidence investigating the functional significance of GPCR dimerisation came from studies of Class C receptors, and in particular the GABA<sub>B</sub> receptor. Both GABA<sub>B</sub>R1 variants can bind GABA<sub>B</sub> ligands but with 100 fold less affinity than the physiological receptor (Kaupmann et al., 1998), while the GABA<sub>B</sub>R2 subtype expressed alone exhibited no affinity for GABA<sub>B</sub> receptor radioligands (Kaupmann et al., 1998). Only when GABA<sub>B</sub>R1 and GABA<sub>B</sub>R2 were co injected into *Xenopus* oocytes (alongside GIRK subunits),

could GIRK channel activation be observed in response to GABA (Jones KA, 1998), (Kaupmann et al., 1998), (White et al., 1998)). Subsequent studies have revealed that agonist binding occurs only at the GABA<sub>B</sub>R1 Venus fly trap domain (Kniazeff J, 2004) but that it is the GABA<sub>B</sub>R2 subunit responsible for G protein coupling (summarised in (Kniazeff et al., 2002)). This implied communication between the two subunits with conformational changes transmitted through to the GABA<sub>B</sub>R2 subunit following agonist binding (Milligan, 2009). This transactivation is a theme that has been subsequently been explored further by targeted mutagenesis in the mGluR (Brock et al., 2007) and GABA<sub>B</sub> receptor family (Monnier et al., 2011).

Intermolecular trans complementation has been observed for some Class A GPCR's in respect to ligand binding, receptor activation and downstream signalling. Functional complementation has been observed for dopamine D2 receptor dimers in respect to G protein coupling (Han et al., 2009). D2 protomers fused to the chimeric Gαq i5 protein were non-functional unless they were also expressed with wildtype D2 protomers, suggesting this system required dimeric D2 receptors and allosteric cooperativity across the dimer interface. For the Angiotensin II receptor, co-expression of two ligand binding defective mutants with distinct mutations in TM3 or 5, were able to restore a functional ligand binding site (Monnot et al., 1996). However it is worth noting that this reconstituted angiotensin mutant receptor could not correctly couple to G proteins. A peptide consisting of the majority of TM6 of β2AR (implicated to be involved in the intermolecular interactions at the postulated adrenoceptor dimer interface(Huang et al., 2013)) when introduced, can substantially decrease β2-adrenoceptor dimer formation and isoprenaline stimulated adenylyl cyclase activity (ie. functional coupling) (Hebert et al., 1996). The authors suggested that this peptide formed a 'pseudodimer' with receptor monomers mimicking receptor – receptor interactions that could occur in receptor dimerisation. Hebert et al followed up this observation in 1998 using the β2-adrenoceptor C431G mutant (mentioned above) that signals less efficiently than wildtype receptor and is constitutively internalised

(Hebert et al., 1998). Co-expression of the mutant and wild type receptors led to a rescue of function for the mutant with the wildtype receptor having a positive complementary effects in terms of restoring wildtype levels of desensitisation and adenylyl cyclase activity (Hebert et al., 1998). However it is unwise to rely on functional complementation assays alone to confirm dimer formation, because the results of many of the studies above might purely be a consequence of co-expression regenerating a functional “monomeric” unit.

Finally, crosslinking experiments using a range of substituted cysteines have implicated TM4 as a particularly crucial interface in dopamine D2 (Guo et al., 2003),  $\delta$  opioid (in addition to TM5) (Johnston et al., 2011) and 5-HT4 receptors (Berthouze et al., 2007) and an interaction between TM5 and the N terminus of ICL3 in muscarinic M3 receptors (Hu et al., 2012). Selective mutagenesis of ICL2 has also been implicated in partially promoting the dissociation of melanocortin 4 receptors (Piechowski et al., 2013), implying that sites distinct from the helical bundle may also influence dimerisation.

#### **5.1.1.6 Fluorescence based techniques**

Förster Resonance Energy Transfer (FRET) and Bioluminescence Resonance Energy Transfer (BRET) assays can visualise protein-protein interactions occurring in cells, including GPCR dimer formation, at high resolution and sensitivity. They are both real time assays which utilise variants of fluorescent proteins with overlapping emission and excitation spectra (Krasel et al., 2004) to allow almost instantaneous detection and localisation of cellular interactions. In FRET proteins of interest (eg. a receptor monomer) can be tagged with cyan fluorescent protein (CFP) which is excited with 436nm light leading to emission at 480nm wavelength. This energy can be transferred to excite a yellow fluorescent protein (YFP) tagged to another protein of interest with light being emitted at a wavelength of 535nm, provided the distance between the two fluorophores is less than 10nm. The ratio of CFP to YFP emission can be used as an indicator of the degree of interaction between the two tagged proteins of interest, although it is still not possible to determine

the proportion of 'FRET dimers' compared to the total receptor population. BRET is a similar technique to FRET but the CFP donor fluorophore is replaced with a light emitting luciferase (typically derived from *Renilla reniformis*). BRET produces less background fluorescence than FRET but has decreased temporal resolution and requires the addition of the exogenous substrate coelenterazine (Lohse et al., 2008).

For FRET and BRET the orientation and distance of the fluorophores joined to the two interaction partners is crucial, with the spatial detection limit of 10nm or less (Kerppola, 2009) equating to the distance of approximately twice that of GPCR protomer dimensions (Milligan, 2009). As most RET studies simply imply that some GPCR protomers interact, rather than identifying the functional behaviour of the discrete dimer, it can be difficult to use these techniques to identify any altered pharmacology that may arise with dimerization.. It is therefore also difficult to infer the relative proportions of dimers present compared to the total receptor population.

RET based techniques have been used to imply the constitutive dimerisation of receptors such as GABA<sub>B1</sub> and GABA<sub>B2</sub>(Maurel et al., 2004),  $\beta$ 2AR (Angers et al., 2000), adenosine A<sub>2A</sub> (Canals et al., 2004), and the Y receptor subtypes Y1, Y2 and Y5 (Dinger et al., 2003). Large variations have been observed for these techniques in respect to dimer stability with ligand stimulation. For example, agonist-stimulated association of somatostatin (Patel et al., 2002) and melatonin MT<sub>1</sub> and MT<sub>2</sub> (Ayoub et al., 2002) receptors, contrasts with dissociation of  $\beta$ 2AR (Angers et al., 2000),  $\mu$  opioid (Cvejic and Devi, 1997) and Y4 receptors (Dinger et al., 2003). Such studies also do not exclude other clustering events at the plasma membrane, for example prior to endocytosis (see Chapter 4).

FRET techniques have also been used in native tissues. Albizu et al (2010) used time resolved (TR)-FRET in mammary gland tissue, which has a high natural expression of oxytocin receptors (Albizu et al., 2010). In TR-FRET the donor fluorophore europium lanthanide has an improved signal to noise ratio with longer lasting fluorescence so that measurements can be taken after

cellular autofluorescence decays. FRET was observed between the donor-labelled receptor antibody and either fluorescent antagonist, or to a lesser extent, agonist treatment.

Dual colour fluorescence recovery after photobleaching (FRAP) microscopy has also been used to probe the mobility of potential GPCR complexes laterally through the plasma membrane. Anti-YFP antibodies were used to immobilise a defined proportion of extracellular YFP- $\beta$ 1AR or YFP- $\beta$ 2AR's at the plasma membrane (Dorsch et al., 2009), tracking whether the diffusion of a co-expressed receptor population (tagged only with C terminal intracellular CFP that did not bind the antibody directly) was also retarded. The authors suggested that although both adrenoceptor subtypes appeared to form homodimers, the lifespan of dimer stability was markedly different with transient associations observed for  $\beta$ 1AR whilst  $\beta$ 2AR showed more stable interactions. This is consistent with suggestions of even higher order  $\beta$ 2AR oligomer formation as stable tetramers in reconstituted systems (Fung JJ, 2009).

Single molecule imaging using total internal reflection microscopy (TIRF) with fluorescent receptors and ligands has identified transient dimerisation of muscarinic M1 (Hern et al., 2010) and *N* formyl peptide receptors (Kasai et al., 2011), which both show dynamic association and dissociation (lifetime 0.5 and 5 s respectively). TIRF combined with Snap labelling also revealed transient homo tetramer formation of  $\beta$ 1 and  $\beta$ 2-adrenoceptors (lifetime  $\sim$ 5secs), the propensity of which differed with receptor subtype and expression levels (Calebiro et al., 2013). Molecular brightness estimates derived from PCH analysis (see Chapter 4), have also implicated that a range of Class A GPCRs including  $\beta$ 2AR and  $\alpha_{1B}$  adrenoceptors, muscarinic M<sub>1</sub> and M<sub>2</sub>, dopamine D1 and 5-HT<sub>2A</sub> and <sub>2B</sub> receptors that have been implied to be stable over a 10 fold expression level (Herrick-Davis et al., 2013).

### **5.1.2 The use of BiFC to constrain GPCRs as defined dimers of precise composition**

The  $\beta$ 2AR is a prime example of how different fluorescence based techniques can generate discrepancies in measurements of the extent, stability and influence of agonist on dimerisation. Some of these differences are likely to arise from the precise molecular composition of dimeric complexes during the receptor lifespan being unknown. The use of BiFC to constrain receptors as dimers is therefore advantageous as it unambiguously defines an interacting protein-protein complex, which can then be studied functionally, as previously demonstrated for the investigation of Y receptor and  $\beta$ -arrestin2 interactions using quantitative plate reader imaging or FCS (Chapters 3 and 4).

BiFC has been used previously to indicate the existence and localisation of adenosine  $A_{2A}$  receptor dimers in a specialised neuronal cell line (Vidi et al., 2008b). Additionally multicolour BiFC, using YFP and CFP tags, has also implied the coexistence of dopamine D2 homodimers and  $A_{2A}$  homodimers in neuronal cell lines (Przybyla and Watts, 2010). Higher order oligomers of D2 receptors (comprising a minimum of 4 D2 receptor protomers) have also been observed in HEK293T using combined fluorescence (BiFC) and luminescence (BiLC) complementation (Guo et al., 2008), together with BRET. BiFC has also been used in combination with both FRET (Vidi et al., 2008b) and BRET (Gandia et al., 2008) to identify higher order complexes of  $A_{2A}$  receptors.

In this and the following chapter, BiFC was used to identify the pharmacological and functional properties of specific Y1 receptor or  $\beta$ 2AR dimerisation. The irreversible nature of BiFC was exploited in order to constrain receptors as dimers of precise composition due to the requirement for both tagged protomers (protomer A tagged with Yn; protomer B tagged with Yc; Figure 5.1) to contribute to producing a fluorescent signal identifying a defined interaction between known receptors (a 'BiFC dimer'; protomer A+B). This allowed the quantification of the agonist induced internalisation of these 'BiFC dimer' complexes to be used as a readout of dimer function. Details of the system are described below.

### 5.1.3 The combined use of Snap receptor labelling with BiFC for multiplex readouts of BiFC dimer and individual protomer function

Here Snap labelling was also used in conjunction with BiFC to allow the simultaneous measurement of the internalisation of both Snap labelled protomer A receptor and BiFC dimer populations within the same cells, applied to Y1 and  $\beta$ 2AR homodimers. Snap labelling of protomer A alone enabled the specific N terminal labelling of the total receptor-Yn population expressed at the cell surface, be that monomers, dimers or higher order oligomers (Figure 5.1; e.g. Snap Y1-Yn, protomer A).

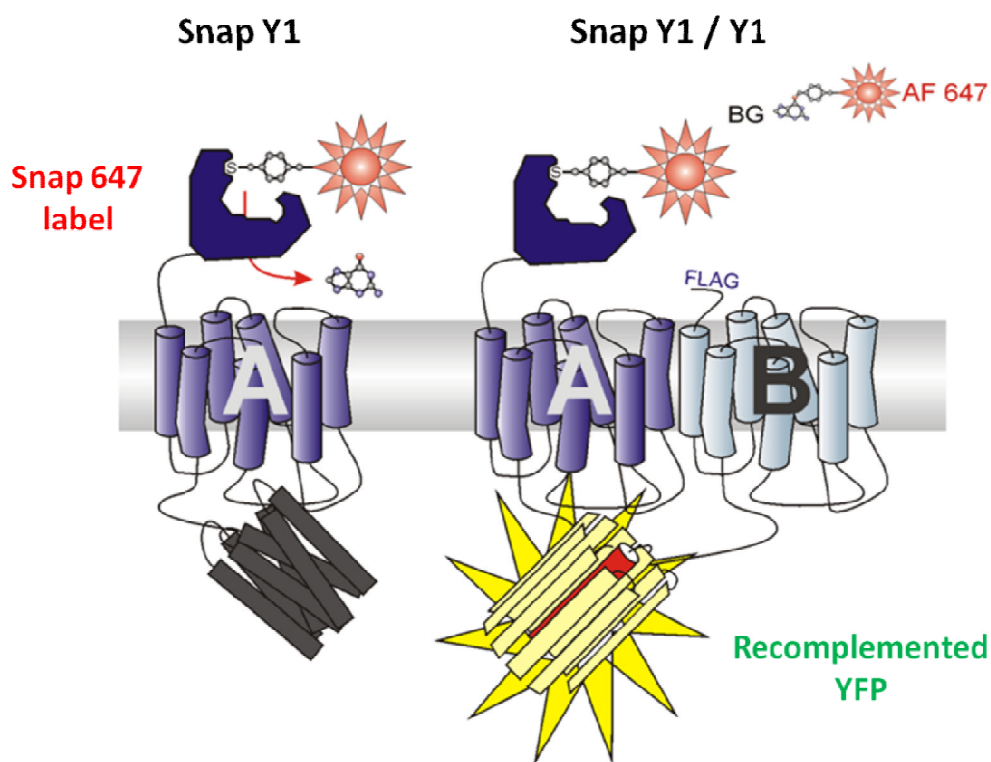


**Figure 5.1: The use of combined Snap labelling and bimolecular fluorescence complementation (BiFC) to constrain receptors as dimers of precise composition**

The schematic illustrates how HEK293T cells were stably transfected with a clonal GPCR protomer (A) expressing an N terminal Snap tag. The Snap tag allowed the surface expression of Snap labelled receptor to be imaged using the Cy5 filter settings of a confocal plater reader (B). To investigate the internalisation of receptor dimers, Snap-protomer A can be co-expressed with an additional FLAG labelled protomer B. Both protomers (A and B) are tagged at their C terminus with a fragment of YFP. Recomplemented YFP produced a fluorescent signal identifying a discrete interaction between receptors of known composition ('BiFC dimer').

## 5.2 Chapter aims

The first aim of this chapter was to ascertain whether the function and pharmacology of example class A GPCRs constrained as BiFC dimers (the NPY Y1 receptor and  $\beta$ 2-adrenoceptor;  $\beta$ 2AR) could be assessed by quantifying their agonist-promoted internalisation. Secondly the roles of ligand binding sites and intracellular domains of individual protomers governing BiFC dimer internalisation were assessed by targeted site directed mutagenesis. Given previous results seen for the Y1 receptor (Chapter 3) (Ouedraogo et al., 2008, Kilpatrick et al., 2010) and  $\beta$ 2AR (Moore et al., 2007), internalisation of BiFC dimers is expected to be a  $\beta$ -arrestin dependent process. However unlike the many studies that have probed the stoichiometry of G protein recruitment to GPCR dimers, the nature of their interaction with  $\beta$ -arrestins is still largely unknown even in respect to the 'model' Class A GPCR rhodopsin (Hanson et al., 2007a, Tsukamoto et al., 2010, Sommer et al., 2011).

Therefore the use of targeted mutations within individual receptor protomers, that selectively aim to disrupt the receptor- $\beta$ -arrestin2 interface, should provide some indirect insight into the mode of  $\beta$ -arrestin2 recruitment to BiFC constrained Y1 or  $\beta$ 2-adrenoceptor dimers.

## 5.3 Results

### 5.3.1 Snap and BiFC fragment tagged Y1 receptors are functional in respect to ligand binding and G protein coupling

Competition binding experiments using the radiolabelled agonist [<sup>125</sup>I] PYY were first performed in order to verify the expression and functional properties of HEK293T cell lines expressing either Snap Y1 receptor-Yn alone (clonal line, termed Snap Y1 throughout) or co-expressing both Snap Y1-Yn and FLAG Y1-Yc constructs (termed Snap Y1/Y1 throughout) (Figure 5.1). Membranes were freshly prepared from both cell lines following the assay protocol detailed in Chapter 2, section 2.2.3). Both membrane preparations isolated from Snap Y1 or Snap Y1/Y1 cell lines showed specific [<sup>125</sup>I] PYY binding which was inhibited by competition with the unlabelled agonist (PYY; A) and antagonist (BIBO3304; B) co-incubation (Figure 5.2). Functional estimates of ligand binding affinities (pK<sub>i</sub>) were calculated using the Cheng-Prusoff equation (Chapter 2, section 2.2.10.1). The affinities of PYY (estimated pK<sub>i</sub> 9.4-9.5 ± 0.1; n=3-4; Table 1) were comparable for both cell lines. Observed affinities for BIBO3304 were also comparable for both cell lines. Additionally [<sup>125</sup>I] PYY binding was sensitive to GTPγS treatment in both cases (C), indicating functional coupling of the expressed receptors to G proteins. Bmax estimates for both cell lines were also comparable in respect to receptor expression.

The Y1 receptor subtype preferentially couples to the G<sub>i</sub> class of G proteins (Herzog et al., 1992), with agonist activation leading to the inhibition of adenylyl cyclase. The resultant decrease in cAMP production acts as a functional readout of this inhibition. The effect of Y1 receptor stimulation on adenylyl cyclase activity was measured by a [<sup>3</sup>H]cAMP accumulation assay (Chapter 2, section 2.2.4), in the presence of forskolin. Forskolin has been shown to activate adenylyl cyclase directly in a receptor independent manner by binding to a hydrophobic pocket close to the enzyme's catalytic site (Tesmer et al., 1997, Tang and Hurley, 1998). The optimal concentration of forskolin was determined in the Y1/Y1 cell line in the presence and absence of

100nM NPY stimulation (Figure 5.3; A), with a control forskolin pEC<sub>50</sub> of 4.8 ± 0.1 (n=2). NPY inhibited these forskolin responses, therefore 30µM forskolin was chosen for use in all subsequent experiments as it produced a sufficient experimental window to measure Y1 mediated inhibitory responses.

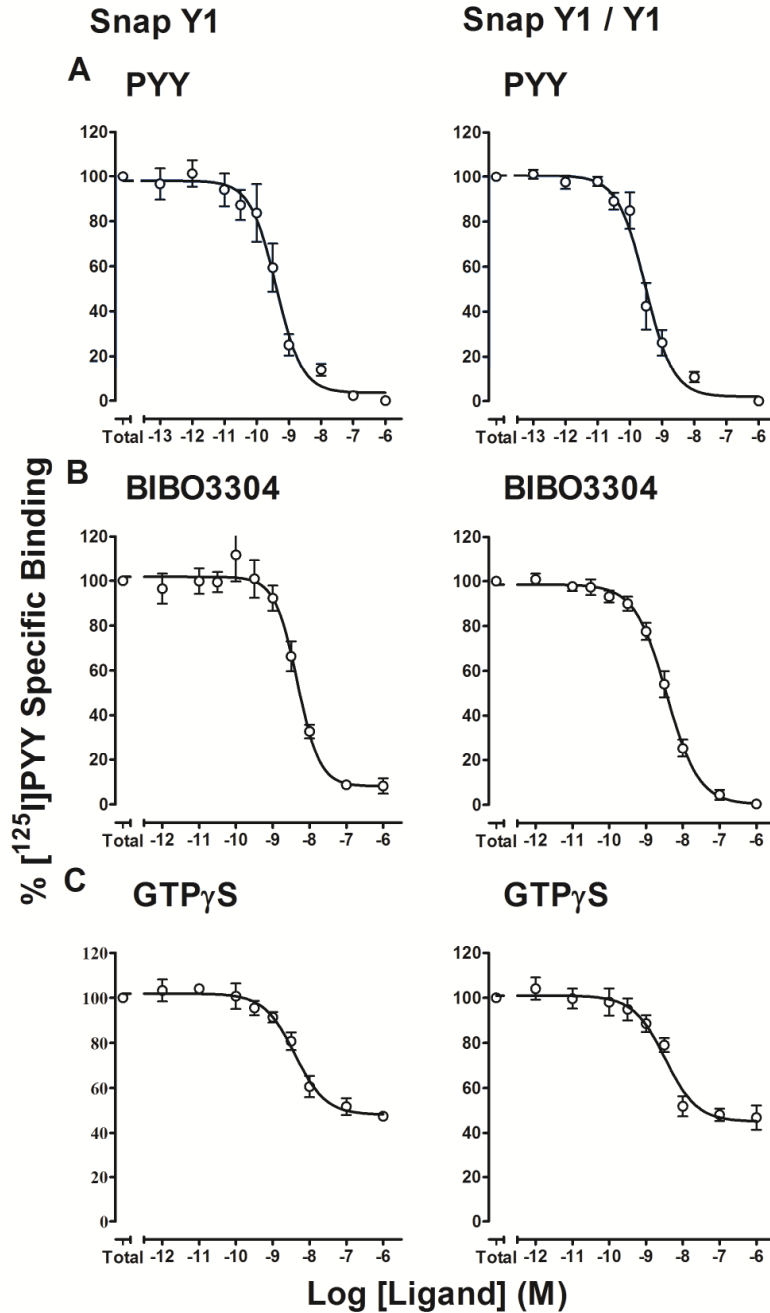


**Figure 5.2:** [<sup>125</sup>I] PYY competition binding experiments performed in membranes isolated from HEK293T cell lines expressing Snap Y1 or Snap Y1/Y1

Membranes were freshly prepared from HEK293T cell lines stably expressing Snap Y1 or Y1/Y1 BiFC dimer constructs (Chapter 2, section 2.2.3). These were incubated with [<sup>125</sup>I] PYY (15pM) and increasing concentrations of unlabelled competing ligand (PYY (A), BIBO3304 (B) or GTP $\gamma$ S (C)), at 22°C for 90min, before membrane bound radioligand was separated using filtration. Retained radioactivity was quantified using a gamma counter and competition displacement curves generated using GraphPad Prism. Pooled data represent a minimum of 3 independent experiments with data expressed as mean  $\pm$  S.E.M. (Hill slopes 0.9-1.1  $\pm$  0.2).

**Table 5.1: Summary of binding parameters for Snap Y1 and Y1 receptor BiFC homodimers**

Cell line	PYY	BIBO3304	GTPγS		Bmax
	pIC <sub>50</sub>	pIC <sub>50</sub>	pIC <sub>50</sub>	% [ <sup>125</sup> I]PYY inhibition	pmol/mg <sup>-1</sup>
Snap Y1	9.4 ± 0.1	8.3 ± 0.1	8.4 ± 0.1	52.6 ± 1.4	2.9 ± 0.4
Snap Y1/Y1	9.5 ± 0.1	8.4 ± 0.1	8.5 ± 0.1	53.2 ± 5.4	3.2 ± 0.8
Snap Y1/Y1Y99A	9.2 ± 0.1	8.4 ± 0.1	8.8 ± 0.1	58.9 ± 6.2	2.7 ± 0.2
Snap Y1/Y15A	9.4 ± 0.1	8.1 ± 0.1	8.3 ± 0.1	47.0 ± 2.2	4.5 ± 0.8
Snap Y1Y5A/Y199A	9.4 ± 0.1	8.4 ± 0.1	8.5 ± 0.2	53.5 ± 6.2	2.7 ± 0.6

All parameters were obtained from [<sup>125</sup>I] PYY competition binding experiments described in the Chapter 2, section 2.2.3.

% inhibition of TSB refers to the displacement by 1μM competing ligand, as a % of the total specific binding (TSB) defined in the absence / presence of 1μM PYY.

Details of Y1 receptor mutations are described in the text.

n =3-4

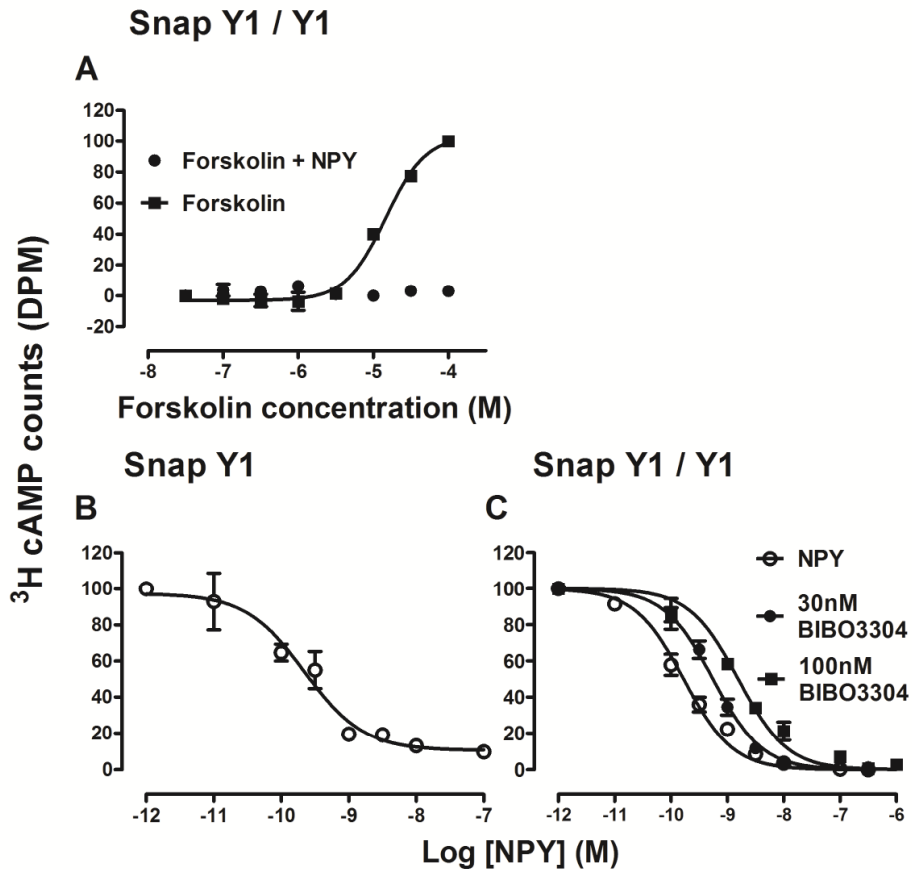


**Figure 5.3: Y1 receptor mediated inhibition of forskolin-stimulated <sup>3</sup>H cAMP accumulation in the Snap Y1 and Y1 / Y1 cell lines**

HEK293T cells stably expressing Snap Y1-Yn with or without co-expression of the Y1-Yc receptor construct were loaded with [<sup>3</sup>H] adenine for 2 hours at 37°C/5% CO<sub>2</sub>, before treatment with a range of forskolin concentrations in the presence or absence of 100nM NPY costimulation (A; 1 h). Snap Y1 (B) or Y1/Y1 BiFC cell lines (C) were loaded with [<sup>3</sup>H] adenine and stimulated with NPY in the presence of 30μM forskolin (1 h at 37°C/5% CO<sub>2</sub>). Y1/Y1 cells were also preincubated with either 30 or 100nM of the Y1 selective antagonist BIBO3304 (30min at 37°C/5% CO<sub>2</sub>), compared to vehicle, prior to stimulation with NPY and forskolin co-stimulation. Double column chromatography was used to isolate [<sup>3</sup>H] cAMP (Chapter 2; section 2.2.4). All responses were normalised to those obtained for forskolin alone (100%) or with 100nM NPY (0%), and are presented as mean ± s.e.m. of n=2-4.

For both Snap Y1 and Snap Y1/Y1 expressing cell lines, stimulation with NPY inhibited the forskolin-stimulated accumulation of [<sup>3</sup>H] cAMP in a concentration dependent manner (Figure 5.3; B and C; open circles) with pEC<sub>50</sub> values of 9.7 ± 0.1 and 9.8 ± 0.1 respectively (n=3-4). Surmountable antagonism of NPY responses in the Snap Y1/Y1 BiFC cell line was observed for BIBO3304 (estimated pK<sub>b</sub> value 7.8-7.9, from shifts in the presence of 30nM or 100nM antagonist; n=2).

### **5.3.2 Y1 receptors constrained as dimers using BiFC internalise in response to agonist stimulation**

Confocal imaging, both manual (Figure 5.4) and automated (Figure 5.5), allowed the expression and localisation of both Snap Y1-Yn receptors and Snap Y1-Yn/Y1-Yc BiFC dimers to be further validated. This was particularly important for the constrained Snap Y1/Y1 BiFC dimers, as both of the previous techniques used (radioligand binding and <sup>3</sup>H-cAMP accumulation assays) did not distinguish between this population and other complexes formed by either the Snap-Y1-Yn or FLAG Y1-Yc promoters within these cells.

Receptor localisation was initially assessed using standard confocal microscopy, labelling the Snap Y1 receptor-population with the membrane impermeant SNAPsurface 647 fluorophore, which is spectrally distinct from the YFP BiFC fluorescence. For both receptor cell lines, under control conditions Snap labelled Y1 receptors (total protomer A; Figure 5.1) and Snap Y1/Y1 receptor BiFC dimers (specifically A+B) were localised predominantly to the plasma membrane (Figure 5.4; A and B). A small amount of constitutive internalisation was observed for both receptor populations. Treatment with the Y1 selective agonist NPY (100nM; 30min at 37°C) resulted in rapid internalisation of both receptor populations with extensive colocalisation (yellow) observed when images were overlaid (Figures 5.4). Similar cellular distribution, and NPY-stimulated internalisation of the Snap-Y1 receptor Yn and BiFC dimer populations, was observed when these cells were imaged using the automated confocal platereader (Figure 5.5 A, B). This method allowed the agonist induced internalisation of both Snap labelled and Y1/Y1 BiFC dimers to be quantified on a per cell basis (see Chapter 2, section 2.2.10.3). A granularity algorithm was applied to either the Snap 647 labelled receptor, or BiFC dimer images, to identify punctuate regions of internalised receptor fluorescence termed 'granules' (Figure 5.5; white spots, analysis panel).

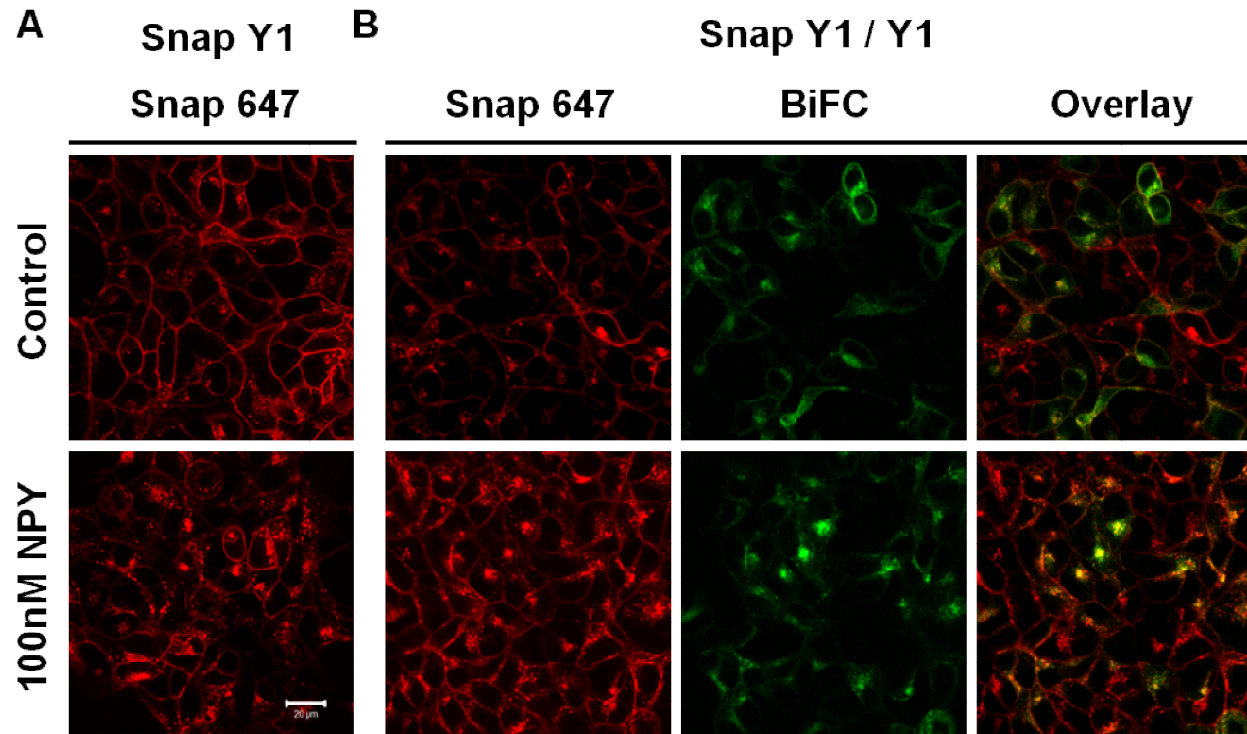


**Figure 5.4: Representative images taken using a LSM510 confocal microscope of Snap Y1 receptors and Y1/Y1 BiFC dimers stably expressed in HEK293T cells**

HEK293T cells stably expressing either Snap Y1 receptor-Yn alone or co-expressed Snap-Y1-Yn and FLAG Y1-Yc constructs were prelabelled with Snap 647 (0.2µM; 30min at 37°C/5% CO<sub>2</sub>) before stimulation with vehicle control (HBS/0.1% BSA) or 100nM NPY (30min at 37°C). Representative images (of at least 3 experiments) taken using a LSM510 confocal microscope showed that under control conditions Snap Y1 receptors expressed alone (A) were localised predominantly to the plasma membrane. A similar pattern of expression was observed for coexpressed Snap Y1 and BiFC dimer receptor populations of the Y1/Y1 BiFC cell line (B). Stimulation with 100nM NPY resulted in rapid internalisation of all receptor populations. For Y1/Y1 BiFC dimers, areas of colocalisation between Snap Y1 receptor and BiFC dimer populations are shown in yellow (overlay panel).

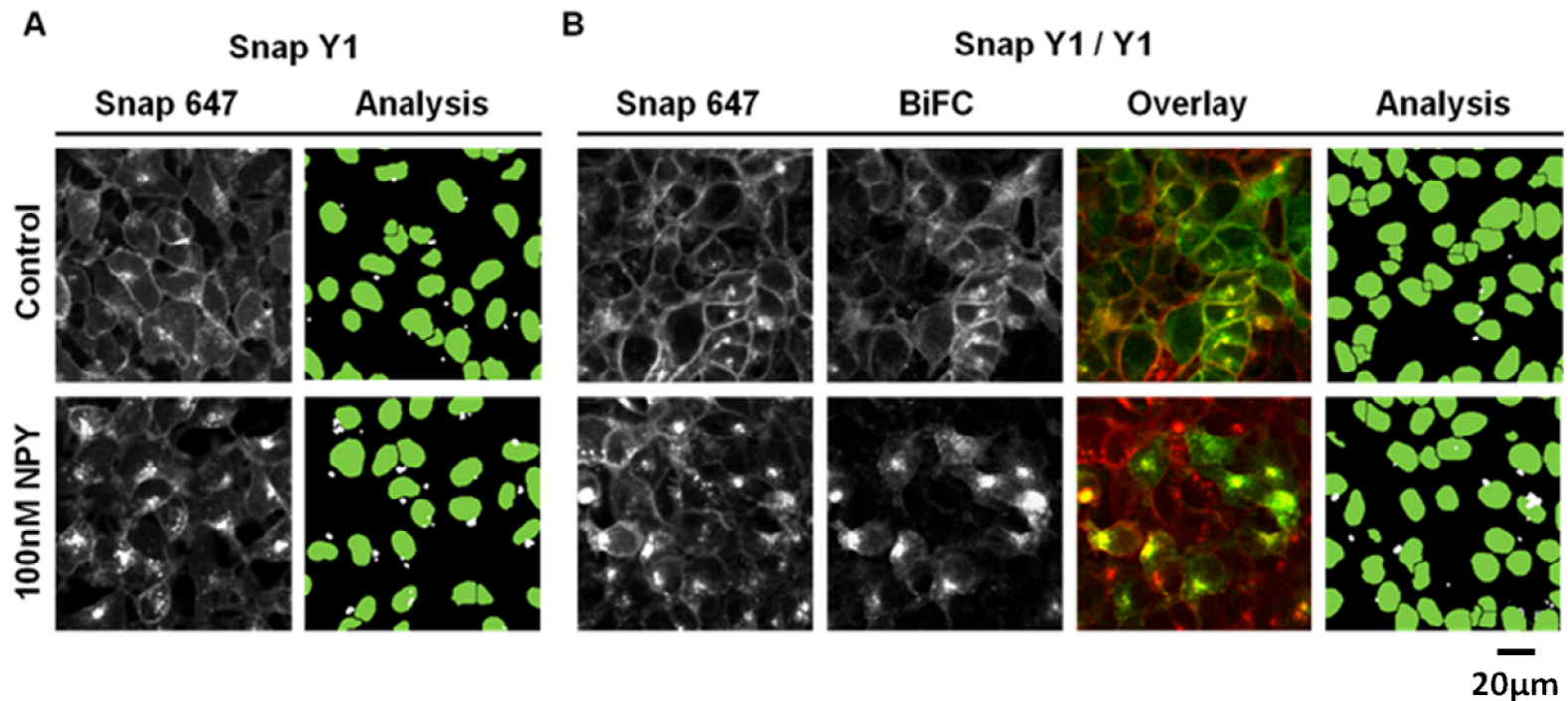


**Figure 5.5: IX Ultra confocal images of Snap Y1 and Y1/Y1 BiFC dimers stably expressed in HEK293T c cells.**

HEK293T cells stably expressing either Snap Y1-Yn receptors alone (A) or Y1/Y1 BiFC dimer constructs (B), were prelabelled with membrane impermeant Snap 647 (0.2µM; 30min at 37°C/5% CO<sub>2</sub>) before stimulation with vehicle control (HBS/0.1% BSA) or 100nM NPY (30min at 37°C). Cells were then fixed, nuclei stained using Hoescht 33342 and imaged. Representative images (cropped as 300x300 pixel regions; n=7-20) were taken using an IX Ultra confocal platerreader for Snap Y1-Yn receptors expressed alone (A) or Snap Y1/Y1 (B) Extensive areas of colocalisation were observed (Yellow; overlay panel). The use of a granularity algorithm to these images allowed quantification of the internalisation of all receptor populations on a per cell basis (granularity panel), with nuclei shown in green (derived from the H33342 images, not shown) and 3-15µm granules identified as white spots.

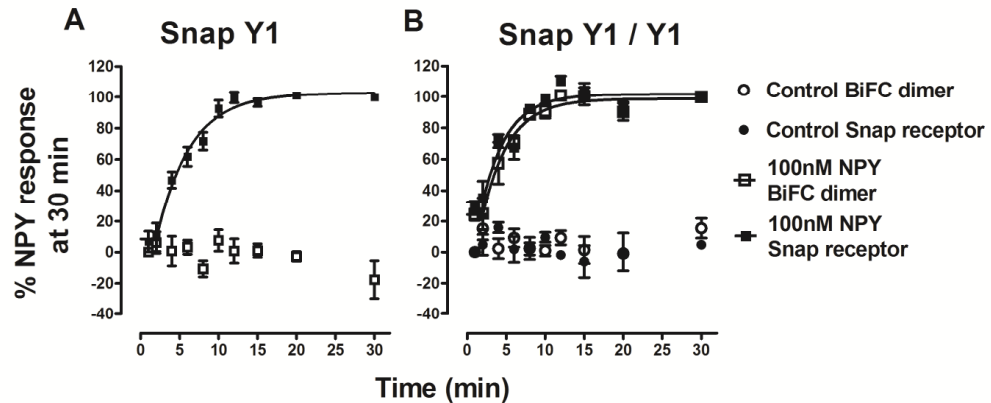


**Figure 5.6: Kinetics of NPY induced internalisation of Snap Y1-Yn receptors and Y1/Y1 BiFC dimers**

Stably transfected HEK293T cells expressing either Snap Y1 (A) or Snap Y1/Y1 BiFC dimers (B) were prelabelled with SNAPsurface 647 (30min at 37°C/5% CO<sub>2</sub>). Cells were then stimulated with either vehicle or 100nM NPY at set time intervals, before responses were terminated by fixation. H33342 labelling, image acquisition and granularity analysis was carried out as described previously. Pooled data (mean ± s.e.m, n = 3-4) were normalised to NPY responses observed at 30 min, and fitted to a 1 site exponential association including a 2min latency period.

A timecourse of agonist stimulated internalisation (NPY, 100nM; Figure 5.6), measured on the IX Ultra plater reader was performed on both Snap Y1 receptor (A) and Y1/Y1 BiFC cell lines (B) to ascertain the optimal length of time required for future assays. Snap Y1-Yn receptors expressed alone (Figure 5.6, A; Snap Y1) or within the Snap Y1/Y1 BiFC cell line (Figure 5.6; B; Snap Y1/Y1), showed comparable kinetics in respect to NPY induced internalisation ( $t_{1/2}$  values of  $5.4 \pm 1.1$  and  $4.2 \pm 0.4$ min respectively, n=4). Additionally no significant difference was observed when comparing to the BiFC dimer populations ( $t_{1/2}$   $4.4 \pm 0.9$ min) of constrained Y1/Y1 BiFC dimers, and these kinetics were also comparable to observations for Y1-YFP internalisation (Kilpatrick et al., 2010). Maximum internalisation responses in both cell lines reached a stable plateau between 20-30 minutes stimulation. An assay length of 30min treatment was therefore deemed optimal for use in subsequent agonist stimulation assays.

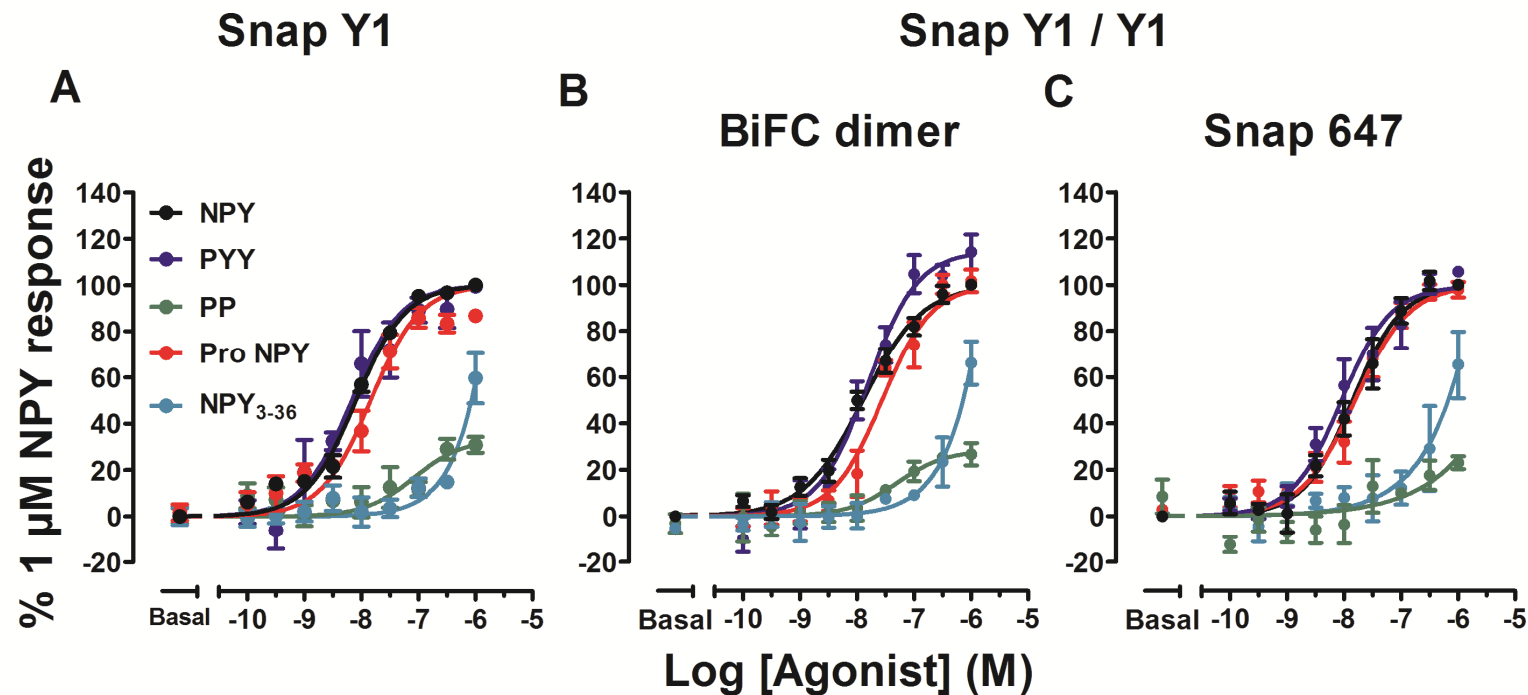


**Figure 5.7: Quantification of the agonist induced internalisation of Snap Y1 or Y1/Y1 BiFC dimers following stimulation with a panel of agonist ligands**  
 HEK293T cells stably expressing Snap Y1 (A) or Snap Y1/Y1 BiFC dimers (B and C) were prelabelled with Snap 647 (30min at 37°C/5% CO<sub>2</sub>), before stimulation with a panel of ligands (30min at 37°C). Receptor internalisation in response to ligands (including [Leu<sup>31</sup>, Pro<sup>34</sup>]NPY, Pro NPY) was determined following granularity analysis of images acquired using an automated confocal plater reader. All data were normalised to negative (basal) and positive (1 $\mu$ M NPY) plate controls. Pooled data shown represented a minimum of 3 independent experiments and are expressed as mean  $\pm$  s.e.m.

**Table 5.2: Summary of potencies and efficacies of a panel of ligands for stimulating the internalisation of Snap Y1 receptors and Y1/**

**BiFC dimers**

Snap Y1			Snap Y1/Y1			
	Snap 647 labelled receptor		BiFC dimer		Snap 647 labelled receptor	
Ligand	pEC <sub>50</sub>	E <sub>max</sub> (%)	pEC <sub>50</sub>	E <sub>max</sub> (%)	pEC <sub>50</sub>	E <sub>max</sub> (%)
NPY	8.1 ± 0.1	100	8.0 ± 0.1	100	8.1 ± 0.1	100
PYY	8.2 ± 0.1	99.4 ± 2.9	8.0 ± 0.2	114.2 ± 7.6	7.8 ± 0.1	105.7 ± 0.6
Leu <sup>31</sup> , Pro <sup>34</sup> NPY	8.0 ± 0.1	86.7 ± 2.4	7.5 ± 0.1	101.7 ± 4.9	7.7 ± 0.1	97.9 ± 3.4
PP	/	29.1 ± 4.1	7.3 ± 0.1	26.4 ± 8.4	7.1 ± 0.1	25.2 ± 3.
NPY <sub>3-36</sub>	/	59.5 ± 10.9	/	56.3 ± 11.8	/	65.3 ± 14.5

All data were expressed as ± standard error of the mean. pEC<sub>50</sub> values were obtained from pooled concentration response curves presented in Figure 5.7.

E<sub>max</sub> responses to each ligand were calculated as a percentage of 1µM NPY responses. n

values for all data 3-20.

/ = responses unable to determined

### **5.3.3 Using BiFC to constrain Y1 receptors as dimers does not result in altered receptor agonist or antagonist pharmacology**

HEK293T cells expressing Snap Y1 or Snap Y1/Y1 BiFC dimers were treated with a panel of agonist ligands (30min at 37°C; Figure 5.7), and the functional internalisation responses were compared. Pooled concentration response curves revealed that the endogenous agonists NPY and PYY were equipotent at Snap Y1 receptors expressed alone (Figure 5.7, A; see Table 5.2), and these potencies were also comparable to those obtained for Snap labelled protomer A (Figure 5.7,C) and BiFC dimer populations in the Snap Y1/Y1 cells (Figure 5.7, B). The selective analogue [Leu<sup>31</sup>, Pro<sup>34</sup>] NPY was a full agonist, with respect to NPY, at both cell lines (see Table 2), with no significant difference observed for Snap labelled protomer A receptor or Snap Y1/Y1 BiFC dimer populations. Both NPY<sub>3-36</sub> and PP showed low potency and efficacy in inducing internalisation of Snap Y1 and Snap Y1/Y1 receptor populations for both cell lines. The rank order of potency for all ligands, both in terms of actual pEC<sub>50</sub> values and relative efficacies was comparable to those previously observed for endocytosis of Y1-GFP receptors (NPY, PP; see chapter 3, Table 3.2) and Y1/β-arrestin2 association measured using BiFC (chapter 3, Table 3.3).

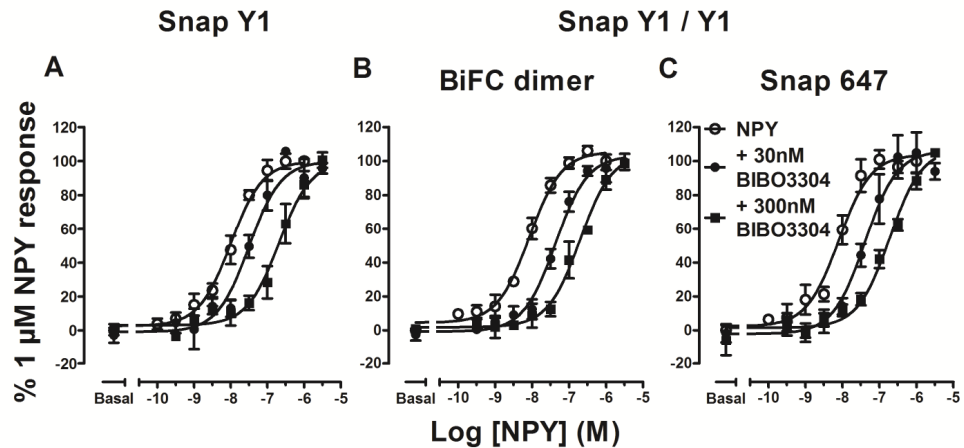


**Figure 5.8: The effect of pretreatment with the Y1 selective antagonist BIBO3304 on the agonist induced internalisation of Snap Y1 or Snap Y1/Y1 BiFC dimers**

HEK293T cells stably expressing Snap Y1 (A) or Snap Y1/Y1 BiFC dimers (B) were prelabelled with SNAPsurface 647 (30min at 37°C/5% CO<sub>2</sub>). Cells were then pretreated with BIBO3304 (30 or 300nM; 30min at 37°C), before being stimulated with NPY (30min at 37°C). Granularity analysis was performed on images obtained using an automated confocal plater reader. Concentration response curves in the presence and absence of BIBO3304 were fitted using GraphPad Prism with shared minimum (basal responses), maximum (1μM NPY responses) and Hill slope constraints. All data were pooled from a minimum of 3 independent experiments, and expressed as mean ± s.e.m

In order to investigate whether constrained Y1 receptor dimers show altered antagonist pharmacology, Snap Y1 receptor and Snap Y1/Y1 BiFC dimer cell lines were pretreated with BIBO3304 (30nM or 300nM for 30min at 37°C). This was followed by stimulation with a concentration response course of NPY (30min at 37°C).

BIBO3304 produced parallel rightward shifts of NPY response curves for Snap Y1 receptors indicative of surmountable antagonism (Figure 5.8, A; estimated  $pK_b$   $7.8 \pm 0.1$  and  $8.1 \pm 0.1$ ;  $n=5$ .) Comparable effects were observed for both Snap protomer A and Snap Y1/Y1 constrained BiFC dimer populations (B and C;  $pK_b$  7.9 - 8.1;  $n = 4$ ).

### 5.3.4 Selective mutagenesis of individual protomers, to disrupt ligand binding or phosphorylation, does not prevent agonist induced internalisation of Y1 receptor BiFC dimers.

The Y1 receptor mutation Y99A has been previously shown to inhibit NPY binding and subsequent receptor internalisation (Sautel et al., 1995, Kilpatrick et al., 2010) (Chapter 3, Figure 3.8). Selective introduction of this mutation into protomer B of Y1 BiFC dimers allowed determination of whether one or both NPY binding sites needed to be occupied for BiFC dimer internalisation (Figure 5.9, A). Additionally, mutations of five C terminal serine/threonine phosphorylation residues in the C terminal domain (Ouedraogo et al., 2008) were also separately introduced into protomer B (Y15A [containing mutations S352A, T353A, S359A, T361A, S362A]; B). This mutant prevents agonist induced internalisation, through inhibition of  $\beta$ -arrestin recruitment (Kilpatrick et al., 2010), equivalent to the Y16A mutant (also including T356A) discussed in Chapter 3 (Figures 3.5, 3.6, 3.8). Expression of the Y15A mutant within a BiFC dimer therefore allowed the number of phosphorylated protomers required for internalisation of BiFC dimers to be investigated.

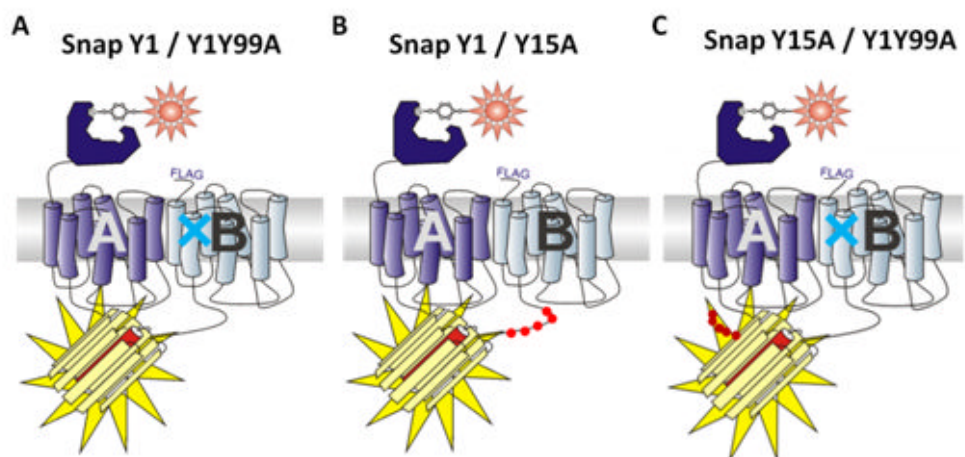


**Figure 5.9: Schematic detailing the position of mutations selectively introduced into Y1 receptor BiFC dimers**

Mutations were selectively introduced into protomer B of Y1/Y1 BiFC dimers. The Y99 residue located at the top of TM2 is involved in NPY binding to the receptor, and was here mutated to alanine (Y1Y99A; A, blue cross). Five serine or threonine residues (B; red spots) located in the Y1 receptor C terminal domain and previously implicated in recruitment of  $\beta$ -arrestin2 to the receptor, were mutated to alanine. A double mutant receptor dimer was created by simultaneously introducing both the Y15A and Y1Y99A mutations into protomer A and B respectively (C).

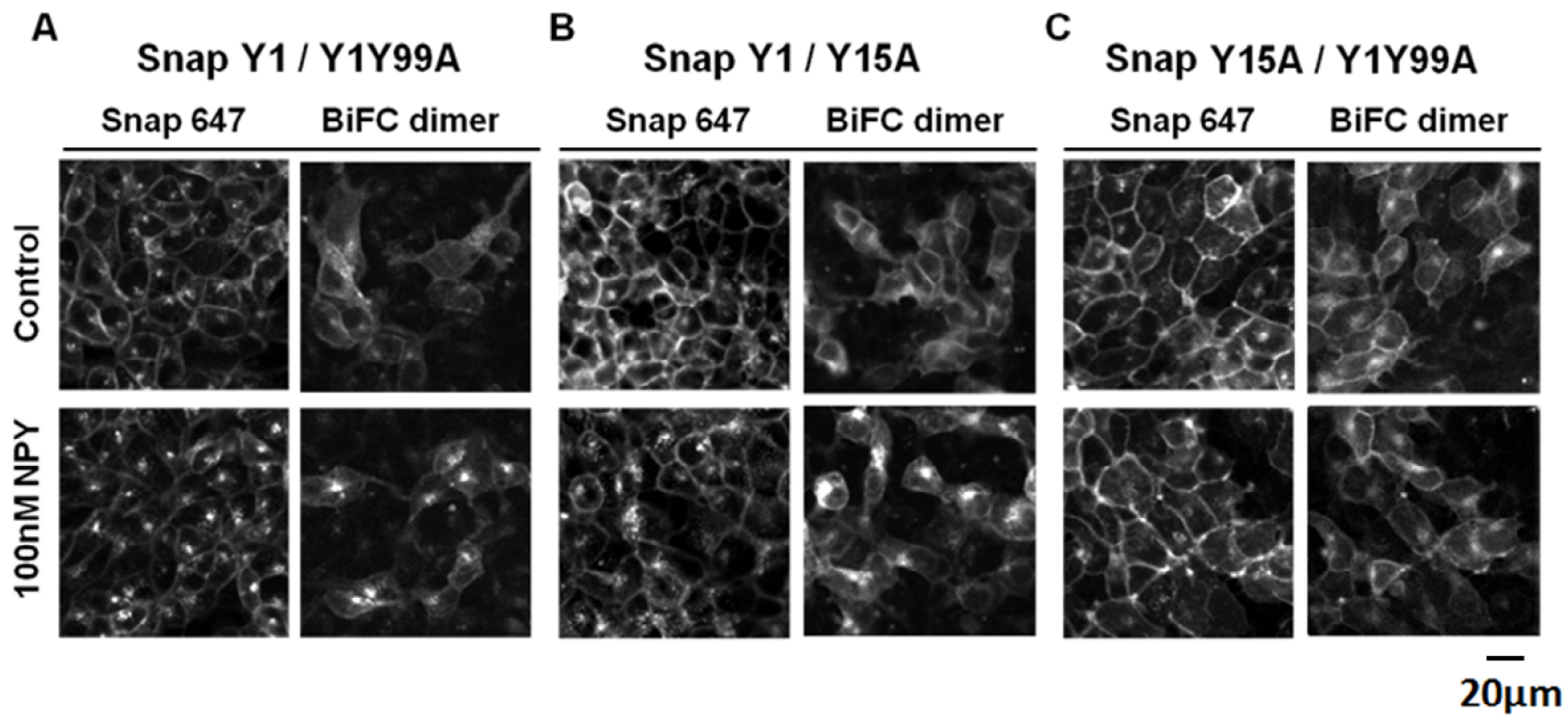


**Figure 5.10: Representative images of Y1/Y1 mutant BiFC dimers taken using a IX Ultra confocal platereader**

HEK293T cells stably expressing Snap Y1/Y1Y99A (A) Snap Y1/Y15A (B) or Snap Y15A/Y1Y99A (C) were prelabelled with SNAPsurface 647 (30min at 37°C/5% CO<sub>2</sub>) before stimulation with vehicle (HBS/0.1% BSA) or 100nM NPY (30min at 37°C). Representative images (cropped as 300x300 pixel regions, from at least 3 experiments) taken using an IX Ultra confocal platereader showed that in control conditions Snap labelled protomer A and BiFC receptor populations for all mutant Snap Y1/Y1 BiFC dimers were localised predominantly to the plasma membrane. Following stimulation with NPY, rapid internalisation was observed for both Snap labelled and BiFC dimer populations of Snap Y1/Y1Y99A and Snap Y1/Y15A BiFC dimers. No discernable internalisation was seen for the double mutant Snap Y1Y5A/Y1Y99A.

Competition binding assays using [<sup>125</sup>I] PYY confirmed expression of both Y1/Y199A and Y1/Y15A cell lines, with binding affinities for PYY and BIBO3304 comparable to those obtained for the Snap Y1/Y1 or Snap Y1-Yn cell lines (see Table 5.1), and binding sensitive to GTPγS treatment.. Estimated Bmax values derived from PYY displacements were also comparable. Automated confocal images, of both Snap Y1/Y1Y99A and Snap Y1/Y15A mutant BiFC homodimers, showed that under control conditions both the Snap labelled and BiFC dimer receptor populations showed predominant plasma membrane expression with some constitutive internalisation (Figure 5.10; A, B), and both populations internalised to colocalised intracellular compartments in response to 100nM NPY. Comparable kinetics of agonist induced internalisation were observed for both populations of Snap Y1/Y199A or Snap Y1/Y15A cell lines ( $t_{1/2}$  values 4.2 - 5.7 min; Figure 5.11). These half times obtained for both mutant BiFC dimer cell lines were also comparable to those seen for Snap Y1 receptors expressed alone (Figure 5.6, A) and Snap Y1/Y1 BiFC dimers (Figure 5.6, B).

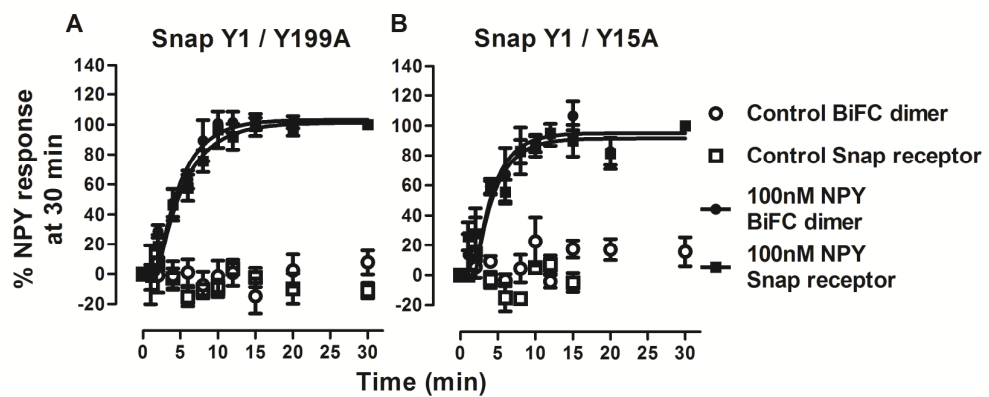


**Figure 5.11: Kinetics of agonist induced internalisation of Snap tagged mutant Y1 receptor BiFC dimers**

Stably transfected HEK293T cells expressing either Snap labelled Y1/Y1Y99A (A) or Y1/Y15A mutant BiFC dimers (B) were prelabelled with SNAPsurface 647 and stimulated with either vehicle or 100nM NPY for different times, as for Figure 6.8. Following image acquisition and data analysis, pooled data (mean  $\pm$  s.e.m, n = 3-4) were normalised to NPY responses observed at 30 min, and fitted to a 1 site exponential association including a 2 min latency period. Graphs represent data from at least 3 independent experiments and are expressed as mean  $\pm$  s.e.m.

Neither mutation inhibited agonist induced internalisation of the mutant BiFC dimers. The Y1 selective agonists NPY and PYY were equipotent at both mutant BiFC dimers ( $pEC_{50}$  values 7.8-8.4;  $n=3-4$ ), with no significant difference observed when comparing mutant BiFC dimer internalisation to that of wildtype Snap Y1/Y1 BiFC dimers or Snap labelled Y1 receptors expressed alone (2 way ANOVA;  $p>0.05$ ). Quantitative comparison of the maximum degree of internalisation ( $R_{max}$ ) was not possible in the normalised data (with  $1\mu M$  NPY set to 100 % in each case). However there was no qualitative difference between the NPY-stimulated cell lines based on inspection the images. In order to investigate whether internalisation of the Snap Y1/Y15A and Snap Y1/Y1Y99A mutant BiFC dimers was due to protomer functional compensation, both mutations were simultaneously introduced into protomer A and B respectively (Snap Y15A/Y1Y99A). [ $^{125}I$ ] PYY competition binding assays confirmed the ability of this Snap Y15A/Y1Y99A mutant BiFC dimer to bind both agonist and antagonist, with binding affinities comparable to those obtained for Snap Y1/Y1 BiFC dimers or Snap labelled Y1 receptors expressed alone (Table 1), and specific [ $^{125}I$ ] PYY binding was also sensitive to GTPyS treatment. However stimulation with NPY or PYY was unable to induce internalisation of either the Snap labelled protomer A or BiFC dimer receptor populations (Figure 5.12, C).

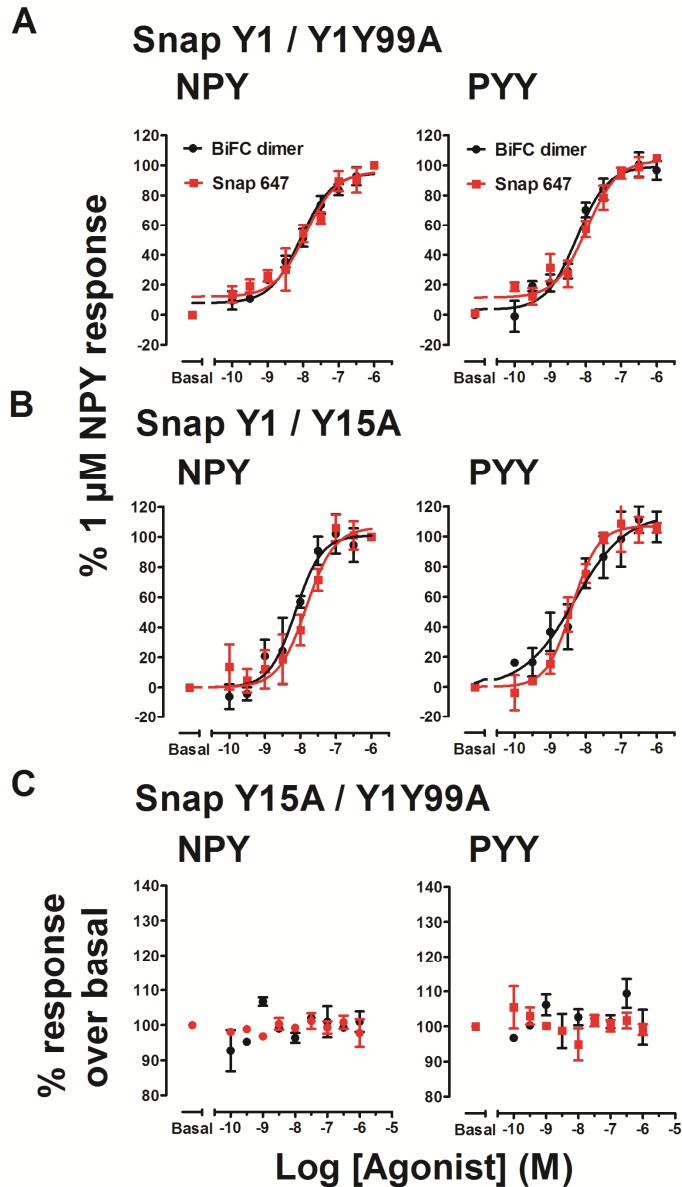


**Figure 5.12: Quantitative analysis of the agonist induced internalisation of Snap tagged Y1 receptor mutant BiFC dimers.**

Mutations adversely affecting ligand binding (Snap Y1/Y1Y99A; A) or  $\beta$ -arrestin dependent internalisation (Snap Y1/Y15A; B) were selectively introduced into protomer B only of Snap Y1/Y1 mutant BiFC dimers. Pooled concentration response curves for internalisation, normalised to 1  $\mu$ M NPY, show that neither set of mutations inhibited the internalisation of mutant BiFC dimers in response to the agonists NPY or PYY (37°C for 30min). Equivalent agonist potencies were obtained for Snap labelled protomer A receptor population (Snap 647, red) and mutant BiFC dimer populations ( $pEC_{50}$  values stated in the text). Simultaneous introduction of the Y15A and Y1Y99A mutations into protomers A and B respectively (Snap Y15A/Y1Y99A) prevented internalisation of the Snap-Y15A-Yn population and Y15A/Y1Y99A BiFC dimer populations in response to either NPY or PYY. As a consequence, data for the Snap Y15A/Y1Y99A BiFC cell line are expressed as fold response over basal (100 %). Data represent n=3-4 experiments.

### 5.3.5 Comparison with BiFC dimer behaviour for a second GPCR – the $\beta$ 2-adrenoceptor

In order to investigate whether observations on Y1 receptor BiFC homodimers were common to other Class A GPCRs, we established a similar BiFC system to constrain the prototypical Class A GPCR, the  $\beta$ 2-adrenoceptor as dimers. A stable clonal population of Snap  $\beta$ 2AR tagged with the Yn fragment, was expressed in HEK293T cells either alone, or in conjunction with FLAG  $\beta$ 2-AR tagged with the complementary Yc fragment.

Automated confocal imaging revealed the expression and localisation of Snap  $\beta$ 2AR populations (Figure 5.13, A) and Snap  $\beta$ 2/ $\beta$ 2AR BiFC dimers (B) within the same cells. Representative images showed that under control conditions all receptor populations were localised to the plasma membrane with regions of localisation shown in yellow (Overlay). Stimulation with the agonist Isoprenaline (10 $\mu$ M; 30 min at 37°C) resulted in rapid internalisation of Snap labelled  $\beta$ 2AR and BiFC dimer populations. As before, automated analysis was performed on both sets of images to allow for the quantification of pharmacological responses of both receptor populations.

A timecourse was performed to compare the kinetics of 10 $\mu$ M isoprenaline induced internalisation of Snap  $\beta$ 2AR receptors expressed alone and Snap  $\beta$ 2AR/ $\beta$ 2AR BiFC dimers (Figure 5.14). For the Snap  $\beta$ 2AR BiFC dimer cell line, a small difference was observed for the half time values of the Snap labelled  $\beta$ 2AR receptor ( $t_{1/2}$  values 13.6  $\pm$  2.1 min; n = 4) and BiFC dimer populations ( $t_{1/2}$  values 6.9  $\pm$  2.3 min; n = 4) however this was not significant (Student's t test p > 0.05). Comparable kinetics were observed for Snap  $\beta$ 2AR when expressed alone ( $t_{1/2}$  values 7.1  $\pm$  1.5 min; n = 6). Timecourse data for Snap  $\beta$ 2/ $\beta$ 2AR BiFC dimers was provided by Dr Nicholas Holliday (University of Nottingham, UK).

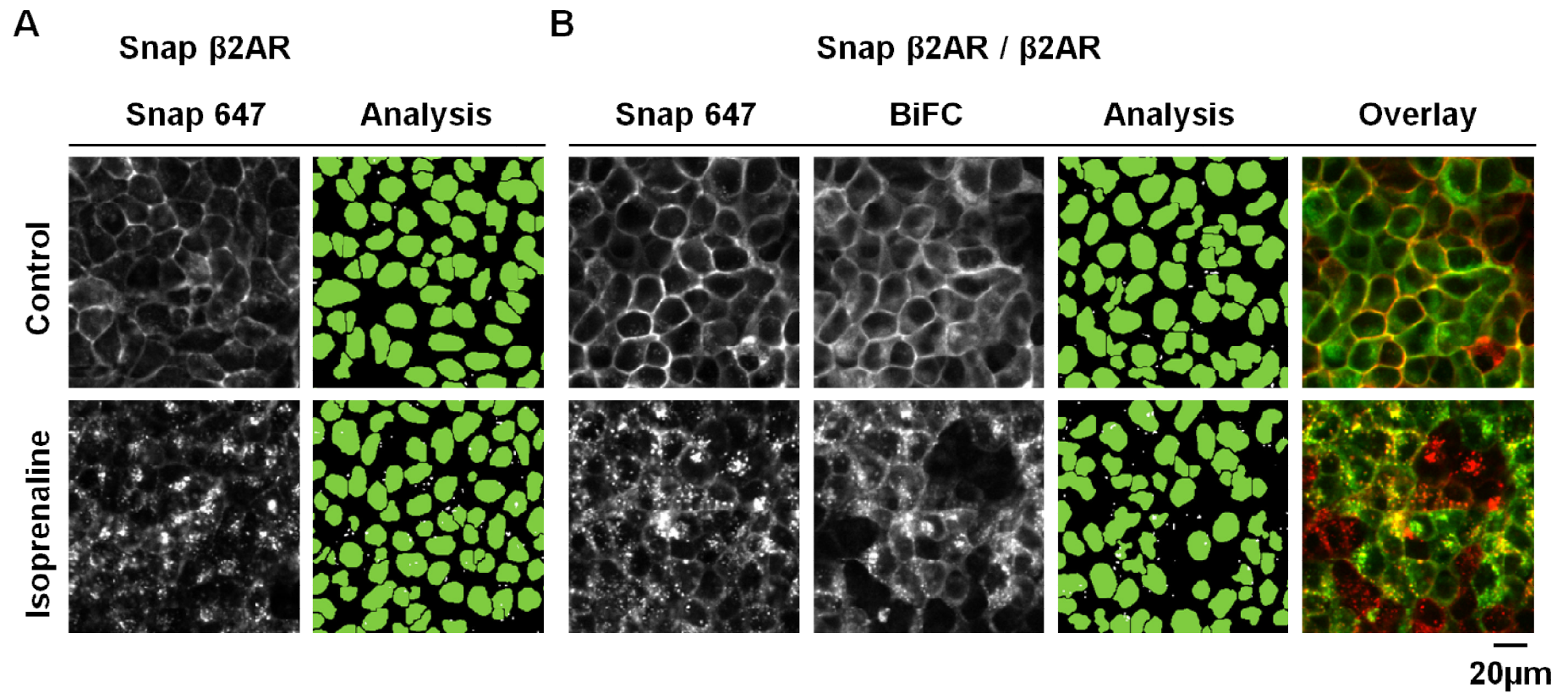


**Figure 5.13: Representative images of  $\beta$ 2AR constrained as dimers using BiFC taken using a IX Ultra confocal platereader**

HEK293T cells stably expressing either Snap  $\beta$ 2AR-Yn alone (A) or Snap  $\beta$ 2AR/ $\beta$ 2AR BiFC dimers (B), were prelabelled with Snap 647 (30min at 37°C/5% CO<sub>2</sub>) before stimulation with vehicle control (HBS/0.1% BSA) or 10 $\mu$ M isoprenaline (30min at 37°C). Representative images (cropped as 300x300 pixel regions) taken using a IX Ultra confocal platereader showed that in control conditions Snap  $\beta$ 2AR-Yn expressed alone (A) showed predominant plasma membrane localisation. Rapid internalisation was observed following stimulation with isoprenaline. A similar pattern of expression was observed for both Snap  $\beta$ 2AR protomer A and the BiFC dimer receptor populations of Snap  $\beta$ 2AR/ $\beta$ 2AR BiFC dimers, with extensive areas of colocalisation observed (Yellow; overlay panel). The use of a granularity algorithm on these images allowed the internalisation of all receptor populations to be quantified on a per cell basis (granularity panel), with nuclei shown in green and 2-15 $\mu$ m granules identified as white spots.

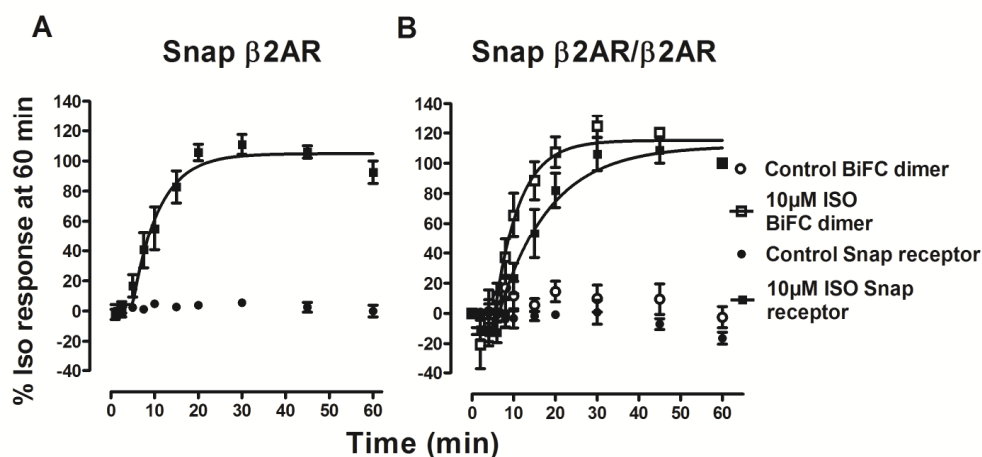


**Figure 5.14: Kinetics of isoprenaline induced internalisation of Snap tagged  $\beta$ 2AR and snap tagged  $\beta$ 2AR/ $\beta$ 2AR BiFC dimers**

Stably transfected HEK293T cells expressing either Snap  $\beta$ 2AR-Yn (A) or Snap  $\beta$ 2AR/ $\beta$ 2AR BiFC dimers (B) were prelabelled with SNAPsurface 647 (30min at 37°C/5% CO<sub>2</sub>). Cells were then stimulated with either vehicle or 10 $\mu$ M isoprenaline at set time intervals, before reactions were terminated using PBS. Cells were then fixed and imaged using an IX Ultra confocal platereader as previously described. Data were normalised to Isoprenaline responses observed at 60min, with a 5min latency period also included during curve fitting. Graphs represent data pooled from at least 3 independent experiments and are expressed as mean  $\pm$  s.e.m. Snap  $\beta$ 2AR/ $\beta$ 2AR timecourse data were provided by Dr Nicholas Holliday (University of Nottingham, UK).

### 5.3.6 Stimulation of Snap $\beta$ 2AR/ $\beta$ 2AR BiFC dimers with a panel of ligands

Snap  $\beta$ 2AR-Yn or Snap  $\beta$ 2AR-Yn/ $\beta$ 2AR-Yc BiFC cell lines were then stimulated with a panel of agonist ligands (30min at 37°C). Pooled concentration response curves showed isoprenaline was equipotent at inducing internalisation at all receptor populations (pEC<sub>50</sub> values 7.1-7.4; n=8-10; Figure 5.15, Table 3). The rank order of potency of ligands was unchanged in each case, being formoterol = salmeterol > isoprenaline > salbutamol. Both salmeterol and salbutamol were partial agonists compared to isoprenaline, and there was no significant change in their relative efficacy for the BiFC dimer internalisation response compared to Snap- $\beta$ 2AR-Yn labelled receptors. In order to investigate whether constraining  $\beta$ 2AR as dimers resulted in altered antagonist pharmacology, Snap  $\beta$ 2 receptor and Snap  $\beta$ 2AR BiFC dimer cell lines were pretreated with the  $\beta$ 2AR antagonist propranolol (10nM for 30min at 37°C). This was followed by stimulation with a concentration response course of isoprenaline (30min at 37°C). Propranolol treatment had no effect alone (Figure 5.16), but resulted in parallel rightward shifts of isoprenaline response curves for Snap  $\beta$ 2AR expressed alone, indicative of surmountable antagonism (Figure 5.16, A; estimated pK<sub>b</sub> 8.9  $\pm$  0.1; n=4). Comparable responses were also observed for both the Snap labelled and BiFC dimer populations of constrained Snap  $\beta$ 2AR/ $\beta$ 2AR BiFC dimers (B; estimated pK<sub>b</sub> values 8.8  $\pm$  0.1 - 9.1  $\pm$  0.1; n = 4).

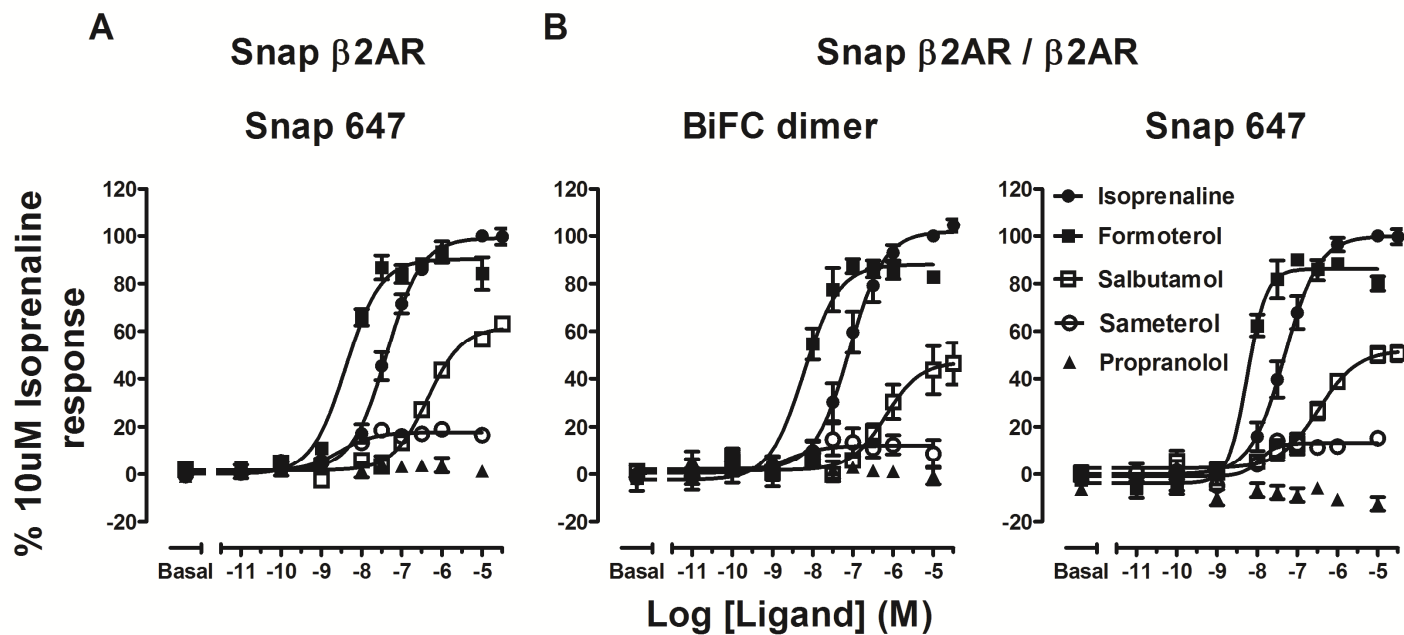


**Figure 5.15: Quantification of the agonist induced internalisation of Snap β2AR-or Snap β2AR/β2AR BiFC dimers following stimulation with a panel of ligands**

HEK293T cells stably expressing either Snap β2AR-Yn alone (A) or Snap labelled β2AR/β2AR BiFC dimers (B) were labelled with 0.2 μM SNAPsurface 647 for 30min at 37°C/5% CO<sub>2</sub>, before stimulation with a panel of ligands (30min at 37°C). Differential responses to ligand were determined following granularity analysis of images acquired using an automated confocal plater reader. All data were normalised to negative (basal responses) and positive (10μM isoprenaline) plate controls. All data were pooled from a minimum of 3 independent experiments, and expressed as mean ± s.e.m.

**Table 5.3: Summary of potencies and efficacies of a panel of ligands for stimulating the internalisation of Snap  $\beta$ 2AR receptors and  $\beta$ 2AR/ $\beta$ 2AR BiFC dimers**

Snap $\beta$ 2AR			Snap $\beta$ 2AR/ $\beta$ 2AR			
	Snap 647 labelled receptor		BiFC dimer		Snap 647 labelled receptor	
Ligand	pEC <sub>50</sub>	E <sub>max</sub> (%)	pEC <sub>50</sub>	E <sub>max</sub> (%)	pEC <sub>50</sub>	E <sub>max</sub> (%)
Isoprenaline	7.4 ± 0.1	100	7.1 ± 0.1	100	7.3 ± 0.1	100
Formoterol	8.4 ± 0.1	84.2 ± 6.8	8.2 ± 0.2	82.8 ± 2.5	8.2 ± 0.1	80.0 ± 2.9
Salbutamol	6.4 ± 0.1	63.3 ± 9.7	6.2 ± 0.1	46.3 ± 8.8	6.2 ± 0.2	50.5 ± 3.2
Salmeterol	8.6 ± 0.1	16.5 ± 6.1	8.6 ± 0.1	8.8 ± 5.6	8.6 ± 0.8	15.2 ± 1.9

All data were expressed as ± standard error of the mean. pEC<sub>50</sub> values were obtained from pooled concentration response curves presented in Figure 5.15.

E<sub>max</sub> responses to each ligand were calculated as a percentage of 1µM NPY responses.

n values for all data 4-10

/ = responses unable to determined

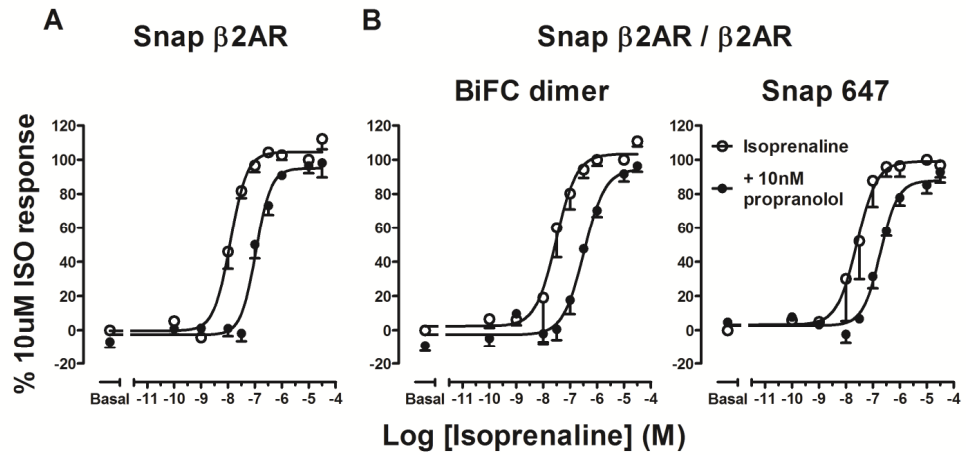


**Figure 5.16: The effect of preincubation with the antagonist propranolol on the agonist induced internalisation of Snap  $\beta$ 2AR receptors and  $\beta$ 2AR/ $\beta$ 2AR BiFC dimers**

HEK293T cells stably expressing Snap  $\beta$ 2AR-Yn (A) or Snap  $\beta$ 2AR/ $\beta$ 2AR BiFC dimers (B) were labelled with SNAPsurface 647 (30min at 37°C/5% CO<sub>2</sub>). Cells were then pretreated with the antagonist propranolol (10nM; 30min at 37°C), followed by stimulation with the agonist isoprenaline (ISO) for 30min at 37°C. Granularity analysis was performed on images obtained using an automated confocal platereader. Concentration response curves in the presence and absence of propranolol were fitted using GraphPad Prism with shared minimum (basal responses), maximum (10 $\mu$ M isoprenaline responses) and Hill slope constraints. All data were pooled from a minimum of 3 independent experiments, and expressed as mean  $\pm$  s.e.m.

### 5.3.7 Introduction of receptor activation mutations selectively introduced into protomer B does not prevent agonist induced internalisation of $\beta$ 2AR BiFC dimers

The NPxxY motif (Asn-Pro-X-X-Tyr) motif is a highly conserved sequence across all Class A GPCRs (Chapter 1, section 1.2.3.2) found at the junction between TM7 and helix 8 (Figure 5.17). This motif has been implicated in maintaining the inactive state of the receptor in addition to influencing receptor expression, sequestration and ligand affinity (Fritze et al., 2003).

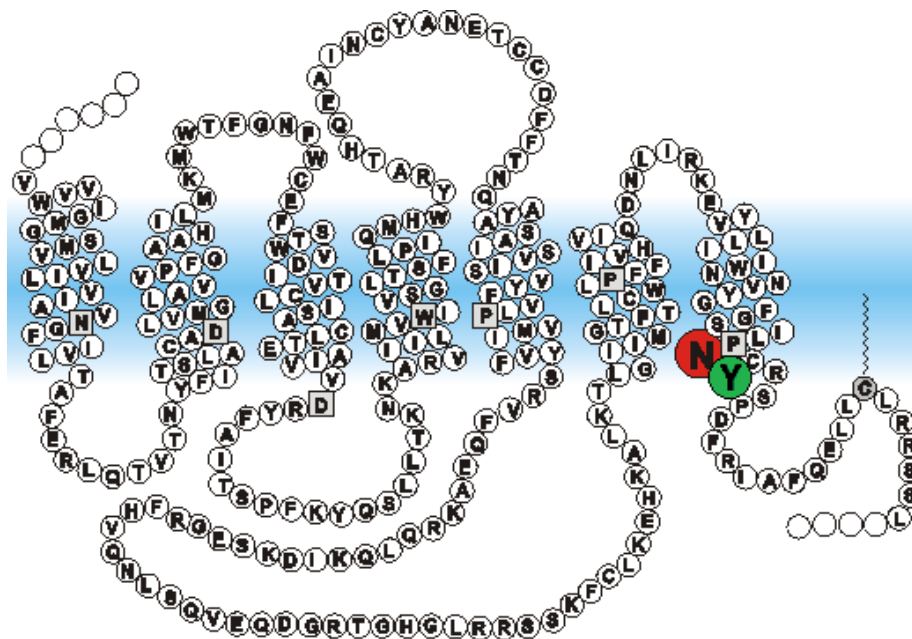


**Figure 5.17: Schematic showing the location of mutations of the NPxxY motif of the human  $\beta$ 2AR**

The position of the NPxxY motif of  $\beta$ 2AR is highlighted, with the N322 shown in red and the Y326 shown in green. Both residues were mutated to alanine when investigating mutant  $\beta$ 2AR BiFC dimers. Square boxes indicate residues highly conserved in the Class A GPCR family. Figure courtesy of Dr Nick Holliday.

Alanine mutations of the asparagine (N322) and tyrosine (N326) residues of the NPxxY motif were introduced into protomer B alone of potential Snap  $\beta$ 2AR/ $\beta$ 2AR BiFC dimers, to examine the effect of inactivating one promoter within the BiFC dimer. As mutation of the tyrosine mutation has already been shown to adversely affect  $\beta$ 2AR internalisation (Barak et al., 1994), agonist

induced internalisation of Snap  $\beta$ 2AR/ $\beta$ 2ARN322A and Snap  $\beta$ 2AR/ $\beta$ 2ARY236A mutant dimers was used as a readout of BiFC dimer function.

In order to investigate the potential effects of NPxxY mutations on  $\beta$ 2AR BiFC dimer function, these mutations were first expressed separately and their internalisation assessed. Mutated receptors containing a N terminal Snap label, but lacking any C terminal modification (ie. the Yn BiFC fragment) were stably expressed in HEK293T cells (Figure 5.18; A, B). Neither the Snap N322A or Snap Y326A mutant receptors were able to internalise in response to stimulation with isoprenaline (30min at 37°C). Responses were 80 ( $\beta$ 2ARN322A) and 61 fold ( $\beta$ 2ARY326A) lower than those observed for wildtype Snap  $\beta$ 2AR internalisation. These data were provided by Dr Nicholas Holliday. Snap  $\beta$ 2AR/ $\beta$ 2ARN322A and Snap  $\beta$ 2AR/ $\beta$ 2ARY326A BiFC dimers were stimulated with a panel of ligands (30min at 37°C) and agonist induced internalisation was quantified using the granularity algorithm. Both mutant BiFC dimers were able to internalise, with the same rank order of agonist potency observed for both Snap  $\beta$ 2AR protomer A and BiFC dimer populations, and preservation of salbutamol and salmeterol partial agonist responses. This ligand selectivity was also the same as observed for Snap  $\beta$ 2AR-Yn expressed alone and Snap  $\beta$ 2AR/ $\beta$ 2AR BiFC dimers (Figure 5.19). Surprisingly neither mutation introduced into protomer B affected the isoprenaline timecourse ( $t_{1/2}$  values 4.0-5.2min; n=4) or relative agonist potency and efficacy of Snap  $\beta$ 2AR BiFC dimer internalisation (Figure 5.18).

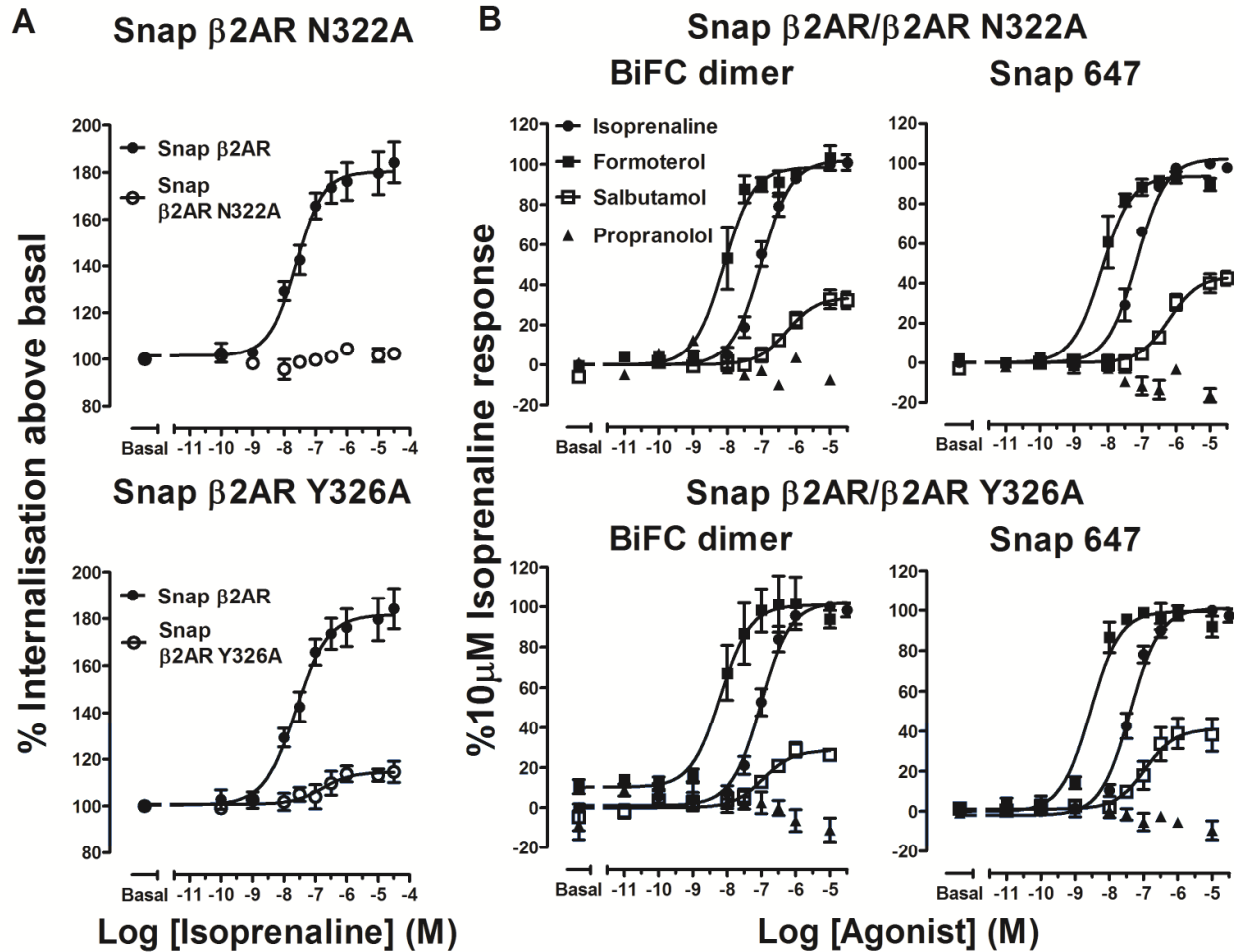


**Figure 5.18: Quantification of the agonist induced internalisation of mutant Snap  $\beta$ 2AR or mutant Snap  $\beta$ 2AR/ $\beta$ 2AR BiFC dimers**

HEK293T cells stably expressing Snap  $\beta$ 2AR receptor constructs were prelabelled with Snap 647 (30min at 37°C/5% CO<sub>2</sub>). Expression of either mutant Snap  $\beta$ 2AR alone (A) allowed the impact of selective NPxxY mutations on receptor internalisation following isoprenaline stimulation (30min at 37°C/5% CO<sub>2</sub>) to be determined. These mutations were then selectively introduced into protomer B of Snap  $\beta$ 2AR/ $\beta$ 2AR BiFC dimers and receptor internalisation was quantified following stimulation with a panel of ligands (30min at 37°C; B). Pooled data are representative of a minimum of 4 independent experiments, expressed as mean  $\pm$  s.e.m.

Snap  $\beta$ 2ARN322A or Snap  $\beta$ 2ARY326A data (A) were provided by Dr Nicholas Holliday.

**Table 5.4: Potencies and efficacies of a panel of ligands for stimulating the internalisation of  $\beta$ 2AR mutant BiFC dimers**

Snap $\beta$ 2AR/ $\beta$ 2ARN322A					Snap $\beta$ 2AR/ $\beta$ 2ARY326A			
	BiFC dimer		Snap 647 labelled receptor		BiFC dimer		Snap 647 labelled receptor	
Ligand	pEC <sub>50</sub>	E <sub>max</sub> (%)	pEC <sub>50</sub>	E <sub>max</sub> (%)	pEC <sub>50</sub>	E <sub>max</sub> (%)	pEC <sub>50</sub>	E <sub>max</sub> (%)
Isoprenaline	7.0 ± 0.1	100	7.1 ± 0.1	100	7.0 ± 0.1	100	7.0 ± 0.1	100
Formoterol	8.1 ± 0.1	103.1 ± 6.1	8.2 ± 0.2	89.7 ± 3.1	8.2 ± 0.2	93.7 ± 4.4	8.6 ± 0.1	91.9 ± 5.2
Salbutamol	6.3 ± 0.1	32.3 ± 4.2	6.2 ± 0.1	42.4 ± 3.5	7.0 ± 0.2	26.2 ± 2.5	6.9 ± 0.2	38.1 ± 8.3

All data were expressed as ± standard error of the mean. pEC<sub>50</sub> values were obtained from pooled concentration response curves presented in Figure 5.18

E<sub>max</sub> responses to each ligand were calculated as a percentage of 1 $\mu$ M NPY responses.

n values for all data 4-8

/ = responses unable to determined

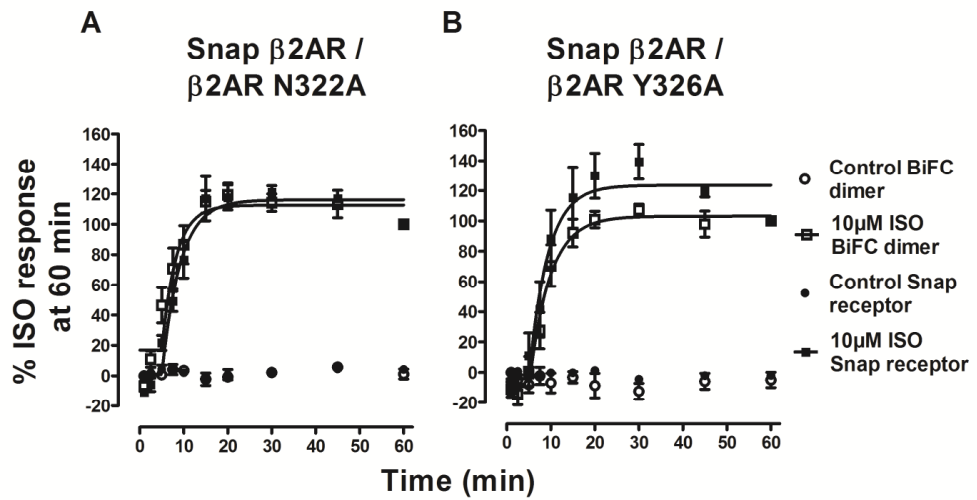


**Figure 5.19: Comparison of the kinetics of the agonist induced internalisation of mutant Snap  $\beta$ 2AR/ $\beta$ 2AR BiFC dimers**

Stably transfected HEK293T cells expressing either Snap  $\beta$ 2AR/ $\beta$ 2ARN322A (A) or Snap  $\beta$ 2AR/ $\beta$ 2ARY326A (B) BiFC dimers, were prelabelled with SNAPsurface 647 (30min at 37°C/5% CO<sub>2</sub>). Cells were then stimulated with either vehicle or 10 $\mu$ M isoprenaline (ISO) at set time intervals. Cells were then fixed, nuclei stained using Hoescht prior to imaging using a IX Ultra confocal platerreader. Data were normalised to isoprenaline responses observed at 60min, with a 5min latency period also included. Graphs represent data pooled from at least 4 independent experiments and are expressed as mean  $\pm$  s.e.m.

## 5.4 Discussion

### 5.4.1 Summary of main findings

In this chapter, BiFC was used to constrain both Y1 receptors and  $\beta$ 2-adrenoceptors as homodimers of precise composition. This allowed a functional readout (agonist-stimulated internalisation) of quantitative pharmacology for these dimers, in a multiplex assay which also monitored in the same cells (using the Snap tag system) the behaviour of the total population of one promoter (“A” - be that monomers, dimers or higher order oligomers). For both Snap Y1/Y1 and Snap  $\beta$ 2AR/ $\beta$ 2AR BiFC constrained dimers, agonist-promoted internalisation was unaffected and the properties of agonists (potency, relative efficacy) and antagonists (affinity) were unaltered compared to reference Snap Y1 or Snap  $\beta$ 2AR internalisation responses. We were able to selectively introduce mutations that disrupt ligand binding, receptor activation, or phosphorylation into one protomer of a BiFC dimer only. These experiments indicated that one ligand binding site, and one functioning receptor protomer was sufficient to induce agonist internalisation of the BiFC dimer. Moreover the lack of functional rescue between ligand binding and phosphorylation mutants in different promoters of the Y1/Y1 BiFC dimer provides indirect evidence against asymmetric recruitment of the internalisation adaptor  $\beta$ -arrestin to the dimer.

### 5.4.2 Y1 or $\beta$ 2AR receptors when constrained as precise homodimers of defined composition, are able to internalise in response to ligand

The nature of complementation assays is artificial in that it essentially creates an irreversible fusion protein between the tagged proteins of interest. However this property was successfully exploited here to constrain the Class A GPCR's subtypes of native Y1 or  $\beta$ 2AR as dimers of precise composition, due to the need for both Yn and Yc fluorescently tagged receptor protomers to associate in order to reform full length YFP (Kerppola, 2009). Observed YFP fluorescence ('BiFC' Figure 5.4, 5.5) was therefore considered a marker of protomer dimerisation, with the quantitative measurement of BiFC dimer

internalisation acting as a readout of dimer function. It is worth emphasising that due to the irreversible trapping of what may be transient protomer interactions, BiFC formation cannot be used in this context as a measure of the extent such receptors form dimers – the purpose instead was to obtain a specific readout of the function (and hence pharmacology) of a particular dimer combination. It is likely that the proportion of BiFC dimers formed is small relative to the total receptor population (discussed further in Chapter 6). Therefore, unlike measurements of whole population responses (such as radioligand binding or cAMP accumulation), in which particular dimer contributions to signalling might be obscured, measurements of BiFC dimer endocytosis uniquely defined responses attributable to this population.

The combined use of Snap labelling also allowed the simultaneous investigation of responses of the total receptor protomer A population (be that monomers, dimers or higher order oligomers) to be compared within the same cell (Figure 5.4, 5.5). Although this is a useful “multiplex” format, there are limitations to the degree to which the “Snap protomer A” and “BiFC dimer” responses are separated. The first is that the Snap labelling will also label the BiFC dimer under investigation, as well as all other protomer A species. The second is that the use of mixed receptor-Yc (protomer B) populations means that the expression of this protomer varied on a cell by cell basis – with some cells (a minority) within the line expressing only the protomer A at detectable levels. Finally the system does not exclude the possibility of higher order oligomers,, in which the BiFC dimers might participate..

The formation of BiFC dimers did not adversely affect cell surface receptor expression, consistent with previous uses of BiFC to investigate adenosine A<sub>2A</sub> homodimers (Vidi et al., 2008b). As indicated above, the presence of plasma membrane BiFC dimers demonstrates that these complexes are not retained in the ER during synthesis and are expressed successfully, but does not exclude trapping of transient, rather than constitutive, interactions by the complementing YFP tags. However techniques with a real time reversible

readout such as BRET, have supported the idea that Y1 receptors (Dinger et al., 2003) and  $\beta$ 2ARs (Angers et al., 2000) can form constitutive dimers prior to membrane expression or ligand stimulation.

The unaffected internalisation of Snap Y1/Y1 and Snap  $\beta$ 2AR/ $\beta$ 2AR BiFC dimers demonstrated that dissociation of these protomers was not a prerequisite for their endocytosis. Observations from coimmunoprecipitation and RET studies of  $\beta$ 2AR (Angers et al., 2000, Hebert et al., 1998), dopamine D2 receptors (Guo et al., 2008) and serotonin 5-HT<sub>2C</sub> receptors (Mancia et al., 2008) have suggested that for these receptors, agonist stimulation has little effect on the dissociation of dimers. However the effect of agonist can vary substantially with GPCR subtype investigated and the experimental approach carried out (Grant et al., 2004). Agonist stimulation has been shown to induce the dissociation of preformed dimers of  $\beta$ 2AR (Lan et al., 2011),  $\delta$  opioid (Cvejic and Devi, 1997), human thyrotropin (Latif et al., 2002), the Class B GPCR type A cholecystokinin receptor (Cheng and Miller, 2001), and interestingly the NPY Y4 receptors (Berglund et al., 2003a).

Lambert (2010) has suggested that these discrepancies on the influence of agonist, may be due to Class A GPCRs existing in a dynamic equilibrium (Lambert, 2010), with dimers being essentially transient. The recruitment of affinity tagged  $\beta$ 2AR or  $\mu$  opioid receptors into an artificial membrane microdomain has suggested they are unable to corecruit untagged receptors (Gavalas et al., 2013) compared to mGluR constitutive dimer controls. This was consistent with FRAP studies of dopamine D2 protomers indicating that they are unable to influence each one another's lateral diffusion within the membrane (Fonseca and Lambert, 2009). These data suggest that Class A GPCR dimerisation is unstable, with the monomer:dimer equilibrium favouring dissociation implying that protomer-protomer interactions are relatively weak. However FRAP studies of the diffusion of subtypes of  $\beta$ -adrenoceptors has disputed this, as the equilibrium of monomers:dimers for  $\beta$ 2AR here favoured association even at subphysiological expression levels

(Dorsch et al., 2009). This reconciles with studies of  $\beta$ 2AR homodimers (Sartania et al., 2007) and yeast  $\alpha$  factor pheromone homodimers (Yesilaltay and Jenness, 2000) showing they are capable of undergoing agonist induced internalisation. BiFC studies have also shown that stimulation of D2/D2 homodimers in a neuronal cell model, with the D2 select agonist quinpirole resulted in internalisation of both dimeric populations (Vidi et al., 2008a).  $A_{2A}/A_{2A}$  homodimers also present were unaffected by D2 stimulation as expected. Equally there is evidence that GPCR heterodimers can result in unique modifications to the endocytosis and trafficking of receptors (see Chapter 6).

Dimer stability has been suggested to differ with receptor subtype (Dorsch et al., 2009, Calebiro et al., 2013) while single fluorescent molecule imaging using fluorescent proteins or ligands has also implied that the half life of dimers may vary from 0.5secs for M1 muscarinic receptors. (Hern et al., 2010) to 5 secs for  $\beta$ 2AR (Calebiro et al., 2013) with dimers only making up a small proportion of the total receptor population expressed (estimated as 30% for muscarinic M1 receptors (Hern et al., 2010)). Interestingly there are suggestions that the predominant receptor form may also be influenced by receptor expression levels (Kasai et al., 2011, Calebiro et al., 2013), with dimers the prevalent form at high receptor expression, most likely due to greater receptor proximity increasing the likelihood of associations. Additionally the plasticity of the plasma membrane could facilitate any dynamic dimer association/dissociation events (Casado et al., 2009a). Plasticity for receptors in respect to their oligomer state in combination with the point in receptor life cycle that measurements are made could impact observations on agonist effects.

Therefore although observations here show that Snap Y1 or  $\beta$ 2AR BiFC dimers can internalise, this does not exclude the possibility that Y1 or  $\beta$ 2AR monomers could also internalise. However it does clearly demonstrate that using BiFC to irreversibly constrain the dimeric state had no effect on

endocytosis and that dissociation of Y1 or  $\beta$ 2AR dimers is therefore not a prerequisite for their internalisation.

#### **5.4.4: BiFC constrained Class A GPCR dimers do not show altered pharmacology in respect to agonists or antagonists.**

##### **5.4.4.1 Unaltered agonist and antagonist pharmacology**

Competitive [ $^{125}$ I] PYY binding showed confirmed that Snap Y1/Y1 cell lines were functional in respect to agonist and antagonist ligand binding affinities and G protein coupling (Table 5.1). Affinity estimates for PYY were comparable to those previously obtained for human and rhesus monkey Y1 receptors in radioligand competition binding assays (Berglund et al., 2003b, Gehlert et al., 1997, Larhammar et al., 1992) and the Y1-GFP or Y1/ $\beta$ -arrestin2 cell lines previously characterised in chapter 3 (Kilpatrick et al., 2010). Additionally the kinetics and agonist rank potencies in respect to internalisation of Snap Y1/Y1 or Snap  $\beta$ 2AR BiFC dimer cell lines were comparable to their Snap Receptor-Yn counterparts and were consistent with previous observations of Y1 receptor (Chapter 3, Tables 3.2 and 3.3) (Wahlestedt et al., 1992, Wahlestedt et al., 1990a) or  $\beta$ 2AR pharmacology (Baker, 2010, Baker, 2005). NPY potencies (as pEC<sub>50</sub>) determined by cAMP accumulation assays were increased compared to internalisation assays for Snap Y1-Yn/Y1-Yc cell lines, likely reflecting the reduced receptor reserve for receptor internalisation compared to the downstream amplification that occurs in cAMP assays. Potencies in cAMP assays were comparable with previous observations for the Y1 receptor (Mullins et al., 2001).

Using BiFC to trap  $\beta$ 2AR dimers had no effect on the affinity of propranolol when compared to the total Snap  $\beta$ 2AR expressed in the same cells or more general  $\beta$ 2AR measurements (Baker, 2010). Equally BIBO3304 was a competitive reversible antagonist of NPY induced inhibition of cAMP accumulation in Snap Y1/Y1 cells and internalisation of Y1/Y1 BiFC dimers. However estimated pK<sub>b</sub> values for both assays, although comparable, were lower than expected based on previous observations (Wieland et al., 1998)

and results obtained from the Y1/A2 cell line (chapter 3, Figure 3.10). However this reduction was also seen for Snap Y1 receptors expressed alone, suggesting that this was not an exclusive consequence of the formation of BiFC dimers and more likely a due to internalisation assays not being performed at receptor-ligand equilibrium.

#### **5.4.4.2 No functional evidence for co-operativity between homo-dimer binding sites.**

Dimerisation of GPCRs may present new pharmacological targets that could be exploited in drug therapies. Altered pharmacology distinct from that typically ascribed to the monomeric form of the receptor, has been observed for some Class A GPCRs (4.1.3). As homodimers are composed of two identical protomers they, unlike heterodimers, have two identical orthosteric binding sites each with theoretically the same selectivity for the same ligand. The apparent transient nature of dimerisation (Lambert, 2010) therefore suggests that potential interactions across the dimer interface may contribute to alterations in signalling and pharmacology.

No changes in agonist and antagonist pharmacology were generally observed for BiFC dimers, but this also raises a question. If cooperativity is occurring for homodimers what would be expected in internalisation data? The only way in which this might be revealed by comparison between Snap receptor and BiFC dimer responses, would be if BiFC were to change the proportion of dimers that are present. If Snap Y1/Y1 or  $\beta$ 2AR/ $\beta$ 2AR dimers were stable anyway, without the presence of the BiFC tags, then there would be no difference observed between measurements for BiFC dimer versus those of Snap Y1-Yn or  $\beta$ 2AR, expressed in the same cells or independently. However as dimerisation is proposed to be a dynamic process (Lambert, 2010, Hern et al., 2010), it is not unreasonable to suggest that dimer formation might be promoted using the BiFC system. If positive cooperativity were occurring between the respective protomer ligand binding sites this would therefore manifest in internalisation data as increases in potency and/or increases in Hill Slopes of curve fits for the BiFC dimer population relative to the Snap

receptor-Yn population. None of the BiFC dimers investigated showed evidence for this, or increases in the relative efficacies of partial agonists such as PP (Y1) or salmeterol ( $\beta$ 2AR).

Negative cooperativity across dimer interfaces implies that only one agonist binding site can be occupied at any one time and has been observed for dopamine D2 (Vivo et al., 2006) and glycoprotein hormone receptors (Urizar et al., 2005). However this would likely be undetectable in internalisation assays in terms of changes in ligand potency or efficacy.

No evidence was seen for cooperativity in respect to changes in antagonism, with surmountable antagonism explained largely by classical pharmacology. Although BIBO3304 affinity measures were lower at both Snap Y1 and Snap Y1/Y1 BiFC dimers, this is likely to be a consequence of non equilibrium conditions. Therefore the influence of cooperativity on BiFC homodimer pharmacology is largely inconclusive, and will be revisited in respect to Y receptor BiFC heterodimer pharmacology in Chapter 6. The BiFC system here has the advantage that, unlike radioligand binding and cAMP accumulation assays, it can distinguish responses of the distinct dimeric population from that of the whole receptor population within the same cell. Therefore the quantification of internalisation as a readout of receptor function is robust as it allowed responses to be directly attributed to this small defined population that are typically hidden in whole population measures (see Chapter 6 for further detail).

#### **5.4.5 The use of selective mutations to probe ligand binding site stoichiometry required to facilitate BiFC dimer internalisation**

Similar to G proteins,  $\beta$ -arrestins are allosteric effectors which can stabilise the high affinity state of the agonist bound receptor. Although evidence suggests that the minimal functional unit for G protein binding is largely believed to be a 1:1 stoichiometry (ie. bound to a receptor monomer(Whorton et al., 2007, Rasmussen et al., 2011a)), this cannot be assumed as true for binding of all effector proteins, such as  $\beta$ -arrestin.

Binding could occur in a 4 potential modes 1:1 (receptor monomer:arrestin monomer), 2:2 (receptor dimer:dimeric arrestin), 2:1a (Asymmetric whereby arrestin interacts across the receptor dimer) and 2:1b (Asymmetric whereby both arrestin domains interact with the same protomer) (Figure 5.20). The use of selective mutations which target the distinct regions of receptor- $\beta$ -arrestin association were used to probe the nature of this interaction.

#### **5.4.5.1 A mutation affecting ligand binding**

The Y99 residue implicated in ligand binding at the Y1 receptor was selectively mutated in protomer B only of a potential BiFC dimer (Figure 5.9), allowing the stoichiometry of ligand binding site occupancy required to induce dimer internalisation to be investigated. The extent of ligand occupancy of a GPCR dimer is important, as ligand binding at one site may have cooperative effects upon binding to the orthosteric site of the second protomer (Birdsall, 2010). The Y99A mutation at the Y1 receptor has been shown to abolish agonist binding and so inhibit the ability of this mutant receptor to recruit  $\beta$ -arrestin2 (Chapter 3; Figure 3.16). However the Y1/Y1Y99A mutant BiFC dimer, was capable of internalising to agonist with kinetics and potencies comparable to those observed for Y1/Y1 BiFC dimers, Snap Y1-Yn expressed alone or superfolder GFP tagged receptors (Chapter 3). Coexpression of the Y1Y99A-Yc mutant receptor did not alter the ability of Snap Y1/Y1Y99A cells to bind ligand and couple to G protein with  $pIC_{50}$  values as expected. However the small proportion of Y1Y99A-Yc expressed in these cells relative to the Snap Y1-Yn clonal population might mean that potential changes indicating altered cooperativity – for example in Hill slopes – were unlikely to be detectable in these assays.

These results suggested that only one functional agonist binding site was required to support endocytosis with the wildtype agonist bound protomer providing the necessary “active” conformation and or C terminal phosphorylated residues required. Previous observations of  $\beta$ 2AR (Sartania et al., 2007) or complement 5a receptors (Rabiet et al., 2008) have supported this conclusion, whereby coexpression of a binding deficient mutant receptor

alongside a wildtype protomer, resulted in a dimer still capable of undergoing agonist induced internalisation. Additionally BRET observations of angiotensin 1 receptor (AT1) dimers, whereby a wild type protomer was coexpressed alongside a ligand binding deficient mutant, resulted in a 'BRET dimer' that was able to recruit  $\beta$ -arrestin2 in response to agonist stimulation (Hansen et al., 2004). Asymmetrical ligand occupancy has also been observed for dopamine D2 receptor homodimers, with maximal activation occurring with agonist binding to a single protomer only (Han et al., 2009).

#### **5.4.5.2 Mutations targeting $\beta$ -arrestin2 recruitment**

Although the mode of G protein binding to GPCR dimers is beginning to be elucidated, the stoichiometry and symmetry of  $\beta$ -arrestin recruitment is much less clear, with the bi-lobed structure of arrestin suggesting the possibility of multiple modes of binding (Figure 5.20 ;(Chapter 1, 1.6.1) (Gurevich and Gurevich, 2004, Nobles et al., 2007). Selective mutations of residues expected to affect interaction with the  $\beta$ -arrestin2 activation sensor ( $\beta$ 2ARN322A or  $\beta$ 2ARY326A) were used to probe this. None of the mutations prevented agonist induced internalisation of BiFC dimers, indicative of an asymmetric recruitment of  $\beta$ -arrestin2 to the dimer, so that only one functional protomer within a dimer was needed for internalisation. The phosphorylation negative mutant Y15A that targets the phosphorylation sensor of  $\beta$ -arrestin2 also did not prevent agonist induced internalisation of Snap Y1/Y15A BiFC dimers. This also suggested a 2:1 stoichiometry of  $\beta$ -arrestin2 binding. Similar results have been observed for complement 5a receptor dimers, whereby a phosphorylation deficient protomer did not internalise when individually expressed, but was able to when coexpressed with a wildtype protomer (Rabiet et al., 2008). This conclusion also assumes that GRKs are able to be recruited to and phosphorylate the unmodified protomer. Additional binding modes utilising the mutated protomer may still also be possible, as although GRKs increase the affinity of  $\beta$ -arrestin for GPCRs (Luttrell and Lefkowitz, 2002), internalisation can still occur in the absence of phosphorylation.

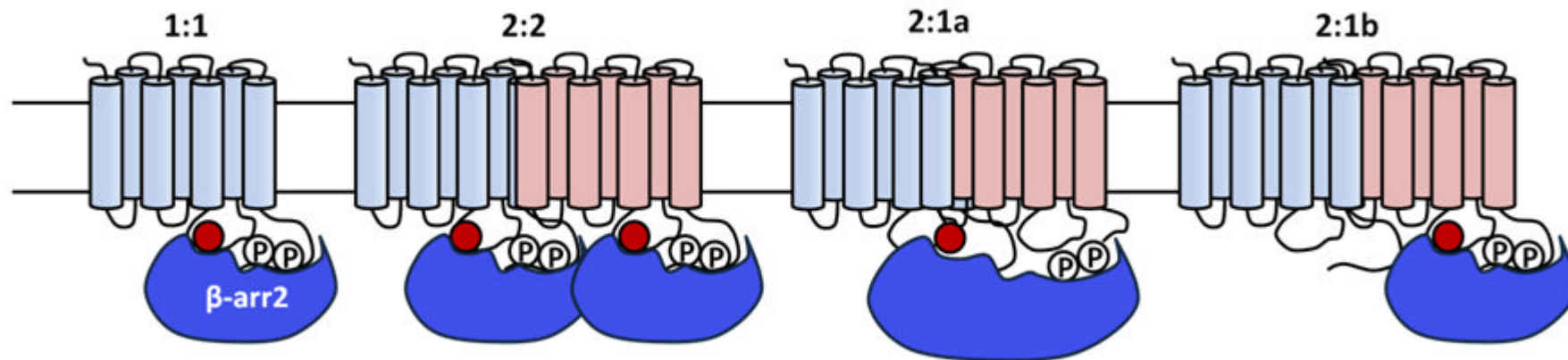


**Figure 5.20: Potential modes of binding of  $\beta$ -arrestin2 to dimeric GPCRs**

Stylised schematic shows the potential modes of binding possible for  $\beta$ -arrestin2 recruitment to GPCRs, with stoichiometries in respect to receptor:arrestin indicated. In a 1:1 stoichiometry monomeric receptor interacts with monomeric  $\beta$ -arrestin so that both its activation (red circle) and phosphate (P) are engaged simultaneously. 2:2 refers to dimeric receptor (blue and pink protomers) binding 2 molecules (or dimeric) arrestin. A 2:1a conformation is whereby dimeric receptor interacts with one molecule of arrestin which bridges the dimer interface to engage both its domains with individual receptor protomers. Finally in a 2:1b stoichiometry, one arrestin binds exclusively to one protomer of the dimer. Respective size of proteins is not to scale.

The bi-lobed structure of arrestin, may support  $\beta$ -arrestin binding to a dimer by interacting with the 2 monomers across its 70 Ångstrom span (Fotiadis et al., 2006) (Gurevich and Gurevich, 2006) (Figure 5.20; stoichiometry 2:1a). Fotiadis et al (2006) have used modelling studies to predict the nature of  $\beta$ -arrestin2 recruitment to an assumed rhodopsin dimer (Fotiadis et al., 2006). They suggest that the dimension and structure of  $\beta$ -arrestin2 would support binding of one molecule to a rhodopsin dimer via dual engagement of the activation and phosphorylation domains of  $\beta$ -arrestin2. However these conclusions are largely based on molecular models of inactive arrestin and may not reflect physiological events, particularly with the recently resolved crystal structure of  $\beta$ -arrestin1 (bound to a peptide fragment of the C terminus of Vasopressin V2 receptor stabilised with an Fab30 antibody fragment) highlighting the profoundly different conformations between the two states (Shukla et al., 2013).

The use of the BiFC system here allowed the direct investigation of the binding model proposed by Fotiadis (Fotiadis et al., 2006) by combining binding site and phosphorylation site mutants in individual Y1 protomers of a BiFC dimer (Snap Y15A/Y1Y99A). If the model proposed by Fotiadis et al., (Fotiadis et al., 2006) is correct then a functional response would only be seen if the activation domain and phosphorylation sensors of  $\beta$ -arrestin engage the phosphorylation deficient protomer (Y15A) and ligand binding deficient protomer (Y1Y99A) respectively. However no functional rescue was seen for Snap Y15A/Y1Y99A, suggesting that the Fotiadis 2:1 model is incorrect and that at least one protomer within a dimer must be both agonist occupied and phosphorylated. However this conclusion depends on the assumption that GRK phosphorylation of the constrained BiFC dimer, and especially the C tail of the Y1Y99A protomer, can proceed. Alternatively, the documented preference of GRKs for agonist occupied receptors (Premont and Gainetdinov, 2007) might limit phosphorylation only to the agonist-occupied protomer – so that the Snap Y15A/Y1Y99A dimer cannot then be phosphorylated. One way to test whether the lack of functional rescue genuinely reveals information

about  $\beta$ -arrestin binding stoichiometry would be to incorporate mutations in the Y1Y99A protomer that also mimic the negative charges of C tail phosphorylation (e.g. substitutions by Glu / Asp). This would reduce the need to consider the intervening GRK step, and if such a mutant restored internalisation of a Snap Y15A/Y1Y99A phosphorylated dimer, the Fotiadis 2:1 model could be re-evaluated.

#### **5.4.6 Reconciling the data from selective mutagenesis of BiFC dimers with proposed modes of $\beta$ -arrestin2 recruitment**

The recently solved crystal structure of active  $\beta$ -arrestin1 bound to a 24 amino acid peptide of the Vasopressin C terminus, suggests that the extensive contacts between the peptide and  $\beta$ -arrestin1 N terminus would likely sterically occlude binding of a second arrestin molecule to the same 'protomer' (Shukla et al., 2013). Evidence from the 'model' Class A GPCR rhodopsin isolated in nanodiscs has also indicated a 1:1 binding stoichiometry of arrestin (visual) with phosphorylated active monomeric rhodopsin (Hanson et al., 2007b, Bayburt et al., 2011, Tsukamoto et al., 2010) that occurs at low nanomolar affinity (Bayburt et al., 2011). Additionally pull down studies of rhodopsin isolated from bovine rod outer segments, as well as *in vivo* transgenic mice studies, have also indicated 1:1 binding saturations even at high arrestin:receptor expression ratios (Hanson et al., 2007a). Due to the physiological role of rod photoreceptors they are advantageous for investigating stoichiometries as both arrestin and rhodopsin are expressed at very high levels. However whilst these observations dispute a 2:1 stoichiometry they do not rule out 2:2 or the formation of even larger complexes (eg. 3:3 or 4:4 (Tsukamoto et al., 2010). Rhodopsin has historically been viewed as the 'model Class A GPCR', however care must be taken when applying observations derived from them to other Class A GPCRs as the 'all or nothing' activation of rhodopsin cannot necessarily describe the degrees of activation and range of conformational states at other GPCRs (Rasmussen et al., 2007b).

Atomic force microscopy has also revealed that *in vivo* rhodopsin formed dimers arranged in organised rows (Fotiadis et al., 2003) suggesting they may support alternative modes of binding. Maurice et al (Maurice et al., 2011) have suggested that the particular binding stoichiometry may change with the receptor dimer and the presence of other effector proteins. A further possibility is that the stoichiometry of binding changes with the activation density of receptors. In native disc membranes at low photoactivation densities stoichiometry was measured as 1:1 arrestin: receptor monomer. Whereas at high photoactivation densities the stoichiometry increased to 2:1 (2 rhodopsin:1 arrestin) (Sommer et al., 2011, Satoh et al., 2010).

The ability of Snap Y1/Y1Y99A BiFC dimers to internalise but the failure of Snap Y15A/Y1Y99A BiFC dimers does not support a 2:2 stoichiometry of 2 activated and or phosphorylated Y1 receptor protomers recruiting 2 molecules of  $\beta$ -arrestin. Instead they are most consistent with 2 receptors binding to 1  $\beta$ -arrestin molecule, whereby both the activation and phosphorylation domains of  $\beta$ -arrestin bind just one of the receptor protomers within the BiFC dimer (discounting the model of (Fotiadis et al., 2006)). An equivalent mutant AT<sub>1</sub> receptor dimer also consisting of a ligand binding deficient protomer and an internalisation deficient protomer has been shown to recruit  $\beta$ -arrestin2 but not G protein (Szalai et al., 2012). This again suggests that for some GPCR dimers, ligand binding to one protomer alone is sufficient to induce  $\beta$ -arrestin2 recruitment with cooperative effects which are propagated through the protomer-protomer interface and reconciles with responses for Snap Y1/Y1Y99A BiFC dimers. However here the authors postulate an asymmetric mode of 2:1  $\beta$ -arrestin2 recruitment to the protomer unoccupied by ligand (ie. to the ligand binding deficient protomer) which can support  $\beta$ -arrestin2 recruitment via its intact C terminus.

Although the lack of internalisation of the Y15A/Y1Y99A mutant BiFC dimer does not support this conclusion, a 2:1 a stoichiometry may represent the mode of  $\beta$ -arrestin2 binding to Snap Y1/Y1Y99A,  $\beta$ 2AR/ $\beta$ 2ARN322A or  $\beta$ 2AR/ $\beta$ 2ARY326A mutant BiFC dimers. However there are two limitations to

this conclusion. Firstly, the quantification of BiFC dimer internalisation is only an indirect measure of  $\beta$ -arrestin2 recruitment. Therefore future studies could combine BiFC with BRET to directly measure this association (See Chapter 7, Final discussion). Secondly the use of BiFC artificially constrains receptors as dimers, therefore it cannot be used to resolve the stoichiometry of  $\beta$ -arrestin binding to native receptors and whether this reconciles with a 1:1 essentially monomeric internalisation or a 2:1 mode for a dimer as suggested from these results. Nevertheless, as indicated in the next chapter, application of this system to Y receptor heterodimers can reveal interactions between the promoters which result in novel pharmacological responses.

## **Chapter 6 – The use of BiFC to constrain GPCRs as heterodimers of precise composition in order to investigate potential dimer specific modified pharmacology**

### **6.1 Introduction**

The pharmacological possibilities presented by GPCR homodimerisation are potentially expanded further by heterodimer formation. As heterodimerisation involves the association of two structurally discrete GPCR subtypes (whether closely or distantly related), often with differing ligand selectivity and downstream signalling outcomes, the pharmacological properties of heterodimerisation may be distinct from that seen for either monomer or homodimer forms (Ayoub and Pflieger, 2010). This raises the possibilities that heterodimers may represent novel pharmacological targets, and that therapies selectively targeting them may show greater selectivity and efficacy.

#### **6.1.1 The evidence for the existence of GPCR heterodimerisation**

As for the GPCR Class A homodimerisation, there are many strands of evidence suggesting the formation of heterodimers. Here is a summary of some key examples from heterologous cell lines and in native tissue samples.

##### **6.1.1.1 Coimmunoprecipitation assays**

As for GPCR homodimerisation, many of the initial indications of heterodimerisation have come from biochemical techniques, such as coimmunoprecipitation using differentially epitope tagged receptor subtypes coexpressed in heterologous cell lines. For the Class C GPCR receptors, which must form obligate dimers to function, coimmunoprecipitation revealed the association of GABA<sub>B</sub>R1 and GABA<sub>B</sub>R2 receptor subtypes (Kaupmann et al., 1998) as well as heterodimer pairings of bitter and sweet taste receptor

subtypes (Kuhn et al., 2010). For Class A GPCRs, coimmunoprecipitation has implied heterodimer formation of a variety of closely related receptor subtypes. For example within the opioid receptor family, coimmunoprecipitation of  $\delta$  and  $\kappa$  (Jordan and Devi, 1999) and  $\delta$  and  $\mu$  (George et al., 2000) subtypes has been documented. Coimmunoprecipitation has also been observed for  $\beta$ 1 and  $\beta$ 2 adrenoceptors (Lavoie et al., 2002) as well as the dopamine receptor subtypes D2 and D3 (Scarselli et al., 2001) and D1 and D3 (Zeng et al., 2006). Coimmunoprecipitation has also been seen for distantly related GPCR subtypes, such as the chemokine R5 (CCR5) and  $\mu$  opioid receptors (Suzuki et al., 2002), the adenosine  $A_{2A}$  and dopamine D2 receptors (Hillion et al., 2002), and the adenosine A1 receptor with multiple receptors including thromboxane  $A_2R\alpha$  receptors (Mizuno et al., 2012), dopamine D1 receptors (Gines et al., 2000), purinergic  $P_2Y_1$  receptors (Yoshioka et al., 2001) and the  $\beta$ -adrenoceptor subtypes  $\beta$ 1 and  $\beta$ 2 (Chandrasekera et al., 2013).

The majority of coimmunoprecipitation studies investigating GPCR heterodimerisation have been performed in overexpressing heterologous cell lines, such as HEK293T, COS-7 or a mouse derived fibroblast cell line (Gines et al., 2000). However coimmunoprecipitation from native tissue samples has identified  $GABA_B R1/R2$  (Kaupmann et al., 1998) and dopamine D1/D3 heterodimers (Zeng et al., 2006). Human heart tissue lysate also revealed distinct populations of adenosine A1 constitutive heterodimers with either  $\beta$ 1 or  $\beta$ 2 adrenoceptors (Chandrasekera et al., 2013). Additionally homogenates isolated from rat striatum have implicated the association of mGluR5, D2 and  $A_{2A}$  receptors as potential trimer complexes (Cabello et al., 2009).

For the majority of observations, specific 'heterodimeric complexes' were identified from membrane isolations where tagged receptors were initially coexpressed, and not when two cell preparations expressing different receptor subtypes were mixed prior to solubilisation. This indicates that coimmunoprecipitation of complexes was not a consequence of the assay protocol used. However coimmunoprecipitation still requires that receptor

complexes are solubilised from the membrane during isolation, and this process might lead to artificial aggregation of the receptor hydrophobic membrane spanning domains. Thus such observations need to be supported by additional techniques, particularly those which provide evidence for heterodimerisation in living cells and *in vivo*.

#### **6.1.1.2 Evidence from fluorescent based approaches**

Observations using fluorescence based techniques, such as FRET and BRET, have implied the association of coexpressed fluorescently tagged receptor subtypes in living cells. These associations may be between closely or distantly related subtypes and have been interpreted as evidence of heterodimer formation.

BRET and FRET studies have indicated interactions between the closely related GPCR Class A subtypes Y1 and Y5 (Gehlert et al., 2007),  $\beta$ 1 and  $\beta$ 2-adrenoceptors (Mercier et al., 2002), melatonin MT<sub>1</sub> and MT<sub>2</sub> (Ayoub et al., 2002), vasopressin V1a and V2 (Terrillon et al., 2003), cannabinoid CB<sub>1</sub> and CB<sub>2</sub> subtypes (Callen et al., 2012), the dopamine subtypes D1 and D3 (Marcellino et al., 2008), D2 and D3 (Pou et al., 2012), and D2 and D5 (So et al., 2009) and chemokine CXCR1 and CXCR2 receptors (Wilson et al., 2005). Both techniques have also implied heterodimerisation of distantly related subtypes such as the  $\beta$ 2 adrenoceptor and  $\delta$  opioid, the  $\beta$ 2 adrenoceptor and  $\kappa$  opioid (Wilson et al., 2005), the  $\alpha$ <sub>1A</sub> adrenoceptor and  $\mu$  opioid receptors (Villardaga et al., 2008) and  $\alpha$ 1B adrenoceptor and dopamine D4 receptors (Gonzalez et al., 2012). FRET has also been used to identify heterodimers of CB<sub>1</sub> and orexin OX<sub>1</sub> receptors in intracellular endosomes of HEK293TR cells (Ellis et al., 2006). This was interpreted as reflecting post endocytic trafficking of heterodimeric receptors from the cell surface, due to the constitutive internalisation observed for CB<sub>1</sub> receptors. In addition these compartments may be a route to traffic complexes that are formed in the ER to the cell surface. Follow up TR-FRET studies using combined SNAP and CLIP N terminal protomer labelling confirmed stable cell surface expression of these heterodimers (Ward et al., 2011). Additionally TR-FRET using N terminal SNAP

and CLIP tagged receptors has identified specific ghrelin (GHSR1a) and D2 receptor heterodimers colocalised at the cell surface of HEK293T cells (Kern et al., 2012).

Heterodimers of adenosine  $A_{2A}$  and D2L receptors have also been identified using both BRET and FRET (Canals et al., 2003). Additionally the use of BiFC identified heterodimers were localised at the cell membrane and within endosomes in a neuronal cell model (Vidi et al., 2008a). This study was also the first to use BiFC to monitor the ligand induced modulation of GPCR oligomerisation, with long term ligand exposure influencing the balance of  $A_{2A}$ /D2L heterodimers,  $A_{2A}$  or D2L homodimers. Multicolour BiFC has also illustrated interactions of  $CB_1$  and D2L receptors in a neuronal cell model, which were regulated by  $CB_1$  selective ligands (Przybyla and Watts, 2010). Complexes of this heterodimer pairing have also been identified using FRET and BRET techniques in HEK293T cells (Navarro et al., 2008) in keeping with previous observations of  $CB_1$  and D2L receptor colocalisation *in situ* in rat striatum (reviewed in (Blume et al., 2013)). The combined use of BiFC and BRET has also suggested the occurrence of higher order hetero-trimers of  $CB_1$ , D2 and  $A_{2A}$  receptors (Navarro et al., 2008) and mGluR5, D2 and  $A_{2A}$  receptors (Cabello et al., 2009) in HEK293T cells. However the use of BiFC has largely been limited to the identification of the existence of GPCR dimers, as opposed to investigating their functional relevance.

Many fluorescence based techniques are difficult to implement in native tissues, as in contrast to heterologous cell lines it is difficult to control receptor expression levels or easily introduce engineered fluorescently tagged receptors (Ferre et al., 2014). To circumvent this, techniques utilising GPCR specific antibodies have been developed. A proximity ligation assay has implied close association of  $A_{2A}$  and D2 receptors in rat brain slices (Trifilieff et al., 2011) and  $CB_1$  and  $CB_2$  subtypes in the rat brain pineal gland and nucleus accumbens (Callen et al., 2012). Here primary antibodies recognising either protomer of a proposed heterodimer, are labelled with secondary antibodies conjugated to complementary oligonucleotide sequences. These sequences

are then ligated, amplified and visualised using a fluorescent probe. 'Heterodimer specific' monoclonal antibodies have also been generated which selectively recognise an epitope spanning both protomers of a heterodimer but shows no specific binding when one of the protomers is removed (Gupta et al., 2010). However designing such a selective epitope is in practice difficult, and is particularly dependent on the GPCR region against which the epitope is designed.

A less complicated use of antibodies is to conjugate them to fluorescentRET partners. This has been used to identify CB1 and AT1 receptor heteromers in isolated rat hepatic stellate cells (Rozenfeld et al., 2011) and morphine induced changes in expression of  $\mu/\delta$  opioid heteromers in rat brain sections (Gupta et al., 2010). It is worth noting that antibody based techniques rely on high expression levels of receptors and their bivalent nature may inadvertently promote receptor associations (Ward et al., 2011). However if highly selective, they are a potentially important tool to identify association of receptor subtypes in native tissue. TR-FRET using fluorescent ligands has also identified heterodimers of ghrelin (GHSR1a) and dopamine D2 receptors in mouse hypothalamic neurons (Kern et al., 2012). Antibody tagged dopamine D2 protomers were identified using a secondary antibody conjugated to fluorescent terbium cryptate, which acted as the donor fluorophore to excite the fluorescently labelled agonist ghrelin (acceptor).

Fluorescence based techniques, although useful in identifying receptor-receptor interactions, are dependent on the proximity and orientation of the probes used. Therefore close receptor proximity can only imply, not confirm, the formation of specific heterodimers and should be used in conjunction with other functional methods. Additionally these techniques (or coimmunoprecipitation) cannot distinguish the proportion of heterodimers present at the cell surface compared to other receptor species (be that monomers, homodimers or higher order oligomers).

### 6.1.1.3 Altered receptor trafficking during synthesis and maturation

The level of receptor expression at the cell surface is largely determined by the balance of intracellular trafficking mechanisms such as export from the endoplasmic reticulum, endocytosis and degradation. GPCR dimerisation has been implicated as a mechanism to facilitate trafficking of receptors through the endoplasmic reticulum and Golgi apparatus following biosynthesis and assist plasma membrane expression. Evidence from obligate dimers of the Class C GPCR family, such as the GABA<sub>B</sub> receptor, has supported this assertion. As discussed in Chapter 5, the GABA<sub>B</sub>R2 subunit effectively masks the intracellular retention signal on the GABA<sub>B</sub>R1 subunit (summarised in (Kniazeff et al., 2002)) so that only via dimerisation is the GABA<sub>B</sub> receptor able to be expressed at the cell surface.

This functional complementation has also been observed for heterodimers of Class A GPCRs, when these receptors were engineered to contain ER retention motifs. The chemokine receptor subtypes CXCR1 and CXCR2 have been shown previously to form constitutive heterodimers that are expressed at the cell surface (Wilson et al., 2005). In addition when expressed independently, both subtypes reach the cell surface correctly. The addition of an ER retention signal from the  $\alpha_{2C}$  adrenoceptor to a HA tagged CXCR1 sequence resulted in a receptor that is not trafficked to the plasma membrane and is retained intracellularly. Coexpression of this mutant with a FLAG tagged CXCR2 subtype resulted in a heterodimer with decreased cell surface expression (approximately a 50% decrease in expression when compared to CXCR2 alone). Additionally co-expression of receptor subtypes showing high cell surface expression with subtypes that are poorly expressed has been shown to promote the translocation of the second protomer to the cell surface. For example coexpression of the  $\alpha_{1D}$ -adrenoceptor, which is almost exclusively intracellular localised, with either the  $\alpha_{1B}$ -adrenoceptor (Hague et al., 2004) or the  $\beta_2$ -adrenoceptor (Uberti et al., 2005) was shown to increase its cell surface expression in luminometer assays. Equally, the  $\beta_2$ -adrenoceptor is able to act as a molecular chaperone facilitating cell surface expression of an

intracellular localised olfactory receptor (Hague et al., 2004), although this study, and other examples of “rescued expression”, might be a consequence of receptor over expression.

#### **6.1.1.4 Altered ligand binding**

Evidence for potential allosteric communication across a heterodimer interface can be inferred by investigating ligand binding. If the affinity of a ligand binding to a receptor coexpressed within a dimer is significantly modified from that seen for the receptor expressed alone, this would suggest that the presence of the second protomer is influencing binding.

This allosteric modulation can be ligand dependent, whereby binding of ligand at protomer A influences binding at the orthosteric binding site of protomer B (Kenakin and Miller, 2010).. One of the earliest observations of modified ligand binding affinities at GPCR complexes came from coexpression studies of  $A_{2A}$  and D2 receptors (Ferre et al., 1991). Here coincubation with the  $A_{2A}$  selective agonist CGS21680 decreased the ability of dopamine to compete with [ $^3$ H] raclopride for the D2 orthosteric binding site. The addition of an  $A_{2A}$  receptor antagonist was able to restore the binding affinity of dopamine, suggesting that the  $A_{2A}$  site was allosterically modulating binding at the D2 orthosteric site. Comparable changes in affinity at selective protomers have been observed for some heterodimers including  $A_{2A}$ /dopamine D3 (Torvinen et al., 2005), D1/D3 (Marcellino et al., 2008), the  $\beta$ 1AR or  $\beta$ 2AR protomer of  $\beta$ 1AR/A1 or  $\beta$ 2/A1 heterodimers (Chandrasekera et al., 2013) and reciprocal changes for either protomer of  $\delta/\mu$  opioid heterodimers (Gomes et al., 2013). Additionally modification of ligand affinities was also seen for adenosine A1/A2 receptor heterodimers expressed both in heterologous cell lines and endogenous receptors expressed in native pre and post synaptic neurons (Ciruela et al., 2006). However it is worth pointing out that ligand based studies are often dependent on the subtype selectivity of the ligands being sufficient to assume that only one protomer binding site is occupied. For closely related receptor subtypes, such as the opioid family, such distinct selectivity is not always possible.

Alternatively allosterism at GPCR heterodimers, may be ligand independent whereby the unoccupied protomer A – the receptor itself - may act as an allosteric modulator of protomer B via a direct physical interaction (Kenakin and Miller, 2010). For example GPR50, an orphan GPCR, constitutively heterodimerises with melatonin MT1 receptors leading to abolition of high affinity binding and G protein coupling of the MT1 protomer (Levoye et al., 2006). This negative modulation is suggested to be due to a steric inhibition of MT1 by the large C terminal tail of the GPR50 receptor.

Alterations in ligand binding affinities have not been observed for all documented GPCR heterodimers. Notable exceptions include association of the NPY Y1 and Y5 receptor subtypes (Gehlert et al., 2007),  $\beta$ 2AR and  $\delta$  opioid receptors;  $\beta$ 2AR and  $\kappa$  opioid receptors (Jordan et al., 2001), the  $\beta$ 2AR and  $\beta$ 3ARs (Breit et al., 2004) and  $\mu$  opioid and neurokinin 1 receptor receptors (Pfeiffer et al., 2003). Affinity ( $K_d$ ) is the ratio of ligand association and dissociation rate constants at equilibrium. Therefore alterations in ligand dissociation rates may better reflect dynamic heterodimer allosterism (May et al., 2007). Insights from the chemokine receptor family, has supported this assertion by using infinite dilution to measure the dissociation kinetics of a radioligand specific to one protomer of a CCR2/CCR5 (Springael et al., 2006) or CCR2/CXCR4 heterodimer (Sohy et al., 2007), and then demonstrating the effects of an unlabelled ligand binding the second protomer. In both cases radioligand dissociation kinetics from the CCR2 protomer were found to be affected by ligand binding to partner protomer, but this allosteric effect was only seen when both receptors were expressed. Comparison with infinite dilution conditions also implied strong cooperativity between protomer binding sites of adenosine A3 dimers, with the effects of competing ligands manifested as changes in ligand dissociation rates at the single cell level (May et al., 2011). This cooperativity was decreased when one of the protomers contained a mutation to prevent ligand binding, suggesting that allosterism was a consequence of communication between protomer orthosteric binding sites.

Effects of ligand binding on GPCR dimers can often be difficult to extract from measures of cell population binding studies, as it is difficult to ascribe effects directly to a dimeric population that may be both transient and (particularly for heterodimers) a small proportion of the overall receptor species. For example as discussed in Chapter 5, TIRF studies of M1 muscarinic receptors suggested that the homodimeric state of these receptors only represent up to 30% of the total population at any time (Hern et al., 2010).

In addition to using ligands selective for one protomer of a heterodimer to probe function, heterodimer selective ligands have been suggested. These ligands have been hypothesised to have greater affinity for binding the heterodimer form than respective monomer or homodimers. Examples of these include 6'-guanidinonaltrindole (6'GNTI), which has been shown to induce intracellular  $Ca^{2+}$  to a greater extent when stimulating  $\delta/\mu$  opioid heterodimers than either species expressed alone, and also have selective analgesic effects in the spinal cord (Waldhoer et al., 2005). A purportedly highly selective dopamine D1-D2 ligand that activates novel  $G_{q/11}$  signalling by acting as a full agonist at D1 and a partial at D2 receptors (Rashid et al., 2007) has also been proposed. However the selectivity of this ligand has been questioned, as paradoxical signalling effects have been observed *in vivo* and it has been shown to have high affinity for other unrelated GPCR subtypes (Chun et al., 2013). Bivalent ligands, whereby two distinct pharmacophores are linked by a spacer, have also been developed which are proposed to bridge the dimer and either target both orthosteric sites or bind one and a distinct allosteric site (Hiller et al., 2013). Examples include those that target opioid receptor subtypes ( $\delta/\mu$ ; (Daniels et al., 2005b) and  $\kappa/\delta$  respectively (Daniels et al., 2005a)). However the main issue of these heterodimer selective bivalent ligands in addition to selectivity is their relatively large size limits therapeutic uses and restricts them to *in vitro* tools.

#### **6.1.1.5 Altered internalisation**

Heterodimerisation has been implicated in altering the endocytosis of one or both protomers within the complex. Evidence suggests that for some

heterodimer combinations binding of a single ligand to one protomer is sufficient to support the co-internalisation of the entire heterodimeric complex. For example, treatment of  $\beta$ 2AR/ $\delta$  opioid receptor heterodimers with the  $\beta$ 2-adrenoceptor agonist isoprenaline, resulted in occupancy of the  $\beta$ 2AR orthosteric binding site and internalisation of both receptor populations. Reciprocal responses were also observed following stimulation with the  $\delta$  opioid agonist etorphine (Jordan et al., 2001). As isoprenaline is structurally distinct from etorphine, this suggests that either ligand is activating its cognate orthosteric site selectively.

Similar effects have been seen with coexpression of  $\delta$  opioid and neurokinin NK<sub>1</sub> receptors, in response to stimulation with the  $\delta$  selective agonist DAMGO or the NK<sub>1</sub> agonist substance P (Pfeiffer et al., 2003). Cointernalisation has also been observed for orexin (OX<sub>1</sub>) and CB<sub>1</sub> heterodimers, whereby stimulation with orexin A was able to stimulate the internalisation of the CB<sub>1</sub> receptor population even though it has no direct affinity for this receptor (Ward et al., 2011). Interestingly this effect was only seen when these receptors were coexpressed and orexin A was more potent at inducing the internalisation of the CB<sub>1</sub> population than the total OX<sub>1</sub> receptor population (which is presumed to be a mixture of monomers, homodimers and oligomers). These data are consistent with the previous observation in this thesis, that ligand occupancy at one protomer within a defined dimer is able to drive agonist induced endocytosis of the dimeric complex (Snap Y1/Y1Y99A BiFC dimer; Chapter 5, Figure 5.13).

Detrimental effects upon internalisation as a consequence of heterodimerisation have also been observed. For example rapid internalisation in response to agonist stimulation has been observed for the  $\beta$ 2-adrenoceptor subtype ((von Zastrow and Kobilka, 1992) ; see Chapter 5, Figure 5.15) when expressed independently. Conversely both the  $\beta$ 1 and  $\beta$ 3 adrenoceptor subtypes both internalise to a much lesser extent. However coexpression of the  $\beta$ 2 subtype with either the  $\beta$ 1 (Lavoie et al., 2002) or the  $\beta$ 3 adrenoceptor subtypes (Breit et al., 2004) resulted in heterodimers that

were unable to undergo agonist promoted endocytosis. A similar effect has been observed when the  $\beta$ 2-adrenoceptor was coexpressed with the distantly related internalisation resistant  $\kappa$  opioid receptor. No heterodimer internalisation was observed following stimulation with either subtype selective ligand suggesting the  $\beta$ 2AR subtype has adopted the internalisation profile of the  $\kappa$  subtype (Jordan et al., 2001). These data suggested that one protomer of a heterodimer (in this case  $\beta$ 1,  $\beta$ 3 or  $\kappa$  opioid subtypes) was able to act as a dominant negative modulator of agonist induced internalisation of the other.

Interestingly ligand induced internalisation has also been used as a measure of the dynamic equilibrium between heterodimer and homodimer species within the same cells. Treatment of  $A_{2A}/D2$  heterodimers with the D2 receptor agonist quinpirole resulted in cointernalisation of the heterodimer complex (Hillion et al., 2002). However long term stimulation induced a change in the proportion of  $A_{2A}/D2$  heterodimers relative to  $A_{2A}/A_{2A}$  homodimers (Vidi et al., 2008a). These observations do raise the question of whether cointernalisation is directly attributable to a physical association between coexpressed receptors. An alternative method could be that activation of one protomer may lead to intracellular signalling pathways that induce an independent internalisation of the second protomer driven by PKA or PKC mediated phosphorylation.

#### **6.1.1.6 Altered G protein coupling and signalling**

Phenotypic changes in downstream signalling outcomes have been observed for some heterodimer pairings. These changes may reflect modifications in effector protein coupling to dimers, in conjunction with the intrinsic efficacy of ligands for stabilising a particular receptor conformation which favours coupling to distinct signalling pathways (Ferre et al., 2014). This phenomenon, termed functional selectivity, has been observed for some heterodimer pairings whereby changes in the nature of G protein or  $\beta$ -arrestin coupling can result in distinct physiological outcomes – often assuming an asymmetric mode of coupling (see Chapter 5, section 5.1.1.3).

For some GPCR heterodimers, the G protein class to which protomer A preferentially couples is modified so that it adopts the  $G_{\alpha}$  subunit preferentially bound by protomer B. For example coexpression of the dopamine D1 receptor with histamine H3 receptors in neuroblastoma cells resulted in a switch from  $G_{\alpha_s}$  to  $G_{\alpha_i}$  driven MAPK signalling for the D2 protomer, while H3 agonists allosterically inhibited dopamine D1 mediated G protein and  $\beta$ -arrestin2 mediated signalling (Moreno et al., 2014). A proposed physiological consequence of this modified signalling is that this histamine dimer is able to inhibit dopamine D1 receptor mediated cell death. This switch in G protein coupling was also observed for  $\beta$ 2AR/ $\beta$ 3AR heterodimers, whereby  $G_{\alpha_i}$  coupling, typically observed in addition to  $G_{\alpha_s}$  coupling for both individual subtypes, was not seen for the heterodimer but  $G_{\alpha_s}$  recruitment was preserved (Breit et al., 2004). Similar effects have also been seen for another adrenergic heterodimer, the  $\beta$ 1AR/ $\beta$ 2AR, but here G protein coupling reflected a  $\beta$ 1AR like phenotype with ERK phosphorylation used as a readout (Lavoie et al., 2002). This suggests that G protein coupling to a receptor protomer (eg. the  $\beta$ 2AR) can be distantly modified depending on the second protomer coexpressed, which further increases the potential for novel pharmacology arising from heterodimerisation.

Heterodimerisation has also been suggested to switch G protein coupling to a class that is completely atypical for either protomer. For example dopamine D1 and D2 receptors, typically couple to  $G_{\alpha_s}$  and  $G_{\alpha_i}$  classes respectively. However the D1/D2 heterodimer shows novel coupling to the  $G_{\alpha_q}$  class, facilitating the elevation of intracellular calcium levels in transfected cells and rat brain striatum (Rashid et al., 2007). However this change in G protein coupling may not reflect physical heterodimer formation, but has been suggested to instead be a consequence of the expression level of  $G_{\alpha_q}$  or downstream signalling crosstalk (Chun et al., 2013).

Signalling switching has also been indicated for  $CB_1/AT_1$  (Rozenfeld et al., 2011) and  $\delta/\mu$  opioid heterodimers (Rozenfeld and Devi, 2007). An additional modification of  $\delta$  and  $\mu$  opioid receptor heterodimerisation that has

unwanted physiological effects is a switch in the nature of effector protein coupling. When expressed alone  $\mu$  opioid receptors stimulated with morphine results in G protein dependent signalling and ultimately analgesia (Raehal et al., 2011). Coexpression of  $\mu$  and  $\delta$  opioid receptors however resulted in morphine directed  $\beta$ -arrestin2 dependent signalling and leading to greater tolerance of chronic morphine induced analgesia (Rozenfeld and Devi, 2010). This outcome was specific to the presence of the  $\delta$  opioid subtype as treatment with a  $\delta$  selective antagonist restored G protein directed signalling and morphine induced analgesia. The intrinsic affinity of the ligand used can also allosterically influence the direction of signalling bias. The angiotensin AT<sub>1</sub> receptor agonist [Sar1,Ile4,Ile8] angiotensin II, shows  $\beta$ -arrestin2 signalling bias at AT<sub>1</sub> receptors expressed alone (Violin et al., 2010). By binding to the AT<sub>1</sub> receptor orthosteric ligand binding site of AT<sub>1</sub>/bradykinin B2 heterodimers, this agonist showed lateral allosteric modulation of signalling at the B2 subtype by inhibiting G <sub>$\alpha$ i/o</sub> signalling and promoting  $\beta$ -arrestin2 recruitment and heterodimer cointernalisation (Wilson et al., 2013). However this heterodimer pairing has been difficult to replicate by other groups in both the same and different cell systems (Hansen et al., 2009).

For some heterodimer pairings, allosteric modulation of protomer A by protomer B results is able to potentiate signalling responses originating at protomer B. An example of this which may have physiological implications in the control of feeding responses is the ghrelin GHSR1a and dopamine D2 receptor heterodimer (Kern et al., 2012) implicated in the promotion of anorexigenic effects. Stimulation of this heterodimer with the dopamine or another D2 receptor agonist cabergoline, led to a PLC mediated increase in intracellular calcium mobilisation via G $\beta\gamma$  activation. This effect was seen in the absence of ghrelin costimulation or the presence of a neutral GHSR1a antagonist, suggesting that it is the GHSR1a subtype itself that is allosterically modulating binding to the D2 subtype. However a caveat to this is that the ghrelin receptor has a high degree of constitutive activity in the absence of

stimulation, which may complicate interpretations of dimer specific pharmacology.

The orexin 1 (OX<sub>1</sub>) / CB<sub>1</sub> heterodimer has also been suggested to mediate the stimulation of food intake. The presence of the CB<sub>1</sub> subtype increased the potency of the agonist orexin A at the OX<sub>1</sub> receptor in respect to internalisation (10 fold increase; (Ward et al., 2011) and MAPK signalling (100 fold; (Hilairt et al., 2003)). This allosteric potentiation of OX<sub>1</sub> signalling was specifically blocked by the CB<sub>1</sub> selective antagonist rimonabant, a known inhibitor of food intake, suggesting the OX<sub>1</sub> / CB<sub>1</sub> heterodimer may be a valid target for anti obesity therapies.

Dual antagonism has also been observed for many GPCR Class A heterodimers. This is where antagonists targeting protomer A of the dimer can inhibit signalling originating from agonist binding to the unrelated protomer B and vice versa. This effect has been observed for heterodimers of  $\alpha_{1B}$  adrenoceptor and dopamine D4 receptors in respect to phosphorylation of Akt (Gonzalez et al., 2012), and histidine H3 and dopamine D1 receptors (Ferrada et al., 2009). The proposed heterodimerisation of  $\beta$ 2AR and AT<sub>1</sub> receptors in mouse cardiomyocytes and whole animals has suggested this effect may have clinical relevance as here cross antagonism resulted in inhibition of heart rate and cardiac contractility (Barki-Harrington et al., 2003). This bidirectional antagonism has also been observed for CB<sub>1</sub>/CB<sub>2</sub> heterodimers expressed in the neuroblastoma cell line SH-SY5Y (Callen et al., 2012). Additionally when expressed individually both CB<sub>1</sub> and CB<sub>2</sub> subtypes have been shown to increase the phosphorylation of Akt and stimulate neurite growth. However coactivation of both protomers of the CB<sub>1</sub>/CB<sub>2</sub> heterodimer inhibits this response, suggesting negative crosstalk is occurring at this heterodimer in respect to Akt phosphorylation.

It is therefore likely that the functional consequences of GPCR heterodimerisation vary greatly depending on the receptor pairing and potentially the specific ligand stimulation (Ferre et al., 2014). The extent of modification of responses due to allosteric interactions within the dimer can

therefore vary from subtle changes in the efficacy of existing responses to profound changes in signal switching. There are also suggestions that functional selectivity may give rise to novel pharmacological targets with distinct physiological implications.

A caveat for many of these observations from whole population measures is they do not define the molecular composition of discrete receptor complexes. This makes it difficult to attribute functional responses directly to heterodimeric populations. Altered pharmacology may therefore be due to intracellular signalling crosstalk as opposed to the defined physical interactions of receptors (see D1-D2 controversy described above). This has been proposed to explain the GABA<sub>B</sub> receptor G<sub>αi</sub> potentiation of mGluR G<sub>αq</sub> signalling, whereby alteration in signalling is actually due to a temporal integration of signalling at PLC rather than receptor association (Rives et al., 2009). Additionally overexpression of histamine or β<sub>2</sub>AR receptors in CHO K1 cells attenuated the signalling of other G<sub>s</sub> coupled receptors without physical interactions occurring. Effects were ascribed instead to receptors sequestering the pool of G protein away from other receptors present and leading to changes in specificity (Prezeau et al., 2010).

## 6.2 Aims of this chapter

Extensive evidence has therefore suggested that coexpression of two distinct receptor subtypes can result in altered pharmacology. However it is often difficult to identify responses directly attributable to heterodimerisation as opposed to a consequence of signalling crosstalk arising from the co-expressed, but physically independent receptors. Here HEK293T cells coexpressing the NPY Y1 receptor with the related subtypes Y5 (Y1/Y5) or Y4 (Y1/Y4) or the unrelated receptor  $\beta$ 2-adrenoceptor (Y1/ $\beta$ 2AR), were used to investigate potential novel pharmacology attributable to receptor heterodimerisation. As highlighted in chapter 4, BiFC was used to irreversibly constrain these receptor pairings as dimers of precise composition allowing a readout of pharmacology for a molecular heterodimer. The combined use of SNAPsurface 647 labelling of the Y1 receptor protomer only, allowed BiFC heterodimer responses to be simultaneously compared to responses of the total Y1 receptor population in the same cells. Quantification of the agonist induced internalisation of both the Snap labelled Y1 and BiFC dimer populations were used as a readout of function.

As both protomers of the heterodimer have discrete orthosteric ligand binding sites, the use of subtype selective ligands facilitated the targeted activation of either protomer within the dimer. This allowed potential allosteric interactions between the two heterodimer orthosteric binding sites in response to agonist or antagonist stimulation to be investigated. Additionally, standard competition radioligand binding and inhibition of cAMP accumulation assays were used to investigate potential changes in subtype selective ligand binding affinities or downstream signalling for the co-expressed receptors at the level of cell populations. Overall these experiments demonstrated that the Snap Y1/Y5 heterodimer, implicated in the regulation of feeding responses but not other pairings investigated, is associated with modified agonist and antagonist pharmacology.

## 6.3 Results

### 6.3.1 Cell surface expression and ligand binding of co-expressed BiFC fragment tagged Y1 receptor-containing heterodimers.

HEK293T cells stably expressing clonal Snap Y1-Yn receptor (protomer A, see Chapter 5, Figure 5.1) were stably cotransfected with a second FLAG tagged Y5 or Y4 receptor subtype, or the less closely related class A  $\beta$ 2AR or dopamine D2 receptor (long variant), each fused at the C terminus to the complementary Yc BiFC fragment (Receptor-Yc; protomer B). This generated Y1/Y5, Y1/Y4, Y1/ $\beta$ 2AR or Y1/D2 cell lines.

Prelabelling with SNAPsurface 647 (0.2 $\mu$ M) allowed the Snap Y1-Yn receptor population to be identified, representing the total receptor population. BiFC fragment tags allowed the simultaneous identification of discrete populations of Snap Y1/Y5, Y1/Y4, Y1/ $\beta$ 2AR or Y1/D2 receptor heterodimers in the same cells, via imaging of recomplemented YFP fluorescence as previously described in Chapter 5. Automated confocal imaging initially confirmed the expression and localisation of these BiFC heterodimers. Under control conditions both the Snap labelled Y1 receptor population and the BiFC dimer populations of Y1/Y5 (Figure 6.1, A) Y1/Y4 (B) and Y1/ $\beta$ 2AR (C) receptor cell lines, were predominantly localised to the plasma membrane, with areas of colocalisation observed. A small degree of constitutive internalisation was also observed. Treatment with the Y1 receptor selective agonist NPY (100nM; 30min at 37°C) showed that both the Snap Y1 receptor population and three BiFC heterodimer pairings (Y1/Y5, Y1/Y4 and Y1/ $\beta$ 2AR) were capable of rapidly internalising in response to agonist stimulation, with extensive regions of colocalisation observed. However Snap Y1/D2 BiFC dimer expression did not share this distribution, with predominant intracellular BiFC fluorescence observed for both control and NPY stimulated conditions (D), despite continued plasma membrane labelling of Snap-tagged Y1-Yn receptors. This suggested that these Y1/D2 dimers were not correctly trafficked to the cell surface and had been retained within the cell post synthesis. Following this

observation, the Y1/D2 BiFC dimer pairing was not investigated further. Standard confocal microscopy of Snap Y1/Y5 and Snap Y1/Y4 BiFC dimers also revealed similar receptor distribution and NPY stimulated internalisation (Figure 6.2, A and B).

The functional properties of HEK293T cell lines expressing Snap Y1/Y5, Y1/Y4 and Y1/ $\beta$ 2AR BiFC heterodimers, were further validated with competition binding experiments using the radiolabelled agonist [ $^{125}$ I] PYY, capable of binding Y1, Y4 or Y5 receptors with high affinity (Lundell et al., 1995, Gerald et al., 1996). Membranes were freshly prepared from these cell lines as described in Chapter 2, section 2.2.4. Snap Y1/Y5 (Figure 5.2, A), Y1/Y4 (B) and Y1/ $\beta$ 2AR (C) cell lines all showed specific [ $^{125}$ I] PYY binding which was inhibited by co-incubation with the unlabelled agonist PYY (Figure 6.3). Observed affinities of PYY were comparable across all three cell lines (estimated pIC<sub>50</sub> values in Table 6.1, A-C) and to those observed for Snap Y1-Yn receptors expressed alone or when coexpressed with Y1-Yc cDNA (Y1/Y1 BiFC dimer; see chapter 5, Table 5.1). For the Snap Y1/Y5 cell line, co-incubation with the Y5 selective agonist cPP (1-17)(Ala<sup>31</sup>, Aib<sup>32</sup>) NPY (18-36) (referred to in all legends as cPP-Aib-NPY), resulted in marginal displacement of [ $^{125}$ I] PYY specific binding (defined by 1  $\mu$ M PYY; Table 6.1, A), even at competing ligand concentrations in excess of 300nM (Figure 6.4, A). This was surprising as [ $^{125}$ I] PYY has high affinity for both the Y1 and Y5 receptor binding sites. Y5 receptor antagonist CGP71683 also showed minor inhibition of specific [ $^{125}$ I] PYY binding. However the Y1 selective antagonist BIBO3304 was able to almost fully inhibit specific [ $^{125}$ I] PYY binding at the Snap Y1/Y5 cell line (Figure 6.4, B; Table 6.1, A). This indicated that Y1 receptor binding was the predominant receptor component labelled in Y1/Y5 cell lines (but not Y1/Y4 membranes, see Figure 6.11). Additionally [ $^{125}$ I] PYY binding was sensitive to GTP $\gamma$ S treatment in both Y1/Y5 and Y1/Y4 cell lines, indicating functional coupling of expressed receptors to G<sub>i</sub>.

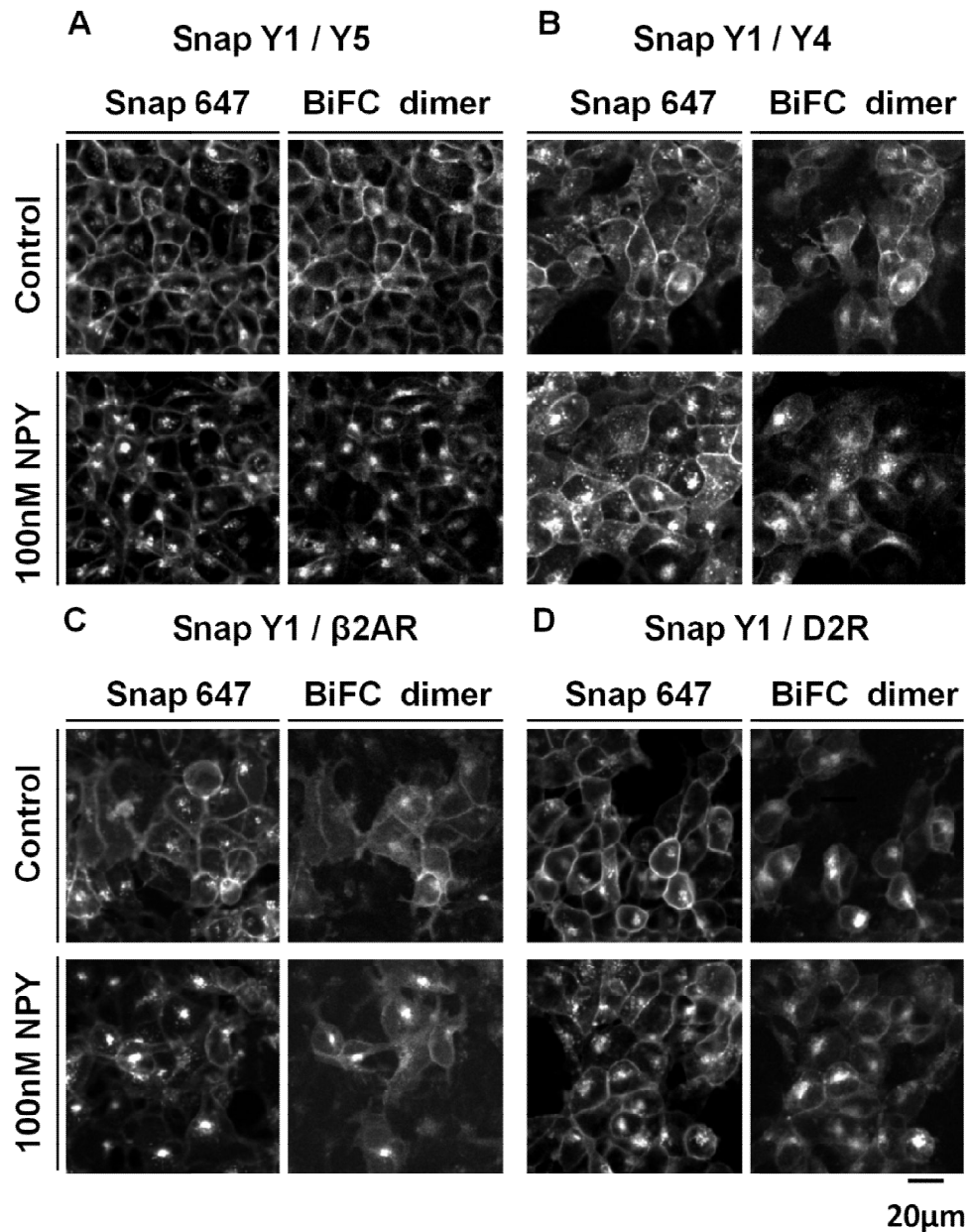


**Figure 6.1: Representative images taken using an IX Ultra confocal platereader of BiFC heterodimers consisting of Snap Y1-Yn receptor constructs coexpressed with FLAG tagged receptor-Yc constructs**

HEK293T cells stably expressing clonal Snap Y1-Yn receptor constructs were coexpressed with FLAG tagged Y5-Yc (A), Y4-Yc (B),  $\beta$ 2AR-Yc (C) or D2L-Yc (D) receptor constructs. The Snap Y1-Yn receptor population was identified by prelabelling with SNAPsurface 647 (0.2 $\mu$ M; 30min at 37°C/5% CO<sub>2</sub>; Snap 647 panel). Simultaneous imaging of recomplemented YFP fluorescence was indicative of the formation of Snap Y1-Yn/receptor-Yc complexes constrained as heterodimers using BiFC (BiFC dimer panel). Cells were stimulated with vehicle control or 100nM NPY (30min at 37°C) prior to fixation, H33342 nuclei staining and imaging using an IX Ultra confocal platereader. Representative images (cropped as a 300x300 pixel region) are taken from at least 3 independent experiments.

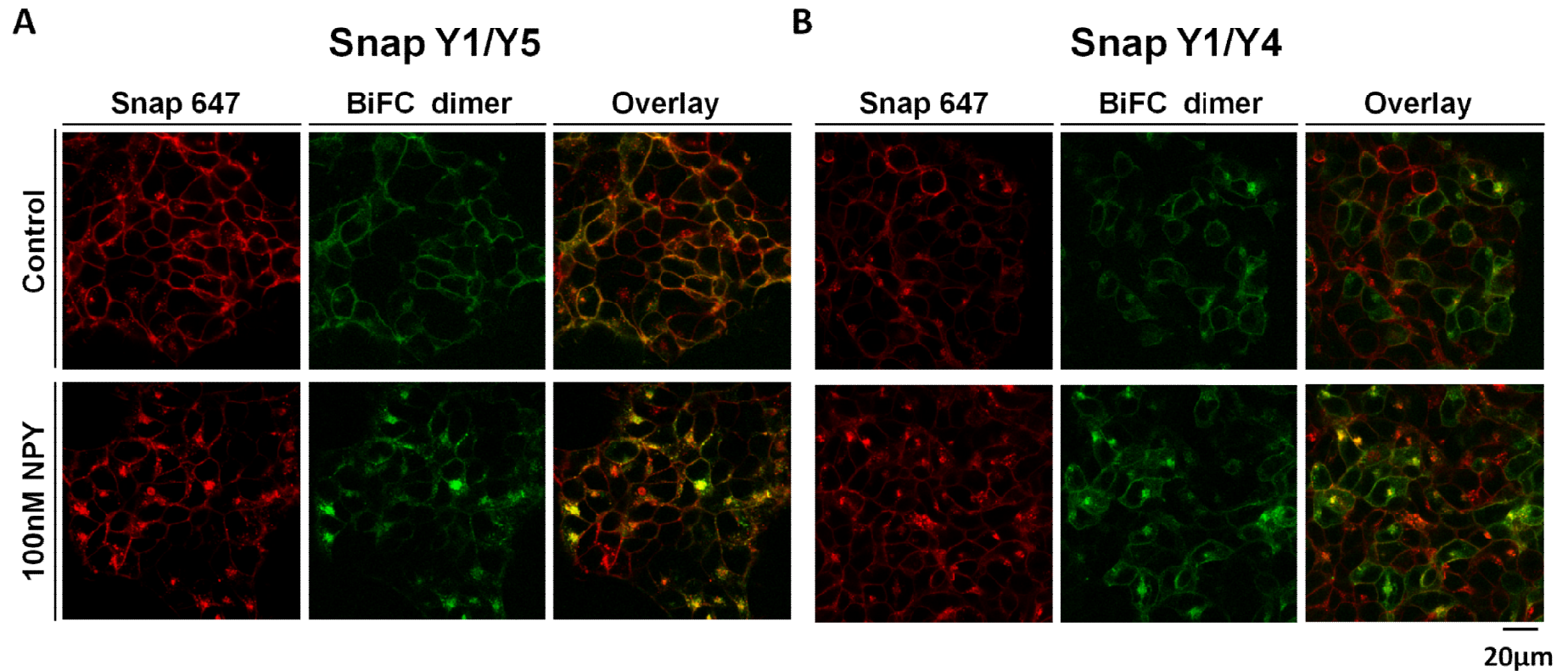


**Figure 6.2: Representative images taken using a LSM510 confocal microscope of Snap Y1/Y5 BiFC dimers stably expressed in HEK293T cells**  
 HEK293T cells stably expressing Snap Y1/Y5 (A) or Snap Y1/Y4 (B), were prelabelled with SNAPsurface 647 (0.2 µM). Representative images (of 3 independent experiments) taken using a LSM510 confocal microscope showed that under control conditions all receptor populations were predominantly localised to the plasma membrane. Stimulation with 100nM NPY (30min at 37°C) resulted in rapid internalisation of all receptor populations. Areas of colocalisation are shown in yellow (overlay panel).

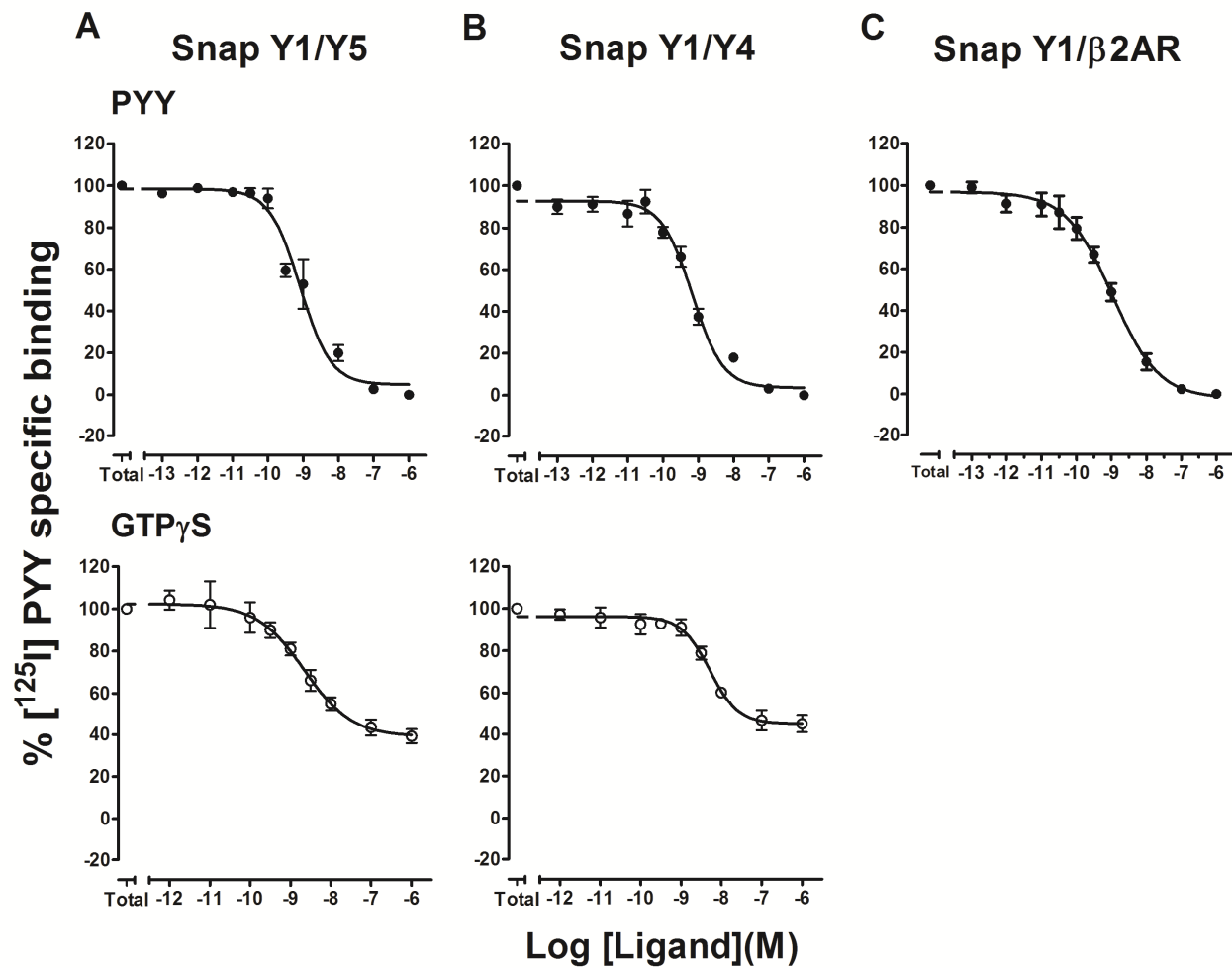


**Figure 6.3: [ $^{125}$ I] PYY competition binding experiments in HEK293T cell lines stably co-expressing BiFC heterodimer constructs.**

Membranes were freshly prepared from HEK293T cell lines stably expressing Snap Y1/Y5 (A), Y1/Y4 (B) or Y1/ $\beta$ 2AR (C) BiFC dimer constructs (see Chapter 2, section 2.2.4). These were incubated with [ $^{125}$ I] PYY (15pM) and increasing concentrations of unlabelled competing agonist PYY or GTP $\gamma$ S for 90min at 22°C. Membrane bound radioligand was separated using filtration and quantified using a gamma counter. Competition displacement curves were generated using GraphPad Prism, with pooled data representing a minimum of 3 independent experiments. pIC<sub>50</sub> and other data were expressed as mean  $\pm$  s.e.m (Table 6.1, A-C; Hill slope range 0.74-0.96).

**Table 6.1A: Summary of ligand binding affinities for HEK293T cells coexpressing Snap Y1-Yn/Y5-Yc**

	PYY	cPP Aib NPY*	BIBO3304	CGP71683	GTP $\gamma$ S
pIC <sub>50</sub>	9.1 ± 0.1	/	8.3 ± 0.1	/	8.7 ± 0.1
%inhibition of TSB	100	11.5 ± 1.1	92.3 ± 0.4	24.0 ± 6.2	60.7 ± 3.3

**Table 6.1B: Summary of ligand binding affinities for HEK293T cells coexpressing Snap Y1-Yn/Y4-Yc**

	PYY	BIBO3304	PP	GTP $\gamma$ S
pIC <sub>50</sub>	9.2 ± 0.1	8.4 ± 0.1	9.6 ± 0.4 (High affinity site); fraction = 41.8% ± 0.2 7.8 ± .0.4 (low affinity site); fraction = 58.2% ± 1.2	8.3 ± 0.1
% inhibition of TSB	100	59.5 ± 2.2	80.8 ± 2.2	45.0 ± 4.1

**Table 6.1C: Summary of ligand binding affinities for HEK293T cells coexpressing Snap Y1-Yn/ $\beta$ 2AR-Yc**

	PYY	BIBO3304	Propranolol	Isoprenaline
pIC <sub>50</sub>	9.2 ± 0.1	8.4 ± 0.1	/	/
% inhibition of TSB	100	97.6 ± 0.5	13.6 ± 12.7	3.7 ± 8.7

% inhibition of TSB refers to the displacement by 1 $\mu$ M competing ligand, as a % of the total specific binding (TSB) defined in the absence / presence of 1  $\mu$ M PYY.

/ = responses unable to determined

n = 2-4

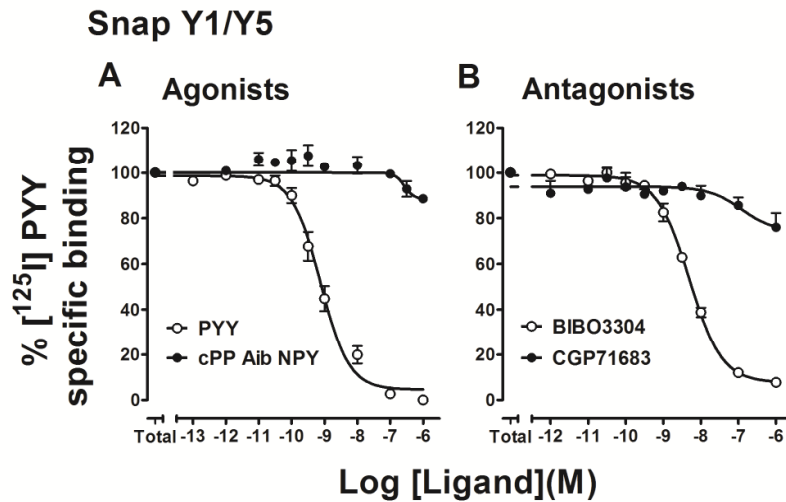


**Figure 6.4: [<sup>125</sup>I] PYY binding experiments in membranes isolated from HEK293T cell lines expressing Snap Y1/Y5 BiFC dimers, and Y1 or Y5 selective competing ligands**  
 Membranes were freshly prepared from HEK293T cell lines stably coexpressing Snap Y1-Yn and Y5-Yc BiFC dimer constructs. These were incubated with [<sup>125</sup>I] PYY (15pM) and increasing concentrations of unlabelled PYY, or Y1 (BIBO3304) or Y5 selective ligands (cPP Aib NPY, CGP71683) for 90min at 22°C. Membrane bound radioligand was separated using filtration and quantified using a gamma counter. Competition displacement curves were generated using GraphPad Prism, with pooled data representing a minimum of 3 independent experiments. pIC<sub>50</sub> data were expressed as mean ± s.e.m (Table 6.1, A; Hill slope range 0.78-0.92). PYY curve replicated from Figure 6.3.

### 6.3.2 Y1 and Y5 receptors BiFC heterodimers show altered pharmacology in respect to Y5 agonist-stimulated internalisation

Using the automated platereader analysis, the kinetics of Snap Y1/Y5 BiFC dimer internalisation in response to NPY were first investigated in timecourse experiments (100nM; 37°C, Figure 6.5). No significant difference was observed in respect to the rate of NPY induced internalisation between the Snap Y1-Yn receptor and Snap Y1/Y5 BiFC dimer populations ( $t_{1/2}$  values of  $4.7 \pm 1.0$  min and  $8.2 \pm 1.8$  min respectively  $n=3$ ; unpaired t test  $P = 0.46$ ). Therefore although 60 min agonist incubations were required for the Y5-GFP cell line (Chapter 3, Figure ), a 30min timecourse was used for Snap Y1/Y5 cells to maintain consistency with other BiFC dimer cell lines.

Whole population studies, such as competition binding, did not identify pharmacology specifically attributable to the Y1/Y5 BiFC dimer population (Figure 6.2). Therefore in order to tease out any effects on agonist pharmacology attributable to heterodimerisation, simultaneous quantification of the internalisation of both Snap labelled Y1 receptor and BiFC Y1/Y5 dimer populations in Snap Y1/Y5 cells was performed, and compared to either receptor expressed alone (Snap Y1-Yn or Y5-GFP, described earlier in chapters 5 and 3 respectively). Pooled concentration response curves normalised to  $1\mu\text{M}$  NPY responses, showed that NPY was a full agonist at both the Snap Y1-Yn receptor and Y1/Y5 BiFC dimer populations, with comparable agonist potencies observed (Figure 6.6, Table 6.2,  $n=14$ ). NPY was also a potent stimulator of Y5-GFP receptor internalisation (Figure 6.6, B).

To investigate this further, agonists showing selectivity for the Y5 receptor subtype over the Y1 subtype were used, namely the endogenous NPY related peptide pancreatic polypeptide (PP) and the Y5 selective agonist cPP (1-17)(Ala<sup>31</sup>, Aib<sup>32</sup>) NPY (18-36). As described in chapter 3, both agonists were potent at inducing the internalisation of Y5-GFP when compared to NPY (see Table 3.2,  $n = 4$ ). However, given that previous data has indicated that agonist occupancy of a single protomer binding site is sufficient for internalisation of the BiFC dimer (Chapter 4), the most striking observation was that both PP

and cPP (1-17)(Ala<sup>31</sup>, Aib<sup>32</sup>) NPY (18-36) agonist responses were significantly altered, relative to NPY in inducing Snap Y1/Y5 BiFC dimer endocytosis. These ligands in addition to a third Y5 selective ligand [D-Trp<sup>32</sup>]NPY were all partial agonists compared to NPY, rather than full agonists, in stimulating Snap Y1/Y5 dimer internalisation (Figure 6.6; Table 6.2). Furthermore these agonists were significantly less potent for example the EC<sub>50</sub> for cPP (1-17)(Ala<sup>31</sup>, Aib<sup>32</sup>) NPY (18-36) was over 300 fold lower in stimulating Snap Y1/Y5 BiFC dimer responses than for Y5-GFP (Table 6.2;  $P < 0.001$ , Student's t test).

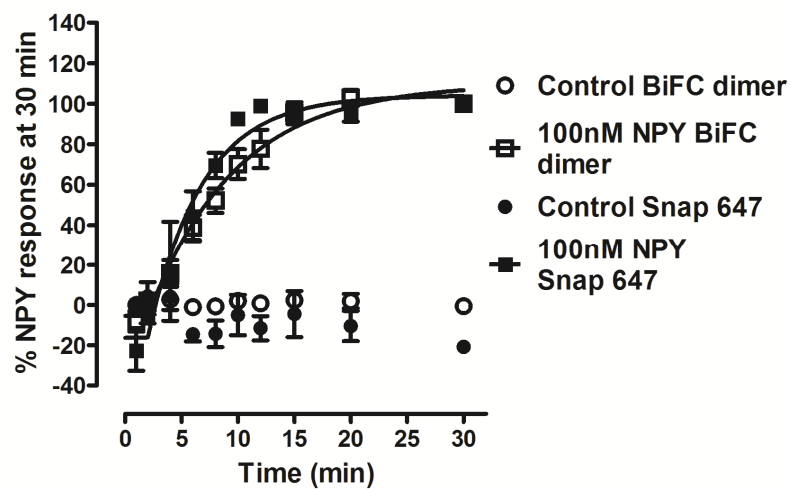


**Figure 6.5: Kinetics of NPY induced internalisation of Snap Y1/Y5 BiFC heterodimers**

Stably transfected HEK293T cells coexpressing Snap Y1/Y5, were prelabelled with SNAPsurface 647 (0.2 $\mu$ M). Cells were then stimulated with vehicle (circles) or 100nM NPY (squares) at set time intervals. H33342 labelling, image acquisition and granularity analysis were performed as previously described to compare internalisation of the Snap-Y1-Yn population (Snap 647) and Y1/Y5 BiFC dimer Pooled data (mean  $\pm$  s.e.m; n = 4) were normalised to NPY responses observed at 30 min and fitted to a 1 site exponential association including a 2 min latency period.

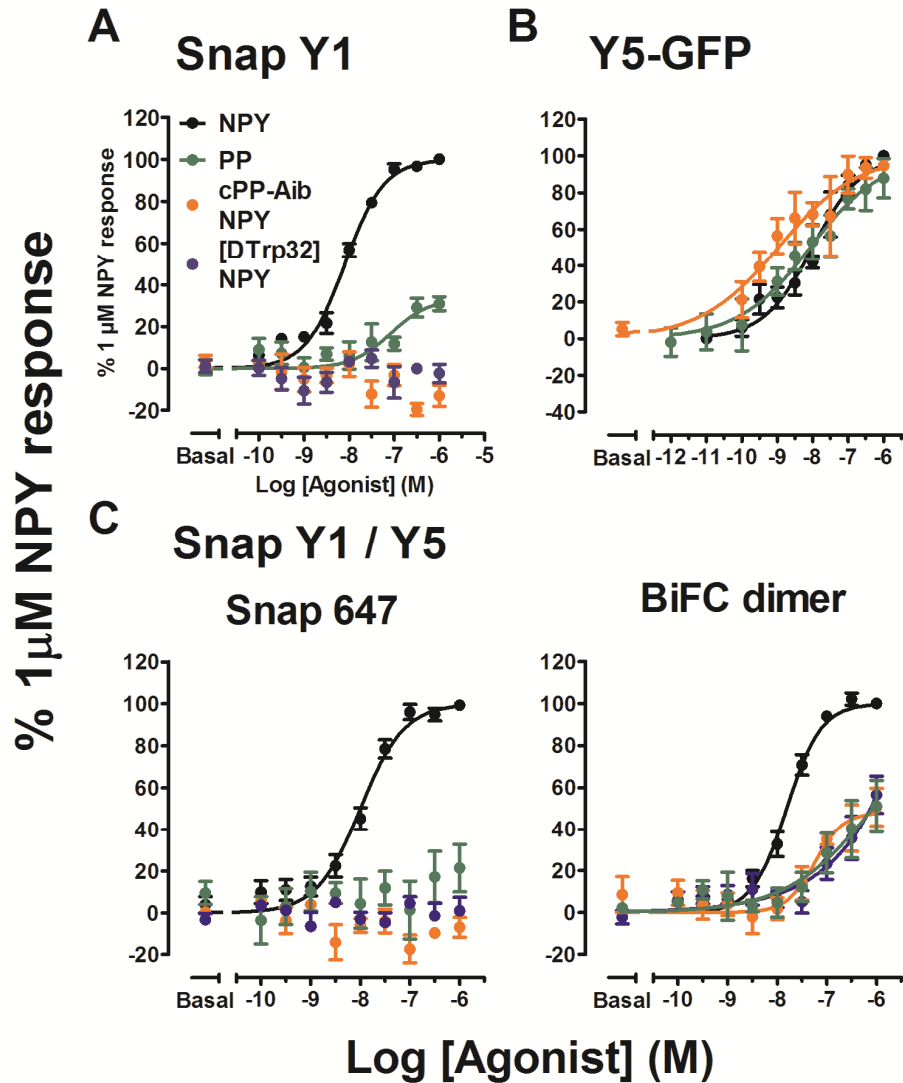


**Figure 6.6: Quantification of the agonist induced internalisation of Y1 or Y5 receptors when expressed alone or constrained as heterodimers using BiFC**

HEK293T cells stably expressing Snap Y1-Yn receptors alone (A), Y5-GFP or Snap Y1/Y5 BiFC dimers (C) were prelabelled with SNAPsurface 647 (0.2 $\mu$ M), before stimulation with a panel of ligands (30min at 37°C). H33342 labelling, image acquisition and granularity analysis of images was performed as previously. All responses were normalised to negative (basal) and positive (1 $\mu$ M NPY) plate controls. Pooled data shown represented a minimum of 3 independent experiments and are expressed as mean  $\pm$  s.e.m. The Y5-GFP data (60min agonist incubation) are repeated from Figure 3.9 for clarity and comparison.

**Table 6.2: Summary of potencies and efficacies of a panel of ligands for stimulating the internalisation of Snap Y1/Y5**

Agonist	Snap Y1 / Y5				Y5-GFP	
	Snap Y1		Y1/Y5 BiFC dimer		pEC <sub>50</sub>	% NPY response
	pEC <sub>50</sub>	% NPY response	pEC <sub>50</sub>	m % NPY response		
NPY	8.0 ± 0.1	100	7.8 ± 0.1	100	8.0 ± 0.1	100
PP		21.4 ± 11.4	/	44.5 ± 11.6	8.1 ± 0.2	87.8 ± 10.7
cPP Aib NPY	/	/	7.2 ± 0.2 <sup>+</sup>	50.6 ± 9.1	9.0 ± 0.1	94.6 ± 1.1
DTrp 32 NPY	/	/	6.4 ± 0.3	56.5 ± 9.0	/	/

+ = potency of cPP Aib NPY pEC<sub>50</sub> value at Snap Y1/Y5 BiFC was significantly different to that for Y5-GFP (p<0.001 \*\*\*).

All data were expressed as ± standard error of the mean. pEC<sub>50</sub> values were obtained from pooled concentration response curves presented in Figure 6.6.

Rmax responses to each ligand were calculated as a percentage of 1µM NPY responses

n= 4-15

/ not able to be determined

### 6.3.3 NPY-induced internalisation of the constrained Y1/Y5 BiFC dimer population is not inhibited by the Y1 receptor selective antagonist BIBO3304

The pharmacology of subtype selective antagonists was next investigated for the Snap Y1/Y5 cell line, initially using [<sup>3</sup>H]cAMP accumulation assays. Stimulation with NPY inhibited forskolin-stimulated accumulation in a concentration dependent manner (Figure 6.7, A) comparable to that observed for Snap Y1 or Snap Y1/Y1 cell lines (Chapter 5, Figure 5.3). Surmountable antagonism of NPY responses was observed in response to pretreatment with the BIBO3304 (estimated pK<sub>b</sub> value 7.6 ± 0.4, from shifts in the presence of 30nM antagonist; n=3). The estimated pK<sub>b</sub> obtained from this was also consistent with previous observations for Snap Y1-Yn receptors expressed alone and when coexpressed with Y1-Yc. Preincubation with CGP71683 had no effect on NPY responses in this assay (B). Therefore in whole population second messenger assays, the Snap Y1-Yn/Y5-Yc cell line showed 'Y1 receptor like' pharmacology in respect to both BIBO3304 and CGP71683.

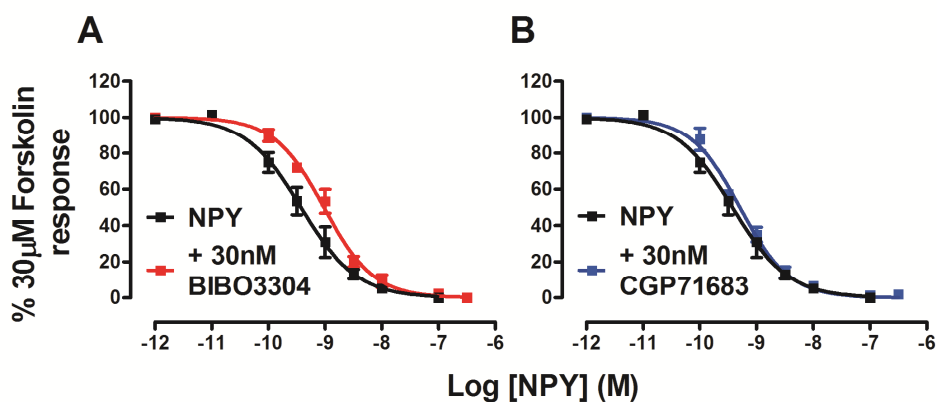


**Figure 6.7: The effect of pretreatment with receptor subtype selective antagonists, on NPY inhibition of forskolin-stimulated [<sup>3</sup>H] cAMP accumulation in the Snap Y1/Y5 cell line.**

HEK293T cells stably coexpressing Snap Y1-Yn/Y5-Yc, were loaded with [<sup>3</sup>H] adenine (2hr; 37°C/5% CO<sub>2</sub>). Cells were then pretreated with vehicle or the Y1 selective antagonist BIBO3304 (A) or the Y5 selective antagonist CGP71683 (B) (30min at 37°C/5 % CO<sub>2</sub>) prior to NPY and 30 µM forskolin costimulation. All responses were normalised to those obtained for forskolin (100%) and 100nM NPY (0%) stimulations and are shown as mean ± s.e.m of 3 independent experiments.

Simultaneous measurement of the internalisation of both Snap Y1 and Snap Y1/Y5 BiFC dimer populations following BIBO3304 pretreatment was then used to investigate potential allosteric modulation of Y1 antagonist pharmacology by Y1 and Y5 receptor association. Following pre-treatment with BIBO3304 (30nM or 300nM; 30min at 37°C) cells were stimulated with NPY (30min at 37°C). Pooled concentration response curves normalised to 1µM NPY responses showed that BIBO3304 produced rightward parallel shifts of NPY induced responses for the Snap-Y1-Yn population indicative of surmountable antagonism (Figure 6.8, Snap 647), and expected based on the known affinity of BIBO3304 for the Y1 receptor subtype (Wieland et al., 1998). Estimated  $pK_b$  values (30nM BIBO3304  $8.2 \pm 0.1$ ,  $n=5$ ; 300nM BIBO3304  $7.8 \pm 0.3$ ,  $n=4$ ) were similar to those observed for Snap Y1-Yn receptors expressed alone, Snap Y1/Y1 homodimers (Chapter 5, Figure 5.9) and Y1-GFP (Chapter 3, section 3.10). However BIBO3304 did not inhibit NPY induced internalisation of the Snap Y1/Y5 BiFC dimer population (Figure 6.8, BiFC dimer) even using concentrations 100x greater (300nM) than the documented  $pK_b$  of BIBO3304 at the Y1 receptor. Notably in the presence of BIBO3304, NPY potency and maximum responses remained largely unchanged (NPY  $pEC_{50}$  values  $7.3 \pm 0.1$ ,  $n=4-5$ ). Given that in the presence of excess BIBO3304, NPY responses might be expected to be driven exclusively via the Y5 binding site, this also contrasts with the markedly reduced potency and partial agonism of Y5 selective agonists previously observed at the Snap Y1/Y5 BiFC dimer.

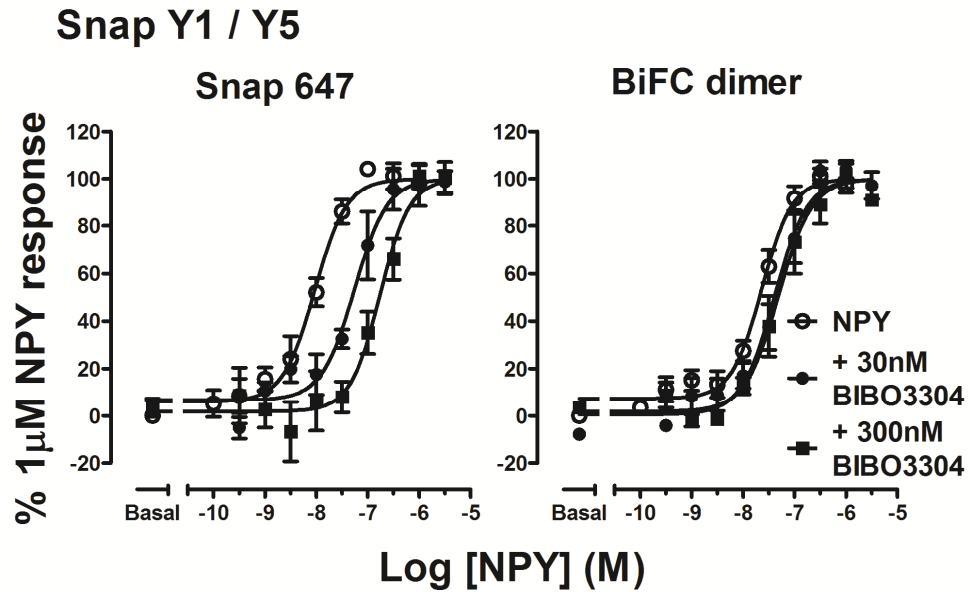


**Figure 6.8: The effect of pretreatment with the Y1 selective antagonist BIBO3304 on the agonist induced internalisation of Snap Y1/Y5 BiFC heterodimers**

HEK293T cells stably expressing Snap Y1/Y5 BiFC dimers were pre labelled with SNAPsurface 647 (0.2 $\mu$ M). Cells were then pretreated with BIBO3304 (30 or 300nM; 30min at 37°C), followed by stimulation with NPY (30min at 37°C). H33342 labelling, image acquisition and quantification of receptor internalisation was performed as previously described. NPY concentration response curves in the presence and absence of BIBO3304 were fitted using GraphPad Prism with shared minimum (basal responses), maximum (1 $\mu$ M NPY responses) and Hill slope (1.0) constraints. All data were pooled from a minimum of 3 independent experiments, and expressed as mean  $\pm$  s.e.m.

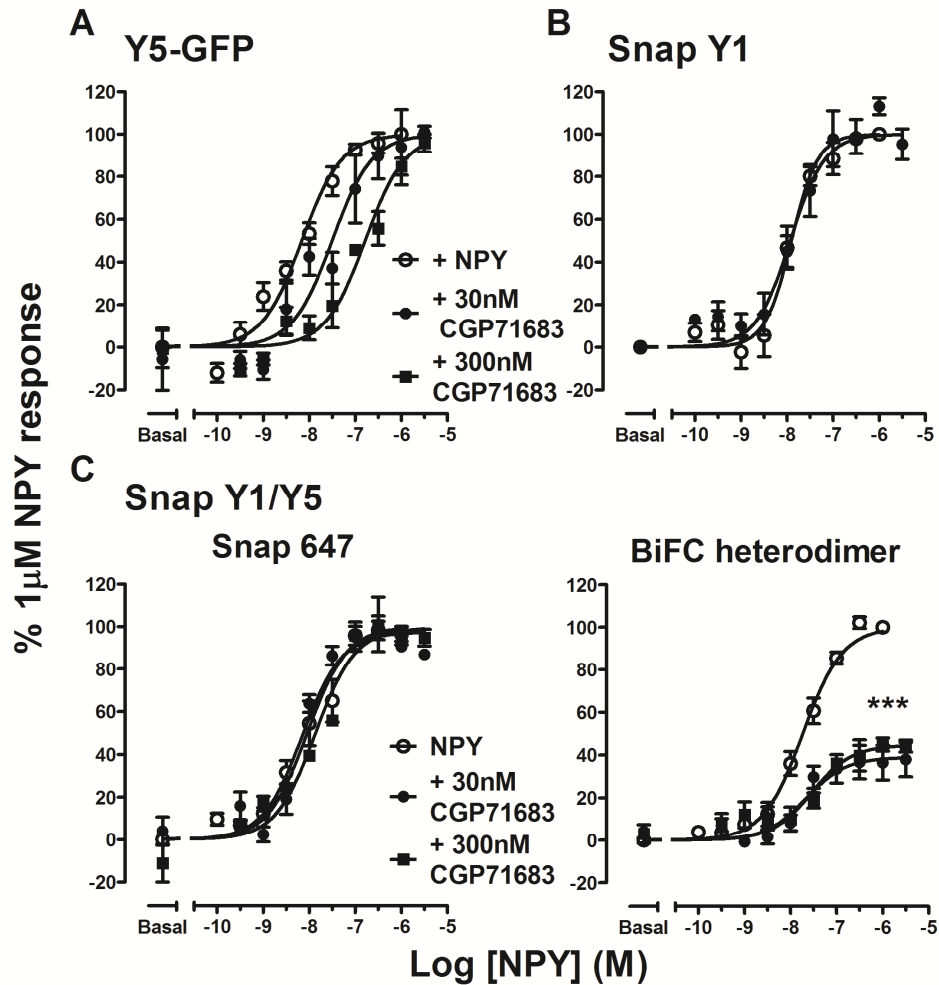


**Figure 6.9: The effect of pretreatment with the Y5 selective antagonist CGP71683 on NPY induced internalisation of Snap Y1/Y5 BiFC heterodimers**

HEK293TR cells stably expressing Y5-GFP (A), and HEK293T cells stably expressing Snap Y1 (B) or Snap Y1/Y5 BiFC dimers (C), were pretreated with the Y5 receptor selective antagonist CGP71683 (30 or 300nM; 30min at 37°C). Cells were then stimulated with NPY (30min at 37°C). H33342 labelling, image acquisition and quantification of receptor internalisation was performed as previously described. NPY concentration response curves in the presence and absence of CGP71683 were fitted using GraphPad Prism with shared minimum (basal responses) and maximum (1µM NPY responses) constraints with Hill slopes set to 1. All data were pooled from a minimum of 3 independent experiments, and expressed as mean  $\pm$  s.e.m. \*\*\* ( $P < 0.001$ , 1 way ANOVA responses compared to 1 µM NPY).

### **6.3.4 Y5 receptor selective antagonists produce insurmountable inhibition of Snap Y1/Y5 BiFC dimer internalisation, contrasting with the expected competitive pharmacology observed for Y5 receptors expressed alone**

The specific pharmacology of Snap Y1/Y5 BiFC heterodimers was next investigated in respect to the Y5 selective non peptide antagonist CGP71683. As previously indicated in population studies using [<sup>125</sup>I]PYY binding and cAMP assays, this antagonist had limited effects in Snap Y1/Y5 cells, presumably reflecting the predominant expression overall of Snap-Y1-Yn compared to Y5-Yc receptors. Thus, in order to probe potential dimer specific pharmacology that may be masked in whole population studies for CGP71683, quantification of the NPY induced internalisation of both the Snap Y1 receptor and Y1/Y5 BiFC dimer populations following pretreatment was next assessed.. For comparison, CGP71683 (30nM or 300nM) showed surmountable competitive antagonism of NPY stimulated Y5-GFP internalisation (Figure 5.9; estimated pK<sub>b</sub> 7.8-8.2 ± 0.1; n=4; also see Chapter 3, Figure 3.10).

At these concentrations, CGP71683 had no significant effect on NPY induced endocytosis of Snap Y1 receptors expressed alone (B) or when coexpressed with Y5-Yc (Snap 647, C) as expected based upon the selectivity of CGP71683 for the Y5 receptor subtype over the Y1 receptor (Criscione et al., 1998). However for the Y1/Y5 BiFC dimer receptor population, the nature of CGP71683 antagonism had changed to non-surmountable inhibition with significantly reduced maximal NPY responses (1 µM in the presence of 30nM CGP71683 37.9 ± 8.0%; \*\*\* *P* < 0.001 1 way ANOVA compared to 1 µM NPY control; n=4) but potencies remained comparable with control curves (NPY pEC<sub>50</sub> 7.7-8.1; n=4-7). Similar results were observed when the concentration of CGP71683 was increased to 300nM (NPY Rmax of 44.1 ± 2.8 %; pEC<sub>50</sub> 7.6-7.9; n=4). Thus increasing the concentration of CGP71683 pre-treatment from 30 to 300 nM did not further reduce maximal NPY responses at the Y1/Y5 BiFC dimer, showing that this insurmountable antagonism was saturable. In order to ensure that this alteration in the nature of CGP71683 antagonism was not due to a steric effect of a particular class of antagonist binding, two

structurally unrelated Y5 selective antagonists, L-182,504 (Kanatani et al., 2000) and NPY5RA972 (Block et al., 2002) were also investigated. Both antagonists were unable to affect NPY induced internalisation of the Snap Y1 receptor population in Snap Y1/Y5 expressing cells. However both compounds showed insurmountable inhibition of Y1/Y5 BiFC dimer internalisation with a significant reduction in maximal NPY responses observed (Figure 6.10 A, B).

## Snap Y1 / Y5

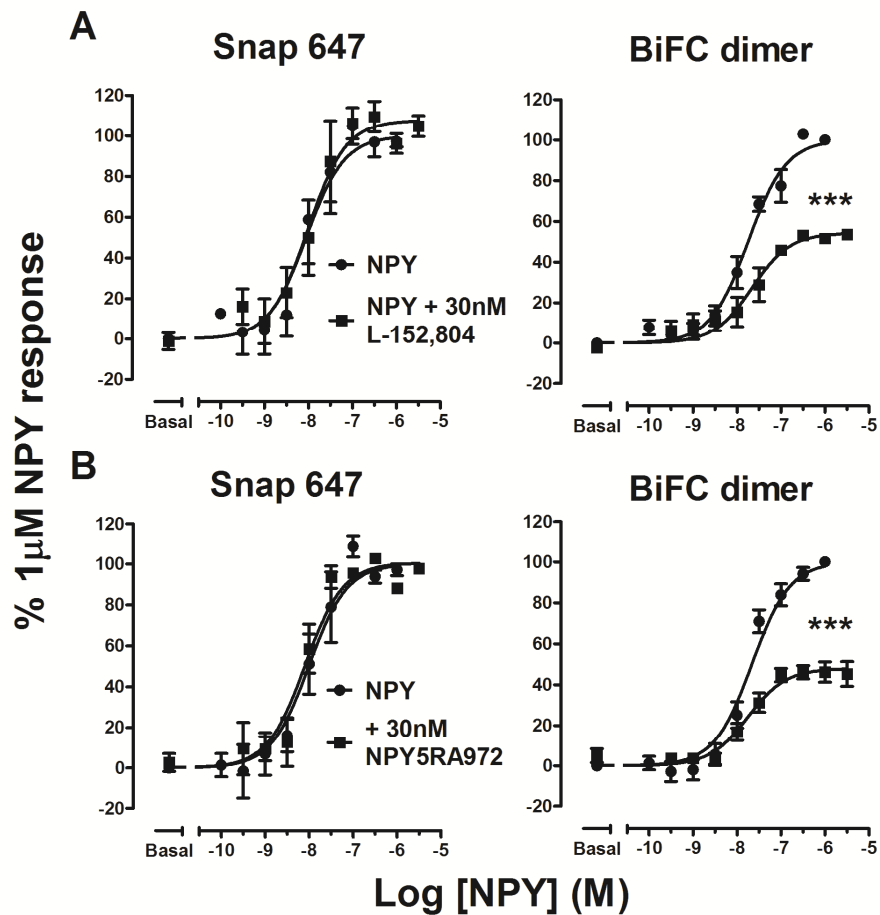


**Figure 6.10: The effect of pretreatment with structurally distinct Y5 receptor selective antagonists on NPY induced internalisation of Snap Y1/Y5 BiFC heterodimers**

HEK293T cells stably expressing Snap Y1/Y5 BiFC dimers were pre labelled with SNAPsurface 647 (0.2 $\mu$ M), followed by pretreatment with L182,504 or NPY5RA972 (30nM; 30min at 37°C). Cells were then stimulated with NPY (30min at 37°C). H33342 labelling, image acquisition and quantification of receptor internalisation was performed. NPY concentration response curves in the presence and absence of antagonist were fitted using GraphPad Prism with shared minimum (basal responses) and Hill slopes of 1. All data were pooled from a minimum of 3 independent experiments, and expressed as mean  $\pm$  s.e.m

### 6.3.5 Y1 and Y4 receptors as BiFC heterodimers exhibit agonist responses consistent with their binding sites acting independently

The unlabelled Y4 receptor selective agonist PP was able to displace specific [<sup>125</sup>I] PYY binding in a concentration dependent manner in membranes prepared from the Y1/Y4 receptor cell line (Figure 6.11, B, Table 6.1, B). However, unlike displacement seen for the Snap Y1 cell line (A), displacement at Snap Y1/Y4 preferentially fit to a 2 site model representing high (estimated pIC<sub>50</sub> 9.6 ± 0.4; 41.8% ± 0.2 fraction of fit; n=4) and low affinity (7.8 ± 0.3; 58.2% fraction) PP binding sites within the whole population. Interestingly the estimated pIC<sub>50</sub> value of the lower affinity site corresponded to the pIC<sub>50</sub> value obtained for PP competition at Snap Y1-Yn receptors expressed alone (1 site fit; 7.9 ± 0.3, n=3). BIBO3304 was able to displace only the Y1 receptor bound [<sup>125</sup>I] PYY at the Snap Y1/Y4 cell line (C). This degree of displacement (Table 6.1, B) was consistent with the fraction of low affinity binding observed for Snap Y1/Y4 in respect to PP induced displacement. This suggested that under the conditions used, specific [<sup>125</sup>I] PYY binding to Snap Y1/Y4 membranes represented relatively even labelling of the Y1 and Y4 receptor populations.

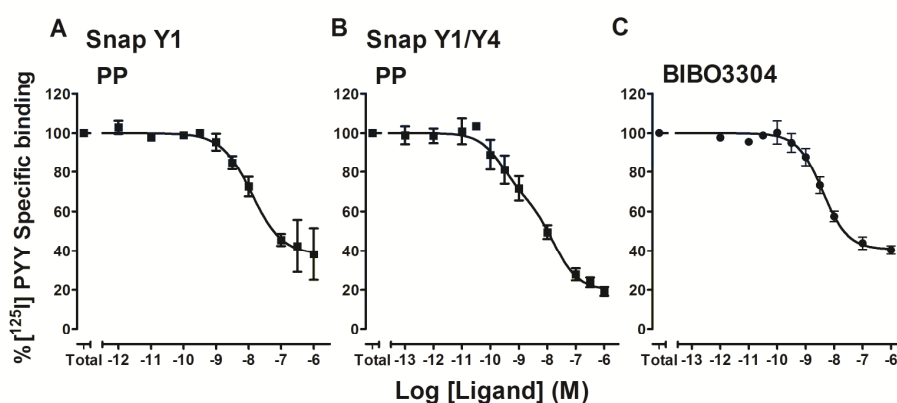


**Figure 6.11: Competition binding experiments using [<sup>125</sup>I] PYY in membranes isolated from HEK293T cells stably expressing Snap Y1-Yn alone or Snap Y1/Y4**

Membranes freshly prepared from HEK293T cell lines stably expressing Snap Y1-Yn alone (A) or Snap Y1-Yn/Y4-Yc (B and C) were incubated with [<sup>125</sup>I] PYY (15pM) and increasing concentrations of unlabelled competing PP or BIBO3304 for 90min at 22°C. Competition displacement curves were generated using GraphPad Prism, with responses in the Snap Y1/Y4 cell line for PP preferentially fitted to a 2 site binding model and Snap Y1 and Snap Y1/Y4 BIBO3304 responses fitted to a 1 site model (Hill slopes 0.92-0.97). Pooled data are presented representing a minimum of 3 independent experiments with data expressed as mean ± s.e.m.

Automated confocal imaging revealed Y1/Y4 BiFC dimers internalised in response to either NPY or PP stimulation (Figure 6.12). However the Snap Y1-Yn population within the same cells only did so in response to NPY. Quantification of internalisation of the BiFC dimer population revealed that PP responses were slightly reduced in respect to the NPY maximum (Figure 6.13, C BiFC dimer; Table 6.3). Limited PP responses, at high concentration, were observed for the Snap Y1 population measured at the same time in the Y1/Y4 cell line (Snap 647;  $21.3\% \pm 5.3$  of  $1\mu\text{M}$  NPY responses) and Y1-GFP (A). These responses were also similar to those obtained for the Snap Y1-Yn receptor populations of Y1/Y1 (Chapter 5, Table 5.2) and Y1/Y5 BiFC dimers (Figure 6.6). The potency of PP responses at the BiFC population of Y1/Y4 heterodimers was significantly reduced (Table 6.3) compared to that seen for inducible Y4-GFP receptor endocytosis, in which internalisation was observed in response to PP (Figure 6.13, B; Table 6.3) but only with high concentrations of NPY.

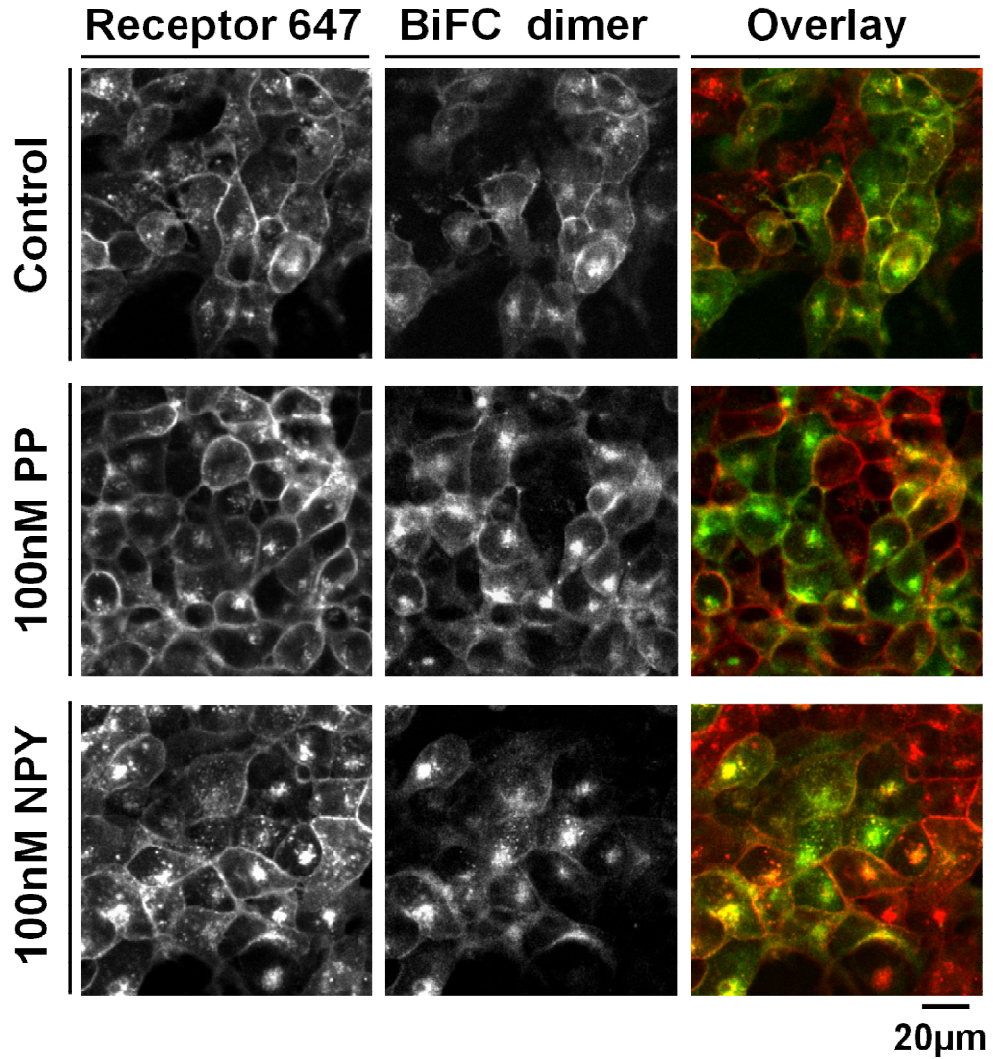


**Figure 6.12: IX Ultra confocal images of Snap Y1/Y4 BiFC dimers stably expressed in HEK293T cells**

HEK293T cells stably coexpressing Snap Y1/Y4 were prelabelled with SNAPsurface 647 (0.2μM) before stimulation with vehicle, 100nM PP or 100nM NPY (30min at 37°C). Representative images from a minimum of 4 independent experiments, were taken using an IX Ultra confocal platereader and are shown as cropped 300x300 pixel regions. Extensive areas of colocalisation between Snap Y1 receptor and BiFC dimer populations are shown in yellow (overlay panel).

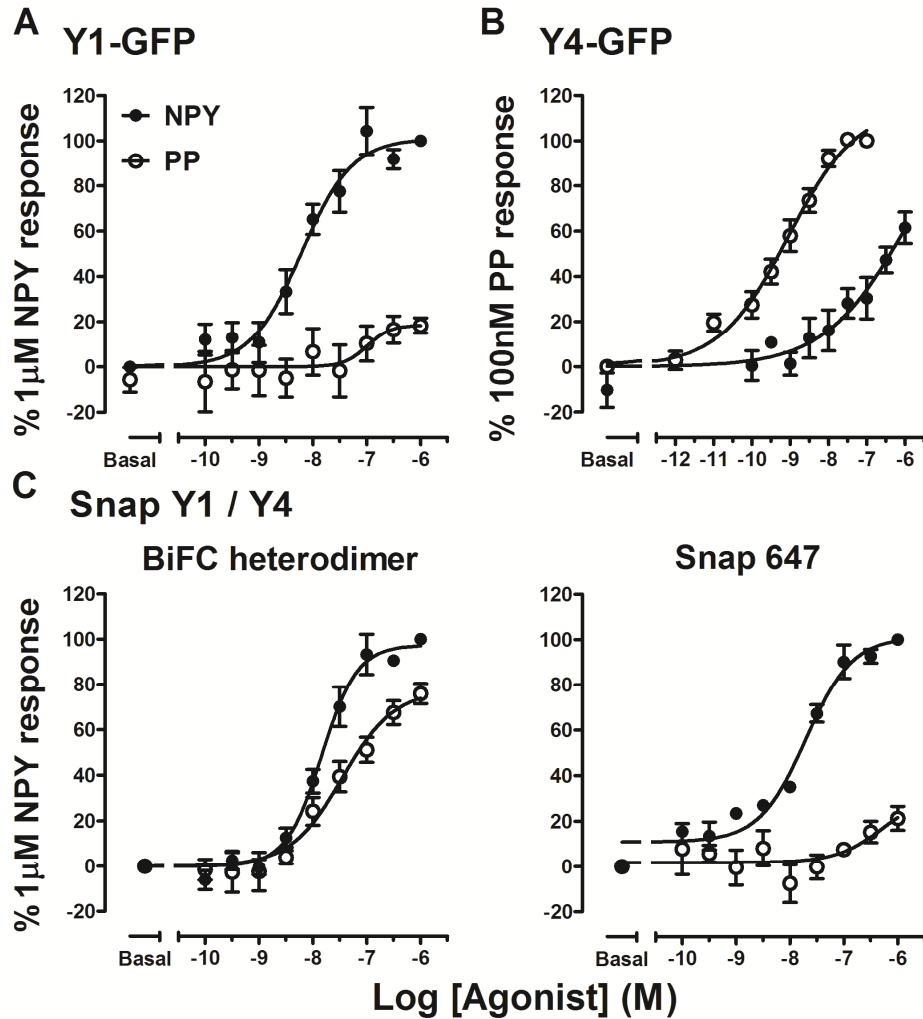


**Figure 6.13: Quantification of the agonist induced internalisation of Y1 or Y4 receptors when expressed alone or constrained as dimers using BiFC**

HEK293T cells stably expressing Snap Y1-Yn (A), Y4-GFP (B) or Snap Y1/Y4 BiFC dimers (C) were prelabelled with SNAPsurface 647 (0.2 $\mu$ M), before stimulation with NPY or PP (30 min at 37°C). H33342 labelling, image acquisition and receptor internalisation was determined following granularity analysis of images acquired using an automated confocal plate reader. All responses were normalised to negative (basal) and positive (1 $\mu$ M NPY for Snap Y1 and Snap Y1/Y4 BiFC dimers; 100nM PP for Y4-GFP) plate controls. Pooled data shown represented a minimum of 3 independent experiments and are expressed as mean  $\pm$  s.e.m. Data for Y4-GFP are repeated from Figure 3.9 for comparison.

**Table 6.3: Summary of potencies and efficacies of a panel of ligands for stimulating the internalisation of Snap Y1/Y4**

Agonist	Snap Y1 / Y4				Y4-GFP	
	Snap Y1		Y1/Y4 BiFC dimer		pEC <sub>50</sub>	% NPY response
	pEC <sub>50</sub>	% NPY response	pEC <sub>50</sub>	% NPY response		
NPY	7.7 ± 0.1	100	7.8 ± 0.1	100	/	61.4 ± 6.9
PP	/	21.3 ± 5.3	7.5 ± 0.2 <sup>+</sup>	75.9 ± 4.4	9.1 ± 0.2	100

+ = potency of PP pEC<sub>50</sub> value at Snap Y1/Y4 BiFC was significantly different to that for Y4-GFP (p<0.001 \*\*\*).

All data were expressed as ± standard error of the mean. pEC<sub>50</sub> values were obtained from pooled concentration response curves presented in Figure 6.13.

Rmax responses to each ligand were calculated as a percentage of 1µM NPY responses for Snap Y1/Y4 cell lines or 100nM PP for Y4-GFP

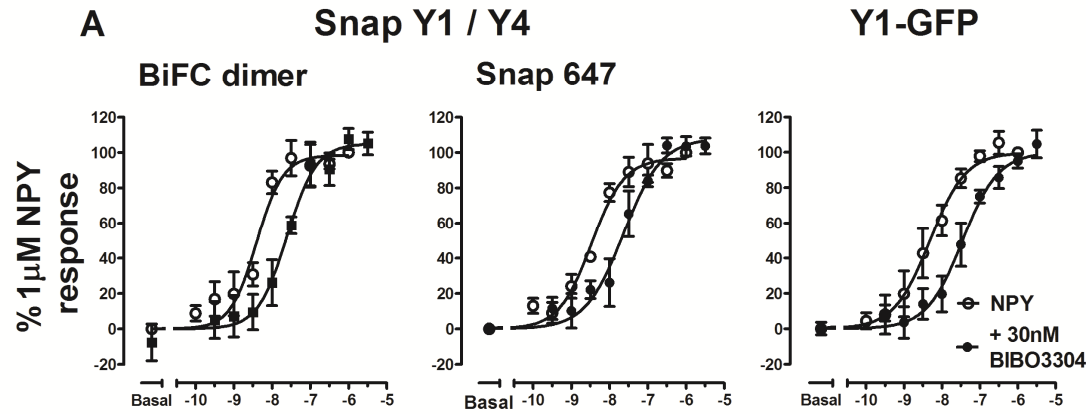
n= 4

/ not able to be determined

### **6.3.6 Constrained NPY Y1/Y4 BiFC heterodimers show Y1 selective antagonist pharmacology also consistent with the Y1 and Y4 orthosteric binding sites acting independently.**

In order to investigate whether constrained NPY receptor heterodimers exhibited novel antagonist pharmacology, Snap Y1/Y4 expressing cells were pre-treated with BIBO3304 (30nM; 30min at 37°C) followed by incubation with NPY or PP (30min at 37°C). Pooled concentration response curves quantifying receptor internalisation in Snap Y1/Y4 cells, (Figure 6.14, A), showed that antagonist treatment produced a 10 fold rightward parallel shift of NPY concentration response curves for both the Snap Y1 receptor-Yn and Snap Y1/Y4 BiFC dimer populations. This was indicative of competitive reversible antagonism (estimated  $pK_b$  of BiFC dimer  $8.5 \pm 0.2$ ; Snap Y1 population  $8.4 \pm 0.2$ ,  $n=4$ ) and was similar to results obtained for the inducible GFP tagged Y1 receptor cell line (estimated  $pK_b$   $8.6 \pm 0.2$ ,  $n=4$ ), and the documented affinity of BIBO3304 for the Y1 receptor (Kilpatrick et al., 2010). However pre-treatment with BIBO3304 had no effect on PP induced internalisation of the Snap Y1 receptor or Snap Y1/Y4 BiFC dimer populations (B). The lack of BIBO3304 effect on PP responses observed in inducible Y4-GFP receptors was consistent with a BIBO3304  $K_i > 1\mu\text{M}$  for the Y4 receptor subtype that has been previously reported (Wieland et al., 1998).

**NPY ± 30nM BIBO3304**



**PP ± 30nM BIBO3304**

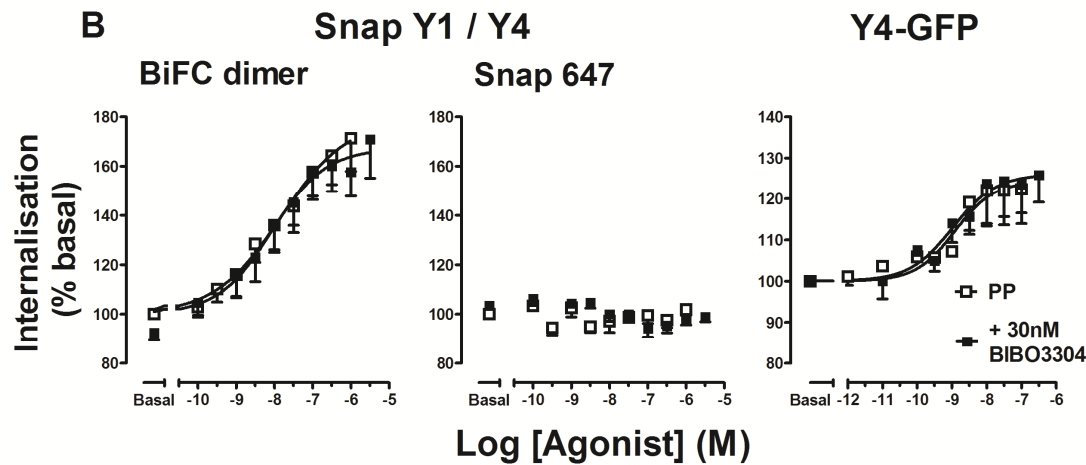


**Figure 6.14: The effect of pretreatment with the antagonist BIBO3304 on the agonist induced internalisation of Y1 and Y4 receptor subtypes expressed alone or when constrained as a heterodimer using BiFC**

GFP tagged Y1 or Y4 receptor and Snap Y1/Y4 BiFC dimer cell lines were pretreated with the Y1 selective antagonist BIBO3304 (30nM; 30min at 37°C) prior to stimulation with either NPY (Snap Y1/Y4; Y1-GFP (A)) or PP (Snap Y1/Y4; Y4-GFP (B)). H33342 labelling, image acquisition and quantification of receptor internalisation was performed as previously described. NPY concentration response curves in the presence and absence of BIBO3304 were fitted using GraphPad Prism with shared Hill slopes. Responses to NPY were normalised to minimum (basal responses) and maximum (1µM NPY responses), whilst responses to PP were expressed as percentage fold over basal (as PP had no effect on the Snap-Y1-Yn populations). All data were pooled from a minimum of 3 independent experiments, and expressed as mean ± s.e.m.

### **6.3.7 The pharmacology of NPY Y1/ $\beta$ 2AR BiFC heterodimers was consistent with independent orthosteric binding sites.**

HEK293T cells stably coexpressing Snap Y1-Yn and  $\beta$ 2AR-Yc receptor constructs were used to investigate whether modified pharmacology was observed when closely related GPCR subtypes were constrained as BiFC dimers. The substantially different structures of Y1 peptide and  $\beta$ 2AR monoamine ligands meant that there was high confidence in the selectivity of either ligand for its cognate orthosteric site.

In competition binding experiments using membranes freshly prepared from these cells, specific [ $^{125}$ I] PYY binding was competed by Y1 selective agonist (PYY) or antagonist (BIBO3304; Figure 6.15, Table 6.1, C). Estimated pIC<sub>50</sub> values were consistent with previous observations for Snap Y1 receptors expressed alone or when coexpressed with Y1-Yc (Y1/Y1 BiFC dimer; Chapter 5, Table 5.1). However co-incubation with a  $\beta$ 2AR selective agonist (isoprenaline) or antagonist (propranolol) did not inhibit specific [ $^{125}$ I] PYY binding, suggesting that in measurements accessing the whole receptor population, as expected a 'Y1 receptor like' phenotype was observed in respect to ligand binding.

Representative images taken using an IX Ultra confocal plate reader, confirmed predominant plasma membrane expression of both the Snap Y1 receptor and Snap Y1/ $\beta$ 2AR BiFC populations under control conditions (Figure 6.16, control). Stimulation with NPY was able to induce the internalisation of both the Snap Y1 receptor and Y1/ $\beta$ 2AR BiFC dimer population in a concentration dependent manner (Figure 6.17; BiFC dimer; Table 6.4). As expected isoprenaline had no activity at the Snap Y1 receptor population, but was able to induce the internalisation of the Y1/ $\beta$ 2AR BiFC dimer population (Figure 6.17; 10 $\mu$ M ISO panel) in a concentration dependent manner with a pEC<sub>50</sub> value consistent with that observed for Snap  $\beta$ 2AR-Yn expressed alone or when coexpressed with  $\beta$ 2AR-Yc (Chapter 5, Table 5.3).

## Snap Y1 / $\beta$ 2AR

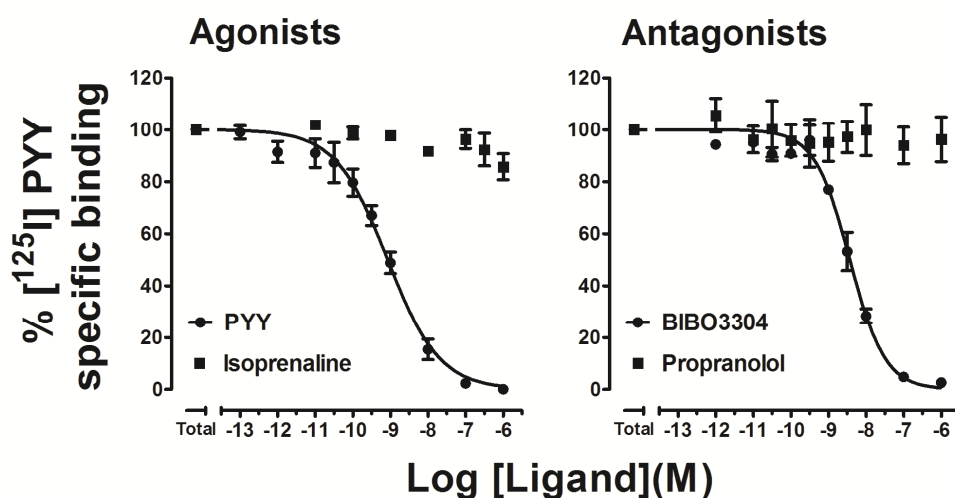


**Figure 6.15: Competition binding assay using [<sup>125</sup>I] PYY and unlabelled receptor subtype selective ligands in membranes derived from HEK293T cells stably expressing Snap Y1 /  $\beta$ 2AR receptor constructs**

Membranes were freshly prepared from HEK293T cell lines stably coexpressing Snap Y1-Yn and  $\beta$ 2AR-Yc BiFC dimer constructs and were incubated with [<sup>125</sup>I] PYY (15pM) and increasing concentrations of unlabelled competing Y1 (PYY or BIBO3304) or  $\beta$ 2AR selective ligands (isoprenaline or propranolol) for 90min at 22°C. Membrane bound radioligand was separated using filtration and quantified using a gamma counter. Competition displacement curves were generated using GraphPad Prism, with pooled data representing a minimum of 3 independent experiments. Data was expressed as mean  $\pm$  s.e.m (Hill slope range 0.70-1.1).

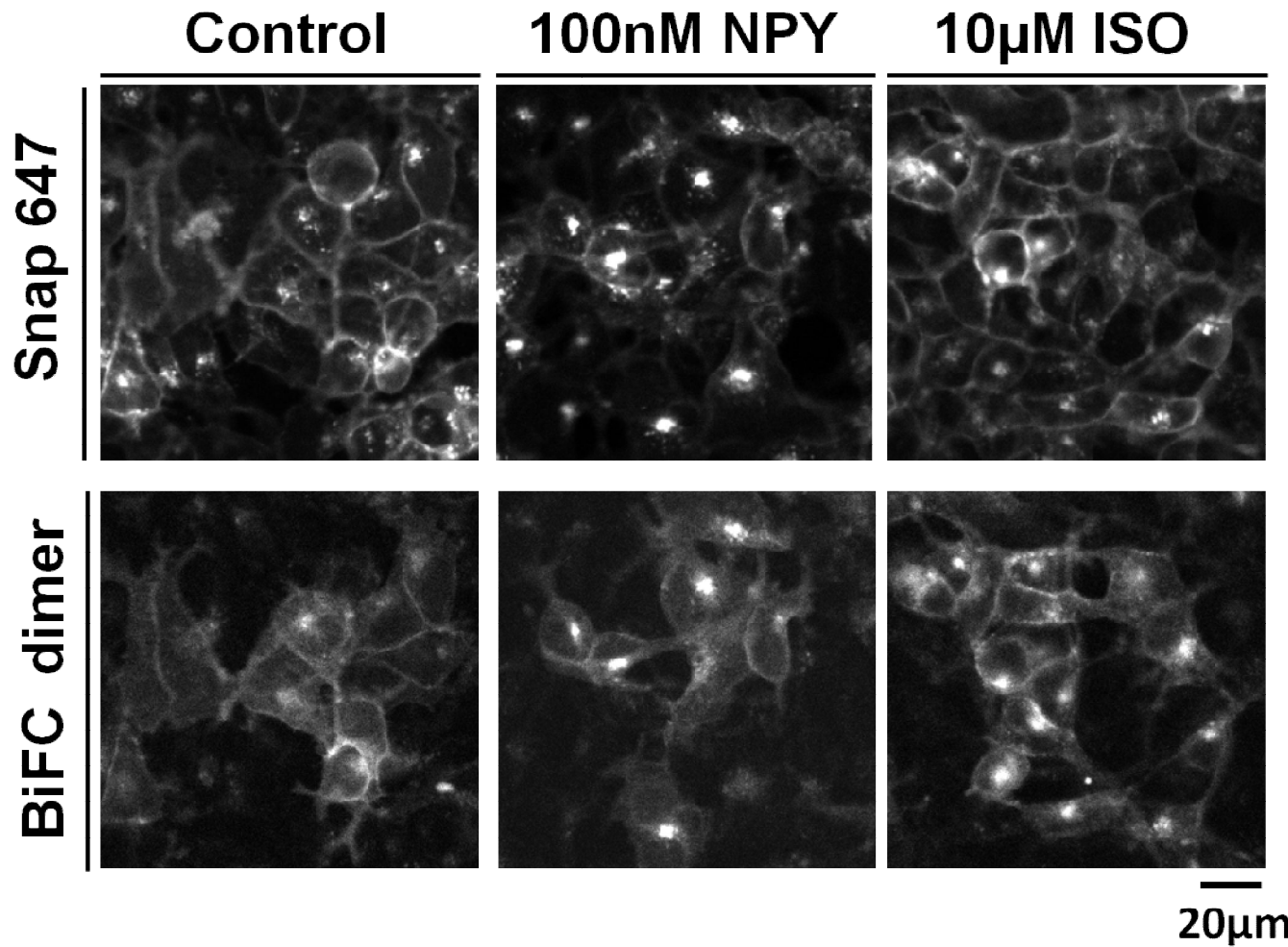


**Figure 6.16: IX Ultra confocal platereader representative images of Snap Y1/ $\beta$ 2AR BiFC heterodimers stimulated with subtype selective agonists**

HEK293T cells stably coexpressing Snap Y1-Yn and FLAG  $\beta$ 2AR-Yc, were prelabelled with SNAPsurface 647 (0.2 $\mu$ M) before stimulation with vehicle, 100nM NPY or 10 $\mu$ M isoprenaline (ISO, 30min at 37°C). Representative images, from a minimum of 4 independent experiments, were taken using a IX Ultra confocal platereader and are shown as cropped 300x300 pixel regions.

## Snap Y1 / $\beta$ 2AR

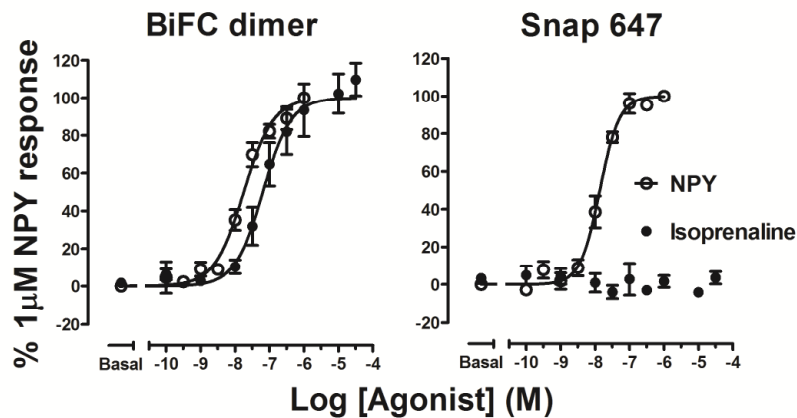


**Figure 6.17: Quantification of Snap Y1/ $\beta$ 2AR BiFC dimer internalisation following stimulation with receptor subtype selective agonists**

Snap Y1/ $\beta$ 2AR BiFC heterodimers were prelabelled with SNAPsurface BG647 (0.2 $\mu$ M) prior to stimulation with NPY or isoprenaline (30min at 37°C). H33342 labelling, image acquisition and quantification of receptor internalisation was performed as previously described. Responses were normalised to minimum (basal) and maximum (1 $\mu$ M NPY) with shared Hill slope constraints. All data were pooled from a minimum of 4 independent experiments, and expressed as mean  $\pm$  s.e.m..

In order to investigate whether constraining Y1/ $\beta$ 2AR as dimers using BiFC resulted in altered antagonist pharmacology, cells were pretreated with either the Y1 selective antagonist BIBO3304 (30nM for 30min at 37°C) or the  $\beta$ 2AR selective propranolol (10nM for 30min at 37°C). This was followed by stimulation with a concentration response course of NPY or isoprenaline (30 min at 37°C). BIBO3304 pretreatment was able to inhibit the NPY induced internalisation of both the Snap Y1 receptor and Y1/ $\beta$ 2AR BiFC dimer populations indicative of surmountable antagonism (Figure 6.18, A; estimated  $pK_b$  8.1  $\pm$  0.1 BiFC dimer; 8.1  $\pm$  0.1 Snap  $\beta$ 2AR; n=4). However BIBO3304 pretreatment was not able to inhibit isoprenaline induced internalisation of the Y1/ $\beta$ 2AR BiFC dimer population (B; isoprenaline  $pEC_{50}$  values 7.0  $\pm$  0.1; +30nM BIBO3304 7.2  $\pm$  0.2; n=4).

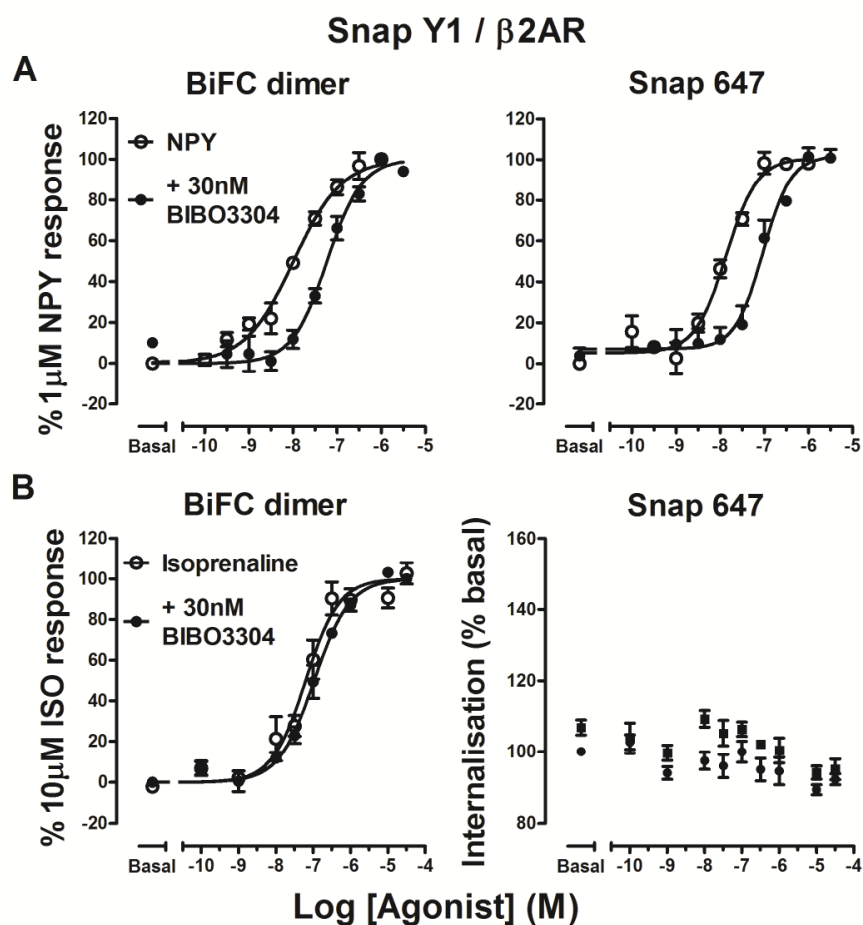


**Figure 6.18: The effect of pretreatment with the antagonist BIBO3304 on the internalisation of Snap Y1/ $\beta$ 2AR BiFC dimers in response to subtype selective agonists**

Snap Y1/ $\beta$ 2AR BiFC dimers were pretreated with the Y1 selective antagonist BIBO3304 (30nM; 30min at 37°C) prior to stimulation with either NPY or isoprenaline. H33342 labelling, image acquisition and quantification of receptor internalisation was performed as previously described. Concentration response curves in the presence and absence of BIBO3304 were fitted using GraphPad Prism with shared Hill slopes and normalised to 1 $\mu$ M NPY or 10 $\mu$ M isoprenaline. Responses for Snap Y1-Yn in respect to isoprenaline were expressed as fold responses over basal (where basal is 100%). All data were pooled from 4 independent experiments, and expressed as mean  $\pm$  s.e.m.

## Snap Y1 / $\beta$ 2AR

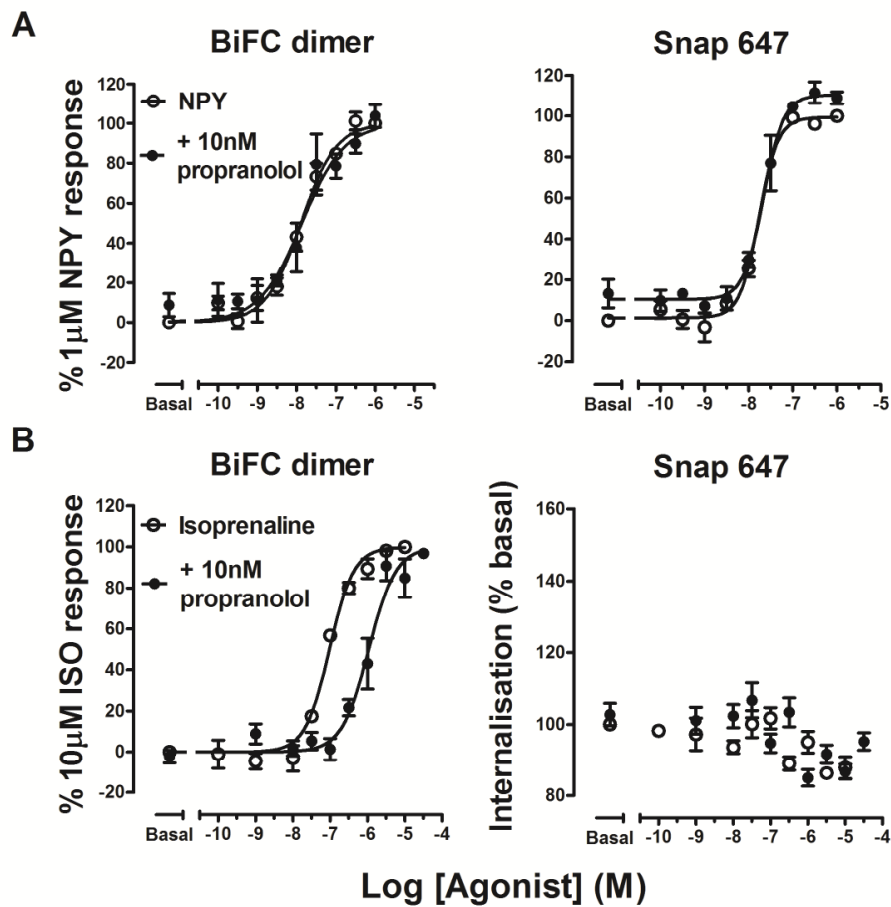


**Figure 6.19: The effect of pretreatment with the  $\beta$ 2AR selective antagonist propranolol on the internalisation of Snap Y1/ $\beta$ 2AR BiFC dimers in response to subtype selective agonists**

Snap Y1/ $\beta$ 2AR BiFC dimers were pretreated with the  $\beta$ 2AR selective antagonist propranolol (10nM; 30min at 37°C) prior to stimulation with either NPY or Isoprenaline. H33342 labelling, image acquisition and quantification of receptor internalisation was performed as previously described. Concentration response curves in the presence and absence of propranolol were fitted using GraphPad Prism with shared Hill slopes and normalised to 1 $\mu$ M NPY or 10 $\mu$ M Isoprenaline Responses for Snap Y1-Yn in respect to isoprenaline were expressed as fold responses over basal (where basal is 100%). All data were pooled from 4 independent experiments, and expressed as mean  $\pm$  s.e.m.

**Table 6.4: Summary of potencies and efficacies of a panel of ligands for stimulating the internalisation of Snap Y1/ $\beta$ 2AR**

	Snap Y1 / $\beta$ 2AR			
Agonist	Snap Y1		Y1/ $\beta$ 2AR BiFC dimer	
	pEC <sub>50</sub>	% NPY response	pEC <sub>50</sub>	% NPY response
NPY	7.9 $\pm$ 0.1	100	7.8 $\pm$ 0.1	100
Isoprenaline	/	3.5 $\pm$ 3.3	7.2 $\pm$ 0.1	109.7 $\pm$ 8.7

All data were expressed as  $\pm$  standard error of the mean. pEC<sub>50</sub> values were obtained from pooled concentration response curves presented in Figure 6.17.

E<sub>max</sub> responses to each ligand were calculated as a percentage of 1 $\mu$ M NPY responses.

/ not able to be determined

n= 4

Equally, pretreatment with the  $\beta$ 2AR selective antagonist propranolol was not able to inhibit NPY induced internalisation of either the Snap Y1 receptor (NPY  $pEC_{50}$  values  $7.8 \pm 0.1$ ) or Y1/ $\beta$ 2AR BiFC dimer populations (Figure 6.19, A; NPY  $pEC_{50}$  values  $7.9 \pm 0.1$ ; n=4). Propranolol was able to selectively inhibit the Isoprenaline induced internalisation of the Y1/ $\beta$ 2AR BiFC dimer population, with rightward parallel shifts in responses seen indicative of surmountable antagonism (B; estimated  $pK_b$   $9.2 \pm 0.2$ ; n=4).

## 6.4 Discussion

### 6.4.1 Summary of main findings

In this chapter BiFC was successfully used to constrain Y1/Y5, Y1/Y4 and Y1/ $\beta$ 2AR subtypes as heterodimers of precise composition, which were able to internalise in response to selective agonist stimulation. In [<sup>125</sup>I]PYY competition binding assays, Snap Y1/Y5 and Snap Y1/ $\beta$ 2AR membranes showed profiles consistent with a Y1 receptor like pharmacology, whilst a mixed profile, suggestive of both Y1 and Y4 receptor components, was obtained from the Snap Y1/Y4 cell line. Equally, cAMP assays in Snap Y1/Y5 cells indicated predominantly Y1 mediated responses. Thus as expected, the trapped heterodimers visualised by BiFC (especially for Snap Y1/Y5) represented a small proportion of the total receptor population, and that as a consequence, cell population studies may mask dimer specific responses. However the combined use of Snap labelling and BiFC allowed the discrete quantification of responses of the constrained BiFC dimer or reference Snap -Y1-Yn receptor populations simultaneously within the same cells, with internalisation of both populations used as a readout of function. This revealed modified agonist and antagonist pharmacology of Snap Y1/Y5 BiFC dimers compared to the responses of either receptor expressed alone. The most striking alteration observed for constrained Snap Y1/Y5 BiFC dimers, was a switch in the nature of antagonism for Y5 receptor selective antagonists from surmountable to insurmountable. Changes in pharmacology were also observed at this dimer pairing in respect to the action of the Y1 selective antagonist BIBO3304, and to the relative potency and efficacy of Y5 selective agonists. When viewed in combination, these altered properties suggest allosteric interactions occurring across the Snap Y1/Y5 receptor dimer interface. Furthermore, the specificity of such interactions was suggested by the fact that modified pharmacology was only seen for the Snap Y1/Y5 combination, with responses for

Snap Y1/Y4 or Snap Y1/ $\beta$ 2AR BiFC dimers largely reconcilable with their orthosteric binding sites acting independently.

As altered pharmacology was only observed for the Y1/Y5 BiFC dimer alone, formation of these dimers may have an impact on the control of central feeding responses *in vivo* by the combined signalling of Y1 and Y5 subtypes, and the limited efficacy of highly selective Y1 or Y5 receptor antagonists in inhibiting these responses. Equally this system raises the possibility of screening for novel Y1/Y5 heterodimer selective anti obesity therapies.

#### **6.4.2 Y receptor subtypes and Y1/ $\beta$ 2AR receptors constrained as heterodimers using BiFC were correctly expressed and capable of binding NPY ligands**

In order to study Y receptor heterodimers, the subtypes Y1 and Y5 were chosen as a primary focus, as this pairing has previously been implicated in co-promoting central feeding responses (Chapter 1, section 1.8.4.1) and immunohistochemistry showing coexpression of these subtypes within the same cells of the hypothalamus (Wolak et al., 2003) raises the potential for functional heterodimerisation.

The Y1 and Y4 pairing were also chosen as in contrast, these receptors have opposing effects in the central control of appetite, where the Y4 receptor has been implicated in inducing satiety (Chapter 1, section 1.8.4.2). However both Y1 and Y4 receptors are co-expressed in epithelial cells of the gastrointestinal tract, where they bind PP and PYY released postprandially, and promote antisecretory effects (Cox, 2007).

Additionally these subtypes have distinct ligand selectivity profiles, particularly in respect to PP binding (Chapter 3, Table 3.2 and 3.3). For both Y receptor heterodimers, the use of selective ligands with high affinities for the distinct subtypes was exploited in order to selectively target orthosteric ligand binding sites within the dimer. When combined with BiFC, this allowed potential pharmacological effects of ligand occupancy and potential cooperativity to be investigated at a constrained heterodimer complex of known composition. The

current lack of a wholly Y1 selective agonist was unfortunate as it did not allow reciprocal effects, particularly in respect to the Y1/Y5 BiFC dimer to be investigated.

The  $\beta$ 2AR was also chosen to be constrained with Y1 receptors within a BiFC dimer, as both receptors are coexpressed at some sympathetic synapses and have been implicated in co-regulating vasoconstriction in vascular smooth muscle cells (Wahlestedt et al., 1990b). Additionally the ligands of both these subtypes are structurally distinct (peptide vs monomamines) allowing selective orthosteric ligand bind site targeting.

BiFC was successfully used to constrain these subtypes as heterodimers of precise composition. As in Chapter 5, the intention here was not to identify to what extent such dimers form, but instead to investigate the pharmacology of complexes constrained in a defined 1:1 stoichiometry. All BiFC dimer heterodimer combinations, with the exception of Snap Y1/D2L, were correctly expressed at the cell surface and functional in respect to PYY binding with affinities consistent with previous observations for Snap Y1-Yn alone, Snap Y1-Y1 homodimers (Chapter 5, Table 5.1) and Y1-GFP (Chapter 3, Table 3.1).

Like Snap Y1/Y1 BiFC homodimers (Chapter 4), constrained Snap Y1/Y5, Y1/Y4 and Y1/ $\beta$ 2AR BiFC dimer populations were all able to rapidly internalise in response to NPY stimulation with comparable potencies to that observed for unconstrained Snap labelled Y1-Yn receptors within the same cells. Extensive areas of colocalisation were also observed, suggesting that both receptor populations internalised to the same intracellular compartments. These observations suggested that the use of BiFC to constrain GPCRs as heterodimers did not adversely affect their expression or endocytosis, which was comparable to Snap Y1/Y1 BiFC dimers, Y1 receptor oligomers (Dinger et al., 2003, Gehlert et al., 2007) and previous uses of BiFC to identify D2L and A<sub>2A</sub> heterodimers in a neuronal cell line (Vidi et al., 2008a). However as for previous observations of BiFC constrained D1 and A<sub>2A</sub> heterodimers (Vidi et al., 2008a), Snap Y1/D2L BiFC

dimers were retained within the cell. This suggests a degree of selectivity in that where receptor pairings are not appropriate, BiFC dimers can form but fail to reach to the cell surface.

In competition radioligand binding studies of Snap Y1-Yn/Y5-Yc derived membranes, a predominantly 'Y1 receptor like' pharmacology was observed in respect to subtype selective agonists and antagonists. The lack of Y5 receptor responses was not due to a lack of binding of the radioligand, as [<sup>125</sup>I] PYY has been previously shown to bind to this subtype with an affinity comparable to that seen for the Y1 receptor (Gerald et al., 1996). This implied that the expression of the Snap Y1-Yn receptor population was substantially greater than the Y5-Yc receptor. In whole population measures, the functional behaviour Snap Y1-Yn population may therefore be masking any alterations in pharmacology attributable to the formation of heterodimers.

For Y1-Yn/Y4-Yc coexpressing cells the preferential two site fit observed for PP inhibition of specific [<sup>125</sup>I] PYY binding reflected the differing affinities of PP for the co-expressed Y1 and Y4 protomer orthosteric binding sites (Chapter 3, Table 3.2, 3.3). This was further confirmed by selective BIBO3304 displacement of Y1 binding. The fraction of specific binding displaced, was almost identical to the binding fraction of the high affinity site for PP. Therefore the high affinity site likely represents PP binding to the Y4 receptor protomer as the IC<sub>50</sub> value obtained here is comparable to previous observations of PP binding affinity to human Y4 receptors ((Gehlert et al., 1997)). Likewise the IC<sub>50</sub> value obtained for the low affinity site is similar to PP binding to rat Y1 receptors (Chapter 3, Table 3.1; (Gehlert et al., 1997)). This is consistent with the known order of selectivity of PP for the Y receptor subtypes, and likely represents PP binding independently to either the Y1 or Y4 orthosteric ligand binding sites of the whole expressed receptor population. [<sup>125</sup>I] PYY binding assays in Y1/Y4 membranes therefore appeared to reflect a relatively greater expression of the Y4 receptor when compared to the Y5-Yc construct in this Snap Y1-Yn coexpressed system. The

exact proportions are hard to assess, because the higher documented affinity of Y4 receptors for [<sup>125</sup>I] PYY (Lundell et al., 1995) compared to the Y1 subtype (Larhammar et al., 1992) (pK<sub>d</sub> values 9.8 vs 9.1 respectively), means that at the concentration of radioligand used (15pM) a greater proportion of Y4 receptors would be labelled than Y1 within the sample.

For the Y1/β2AR cell line, a 'Y1 receptor like' pharmacology was also observed in respect to competition binding as expected due to the lack of affinity the β2AR orthosteric site has for [<sup>125</sup>I] PYY, and no allosteric influence of competing β2AR agonists or antagonists was detected

#### **6.4.3 Pharmacology consistent with the Y1 receptor subtype was observed in inhibition of cAMP accumulation experiments for the Snap Y1/Y5 cell line**

Similar to observations in [<sup>125</sup>I] PYY binding, a 'Y1 receptor like' pharmacology was also observed for the Y1/Y5 cell line in respect to inhibition of cAMP accumulation. For example, BIBO3304 showed surmountable antagonism of NPY responses. It is worth noting that BIBO3304 showed slightly reduced affinity (3 – 10 fold) in cAMP accumulation, than expected from previous work (Wieland et al., 1998). This might be attributed to a portion of the response being mediated via BIBO-insensitive Y5 receptors. However as discussed in Chapter 5, similarly lower affinity was also observed for BIBO3304 in radioligand binding assays, Snap Y1/Y1 BiFC homodimers, and Snap Y1 receptors expressed alone (Chapter 5, Figure 5.9), Y1-GFP and Y1/A2 (Chapter 3), suggesting BIBO3304 were relatively internally consistent. Equally the lack of inhibition observed for CGP71683 in cAMP accumulation assays reflected the reduced Y5 receptor expression in the Snap Y1/Y5 cell line compared to the Snap Y1-Yn receptor as indicated by radioligand binding.

Although modified pharmacology has been observed in cell systems for the Y1 / Y5 receptor combination (Gehlert et al., 2007; see below), in this work, whole population studies could not distinguish heterodimer specific responses from those of monomeric receptor or homodimer populations likely also present.

#### **6.4.4 The combined use of Snap labelling and BiFC revealed altered ligand pharmacology of constrained Y1/Y5 BiFC dimers previously unseen in whole population measures**

BRET studies have previously suggested Y1 and Y5 receptor can interact (Gehlert et al., 2007), but this can only infer the formation of distinct functional heterodimers. This is where the use of BiFC was advantageous as it discretely identified the Y1 / Y5 complexes due to the need for both fragment tagged protomers to contribute to fluorescence production. The irreversibility of BiFC meant that both Y1 and Y5 receptors were constrained as dimers, in a defined 1:1 stoichiometry. Notably, because BiFC is an inefficient process (for example due to its proximity and orientation limits and the likelihood that not all complemented YFP will be matured and fluorescent (Hallworth and Nichols, 2012)), and population studies established a significant excess of Snap-Y1-Yn receptors, the levels of Snap Y1/Y5 BiFC dimers must represent a small proportion of the total Y receptor contingent on the surface. Thus using agonist induced receptor internalisation as a readout of function enabled responses of the “Y1/Y5 BiFC dimer” to be assessed in a way which is impossible in population experiments, and also allowed comparisons to responses of the Snap labelled total Y1 receptor population simultaneously in the same cells. Therefore the alterations in both agonist and antagonist pharmacology observed for the Snap Y1/Y5 BiFC population could be assigned to the behaviour of the specific molecular dimer.

First, constrained Snap Y1/Y5 BiFC dimers showed altered pharmacology for Y5 subtype selective agonists such as cPP(1-17)(Ala<sup>31</sup>,Aib<sup>32</sup>) NPY(18-36) or D-Trp<sup>32</sup> NPY (Balasubramaniam et al., 1994) which became markedly less potent and had lower ability to stimulate internalisation than NPY (compared to observations in Y5-GFP cells). These altered responses for Snap Y1/Y5 BiFC heterodimers, suggested that coexpression of the Snap Y1-Yn was adversely influencing the binding of Y5 selective ligands to the Y5 receptor orthosteric binding site. This

was not evident in previous results where the Y5 selective agonist cPP(1-17) NPY(19-23, Ala<sup>31</sup>,Aib<sup>32</sup>) and Gln<sup>34</sup> hPP showed greater efficacy in inhibiting forskolin induced cAMP accumulation at a AV-12 cell line coexpressing both Y1 and Y5 receptors when compared to Y5 receptors expressed alone (Gehlert et al., 2007). Taken alone however these data on Y5 agonists are not sufficient to confirm an allosteric interaction. As determined in Chapter 5, agonist occupancy of one binding site is sufficient to drive internalisation of Snap Y1/Y1 BiFC dimers, supported by other studies (Rovira et al., 2009). Indeed Y5 agonist stimulated internalisation of the Snap Y1/Y5 BiFC dimer must occur in this manner, since these agonists were inactive at the Snap-Y1-Yn protomer. Conceivably, reduced ability of Y5 receptors to undergo endocytosis compared to Y1 might confer these agonist-selective properties on the Snap Y1/Y5 dimer, and the use of a 60min agonist incubation period for Y5-GFP and previously observations of reduced kinetics of endocytosis (Bohme et al., 2008, Parker et al., 2003) may suggest this. However, the same low potency partial agonism of PP-Aib-NPY and PP, relative to NPY, was still observed in Snap Y1/Y5 cells when internalisation was instead measured at 60 min (Dr N Holliday, personal communication).

Therefore additional evidence for allosteric communication between Y1 and Y5 receptors was required, and provided by the modified antagonist pharmacology that is directly attributable to the Snap Y1/Y5 BiFC dimer. The switch in the nature of inhibition of structurally unrelated Y5 selective antagonists from surmountable in single receptor systems (Y5-GFP) to insurmountable at the Snap Y1/Y5 BiFC dimer population is strong evidence that the presence of the Y1 receptor was influencing the Y5 receptor orthosteric ligand binding site. For two orthosteric sites acting independently, and given that only one binding site (e.g. Y1) needs to be occupied by NPY for maximum Snap Y1/Y5 internalisation, the prediction would be that antagonists such as CGP71683 would have become inactive, because they had no effect on the Snap-Y1-Yn population. However clearly this did not occur. Interestingly, a similar switch from reversible to

irreversible antagonism was also observed for the Y5 selective antagonist, Novartis-1, in AV-12 cell populations coexpressing both the Y1 and Y5 receptor subtypes by (Gehlert et al., 2007) – the detection of this phenomenon in cell populations may be because Y1 and Y5 receptor expression levels were better matched (see section 6.4.3 on cAMP). In addition both receptors in that study did possess a C terminal fluorescent protein tag to allow BRET identification of potential dimers, but were not irreversibly constrained, ruling out an artefact from the use of BiFC in this study. Instead identification of these antagonist properties at the level of a molecularly defined dimer is new evidence that they derive from physical association between the receptors, rather than indirectly via signalling cross talk.

The modified pharmacology also observed for the Y1 selective antagonist BIBO3304 again suggested that Y1 and Y5 receptor heterodimerisation has functional implications for ligand binding. Surmountable antagonism was observed for the Snap Y1-Yn receptor population alone, but BIBO3304 was unable to inhibit the NPY induced internalisation of the Snap Y1/Y5 BiFC dimer population in the same cells. Thus the behaviour of Y1 and Y5 receptor antagonists is not reciprocal. BIBO3304 has very low affinity for the Y5 receptor ( $K_i > 1\mu\text{M}$ ) (Wieland et al., 1998), and so Snap Y1/Y5 BiFC dimer internalisation could still be mediated by NPY binding the Y5 protomer. However if this was the case, the behaviour of NPY in stimulating Snap Y1/Y5 BiFC dimer internalisation might be expected to resemble the partial agonism of the Y5 selective agonists (see above), which are equally efficacious in stimulating Y5-GFP receptor endocytosis. Thus the lack of effect of BIBO3304 on NPY potency or maximum response is hard to explain without allosteric modulation. Either the Y5 selective agonists are indeed less active at the Snap Y1/Y5 dimer because of allosteric communication, or co-expression of the Y5 receptor modifies the ability of the Y1 protomer to bind BIBO304. Again, this effect does not appear to be biased towards receptor internalisation readouts (and indirectly  $\beta$ -arrestin recruitment),

or the BiFC approach, as similar results have been observed for the Y1 selective antagonists BIBP3226 and LY366258 in respect to the agonist mediated inhibition of cAMP synthesis by coexpressed Y1 and Y5 receptors when compared to Y1 receptors expressed alone (Gehlert et al., 2007). While in the Gehlert study it was impossible to rule out the possibility that Y5 receptor stimulation by NPY was maintaining responses in the presence of Y1 antagonists, this study again pinpoints the lack of Y1 antagonist effect to the physical properties of the Snap Y1/Y5 dimer. The extensive modified agonist and particularly antagonist pharmacology observed for Snap Y1/Y5 BiFC heterodimers, was therefore likely to be a consequence of the distinct association of Y1 and Y5 receptor subtypes. Interestingly modified signalling for both Y1 and Y5 selective antagonists seen here and by (Gehlert et al., 2007) exhibited a ceiling effect, whereby even using concentrations of antagonist 100 fold that of their documented  $pK_b$ 's did not result in further changes in responses. This phenomenon of saturation is indicative of allosteric modulation (Langmead and Christopoulos, 2014). This suggested that both the Y1 and Y5 orthosteric ligand binding sites of the heterodimer were both amenable to allosteric modulation, whereby ligand binding to one protomer (eg. the Y1), induces a conformational change within the dimer so that the affinity of ligand binding to the second site (Y5) is either positively or negatively modulated and vice versa. Observations from other GPCR heterodimers, suggest that it is possible to obtain modified pharmacology that is functionally specific. For example coexpression of  $\beta_2/\beta_3$  adrenoceptors resulted in marked changes in the agonist induced internalisation of the  $\beta_2$  adrenoceptor protomer (Breit et al., 2004), but with no changes in respect to ligand binding affinities at either protomer or the ability of the  $\beta_2$  adrenoceptor protomer to functionally couple to  $G_{\alpha_s}$ . It is therefore likely that the signalling pathway that is modified can vary greatly depending with receptor pairing and potentially the specific ligand stimulation used (Ferre et al., 2014) – this might be expected given the distinct ways in which effectors (G proteins or arrestins for example) might

interact with such heterodimers. As we have highlighted in this study, the caveat in proposing functionally selective effects is the extent to which the specific dimer pairing can be isolated from other receptor combinations for the different signalling endpoints. Future investigations (see Chapter 7) might adapt the BiFC system in combination with RET to examine signalling of the Snap Y1 / Y5 pairs directly with G proteins or arrestins.

A potential mechanism to propagate allosteric effects across a GPCR Class A dimer, such as the Y1/Y5 BiFC dimer, is physical interaction between the two protomers of the dimer, such as that observed for the melatonin MT<sub>1</sub> receptor and GPR50 receptor. There are 3 main sites most likely to be the location of dimer interfaces. Firstly the analysis of X-ray structures such as the  $\mu$  and  $\kappa$  opioid (Wu et al., 2012, Manglik et al., 2012), chemokine CXCR4 (Wu et al., 2010) and  $\beta$ 1-adrenoceptor (Huang et al., 2013) which all crystallised as dimers and/or tetramers, suggested that the transmembrane helices may be such sites (section 5.1.1.4). Interactions of TM1 with helix 8 and TM4 with TM56 appear to be particularly conserved (Huang et al., 2013, Manglik et al., 2012). Many of these observations are supportive of previous interaction candidates suggested from biochemical studies (Johnston et al., 2012)(Section 5.1.1.5). The TM helices are relatively rigid, so questions remain whether these regions would be sufficiently influenced upon domain formation to propagate a conformational change that would be sufficient to affect both protomer binding sites. A second potential interface site is within the N terminus and/or extracellular loops. ECL2 has been implicated as the primary region that defines ligand specificity by governing access to the binding pocket (section 1.2.2.2). For example, for binding of neuropeptides by Y receptors a critical highly conserved (in Y subtypes) Asp 6.59 of ECL3 binds to the amidated C terminus of NPY (Walker et al., 1994, Merten et al., 2007) and for the Y1 receptor only an additional connection involving His7.31 of ECL3 (Akerberg et al., 2010) is also crucial. If dimerisation involved these ECL regions, the high degree of influence they hold over ligand access and binding

would likely allow conformational changes/cooperative effects to be propagated from one protomer binding site to the other.

Lastly the intracellular regions govern the binding of effector proteins such as G proteins and  $\beta$ -arrestins. As these effectors are allosteric modulators in their own right, this means that if dimerisation were governed by the intracellular domains, then these allosteric effects which influence ligand binding could be readily transduced through the dimer structure. This reconciles with the observations of Maurice et al., 2011 (Maurice et al., 2011) who suggested that some cooperative effects ascribed to dimerisation, may instead be due to sequential or spatial binding of effector molecules such as G proteins and  $\beta$ -arrestins to distinct receptor populations. It is unlikely that the presence of the BiFC tags is affecting this as only the Snap Y1/Y5 BiFC, and not the Y1/Y4 or Y1/ $\beta$ 2AR dimer pairing showed any modification of pharmacology when constrained. It is unlikely that the Snap Y1/Y5 BiFC dimer is adopting a conformation that sterically affects  $\beta$ -arrestin2 binding affinity, as potencies for NPY at inducing internalisation of this BiFC dimer population were comparable to Snap Y1-Yn expressed alone (Chapter 5, Table 5.2) or when BiFC was used to investigate  $\beta$ -arrestin2 recruitment to the Y1 or Y5 receptor (Y1/A2; Chapter 3, Table 3.3). One consideration is that the evidence from Y1 homodimer mutagenesis (Chapter 5) argues against asymmetric binding of arrestin molecular sensors to different protomers of the dimer (with caveats, for example the ability of GRKs to phosphorylate such dimers) – a 1:2 stoichiometry would be the most plausible manner for modified dimer properties to occur via this mechanism. However heterodimer specific intracellular domains could still modify the way in which effectors are recruited to individual protomers by other means. The use of selective mutagenesis of single protomers within a BiFC dimer (Chapter 5) provides a unique mechanism to investigate which regions of the receptor are responsible for communicating allosteric effects (see Chapter 7).

There is also the potential that observations of altered signalling for heterodimers are actually a consequence of downstream signalling cross talk between receptors in close proximity. This is a particular concern when studying receptors expressed in heterologous cell lines, as receptor expression levels often exceed those found physiologically, and use population measurements which derive from the entire cohort of receptors on the cell surface. However as the modified signalling observed here for Y1/Y5 has been seen using a constrained system (BiFC) whereby protomer stoichiometries are defined (1:1) the impact of cross talk, although not wholly eliminated, is certainly less likely.

#### **6.4.5 Snap Y1/Y4 and Y1/ $\beta$ 2AR BiFC dimers showed agonist and antagonist pharmacology consistent with their orthosteric ligand binding sites acting independently**

The observations that Snap Y1/Y5 dimers showed allosterically modified pharmacology were given greater weight in that these changes were specific to that heterodimer. In general, the BiFC system applied to Snap Y1/Y4 or Snap Y1/ $\beta$ 2AR heterodimers did not reveal altered pharmacology.

When using the Snap-BiFC system to quantify internalisation, agonist responses for NPY and PP at the Snap Y1 or Snap Y1/Y4 BiFC dimer populations or isoprenaline at the Snap Y1/ $\beta$ 2AR BiFC dimer could be explained by the known ligand selectivity's of Y1, Y4 or  $\beta$ 2AR and were largely consistent with those previously seen for the Y1 (Y1-GFP; Chapter 3, Figure ), Y4 (Chapter 3, Figure 3.9) or  $\beta$ 2AR receptors (Chapter 5, Figure 5.15) expressed alone. It was observed that PP was significantly less potent (more than 10 fold) for the Snap Y1/Y4 dimer than might be expected from its effects in Y4-GFP expressing cells. However in the absence of a greater range of Y4 selective ligands (both agonists and antagonists), this finding alone cannot be sufficient evidence for an allosteric effect. Instead, when considering the effects of antagonists (and in marked contrast to the Snap Y1/Y5 system), both Y1/Y4 and Y1/ $\beta$ 2AR BiFC dimers displayed surmountable antagonism to BIBO3304 and propranolol respectively, but only when the

relevant orthosteric agonist (NPY or isoprenaline) was used, consistent with the protomer binding sites acting independently.

#### **6.4.6 Potential physiological implications of modified pharmacology of Y1/Y5 receptor heterodimers**

The control of food intake in response to NPY is driven largely by the combined action of Y1 and Y5 receptors in neurons of the paraventricular nucleus of the hypothalamus. The modified pharmacology (particularly in respect to antagonists) of these heterodimers seen both here and by other groups (Gehlert et al., 2007), might explain the poor clinical efficacy of antagonist therapies that are highly selective for either subtype (Chapter 1, section 1.8.6.1). Gehlert et al., 2007 observed that only dual treatment with both Y1 and Y5 selective antagonists resulted in significant decreases in the agonist induced internalisation of coexpressed subtypes. This evidence suggests that a therapeutic agent which co-targets both subtypes may have greater success.

This hypothesis is supported by the overlapping mRNA and protein expression of both receptors in a range of brain regions (Parker and Herzog, 1999) with *in situ* immunohistochemistry suggesting this coexpression is within the same cells and nerve fibres (Wolak et al., 2003). The formation of Y1/Y5 heterodimers may therefore be a mechanism by which these receptors co-regulate feeding. Additionally the presence of functional Y1/Y5 heterodimers may explain some of the paradoxical results seen in knockout studies of either subtype (Chapter 1, section 1.8.4.1). For example, germline knock outs of either subtype in mice resulted in late onset obesity with either no change or increases in food intake (Kushi et al., 1998, Marsh et al., 1998). In the context of receptor dimerisation, this may reflect changes in the proportion of homodimer or heterodimer species present. Hypothalamic knock out of both subtypes in mice, resulted in decreased spontaneous and fast induced food intake, increased body weight and adiposity when fed a high fat diet, supporting the hypothesis that it is the combined action of both receptors which drives hyperphagia *in vivo* (Nguyen et al., 2012, Lecklin et

al., 2002). Additionally a series of experiments performed in wildtype and Y1 receptor knock mice fed a high fat diet have illustrated that co-administration of Y1 and Y5 receptor antagonists resulted in greater anti obesity effects than when either subtype was targeted alone (Mashiko et al., 2009). However the documented poor bioavailability of many Y receptor antagonists suggests that simultaneous administration may not show as great an efficacy in human studies. However care must be taken when interpreting *in vivo* observations of co-regulation as direct evidence for dimerisation, as other explanations might be sufficient. For example alterations in the action of antagonists, may simply be explained by coexpression of both subtypes in close proximity without necessarily implying the need for direct physical associations. Close proximity of receptors does not necessarily imply co-regulation as signalling at both receptors may instead be temporally regulated. For example the rate of agonist induced internalisation (Bohme et al., 2008) and  $\beta$ -arrestin2 recruitment of singularly expressed Y5 receptors are slower than that of Y1 (Berglund et al., 2003b). Additionally both Y1 and Y5 receptors have been shown to individually regulate multiple aspects of metabolism beyond the induction of feeding, and these effects are not limited to the hypothalamus.

As we have shown, the Y1/Y5 BiFC constrained heterodimer exhibits modified pharmacology. It is difficult to unambiguously identify heterodimer populations in coexpression systems due to the likely mixture of monomer, homodimer and higher order oligomers also present and the proposed transience of dimers (Lambert, 2010). However designing heterodimer selective bivalent ligands which bridge the dimer structure may provide an answer to this. Additionally bivalent ligands have the potential to increase the potency, efficacy and/or selectivity of pharmacotherapies. Such ligands have been developed for the opioid receptor subtypes  $\delta/\mu$  (Daniels et al., 2005b) and  $\kappa/\delta$  (Daniels et al., 2005a), which have been shown to promote greater analgesia than morphine. However as the majority of these ligands are tested in coexpression systems, the actual 'dimeric

complex' responsible is not clearly defined. For example the dopamine D1-D2 heterodimer selective agonist SKF83959, was proposed to show heterodimer selective pharmacology when receptors were coexpressed in HEK293T cells, but subsequent screening revealed profound cross selectivity with other GPCRs (Chun et al., 2013). The BiFC system provides a way to screen such compounds at clearly defined heterodimers, allowing any selective responses that are identified to be then further investigated.

## Chapter 7: Final discussion

The prevalence of obesity has increased globally over the past three decades (Finucane et al., 2011) and has been implicated as a causative factor in a range of health problems including cardiovascular disease, cancer and type II diabetes (reviewed in (Mitchell et al., 2011)). There is therefore a largely unmet demand for anti obesity therapies that are effective at delivering long term weight loss and are safe.

The NPY Y receptor family of GPCRs has been shown to contribute to the central control of feeding responses. In particular the subtypes Y1 and Y5 have been shown to mediate NPY induced hyperphagia, lipogenesis and insulin resistance. Immunohistochemistry techniques have implied that these subtypes are coexpressed in the same cells of the paraventricular neurons (Wolak et al., 2003), with knock out studies suggesting a co-regulation between subtypes in respect to feeding responses (Nguyen et al., 2012). This co-regulation has been suggested to be due to the formation of Y1/Y5 heterodimers (Gehlert et al., 2007), which may account for the limited efficacy of antagonist therapies selective for either subtype in clinical trials.

The functional role of GPCR dimerisation is still currently in debate particularly in respect to physiological relevance. Dimerisation has the potential to offer novel pharmacological targets, and account for pathway specific signalling by some ligands both of which might increase the efficacy and selectivity of future GPCR based therapies. A wide array of biochemical, fluorescence based and kinetic data have suggested that the formation of dimers can alter the pharmacology of GPCR subtypes in respect to expression, ligand binding, coupling of effector proteins and downstream signalling. However many of these modifications might instead be explained as consequences of receptor coexpression, such as intracellular signalling cross talk, as opposed to representing a genuine physical interaction.

There is therefore a need to unambiguously identify the precise molecular makeup of signalling complexes.

This thesis explored the way this could be achieved using bimolecular fluorescence complementation (BiFC) to constrain protein-protein interactions as complexes of defined composition – either Y receptor dimers, or receptors and  $\beta$ -arrestin. The use of BiFC in conjunction with high content imaging and selective mutagenesis, initially allowed the quantification of the pharmacology of the association of Y receptor subtypes with  $\beta$ -arrestin2. Responses largely correlated with those observed for the pharmacology of Y receptor agonist induced internalisation, suggesting that it is the recruitment of  $\beta$ -arrestin2 that largely drives endocytosis of Y receptors. This conclusion was supported by single molecule imaging studies, such as FCS and PCH, whereby agonist occupancy resulted in a slowing of receptor diffusion, interpreted as clustering of activated receptors prior to their endocytosis. These FCS observations supported a well established endocytic pathway dependent upon  $\beta$ -arrestin and the recruitment of clathrin coated pits (Goodman et al., 1996, Luttrell and Gesty-Palmer, 2010). Understanding the molecular mechanisms of receptor effector protein interactions is particularly important in light of the ability of  $\beta$ -arrestin2 to act as a signalling component in its own right with potentially beneficial therapeutic outcomes (Violin et al., 2010). To further investigate the effect of Y receptor –  $\beta$ -arrestin interactions, a novel version of BiFC using superfolder GFP fragments was used for the first time in FCS. This revealed slow mobility of discretely defined Y1 receptor/ $\beta$ -arrestin2 complexes and their clustering prior to endocytosis. Molecular brightness analysis using PCH indicated a symmetrical mode of recruitment of  $\beta$ -arrestin2 to individual Y1 receptor complexes which were potentially oligomeric in nature. Single molecule imaging using BiFC therefore allowed the investigation of defined Y receptor/  $\beta$ -arrestin2 complexes at the plasma membrane prior to endocytosis. However questions remain as to the downstream intracellular signalling properties of these discrete complexes (for

example to ERK signalling). Investigating this is the key to understanding potential agonist directed signalling bias. The use of two colour cross correlation FCS may be an option. Here two detection channels separate the emission from two spectrally distinct fluorophores, and the fluctuations from both can each be autocorrelated (Briddon and Hill, 2007). Cross correlation between the two channels can also be performed to give an indication of interaction between the two distinctly labelled species (which does not rely on proximity rather co-diffusion). Therefore this technique could use BiFC (ie reconstituted YFP) alongside intracellular protein such as ERK, clathrin or caveolin labelled with spectrally distinct fluorophores (such as Cy5) to investigate potential changes in downstream signalling partners associated with discretely identified BiFC dimer pairings or receptor-arrestin complexes based on co-diffusion. Additionally PCH identified both clustered Y receptor/ $\beta$ -arrestin2 complexes (component 2) but single units (ie. not clustered) complexes were also identified. These units were presumably not associated with clathrin coated pits, therefore questions remain as to what these complexes represent and what they are interacting with.

The use of conventional fluorescence microscopy is of too low spatial resolution to adequately determine interactions of BiFC complexes with downstream partners. This is due to the diffraction limit of light being comparable or larger than the size of many subcellular proteins (Huang et al., 2009). However recent advances in microscopy techniques, so called 'super resolution' have demonstrated order of magnitude improvements in spatial resolution. One of these, termed photoactivated localisation microscopy (PALM) uses fluorophores that switch between bright and dark states to allow these molecules to be activated at different time points within a diffraction limited region, so that single fluorescence molecules can be individually activated, imaged, localised and deactivated allowing the fraction of molecules in the fluorescent state at any one time to be controlled to increase optic resolution. The coordinates of many individual fluorescent molecules can then be mapped and images reconstructed.

Recently BiFC-PALM, using photactivatable recomplemented mCherry has been used to visualise the nanoscale interaction and localisation of the GTPase Ras with its downstream effector Raf and indicated clustering of these complexes (Nickerson et al., 2014). A range of photoactivatable and photoconvertible fluorescent proteins have been shown to be suitable for BiFC, suggesting that super resolution imaging of BiFC complexes could provide more detailed information on the localisation of these complexes following endocytosis and the degree of clustering that occurs.

Quantification of internalisation using high content imaging was also used to investigate the function of GPCR dimerisation, with Snap labelling also used to allow comparison with responses of the total receptor population (be that monomers, dimers or oligomers). This revealed that constrained BiFC dimers were capable of undergoing agonist induced endocytosis, countering the notion that GPCR dimers must dissociate prior to internalisation (Lambert, 2010). Selective mutagenesis of one protomer of the dimer showed that occupation of one ligand binding site (Y1/Y1Y99A) and the phosphorylation of one protomer C terminus (Y1/Y15A) was sufficient to support this. The chief limitation to these observations is that the inherent irreversibility of BiFC essentially creates a fusion protein between the two protomers. Hence, it is difficult to exclude the possibility that internalisation of the wildtype protomer 'drags' the mutant protomer with it Co-internalisation of wildtype/mutant Y1 homodimers in the absence of BiFC tagging would go some way to answering this. Alternatively the use of an unrelated well characterised monomeric receptor as the second protomer, such as CD86, would allow this question to be further addressed, provided that the differences in receptor structures (for example CD86 only has a single TM domain) does not adversely affect expression of complexes.

The work of Chapters 4 and 5 indirectly suggested a single Y receptor protomer was sufficient to recruit  $\beta$ -arrestins, whether or not the receptors were joined as a BiFC homo-dimer. This argues against an asymmetric recruitment of  $\beta$ -arrestin

to a GPCR dimer, whereby the activation and phosphorylation sensors of  $\beta$ -arrestin engage with separate protomers of the dimer as proposed by Fotiadis et al., (Fotiadis et al., 2006).

However it is worth noting that BiFC here identified two protomers in a dimer as a unit, but that does not eliminate the possibility that higher order oligomers (such as trimers or tetramers) are present. This higher order oligomerisation may affect the potential mode of  $\beta$ -arrestin recruitment. Additionally the mode of recruitment may change with experimental/physiological conditions. For example this may be ligand dependent, particularly when the evidence of ligand induced receptor 'phosphorylation barcodes' altering  $\beta$ -arrestin signalling is also considered (Nobles et al., 2011). In addition there is also evidence from rhodopsin studies, that the stoichiometry of arrestin recruitment changes with the proportion of activated receptors (Sommer et al., 2011). This suggests there may be a degree of structural plasticity in  $\beta$ -arrestin recruitment with multiple modes possible.

Additionally as internalisation is an indirect measure of  $\beta$ -arrestin recruitment to BiFC constrained dimers, this assumes that GRKs are able to phosphorylate a non ligand occupied receptor protomer. To address this issue mutations that mimic phosphorylation could be introduced into the Y1Y99A protomer which would remove the need for GRK phosphorylation. If this mutant (ie. Y1Y99A + phosphorylation) when coexpressed with the Y15A (phosphorylation negative) protomer was able to restore dimer internalisation, this would show an asymmetric mode of  $\beta$ -arrestin recruitment is possible.

Combining BiFC with BRET would also provide a more accurate assessment of the association of  $\beta$ -arrestin2, or other effector proteins, with discrete GPCR dimers. The luminescent donor can be attached to  $\beta$ -arrestin2 with the fluorescence acceptor being reconstituted YFP (ie. GPCR BiFC dimer). The advantage of BRET is that it can provide a real time measurement of  $\beta$ -arrestin2 recruitment. The fold change in fluorescence produced in BRET assays is typically small

(Salahpour et al., 2012), which is a potential problem for sensitivity when the relatively low expression of the BiFC dimer population in these cell lines is also considered. A solution to this may be the use of the newer luminescent donors with increased quantum yields and longer lifespans of emission, such as the mutant form of luciferase RLuc8 (De et al., 2007) or the engineered luciferase reporter NanoLuc (Hall et al., 2012). However a caveat to using these brighter luciferase variants is that overexpression may make it very difficult to differentiate a specific BRET from the general luciferase emission.

Quantification of BiFC Y1 heterodimer internalisation (Chapter 6), revealed modified pharmacology for constrained Y1/Y5 BiFC dimers that was unseen in whole receptor population studies, or for other Y1 heterodimer combinations. The most striking alteration was a switching in the nature of Y5 selective antagonism from surmountable at single receptor expression systems to insurmountable at the Y1/Y5 BiFC dimer. This alteration was independent of the structure of the Y5 antagonist used, and was not replicated by Y1 antagonist data, where BIBO3304 became ineffective. The fact that these effects were able to be measured from the responses of a well defined BiFC dimer strongly suggests an allosteric interaction occurring between the Y1 and Y5 protomers.

There is still a risk that allosteric effects are an artefact of BiFC complementation. However this risk is minimised by the specificity of this allosterism, with no changes observed for Y1 and Y4 or Y1 and  $\beta$ 2AR pairings. To further confirm that altered Y1/Y5 pharmacology was not an artefact of BiFC, co-expression experiments could be performed to investigate the internalisation of co-expressed (but not BiFC joined) partners. However, similar to whole receptor populations studies (Chapter 6) coexpression studies may still be unable to detect the specific responses of a Y1/Y5 heterodimer from that of the other Y1 and Y5 receptor species that are likely to be present. For example, even if these receptors were expressed at equivalent levels and showed an equal propensity to form stable dimers, the heterodimer component would form only 50% of a

population that also included Y1/Y1 and Y5/Y5 homodimers. This illustrates the strength of the BiFC technique whereby responses can be attributed to a discrete dimer population without the confounding influence of monomer or homodimer internalisation responses.

It is also worth noting that Gehlert et al., (2007) observed comparable changes that support those observed in this study, in the nature of Y1 and Y5 selective antagonists in respect to cAMP accumulation using coexpressed untagged Y1 and Y5 receptors (Gehlert et al., 2007), albeit these experiments were performed in AV-12 cells, not HEK293T as here, with unknown levels of respective absolute expression. The structure of the Y5 receptor is most divergent of all the Y subtypes, in that it has a longer intracellular loop 3 and a shorter C terminal tail (Michel et al., 1998), and historically this subtype (whether tagged or not) has proven the most challenging to express recombinantly. Competition radioligand binding assays indicated that the population of FLAG Y5-Yc receptors was substantially lower than the Snap Y1-Yn population also expressed in the same cells, and this potentially differed from the Y1/Y4 and Y1/ $\beta$ 2AR (where  $\beta$ 2AR expression was not specifically measured) controls. In each case the presence of the N terminal FLAG tag prior to the start of the receptor-Yc cDNA could facilitate the monitoring of this receptor population using antibody live labelling techniques. A primary antibody that selectively recognises the FLAG tag epitope is added, followed by a secondary antibody conjugated to a fluorophore. This technique could be used to give a qualitative indication of the membrane localisation of these receptors and the differences in expression levels of receptor-Yc between cell lines. The advantage of antibody labelling is that only receptors that have successfully reached the cell surface are detected due to the membrane impermeance of the antibody. In addition to this the granularity algorithm is actually an indirect measure of internalisation as opposed to other techniques which measure the actual loss of cell surface fluorescence. For example the use of FLAG tag labelling may be a way to quantify the fraction of

labelled receptor-Yc lost from the cell surface using enzyme linked immunosorbent assays (ELISA), with anti-SNAP antibodies identifying the receptor-Yn population. Although these approaches could allow measures of receptor internalisation to be compared between subtypes and supplement granularity data, unlike the BiFC technique used here they do not specifically identify dimeric complexes. Additionally the work of Gehlert et al. (2007) has indicated that coexpression of Y1 and Y5 receptor subtypes increased the rate of Y5 receptor internalisation and can also change the trafficking fate. Again, these data support the idea of a Y1/Y5 heterodimeric receptor complex with unique pharmacology, arrestin recruitment and trafficking properties. However as previously noted, coexpression systems can only imply specific associations of receptors based on proximity. It would therefore be interesting to repeat aspects of this study, using both the combined Snap-BiFC system where the dimeric state is constrained, and the co-expressing Y1 and Y5 cell lines described above. However a caveat to this is that the irreversible nature of BiFC may itself influence trafficking, but it would be interesting to see whether localisation with markers of the endocytic pathway (such as transferrin to identify recycling compartments and lysotracker to identify lysosomes on the degradative pathway) occurs and if trafficking of a known dimer differs from either subtype expressed alone.

As previously detailed in Chapters 5 and 6, multiple regions have been proposed as the site/sites of protomer-protomer interfaces. While transmembrane domain regions might be responsible for determining the structural integrity and stability of the dimer, the extracellular loops are promising (especially for peptide receptors) as a mechanism for allosteric modulation due to their influence over the ligand binding pocket and access of ligands to and from it. Equally the unique intracellular domains of the Y5 receptor compared to the Y1 subtype (e.g. large ICL3) might play a role in allosteric modulation of the dimer by effector proteins such as arrestins – which would then impact on ligand pharmacology. The use of

selective mutagenesis or chimeric receptors at BiFC constrained dimers may allow the effect of particular domains on dimer pharmacology to be investigated. For example exchanging the extracellular loops (e.g. ECL2) of the Y1 and Y5 receptor subtypes might reverse the effects of heterodimerisation on ligand pharmacology observed. A challenge to this technique will be distinguishing effects on dimer allosterism of these mutations from more general effects they may bestow on ligand binding at the orthosteric site. Nevertheless such investigations may be possible using the BiFC system as it would allow the heterodimer specific pharmacology to be probed.

Ultimately, for validating the role of the Y1/Y5 heterodimer in native cells and tissues (e.g. on feeding responses) and the potential therapeutic targeting of this pairing in the future, the development of heterodimer selective ligands is required. For some types of heterodimer ligands, selectivity could simply be achieved because the ligand influences allosteric communication between the receptor protomers. For example, this phenomenon has been recently observed at functionally constrained dopamine D2 dimers, whereby binding of the bivalent ligand SB269652 to one protomer orthosteric ligand binding site allows it to allosterically modulate the binding of dopamine to the second orthosteric site (Lane et al., 2014). In order to do this SB269652 must bind at a secondary site found at the extracellular end of TM2 and TM7. Interestingly the introduction of a ligand binding mutation into the second protomer switched the nature of SB269652 pharmacology in respect to dopamine signalling from allosteric to competitive. Potential bivalent ligands are already identified for the Y receptor family, such as the dimeric C terminal NPY analogue GR231118, which is highly potent Y1 receptor antagonist (Dumont and Quirion, 2000, Kilpatrick et al., 2010), and of much greater affinity at this receptor than its monomeric components. However the size of GR231118 makes it unlikely that it would be able to simultaneously bridge both orthosteric binding sites of a Y1 receptor dimer. However this does not mean that dimerisation does not impact GR231118

pharmacology. The twin pharmacophores mean that when one C terminal domain of GR231118 is docked at one protomer, it acts as a tethered ligand increasing the local “concentration” of the second C terminal domain in the environment of the second protomer. This mechanism could be tested using the BiFC system and the Y1/Y99A dimer (with only one GR231118 binding site), allowing the mode of GR231118 antagonism to be assessed at both Snap Y1/Y1 or Y1/Y1Y99A homodimers, in a manner similar to the work of Lane et al., 2014 (Lane et al., 2014). If such a mechanism exists, the ability to synthesise chimeric dimer GR231118 peptides (Mountford et al., 2014) in which one arm of the peptide incorporates Y5 selective amino acids (e.g. Ala31, Aib32) (Cabrele et al., 2000) may be a strategy to develop Y1/Y5 selective antagonists.

Although no indications of cooperativity were observed for the Snap Y1/Y1 homodimer pairings, this effect is typically difficult to observe using radioligand binding techniques as both orthosteric sites are identical. The use of fluorescent ligand single cell binding kinetics comparing infinite dilution with the presence of potential allosteric modulators, may be a way to investigate this.. For example both monovalent and bivalent fluorescent GR231118 based antagonists have recently been developed with nanomolar affinity for the Y1 receptor (Mountford et al., 2014). May et al (2007) has suggested that alterations in dissociation rates may better reflect dimer allosterism with conformation changes of protomer A occurring in response to ligand binding at protomer B, with the second site effectively acting as an allosteric modulator (May et al., 2007). This technique has previously been used to illustrate strong cooperative interactions between orthosteric binding sites of adenosine A<sub>3</sub> receptors (May et al., 2011), which was manifested as changes in fluorescent ligand dissociation rates. For example comparison between existing monomeric and dimeric ligand, and the use of the Snap Y1/Y1Y99A co-expressing cells here would allow the potential extent of cooperativity across the dimer interface to be investigated.

Other Y receptor dimer combinations may also have future therapeutic benefit. For example the Y2/Y4 receptor subtypes have been shown to work in concert to regulate PP or PYY induced satiety. Currently the lack of truly subject selective ligands for either protomer makes it difficult to investigate these dimers to the same extent *in vitro*, although there are indications that the introduction of  $\beta$ -amino acids may lead to the synthesis of compounds with high Y4 selectivity in the future (Berlicki et al., 2013). A more general issue for Y2/Y4 ligands (as experienced for the Y2/Y4 obinipitide) is that they are agonists, and are thus prone to limiting side effects such as nausea. Thus, in revealing modified pharmacology observed for Y1/Y5 hetero-dimers, the work in this thesis may offer one approach for re-evaluation of the role and targeting of these receptors in the central control of appetite. Functional dimerisation may explain the failure of current therapies that only target either subtype. The BiFC system therefore offers opportunities to screen and identify Y1/Y5 heterodimer selective ligands in the future, which if efficacious in animal models, may be a valid therapeutic option for the treatment of obesity.

## References

- ABBOTT, C. R., SMALL, C. J., KENNEDY, A. R., NEARY, N. M., SAJEDI, A., GHATEI, M. A. & BLOOM, S. R. 2005. Blockade of the neuropeptide Y Y2 receptor with the specific antagonist BIIE0246 attenuates the effect of endogenous and exogenous peptide YY(3-36) on food intake. *Brain Res*, 1043, 139-44.
- ACHARYA, S., SAAD, Y. & KARNIK, S. S. 1997. Transducin-alpha C-terminal peptide binding site consists of C-D and E-F loops of rhodopsin. *J Biol Chem*, 272, 6519-24.
- ADRIAN, T. E., BLOOM, S. R., HERMANSEN, K. & IVERSEN, J. 1978. Pancreatic polypeptide, glucagon and insulin secretion from the isolated perfused canine pancreas. *Diabetologia*, 14, 413-7.
- AHMED, M. R., ZHAN, X., SONG, X., KOOK, S., GUREVICH, V. V. & GUREVICH, E. V. 2011. Ubiquitin ligase parkin promotes Mdm2-arrestin interaction but inhibits arrestin ubiquitination. *Biochemistry*, 50, 3749-63.
- AKABAYASHI, A., LEVIN, N., PAEZ, X., ALEXANDER, J. T. & LEIBOWITZ, S. F. 1994. Hypothalamic neuropeptide Y and its gene expression: relation to light/dark cycle and circulating corticosterone. *Mol Cell Neurosci*, 5, 210-8.
- AKERBERG, H., FALLMAR, H., SJODIN, P., BOUKHARTA, L., GUTIERREZ-DE-TERAN, H., LUNDELL, I., MOHELL, N. & LARHAMMAR, D. 2010. Mutagenesis of human neuropeptide Y/peptide YY receptor Y2 reveals additional differences to Y1 in interactions with highly conserved ligand positions. *Regul Pept*, 163, 120-9.
- ALBIZU, L., COTTET, M., KRALIKOVA, M., STOEVE, S., SEYER, R., BRABET, I., ROUX, T., BAZIN, H., BOURRIER, E., LAMARQUE, L., BRETON, C., RIVES, M. L., NEWMAN, A., JAVITCH, J., TRINQUET, E., MANNING, M., PIN, J. P., MOUILLAC, B. & DURROUX, T. 2010. Time-resolved FRET between GPCR ligands reveals oligomers in native tissues. *Nat Chem Biol*, 6, 587-94.
- ALLISON, S. J. & HERZOG, H. 2006. NPY and bone. *EXS*, 171-82.
- ANGERS, S., SALAHPOUR, A. & BOUVIER, M. 2002. Dimerization: an emerging concept for G protein-coupled receptor ontogeny and function. *Annu Rev Pharmacol Toxicol*, 42, 409-35.
- ANGERS, S., SALAHPOUR, A., JOLY, E., HILAIRET, S., CHELSKY, D., DENNIS, M. & BOUVIER, M. 2000. Detection of beta 2-adrenergic receptor dimerization in living cells using bioluminescence resonance energy transfer (BRET). *Proc Natl Acad Sci U S A*, 97, 3684-9.
- ASAKAWA, A., INUI, A., UENO, N., FUJIMIYA, M., FUJINO, M. A. & KASUGA, M. 1999. Mouse pancreatic polypeptide modulates food intake, while not influencing anxiety in mice. *Peptides*, 20, 1445-8.
- AULD, D. S., JOHNSON, R. L., ZHANG, Y. Q., VEITH, H., JADHAV, A., YASGAR, A., SIMEONOV, A., ZHENG, W., MARTINEZ, E. D., WESTWICK, J. K., AUSTIN, C. P. & INGLESE, J. 2006. Fluorescent protein-based cellular assays analyzed by laser-scanning microplate cytometry in 1536-well plate format. *Methods Enzymol*, 414, 566-89.
- AVISSAR, S., AMITAI, G. & SOKOLOVSKY, M. 1983. Oligomeric structure of muscarinic receptors is shown by photoaffinity labeling: subunit

- assembly may explain high- and low-affinity agonist states. *Proc Natl Acad Sci U S A*, 80, 156-9.
- AXELROD, D., KOPPEL, D. E., SCHLESSINGER, J., ELSON, E. & WEBB, W. W. 1976. Mobility measurement by analysis of fluorescence photobleaching recovery kinetics. *Biophys J*, 16, 1055-69.
- AYOUB, M. A., COUTURIER, C., LUCAS-MEUNIER, E., ANGERS, S., FOSSIER, P., BOUVIER, M. & JOCKERS, R. 2002. Monitoring of ligand-independent dimerization and ligand-induced conformational changes of melatonin receptors in living cells by bioluminescence resonance energy transfer. *J Biol Chem*, 277, 21522-8.
- AYOUB, M. A. & PFLEGER, K. D. 2010. Recent advances in bioluminescence resonance energy transfer technologies to study GPCR heteromerization. *Curr Opin Pharmacol*, 10, 44-52.
- AZZI, M., CHAREST, P. G., ANGERS, S., ROUSSEAU, G., KOHOUT, T., BOUVIER, M. & PINEYRO, G. 2003. Beta-arrestin-mediated activation of MAPK by inverse agonists reveals distinct active conformations for G protein-coupled receptors. *Proc Natl Acad Sci U S A*, 100, 11406-11.
- BABILON, S., MORL, K. & BECK-SICKINGER, A. G. 2013. Towards improved receptor targeting: anterograde transport, internalization and postendocytic trafficking of neuropeptide Y receptors. *Biol Chem*, 394, 921-36.
- BADER, R., BETTIO, A., BECK-SICKINGER, A. G. & ZERBE, O. 2001. Structure and dynamics of micelle-bound neuropeptide Y: comparison with unligated NPY and implications for receptor selection. *J Mol Biol*, 305, 307-29.
- BAI, F. L., YAMANO, M., SHIOTANI, Y., EMSON, P. C., SMITH, A. D., POWELL, J. F. & TOHYAMA, M. 1985. An arcuate-paraventricular and -dorsomedial hypothalamic neuropeptide Y-containing system which lacks noradrenaline in the rat. *Brain Res*, 331, 172-5.
- BAILLIE, G. S., SOOD, A., MCPHEE, I., GALL, I., PERRY, S. J., LEFKOWITZ, R. J. & HOUSLAY, M. D. 2003. beta-Arrestin-mediated PDE4 cAMP phosphodiesterase recruitment regulates beta-adrenoceptor switching from Gs to Gi. *Proc Natl Acad Sci U S A*, 100, 940-5.
- BAKER, J. G. 2005. The selectivity of beta-adrenoceptor antagonists at the human beta1, beta2 and beta3 adrenoceptors. *Br J Pharmacol*, 144, 317-22.
- BAKER, J. G. 2010. The selectivity of beta-adrenoceptor agonists at human beta1-, beta2- and beta3-adrenoceptors. *Br J Pharmacol*, 160, 1048-61.
- BALARAMAN, G. S., BHATTACHARYA, S. & VAIDEHI, N. 2010. Structural insights into conformational stability of wild-type and mutant beta1-adrenergic receptor. *Biophys J*, 99, 568-77.
- BALASUBRAMANIAM, A., MULLINS, D. E., LIN, S., ZHAI, W., TAO, Z., DHAWAN, V. C., GUZZI, M., KNITTEL, J. J., SLACK, K., HERZOG, H. & PARKER, E. M. 2006. Neuropeptide Y (NPY) Y4 receptor selective agonists based on NPY(32-36): development of an anorectic Y4 receptor selective agonist with picomolar affinity. *J Med Chem*, 49, 2661-5.
- BALASUBRAMANIAM, A., SHERIFF, S., JOHNSON, M. E., PRABHAKARAN, M., HUANG, Y., FISCHER, J. E. & CHANCE, W. T. 1994. [D-TRP32]neuropeptide Y: a competitive antagonist of NPY in rat hypothalamus. *J Med Chem*, 37, 811-5.

- BALASUBRAMANIAM, A. A. 1997. Neuropeptide Y family of hormones: receptor subtypes and antagonists. *Peptides*, 18, 445-57.
- BALLESTEROS, J. & WEINSTEIN, H. 1995. *Integrated methods for the construction of three-dimensional models and computational probing of structure-function relations in G protein-coupled receptors.*
- BALLESTEROS, J. A., JENSEN, A. D., LIAPAKIS, G., RASMUSSEN, S. G., SHI, L., GETHER, U. & JAVITCH, J. A. 2001. Activation of the beta 2-adrenergic receptor involves disruption of an ionic lock between the cytoplasmic ends of transmembrane segments 3 and 6. *J Biol Chem*, 276, 29171-7.
- BANCAUD, A., HUET, S., DAIGLE, N., MOZZICONACCI, J., BEAUDOUIN, J. & ELLENBERG, J. 2009. Molecular crowding affects diffusion and binding of nuclear proteins in heterochromatin and reveals the fractal organization of chromatin. *EMBO J*, 28, 3785-98.
- BANERES, J. L. & PARELLO, J. 2003. Structure-based analysis of GPCR function: evidence for a novel pentameric assembly between the dimeric leukotriene B4 receptor BLT1 and the G-protein. *J Mol Biol*, 329, 815-29.
- BARAK, L. S., FERGUSON, S. S., ZHANG, J. & CARON, M. G. 1997a. A beta-arrestin/green fluorescent protein biosensor for detecting G protein-coupled receptor activation. *J Biol Chem*, 272, 27497-500.
- BARAK, L. S., FERGUSON, S. S., ZHANG, J., MARTENSON, C., MEYER, T. & CARON, M. G. 1997b. Internal trafficking and surface mobility of a functionally intact beta2-adrenergic receptor-green fluorescent protein conjugate. *Mol Pharmacol*, 51, 177-84.
- BARAK, L. S., TIBERI, M., FREEDMAN, N. J., KWATRA, M. M., LEFKOWITZ, R. J. & CARON, M. G. 1994. A highly conserved tyrosine residue in G protein-coupled receptors is required for agonist-mediated beta 2-adrenergic receptor sequestration. *J Biol Chem*, 269, 2790-5.
- BARANOWSKA, B., WOLINSKA-WITORT, E., MARTYNSKA, L., CHMIELOWSKA, M. & BARANOWSKA-BIK, A. 2005. Plasma orexin A, orexin B, leptin, neuropeptide Y (NPY) and insulin in obese women. *Neuro Endocrinol Lett*, 26, 293-6.
- BARD, J. A., WALKER, M. W., BRANCHEK, T. A. & WEINSHANK, R. L. 1995. Cloning and functional expression of a human Y4 subtype receptor for pancreatic polypeptide, neuropeptide Y, and peptide YY. *J Biol Chem*, 270, 26762-5.
- BARKI-HARRINGTON, L., LUTTRELL, L. M. & ROCKMAN, H. A. 2003. Dual inhibition of beta-adrenergic and angiotensin II receptors by a single antagonist: a functional role for receptor-receptor interaction in vivo. *Circulation*, 108, 1611-8.
- BATTERHAM, R. L., COHEN, M. A., ELLIS, S. M., LE ROUX, C. W., WITHERS, D. J., FROST, G. S., GHATEI, M. A. & BLOOM, S. R. 2003a. Inhibition of food intake in obese subjects by peptide YY3-36. *N Engl J Med*, 349, 941-8.
- BATTERHAM, R. L., COWLEY, M. A., SMALL, C. J., HERZOG, H., COHEN, M. A., DAKIN, C. L., WREN, A. M., BRYNES, A. E., LOW, M. J., GHATEI, M. A., CONE, R. D. & BLOOM, S. R. 2002. Gut hormone PYY(3-36) physiologically inhibits food intake. *Nature*, 418, 650-4.
- BATTERHAM, R. L., HEFFRON, H., KAPOOR, S., CHIVERS, J. E., CHANDARANA, K., HERZOG, H., LE ROUX, C. W., THOMAS, E. L., BELL, J. D. &

- WITHERS, D. J. 2006. Critical role for peptide YY in protein-mediated satiation and body-weight regulation. *Cell Metab*, 4, 223-33.
- BATTERHAM, R. L., LE ROUX, C. W., COHEN, M. A., PARK, A. J., ELLIS, S. M., PATTERSON, M., FROST, G. S., GHATEI, M. A. & BLOOM, S. R. 2003b. Pancreatic polypeptide reduces appetite and food intake in humans. *J Clin Endocrinol Metab*, 88, 3989-92.
- BAYBURT, T. H., LEITZ, A. J., XIE, G., OPRIAN, D. D. & SLIGAR, S. G. 2007. Transducin activation by nanoscale lipid bilayers containing one and two rhodopsins. *J Biol Chem*, 282, 14875-81.
- BAYBURT, T. H., VISHNIVETSKIY, S. A., MCLEAN, M. A., MORIZUMI, T., HUANG, C. C., TESMER, J. J., ERNST, O. P., SLIGAR, S. G. & GUREVICH, V. V. 2011. Monomeric rhodopsin is sufficient for normal rhodopsin kinase (GRK1) phosphorylation and arrestin-1 binding. *J Biol Chem*, 286, 1420-8.
- BENOVIC, J. L. & VON ZASTROW, M. 2014. Editorial overview: Cell regulation: The ins and outs of G protein-coupled receptors. *Curr Opin Cell Biol*, 27, v-vi.
- BERGLUND, M. M., LUNDELL, I., ERIKSSON, H., SOLL, R., BECK-SICKINGER, A. G. & LARHAMMAR, D. 2001. Studies of the human, rat, and guinea pig Y4 receptors using neuropeptide Y analogues and two distinct radioligands. *Peptides*, 22, 351-6.
- BERGLUND, M. M., SCHOBER, D. A., ESTERMAN, M. A. & GEHLERT, D. R. 2003a. Neuropeptide Y Y4 receptor homodimers dissociate upon agonist stimulation. *J Pharmacol Exp Ther*, 307, 1120-6.
- BERGLUND, M. M., SCHOBER, D. A., STATNICK, M. A., MCDONALD, P. H. & GEHLERT, D. R. 2003b. The use of bioluminescence resonance energy transfer 2 to study neuropeptide Y receptor agonist-induced beta-arrestin 2 interaction. *J Pharmacol Exp Ther*, 306, 147-56.
- BERLICKI, L., KASKE, M., GUTIERREZ-ABAD, R., BERNHARDT, G., ILLA, O., ORTUNO, R. M., CABRELE, C., BUSCHAUER, A. & REISER, O. 2013. Replacement of Thr32 and Gln34 in the C-terminal neuropeptide Y fragment 25-36 by cis-cyclobutane and cis-cyclopentane beta-amino acids shifts selectivity toward the Y(4) receptor. *J Med Chem*, 56, 8422-31.
- BERNTSON, G. G., ZIPF, W. B., O'DORISIO, T. M., HOFFMAN, J. A. & CHANCE, R. E. 1993. Pancreatic polypeptide infusions reduce food intake in Prader-Willi syndrome. *Peptides*, 14, 497-503.
- BERTHOUZE, M., RIVAIL, L., LUCAS, A., AYOUB, M. A., RUSSO, O., SICSIC, S., FISCHMEISTER, R., BERQUE-BESTEL, I., JOCKERS, R. & LEZOUALC'H, F. 2007. Two transmembrane Cys residues are involved in 5-HT4 receptor dimerization. *Biochem Biophys Res Commun*, 356, 642-7.
- BHATTACHARYA, S., HALL, S. E. & VAIDEHI, N. 2008. Agonist-induced conformational changes in bovine rhodopsin: insight into activation of G-protein-coupled receptors. *J Mol Biol*, 382, 539-55.
- BIRDSALL, N. J. 2010. Class A GPCR heterodimers: evidence from binding studies. *Trends Pharmacol Sci*, 31, 499-508.
- BLOCK, M. H., BOYER, S., BRAILSFORD, W., BRITAIN, D. R., CARROLL, D., CHAPMAN, S., CLARKE, D. S., DONALD, C. S., FOOTE, K. M., GODFREY, L., LADNER, A., MARSHAM, P. R., MASTERS, D. J., MEE, C. D., O'DONOVAN, M. R., PEASE, J. E., PICKUP, A. G., RAYNER, J. W., ROBERTS, A., SCHOFIELD, P., SULEMAN, A. & TURNBULL, A. V. 2002.

- Discovery and optimization of a series of carbazole ureas as NPY5 antagonists for the treatment of obesity. *J Med Chem*, 45, 3509-23.
- BLUME, L. C., BASS, C. E., CHILDERS, S. R., DALTON, G. D., ROBERTS, D. C., RICHARDSON, J. M., XIAO, R., SELLEY, D. E. & HOWLETT, A. C. 2013. Striatal CB1 and D2 receptors regulate expression of each other, CRIP1A and delta opioid systems. *J Neurochem*, 124, 808-20.
- BLUNDELL, T. L., PITTS, J. E., TICKLE, I. J., WOOD, S. P. & WU, C. W. 1981. X-ray analysis (1.4-Å resolution) of avian pancreatic polypeptide: Small globular protein hormone. *Proc Natl Acad Sci U S A*, 78, 4175-9.
- BOCKENHAUER, S., FURSTENBERG, A., YAO, X. J., KOBILKA, B. K. & MOERNER, W. E. 2011. Conformational dynamics of single G protein-coupled receptors in solution. *J Phys Chem B*, 115, 13328-38.
- BOEY, D., HEILBRONN, L., SAINSBURY, A., LAYBUTT, R., KRIKETOS, A., HERZOG, H. & CAMPBELL, L. V. 2006. Low serum PYY is linked to insulin resistance in first-degree relatives of subjects with type 2 diabetes. *Neuropeptides*, 40, 317-24.
- BOHME, I., STICHEL, J., WALTHER, C., MORL, K. & BECK-SICKINGER, A. G. 2008. Agonist induced receptor internalization of neuropeptide Y receptor subtypes depends on third intracellular loop and C-terminus. *Cell Signal*, 20, 1740-9.
- BOROWSKY, B., WALKER, M. W., BARD, J., WEINSHANK, R. L., LAZ, T. M., VAYSSE, P., BRANCHEK, T. A. & GERALD, C. 1998. Molecular biology and pharmacology of multiple NPY Y5 receptor species homologs. *Regul Pept*, 75-76, 45-53.
- BOUVIER, M., HAUSDORFF, W. P., DE BLASI, A., O'DOWD, B. F., KOBILKA, B. K., CARON, M. G. & LEFKOWITZ, R. J. 1988. Removal of phosphorylation sites from the beta 2-adrenergic receptor delays onset of agonist-promoted desensitization. *Nature*, 333, 370-3.
- BRAUN, L., CHRISTOPHE, T. & BOULAY, F. 2003. Phosphorylation of key serine residues is required for internalization of the complement 5a (C5a) anaphylatoxin receptor via a beta-arrestin, dynamin, and clathrin-dependent pathway. *J Biol Chem*, 278, 4277-85.
- BREIT, A., LAGACE, M. & BOUVIER, M. 2004. Hetero-oligomerization between beta2- and beta3-adrenergic receptors generates a beta-adrenergic signaling unit with distinct functional properties. *J Biol Chem*, 279, 28756-65.
- BRIDDON, S. J., GANDIA, J., AMARAL, O. B., FERRE, S., LLUIS, C., FRANCO, R., HILL, S. J. & CIRUELA, F. 2008. Plasma membrane diffusion of G protein-coupled receptor oligomers. *Biochim Biophys Acta*, 1783, 2262-8.
- BRIDDON, S. J. & HILL, S. J. 2007. Pharmacology under the microscope: the use of fluorescence correlation spectroscopy to determine the properties of ligand-receptor complexes. *Trends Pharmacol Sci*, 28, 637-45.
- BRIDDON, S. J., MIDDLETON, R. J., CORDEAUX, Y., FLAVIN, F. M., WEINSTEIN, J. A., GEORGE, M. W., KELLAM, B. & HILL, S. J. 2004a. Quantitative analysis of the formation and diffusion of A1-adenosine receptor-antagonist complexes in single living cells. *Proc Natl Acad Sci U S A*, 101, 4673-8.
- BRIDDON, S. J., MIDDLETON, R. J., YATES, A. S., GEORGE, M. W., KELLAM, B. & HILL, S. J. 2004b. Application of fluorescence correlation spectroscopy to the measurement of agonist binding to a G-protein

- coupled receptor at the single cell level. *Faraday Discuss*, 126, 197-207; discussion 245-54.
- BROCK, C., OUESLATI, N., SOLER, S., BOUDIER, L., RONDARD, P. & PIN, J. P. 2007. Activation of a dimeric metabotropic glutamate receptor by intersubunit rearrangement. *J Biol Chem*, 282, 33000-8.
- BRZOBOHATY, B. & KOVAC, L. 1986. Factors enhancing genetic transformation of intact yeast cells modify cell wall porosity. *J Gen Microbiol*, 132, 3089-93.
- BUSILLO, J. M., ARMANDO, S., SENGUPTA, R., MEUCCI, O., BOUVIER, M. & BENOVIC, J. L. 2010. Site-specific phosphorylation of CXCR4 is dynamically regulated by multiple kinases and results in differential modulation of CXCR4 signaling. *J Biol Chem*, 285, 7805-17.
- BUTCHER, A. J., PRIHANDOKO, R., KONG, K. C., MCWILLIAMS, P., EDWARDS, J. M., BOTTRILL, A., MISTRY, S. & TOBIN, A. B. 2011. Differential G-protein-coupled receptor phosphorylation provides evidence for a signaling bar code. *J Biol Chem*, 286, 11506-18.
- CABANTOUS, S. & WALDO, G. S. 2006. In vivo and in vitro protein solubility assays using split GFP. *Nat Methods*, 3, 845-54.
- CABELLO, N., GANDIA, J., BERTARELLI, D. C., WATANABE, M., LLUIS, C., FRANCO, R., FERRE, S., LUJAN, R. & CIRUELA, F. 2009. Metabotropic glutamate type 5, dopamine D2 and adenosine A2a receptors form higher-order oligomers in living cells. *J Neurochem*, 109, 1497-507.
- CABRELE, C. & BECK-SICKINGER, A. G. 2000. Molecular characterization of the ligand-receptor interaction of the neuropeptide Y family. *J Pept Sci*, 6, 97-122.
- CABRELE, C., LANGER, M., BADER, R., WIELAND, H. A., DOODS, H. N., ZERBE, O. & BECK-SICKINGER, A. G. 2000. The first selective agonist for the neuropeptide YY5 receptor increases food intake in rats. *J Biol Chem*, 275, 36043-8.
- CALEBIRO, D., RIEKEN, F., WAGNER, J., SUNGKAWORN, T., ZABEL, U., BORZI, A., COCUCCI, E., ZURN, A. & LOHSE, M. J. 2013. Single-molecule analysis of fluorescently labeled G-protein-coupled receptors reveals complexes with distinct dynamics and organization. *Proc Natl Acad Sci U S A*, 110, 743-8.
- CALLEN, L., MORENO, E., BARROSO-CHINEA, P., MORENO-DELGADO, D., CORTES, A., MALLOL, J., CASADO, V., LANCIEGO, J. L., FRANCO, R., LLUIS, C., CANELA, E. I. & MCCORMICK, P. J. 2012. Cannabinoid receptors CB1 and CB2 form functional heteromers in brain. *J Biol Chem*, 287, 20851-65.
- CANALS, M., BURGUENO, J., MARCELLINO, D., CABELLO, N., CANELA, E. I., MALLOL, J., AGNATI, L., FERRE, S., BOUVIER, M., FUXE, K., CIRUELA, F., LLUIS, C. & FRANCO, R. 2004. Homodimerization of adenosine A2A receptors: qualitative and quantitative assessment by fluorescence and bioluminescence energy transfer. *J Neurochem*, 88, 726-34.
- CANALS, M., MARCELLINO, D., FANELLI, F., CIRUELA, F., DE BENEDETTI, P., GOLDBERG, S. R., NEVE, K., FUXE, K., AGNATI, L. F., WOODS, A. S., FERRE, S., LLUIS, C., BOUVIER, M. & FRANCO, R. 2003. Adenosine A2A-dopamine D2 receptor-receptor heteromerization: qualitative and quantitative assessment by fluorescence and bioluminescence energy transfer. *J Biol Chem*, 278, 46741-9.
- CASADO, V., CORTES, A., MALLOL, J., PEREZ-CAPOTE, K., FERRE, S., LLUIS, C., FRANCO, R. & CANELA, E. I. 2009a. GPCR homomers and

- heteromers: a better choice as targets for drug development than GPCR monomers? *Pharmacol Ther*, 124, 248-57.
- CASADO, V., FERRADA, C., BONAVENTURA, J., GRACIA, E., MALLOL, J., CANELA, E. I., LLUIS, C., CORTES, A. & FRANCO, R. 2009b. Useful pharmacological parameters for G-protein-coupled receptor homodimers obtained from competition experiments. Agonist-antagonist binding modulation. *Biochem Pharmacol*, 78, 1456-63.
- CERDA-REVERTER, J. M. & LARHAMMAR, D. 2000. Neuropeptide Y family of peptides: structure, anatomical expression, function, and molecular evolution. *Biochem Cell Biol*, 78, 371-92.
- CEZANNE, L., LECAT, S., LAGANE, B., MILLOT, C., VOLLMER, J. Y., MATTHES, H., GALZI, J. L. & LOPEZ, A. 2004. Dynamic confinement of NK2 receptors in the plasma membrane. Improved FRAP analysis and biological relevance. *J Biol Chem*, 279, 45057-67.
- CHABRE, M., DETERRE, P. & ANTONNY, B. 2009. The apparent cooperativity of some GPCRs does not necessarily imply dimerization. *Trends Pharmacol Sci*, 30, 182-7.
- CHABRE, M. & LE MAIRE, M. 2005. Monomeric G-protein-coupled receptor as a functional unit. *Biochemistry*, 44, 9395-403.
- CHANDRASEKERA, P. C., WAN, T. C., GIZEWSKI, E. T., AUCHAMPACH, J. A. & LASLEY, R. D. 2013. Adenosine A1 receptors heterodimerize with beta1- and beta2-adrenergic receptors creating novel receptor complexes with altered G protein coupling and signaling. *Cell Signal*, 25, 736-42.
- CHEN, Y., MULLER, J. D., SO, P. T. & GRATTON, E. 1999. The photon counting histogram in fluorescence fluctuation spectroscopy. *Biophys J*, 77, 553-67.
- CHEN, Y. J., OLDFIELD, S., BUTCHER, A. J., TOBIN, A. B., SAXENA, K., GUREVICH, V. V., BENOVIC, J. L., HENDERSON, G. & KELLY, E. 2013. Identification of phosphorylation sites in the COOH-terminal tail of the mu-opioid receptor. *J Neurochem*, 124, 189-99.
- CHENG, Z. J. & MILLER, L. J. 2001. Agonist-dependent dissociation of oligomeric complexes of G protein-coupled cholecystokinin receptors demonstrated in living cells using bioluminescence resonance energy transfer. *J Biol Chem*, 276, 48040-7.
- CHEREZOV, V., ROSENBAUM, D. M., HANSON, M. A., RASMUSSEN, S. G., THIAN, F. S., KOBILKA, T. S., CHOI, H. J., KUHN, P., WEIS, W. I., KOBILKA, B. K. & STEVENS, R. C. 2007. High-resolution crystal structure of an engineered human beta2-adrenergic G protein-coupled receptor. *Science*, 318, 1258-65.
- CHERFELS, J. & ZEGHOUF, M. 2013. Regulation of small GTPases by GEFs, GAPs, and GDIs. *Physiol Rev*, 93, 269-309.
- CHEUNG, B. M., CHEUNG, T. T. & SAMARANAYAKE, N. R. 2013. Safety of antiobesity drugs. *Ther Adv Drug Saf*, 4, 171-81.
- CHIEN, E. Y., LIU, W., ZHAO, Q., KATRITCH, V., HAN, G. W., HANSON, M. A., SHI, L., NEWMAN, A. H., JAVITCH, J. A., CHEREZOV, V. & STEVENS, R. C. 2010. Structure of the human dopamine D3 receptor in complex with a D2/D3 selective antagonist. *Science*, 330, 1091-5.
- CHUN, L. S., FREE, R. B., DOYLE, T. B., HUANG, X. P., RANKIN, M. L. & SIBLEY, D. R. 2013. D1-D2 dopamine receptor synergy promotes calcium signaling via multiple mechanisms. *Mol Pharmacol*, 84, 190-200.

- CHUNG, K. Y., RASMUSSEN, S. G., LIU, T., LI, S., DEVREE, B. T., CHAE, P. S., CALINSKI, D., KOBILKA, B. K., WOODS, V. L., JR. & SUNAHARA, R. K. 2011. Conformational changes in the G protein Gs induced by the beta2 adrenergic receptor. *Nature*, 477, 611-5.
- CIRUELA, F., CASADO, V., RODRIGUES, R. J., LUJAN, R., BURGUENO, J., CANALS, M., BORYCZ, J., REBOLA, N., GOLDBERG, S. R., MALLOL, J., CORTES, A., CANELA, E. I., LOPEZ-GIMENEZ, J. F., MILLIGAN, G., LLUIS, C., CUNHA, R. A., FERRE, S. & FRANCO, R. 2006. Presynaptic control of striatal glutamatergic neurotransmission by adenosine A1-A2A receptor heteromers. *J Neurosci*, 26, 2080-7.
- CIRUELA, F., VALLANO, A., CUFFI, M. L., CARBONELL, L., SANCHEZ, S., ARNAU, J. M., TASCA, C., FERNANDEZ-DUENAS, V. & GOMEZ-SOLER, M. 2014. Deciphering G Protein-Coupled Receptor Biology With Fluorescence-Based Methods. *Curr Pharm Biotechnol*.
- CLARK, J. T., KALRA, P. S., CROWLEY, W. R. & KALRA, S. P. 1984. Neuropeptide Y and human pancreatic polypeptide stimulate feeding behavior in rats. *Endocrinology*, 115, 427-9.
- COHEN, F. R., LAZARENO, S. & BIRDSALL, N. J. 1996. The effects of saponin on the binding and functional properties of the human adenosine A1 receptor. *Br J Pharmacol*, 117, 1521-9.
- CORDEAUX, Y., BRIDDON, S. J., ALEXANDER, S. P., KELLAM, B. & HILL, S. J. 2008. Agonist-occupied A3 adenosine receptors exist within heterogeneous complexes in membrane microdomains of individual living cells. *FASEB J*, 22, 850-60.
- CORMACK, B. P., VALDIVIA, R. H. & FALKOW, S. 1996. FACS-optimized mutants of the green fluorescent protein (GFP). *Gene*, 173, 33-8.
- CORRIDEN, R., KILPATRICK, L. E., KELLAM, B., BRIDDON, S. J. & HILL, S. J. 2014. Kinetic analysis of antagonist-occupied adenosine-A3 receptors within membrane microdomains of individual cells provides evidence of receptor dimerization and allostereism. *FASEB J*.
- COX, H. M. 2007. Neuropeptide Y receptors; antiseecretory control of intestinal epithelial function. *Auton Neurosci*, 133, 76-85.
- CRAMERI, A., WHITEHORN, E. A., TATE, E. & STEMMER, W. P. 1996. Improved green fluorescent protein by molecular evolution using DNA shuffling. *Nat Biotechnol*, 14, 315-9.
- CRISCIONE, L., RIGOLLIER, P., BATZL-HARTMANN, C., RUEGER, H., STRICKER-KRONGRAD, A., WYSS, P., BRUNNER, L., WHITEBREAD, S., YAMAGUCHI, Y., GERALD, C., HEURICH, R. O., WALKER, M. W., CHIESI, M., SCHILLING, W., HOFBAUER, K. G. & LEVENS, N. 1998. Food intake in free-feeding and energy-deprived lean rats is mediated by the neuropeptide Y5 receptor. *J Clin Invest*, 102, 2136-45.
- CVEJIC, S. & DEVI, L. A. 1997. Dimerization of the delta opioid receptor: implication for a role in receptor internalization. *J Biol Chem*, 272, 26959-64.
- DAMIAN, M., MARY, S., MARTIN, A., PIN, J. P. & BANERES, J. L. 2008. G protein activation by the leukotriene B4 receptor dimer. Evidence for an absence of trans-activation. *J Biol Chem*, 283, 21084-92.
- DANIELS, A. J., GRIZZLE, M. K., WIARD, R. P., MATTHEWS, J. E. & HEYER, D. 2002. Food intake inhibition and reduction in body weight gain in lean and obese rodents treated with GW438014A, a potent and selective NPY-Y5 receptor antagonist. *Regul Pept*, 106, 47-54.

- DANIELS, A. J., MATTHEWS, J. E., SLEPETIS, R. J., JANSEN, M., VIVEROS, O. H., TADEPALLI, A., HARRINGTON, W., HEYER, D., LANDAVAZO, A., LEBAN, J. J. & SPALTENSTEIN, A. 1995. High-affinity neuropeptide Y receptor antagonists. *Proc Natl Acad Sci U S A*, 92, 9067-71.
- DANIELS, D. J., KULKARNI, A., XIE, Z., BHUSHAN, R. G. & PORTOGHESE, P. S. 2005a. A bivalent ligand (KDAN-18) containing delta-antagonist and kappa-agonist pharmacophores bridges delta2 and kappa1 opioid receptor phenotypes. *J Med Chem*, 48, 1713-6.
- DANIELS, D. J., LENARD, N. R., ETIENNE, C. L., LAW, P. Y., ROERIG, S. C. & PORTOGHESE, P. S. 2005b. Opioid-induced tolerance and dependence in mice is modulated by the distance between pharmacophores in a bivalent ligand series. *Proc Natl Acad Sci U S A*, 102, 19208-13.
- DE, A., LOENING, A. M. & GAMBHIR, S. S. 2007. An improved bioluminescence resonance energy transfer strategy for imaging intracellular events in single cells and living subjects. *Cancer Res*, 67, 7175-83.
- DEUPI, X. & STANDFUSS, J. 2011. Structural insights into agonist-induced activation of G-protein-coupled receptors. *Curr Opin Struct Biol*, 21, 541-51.
- DEWIRE, S. M., AHN, S., LEFKOWITZ, R. J. & SHENOY, S. K. 2007. Beta-arrestins and cell signaling. *Annu Rev Physiol*, 69, 483-510.
- DIEKMANN, S. & HOISCHEN, C. 2014. Biomolecular dynamics and binding studies in the living cell. *Phys Life Rev*, 11, 1-30.
- DING, X., ZHAO, X. & WATTS, A. 2013. G-protein-coupled receptor structure, ligand binding and activation as studied by solid-state NMR spectroscopy. *Biochem J*, 450, 443-57.
- DINGER, M. C., BADER, J. E., KOBOR, A. D., KRETZSCHMAR, A. K. & BECK-SICKINGER, A. G. 2003. Homodimerization of neuropeptide y receptors investigated by fluorescence resonance energy transfer in living cells. *J Biol Chem*, 278, 10562-71.
- DOAN, T., MENDEZ, A., DETWILER, P. B., CHEN, J. & RIEKE, F. 2006. Multiple phosphorylation sites confer reproducibility of the rod's single-photon responses. *Science*, 313, 530-3.
- DOHERTY, G. J. & MCMAHON, H. T. 2009. Mechanisms of endocytosis. *Annu Rev Biochem*, 78, 857-902.
- DONALDSON, J., BROWN, A. M. & HILL, S. J. 1989. Temporal changes in the calcium-dependence of the histamine H1-receptor-stimulation of cyclic AMP accumulation in guinea-pig cerebral cortex. *Br J Pharmacol*, 98, 1365-75.
- DORE, A. S., OKRASA, K., PATEL, J. C., SERRANO-VEGA, M., BENNETT, K., COOKE, R. M., ERREY, J. C., JAZAYERI, A., KHAN, S., TEHAN, B., WEIR, M., WIGGIN, G. R. & MARSHALL, F. H. 2014. Structure of class C GPCR metabotropic glutamate receptor 5 transmembrane domain. *Nature*, 511, 557-62.
- DORE, A. S., ROBERTSON, N., ERREY, J. C., NG, I., HOLLENSTEIN, K., TEHAN, B., HURRELL, E., BENNETT, K., CONGREVE, M., MAGNANI, F., TATE, C. G., WEIR, M. & MARSHALL, F. H. 2011. Structure of the adenosine A(2A) receptor in complex with ZM241385 and the xanthines XAC and caffeine. *Structure*, 19, 1283-93.
- DORSCH, S., KLOTZ, K. N., ENGELHARDT, S., LOHSE, M. J. & BUNEMANN, M. 2009. Analysis of receptor oligomerization by FRAP microscopy. *Nat Methods*, 6, 225-30.

- DUMONT, Y., CADIEUX, A., DOODS, H., FOURNIER, A. & QUIRION, R. 2000. Potent and selective tools to investigate neuropeptide Y receptors in the central and peripheral nervous systems: BIB03304 (Y1) and CGP71683A (Y5). *Can J Physiol Pharmacol*, 78, 116-25.
- DUMONT, Y., JACQUES, D., BOUCHARD, P. & QUIRION, R. 1998. Species differences in the expression and distribution of the neuropeptide Y Y1, Y2, Y4, and Y5 receptors in rodents, guinea pig, and primates brains. *J Comp Neurol*, 402, 372-84.
- DUMONT, Y. & QUIRION, R. 2000. [(125)I]-GR231118: a high affinity radioligand to investigate neuropeptide Y Y(1) and Y(4) receptors. *Br J Pharmacol*, 129, 37-46.
- DUMONT, Y., THAKUR, M., BECK-SICKINGER, A., FOURNIER, A. & QUIRION, R. 2003. Development and characterization of a highly selective neuropeptide Y Y5 receptor agonist radioligand: [125I][hPP1-17, Ala31, Aib32]NPY. *Br J Pharmacol*, 139, 1360-8.
- DUNHAM, T. D. & FARRENS, D. L. 1999. Conformational changes in rhodopsin. Movement of helix f detected by site-specific chemical labeling and fluorescence spectroscopy. *J Biol Chem*, 274, 1683-90.
- EKBLAD, E. & SUNDLER, F. 2002. Distribution of pancreatic polypeptide and peptide YY. *Peptides*, 23, 251-61.
- EL MOUSTAINE, D., GRANIER, S., DOUMAZANE, E., SCHOLLER, P., RAHMEH, R., BRON, P., MOUILLAC, B., BANERES, J. L., RONDARD, P. & PIN, J. P. 2012. Distinct roles of metabotropic glutamate receptor dimerization in agonist activation and G-protein coupling. *Proc Natl Acad Sci U S A*, 109, 16342-7.
- ELLIS, J., PEDIANI, J. D., CANALS, M., MILASTA, S. & MILLIGAN, G. 2006. Orexin-1 receptor-cannabinoid CB1 receptor heterodimerization results in both ligand-dependent and -independent coordinated alterations of receptor localization and function. *J Biol Chem*, 281, 38812-24.
- ELMQUIST, J. K., AHIMA, R. S., ELIAS, C. F., FLIER, J. S. & SAPER, C. B. 1998. Leptin activates distinct projections from the dorsomedial and ventromedial hypothalamic nuclei. *Proc Natl Acad Sci U S A*, 95, 741-6.
- ERONDU, N., GANTZ, I., MUSSER, B., SURYAWANSHI, S., MALLICK, M., ADDY, C., COTE, J., BRAY, G., FUJIOKA, K., BAYS, H., HOLLANDER, P., SANABRIA-BOHORQUEZ, S. M., ENG, W., LANGSTROM, B., HARGREAVES, R. J., BURNS, H. D., KANATANI, A., FUKAMI, T., MACNEIL, D. J., GOTTESDIENER, K. M., AMATRUDA, J. M., KAUFMAN, K. D. & HEYMSFIELD, S. B. 2006. Neuropeptide Y5 receptor antagonism does not induce clinically meaningful weight loss in overweight and obese adults. *Cell Metab*, 4, 275-82.
- ESCRIBA, P. V., WEDEGAERTNER, P. B., GONI, F. M. & VOGLER, O. 2007. Lipid-protein interactions in GPCR-associated signaling. *Biochim Biophys Acta*, 1768, 836-52.
- FABRY, M., LANGER, M., ROTHEN-RUTISHAUSER, B., WUNDERLI-ALLENSPACH, H., HOCKER, H. & BECK-SICKINGER, A. G. 2000. Monitoring of the internalization of neuropeptide Y on neuroblastoma cell line SK-N-MC. *Eur J Biochem*, 267, 5631-7.
- FERGUSON, S. S., DOWNEY, W. E., 3RD, COLAPIETRO, A. M., BARAK, L. S., MENARD, L. & CARON, M. G. 1996. Role of beta-arrestin in mediating agonist-promoted G protein-coupled receptor internalization. *Science*, 271, 363-6.

- FERMINI, B. & FOSSA, A. A. 2003. The impact of drug-induced QT interval prolongation on drug discovery and development. *Nat Rev Drug Discov*, 2, 439-47.
- FERRADA, C., MORENO, E., CASADO, V., BONGERS, G., CORTES, A., MALLOL, J., CANELA, E. I., LEURS, R., FERRE, S., LLUIS, C. & FRANCO, R. 2009. Marked changes in signal transduction upon heteromerization of dopamine D1 and histamine H3 receptors. *Br J Pharmacol*, 157, 64-75.
- FERRE, S., CASADO, V., DEVI, L. A., FILIZOLA, M., JOCKERS, R., LOHSE, M. J., MILLIGAN, G., PIN, J. P. & GUITART, X. 2014. G protein-coupled receptor oligomerization revisited: functional and pharmacological perspectives. *Pharmacol Rev*, 66, 413-34.
- FERRE, S., VON EULER, G., JOHANSSON, B., FREDHOLM, B. B. & FUXE, K. 1991. Stimulation of high-affinity adenosine A2 receptors decreases the affinity of dopamine D2 receptors in rat striatal membranes. *Proc Natl Acad Sci U S A*, 88, 7238-41.
- FERRIS, C. D. & SNYDER, S. H. 1992. IP3 receptors. Ligand-activated calcium channels in multiple forms. *Adv Second Messenger Phosphoprotein Res*, 26, 95-107.
- FETISSOV, S. O., KOPP, J. & HOKFELT, T. 2004. Distribution of NPY receptors in the hypothalamus. *Neuropeptides*, 38, 175-88.
- FIELD, B. C., CHAUDHRI, O. B. & BLOOM, S. R. 2010. Bowels control brain: gut hormones and obesity. *Nat Rev Endocrinol*, 6, 444-53.
- FINUCANE, M. M., STEVENS, G. A., COWAN, M. J., DANAEI, G., LIN, J. K., PACIOREK, C. J., SINGH, G. M., GUTIERREZ, H. R., LU, Y., BAHALIM, A. N., FARZADFAR, F., RILEY, L. M. & EZZATI, M. 2011. National, regional, and global trends in body-mass index since 1980: systematic analysis of health examination surveys and epidemiological studies with 960 country-years and 9.1 million participants. *Lancet*, 377, 557-67.
- FONSECA, J. M. & LAMBERT, N. A. 2009. Instability of a class A G protein-coupled receptor oligomer interface. *Mol Pharmacol*, 75, 1296-9.
- FOTIADIS, D., JASTRZEBSKA, B., PHILIPPSSEN, A., MULLER, D. J., PALCZEWSKI, K. & ENGEL, A. 2006. Structure of the rhodopsin dimer: a working model for G-protein-coupled receptors. *Curr Opin Struct Biol*, 16, 252-9.
- FOTIADIS, D., LIANG, Y., FILIPEK, S., SAPERSTEIN, D. A., ENGEL, A. & PALCZEWSKI, K. 2003. Atomic-force microscopy: Rhodopsin dimers in native disc membranes. *Nature*, 421, 127-8.
- FRITZE, O., FILIPEK, S., KUKSA, V., PALCZEWSKI, K., HOFMANN, K. P. & ERNST, O. P. 2003. Role of the conserved NPxxY(x)5,6F motif in the rhodopsin ground state and during activation. *Proc Natl Acad Sci U S A*, 100, 2290-5.
- FUHLENDORFF, J., GETHER, U., AAKERLUND, L., LANGELAND-JOHANSEN, N., THOGERSEN, H., MELBERG, S. G., OLSEN, U. B., THASTRUP, O. & SCHWARTZ, T. W. 1990. [Leu31, Pro34]neuropeptide Y: a specific Y1 receptor agonist. *Proc Natl Acad Sci U S A*, 87, 182-6.
- FUJIMIYA, M. & INUI, A. 2000. Peptidergic regulation of gastrointestinal motility in rodents. *Peptides*, 21, 1565-82.
- FUJIWARA, T., RITCHIE, K., MURAKOSHI, H., JACOBSON, K. & KUSUMI, A. 2002. Phospholipids undergo hop diffusion in compartmentalized cell membrane. *J Cell Biol*, 157, 1071-81.
- FUNG JJ, D. X., PRADO L, YAO XJ, VELEZ-RUIZ GA, DEVREE BT, SUNAHARA RK, KOBILKA BK 2009. Ligand-regulated oligomerization of  $\beta_2$ -

- adrenoceptors in a model lipid bilayer. *The EMBO Journal*, 28, 3315-3328.
- GANDIA, J., GALINO, J., AMARAL, O. B., SORIANO, A., LLUIS, C., FRANCO, R. & CIRUELA, F. 2008. Detection of higher-order G protein-coupled receptor oligomers by a combined BRET-BiFC technique. *FEBS Lett*, 582, 2979-84.
- GAO, J., GHIBAUDI, L. & HWA, J. J. 2004. Selective activation of central NPY Y1 vs. Y5 receptor elicits hyperinsulinemia via distinct mechanisms. *Am J Physiol Endocrinol Metab*, 287, E706-11.
- GARLAND, S. L. 2013. Are GPCRs still a source of new targets? *J Biomol Screen*, 18, 947-66.
- GAVALAS, A., LAN, T. H., LIU, Q., CORREA, I. R., JR., JAVITCH, J. A. & LAMBERT, N. A. 2013. Segregation of family A G protein-coupled receptor protomers in the plasma membrane. *Mol Pharmacol*, 84, 346-52.
- GEHLERT, D. R., BEAVERS, L. S., JOHNSON, D., GACKENHEIMER, S. L., SCHOBBER, D. A. & GADSKI, R. A. 1996a. Expression cloning of a human brain neuropeptide Y Y2 receptor. *Mol Pharmacol*, 49, 224-8.
- GEHLERT, D. R. & GACKENHEIMER, S. L. 1997. Differential distribution of neuropeptide Y Y1 and Y2 receptors in rat and guinea-pig brains. *Neuroscience*, 76, 215-24.
- GEHLERT, D. R., GACKENHEIMER, S. L., SCHOBBER, D. A., BEAVERS, L., GADSKI, R., BURNETT, J. P., MAYNE, N., LUNDELL, I. & LARHAMMAR, D. 1996b. The neuropeptide Y Y1 receptor selective radioligand, [<sup>125</sup>I][Leu<sup>31</sup>,Pro<sup>34</sup>]peptide YY, is also a high affinity radioligand for human pancreatic polypeptide 1 receptors. *Eur J Pharmacol*, 318, 485-90.
- GEHLERT, D. R., SCHOBBER, D. A., GACKENHEIMER, S. L., BEAVERS, L., GADSKI, R., LUNDELL, I. & LARHAMMAR, D. 1997. [<sup>125</sup>I]Leu<sup>31</sup>, Pro<sup>34</sup>-PYY is a high affinity radioligand for rat PP1/Y4 and Y1 receptors: evidence for heterogeneity in pancreatic polypeptide receptors. *Peptides*, 18, 397-401.
- GEHLERT, D. R., SCHOBBER, D. A., MORIN, M. & BERGLUND, M. M. 2007. Co-expression of neuropeptide Y Y1 and Y5 receptors results in heterodimerization and altered functional properties. *Biochem Pharmacol*, 74, 1652-64.
- GEORGE, M., RAJARAM, M. & SHANMUGAM, E. 2014. New and emerging drug molecules against obesity. *J Cardiovasc Pharmacol Ther*, 19, 65-76.
- GEORGE, S. R., FAN, T., XIE, Z., TSE, R., TAM, V., VARGHESE, G. & O'DOWD, B. F. 2000. Oligomerization of mu- and delta-opioid receptors. Generation of novel functional properties. *J Biol Chem*, 275, 26128-35.
- GERALD, C., WALKER, M. W., CRISCIONE, L., GUSTAFSON, E. L., BATZLHARTMANN, C., SMITH, K. E., VAYSSE, P., DURKIN, M. M., LAZ, T. M., LINEMEYER, D. L., SCHAFFHAUSER, A. O., WHITEBREAD, S., HOFBAUER, K. G., TABER, R. I., BRANCHEK, T. A. & WEINSHANK, R. L. 1996. A receptor subtype involved in neuropeptide-Y-induced food intake. *Nature*, 382, 168-71.
- GERALD, C., WALKER, M. W., VAYSSE, P. J., HE, C., BRANCHEK, T. A. & WEINSHANK, R. L. 1995. Expression cloning and pharmacological characterization of a human hippocampal neuropeptide Y/peptide YY Y2 receptor subtype. *J Biol Chem*, 270, 26758-61.

- GESTY-PALMER, D., CHEN, M., REITER, E., AHN, S., NELSON, C. D., WANG, S., ECKHARDT, A. E., COWAN, C. L., SPURNEY, R. F., LUTTRELL, L. M. & LEFKOWITZ, R. J. 2006. Distinct beta-arrestin- and G protein-dependent pathways for parathyroid hormone receptor-stimulated ERK1/2 activation. *J Biol Chem*, 281, 10856-64.
- GHANOUNI, P., STEENHUIS, J. J., FARRENS, D. L. & KOBILKA, B. K. 2001. Agonist-induced conformational changes in the G-protein-coupling domain of the beta 2 adrenergic receptor. *Proc Natl Acad Sci U S A*, 98, 5997-6002.
- GHOSH, R. N., CHEN, Y. T., DEBIASIO, R., DEBIASIO, R. L., CONWAY, B. R., MINOR, L. K. & DEMAREST, K. T. 2000. Cell-based, high-content screen for receptor internalization, recycling and intracellular trafficking. *Biotechniques*, 29, 170-5.
- GICQUIAUX, H., LECAT, S., GAIRE, M., DIETERLEN, A., MELY, Y., TAKEDA, K., BUCHER, B. & GALZI, J. L. 2002. Rapid internalization and recycling of the human neuropeptide Y Y(1) receptor. *J Biol Chem*, 277, 6645-55.
- GILMAN, A. G. 1984. G proteins and dual control of adenylate cyclase. *Cell*, 36, 577-9.
- GIMENEZ, L. E., KOOK, S., VISHNIVETSKIY, S. A., AHMED, M. R., GUREVICH, E. V. & GUREVICH, V. V. 2012. Role of receptor-attached phosphates in binding of visual and non-visual arrestins to G protein-coupled receptors. *J Biol Chem*, 287, 9028-40.
- GINES, S., HILLION, J., TORVINEN, M., LE CROM, S., CASADO, V., CANELA, E. I., RONDIN, S., LEW, J. Y., WATSON, S., ZOLI, M., AGNATI, L. F., VERNIERA, P., LLUIS, C., FERRE, S., FUXE, K. & FRANCO, R. 2000. Dopamine D1 and adenosine A1 receptors form functionally interacting heteromeric complexes. *Proc Natl Acad Sci U S A*, 97, 8606-11.
- GOLEBIEWSKA, U., JOHNSTON, J. M., DEVI, L., FILIZOLA, M. & SCARLATA, S. 2011. Differential response to morphine of the oligomeric state of mu-opioid in the presence of delta-opioid receptors. *Biochemistry*, 50, 2829-37.
- GOMES, I., FUJITA, W., GUPTA, A., SALDANHA, S. A., NEGRI, A., PINELLO, C. E., EBERHART, C., ROBERTS, E., FILIZOLA, M., HODDER, P. & DEVI, L. A. 2013. Identification of a mu-delta opioid receptor heteromer-biased agonist with antinociceptive activity. *Proc Natl Acad Sci U S A*, 110, 12072-7.
- GONZALEZ, S., MORENO-DELGADO, D., MORENO, E., PEREZ-CAPOTE, K., FRANCO, R., MALLOL, J., CORTES, A., CASADO, V., LLUIS, C., ORTIZ, J., FERRE, S., CANELA, E. & MCCORMICK, P. J. 2012. Circadian-related heteromerization of adrenergic and dopamine D(4) receptors modulates melatonin synthesis and release in the pineal gland. *PLoS Biol*, 10, e1001347.
- GOODMAN, O. B., JR., KRUPNICK, J. G., SANTINI, F., GUREVICH, V. V., PENN, R. B., GAGNON, A. W., KEEN, J. H. & BENOVIĆ, J. L. 1996. Beta-arrestin acts as a clathrin adaptor in endocytosis of the beta2-adrenergic receptor. *Nature*, 383, 447-50.
- GRACE, C. R., PERRIN, M. H., DIGRUCCIO, M. R., MILLER, C. L., RIVIER, J. E., VALE, W. W. & RIEK, R. 2004. NMR structure and peptide hormone binding site of the first extracellular domain of a type B1 G protein-coupled receptor. *Proc Natl Acad Sci U S A*, 101, 12836-41.

- GRANDOCH, M., ROSCIONI, S. S. & SCHMIDT, M. 2010. The role of Epac proteins, novel cAMP mediators, in the regulation of immune, lung and neuronal function. *Br J Pharmacol*, 159, 265-84.
- GRANIER, S., MANGLIK, A., KRUSE, A. C., KOBILKA, T. S., THIAN, F. S., WEIS, W. I. & KOBILKA, B. K. 2012. Structure of the delta-opioid receptor bound to naltrindole. *Nature*, 485, 400-4.
- GRANT, M., COLLIER, B. & KUMAR, U. 2004. Agonist-dependent dissociation of human somatostatin receptor 2 dimers: a role in receptor trafficking. *J Biol Chem*, 279, 36179-83.
- GRAY, P. C., SCOTT, J. D. & CATTERALL, W. A. 1998. Regulation of ion channels by cAMP-dependent protein kinase and A-kinase anchoring proteins. *Curr Opin Neurobiol*, 8, 330-4.
- GREASLEY, P. J., FANELLI, F., ROSSIER, O., ABUIN, L. & COTECCHIA, S. 2002. Mutagenesis and modelling of the alpha(1b)-adrenergic receptor highlight the role of the helix 3/helix 6 interface in receptor activation. *Mol Pharmacol*, 61, 1025-32.
- GUO, W., SHI, L. & JAVITCH, J. A. 2003. The fourth transmembrane segment forms the interface of the dopamine D2 receptor homodimer. *J Biol Chem*, 278, 4385-8.
- GUO, W., URIZAR, E., KRALIKOVA, M., MOBAREC, J. C., SHI, L., FILIZOLA, M. & JAVITCH, J. A. 2008. Dopamine D2 receptors form higher order oligomers at physiological expression levels. *EMBO J*, 27, 2293-304.
- GUPTA, A., MULDER, J., GOMES, I., ROZENFELD, R., BUSHLIN, I., ONG, E., LIM, M., MAILLET, E., JUNEK, M., CAHILL, C. M., HARKANY, T. & DEVI, L. A. 2010. Increased abundance of opioid receptor heteromers after chronic morphine administration. *Sci Signal*, 3, ra54.
- GUREVICH, E. V. & GUREVICH, V. V. 2006. Arrestins: ubiquitous regulators of cellular signaling pathways. *Genome Biol*, 7, 236.
- GUREVICH, V. V. & GUREVICH, E. V. 2004. The molecular acrobatics of arrestin activation. *Trends Pharmacol Sci*, 25, 105-11.
- GUREVICH, V. V. & GUREVICH, E. V. 2008. GPCR monomers and oligomers: it takes all kinds. *Trends Neurosci*, 31, 74-81.
- GUREVICH, V. V. & GUREVICH, E. V. 2013. Structural determinants of arrestin functions. *Prog Mol Biol Transl Sci*, 118, 57-92.
- HAGA, K., KRUSE, A. C., ASADA, H., YURUGI-KOBAYASHI, T., SHIROISHI, M., ZHANG, C., WEIS, W. I., OKADA, T., KOBILKA, B. K., HAGA, T. & KOBAYASHI, T. 2012. Structure of the human M2 muscarinic acetylcholine receptor bound to an antagonist. *Nature*, 482, 547-51.
- HAGUE, C., UBERTI, M. A., CHEN, Z., HALL, R. A. & MINNEMAN, K. P. 2004. Cell surface expression of alpha1D-adrenergic receptors is controlled by heterodimerization with alpha1B-adrenergic receptors. *J Biol Chem*, 279, 15541-9.
- HALL, M. P., UNCH, J., BINKOWSKI, B. F., VALLEY, M. P., BUTLER, B. L., WOOD, M. G., OTTO, P., ZIMMERMAN, K., VIDUGIRIS, G., MACHLEIDT, T., ROBERS, M. B., BENINK, H. A., EGGERS, C. T., SLATER, M. R., MEISENHEIMER, P. L., KLAUBERT, D. H., FAN, F., ENCELL, L. P. & WOOD, K. V. 2012. Engineered luciferase reporter from a deep sea shrimp utilizing a novel imidazopyrazinone substrate. *ACS Chem Biol*, 7, 1848-57.
- HALLS, M. L. & COOPER, D. M. 2010. Sub-picomolar relaxin signalling by a pre-assembled RXFP1, AKAP79, AC2, beta-arrestin 2, PDE4D3 complex. *EMBO J*, 29, 2772-87.

- HALLWORTH, R. & NICHOLS, M. G. 2012. Prestin in HEK cells is an obligate tetramer. *J Neurophysiol*, 107, 5-11.
- HAN, Y., MOREIRA, I. S., URIZAR, E., WEINSTEIN, H. & JAVITCH, J. A. 2009. Allosteric communication between protomers of dopamine class A GPCR dimers modulates activation. *Nat Chem Biol*, 5, 688-95.
- HANSEN, J. L., HANSEN, J. T., SPEERSCHNEIDER, T., LYGNSO, C., ERIKSTRUP, N., BURSTEIN, E. S., WEINER, D. M., WALTHER, T., MAKITA, N., IIRI, T., MERTEN, N., KOSTENIS, E. & SHEIKH, S. P. 2009. Lack of evidence for AT1R/B2R heterodimerization in COS-7, HEK293, and NIH3T3 cells: how common is the AT1R/B2R heterodimer? *J Biol Chem*, 284, 1831-9.
- HANSEN, J. L., THEILADE, J., HAUNSO, S. & SHEIKH, S. P. 2004. Oligomerization of wild type and nonfunctional mutant angiotensin II type I receptors inhibits galphaq protein signaling but not ERK activation. *J Biol Chem*, 279, 24108-15.
- HANSON, M. A., ROTH, C. B., JO, E., GRIFFITH, M. T., SCOTT, F. L., REINHART, G., DESALE, H., CLEMONS, B., CAHALAN, S. M., SCHUERER, S. C., SANNA, M. G., HAN, G. W., KUHN, P., ROSEN, H. & STEVENS, R. C. 2012. Crystal structure of a lipid G protein-coupled receptor. *Science*, 335, 851-5.
- HANSON, S. M., FRANCIS, D. J., VISHNIVETSKIY, S. A., KOLOBOVA, E. A., HUBBELL, W. L., KLUG, C. S. & GUREVICH, V. V. 2006. Differential interaction of spin-labeled arrestin with inactive and active phosphorhodopsin. *Proc Natl Acad Sci U S A*, 103, 4900-5.
- HANSON, S. M., GUREVICH, E. V., VISHNIVETSKIY, S. A., AHMED, M. R., SONG, X. & GUREVICH, V. V. 2007a. Each rhodopsin molecule binds its own arrestin. *Proc Natl Acad Sci U S A*, 104, 3125-8.
- HANSON, S. M., VAN EPS, N., FRANCIS, D. J., ALTENBACH, C., VISHNIVETSKIY, S. A., ARSHAVSKY, V. Y., KLUG, C. S., HUBBELL, W. L. & GUREVICH, V. V. 2007b. Structure and function of the visual arrestin oligomer. *EMBO J*, 26, 1726-36.
- HANYALOGLU, A. C. & VON ZASTROW, M. 2008. Regulation of GPCRs by endocytic membrane trafficking and its potential implications. *Annu Rev Pharmacol Toxicol*, 48, 537-68.
- HASBI, A., DEVOST, D., LAPORTE, S. A. & ZINGG, H. H. 2004. Real-time detection of interactions between the human oxytocin receptor and G protein-coupled receptor kinase-2. *Mol Endocrinol*, 18, 1277-86.
- HAUPTS, U., MAITI, S., SCHWILLE, P. & WEBB, W. W. 1998. Dynamics of fluorescence fluctuations in green fluorescent protein observed by fluorescence correlation spectroscopy. *Proc Natl Acad Sci U S A*, 95, 13573-8.
- HAYNES, A. C., ARCH, J. R., WILSON, S., MCCLUE, S. & BUCKINGHAM, R. E. 1998. Characterisation of the neuropeptide Y receptor that mediates feeding in the rat: a role for the Y5 receptor? *Regul Pept*, 75-76, 355-61.
- HEBERT, T. E., LOISEL, T. P., ADAM, L., ETHIER, N., ONGE, S. S. & BOUVIER, M. 1998. Functional rescue of a constitutively desensitized beta2AR through receptor dimerization. *Biochem J*, 330 ( Pt 1), 287-93.
- HEBERT, T. E., MOFFETT, S., MORELLO, J. P., LOISEL, T. P., BICHET, D. G., BARRET, C. & BOUVIER, M. 1996. A peptide derived from a beta2-adrenergic receptor transmembrane domain inhibits both receptor dimerization and activation. *J Biol Chem*, 271, 16384-92.

- HEGENER, O., PRENNER, L., RUNKEL, F., BAADER, S. L., KAPPLER, J. & HABERLEIN, H. 2004. Dynamics of beta2-adrenergic receptor-ligand complexes on living cells. *Biochemistry*, 43, 6190-9.
- HEIM, R., CUBITT, A. B. & TSIEN, R. Y. 1995. Improved green fluorescence. *Nature*, 373, 663-4.
- HELSEN, C. & CLAESSENS, F. 2014. Looking at nuclear receptors from a new angle. *Mol Cell Endocrinol*, 382, 97-106.
- HENRY, M., GHIBAUDI, L., GAO, J. & HWA, J. J. 2005. Energy metabolic profile of mice after chronic activation of central NPY Y1, Y2, or Y5 receptors. *Obes Res*, 13, 36-47.
- HERN, J. A., BAIG, A. H., MASHANOV, G. I., BIRDSALL, B., CORRIE, J. E., LAZARENO, S., MOLLOY, J. E. & BIRDSALL, N. J. 2010. Formation and dissociation of M1 muscarinic receptor dimers seen by total internal reflection fluorescence imaging of single molecules. *Proc Natl Acad Sci U S A*, 107, 2693-8.
- HERRICK-DAVIS, K., GRINDE, E., COWAN, A. & MAZURKIEWICZ, J. E. 2013. Fluorescence correlation spectroscopy analysis of serotonin, adrenergic, muscarinic, and dopamine receptor dimerization: the oligomer number puzzle. *Mol Pharmacol*, 84, 630-42.
- HERRICK-DAVIS, K., GRINDE, E., LINDSLEY, T., COWAN, A. & MAZURKIEWICZ, J. E. 2012. Oligomer size of the serotonin 5-hydroxytryptamine 2C (5-HT<sub>2C</sub>) receptor revealed by fluorescence correlation spectroscopy with photon counting histogram analysis: evidence for homodimers without monomers or tetramers. *J Biol Chem*, 287, 23604-14.
- HERZOG, H., HORT, Y. J., BALL, H. J., HAYES, G., SHINE, J. & SELBIE, L. A. 1992. Cloned human neuropeptide Y receptor couples to two different second messenger systems. *Proc Natl Acad Sci U S A*, 89, 5794-8.
- HIGUCHI, H., NIKI, T. & SHIYI, T. 2008. Feeding behavior and gene expression of appetite-related neuropeptides in mice lacking for neuropeptide Y Y5 receptor subclass. *World J Gastroenterol*, 14, 6312-7.
- HILAIRET, S., BOUABOULA, M., CARRIERE, D., LE FUR, G. & CASELLAS, P. 2003. Hypersensitization of the Orexin 1 receptor by the CB1 receptor: evidence for cross-talk blocked by the specific CB1 antagonist, SR141716. *J Biol Chem*, 278, 23731-7.
- HILLER, C., KUHORN, J. & GMEINER, P. 2013. Class A G-protein-coupled receptor (GPCR) dimers and bivalent ligands. *J Med Chem*, 56, 6542-59.
- HILLION, J., CANALS, M., TORVINEN, M., CASADO, V., SCOTT, R., TERASMAA, A., HANSSON, A., WATSON, S., OLAH, M. E., MALLOL, J., CANELA, E. I., ZOLI, M., AGNATI, L. F., IBANEZ, C. F., LLUIS, C., FRANCO, R., FERRE, S. & FUXE, K. 2002. Coaggregation, cointernalization, and codesensitization of adenosine A<sub>2A</sub> receptors and dopamine D<sub>2</sub> receptors. *J Biol Chem*, 277, 18091-7.
- HOLLENSTEIN, K., KEAN, J., BORTOLATO, A., CHENG, R. K., DORE, A. S., JAZAYERI, A., COOKE, R. M., WEIR, M. & MARSHALL, F. H. 2013. Structure of class B GPCR corticotropin-releasing factor receptor 1. *Nature*, 499, 438-43.
- HOLLIDAY, N. D. & COX, H. M. 2003. Control of signalling efficacy by palmitoylation of the rat Y1 receptor. *Br J Pharmacol*, 139, 501-12.

- HOLLIDAY, N. D., LAM, C. W., TOUGH, I. R. & COX, H. M. 2005. Role of the C terminus in neuropeptide Y Y1 receptor desensitization and internalization. *Mol Pharmacol*, 67, 655-64.
- HOLST, B., NYGAARD, R., VALENTIN-HANSEN, L., BACH, A., ENGELSTOFT, M. S., PETERSEN, P. S., FRIMURER, T. M. & SCHWARTZ, T. W. 2010. A conserved aromatic lock for the tryptophan rotameric switch in TM-VI of seven-transmembrane receptors. *J Biol Chem*, 285, 3973-85.
- HOLZER, P., REICHMANN, F. & FARZI, A. 2012. Neuropeptide Y, peptide YY and pancreatic polypeptide in the gut-brain axis. *Neuropeptides*.
- HOWELL, O. W., SCHARFMAN, H. E., HERZOG, H., SUNDSTROM, L. E., BECK-SICKINGER, A. & GRAY, W. P. 2003. Neuropeptide Y is neuroproliferative for post-natal hippocampal precursor cells. *J Neurochem*, 86, 646-59.
- HU, C. D., CHINENOV, Y. & KERPPOLA, T. K. 2002. Visualization of interactions among bZIP and Rel family proteins in living cells using bimolecular fluorescence complementation. *Mol Cell*, 9, 789-98.
- HU, C. D. & KERPPOLA, T. K. 2003. Simultaneous visualization of multiple protein interactions in living cells using multicolor fluorescence complementation analysis. *Nat Biotechnol*, 21, 539-45.
- HU, J., THOR, D., ZHOU, Y., LIU, T., WANG, Y., MCMILLIN, S. M., MISTRY, R., CHALLISS, R. A., COSTANZI, S. & WESS, J. 2012. Structural aspects of M(3) muscarinic acetylcholine receptor dimer formation and activation. *FASEB J*, 26, 604-16.
- HUANG, B., BATES, M. & ZHUANG, X. 2009. Super-resolution fluorescence microscopy. *Annu Rev Biochem*, 78, 993-1016.
- HUANG, B., PERROUD, T. D. & ZARE, R. N. 2004. Photon counting histogram: one-photon excitation. *Chemphyschem*, 5, 1523-31.
- HUANG, J., CHEN, S., ZHANG, J. J. & HUANG, X. Y. 2013. Crystal structure of oligomeric beta1-adrenergic G protein-coupled receptors in ligand-free basal state. *Nat Struct Mol Biol*, 20, 419-25.
- HUANG, W., OSMAN, R. & GERSHENGORN, M. C. 2005. Agonist-induced conformational changes in thyrotropin-releasing hormone receptor type I: disulfide cross-linking and molecular modeling approaches. *Biochemistry*, 44, 2419-31.
- HUANG, X. F., HAN, M. & STORLIEN, L. H. 2003. The level of NPY receptor mRNA expression in diet-induced obese and resistant mice. *Brain Res Mol Brain Res*, 115, 21-8.
- HUBBARD, S. R. & MILLER, W. T. 2007. Receptor tyrosine kinases: mechanisms of activation and signaling. *Curr Opin Cell Biol*, 19, 117-23.
- HUTTENRAUCH, F., POLLOK-KOPP, B. & OPPERMANN, M. 2005. G protein-coupled receptor kinases promote phosphorylation and beta-arrestin-mediated internalization of CCR5 homo- and hetero-oligomers. *J Biol Chem*, 280, 37503-15.
- ILLES, P. & REGENOLD, J. T. 1990. Interaction between neuropeptide Y and noradrenaline on central catecholamine neurons. *Nature*, 344, 62-3.
- INSEL, P. A., HEAD, B. P., PATEL, H. H., ROTH, D. M., BUNDEY, R. A. & SWANEY, J. S. 2005. Compartmentation of G-protein-coupled receptors and their signalling components in lipid rafts and caveolae. *Biochem Soc Trans*, 33, 1131-4.
- ISHIHARA, A., KANATANI, A., OKADA, M., HIDAKA, M., TANAKA, T., MASHIKO, S., GOMORI, A., KANNO, T., HATA, M., KANESAKA, M.,

- TOMINAGA, Y., SATO, N. A., KOBAYASHI, M., MURAI, T., WATANABE, K., ISHII, Y., FUKURODA, T., FUKAMI, T. & IHARA, M. 2002. Blockade of body weight gain and plasma corticosterone levels in Zucker fatty rats using an orally active neuropeptide Y Y1 antagonist. *Br J Pharmacol*, 136, 341-6.
- ISHIHARA, A., TANAKA, T., KANATANI, A., FUKAMI, T., IHARA, M. & FUKURODA, T. 1998. A potent neuropeptide Y antagonist, 1229U91, suppressed spontaneous food intake in Zucker fatty rats. *Am J Physiol*, 274, R1500-4.
- ISHIKAWA-ANKERHOLD, H. C., ANKERHOLD, R. & DRUMMEN, G. P. 2012. Advanced fluorescence microscopy techniques--FRAP, FLIP, FLAP, FRET and FLIM. *Molecules*, 17, 4047-132.
- JAAKOLA, V. P., GRIFFITH, M. T., HANSON, M. A., CHEREZOV, V., CHIEN, E. Y., LANE, J. R., IJZERMAN, A. P. & STEVENS, R. C. 2008. The 2.6 angstrom crystal structure of a human A2A adenosine receptor bound to an antagonist. *Science*, 322, 1211-7.
- JAGER, S., PALCZEWSKI, K. & HOFMANN, K. P. 1996. Opsin/all-trans-retinal complex activates transducin by different mechanisms than photolyzed rhodopsin. *Biochemistry*, 35, 2901-8.
- JASTRZEBSKA, B., ORBAN, T., GOLCZAK, M., ENGEL, A. & PALCZEWSKI, K. 2013. Asymmetry of the rhodopsin dimer in complex with transducin. *FASEB J*, 27, 1572-84.
- JOHNSON, J. D., CAMPISI, J., SHARKEY, C. M., KENNEDY, S. L., NICKERSON, M. & FLESHNER, M. 2005. Adrenergic receptors mediate stress-induced elevations in extracellular Hsp72. *J Appl Physiol* (1985), 99, 1789-95.
- JOHNSON, M. 2006. Molecular mechanisms of beta(2)-adrenergic receptor function, response, and regulation. *J Allergy Clin Immunol*, 117, 18-24; quiz 25.
- JOHNSTON, J. M., ABURI, M., PROVASI, D., BORTOLATO, A., URIZAR, E., LAMBERT, N. A., JAVITCH, J. A. & FILIZOLA, M. 2011. Making structural sense of dimerization interfaces of delta opioid receptor homodimers. *Biochemistry*, 50, 1682-90.
- JOHNSTON, J. M., WANG, H., PROVASI, D. & FILIZOLA, M. 2012. Assessing the relative stability of dimer interfaces in g protein-coupled receptors. *PLoS Comput Biol*, 8, e1002649.
- JONES KA, B. B., TAMM JA, CRAIG DA, DURKIN MM, DAI M, YAO W-J, JOHNSON M, GUNWALDSEN C, HUANG L-Y, TANG C, SHEN Q, SALON JA, MORSE K, LAZ T, SMITH KE, NAGARATHNAM D, NOBLE SA, BRANCHEK TA, GERALD C 1998. GABA<sub>B</sub> receptors function as a heteromeric assembly of the subunits GABA<sub>B</sub>R1 and GABA<sub>B</sub>R2. *Nature* 396, 674-678.
- JONGEJAN, A., BRUYSTERS, M., BALLESTEROS, J. A., HAAKSMA, E., BAKKER, R. A., PARDO, L. & LEURS, R. 2005. Linking agonist binding to histamine H1 receptor activation. *Nat Chem Biol*, 1, 98-103.
- JORDAN, B. A. & DEVI, L. A. 1999. G-protein-coupled receptor heterodimerization modulates receptor function. *Nature*, 399, 697-700.
- JORDAN, B. A., TRAPAIDZE, N., GOMES, I., NIVARTHI, R. & DEVI, L. A. 2001. Oligomerization of opioid receptors with beta 2-adrenergic receptors: a role in trafficking and mitogen-activated protein kinase activation. *Proc Natl Acad Sci U S A*, 98, 343-8.

- KALLAL, L. & BENOVIĆ, J. L. 2000. Using green fluorescent proteins to study G-protein-coupled receptor localization and trafficking. *Trends Pharmacol Sci*, 21, 175-80.
- KALRA, S. P., DUBE, M. G., SAHU, A., PHELPS, C. P. & KALRA, P. S. 1991. Neuropeptide Y secretion increases in the paraventricular nucleus in association with increased appetite for food. *Proc Natl Acad Sci U S A*, 88, 10931-5.
- KANATANI, A., HATA, M., MASHIKO, S., ISHIHARA, A., OKAMOTO, O., HAGA, Y., OHE, T., KANNO, T., MURAI, N., ISHII, Y., FUKURODA, T., FUKAMI, T. & IHARA, M. 2001. A typical Y1 receptor regulates feeding behaviors: effects of a potent and selective Y1 antagonist, J-115814. *Mol Pharmacol*, 59, 501-5.
- KANATANI, A., ISHIHARA, A., ASAHİ, S., TANAKA, T., OZAKI, S. & IHARA, M. 1996. Potent neuropeptide Y Y1 receptor antagonist, 1229U91: blockade of neuropeptide Y-induced and physiological food intake. *Endocrinology*, 137, 3177-82.
- KANATANI, A., ISHIHARA, A., IWAASA, H., NAKAMURA, K., OKAMOTO, O., HIDAKA, M., ITO, J., FUKURODA, T., MACNEIL, D. J., VAN DER PLOEG, L. H., ISHII, Y., OKABE, T., FUKAMI, T. & IHARA, M. 2000. L-152,804: orally active and selective neuropeptide Y Y5 receptor antagonist. *Biochem Biophys Res Commun*, 272, 169-73.
- KANATANI, A., KANNO, T., ISHIHARA, A., HATA, M., SAKURABA, A., TANAKA, T., TSUCHIYA, Y., MASE, T., FUKURODA, T., FUKAMI, T. & IHARA, M. 1999. The novel neuropeptide Y Y(1) receptor antagonist J-104870: a potent feeding suppressant with oral bioavailability. *Biochem Biophys Res Commun*, 266, 88-91.
- KANG, D. S., KERN, R. C., PUTHENVEEDU, M. A., VON ZASTROW, M., WILLIAMS, J. C. & BENOVIĆ, J. L. 2009. Structure of an arrestin2-clathrin complex reveals a novel clathrin binding domain that modulates receptor trafficking. *J Biol Chem*, 284, 29860-72.
- KANG, D. S., TIAN, X. & BENOVIĆ, J. L. 2014. Role of beta-arrestins and arrestin domain-containing proteins in G protein-coupled receptor trafficking. *Curr Opin Cell Biol*, 27, 63-71.
- KANNO, T., KANATANI, A., KEEN, S. L., ARAI-OTSUKI, S., HAGA, Y., IWAMA, T., ISHIHARA, A., SAKURABA, A., IWAASA, H., HIROSE, M., MORISHIMA, H., FUKAMI, T. & IHARA, M. 2001. Different binding sites for the neuropeptide Y Y1 antagonists 1229U91 and J-104870 on human Y1 receptors. *Peptides*, 22, 405-13.
- KASAI, R. S., SUZUKI, K. G., PROSSNITZ, E. R., KOYAMA-HONDA, I., NAKADA, C., FUJIWARA, T. K. & KUSUMI, A. 2011. Full characterization of GPCR monomer-dimer dynamic equilibrium by single molecule imaging. *J Cell Biol*, 192, 463-80.
- KASK, P., PALO, K., ULLMANN, D. & GALL, K. 1999. Fluorescence-intensity distribution analysis and its application in biomolecular detection technology. *Proc Natl Acad Sci U S A*, 96, 13756-61.
- KATRITCH, V., CHEREZOV, V. & STEVENS, R. C. 2012. Diversity and modularity of G protein-coupled receptor structures. *Trends Pharmacol Sci*, 33, 17-27.
- KAUPMANN, K., MALITSCHKEK, B., SCHULER, V., HEID, J., FROESTL, W., BECK, P., MOSBACHER, J., BISCHOFF, S., KULIK, A., SHIGEMOTO, R., KARSCHIN, A. & BETTLER, B. 1998. GABA(B)-receptor subtypes assemble into functional heteromeric complexes. *Nature*, 396, 683-7.

- KAYA, A. I., UGUR, O., ALTUNTAS, O., SAYAR, K. & ONARAN, H. O. 2011. Long and short distance movements of beta(2)-adrenoceptor in cell membrane assessed by photoconvertible fluorescent protein dendra2-beta(2)-adrenoceptor fusion. *Biochim Biophys Acta*, 1813, 1511-24.
- KEIRE, D. A., MANNON, P., KOBAYASHI, M., WALSH, J. H., SOLOMON, T. E. & REEVE, J. R., JR. 2000. Primary structures of PYY, [Pro(34)]PYY, and PYY-(3-36) confer different conformations and receptor selectivity. *Am J Physiol Gastrointest Liver Physiol*, 279, G126-31.
- KENAKIN, T. & CHRISTOPOULOS, A. 2013. Measurements of ligand bias and functional affinity. *Nat Rev Drug Discov*, 12, 483.
- KENAKIN, T. & MILLER, L. J. 2010. Seven transmembrane receptors as shapeshifting proteins: the impact of allosteric modulation and functional selectivity on new drug discovery. *Pharmacol Rev*, 62, 265-304.
- KENDALL, R. T. & LUTTRELL, L. M. 2009. Diversity in arrestin function. *Cell Mol Life Sci*, 66, 2953-73.
- KENWORTHY, A. K., NICHOLS, B. J., REMMERT, C. L., HENDRIX, G. M., KUMAR, M., ZIMMERBERG, J. & LIPPINCOTT-SCHWARTZ, J. 2004. Dynamics of putative raft-associated proteins at the cell surface. *J Cell Biol*, 165, 735-46.
- KERN, A., ALBARRAN-ZECKLER, R., WALSH, H. E. & SMITH, R. G. 2012. Apoghrelin receptor forms heteromers with DRD2 in hypothalamic neurons and is essential for anorexigenic effects of DRD2 agonism. *Neuron*, 73, 317-32.
- KERN, R. C., KANG, D. S. & BENOVIC, J. L. 2009. Arrestin2/clathrin interaction is regulated by key N- and C-terminal regions in arrestin2. *Biochemistry*, 48, 7190-200.
- KERPPOLA, T. K. 2008a. Bimolecular fluorescence complementation (BiFC) analysis as a probe of protein interactions in living cells. *Annu Rev Biophys*, 37, 465-87.
- KERPPOLA, T. K. 2008b. Bimolecular fluorescence complementation: visualization of molecular interactions in living cells. *Methods Cell Biol*, 85, 431-70.
- KERPPOLA, T. K. 2009. Visualization of molecular interactions using bimolecular fluorescence complementation analysis: characteristics of protein fragment complementation. *Chem Soc Rev*, 38, 2876-86.
- KERPPOLA, T. K. 2013. Bimolecular fluorescence complementation (BiFC) analysis of protein interactions in live cells. *Cold Spring Harb Protoc*, 2013, 727-31.
- KILPATRICK, L. E., BRIDDON, S. J., HILL, S. J. & HOLLIDAY, N. D. 2010. Quantitative analysis of neuropeptide Y receptor association with beta-arrestin2 measured by bimolecular fluorescence complementation. *Br J Pharmacol*, 160, 892-906.
- KILPATRICK, L. E., BRIDDON, S. J. & HOLLIDAY, N. D. 2012. Fluorescence correlation spectroscopy, combined with bimolecular fluorescence complementation, reveals the effects of beta-arrestin complexes and endocytic targeting on the membrane mobility of neuropeptide Y receptors. *Biochim Biophys Acta*, 1823, 1068-81.
- KILPATRICK, L. E. & HOLLIDAY, N. D. 2012. Dissecting the pharmacology of G protein-coupled receptor signaling complexes using bimolecular fluorescence complementation. *Methods Mol Biol*, 897, 109-38.

- KIM, M., VISHNIVETSKIY, S. A., VAN EPS, N., ALEXANDER, N. S., CLEGHORN, W. M., ZHAN, X., HANSON, S. M., MORIZUMI, T., ERNST, O. P., MEILER, J., GUREVICH, V. V. & HUBBELL, W. L. 2012. Conformation of receptor-bound visual arrestin. *Proceedings of the National Academy of Sciences*, 109, 18407-18412.
- KIM, Y. M. & BENOVIC, J. L. 2002. Differential roles of arrestin-2 interaction with clathrin and adaptor protein 2 in G protein-coupled receptor trafficking. *J Biol Chem*, 277, 30760-8.
- KIRCHBERG, K., KIM, T. Y., MOLLER, M., SKEGRO, D., DASARA RAJU, G., GRANZIN, J., BULDT, G., SCHLESINGER, R. & ALEXIEV, U. 2011. Conformational dynamics of helix 8 in the GPCR rhodopsin controls arrestin activation in the desensitization process. *Proc Natl Acad Sci U S A*, 108, 18690-5.
- KISSELEV, O. G., MCDOWELL, J. H. & HARGRAVE, P. A. 2004. The arrestin-bound conformation and dynamics of the phosphorylated carboxy-terminal region of rhodopsin. *FEBS Lett*, 564, 307-11.
- KLAPSTEIN, G. J. & COLMERS, W. F. 1993. On the sites of presynaptic inhibition by neuropeptide Y in rat hippocampus in vitro. *Hippocampus*, 3, 103-11.
- KNIAZEFF J, B. A.-S., MAUREL D, ANSANAY H, PREZEAU L, PIN JP 2004. Closed state of both binding domains of homodimeric mGlu receptors is required for full activity. *Nature Structural and Molecular Biology*, 11, 706-713.
- KNIAZEFF, J., GALVEZ, T., LABESSE, G. & PIN, J. P. 2002. No ligand binding in the GB2 subunit of the GABA(B) receptor is required for activation and allosteric interaction between the subunits. *J Neurosci*, 22, 7352-61.
- KOBILKA, B. K. & DEUPI, X. 2007. Conformational complexity of G-protein-coupled receptors. *Trends Pharmacol Sci*, 28, 397-406.
- KOCAN, M., SEE, H. B., SAMPAIO, N. G., EIDNE, K. A., FELDMAN, B. J. & PFLEGER, K. D. 2009. Agonist-independent interactions between beta-arrestins and mutant vasopressin type II receptors associated with nephrogenic syndrome of inappropriate antidiuresis. *Mol Endocrinol*, 23, 559-71.
- KOCAN, M., SEE, H. B., SEEBER, R. M., EIDNE, K. A. & PFLEGER, K. D. 2008. Demonstration of improvements to the bioluminescence resonance energy transfer (BRET) technology for the monitoring of G protein-coupled receptors in live cells. *J Biomol Screen*, 13, 888-98.
- KODAMA, Y. & HU, C. D. 2010. An improved bimolecular fluorescence complementation assay with a high signal-to-noise ratio. *Biotechniques*, 49, 793-805.
- KODAMA, Y. & HU, C. D. 2012. Bimolecular fluorescence complementation (BiFC): a 5-year update and future perspectives. *Biotechniques*, 53, 285-98.
- KOLINSKI, M. & FILIPEK, S. 2010. Study of a structurally similar kappa opioid receptor agonist and antagonist pair by molecular dynamics simulations. *J Mol Model*, 16, 1567-76.
- KOMMADDI, R. P. & SHENOY, S. K. 2013. Arrestins and protein ubiquitination. *Prog Mol Biol Transl Sci*, 118, 175-204.
- KOSUGI, S., KOHN, L. D., AKAMIZU, T. & MORI, T. 1994. The middle portion in the second cytoplasmic loop of the thyrotropin receptor plays a crucial role in adenylate cyclase activation. *Mol Endocrinol*, 8, 498-509.

- KRASEL, C., VILARDAGA, J. P., BUNEMANN, M. & LOHSE, M. J. 2004. Kinetics of G-protein-coupled receptor signalling and desensitization. *Biochem Soc Trans*, 32, 1029-31.
- KRAUSE, J., EVA, C., SEEBURG, P. H. & SPRENGEL, R. 1992. Neuropeptide Y1 subtype pharmacology of a recombinantly expressed neuropeptide receptor. *Mol Pharmacol*, 41, 817-21.
- KRUPNICK, J. G., GOODMAN, O. B., JR., KEEN, J. H. & BENOVIC, J. L. 1997a. Arrestin/clathrin interaction. Localization of the clathrin binding domain of nonvisual arrestins to the carboxy terminus. *J Biol Chem*, 272, 15011-6.
- KRUPNICK, J. G., GUREVICH, V. V. & BENOVIC, J. L. 1997b. Mechanism of quenching of phototransduction. Binding competition between arrestin and transducin for phosphorhodopsin. *J Biol Chem*, 272, 18125-31.
- KRUSE, A. C., HU, J., PAN, A. C., ARLOW, D. H., ROSENBAUM, D. M., ROSEMOND, E., GREEN, H. F., LIU, T., CHAE, P. S., DROR, R. O., SHAW, D. E., WEIS, W. I., WESS, J. & KOBILKA, B. K. 2012. Structure and dynamics of the M3 muscarinic acetylcholine receptor. *Nature*, 482, 552-6.
- KUDER, K. & KIEC-KONONOWICZ, K. 2008. Fluorescent GPCR ligands as new tools in pharmacology. *Curr Med Chem*, 15, 2132-43.
- KUHN, C., BUFE, B., BATRAM, C. & MEYERHOF, W. 2010. Oligomerization of TAS2R bitter taste receptors. *Chem Senses*, 35, 395-406.
- KUSHI, A., SASAI, H., KOIZUMI, H., TAKEDA, N., YOKOYAMA, M. & NAKAMURA, M. 1998. Obesity and mild hyperinsulinemia found in neuropeptide Y-Y1 receptor-deficient mice. *Proc Natl Acad Sci U S A*, 95, 15659-64.
- KUSZAK, A. J., PITCHIAYA, S., ANAND, J. P., MOSBERG, H. I., WALTER, N. G. & SUNAHARA, R. K. 2009. Purification and functional reconstitution of monomeric mu-opioid receptors: allosteric modulation of agonist binding by Gi2. *J Biol Chem*, 284, 26732-41.
- LAMBERT, N. 2010. GPCR Dimers Fall Apart. *Science Signaling*, 3, 1-3.
- LAN, H., DURAND, C. J., TEETER, M. M. & NEVE, K. A. 2006. Structural determinants of pharmacological specificity between D(1) and D(2) dopamine receptors. *Mol Pharmacol*, 69, 185-94.
- LAN, T. H., KURAVI, S. & LAMBERT, N. A. 2011. Internalization dissociates beta2-adrenergic receptors. *PLoS One*, 6, e17361.
- LANE, J. R., DONTAMSETTI, P., SHONBERG, J., DRAPER-JOYCE, C. J., DENTRY, S., MICHINO, M., SHI, L., LOPEZ, L., SCAMMELLS, P. J., CAPUANO, B., SEXTON, P. M., JAVITCH, J. A. & CHRISTOPOULOS, A. 2014. A new mechanism of allostery in a G protein-coupled receptor dimer. *Nat Chem Biol*, 10, 745-52.
- LANGMEAD, C. J. & CHRISTOPOULOS, A. 2014. Functional and structural perspectives on allosteric modulation of GPCRs. *Curr Opin Cell Biol*, 27, 94-101.
- LAPORTE, S. A., OAKLEY, R. H., ZHANG, J., HOLT, J. A., FERGUSON, S. S., CARON, M. G. & BARAK, L. S. 1999. The beta2-adrenergic receptor/betaarrestin complex recruits the clathrin adaptor AP-2 during endocytosis. *Proc Natl Acad Sci U S A*, 96, 3712-7.
- LARHAMMAR, D., BLOMQVIST, A. G., YEE, F., JAZIN, E., YOO, H. & WAHLESTED, C. 1992. Cloning and functional expression of a human neuropeptide Y/peptide YY receptor of the Y1 type. *J Biol Chem*, 267, 10935-8.

- LATIF, R., GRAVES, P. & DAVIES, T. F. 2002. Ligand-dependent inhibition of oligomerization at the human thyrotropin receptor. *J Biol Chem*, 277, 45059-67.
- LAVOIE, C., MERCIER, J. F., SALAHPOUR, A., UMAPATHY, D., BREIT, A., VILLENEUVE, L. R., ZHU, W. Z., XIAO, R. P., LAKATTA, E. G., BOUVIER, M. & HEBERT, T. E. 2002. Beta 1/beta 2-adrenergic receptor heterodimerization regulates beta 2-adrenergic receptor internalization and ERK signaling efficacy. *J Biol Chem*, 277, 35402-10.
- LE ROY, C. & WRANA, J. L. 2005. Clathrin- and non-clathrin-mediated endocytic regulation of cell signalling. *Nat Rev Mol Cell Biol*, 6, 112-26.
- LECAT, S., OUEDRAOGO, M., CHERRIER, T., NOULET, F., RONDE, P., GLASSER, N., GALZI, J. L., MELY, Y., TAKEDA, K. & BUCHER, B. 2011. Contribution of a tyrosine-based motif to cellular trafficking of wild-type and truncated NPY Y(1) receptors. *Cell Signal*, 23, 228-38.
- LECKLIN, A., LUNDELL, I., PAANANEN, L., WIKBERG, J. E., MANNISTO, P. T. & LARHAMMAR, D. 2002. Receptor subtypes Y1 and Y5 mediate neuropeptide Y induced feeding in the guinea-pig. *Br J Pharmacol*, 135, 2029-37.
- LEIBOWITZ, S. F., SLADEK, C., SPENCER, L. & TEMPEL, D. 1988. Neuropeptide Y, epinephrine and norepinephrine in the paraventricular nucleus: stimulation of feeding and the release of corticosterone, vasopressin and glucose. *Brain Res Bull*, 21, 905-12.
- LENNE, P. F., WAWREZINIECK, L., CONCHONAUD, F., WURTZ, O., BONED, A., GUO, X. J., RIGNEAULT, H., HE, H. T. & MARGUET, D. 2006. Dynamic molecular confinement in the plasma membrane by microdomains and the cytoskeleton meshwork. *EMBO J*, 25, 3245-56.
- LEVOYE, A., DAM, J., AYOUB, M. A., GUILLAUME, J. L., COUTURIER, C., DELAGRANGE, P. & JOCKERS, R. 2006. The orphan GPR50 receptor specifically inhibits MT1 melatonin receptor function through heterodimerization. *EMBO J*, 25, 3012-23.
- LICHT, S. S., SONNLEITNER, A., WEISS, S. & SCHULTZ, P. G. 2003. A rugged energy landscape mechanism for trapping of transmembrane receptors during endocytosis. *Biochemistry*, 42, 2916-25.
- LINDNER, D., STICHEL, J. & BECK-SICKINGER, A. G. 2008. Molecular recognition of the NPY hormone family by their receptors. *Nutrition*, 24, 907-17.
- LINDNER, D., WALTHER, C., TENNEMANN, A. & BECK-SICKINGER, A. G. 2009. Functional role of the extracellular N-terminal domain of neuropeptide Y subfamily receptors in membrane integration and agonist-stimulated internalization. *Cell Signal*, 21, 61-8.
- LIPPINCOTT-SCHWARTZ, J., ALTAN-BONNET, N. & PATTERSON, G. H. 2003. Photobleaching and photoactivation: following protein dynamics in living cells. *Nat Cell Biol*, Suppl, S7-14.
- LOHSE, M. J., BENOVIC, J. L., CODINA, J., CARON, M. G. & LEFKOWITZ, R. J. 1990. beta-Arrestin: a protein that regulates beta-adrenergic receptor function. *Science*, 248, 1547-50.
- LOHSE, M. J., HEIN, P., HOFFMANN, C., NIKOLAEV, V. O., VILARDAGA, J. P. & BUNEMANN, M. 2008. Kinetics of G-protein-coupled receptor signals in intact cells. *Br J Pharmacol*, 153 Suppl 1, S125-32.
- LUNDELL, I., BLOMQVIST, A. G., BERGLUND, M. M., SCHOBER, D. A., JOHNSON, D., STATNICK, M. A., GADSKI, R. A., GEHLERT, D. R. & LARHAMMAR, D. 1995. Cloning of a human receptor of the NPY

- receptor family with high affinity for pancreatic polypeptide and peptide YY. *J Biol Chem*, 270, 29123-8.
- LUNDELL, I., RABE BERNHARDT, N., JOHNSON, A. K. & LARHAMMAR, D. 2011. Internalization studies of chimeric neuropeptide Y receptors Y1 and Y2 suggest complex interactions between cytoplasmic domains. *Regul Pept*, 168, 50-8.
- LUNDELL, I., STATNICK, M. A., JOHNSON, D., SCHOBER, D. A., STARBACK, P., GEHLERT, D. R. & LARHAMMAR, D. 1996. The cloned rat pancreatic polypeptide receptor exhibits profound differences to the orthologous receptor. *Proc Natl Acad Sci U S A*, 93, 5111-5.
- LUTTRELL, L. M. & GESTY-PALMER, D. 2010. Beyond desensitization: physiological relevance of arrestin-dependent signaling. *Pharmacol Rev*, 62, 305-30.
- LUTTRELL, L. M. & LEFKOWITZ, R. J. 2002. The role of beta-arrestins in the termination and transduction of G-protein-coupled receptor signals. *J Cell Sci*, 115, 455-65.
- MANCIA, F., ASSUR, Z., HERMAN, A. G., SIEGEL, R. & HENDRICKSON, W. A. 2008. Ligand sensitivity in dimeric associations of the serotonin 5HT<sub>2c</sub> receptor. *EMBO Rep*, 9, 363-9.
- MANGLIK, A., KRUSE, A. C., KOBILKA, T. S., THIAN, F. S., MATHIESEN, J. M., SUNAHARA, R. K., PARDO, L., WEIS, W. I., KOBILKA, B. K. & GRANIER, S. 2012. Crystal structure of the micro-opioid receptor bound to a morphinan antagonist. *Nature*, 485, 321-6.
- MARCELLINO, D., FERRE, S., CASADO, V., CORTES, A., LE FOLL, B., MAZZOLA, C., DRAGO, F., SAUR, O., STARK, H., SORIANO, A., BARNES, C., GOLDBERG, S. R., LLUIS, C., FUXE, K. & FRANCO, R. 2008. Identification of dopamine D1-D3 receptor heteromers. Indications for a role of synergistic D1-D3 receptor interactions in the striatum. *J Biol Chem*, 283, 26016-25.
- MARGETA-MITROVIC, M., JAN, Y. N. & JAN, L. Y. 2000. A trafficking checkpoint controls GABA(B) receptor heterodimerization. *Neuron*, 27, 97-106.
- MARION, S., OAKLEY, R. H., KIM, K. M., CARON, M. G. & BARAK, L. S. 2006. A beta-arrestin binding determinant common to the second intracellular loops of rhodopsin family G protein-coupled receptors. *J Biol Chem*, 281, 2932-8.
- MARKS, J. L., PORTE, D., JR., STAHL, W. L. & BASKIN, D. G. 1990. Localization of insulin receptor mRNA in rat brain by in situ hybridization. *Endocrinology*, 127, 3234-6.
- MARSH, D. J., HOLLOPETER, G., KAFER, K. E. & PALMITER, R. D. 1998. Role of the Y5 neuropeptide Y receptor in feeding and obesity. *Nat Med*, 4, 718-21.
- MASHIKO, S., MORIYA, R., ISHIHARA, A., GOMORI, A., MATSUSHITA, H., EGASHIRA, S., IWAASA, H., TAKAHASHI, T., HAGA, Y., FUKAMI, T. & KANATANI, A. 2009. Synergistic interaction between neuropeptide Y1 and Y5 receptor pathways in regulation of energy homeostasis. *Eur J Pharmacol*, 615, 113-7.
- MASRI, B., SALAHPOUR, A., DIDRIKSEN, M., GHISI, V., BEAULIEU, J. M., GAINETDINOV, R. R. & CARON, M. G. 2008. Antagonism of dopamine D2 receptor/beta-arrestin 2 interaction is a common property of clinically effective antipsychotics. *Proc Natl Acad Sci U S A*, 105, 13656-61.

- MATTHEWS, J. E., JANSEN, M., LYERLY, D., COX, R., CHEN, W. J., KOLLER, K. J. & DANIELS, A. J. 1997. Pharmacological characterization and selectivity of the NPY antagonist GR231118 (1229U91) for different NPY receptors. *Regul Pept*, 72, 113-9.
- MAUREL, D., KNIAZEFF, J., MATHIS, G., TRINQUET, E., PIN, J. P. & ANSANAY, H. 2004. Cell surface detection of membrane protein interaction with homogeneous time-resolved fluorescence resonance energy transfer technology. *Anal Biochem*, 329, 253-62.
- MAURICE, P., KAMAL, M. & JOCKERS, R. 2011. Asymmetry of GPCR oligomers supports their functional relevance. *Trends Pharmacol Sci*, 32, 514-20.
- MAY, L. T., BRIDGE, L. J., STODDART, L. A., BRIDDON, S. J. & HILL, S. J. 2011. Allosteric interactions across native adenosine-A3 receptor homodimers: quantification using single-cell ligand-binding kinetics. *FASEB J*, 25, 3465-76.
- MAY, L. T., LEACH, K., SEXTON, P. M. & CHRISTOPOULOS, A. 2007. Allosteric modulation of G protein-coupled receptors. *Annu Rev Pharmacol Toxicol*, 47, 1-51.
- MCCOY, K. L., GYONEVA, S., VELLANO, C. P., SMRCKA, A. V., TRAYNELIS, S. F. & HEPLER, J. R. 2012. Protease-activated receptor 1 (PAR1) coupling to G(q/11) but not to G(i/o) or G(12/13) is mediated by discrete amino acids within the receptor second intracellular loop. *Cell Signal*, 24, 1351-60.
- MCCREA, K., WISIALOWSKI, T., CABRELE, C., CHURCH, B., BECK-SICKINGER, A., KRAEGER, E. & HERZOG, H. 2000. 2-36[K4,RYYS(19-23)]PP a novel Y5-receptor preferring ligand with strong stimulatory effect on food intake. *Regul Pept*, 87, 47-58.
- MCGAVIGAN, A. K. & MURPHY, K. G. 2012. Gut hormones: the future of obesity treatment? *Br J Clin Pharmacol*, 74, 911-9.
- MCGUIRE, H., AUROUSSEAU, M. R., BOWIE, D. & BLUNCK, R. 2012. Automating single subunit counting of membrane proteins in mammalian cells. *J Biol Chem*, 287, 35912-21.
- MCLEAN, A. J. & MILLIGAN, G. 2000. Ligand regulation of green fluorescent protein-tagged forms of the human beta(1)- and beta(2)-adrenoceptors; comparisons with the unmodified receptors. *Br J Pharmacol*, 130, 1825-32.
- MCNALLY, J. G. 2008. Quantitative FRAP in analysis of molecular binding dynamics in vivo. *Methods Cell Biol*, 85, 329-51.
- MEDEIROS, P. J. & JACKSON, D. N. 2013. Neuropeptide Y Y5-receptor activation on breast cancer cells acts as a paracrine system that stimulates VEGF expression and secretion to promote angiogenesis. *Peptides*, 48C, 106-113.
- MEISSNER, O. & HABERLEIN, H. 2003. Lateral mobility and specific binding to GABA(A) receptors on hippocampal neurons monitored by fluorescence correlation spectroscopy. *Biochemistry*, 42, 1667-72.
- MERCIER, J. F., SALAHPOUR, A., ANGERS, S., BREIT, A. & BOUVIER, M. 2002. Quantitative assessment of beta 1- and beta 2-adrenergic receptor homo- and heterodimerization by bioluminescence resonance energy transfer. *J Biol Chem*, 277, 44925-31.
- MERTEN, N., LINDNER, D., RABE, N., ROMPLER, H., MORL, K., SCHONEBERG, T. & BECK-SICKINGER, A. G. 2007. Receptor subtype-specific docking of Asp6.59 with C-terminal arginine residues in Y receptor ligands. *J Biol Chem*, 282, 7543-51.

- MICHEL, M. C., BECK-SICKINGER, A., COX, H., DOODS, H. N., HERZOG, H., LARHAMMAR, D., QUIRION, R., SCHWARTZ, T. & WESTFALL, T. 1998. XVI. International Union of Pharmacology recommendations for the nomenclature of neuropeptide Y, peptide YY, and pancreatic polypeptide receptors. *Pharmacol Rev*, 50, 143-50.
- MICHNICK, S. W., EAR, P. H., LANDRY, C., MALLESHAIAH, M. K. & MESSIER, V. 2011. Protein-fragment complementation assays for large-scale analysis, functional dissection and dynamic studies of protein-protein interactions in living cells. *Methods Mol Biol*, 756, 395-425.
- MILLIGAN, G. 2009. G protein-coupled receptor hetero-dimerization: contribution to pharmacology and function. *Br J Pharmacol*, 158, 5-14.
- MITCHELL, N. S., CATENACCI, V. A., WYATT, H. R. & HILL, J. O. 2011. Obesity: overview of an epidemic. *Psychiatr Clin North Am*, 34, 717-32.
- MIZUNO, N., SUZUKI, T., HIRASAWA, N. & NAKAHATA, N. 2012. Hetero-oligomerization between adenosine A(1) and thromboxane A(2) receptors and cellular signal transduction on stimulation with high and low concentrations of agonists for both receptors. *Eur J Pharmacol*, 677, 5-14.
- MOLLEREAU, C., GOUARDERES, C., DUMONT, Y., KOTANI, M., DETHEUX, M., DOODS, H., PARMENTIER, M., QUIRION, R. & ZAJAC, J. M. 2001. Agonist and antagonist activities on human NPFF(2) receptors of the NPY ligands GR231118 and BIBP3226. *Br J Pharmacol*, 133, 1-4.
- MONKS, S. A., KARAGIANIS, G., HOWLETT, G. J. & NORTON, R. S. 1996. Solution structure of human neuropeptide Y. *J Biomol NMR*, 8, 379-90.
- MONNIER, C., TU, H., BOURRIER, E., VOL, C., LAMARQUE, L., TRINQUET, E., PIN, J. P. & RONDARD, P. 2011. Trans-activation between 7TM domains: implication in heterodimeric GABAB receptor activation. *EMBO J*, 30, 32-42.
- MONNOT, C., BIHOREAU, C., CONCHON, S., CURNOW, K. M., CORVOL, P. & CLAUSER, E. 1996. Polar residues in the transmembrane domains of the type 1 angiotensin II receptor are required for binding and coupling. Reconstitution of the binding site by co-expression of two deficient mutants. *J Biol Chem*, 271, 1507-13.
- MOORE, C. A., MILANO, S. K. & BENOVIC, J. L. 2007. Regulation of receptor trafficking by GRKs and arrestins. *Annu Rev Physiol*, 69, 451-82.
- MOREIRA, I. S. 2014. Structural features of the G-protein/GPCR interactions. *Biochim Biophys Acta*, 1840, 16-33.
- MORENO, E., MORENO-DELGADO, D., NAVARRO, G., HOFFMANN, H. M., FUENTES, S., ROSELL-VILAR, S., GASPERINI, P., RODRIGUEZ-RUIZ, M., MEDRANO, M., MALLOL, J., CORTES, A., CASADO, V., LLUIS, C., FERRE, S., ORTIZ, J., CANELA, E. & MCCORMICK, P. J. 2014. Cocaine disrupts histamine H3 receptor modulation of dopamine D1 receptor signaling: sigma1-D1-H3 receptor complexes as key targets for reducing cocaine's effects. *J Neurosci*, 34, 3545-58.
- MORRIS, B. J. 1989. Neuronal localisation of neuropeptide Y gene expression in rat brain. *J Comp Neurol*, 290, 358-68.
- MOUNTFORD, S. J., LIU, M., ZHANG, L., GROENEN, M., HERZOG, H., HOLLIDAY, N. D. & THOMPSON, P. E. 2014. Synthetic routes to the Neuropeptide Y Y1 receptor antagonist 1229U91 and related analogues for SAR studies and cell-based imaging. *Org Biomol Chem*, 12, 3271-81.

- MULLINS, D., KIRBY, D., HWA, J., GUZZI, M., RIVIER, J. & PARKER, E. 2001. Identification of potent and selective neuropeptide Y Y(1) receptor agonists with orexigenic activity in vivo. *Mol Pharmacol*, 60, 534-40.
- MUSNIER, A., BLANCHOT, B., REITER, E. & CRÉPIEUX, P. 2010. GPCR signalling to the translation machinery. *Cellular Signalling*, 22, 707-716.
- NAGAI, T., IBATA, K., PARK, E. S., KUBOTA, M., MIKOSHIBA, K. & MIYAWAKI, A. 2002. A variant of yellow fluorescent protein with fast and efficient maturation for cell-biological applications. *Nat Biotechnol*, 20, 87-90.
- NAVARRO, G., CARRIBA, P., GANDIA, J., CIRUELA, F., CASADO, V., CORTES, A., MALLOL, J., CANELA, E. I., LLUIS, C. & FRANCO, R. 2008. Detection of heteromers formed by cannabinoid CB1, dopamine D2, and adenosine A2A G-protein-coupled receptors by combining bimolecular fluorescence complementation and bioluminescence energy transfer. *ScientificWorldJournal*, 8, 1088-97.
- NAVEILHAN, P., HASSANI, H., CANALS, J. M., EKSTRAND, A. J., LAREFALK, A., CHHAJLANI, V., ARENAS, E., GEDDA, K., SVENSSON, L., THOREN, P. & ERNFORS, P. 1999. Normal feeding behavior, body weight and leptin response require the neuropeptide Y Y2 receptor. *Nat Med*, 5, 1188-93.
- NELSON, C. D., PERRY, S. J., REGIER, D. S., PRESCOTT, S. M., TOPHAM, M. K. & LEFKOWITZ, R. J. 2007. Targeting of diacylglycerol degradation to M1 muscarinic receptors by beta-arrestins. *Science*, 315, 663-6.
- NEUSCHAFER-RUBE, F., HERMOSILLA, R., REHWALD, M., RONNSTRAND, L., SCHULEIN, R., WERNSTEDT, C. & PUSCHEL, G. P. 2004. Identification of a Ser/Thr cluster in the C-terminal domain of the human prostaglandin receptor EP4 that is essential for agonist-induced beta-arrestin1 recruitment but differs from the apparent principal phosphorylation site. *Biochem J*, 379, 573-85.
- NGUYEN, A. D., MITCHELL, N. F., LIN, S., MACIA, L., YULYANINGSIH, E., BALDOCK, P. A., ENRIQUEZ, R. F., ZHANG, L., SHI, Y. C., ZOLOTUKHIN, S., HERZOG, H. & SAINSBURY, A. 2012. Y1 and Y5 receptors are both required for the regulation of food intake and energy homeostasis in mice. *PLoS One*, 7, e40191.
- NICKERSON, A., HUANG, T., LIN, L. J. & NAN, X. 2014. Photoactivated localization microscopy with bimolecular fluorescence complementation (BiFC-PALM) for nanoscale imaging of protein-protein interactions in cells. *PLoS One*, 9, e100589.
- NOBLES, K. N., GUAN, Z., XIAO, K., OAS, T. G. & LEFKOWITZ, R. J. 2007. The active conformation of beta-arrestin1: direct evidence for the phosphate sensor in the N-domain and conformational differences in the active states of beta-arrestins1 and -2. *J Biol Chem*, 282, 21370-81.
- NOBLES, K. N., XIAO, K., AHN, S., SHUKLA, A. K., LAM, C. M., RAJAGOPAL, S., STRACHAN, R. T., HUANG, T. Y., BRESSLER, E. A., HARA, M. R., SHENOY, S. K., GYGI, S. P. & LEFKOWITZ, R. J. 2011. Distinct phosphorylation sites on the beta(2)-adrenergic receptor establish a barcode that encodes differential functions of beta-arrestin. *Sci Signal*, 4, ra51.
- NYGAARD, R., ZOU, Y., DROR, R. O., MILDORF, T. J., ARLOW, D. H., MANGLIK, A., PAN, A. C., LIU, C. W., FUNG, J. J., BOKOCH, M. P., THIAN, F. S., KOBILKA, T. S., SHAW, D. E., MUELLER, L., PROSSER, R.

- S. & KOBILKA, B. K. 2013. The dynamic process of beta(2)-adrenergic receptor activation. *Cell*, 152, 532-42.
- OFFERMANN, S., LAUGWITZ, K. L., SPICHER, K. & SCHULTZ, G. 1994. G proteins of the G12 family are activated via thromboxane A2 and thrombin receptors in human platelets. *Proc Natl Acad Sci U S A*, 91, 504-8.
- OLDHAM, W. M. & HAMM, H. E. 2008. Heterotrimeric G protein activation by G-protein-coupled receptors. *Nat Rev Mol Cell Biol*, 9, 60-71.
- ONUOHA, G. N., NUGENT, A. M., HUNTER, S. J., ALPAR, E. K., MCENEANEY, D. J., CAMPBELL, N. P., SHAW, C., BUCHANAN, K. D. & NICHOLLS, D. P. 2000. Neuropeptide variability in man. *Eur J Clin Invest*, 30, 570-7.
- ORMO, M., CUBITT, A. B., KALLIO, K., GROSS, L. A., TSIEN, R. Y. & REMINGTON, S. J. 1996. Crystal structure of the Aequorea victoria green fluorescent protein. *Science*, 273, 1392-5.
- ORTIZ, A. A., MILARDO, L. F., DECARR, L. B., BUCKHOLZ, T. M., MAYS, M. R., CLAUS, T. H., LIVINGSTON, J. N., MAHLE, C. D. & LUMB, K. J. 2007. A novel long-acting selective neuropeptide Y2 receptor polyethylene glycol-conjugated peptide agonist reduces food intake and body weight and improves glucose metabolism in rodents. *J Pharmacol Exp Ther*, 323, 692-700.
- OUEDRAOGO, M., LECAT, S., ROCHDI, M. D., HACHET-HAAS, M., MATTHES, H., GICQUIAUX, H., VERRIER, S., GAIRE, M., GLASSER, N., MELY, Y., TAKEDA, K., BOUVIER, M., GALZI, J. L. & BUCHER, B. 2008. Distinct motifs of neuropeptide Y receptors differentially regulate trafficking and desensitization. *Traffic*, 9, 305-24.
- OZAWA, K., WHALEN, E. J., NELSON, C. D., MU, Y., HESS, D. T., LEFKOWITZ, R. J. & STAMLER, J. S. 2008. S-nitrosylation of beta-arrestin regulates beta-adrenergic receptor trafficking. *Mol Cell*, 31, 395-405.
- PADGETT, C. L. & SLESINGER, P. A. 2010. GABAB receptor coupling to G-proteins and ion channels. *Adv Pharmacol*, 58, 123-47.
- PAGE, K. M., CURTIS, C. A., JONES, P. G. & HULME, E. C. 1995. The functional role of the binding site aspartate in muscarinic acetylcholine receptors, probed by site-directed mutagenesis. *Eur J Pharmacol*, 289, 429-37.
- PAING, M. M., STUTTS, A. B., KOHOUT, T. A., LEFKOWITZ, R. J. & TREJO, J. 2002. beta -Arrestins regulate protease-activated receptor-1 desensitization but not internalization or Down-regulation. *J Biol Chem*, 277, 1292-300.
- PALCZEWSKI, K. 2006. G protein-coupled receptor rhodopsin. *Annu Rev Biochem*, 75, 743-67.
- PALCZEWSKI, K., BUCZYLSKO, J., IMAMI, N. R., MCDOWELL, J. H. & HARGRAVE, P. A. 1991. Role of the carboxyl-terminal region of arrestin in binding to phosphorylated rhodopsin. *J Biol Chem*, 266, 15334-9.
- PALCZEWSKI, K., KUMASAKA, T., HORI, T., BEHNKE, C. A., MOTOSHIMA, H., FOX, B. A., LE TRONG, I., TELLER, D. C., OKADA, T., STENKAMP, R. E., YAMAMOTO, M. & MIYANO, M. 2000. Crystal structure of rhodopsin: A G protein-coupled receptor. *Science*, 289, 739-45.
- PALS-RYLAARSDAM, R., GUREVICH, V. V., LEE, K. B., PTASIENSKI, J. A., BENOVIC, J. L. & HOSEY, M. M. 1997. Internalization of the m2 muscarinic acetylcholine receptor. Arrestin-independent and -dependent pathways. *J Biol Chem*, 272, 23682-9.

- PARK, J. H., SCHEERER, P., HOFMANN, K. P., CHOE, H. W. & ERNST, O. P. 2008. Crystal structure of the ligand-free G-protein-coupled receptor opsin. *Nature*, 454, 183-7.
- PARKER, E. M., BABIJ, C. K., BALASUBRAMANIAM, A., BURRIER, R. E., GUZZI, M., HAMUD, F., MUKHOPADHYAY, G., RUDINSKI, M. S., TAO, Z., TICE, M., XIA, L., MULLINS, D. E. & SALISBURY, B. G. 1998. GR231118 (1229U91) and other analogues of the C-terminus of neuropeptide Y are potent neuropeptide Y Y1 receptor antagonists and neuropeptide Y Y4 receptor agonists. *Eur J Pharmacol*, 349, 97-105.
- PARKER, M. S., SAH, R., SHERIFF, S., BALASUBRAMANIAM, A. & PARKER, S. L. 2005. Internalization of cloned pancreatic polypeptide receptors is accelerated by all types of Y4 agonists. *Regul Pept*, 132, 91-101.
- PARKER, R. M. & HERZOG, H. 1999. Regional distribution of Y-receptor subtype mRNAs in rat brain. *Eur J Neurosci*, 11, 1431-48.
- PARKER, S. L., KANE, J. K., PARKER, M. S., BERGLUND, M. M., LUNDELL, I. A. & LI, M. D. 2001. Cloned neuropeptide Y (NPY) Y1 and pancreatic polypeptide Y4 receptors expressed in Chinese hamster ovary cells show considerable agonist-driven internalization, in contrast to the NPY Y2 receptor. *Eur J Biochem*, 268, 877-86.
- PARKER, S. L., PARKER, M. S., BUSCHAUER, A. & BALASUBRAMANIAM, A. 2003. Ligand internalization by cloned neuropeptide Y Y5 receptors excludes Y2 and Y4 receptor-selective peptides. *Eur J Pharmacol*, 474, 31-42.
- PARKER, S. L., PARKER, M. S., LUNDELL, I., BALASUBRAMANIAM, A., BUSCHAUER, A., KANE, J. K., YALCIN, A. & BERGLUND, M. M. 2002. Agonist internalization by cloned Y1 neuropeptide Y (NPY) receptor in Chinese hamster ovary cells shows strong preference for NPY, endosome-linked entry and fast receptor recycling. *Regul Pept*, 107, 49-62.
- PATEL, R. C., KUMAR, U., LAMB, D. C., EID, J. S., ROCHEVILLE, M., GRANT, M., RANI, A., HAZLETT, T., PATEL, S. C., GRATTON, E. & PATEL, Y. C. 2002. Ligand binding to somatostatin receptors induces receptor-specific oligomer formation in live cells. *Proc Natl Acad Sci U S A*, 99, 3294-9.
- PATTERSON, G. H. 2007. Fluorescent proteins for cell biology. *Methods Mol Biol*, 411, 47-80.
- PEDELACQ, J. D., CABANTOUS, S., TRAN, T., TERWILLIGER, T. C. & WALDO, G. S. 2006. Engineering and characterization of a superfolder green fluorescent protein. *Nat Biotechnol*, 24, 79-88.
- PEDRAGOSA-BADIA, X., STICHEL, J. & BECK-SICKINGER, A. G. 2013. Neuropeptide Y receptors: how to get subtype selectivity. *Front Endocrinol (Lausanne)*, 4, 5.
- PEDRAZZINI, T., SEYDOUX, J., KUNSTNER, P., AUBERT, J. F., GROUZMANN, E., BEERMANN, F. & BRUNNER, H. R. 1998. Cardiovascular response, feeding behavior and locomotor activity in mice lacking the NPY Y1 receptor. *Nat Med*, 4, 722-6.
- PEETERS, M. C., VAN WESTEN, G. J., GUO, D., WISSE, L. E., MULLER, C. E., BEUKERS, M. W. & IJZERMAN, A. P. 2011. GPCR structure and activation: an essential role for the first extracellular loop in activating the adenosine A2B receptor. *FASEB J*, 25, 632-43.

- PEGG, A. E. 2011. Multifaceted roles of alkyltransferase and related proteins in DNA repair, DNA damage, resistance to chemotherapy, and research tools. *Chem Res Toxicol*, 24, 618-39.
- PELLISSIER, L. P., BARTHET, G., GAVEN, F., CASSIER, E., TRINQUET, E., PIN, J. P., MARIN, P., DUMUIS, A., BOCKAERT, J., BANERES, J. L. & CLAEYSEN, S. 2011. G protein activation by serotonin type 4 receptor dimers: evidence that turning on two protomers is more efficient. *J Biol Chem*.
- PFEIFFER, M., KIRSCHT, S., STUMM, R., KOCH, T., WU, D., LAUGSCH, M., SCHRODER, H., HOLLT, V. & SCHULZ, S. 2003. Heterodimerization of substance P and mu-opioid receptors regulates receptor trafficking and resensitization. *J Biol Chem*, 278, 51630-7.
- PHENG, L. H., DUMONT, Y., FOURNIER, A., CHABOT, J. G., BEAUDET, A. & QUIRION, R. 2003. Agonist- and antagonist-induced sequestration/internalization of neuropeptide Y Y1 receptors in HEK293 cells. *Br J Pharmacol*, 139, 695-704.
- PHILIP, F., SENGUPTA, P. & SCARLATA, S. 2007. Signaling through a G Protein-coupled receptor and its corresponding G protein follows a stoichiometrically limited model. *J Biol Chem*, 282, 19203-16.
- PIECHOWSKI, C. L., REDIGER, A., LAGEMANN, C., MUHLHAUS, J., MULLER, A., PRATZKA, J., TARNOW, P., GRUTERS, A., KRUDE, H., KLEINAU, G. & BIEBERMANN, H. 2013. Inhibition of melanocortin-4 receptor dimerization by substitutions in intracellular loop 2. *J Mol Endocrinol*, 51, 109-18.
- PIERCE, K. L., PREMONT, R. T. & LEFKOWITZ, R. J. 2002. Seven-transmembrane receptors. *Nat Rev Mol Cell Biol*, 3, 639-50.
- PIN, J. P., NEUBIG, R., BOUVIER, M., DEVI, L., FILIZOLA, M., JAVITCH, J. A., LOHSE, M. J., MILLIGAN, G., PALCZEWSKI, K., PARMENTIER, M. & SPEDDING, M. 2007. International Union of Basic and Clinical Pharmacology. LXVII. Recommendations for the recognition and nomenclature of G protein-coupled receptor heteromultimers. *Pharmacol Rev*, 59, 5-13.
- PITTNER, R. A., MOORE, C. X., BHAVSAR, S. P., GEDULIN, B. R., SMITH, P. A., JODKA, C. M., PARKES, D. G., PATERNITI, J. R., SRIVASTAVA, V. P. & YOUNG, A. A. 2004. Effects of PYY[3-36] in rodent models of diabetes and obesity. *Int J Obes Relat Metab Disord*, 28, 963-71.
- PORRELLO, E. R., PFLEGER, K. D., SEEBER, R. M., QIAN, H., ORO, C., ABOGADIE, F., DELBRIDGE, L. M. & THOMAS, W. G. 2011. Heteromerization of angiotensin receptors changes trafficking and arrestin recruitment profiles. *Cell Signal*, 23, 1767-76.
- POU, C., MANNOURY LA COUR, C., STODDART, L. A., MILLAN, M. J. & MILLIGAN, G. 2012. Functional homomers and heteromers of dopamine D2L and D3 receptors co-exist at the cell surface. *J Biol Chem*, 287, 8864-78.
- POULIN, B., BUTCHER, A., MCWILLIAMS, P., BOURGOGNON, J. M., PAWLAK, R., KONG, K. C., BOTTRILL, A., MISTRY, S., WESS, J., ROSETHORNE, E. M., CHARLTON, S. J. & TOBIN, A. B. 2010. The M3-muscarinic receptor regulates learning and memory in a receptor phosphorylation/arrestin-dependent manner. *Proc Natl Acad Sci U S A*, 107, 9440-5.
- PRALONG, F. P., GONZALES, C., VOIROL, M. J., PALMITER, R. D., BRUNNER, H. R., GAILLARD, R. C., SEYDOUX, J. & PEDRAZZINI, T. 2002. The

- neuropeptide Y Y1 receptor regulates leptin-mediated control of energy homeostasis and reproductive functions. *FASEB J*, 16, 712-4.
- PRASHER, D. C., ECKENRODE, V. K., WARD, W. W., PRENDERGAST, F. G. & CORMIER, M. J. 1992. Primary structure of the *Aequorea victoria* green-fluorescent protein. *Gene*, 111, 229-33.
- PREMONT, R. T. & GAINETDINOV, R. R. 2007. Physiological roles of G protein-coupled receptor kinases and arrestins. *Annu Rev Physiol*, 69, 511-34.
- PREZEAU, L., RIVES, M. L., COMPS-AGRAR, L., MAUREL, D., KNIAZEFF, J. & PIN, J. P. 2010. Functional crosstalk between GPCRs: with or without oligomerization. *Curr Opin Pharmacol*, 10, 6-13.
- PRZYBYLA, J. A. & WATTS, V. J. 2010. Ligand-induced regulation and localization of cannabinoid CB1 and dopamine D2L receptor heterodimers. *J Pharmacol Exp Ther*, 332, 710-9.
- PUCA, L. & BROU, C. 2014. Alpha-arrestins - new players in Notch and GPCR signaling pathways in mammals. *J Cell Sci*, 127, 1359-67.
- RABIET, M. J., HUET, E. & BOULAY, F. 2008. Complement component 5a receptor oligomerization and homologous receptor down-regulation. *J Biol Chem*, 283, 31038-46.
- RAEHAL, K. M., SCHMID, C. L., GROER, C. E. & BOHN, L. M. 2011. Functional selectivity at the mu-opioid receptor: implications for understanding opioid analgesia and tolerance. *Pharmacol Rev*, 63, 1001-19.
- RAJAGOPAL, S., KIM, J., AHN, S., CRAIG, S., LAM, C. M., GERARD, N. P., GERARD, C. & LEFKOWITZ, R. J. 2010. Beta-arrestin- but not G protein-mediated signaling by the "decoy" receptor CXCR7. *Proc Natl Acad Sci U S A*, 107, 628-32.
- RAMAN, D., OSAWA, S. & WEISS, E. R. 1999. Binding of arrestin to cytoplasmic loop mutants of bovine rhodopsin. *Biochemistry*, 38, 5117-23.
- RANG, H. P. 2003. *Pharmacology*, Churchill Livingstone.
- RASHID, A. J., SO, C. H., KONG, M. M., FURTAK, T., EL-GHUNDI, M., CHENG, R., O'DOWD, B. F. & GEORGE, S. R. 2007. D1-D2 dopamine receptor heterooligomers with unique pharmacology are coupled to rapid activation of Gq/11 in the striatum. *Proc Natl Acad Sci U S A*, 104, 654-9.
- RASMUSSEN, S. G., CHOI, H. J., FUNG, J. J., PARDON, E., CASAROSA, P., CHAE, P. S., DEVREE, B. T., ROSENBAUM, D. M., THIAN, F. S., KOBILKA, T. S., SCHNAPP, A., KONETZKI, I., SUNAHARA, R. K., GELLMAN, S. H., PAUTSCH, A., STEYAERT, J., WEIS, W. I. & KOBILKA, B. K. 2011a. Structure of a nanobody-stabilized active state of the beta(2) adrenoceptor. *Nature*, 469, 175-80.
- RASMUSSEN, S. G., CHOI, H. J., ROSENBAUM, D. M., KOBILKA, T. S., THIAN, F. S., EDWARDS, P. C., BURGHAMMER, M., RATNALA, V. R., SANISHVILI, R., FISCHETTI, R. F., SCHERTLER, G. F., WEIS, W. I. & KOBILKA, B. K. 2007a. Crystal structure of the human beta2 adrenergic G-protein-coupled receptor. *Nature*, 450, 383-7.
- RASMUSSEN, S. G., DEVREE, B. T., ZOU, Y., KRUSE, A. C., CHUNG, K. Y., KOBILKA, T. S., THIAN, F. S., CHAE, P. S., PARDON, E., CALINSKI, D., MATHIESEN, J. M., SHAH, S. T., LYONS, J. A., CAFFREY, M., GELLMAN, S. H., STEYAERT, J., SKINIOTIS, G., WEIS, W. I., SUNAHARA, R. K. & KOBILKA, B. K. 2011b. Crystal structure of the beta2 adrenergic receptor-Gs protein complex. *Nature*, 477, 549-55.

- RASMUSSEN, S. G. F., CHOI, H.-J., ROSENBAUM, D. M., KOBILKA, T. S., THIAN, F. S., EDWARDS, P. C., BURGHAMMER, M., RATNALA, V. R. P., SANISHVILI, R., FISCHETTI, R. F., SCHERTLER, G. F. X., WEIS, W. I. & KOBILKA, B. K. 2007b. Crystal structure of the human [bgr]2 adrenergic G-protein-coupled receptor. *Nature*, 450, 383-387.
- REICH, N. C. 2007. STAT dynamics. *Cytokine Growth Factor Rev*, 18, 511-8.
- REUVEN, E. M., FINK, A. & SHAI, Y. 2014. Regulation of innate immune responses by transmembrane interactions: Lessons from the TLR family. *Biochim Biophys Acta*, 1838, 1586-1593.
- RICHARDSON, M. D., BALIUS, A. M., YAMAGUCHI, K., FREILICH, E. R., BARAK, L. S. & KWATRA, M. M. 2003. Human substance P receptor lacking the C-terminal domain remains competent to desensitize and internalize. *J Neurochem*, 84, 854-63.
- RIVES, M. L., VOL, C., FUKAZAWA, Y., TINEL, N., TRINQUET, E., AYOUB, M. A., SHIGEMOTO, R., PIN, J. P. & PREZEAU, L. 2009. Crosstalk between GABAB and mGlu1a receptors reveals new insight into GPCR signal integration. *EMBO J*, 28, 2195-208.
- ROMANO, C., YANG, W. L. & O'MALLEY, K. L. 1996. Metabotropic glutamate receptor 5 is a disulfide-linked dimer. *J Biol Chem*, 271, 28612-6.
- ROMO, T. D., GROSSFIELD, A. & PITMAN, M. C. 2010. Concerted interconversion between ionic lock substates of the beta(2) adrenergic receptor revealed by microsecond timescale molecular dynamics. *Biophys J*, 98, 76-84.
- ROSE, P. M., LYNCH, J. S., FRAZIER, S. T., FISHER, S. M., CHUNG, W., BATTAGLINO, P., FATHI, Z., LEIBEL, R. & FERNANDES, P. 1997. Molecular genetic analysis of a human neuropeptide Y receptor. The human homolog of the murine "Y5" receptor may be a pseudogene. *J Biol Chem*, 272, 3622-7.
- ROSE, R. H., BRIDDON, S. J. & HILL, S. J. 2012. A novel fluorescent histamine H(1) receptor antagonist demonstrates the advantage of using fluorescence correlation spectroscopy to study the binding of lipophilic ligands. *Br J Pharmacol*, 165, 1789-800.
- ROSE RH, B. S., HOLLIDAY ND. 2010. Bimolecular fluorescence complementation: lighting up seven transmembrane domain receptor signalling networks. *British Journal of Pharmacology*, 159, 738-750.
- ROSENBAUM, D. M., CHEREZOV, V., HANSON, M. A., RASMUSSEN, S. G., THIAN, F. S., KOBILKA, T. S., CHOI, H. J., YAO, X. J., WEIS, W. I., STEVENS, R. C. & KOBILKA, B. K. 2007. GPCR engineering yields high-resolution structural insights into beta2-adrenergic receptor function. *Science*, 318, 1266-73.
- ROVIRA, X., VIVO, M., SERRA, J., ROCHE, D., STRANGE, P. G. & GIRALDO, J. 2009. Modelling the interdependence between the stoichiometry of receptor oligomerization and ligand binding for a coexisting dimer/tetramer receptor system. *Br J Pharmacol*, 156, 28-35.
- ROZENFELD, R. & DEVI, L. A. 2007. Receptor heterodimerization leads to a switch in signaling: beta-arrestin2-mediated ERK activation by mu-delta opioid receptor heterodimers. *FASEB J*, 21, 2455-65.
- ROZENFELD, R. & DEVI, L. A. 2010. Receptor heteromerization and drug discovery. *Trends Pharmacol Sci*, 31, 124-30.
- ROZENFELD, R., GUPTA, A., GAGNIDZE, K., LIM, M. P., GOMES, I., LEE-RAMOS, D., NIETO, N. & DEVI, L. A. 2011. AT1R-CB(1)R

- heteromerization reveals a new mechanism for the pathogenic properties of angiotensin II. *EMBO J*, 30, 2350-63.
- SAINSBURY, A., BALDOCK, P. A., SCHWARZER, C., UENO, N., ENRIQUEZ, R. F., COUZENS, M., INUI, A., HERZOG, H. & GARDINER, E. M. 2003. Synergistic effects of Y2 and Y4 receptors on adiposity and bone mass revealed in double knockout mice. *Mol Cell Biol*, 23, 5225-33.
- SAINSBURY, A., SCHWARZER, C., COUZENS, M., FETISSOV, S., FURTINGER, S., JENKINS, A., COX, H. M., SPERK, G., HOKFELT, T. & HERZOG, H. 2002. Important role of hypothalamic Y2 receptors in body weight regulation revealed in conditional knockout mice. *Proc Natl Acad Sci U S A*, 99, 8938-43.
- SALAHPOUR, A., ESPINOZA, S., MASRI, B., LAM, V., BARAK, L. S. & GAINETDINOV, R. R. 2012. BRET biosensors to study GPCR biology, pharmacology, and signal transduction. *Front Endocrinol (Lausanne)*, 3, 105.
- SALOMON, Y., LONDOS, C. & RODBELL, M. 1974. A highly sensitive adenylate cyclase assay. *Anal Biochem*, 58, 541-8.
- SAMAMA, P., COTECCHIA, S., COSTA, T. & LEFKOWITZ, R. J. 1993. A mutation-induced activated state of the beta 2-adrenergic receptor. Extending the ternary complex model. *J Biol Chem*, 268, 4625-36.
- SARTANIA, N., APPELBE, S., PEDIANI, J. D. & MILLIGAN, G. 2007. Agonist occupancy of a single monomeric element is sufficient to cause internalization of the dimeric beta2-adrenoceptor. *Cell Signal*, 19, 1928-38.
- SATO, T., KOBAYASHI, H., NAGAO, T. & KUROSE, H. 1999. Ser203 as well as Ser204 and Ser207 in fifth transmembrane domain of the human beta2-adrenoceptor contributes to agonist binding and receptor activation. *Br J Pharmacol*, 128, 272-4.
- SATO, Y., KUROSE, H., ISOGAYA, M. & NAGAO, T. 1996. Molecular characterization of pharmacological properties of T-0509 for beta-adrenoceptors. *Eur J Pharmacol*, 315, 363-7.
- SATOH, A. K., XIA, H., YAN, L., LIU, C. H., HARDIE, R. C. & READY, D. F. 2010. Arrestin translocation is stoichiometric to rhodopsin isomerization and accelerated by phototransduction in *Drosophila* photoreceptors. *Neuron*, 67, 997-1008.
- SAULIERE, A., GAIBELET, G., MILLOT, C., MAZERES, S., LOPEZ, A. & SALOME, L. 2006. Diffusion of the mu opioid receptor at the surface of human neuroblastoma SH-SY5Y cells is restricted to permeable domains. *FEBS Lett*, 580, 5227-31.
- SAUTEL, M., MARTINEZ, R., MUNOZ, M., PEITSCH, M. C., BECK-SICKINGER, A. G. & WALKER, P. 1995. Role of a hydrophobic pocket of the human Y1 neuropeptide Y receptor in ligand binding. *Mol Cell Endocrinol*, 112, 215-22.
- SAUTEL, M., RUDOLF, K., WITTNEBEN, H., HERZOG, H., MARTINEZ, R., MUNOZ, M., EBERLEIN, W., ENGEL, W., WALKER, P. & BECK-SICKINGER, A. G. 1996. Neuropeptide Y and the nonpeptide antagonist BIBP 3226 share an overlapping binding site at the human Y1 receptor. *Mol Pharmacol*, 50, 285-92.
- SAVARESE, T. M. & FRASER, C. M. 1992. In vitro mutagenesis and the search for structure-function relationships among G protein-coupled receptors. *Biochem J*, 283 ( Pt 1), 1-19.

- SCARSELLI, M., NOVI, F., SCHALLMACH, E., LIN, R., BARAGLI, A., COLZI, A., GRIFFON, N., CORSINI, G. U., SOKOLOFF, P., LEVENSON, R., VOGEL, Z. & MAGGIO, R. 2001. D2/D3 dopamine receptor heterodimers exhibit unique functional properties. *J Biol Chem*, 276, 30308-14.
- SCHEER, A., COSTA, T., FANELLI, F., DE BENEDETTI, P. G., MHAOUTY-KODJA, S., ABUIN, L., NENNIGER-TOSATO, M. & COTECCHIA, S. 2000. Mutational analysis of the highly conserved arginine within the Glu/Asp-Arg-Tyr motif of the alpha(1b)-adrenergic receptor: effects on receptor isomerization and activation. *Mol Pharmacol*, 57, 219-31.
- SCHEERER, P., PARK, J. H., HILDEBRAND, P. W., KIM, Y. J., KRAUSS, N., CHOE, H. W., HOFMANN, K. P. & ERNST, O. P. 2008. Crystal structure of opsin in its G-protein-interacting conformation. *Nature*, 455, 497-502.
- SCHWARTZ, T. W., HOLST, J. J., FAHRENKRUG, J., JENSEN, S. L., NIELSEN, O. V., REHFELD, J. F., DE MUCKADELL, O. B. & STADIL, F. 1978. Vagal, cholinergic regulation of pancreatic polypeptide secretion. *J Clin Invest*, 61, 781-9.
- SCHWILLE, P. 2001. Fluorescence correlation spectroscopy and its potential for intracellular applications. *Cell Biochem Biophys*, 34, 383-408.
- SHAN, J., WEINSTEIN, H. & MEHLER, E. L. 2010. Probing the structural determinants for the function of intracellular loop 2 in structurally cognate G-protein-coupled receptors. *Biochemistry*, 49, 10691-701.
- SHENOY, S. K. & LEFKOWITZ, R. J. 2003. Trafficking patterns of beta-arrestin and G protein-coupled receptors determined by the kinetics of beta-arrestin deubiquitination. *J Biol Chem*, 278, 14498-506.
- SHERIFF, S., ALI, M., YAHYA, A., HAIDER, K. H., BALASUBRAMANIAM, A. & AMLAL, H. 2010. Neuropeptide Y Y5 receptor promotes cell growth through extracellular signal-regulated kinase signaling and cyclic AMP inhibition in a human breast cancer cell line. *Mol Cancer Res*, 8, 604-14.
- SHI, Y. C., LIN, S., WONG, I. P., BALDOCK, P. A., ALJANOVA, A., ENRIQUEZ, R. F., CASTILLO, L., MITCHELL, N. F., YE, J. M., ZHANG, L., MACIA, L., YULYANINGSIH, E., NGUYEN, A. D., RIEPLER, S. J., HERZOG, H. & SAINSBURY, A. 2010. NPY neuron-specific Y2 receptors regulate adipose tissue and trabecular bone but not cortical bone homeostasis in mice. *PLoS One*, 5, e11361.
- SHIMAMURA, T., SHIROISHI, M., WEYAND, S., TSUJIMOTO, H., WINTER, G., KATRITCH, V., ABAGYAN, R., CHEREZOV, V., LIU, W., HAN, G. W., KOBAYASHI, T., STEVENS, R. C. & IWATA, S. 2011. Structure of the human histamine H1 receptor complex with doxepin. *Nature*, 475, 65-70.
- SHUKLA, A. K., MANGLIK, A., KRUSE, A. C., XIAO, K., REIS, R. I., TSENG, W. C., STAUS, D. P., HILGER, D., UYSAL, S., HUANG, L. Y., PADUCH, M., TRIPATHI-SHUKLA, P., KOIDE, A., KOIDE, S., WEIS, W. I., KOSSIAKOFF, A. A., KOBILKA, B. K. & LEFKOWITZ, R. J. 2013. Structure of active beta-arrestin-1 bound to a G-protein-coupled receptor phosphopeptide. *Nature*, 497, 137-41.
- SHUKLA, A. K., VIOLIN, J. D., WHALEN, E. J., GESTY-PALMER, D., SHENOY, S. K. & LEFKOWITZ, R. J. 2008. Distinct conformational changes in beta-arrestin report biased agonism at seven-transmembrane receptors. *Proc Natl Acad Sci U S A*, 105, 9988-93.

- SJODIN, P., HOLMBERG, S. K., AKERBERG, H., BERGLUND, M. M., MOHELL, N. & LARHAMMAR, D. 2006. Re-evaluation of receptor-ligand interactions of the human neuropeptide Y receptor Y1: a site-directed mutagenesis study. *Biochem J*, 393, 161-9.
- SKAKUN, V. V., ENGEL, R., BORST, J. W., APANASOVICH, V. V. & VISSER, A. J. 2012. Simultaneous diffusion and brightness measurements and brightness profile visualization from single fluorescence fluctuation traces of GFP in living cells. *Eur Biophys J*, 41, 1055-64.
- SLOTH, B., HOLST, J. J., FLINT, A., GREGERSEN, N. T. & ASTRUP, A. 2007. Effects of PYY1-36 and PYY3-36 on appetite, energy intake, energy expenditure, glucose and fat metabolism in obese and lean subjects. *Am J Physiol Endocrinol Metab*, 292, E1062-8.
- SMITH, N. J. & MILLIGAN, G. 2010. Allosterism at G protein-coupled receptor homo- and heteromers: uncharted pharmacological landscapes. *Pharmacol Rev*, 62, 701-25.
- SO, C. H., VERMA, V., ALIJANIARAM, M., CHENG, R., RASHID, A. J., O'DOWD, B. F. & GEORGE, S. R. 2009. Calcium signaling by dopamine D5 receptor and D5-D2 receptor hetero-oligomers occurs by a mechanism distinct from that for dopamine D1-D2 receptor hetero-oligomers. *Mol Pharmacol*, 75, 843-54.
- SOHY, D., PARMENTIER, M. & SPRINGAEL, J. Y. 2007. Allosteric transinhibition by specific antagonists in CCR2/CXCR4 heterodimers. *J Biol Chem*, 282, 30062-9.
- SOMMER, M. E., HOFMANN, K. P. & HECK, M. 2011. Arrestin-rhodopsin binding stoichiometry in isolated rod outer segment membranes depends on the percentage of activated receptors. *J Biol Chem*, 286, 7359-69.
- SOMMER, M. E., HOFMANN, K. P. & HECK, M. 2012. Distinct loops in arrestin differentially regulate ligand binding within the GPCR opsin. *Nat Commun*, 3, 995.
- SONG, X., COFFA, S., FU, H. & GUREVICH, V. V. 2009. How does arrestin assemble MAPKs into a signaling complex? *J Biol Chem*, 284, 685-95.
- SPRINGAEL, J. Y., LE MINH, P. N., URIZAR, E., COSTAGLIOLA, S., VASSART, G. & PARMENTIER, M. 2006. Allosteric modulation of binding properties between units of chemokine receptor homo- and hetero-oligomers. *Mol Pharmacol*, 69, 1652-61.
- SRIVASTAVA, A., YANO, J., HIROZANE, Y., KEFALA, G., GRUSWITZ, F., SNELL, G., LANE, W., IVETAC, A., AERTGEERTS, K., NGUYEN, J., JENNINGS, A. & OKADA, K. 2014. High-resolution structure of the human GPR40 receptor bound to allosteric agonist TAK-875. *Nature*.
- STANLEY, B. G., KYRKOULI, S. E., LAMPERT, S. & LEIBOWITZ, S. F. 1986. Neuropeptide Y chronically injected into the hypothalamus: a powerful neurochemical inducer of hyperphagia and obesity. *Peptides*, 7, 1189-92.
- STANLEY, B. G. & LEIBOWITZ, S. F. 1985. Neuropeptide Y injected in the paraventricular hypothalamus: a powerful stimulant of feeding behavior. *Proc Natl Acad Sci U S A*, 82, 3940-3.
- STEPHENS, T. W. & CARO, J. F. 1998. To be lean or not to be lean. Is leptin the answer? *Exp Clin Endocrinol Diabetes*, 106, 1-15.
- STRADER, C. D., CANDELORE, M. R., HILL, W. S., SIGAL, I. S. & DIXON, R. A. 1989. Identification of two serine residues involved in agonist activation of the beta-adrenergic receptor. *J Biol Chem*, 264, 13572-8.

- STRADER, C. D., SIGAL, I. S., CANDELORE, M. R., RANDS, E., HILL, W. S. & DIXON, R. A. 1988. Conserved aspartic acid residues 79 and 113 of the beta-adrenergic receptor have different roles in receptor function. *J Biol Chem*, 263, 10267-71.
- SUN, Q. Q., HUGUENARD, J. R. & PRINCE, D. A. 2001. Neuropeptide Y receptors differentially modulate G-protein-activated inwardly rectifying K<sup>+</sup> channels and high-voltage-activated Ca<sup>2+</sup> channels in rat thalamic neurons. *J Physiol*, 531, 67-79.
- SUZUKI, K., RITCHIE, K., KAJIKAWA, E., FUJIWARA, T. & KUSUMI, A. 2005. Rapid hop diffusion of a G-protein-coupled receptor in the plasma membrane as revealed by single-molecule techniques. *Biophys J*, 88, 3659-80.
- SUZUKI, S., CHUANG, L. F., YAU, P., DOI, R. H. & CHUANG, R. Y. 2002. Interactions of opioid and chemokine receptors: oligomerization of mu, kappa, and delta with CCR5 on immune cells. *Exp Cell Res*, 280, 192-200.
- SZALAI, B., BARKAI, L., TURU, G., SZIDONYA, L., VARNAI, P. & HUNYADY, L. 2012. Allosteric interactions within the AT(1) angiotensin receptor homodimer: role of the conserved DRY motif. *Biochem Pharmacol*, 84, 477-85.
- TANG, W. J. & HURLEY, J. H. 1998. Catalytic mechanism and regulation of mammalian adenylyl cyclases. *Mol Pharmacol*, 54, 231-40.
- TER HAAR, E., HARRISON, S. C. & KIRCHHAUSEN, T. 2000. Peptide-in-groove interactions link target proteins to the beta-propeller of clathrin. *Proc Natl Acad Sci U S A*, 97, 1096-100.
- TERRILLON, S. & BOUVIER, M. 2004. Receptor activity-independent recruitment of betaarrestin2 reveals specific signalling modes. *EMBO J*, 23, 3950-61.
- TERRILLON, S., DURROUX, T., MOUILLAC, B., BREIT, A., AYOUB, M. A., TAULAN, M., JOCKERS, R., BARBERIS, C. & BOUVIER, M. 2003. Oxytocin and vasopressin V1a and V2 receptors form constitutive homo- and heterodimers during biosynthesis. *Mol Endocrinol*, 17, 677-91.
- TESMER, J. J., SUNAHARA, R. K., GILMAN, A. G. & SPRANG, S. R. 1997. Crystal structure of the catalytic domains of adenylyl cyclase in a complex with G $\alpha$ .GTP $\gamma$ S. *Science*, 278, 1907-16.
- TORVINEN, M., MARCELLINO, D., CANALS, M., AGNATI, L. F., LLUIS, C., FRANCO, R. & FUXE, K. 2005. Adenosine A2A receptor and dopamine D3 receptor interactions: evidence of functional A2A/D3 heteromeric complexes. *Mol Pharmacol*, 67, 400-7.
- TOUGH, I. R., HOLLIDAY, N. D. & COX, H. M. 2006. Y(4) receptors mediate the inhibitory responses of pancreatic polypeptide in human and mouse colon mucosa. *J Pharmacol Exp Ther*, 319, 20-30.
- TRIFILIEFF, P., RIVES, M. L., URIZAR, E., PISKOROWSKI, R. A., VISHWASRAO, H. D., CASTRILLON, J., SCHMAUSS, C., SLATTMAN, M., GULLBERG, M. & JAVITCH, J. A. 2011. Detection of antigen interactions ex vivo by proximity ligation assay: endogenous dopamine D2-adenosine A2A receptor complexes in the striatum. *Biotechniques*, 51, 111-8.
- TSAO, P. I. & VON ZASTROW, M. 2001. Diversity and specificity in the regulated endocytic membrane trafficking of G-protein-coupled receptors. *Pharmacol Ther*, 89, 139-47.

- TSIEN, R. Y. 1998. The green fluorescent protein. *Annu Rev Biochem*, 67, 509-44.
- TSUKAMOTO, H., SINHA, A., DEWITT, M. & FARRENS, D. L. 2010. Monomeric rhodopsin is the minimal functional unit required for arrestin binding. *J Mol Biol*, 399, 501-11.
- UBERTI, M. A., HAGUE, C., OLLER, H., MINNEMAN, K. P. & HALL, R. A. 2005. Heterodimerization with beta2-adrenergic receptors promotes surface expression and functional activity of alpha1D-adrenergic receptors. *J Pharmacol Exp Ther*, 313, 16-23.
- UNAL, H., JAGANNATHAN, R. & KARNIK, S. S. 2012. Mechanism of GPCR-directed autoantibodies in diseases. *Adv Exp Med Biol*, 749, 187-99.
- UNGER, V. M. & SCHERTLER, G. F. 1995. Low resolution structure of bovine rhodopsin determined by electron cryo-microscopy. *Biophys J*, 68, 1776-86.
- URIBE, A., ZARINAN, T., PEREZ-SOLIS, M. A., GUTIERREZ-SAGAL, R., JARDON-VALADEZ, E., PINEIRO, A., DIAS, J. A. & ULLOA-AGUIRRE, A. 2008. Functional and structural roles of conserved cysteine residues in the carboxyl-terminal domain of the follicle-stimulating hormone receptor in human embryonic kidney 293 cells. *Biol Reprod*, 78, 869-82.
- URIZAR, E., MONTANELLI, L., LOY, T., BONOMI, M., SWILLENS, S., GALES, C., BOUVIER, M., SMITS, G., VASSART, G. & COSTAGLIOLA, S. 2005. Glycoprotein hormone receptors: link between receptor homodimerization and negative cooperativity. *EMBO J*, 24, 1954-64.
- VENKATAKRISHNAN, A. J., DEUPI, X., LEBON, G., TATE, C. G., SCHERTLER, G. F. & BABU, M. M. 2013. Molecular signatures of G-protein-coupled receptors. *Nature*, 494, 185-94.
- VIDI, P. A., CHEMEL, B. R., HU, C. D. & WATTS, V. J. 2008a. Ligand-dependent oligomerization of dopamine D(2) and adenosine A(2A) receptors in living neuronal cells. *Mol Pharmacol*, 74, 544-51.
- VIDI, P. A., CHEN, J., IRUDAYARAJ, J. M. & WATTS, V. J. 2008b. Adenosine A(2A) receptors assemble into higher-order oligomers at the plasma membrane. *FEBS Lett*, 582, 3985-90.
- VIDI, P. A. & WATTS, V. J. 2009. Fluorescent and bioluminescent protein-fragment complementation assays in the study of G protein-coupled receptor oligomerization and signaling. *Mol Pharmacol*, 75, 733-9.
- VILARDAGA, J. P., JEAN-ALPHONSE, F. G. & GARDELLA, T. J. 2014. Endosomal generation of cAMP in GPCR signaling. *Nat Chem Biol*, 10, 700-6.
- VILARDAGA, J. P., NIKOLAEV, V. O., LORENZ, K., FERRANDON, S., ZHUANG, Z. & LOHSE, M. J. 2008. Conformational cross-talk between alpha2A-adrenergic and mu-opioid receptors controls cell signaling. *Nat Chem Biol*, 4, 126-31.
- VIOLIN, J. D., CROMBIE, A. L., SOERGEL, D. G. & LARK, M. W. 2014. Biased ligands at G-protein-coupled receptors: promise and progress. *Trends Pharmacol Sci*, 35, 308-16.
- VIOLIN, J. D., DEWIRE, S. M., YAMASHITA, D., ROMINGER, D. H., NGUYEN, L., SCHILLER, K., WHALEN, E. J., GOWEN, M. & LARK, M. W. 2010. Selectively engaging beta-arrestins at the angiotensin II type 1 receptor reduces blood pressure and increases cardiac performance. *J Pharmacol Exp Ther*, 335, 572-9.

- VISHNIVETSKIY, S. A., FRANCIS, D., VAN EPS, N., KIM, M., HANSON, S. M., KLUG, C. S., HUBBELL, W. L. & GUREVICH, V. V. 2010. The role of arrestin alpha-helix I in receptor binding. *J Mol Biol*, 395, 42-54.
- VISHNIVETSKIY, S. A., GIMENEZ, L. E., FRANCIS, D. J., HANSON, S. M., HUBBELL, W. L., KLUG, C. S. & GUREVICH, V. V. 2011. Few residues within an extensive binding interface drive receptor interaction and determine the specificity of arrestin proteins. *J Biol Chem*, 286, 24288-99.
- VISHNIVETSKIY, S. A., HOSEY, M. M., BENOVIC, J. L. & GUREVICH, V. V. 2004. Mapping the arrestin-receptor interface. Structural elements responsible for receptor specificity of arrestin proteins. *J Biol Chem*, 279, 1262-8.
- VISHNIVETSKIY, S. A., SCHUBERT, C., CLIMACO, G. C., GUREVICH, Y. V., VELEZ, M. G. & GUREVICH, V. V. 2000. An additional phosphate-binding element in arrestin molecule. Implications for the mechanism of arrestin activation. *J Biol Chem*, 275, 41049-57.
- VIVO, M., LIN, H. & STRANGE, P. G. 2006. Investigation of cooperativity in the binding of ligands to the D(2) dopamine receptor. *Mol Pharmacol*, 69, 226-35.
- VOISIN, T., GOUMAIN, M., LORINET, A. M., MAORET, J. J. & LABURTHE, M. 2000. Functional and molecular properties of the human recombinant Y4 receptor: resistance to agonist-promoted desensitization. *J Pharmacol Exp Ther*, 292, 638-46.
- VON ZASTROW, M. & KOBILKA, B. K. 1992. Ligand-regulated internalization and recycling of human beta 2-adrenergic receptors between the plasma membrane and endosomes containing transferrin receptors. *Journal of Biological Chemistry*, 267, 3530-3538.
- WAHLESTEDT, C., GRUNDEMAR, L., HAKANSON, R., HEILIG, M., SHEN, G. H., ZUKOWSKA-GROJEC, Z. & REIS, D. J. 1990a. Neuropeptide Y receptor subtypes, Y1 and Y2. *Ann N Y Acad Sci*, 611, 7-26.
- WAHLESTEDT, C., HAKANSON, R., VAZ, C. A. & ZUKOWSKA-GROJEC, Z. 1990b. Norepinephrine and neuropeptide Y: vasoconstrictor cooperation in vivo and in vitro. *Am J Physiol*, 258, R736-42.
- WAHLESTEDT, C., REGUNATHAN, S. & REIS, D. J. 1992. Identification of cultured cells selectively expressing Y1-, Y2-, or Y3-type receptors for neuropeptide Y/peptide YY. *Life Sci*, 50, PL7-12.
- WALDHOER, M., FONG, J., JONES, R. M., LUNZER, M. M., SHARMA, S. K., KOSTENIS, E., PORTOGHESE, P. S. & WHISTLER, J. L. 2005. A heterodimer-selective agonist shows in vivo relevance of G protein-coupled receptor dimers. *Proc Natl Acad Sci U S A*, 102, 9050-5.
- WALKER, P., MUNOZ, M., MARTINEZ, R. & PEITSCH, M. C. 1994. Acidic residues in extracellular loops of the human Y1 neuropeptide Y receptor are essential for ligand binding. *J Biol Chem*, 269, 2863-9.
- WALTHER, C., NAGEL, S., GIMENEZ, L. E., MORL, K., GUREVICH, V. V. & BECK-SICKINGER, A. G. 2010. Ligand-induced internalization and recycling of the human neuropeptide Y2 receptor is regulated by its carboxyl-terminal tail. *J Biol Chem*, 285, 41578-90.
- WANG, C., WU, H., KATRITCH, V., HAN, G. W., HUANG, X. P., LIU, W., SIU, F. Y., ROTH, B. L., CHEREZOV, V. & STEVENS, R. C. 2013. Structure of the human smoothed receptor bound to an antitumour agent. *Nature*, 497, 338-43.

- WANG, D., TAN, Y. C., KREITZER, G. E., NAKAI, Y., SHAN, D., ZHENG, Y. & HUANG, X. Y. 2006. G proteins G12 and G13 control the dynamic turnover of growth factor-induced dorsal ruffles. *J Biol Chem*, 281, 32660-7.
- WANG, L., GOURCEROL, G., YUAN, P. Q., WU, S. V., MILLION, M., LARAUCHE, M. & TACHE, Y. 2010. Peripheral peptide YY inhibits propulsive colonic motor function through Y2 receptor in conscious mice. *Am J Physiol Gastrointest Liver Physiol*, 298, G45-56.
- WARD, R. J., PEDIANI, J. D. & MILLIGAN, G. 2011. Ligand-induced internalization of the orexin OX(1) and cannabinoid CB(1) receptors assessed via N-terminal SNAP and CLIP-tagging. *Br J Pharmacol*, 162, 1439-52.
- WARNE, T., SERRANO-VEGA, M. J., BAKER, J. G., MOUKHAMETZIANOV, R., EDWARDS, P. C., HENDERSON, R., LESLIE, A. G., TATE, C. G. & SCHERTLER, G. F. 2008. Structure of a beta1-adrenergic G-protein-coupled receptor. *Nature*, 454, 486-91.
- WATSON, S. J., BROWN, A. J. & HOLLIDAY, N. D. 2012. Differential signaling by splice variants of the human free fatty acid receptor GPR120. *Mol Pharmacol*, 81, 631-42.
- WHITE, J. H., WISE, A., MAIN, M. J., GREEN, A., FRASER, N. J., DISNEY, G. H., BARNES, A. A., EMSON, P., FOORD, S. M. & MARSHALL, F. H. 1998. Heterodimerization is required for the formation of a functional GABA(B) receptor. *Nature*, 396, 679-82.
- WHORTON, M. R., BOKOCH, M. P., RASMUSSEN, S. G., HUANG, B., ZARE, R. N., KOBILKA, B. & SUNAHARA, R. K. 2007. A monomeric G protein-coupled receptor isolated in a high-density lipoprotein particle efficiently activates its G protein. *Proc Natl Acad Sci U S A*, 104, 7682-7.
- WHORTON, M. R., JASTRZEBSKA, B., PARK, P. S., FOTIADIS, D., ENGEL, A., PALCZEWSKI, K. & SUNAHARA, R. K. 2008. Efficient coupling of transducin to monomeric rhodopsin in a phospholipid bilayer. *J Biol Chem*, 283, 4387-94.
- WIELAND, H. A., ENGEL, W., EBERLEIN, W., RUDOLF, K. & DOODS, H. N. 1998. Subtype selectivity of the novel nonpeptide neuropeptide Y Y1 receptor antagonist BIBO 3304 and its effect on feeding in rodents. *Br J Pharmacol*, 125, 549-55.
- WILDEN, U., WUST, E., WEYAND, I. & KUHN, H. 1986. Rapid affinity purification of retinal arrestin (48 kDa protein) via its light-dependent binding to phosphorylated rhodopsin. *FEBS Lett*, 207, 292-5.
- WILLESEN, M. G., KRISTENSEN, P. & ROMER, J. 1999. Co-localization of growth hormone secretagogue receptor and NPY mRNA in the arcuate nucleus of the rat. *Neuroendocrinology*, 70, 306-16.
- WILSON, P. C., LEE, M. H., APPLETON, K. M., EL-SHEWY, H. M., MORINELLI, T. A., PETERSON, Y. K., LUTTRELL, L. M. & JAFFA, A. A. 2013. The arrestin-selective angiotensin AT1 receptor agonist [Sar1,Ile4,Ile8]-AngII negatively regulates bradykinin B2 receptor signaling via AT1-B2 receptor heterodimers. *J Biol Chem*, 288, 18872-84.
- WILSON, S., WILKINSON, G. & MILLIGAN, G. 2005. The CXCR1 and CXCR2 receptors form constitutive homo- and heterodimers selectively and with equal apparent affinities. *J Biol Chem*, 280, 28663-74.
- WISLER, J. W., DEWIRE, S. M., WHALEN, E. J., VIOLIN, J. D., DRAKE, M. T., AHN, S., SHENOY, S. K. & LEFKOWITZ, R. J. 2007. A unique

- mechanism of beta-blocker action: carvedilol stimulates beta-arrestin signaling. *Proc Natl Acad Sci U S A*, 104, 16657-62.
- WOLAK, M. L., DEJOSEPH, M. R., CATOR, A. D., MOKASHI, A. S., BROWNFIELD, M. S. & URBAN, J. H. 2003. Comparative distribution of neuropeptide Y Y1 and Y5 receptors in the rat brain by using immunohistochemistry. *The Journal of Comparative Neurology*, 464, 285-311.
- WOLFE, B. L. & TREJO, J. 2007. Clathrin-Dependent Mechanisms of G Protein-coupled Receptor Endocytosis. *Traffic*, 8, 462-470.
- WORTLEY, K. E., GARCIA, K., OKAMOTO, H., THABET, K., ANDERSON, K. D., SHEN, V., HERMAN, J. P., VALENZUELA, D., YANCOPOULOS, G. D., TSCHOP, M. H., MURPHY, A. & SLEEMAN, M. W. 2007. Peptide YY regulates bone turnover in rodents. *Gastroenterology*, 133, 1534-43.
- WU, B., CHIEN, E. Y., MOL, C. D., FENALTI, G., LIU, W., KATRITCH, V., ABAGYAN, R., BROOUN, A., WELLS, P., BI, F. C., HAMEL, D. J., KUHN, P., HANDEL, T. M., CHEREZOV, V. & STEVENS, R. C. 2010. Structures of the CXCR4 chemokine GPCR with small-molecule and cyclic peptide antagonists. *Science*, 330, 1066-71.
- WU, H., WACKER, D., MILENI, M., KATRITCH, V., HAN, G. W., VARDY, E., LIU, W., THOMPSON, A. A., HUANG, X. P., CARROLL, F. I., MASCARELLA, S. W., WESTKAEMPER, R. B., MOSIER, P. D., ROTH, B. L., CHEREZOV, V. & STEVENS, R. C. 2012. Structure of the human kappa-opioid receptor in complex with JD1c. *Nature*, 485, 327-32.
- WU, S., BIRNBAUMER, M. & GUAN, Z. 2008. Phosphorylation analysis of G protein-coupled receptor by mass spectrometry: identification of a phosphorylation site in V2 vasopressin receptor. *Anal Chem*, 80, 6034-7.
- WYATT, D., MALIK, R., VESECKY, A. C. & MARCHESE, A. 2011. Small ubiquitin-like modifier modification of arrestin-3 regulates receptor trafficking. *J Biol Chem*, 286, 3884-93.
- XIAO, K., MCCLATCHY, D. B., SHUKLA, A. K., ZHAO, Y., CHEN, M., SHENOY, S. K., YATES, J. R., 3RD & LEFKOWITZ, R. J. 2007. Functional specialization of beta-arrestin interactions revealed by proteomic analysis. *Proc Natl Acad Sci U S A*, 104, 12011-6.
- XIAO, K., SHENOY, S. K., NOBLES, K. & LEFKOWITZ, R. J. 2004. Activation-dependent conformational changes in {beta}-arrestin 2. *J Biol Chem*, 279, 55744-53.
- XU, B., FALLMAR, H., BOUKHARTA, L., PRUNER, J., LUNDELL, I., MOHELL, N., GUTIERREZ-DE-TERAN, H., AQVIST, J. & LARHAMMAR, D. 2013. Mutagenesis and computational modeling of human G-protein-coupled receptor Y2 for neuropeptide Y and peptide YY. *Biochemistry*, 52, 7987-98.
- YAO, F., SVENSJO, T., WINKLER, T., LU, M., ERIKSSON, C. & ERIKSSON, E. 1998. Tetracycline repressor, tetR, rather than the tetR-mammalian cell transcription factor fusion derivatives, regulates inducible gene expression in mammalian cells. *Hum Gene Ther*, 9, 1939-50.
- YESILALTAY, A. & JENNESS, D. D. 2000. Homo-oligomeric complexes of the yeast alpha-factor pheromone receptor are functional units of endocytosis. *Mol Biol Cell*, 11, 2873-84.
- YOSHIOKA, K., SAITOH, O. & NAKATA, H. 2001. Heteromeric association creates a P2Y-like adenosine receptor. *Proc Natl Acad Sci U S A*, 98, 7617-22.

- ZACHARIAS, D. A., VIOLIN, J. D., NEWTON, A. C. & TSIEN, R. Y. 2002. Partitioning of lipid-modified monomeric GFPs into membrane microdomains of live cells. *Science*, 296, 913-6.
- ZARJEVSKI, N., CUSIN, I., VETTOR, R., ROHNER-JEANRENAUD, F. & JEANRENAUD, B. 1993. Chronic intracerebroventricular neuropeptide-Y administration to normal rats mimics hormonal and metabolic changes of obesity. *Endocrinology*, 133, 1753-8.
- ZENG, C., WANG, Z., LI, H., YU, P., ZHENG, S., WU, L., ASICO, L. D., HOPFER, U., EISNER, G. M., FELDER, R. A. & JOSE, P. A. 2006. D3 dopamine receptor directly interacts with D1 dopamine receptor in immortalized renal proximal tubule cells. *Hypertension*, 47, 573-9.
- ZHANG, J., FERGUSON, S. S., BARAK, L. S., MENARD, L. & CARON, M. G. 1996. Dynamin and beta-arrestin reveal distinct mechanisms for G protein-coupled receptor internalization. *J Biol Chem*, 271, 18302-5.
- ZHANG, L., BIJKER, M. S. & HERZOG, H. 2011. The neuropeptide Y system: pathophysiological and therapeutic implications in obesity and cancer. *Pharmacol Ther*, 131, 91-113.
- ZHANG, L., RIEPLER, S. J., TURNER, N., ENRIQUEZ, R. F., LEE, I. C., BALDOCK, P. A., HERZOG, H. & SAINSBURY, A. 2010. Y2 and Y4 receptor signaling synergistically act on energy expenditure and physical activity. *Am J Physiol Regul Integr Comp Physiol*, 299, R1618-28.
- ZHUANG, T., CHEN, Q., CHO, M. K., VISHNIVETSKIY, S. A., IVERSON, T. M., GUREVICH, V. V. & SANDERS, C. R. 2013. Involvement of distinct arrestin-1 elements in binding to different functional forms of rhodopsin. *Proc Natl Acad Sci U S A*, 110, 942-7.
- ZIPF, W. B., O'DORISIO, T. M., CATALAND, S. & SOTOS, J. 1981. Blunted pancreatic polypeptide responses in children with obesity of Prader-Willi syndrome. *J Clin Endocrinol Metab*, 52, 1264-6.